frontiers | Research Topics

New insights into brain imaging methods for rehabilitation of brain diseases

Edited by
Guang-qing Xu, Ying Shen, Bin Hu and Feng Zhang

Published in
Frontiers in Neuroscience

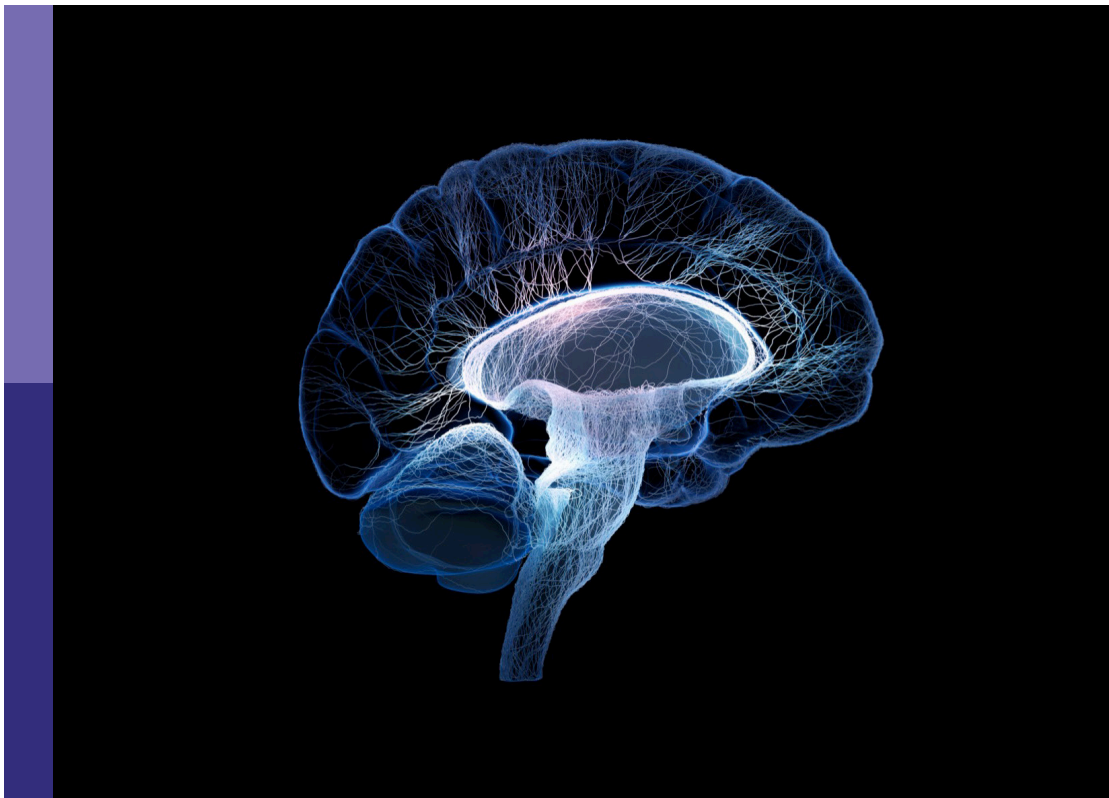

ISSN 1664-8714
ISBN 978-2-8325-4697-0
DOI 10.3389/978-2-8325-4697-0

About Frontiers

Frontiers is more than just an open access publisher of scholarly articles: it is a pioneering approach to the world of academia, radically improving the way scholarly research is managed. The grand vision of Frontiers is a world where all people have an equal opportunity to seek, share and generate knowledge. Frontiers provides immediate and permanent online open access to all its publications, but this alone is not enough to realize our grand goals.

Frontiers journal series

The Frontiers journal series is a multi-tier and interdisciplinary set of open-access, online journals, promising a paradigm shift from the current review, selection and dissemination processes in academic publishing. All Frontiers journals are driven by researchers for researchers; therefore, they constitute a service to the scholarly community. At the same time, the *Frontiers journal series* operates on a revolutionary invention, the tiered publishing system, initially addressing specific communities of scholars, and gradually climbing up to broader public understanding, thus serving the interests of the lay society, too.

Dedication to quality

Each Frontiers article is a landmark of the highest quality, thanks to genuinely collaborative interactions between authors and review editors, who include some of the world's best academicians. Research must be certified by peers before entering a stream of knowledge that may eventually reach the public - and shape society; therefore, Frontiers only applies the most rigorous and unbiased reviews. Frontiers revolutionizes research publishing by freely delivering the most outstanding research, evaluated with no bias from both the academic and social point of view. By applying the most advanced information technologies, Frontiers is catapulting scholarly publishing into a new generation.

What are Frontiers Research Topics?

Frontiers Research Topics are very popular trademarks of the *Frontiers journals series*: they are collections of at least ten articles, all centered on a particular subject. With their unique mix of varied contributions from Original Research to Review Articles, Frontiers Research Topics unify the most influential researchers, the latest key findings and historical advances in a hot research area.

Find out more on how to host your own Frontiers Research Topic or contribute to one as an author by contacting the Frontiers editorial office: frontiersin.org/about/contact

New insights into brain imaging methods for rehabilitation of brain diseases

Topic editors

Guang-qing Xu — The First Affiliated Hospital of Sun Yat-sen University, China
Ying Shen — The First Affiliated Hospital of Nanjing Medical University, China
Bin Hu — University of Calgary, Canada
Feng Zhang — Third Hospital of Hebei Medical University, China

Citation

Xu, G.-q., Shen, Y., Hu, B., Zhang, F., eds. (2024). *New insights into brain imaging methods for rehabilitation of brain diseases*. Lausanne: Frontiers Media SA.
doi: 10.3389/978-2-8325-4697-0

Table of contents

frontiers | Frontiers in Neuroscience

TYPE Editorial
PUBLISHED 20 March 2024
DOI 10.3389/fnins.2024.1397293

OPEN ACCESS

EDITED AND REVIEWED BY
Guo-Yuan Yang,
Shanghai Jiao Tong University, China

*CORRESPONDENCE
Bin Hu
✉ hub@ucalgary.ca

RECEIVED 07 March 2024
ACCEPTED 13 March 2024
PUBLISHED 20 March 2024

CITATION
Hu B (2024) Editorial: New insights into brain imaging methods for rehabilitation of brain diseases. *Front. Neurosci.* 18:1397293. doi: 10.3389/fnins.2024.1397293

Editorial: New insights into brain imaging methods for rehabilitation of brain diseases

Bin Hu*

Department of Clinical Neurosciences, Hotchkiss Brain Institute, Cumming School of Medicine, University of Calgary, Calgary, AB, Canada

KEYWORDS

neurorehabilitation, music therapy, brain imaging interventions, TMS, EEG, fMRI

Editorial on the Research Topic
New insights into brain imaging methods for rehabilitation of brain diseases

This editorial on the Research Topic of Neurorehabilitation aims to concisely present the contributions of each study within the broader context of neurorehabilitation research, showcasing the collaborative effort to advance the field.

First of all the landscape of neurorehabilitation is enriched by the pioneering studies of Wang et al., Zou et al., Yang et al., and their contemporaries, who collectively push the boundaries of our understanding and treatment capabilities for neurological conditions. These researchers harness a variety of innovative methods, from functional near-infrared spectroscopy (fNIRS) to machine learning algorithms, to explore cognitive impairment, motor function recovery, and beyond.

Wang et al.'s nomograms for predicting cognitive impairment post-TBI set a precedent for personalized patient care. Zou et al. and Yang et al. further this narrative by utilizing fNIRS to investigate cognitive impairment and the therapeutic potential of sensory tasks in stroke rehabilitation. The collaborative work of Chen, Zhang, et al. introduces a nuanced understanding of interhemispheric imbalance, advocating for individualized neuromodulation strategies.

In parallel, Lin et al. review the promising effects of noninvasive brain stimulation on dual-task performance, whereas Xiao et al. and Song et al. delve into the realms of music therapy and ultrasonic neuromodulation, revealing new therapeutic avenues. The studies by Yang et al. and Xia et al. emphasize the role of alternative therapies like acupuncture and the physiological insights from acoustic startle priming, broadening the scope of neurorehabilitation strategies.

Moreover, Liu L. et al.'s development of a rodent-specific TMS coil and Zhang et al.'s identification of biological markers for post-stroke depression exemplify the integration of technology and biology in research. Further contributions from Liu S. et al., Chen, Huang, et al., and Zhao et al. focus on the practical applications of these findings in clinical settings, from improving balance and gait in cerebral infarction patients to enhancing diagnostic accuracy for Alzheimer's disease.

The comprehensive analysis by Zhou et al. of oxidative stress in ischemic stroke underlines the importance of addressing biochemical pathways in recovery. Finally, Shen et al.'s study on the effects of focal muscle vibration therapy showcases the potential of physical interventions in activating brain regions for motor function improvement.

Collectively, these studies not only underscore the importance of multidisciplinary approaches in neurorehabilitation but also highlight the potential for significant advances in patient outcomes through the integration of innovative research and clinical practice.

Below I will further comment on the unique contributions made by different groups of contributing authors.

The study by Wang et al. investigates the prediction of cognitive impairment in patients in with mild-to-moderate traumatic brain injury (TBI) through clinical and radiological parameters. They developed nomograms based on identified risk factors, such as age, Glasgow Coma Scale score, education level, hyperlipidemia, temporal lobe contusion, traumatic subarachnoid hemorrhage, very early rehabilitation, and ICU admission, to predict cognitive impairment at 3 and 12 months post-injury. The nomograms demonstrated good discriminative ability, indicating their potential utility in clinical management and intervention planning for TBI patients.

The study by Zou et al. investigates the functional connectivity in post-stroke cognitive impairment patients using functional near-infrared spectroscopy (fNIRS). It compares resting-state functional connectivity among patients with post-stroke cognitive impairment, patients without cognitive impairment, and healthy controls. The findings reveal that patients with cognitive impairment exhibit significantly decreased interhemispheric and intra-right hemispheric functional connectivity, suggesting that fNIRS could be a valuable tool in identifying patients at risk of cognitive impairment following a stroke.

The study by Yang et al. focuses on the impact of a bilateral plantar contact task on dorsolateral prefrontal activation in cerebral infarction patients, under both open and closed eye conditions. Using functional near-infrared spectroscopy (fNIRS), the research found that performing the task with eyes open significantly influenced dorsolateral prefrontal cortex activation, especially on the paralyzed side. These findings suggest that cognitive-motor therapies, which activate cognitive control brain regions through sensory tasks, might be effective in rehabilitating motor functions in cerebral infarction patients.

The study by Chen, Huang, et al. explores the use of functional near-infrared spectroscopy (fNIRS) and transcranial magnetic stimulation (TMS) to assess interhemispheric imbalance and its correlation with motor function recovery after stroke. The research demonstrates that combining TMS and fNIRS metrics provides insights into the role of hemispheric activity in recovery, suggesting potential for developing individualized neuromodulation strategies for stroke rehabilitation.

The study by Lin et al. systematically reviews the effects of noninvasive brain stimulation (NIBS) on dual-task performance across different populations, including healthy young adults, older adults, and individuals with Parkinson's disease (PD) and stroke. The research assesses both transcranial direct current stimulation (tDCS) and repetitive transcranial magnetic stimulation (rTMS), focusing on their impact on balance, mobility, and cognitive function under single-task and dual-task conditions. The findings suggest promising effects of tDCS and rTMS in improving dual-task walking and balance performance across these diverse groups, although the heterogeneity of the studies and limited data prevent definitive conclusions.

In the groundbreaking study conducted by Xiao et al., the team delves into the realm of music therapy, showcasing its profound impact on patients in a minimally conscious state (MCS). This ingenious and high-quality original research not only sheds light on the significant improvements in autonomic nervous system indicators and Glasgow Coma Scale scores but also leads to a pivotal change in clinical practice. By comparing the outcomes among patients receiving music therapy to those provided with familial auditory stimulation or standard care, Xiao et al. reveal the potential of music therapy as a superior rehabilitative intervention. The research convincingly argues for the integration of music therapy into the standard neurorehabilitation protocol, marking a transformative step forward in enhancing the quality of life and recovery prospects for MCS patients. This study stands as a testament to the power of innovative therapeutic approaches in revolutionizing patient care in neurorehabilitation.

The study by Song et al. explores the potential of ultrasonic neuromodulation mediated by mechanosensitive ion channels, highlighting its non-invasive, high-resolution, and targeted approach as an alternative to drug-based and invasive therapies. This perspective outlines the roles of various mechanosensitive ion channels like Piezo and TRP channels in neuronal excitability and biological effects induced by ultrasound, emphasizing the need for deeper understanding and further research in this promising field.

The study by Yang et al. focuses on the effects of acupuncture on brain function in patients with Cerebral Small Vessel Disease Cognitive Impairment (CSVDCI). It utilized amplitude of low-frequency fluctuation (ALFF) analysis in a randomized control trial setting to assess changes in brain activity. The findings suggest that acupuncture treatment significantly modulates the functional activity of certain brain regions in CSVDCI patients, pointing toward its potential utility in enhancing cognitive functions through specific neural mechanisms.

The study by Xia et al. examines the effect of acoustic startle priming (ASP) on the activation of the reticulospinal tract (RST) and its influence on motor response time. Through an innovative approach using functional near-infrared spectroscopy (fNIRS), they observed increased activation in the right dorsolateral prefrontal cortex and changes in frontoparietal activity during ASP tasks. These findings suggest the involvement of the right dorsolateral prefrontal cortex and frontoparietal network in regulating the StartleReact effect and RST facilitation, providing new insights into the neural mechanisms underlying motor control and facilitation.

The study by Liu L. et al. introduces a novel rodent-specific transcranial magnetic stimulation (TMS) coil equipped with a custom shielding device to enhance focal stimulation. This development aims to improve the spatial focus of TMS in animal models, thereby facilitating more precise neuroscientific research. Their findings demonstrate that the shielding device significantly narrows the stimulated area without compromising the intensity of the core magnetic field, potentially enabling more targeted brain area stimulation in rodent studies of neurological disorders.

The study by Zhang et al. focuses on identifying biological features associated with post-stroke depression (PSD) through machine learning algorithms. By analyzing gene expression profiles and employing weighted gene co-expression network analysis

(WGCNA), the research identifies key genes and metabolic pathways linked to PSD. The findings highlight the potential of specific genes, SDHD and FERMT3, as diagnostic and therapeutic biomarkers for PSD, offering new avenues for early diagnosis and treatment strategies in stroke patients.

The study by Liu S. et al. explores the correlation between balance function, plantar pressure distribution, and gait parameters in patients with cerebral infarction in the basal ganglia region. It focuses on analyzing how balance function influences plantar pressure and hemiplegic gait, utilizing the Berg Balance Scale among other measures. The findings indicate a significant relationship between balance function and various gait and pressure parameters, suggesting that interventions aimed at improving balance could enhance gait performance and safety in stroke rehabilitation.

The study by Chen, Huang et al. analyzed spontaneous brain activity in patients with cerebral small vessel disease (cSVD), using amplitude of low-frequency fluctuation (ALFF) in different frequency bands. They found that cSVD patients exhibited significantly lower ALFF, particularly in the cerebellum, hippocampus, and occipital cortex compared to healthy controls, suggesting these regions' involvement in cSVD-related cognitive decline. This research adds to the understanding of cSVD's impact on brain function and its association with cognitive impairment.

The study by Zhao et al. reviews advancements in diagnosing Alzheimer's disease (AD) and mild cognitive impairment (MCI) using 11C-PIB-PET/CT imaging and common neuropsychological tests. It highlights the critical role of early detection and diagnosis through PET/CT imaging in identifying amyloid deposits, which are significant in the pathology of AD and MCI. This approach, combined with neuropsychological assessments, can improve diagnostic accuracy, offering a pathway for early intervention and potentially slowing disease progression.

The study by Zhou et al. provides a comprehensive analysis of hub genes related to oxidative stress in ischemic stroke. Through integrating datasets and employing machine learning methods, they identify key genes and pathways associated with oxidative stress, suggesting potential therapeutic targets. This research underscores the critical role of oxidative stress in stroke pathophysiology and highlights the promise of antioxidant therapy in treatment strategies.

The study by Shen et al. uses functional near-infrared spectroscopy (fNIRS) to examine the effects of focal muscle vibration (FMV) therapy on cortical activity in hemiplegic stroke patients. Specifically, it investigates how FMV applied to the forearm flexor muscles influences cortical regions and correlates with clinical characteristics. The results indicate FMV can activate additional brain cortices, including the prefrontal and sensorimotor areas, potentially supporting its use in stroke rehabilitation to enhance motor function and neural plasticity.

Author contributions

BH: Writing – original draft, Writing – review & editing.

Funding

The author(s) declare that no financial support was received for the research, authorship, and/or publication of this article.

Conflict of interest

The author declares that the research was conducted in the absence of any commercial or financial relationships that could be construed as a potential conflict of interest.

Publisher's note

frontiers | Frontiers in Neuroscience

TYPE Original Research
PUBLISHED 16 February 2023
DOI 10.3389/fnins.2023.1112046

OPEN ACCESS

EDITED BY
Ying Shen,
The First Affiliated Hospital of Nanjing Medical University, China

REVIEWED BY
Hanjun Liu,
Sun Yat-sen University, China
Xi Lu,
China-Japan Friendship Hospital, China

*CORRESPONDENCE
Xiaolin Huang
✉ xiaolinh2006@tjh.tjmu.edu.cn
Xiaohua Han
✉ hanxiao1470@hust.edu.cn

†These authors have contributed equally to this work and share first authorship

SPECIALTY SECTION
This article was submitted to Translational Neuroscience, a section of the journal Frontiers in Neuroscience

RECEIVED 30 November 2022
ACCEPTED 02 February 2023
PUBLISHED 16 February 2023

CITATION
Xia N, He C, Wei X, Li Y-A, Lou W, Gu M, Chen Z, Xu J, Liu Y, Han X and Huang X (2023) Altered frontoparietal activity in acoustic startle priming tasks during reticulospinal tract facilitation: An fNIRS study. *Front. Neurosci.* 17:1112046. doi: 10.3389/fnins.2023.1112046

Altered frontoparietal activity in acoustic startle priming tasks during reticulospinal tract facilitation: An fNIRS study

Nan Xia[1,2†], Chang He[3,4†], Xiupan Wei[1,2], Yang-An Li[1,2], Weiwei Lou[1,2], Minghui Gu[1,2], Zejian Chen[1,2], Jiang Xu[1,2], Yali Liu[1,2], Xiaohua Han[1,2*] and Xiaolin Huang[1,2*]

[1]Department of Rehabilitation Medicine, Tongji Hospital, Tongji Medical College, Huazhong University of Science and Technology, Wuhan, Hubei, China, [2]World Health Organization Collaborating Centre for Training and Research in Rehabilitation, Wuhan, China, [3]Institute of Medical Equipment Science and Engineering, Huazhong University of Science and Technology, Wuhan, Hubei, China, [4]State Key Lab of Digital Manufacturing Equipment and Technology, Institute of Rehabilitation and Medical Robotics, Huazhong University of Science and Technology, Wuhan, Hubei, China

Background: Because it is one of the important pathways for promoting motor recovery after cortical injury, the function of the reticulospinal tract (RST) has received increasing attention in recent years. However, the central regulatory mechanism of RST facilitation and reduction of apparent response time is not well understood.

Objectives: To explore the potential role of RST facilitation in the acoustic startle priming (ASP) paradigm and observe the cortical changes induced by ASP reaching tasks.

Methods: Twenty healthy participants were included in this study. The reaching tasks were performed with their left and right hands. Participants were instructed to get ready after the warning cue and complete the reach as soon as they heard the Go cue. Half of the testing trials were set as control trials with an 80-dB Go cue. The other half of the trials had the Go cue replaced with 114-dB white noise to evoke the StartleReact effect, inducing reticulospinal tract facilitation. The response of the bilateral sternocleidomastoid muscle (SCM) and the anterior deltoid was recorded *via* surface electromyography. Startle trials were labeled as exhibiting a positive or negative StartleReact effect, according to whether the SCM was activated early (30–130 ms after the Go cue) or late, respectively. Functional near-infrared spectroscopy was used to synchronously record the oxyhemoglobin and deoxyhemoglobin fluctuations in bilateral motor-related cortical regions. The β values representing cortical responses were estimated *via* the statistical parametric mapping technique and included in the final analyses.

Results: Separate analyses of data from movements of the left or right side revealed significant activation of the right dorsolateral prefrontal cortex during RST facilitation. Moreover, left frontopolar cortex activation was greater in positive startle trials than in control or negative startle trials during left-side movements. Furthermore, decreased activity of the ipsilateral primary motor cortex in positive startle trials during ASP reaching tasks was observed.

Conclusion: The right dorsolateral prefrontal cortex and the frontoparietal network to which it belongs may be the regulatory center for the StartleReact effect and RST facilitation. In addition, the ascending reticular activating system may be involved. The decreased activity of the ipsilateral primary motor cortex suggests enhanced inhibition of the non-moving side during the ASP reaching task. These findings provide further insight into the SE and into RST facilitation.

KEYWORDS

acoustic startle, functional near-infrared spectroscopy, reticulospinal tract, rehabilitation, frontoparietal cortex

Introduction

As part of the extrapyramidal system, the reticulospinal tract (RST) consists of bundles of axons that convey signals from the reticular formation in the brainstem to the spinal cord; it participates in movement control in humans (Baker, 2011). This descending pathway, together with the more well-known corticospinal tract (CST), constitutes the major control system of human voluntary movement (Brownstone and Chopek, 2018). However, compared to our understanding of the function of the CST, that of the RST has rarely been explored in humans. Based on animal research, the RST is thought to control proximal and axial muscles and be primarily responsible for locomotion (Matsuyama and Drew, 2000) and postural adjustment (Schepens and Drew, 2004). However, some recent studies in humans have revealed extensive participation of the RST in muscle contraction and motor control (Smith et al., 2019; Glover and Baker, 2022), and it plays a pivotal role in the remastering of motor control after brain injury (Zaaimi et al., 2012; Jang et al., 2015). The ipsilateral innervation (Boyne et al., 2021; Fisher et al., 2021; Ko et al., 2021) and abundant plasticity of the RST (Glover and Baker, 2020) provide tremendous potential for the recovery of motor function after CST impairment.

However, few methods or approaches have been developed to measure RST function in humans. Currently, most studies on human motor control by the RST utilize either the ipsilateral motor evoked potentials (iMEPs) *via* transcranial magnetic stimulation (Wassermann et al., 1994; Bawa et al., 2004; Maitland and Baker, 2021), the muscle activation latency after acoustic startle (Rangarajan et al., 2022) or a combination of the two (Smith et al., 2019) to deduce its function from target muscles. Through the cortical-reticulospinal pathway, transcranial magnetic stimulation likely indirectly affects the RST and triggers iMEPs of the target muscle (Fisher et al., 2012). The changes in activation latency and amplitude of iMEPs are believed to reflex RST adaptation during strength training and motor recovery from central nervous system injury (Alagona et al., 2001; Atkinson et al., 2022). Typically, iMEPs exhibit higher trigger thresholds and longer latencies than contralateral MEPs in healthy subjects (Bawa et al., 2004). However, in some patients with subcortical defects, a decreased threshold and shorter activation latency were also observed (Alagona et al., 2001). This phenomenon may be explained by the enhanced involvement of the RST in motor control after stroke (Zaaimi et al., 2012; Choudhury et al., 2019).

Acoustic startle stimuli are also widely used to explore the function of the RST in movement. Using a loud sound (>110 dB) as the start signal of a task can evoke the early initiation of prepared movement at an extremely short latency (DeLuca et al., 2022). This phenomenon is called the StartleReact effect (SE) and is recognized as the result of the rapid transmission of motion commands mainly *via* the RST (Carlsen and Maslovat, 2019). Despite not always occurring simultaneously (Leow et al., 2018), early activation of the sternocleidomastoid muscle (SCM) due to the startle reflex is strongly correlated with early initiation of movement in this paradigm (Maslovat et al., 2021). The SCM activation latency in the time window of 30 to 130 ms provides a convenient marker of the SE (Carlsen et al., 2011; van Lith et al., 2018). Therefore, analyses that simultaneously incorporate SCM response time and limb muscle activity enable better dissection of RST function in motor control (Maslovat et al., 2021). With this approach, researchers have revealed increased motor unit discharge (Skarabot et al., 2022), additional muscle contraction (Fernandez-Del-Olmo et al., 2014), a greater range of motion during motor initiation (McInnes et al., 2020), and even better motor (Rahimi and Honeycutt, 2020) or speech output (Swann et al., 2022) in stroke survivors. Given the hardware demands and technical challenges of this approach, using acoustic startle priming (ASP) to assess the characteristics and adaptation of the RST for motor control may be an easier approach.

In some previous studies, auditory stimuli have been found to modulate cortical excitability (Furubayashi et al., 2000; Lofberg et al., 2014), providing input *via* the ascending reticular activating system to the brain cortex (Saper et al., 2005). Furubayashi et al. (2000) were one of the first to examine the effects of acoustic stimuli on the cortex. Their study revealed transient inhibitory effects of sound stimuli on the motor cortex in the resting state. Subsequent studies further confirmed this inhibitory pathway derived from the RST (Fisher et al., 2004; Kuhn et al., 2004). However, the inhibitory effects detected in the resting state were completely reversed during motor preparation. In people highly prepared for action, corticospinal excitability was increased after loud auditory stimuli (Marinovic et al., 2014). A recent study also revealed that inducing the startle effect at the end of movement promotes motor learning and improves task performance (Leow et al., 2021). However, beneficial effects of ASP cannot be attributed to changes in excitability during preparation. The acoustic stimuli did not evoke significant changes in the ipsilateral motor cortex during preparation in a dual-coil transcranial magnetic stimulation (TMS) paradigm (Marinovic et al., 2015). A more recent study based on

a combined acoustic startle-TMS paradigm further validated the above findings and disentangled evidence of the cortical effects from the startle effect. The different MEP changes in the M1 at rest and during motor preparation induced by acoustic startle may be indirect and regulated by higher-level centers (Chen et al., 2022). Due to the limitation of TMS paradigms, it may be necessary to use imaging techniques to further verify the existence of this regulatory center.

Although the exact neural mechanism by which loud sounds induce the SE is unclear, it most likely involves some known subcortical and cortical pathways in the brain (Marinovic and Tresilian, 2016; Carlsen and Maslovat, 2019). In mammalian studies, two neural pathways (the cortico-striato-pallido-pontine network and an independent circuit from the central nucleus of the amygdala to the pontine reticular nucleus) have been found to participate in the modulation of prepulse inhibition of the auditory startle reflex (Cano et al., 2021; Zhang et al., 2022). Moreover, activity in the supplementary motor area (SMA), supramarginal gyrus, cingulate cortex, anterior insula and cerebellar lobule was also associated with startle stimuli (Mueller-Pfeiffer et al., 2014). Two hypothetical cortical circuits underlying ASP were proposed by Marinovic and Tresilian (2016) i.e., the startle stimuli may transmit information through the thalamus to the auditory cortex *via* the primary auditory pathway and then through other motor cortices to the primary motor cortex (M1) to form motor commands descending to the spinal cord. Additionally, the stimulus signal can directly reach the pontomedullary reticular formation (PMRF) and then the motor cortex *via* the thalamus to complete motor output. With the activation of these subcortical structures, the ascending reticular activation system (ARAS) is likely to be activated, which arises from the PMRF and has extensive connections with the frontal and parietal cortex, including the sensorimotor network (SMN). In addition, some high-level cortical modulation networks identified from resting-state functional magnetic resonance imaging (fMRI) (Yeo et al., 2011) also have confirmed connectivity with the ARAS (Weng et al., 2017; Wijdicks, 2019). Among them, the triple-network model (Menon, 2011) involving the default mode network (DMN) (Buckner, 2013), the lateral frontoparietal network (FPN) (Uddin et al., 2019), and the salience network (SN) (Menon and Uddin, 2010) has received substantial attention. As part of the central executive network, the FPN is located in the dorsolateral prefrontal cortex (dlPFC) and posterior parietal cortex and is involved in working memory, sustained attention, and problem solving. However, the DMN, which includes regions in similar areas, plays the opposite role. The DMN is active when an individual is not focused on external stimuli. The SN acts as an interface between the two networks; it integrates sensory, emotional and cognitive information to balance external stimuli with internal mental processes (Menon, 2011). These large-scale brain networks cover most of the frontal and parietal cortex and some subcortical regions.

Functional magnetic resonance imaging is an excellent method of measuring cortical activity. However, its limited space precludes large-scale arm and torso movements, as needed for the ASP reaching paradigm that we developed (Xia et al., 2021). Additionally, its magnetic field poses a large challenge to recording equipment. Functional near-infrared spectroscopy (fNIRS) provides another method of observing cortical activation during motor tasks. It is a non-invasive neuroimaging technique that detects changes in the oxygenation of hemoglobin in brain tissue *via* differences in optical absorption (Chen et al., 2020). With advances in data processing, it has been widely used to monitor cortical activation during various cognitive and motor tasks (Chen et al., 2020; Huo et al., 2021). Since fNIRS has less environmental limitations and allows a large range of motion during recording, it is a suitable method for dynamic observation of cortical activity during RST facilitation in the ASP reaching tasks.

In the present study, we aimed to investigate the cortical activation features associated with ASP during movement preparation and further explore the location of potential regulatory centers for the SE and RST facilitation. The bilateral prefrontal cortex, frontal cortex, M1, premotor cortex and SMA were regions of interest. The testing paradigm was consistent with our previous experiment, in which participants were first prompted to enter a state of high movement readiness and subsequently received ASP (Xia et al., 2021). We hypothesized that some motor-related cortices would show different activation in the presence of SE. The results of this study will help to reveal the mechanisms of the ASP-induced SE and RST facilitation. Regulatory centers necessary for RST facilitation can guide future in-depth research.

Materials and methods

Participants

A total of 20 volunteers (7 females and 13 males, mean age: 26.26 ± 6.65 years, mean body mass index: 22.80 ± 2.57 kg/m^2) were invited to participate in this study. All participants were healthy, right-handed, and had good tolerance for sudden 114-dB stimuli. Before participation, all subjects signed informed consent forms. Data from this study were part of a former project that was approved by the Ethics Committee of Tongji Hospital (No. TJ-IRB20210648) and preregistered (No. ChiCTR2100048222).

The sample size was estimated *via* G*Power 3.1 software based on the muscle activation latency of the AD after ASP. According to a recent review (DeLuca et al., 2022), the effect size d was set as 0.64, and 17 subjects were needed to detect significance with a paired t test with a power of 0.8 and an α level of 0.05. Accounting for a 15% drop-out rate, 20 subjects were needed.

Experimental procedure

The procedure for this test was exactly the same as that in our previous study (Xia et al., 2021). Participants were asked to sit in front of a blank blackboard in a quiet environment. First, the subject was asked to place their upper limbs next to their trunk and keep their whole bodies relaxed as much as possible. A pallet at 80% of shoulder height was placed on the anterolateral side of the testing limb at a distance of 120% of arm length. Subjects were asked to perform the reaching tasks according to the auditory stimuli from a headphone (Sennheiser HD25-I; Wedemark, Germany). The left and right sides of the subject were tested separately. To maintain sufficient attention during the testing process, three kinds of reaching tasks containing 10 repetitions each were randomly

assigned. These tasks included reaching to tap the center of the pallet and reaching to grasp a tennis ball or a coffee takeaway cup with the palm facing inward. Thus, each participant completed a total of 30 trials on their left and right sides.

After 10 consecutive trials, the subjects were allowed to rest and relax for 1 min. Each trial took approximately 23 s. In the first 5 s of the trial, participants were verbally informed of the upcoming task and then heard an 82-dB warning "beep" continuously for 0.5 s to prompt them to be ready. After 2.5–3 s, a 40-ms Go cue was emitted to initiate the aiming task. This sound clip was randomly placed in the aforementioned 500-ms interval to prevent anticipation. Half of the 30 trials were set as control trials, and their Go cues were the same 40-ms "beep" as the warning cue. However, the other 15 trials (startle trials) used a 40-ms 114-dB white noise clip as the Go cue. The order of control or startle trials was also randomized before each test. A 15-s interval was set between every two trials to allow full relaxation. To complete all reach tasks, participants used their left and right hands to perform 30 trials with 80-dB stimuli (control trials) and 114-dB stimuli (startle trials), with 15 trials each. The Psychtoolbox-3 package within MATLAB (2017b, MathWorks, USA) was used to design and implement those tests. A custom-written program was used to simultaneously trigger the markers on the surface electromyography (sEMG) and fNIRS systems as the Go cue was released.

Surface electromyography and data preprocessing

The Ultium EMG system (Noraxon USA Inc., Scottsdale, AZ, USA) was used to collect the sEMG signals with a sampling rate of 2,000 Hz. Our experimental procedures followed SENIAM recommendations. After the electrodes were connected to the acquisition unit, they were placed on the muscle belly of both (bilateral) SCMs and the anterior deltoid (AD) of the movement side.

Raw sEMG data were processed in MATLAB (2017b, MathWorks, Natick, MA, USA). After data segmentation, the data were bandpass filtered (30–300 Hz) and then notch filtered at 50 Hz. The Teager–Kaiser energy operation was applied to further process the filtered data to achieve higher reliability of muscle onset (Solnik et al., 2010). The threshold method was used to detect the muscle onset time. The threshold was set as the mean + 3 SD of baseline amplitude at a time window of 2,500–500 ms before the Go cue on each trial. The time intervals from the Go cue to muscle onset of SCMs and the AD were recorded as the reaction time and activation latency, respectively, for further analysis.

Trials were first excluded if the AD reaction time did not occur in the time window of 30 to 400 ms after the Go cue. For startle trials, those with a reaction time of either SCM within 30 to 130 ms after the Go cue were marked as a positive startle reaction (SCM^+) (van Lith et al., 2018). Similarly, those without obvious SCM activation in this interval were marked as a negative startle reaction (SCM^-). In addition, taking into account the SCM^+ incidence in the previous study (Xia et al., 2021) and the requirements of fNIRS data analysis, data from subjects with a disproportionately low proportion of SCM^+ trials (<3/15) were considered invalid and excluded from the analysis.

Functional near-infrared spectroscopy (fNIRS) and data preprocessing

During testing, changes in deoxyhemoglobin (HbR) and oxyhemoglobin (HbO) concentrations were monitored *via* a wearable fNIRS device (NIRSport2, Nirx Medical Technologies LLC, Berlin, Germany). Subjects were asked to rest in a quiet sitting position for more than 1 min before starting the test. Forty valid NIRS channels with 16 dual-wavelength LED sources (760 nm and 850 nm) and 16 detectors were placed to cover the bilateral prefrontal cortex, frontal cortex, M1, premotor cortex and SMA. The distance between the first source and detector was 3.1 cm, and the exact distance of the other channels was automatically calculated by nirsLAB software (version 2017.06, NIRx Medical Technologies, Glen Head, NY, USA). The HbR and HbO concentrations at each location were recorded at a sampling rate of 6.1 Hz. The detailed locations of each source and detector as well as the representative Brodmann area and MNI coordinates of each channel are provided in **Figure 1** and **Table 1**.

The fNIRS data were processed *via* nirsLAB software (version 2017.06, NIRx Medical Technologies, Glen Head, NY, USA). During data processing, invalid error trials and tests marked during sEMG data processing were excluded from subsequent analysis. The two 1-min resting periods in each test were truncated. Data from 5 s before to 35 s after the Go cue in each trial were retained for analysis. Data from 100 s before the first trial to 50 s after the last trial were also preserved as a baseline reference. The gain setting (Zhang et al., 2018) and coefficient of variation were set at 7 and 15%, respectively, to improve the signal-to-noise ratio. Datasets with over 10 bad channels (out of 40 total channels) were excluded from further analysis. Discontinuities and spike artifacts were removed with a 5-SD threshold. Then, a bandpass filter at 0.01 to 0.09 Hz (Pinti et al., 2018) was used to filter the remaining data. The intensity data were converted into optical density changes and transformed to relative fluctuations of HbO/HbR concentrations by using the modified Beer-Lambert law (Cope and Delpy, 1988). Both the HbO and HbR signals were chosen for subsequent processing. An event time window of 5 s after each warning cue in each trial was set to calculate the hemodynamic response function with HbO/HbR fluctuations based on a generalized linear model. Within-subject statistical parametric mapping (SPM) was used to estimate the β values of each fNIRS channel.

Statistical analyses

The tasks with the left and right hands were processed and analyzed separately. Due to the similar sEMG responses (Xia et al., 2021), the side differences in the three reaching tasks were neglected in this study. The reaction time of SCM in each kind of trial of each subject was averaged and reported as the mean with standard deviation. The activation latency of AD in the control, SCM^+ and SCM^- trials was averaged for each separate left- or right-side test and reported as the mean with standard deviation. The Shapiro-Wilk test was used to evaluate the normal distribution of variables. After confirming the homogeneity of variance, two-way analyses of variances (ANOVAs) with Bonferroni *post hoc* comparisons were used to identify significant difference in muscle

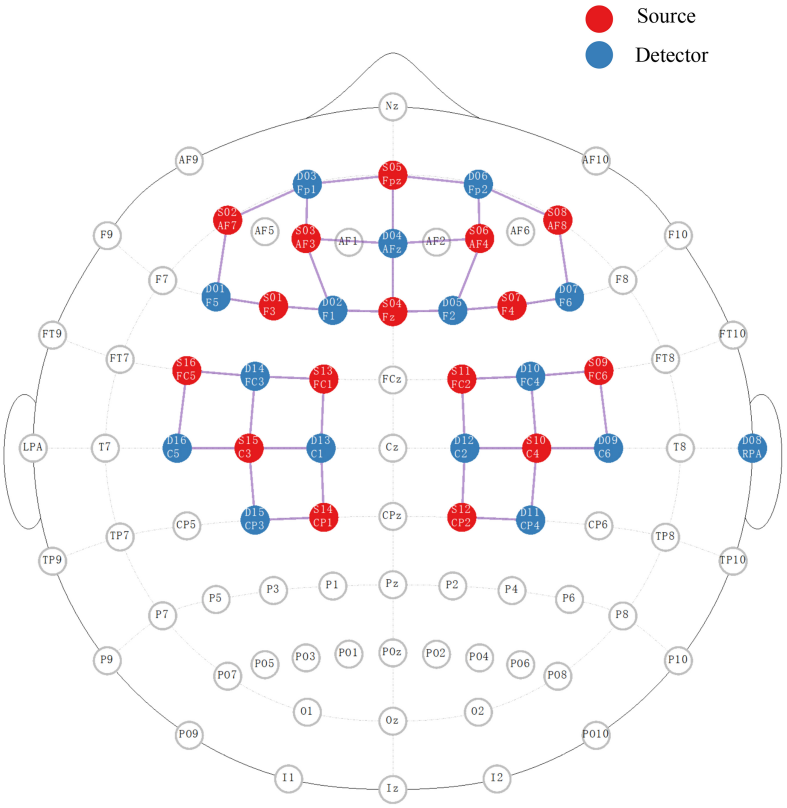

FIGURE 1
The placement of sources and detectors for fNIRS detection in 10/10 EEG system. The red and blue circles represent the ordered sources and detectors, respectively. The pink line between the two represents the active channel used for this study.

reaction time according to trial type and movement side. Two-way ANOVAs with Bonferroni *post hoc* comparisons were used to detect differences in β values of channels in the same model. However, few significant differences in β values within different trials were found. No difference was detected between the left and right movement sides. A further one-way ANOVA for data from each movement side was also performed. However, the only significant differences among the three kinds of trials were in β values from channel 17 on the HbR response. In addition, the large standard deviations of β values from these channels revealed large interindividual variability. Considering that this study involved a within-subjects design, paired *t* tests with a Bonferroni correction ($P < 0.05/2 = 0.025$) were chosen as an alternative method of detecting within-individual differences in β values between pairs among the 3 kinds of trials. SPSS 24.0 software (SPSS, Chicago, IL, USA) was used for statistical analyses, and the significance was set at $P < 0.05$.

Results

Characteristics of valid trials and comparison of muscle activation latency

A total of 40 datasets from the left and right sides of 20 subjects were collected. Among them, 8 datasets were directly excluded from subsequent analysis because there were fewer than 20% of SCM^+ trials (3/15 trials). Similarly, two other datasets were eliminated due to the number of bad channels in the simultaneously collected fNIRS data (>10/40 channels). Of the remaining 900 trials from 30 datasets, 32 trials were further excluded due to apparent early movement initiation (AD reaction time <30 ms) or delayed initiation (AD reaction time >400 ms). Therefore, data from 30 datasets (15 from the left side to 15 from the right side) consisting of 429 control trials, 166 SCM^+ trials, and 273 SCM^- trials were included in the final analyses. Supplementary Material 1 provides the proportion of SCM^+ trials in the left- or right-side movements of each subject. The mean positive startle rate (SCM^+) was approximately 37.95%. The mean SCM response times of the control and $SCM^{+/-}$ trials were 201.62 ± 74.36 ms and 117.31 ± 52.69/141.28 ± 58.95 ms, respectively. Two-way ANOVAs revealed a significant main effect of trial type on SCM response time [$F(2,825) = 111.76$, $P < 0.001$], and the *post hoc* Bonferroni comparisons also revealed significant differences between control and SCM^+ trials ($P < 0.001$) and between SCM^+ and SCM^- trials ($P < 0.001$). No significant difference was found between control and SCM^- trials ($P > 0.05$). Moreover, significant main effects of trial type (SCM^+, SCM^-, or control) [$F(2,867) = 77.88$, $P < 0.001$] and movement side [$F(1,867) = 1.06$, $P = 0.025$] on the AD reaction time were detected. Significant differences between each pair of trials were found in the *post hoc* Bonferroni comparisons ($P < 0.01$). The mean AD

TABLE 1 Coordinates and cortical areas of the fNIRS channels.

Channel no.	Source-detector	10/10_EEG_system	MNI coordinate			Brodmann area	Specificity (%)
			X (mm)	*Y* (mm)	*Z* (mm)		
1	S1-D1	F3-F5	−46	39	26	45–pars triangularis Broca's area	72.56
2	S1-D2	F3-F1	−31	39	41	9–Dorsolateral prefrontal cortex	66.61
3	S2-D1	AF7-F5	−47	46	6	46–Dorsolateral prefrontal cortex	43.20
4	S2-D3	AF7-Fp1	−33	59	−2	11–Orbitofrontal area	32.71
5	S3-D2	AF3-F1	−23	52	32	9–Dorsolateral prefrontal cortex	48.44
6	S3-D3	AF3-FP1	−24	63	9	10–Frontopolar area	69.63
7	S3-D4	AF3-AFz	−12	62	23	10–Frontopolar area	75.76
8	S4-D2	Fz-F1	−9	41	50	9–Dorsolateral prefrontal cortex	63.16
9	S4-D4	Fz-Afz	2	50	39	9–Dorsolateral prefrontal cortex	61.77
10	S4-D5	Fz-F2	10	41	50	9–Dorsolateral prefrontal cortex	68.93
11	S5-D3	Fpz-Fp1	−12	67	0	10–Frontopolar area	54.50
12	S5-D4	Fpz-AFz	1	64	14	10–Frontopolar area	87.48
13	S5-D6	Fpz-Fp2	13	67	0	10–Frontopolar area	54.46
14	S6-D4	AF4-Afz	13	61	24	10–Frontopolar area	72.47
15	S6-D5	AF4-F2	22	52	33	9–Dorsolateral prefrontal cortex	51.52
16	S6-D6	AF4-Fp2	25	63	9	10–Frontopolar area	68.78
17	S7-D5	F4-F2	30	40	41	9–Dorsolateral prefrontal cortex	68.37
18	S7-D7	F4-F6	48	42	22	46–Dorsolateral prefrontal cortex	82.10
19	S8-D6	AF8-Fp2	34	59	−2	10–Frontopolar area	31.08
20	S8-D7	AF8-F6	48	46	5	46–Dorsolateral prefrontal cortex	43.18
21	S9-D9	FC6-C6	66	−3	24	6–Pre-motor and supplementary motor cortex	66.08
22	S9-D10	FC6-FC4	56	12	33	6–Pre-motor and supplementary motor cortex	40.06
23	S10-D9	C4-C6	62	−20	37	2–primary somatosensory cortex	27.65
24	S10-D10	C4-FC4	52	−4	48	6–Pre-motor and supplementary motor cortex	56.87
25	S10-D11	C4-CP4	53	−35	52	40-Supramarginal gyrus part of Wernicke's area	50.04
26	S10-D12	C4-C2	42	−21	62	4–Primary motor cortex	36.77
27	S11-D10	FC2-FC4	39	12	54	6–Pre-motor and supplementary motor cortex	38.21
28	S11-D12	FC2-C2	27	−4	68	6–Pre-motor and supplementary motor cortex	82.46
29	S12-D11	CP2-CP4	39	−49	60	40-Supramarginal gyrus part of Wernicke's area	45.11
30	S12-D12	CP2-C2	28	−36	71	4–Primary motor cortex	31.56
31	S13-D13	FC1-C1	−26	5	68	6–Pre-motor and supplementary motor cortex	81.78
32	S13-D14	FC1-FC3	−38	12	55	6–Pre-motor and supplementary motor cortex	37.52
33	S14-D13	CP1-C1	−27	−36	71	4–Primary Motor Cortex	31.56
34	S14-D15	CP1-CP3	−39	−48	60	40-Supramarginal gyrus part of Wernicke's area	41.82
35	S15-D13	C3-C1	−42	−20	62	4–Primary motor cortex	34.98
36	S15-D14	C3-FC3	−50	−3	50	6–Pre-motor and supplementary motor cortex	61.71
37	S15-D15	C3-CP3	−52	−34	52	40-Supramarginal gyrus part of Wernicke's area	43.32
38	S15-D16	C3-C5	−60	−18	37	3–primary somatosensory cortex	23.83
39	S16-D14	FC5-FC3	−55	12	34	44–part of Broca's area/ 6–Pre-motor and supplementary motor cortex	47.81/35.96
40	S16-D16	FC5-C5	−62	−3	23	43–Subcentral area	47.13

reaction times of $SCM^{\pm}$ trials and control trials in the right-side movements were 132.07 ± 39.97/157.84 ± 43.28 ms and 191.65 ± 72.02 ms, respectively. The mean AD reaction times of $SCM^{+/-}$ trials and control trials in the left-side movements were 134.91 ± 49.04/166.01 ± 47.46 ms and 203.76 ± 70.26 ms, respectively. The activation latency of AD in SCM^{+} trials was approximately 60 ms faster than that in control trials.

Comparisons of β values in fNIRS data among control, SCM^{+}, and SCM^{-} trials

Thirty datasets (15 left-side and 15 right-side) from 17 subjects were included in the analyses. The primary outcome was differences in β values of the 40 channels among control, SCM^{+}, and SCM^{-} trials.

TABLE 2 The results of β value comparisons among control, SCM^+, and SCM^- trials in the positive channels.

Channel	Left and right side tasks	HbO/HbR	Trials	β values ($\times 10^{-5}$)			*Paired-T*	*t*	*Uncorrected P*-values
				Mean	SD	SEM			
			Control	−0.69	18.48	4.62	SCM^+ vs. Control	−2.98	0.009
11	Left	HbR	SCM^+	8.32	21.25	5.30	SCM^+ vs. SCM^-	2.98	0.009
			SCM^-	−3.02	70.78	22.75			
			Control	24.03	271.12	70.00	SCM^+ vs. Control	−2.86	0.013
17	Right	HbR	SCM^+	156.61	350.21	90.42			
			SCM^-	−136.49	274.13	70.78			
			Control	1.72	19.15	4.79	SCM^+ vs. SCM^-	−3.13	0.007
18	Left	HbO	SCM^+	−12.43	35.50	8.88			
			SCM^-	−1.02	32.35	8.09			
			Control	−46.78	920.95	246.14	SCM^+ vs. SCM^-	−3.00	0.010
30	Left	HbO	SCM^+	−280.33	833.95	222.88			
			SCM^-	343	922.36	246.51			
			Control	−171.48	272.07	90.69	SCM^+ vs. SCM^-	−2.96	0.017
33	Right	HbR	SCM^+	9.28	273.11	91.04			
			SCM^-	−281.92	489.79	163.26			

SD and SEM represent standard deviation and standard error of mean, respectively.

In the right-side movements, the one-way ANOVA revealed a significant main effect of trial type [$F(2,42) = 3.57$, $P = 0.037$] on the β values of the HbR response in channel 17. The *post hoc* Bonferroni comparisons suggested significantly higher fluctuation in SCM^+ trials than in SCM^- trials ($P = 0.032$). Although this *post hoc* comparison did not reveal a significant difference between SCM and control trials ($P > 0.05$), the difference between the two kinds of trials was revealed *via* a paired *t* test after Bonferroni correction ($t_{14} = -2.858$, uncorrected $P = 0.013$). Additionally, the HbR responses in SCM^+ trials of channel 33 were significantly smaller than those in control trials ($t_{12} = -2.961$, uncorrected $P = 0.017$). However, no differences were found in the other pairwise comparisons after Bonferroni correction ($P > 0.05$). As shown in Table 1 and Figure 1, channel 17 and channel 33 had specificities of 68.37 and 31.56%, respectively, for the right dlPFC and left M1. No differences were found in the β values of HbR responses in other channels or in HbO responses in all channels ($P > 0.05$).

In the left-side movements, paired *t* tests revealed a significant difference in β values from HbR in channel 11 between SCM^+ trials [$(8.32 \pm 21.21) \times 10^{-5}$] and control trials [$(-0.69 \pm 18.48) \times 10^{-5}$] ($t_{12} = -2.976$, uncorrected $P = 0.009$). A greater response was also found in SCM^+ trials than in SCM^- trials [$(-3.02 \pm 22.75) \times 10^{-5}$] ($t_{11} = 2.976$, uncorrected $P = 0.009$). No difference was found between the SCM and control trials ($P > 0.05$). Channel 11 had a specificity of 54.50% for the left frontopolar area. In the comparison between SCM^+ and SCM^- trials, paired *t* tests revealed significantly larger and smaller HbO responses of SCM^+ trials in channels 18 ($t_{12} = -3.132$, uncorrected $P = 0.007$) and 30 ($t_{12} = -3.002$, uncorrected $P = 0.010$), respectively. However, no differences were found in other pairwise comparisons after Bonferroni correction ($P > 0.05$). The above two channels correspond to the right dlPFC (specificity: 82.10%) and the right M1 (specificity: 31.56%), respectively. The β values of the 3 kinds of trials for every positive channel of HbO/HbR responses are provided in Table 2.

Each trial took approximately 23 s, so the event-related fluctuations in HbO/HbR concentrations of approximately 0.043 Hz were likely to occur in the relevant cortex. The representative results of the block-averaged hemodynamic response in HbR/HbO concentrations of channel 11 (left frontopolar area), channel 18 (right dlPFC) and channel 30 (left M1) during the left-side tests are provided in Figure 2. Figures 2A, B show the hemodynamic responses in HbO/HbR concentrations of channel 11 for control, SCM^+ and SCM^- trials 35 s after the warning cue. Figure 2B further shows the HbR responses. There was a significantly greater response in SCM^+ trials than in the other two trials according to paired *t* tests. Figures 2C–F show the hemodynamic HbO/HbR responses and the positive HbO responses, respectively, during the same period.

Figure 3 displays representative results from one subject and one movement side of statistical parametric mapping analysis of the fNIRS data (HbO and HbR) that were used in pairwise *t* test (1: −1) of brain activation between SCM^+ and SCM^- trials. The differences in activation of the frontal lobe and ipsilateral M1 are shown.

Discussions

Previous studies investigated the facilitating effects of acoustic startle stimuli on cortical and subcortical areas (Mueller-Pfeiffer et al., 2014; Zhang et al., 2022). However, few studies investigated the activation of the non-motor cortex and potential brain

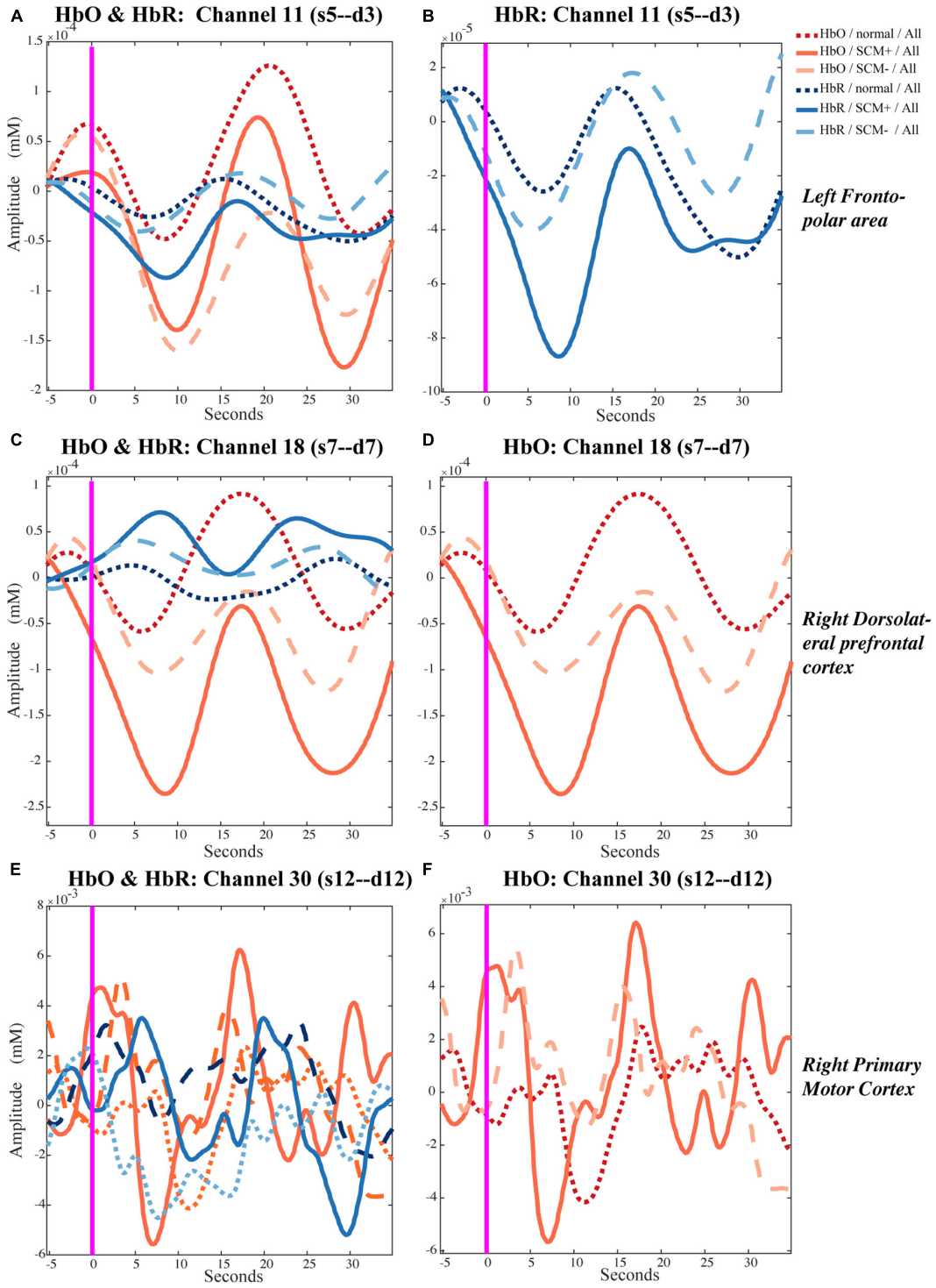

FIGURE 2
Temporal hemodynamic response of HbO and HbR in control, SCM^{+} and SCM^{-} trials. **(A,B)** Show the hemodynamic responses in HbO/HbR concentrations of channel 11 for control, SCM^{+} and SCM^{-} trials 35 s after the warning cue. In panel **(B)** shows the HbR responses. **(C,D)** Show the hemodynamic HbO/HbR responses and the positive HbO responses in channel 18, respectively. **(E,F)** Show the hemodynamic HbO/HbR responses and the positive HbO responses in channel 30, during the same period.

networks. In contrast to commonly used methods of observing brain activation under loud stimuli, we used the ASP motor task to explore the various cortical effects of ASP from movement preparation to movement initiation. As summarized by Marinovic and Tresilian (2016) as the expected moment of motor initiation draws near, preparatory activation of the movement response circuits occurs, and acoustic stimulus-evoked activity can enhance this activation. Sudden stimuli have activating or arousing effects on the sensorimotor system, which could initiate command generation. Moreover, the triggering effect may depend on the

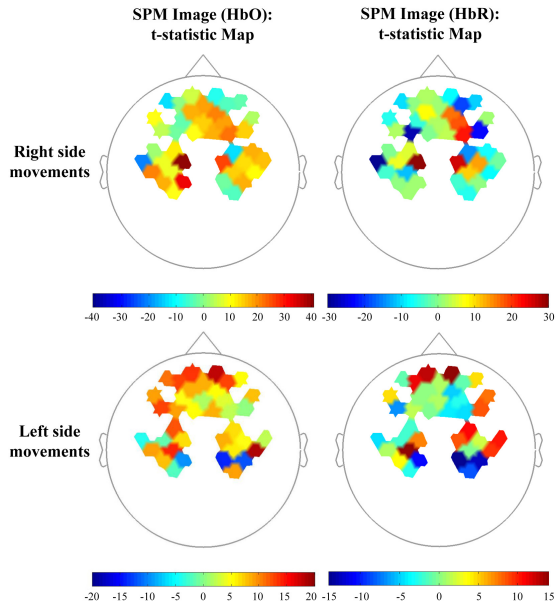

FIGURE 3
Topographic maps in the comparison among control and SCM$^{+/-}$ trials of one subject. The beta images (HbO and HbR) of SCM^{+} and SCM^{-} trials were set as 1 and −1, respectively for the *t*-statistic map.

amplitude and timing of stimuli. Accordingly, the SE is likely regulated by a higher-level network (Chen et al., 2022). Based on our findings, the possible brain network mechanisms leading to ASP are discussed below.

In the present study, we found that ASP reaching trials with successful RST facilitation (SCM^{+} trials) evoked greater cortical activation in prefrontal areas. This result is consistent with the hypothesized existence of a regulatory center for ASP-induced movements (Chen et al., 2022). Moreover, SCM^{+} trials from both left- and right-side movements exhibited greater activation in the right dlPFC than control or SCM^{-} trials. Furthermore, consistent with previous findings that there was no obvious activation of the M1 after acoustic startle stimuli (Mueller-Pfeiffer et al., 2014; Chen et al., 2022), we found a potential inhibitory effect of the startle on the ipsilateral M1 during RST facilitation. The M1 ipsilateral to the movement side showed a smaller HbR/HbO response during the ASP reaching trials.

Additional ASP-induced activation of prefrontal areas

Additional activation in the left frontopolar area (Brodmann area 10) was found during the left-side ASP reaching tasks in SCM^{+} trials. The anterior portion of the prefrontal cortex in the human brain is involved in memory recall, decision-making, and various executive functions (Ramnani and Owen, 2004; Koechlin and Hyafil, 2007). Previous studies have noted that anterior prefrontal activity occurs in motor preparation for a cued movement (Sahyoun et al., 2004). This cortical activity, which represents the level of attentional focus and movement readiness, is obviously closely related to the occurrence of the SE and the reduced reaction time during RST facilitation (Carlsen et al., 2012; Leow et al., 2018). These areas typically play an inhibitory role in motor execution (Brass et al., 2001).

Moreover, the additional activation of the right dlPFC was more prominent in SCM^{+} trials of both left and right ASP reaching tasks. This result highlights the important role of the right dlPFC in RST facilitation. It is well known that the dlPFC plays a key role in motor planning, organization, and regulation (Kaplan et al., 2016). Additionally, the FPN to which the dlPFC belongs serves as a flexible hub to rapidly instantiate task states through interactions with other control and processing networks (Marek and Dosenbach, 2018). This network is activated during motor sequence tasks and contributes to motor learning (Maruyama et al., 2021). Simultaneous activation of the FPN and M1 during motor preparation was also found (Maruyama et al., 2021). In addition, the FPN was also found to receive projections from the ARAS, which is primarily responsible for consciousness (Jang et al., 2021). The connection strength between the FPN and ARAS revealed a clear positive correlation with the state of consciousness. Patients in a vegetative state showed a substantial reduction in the connectivity strength between the PMRF and the frontal cortex (Jang et al., 2021). More precisely, in the ARAS, one dopamine signaling pathway arising from the ventral tegmental area has been proven to play a facilitative role in the frontal cortex (Brown et al., 2011). Additionally, supported by the ARAS, the signal from the PMRF can also reach the motor cortex *via* the thalamus and cause excitability of the motor cortex (Brown et al., 2011; Marinovic and Tresilian, 2016). Thus, after activating the cochlear nucleus by loud acoustic stimuli, an upward signal will reach the PMRF and then activate the FPN and motor cortex.

In addition, the right dlPFC may also be involved in threat-induced anxiety. Greater activity in the right dlPFC was found in subjects who classified themselves as behaviorally inhibited (Shackman et al., 2009). In our experiment, a 114-dB acoustic stimulus was used for the Go cue of the prepared reaching task. In addition to inducing the SE, it also induced a sense of threat and anxiety.

Dissociable contributions of the right and left dlPFC to different task demands have been investigated previously (Kaller et al., 2011), and the right dlPFC may be more involved in the planning of simple tasks such as ASP reaching. Moreover, some evidence also indicates lateralization of the PFN. The left PFN may be more strongly related to language function (Smith et al., 2009) rather than movement. The right dlPFC is also better at reactive inhibition (van Belle et al., 2014). Thus, activation of the right dlPFC did not appear to differ between left and right ASP tasks.

Enhanced inhibitory effect of ASP on the ipsilateral M1

Typically, activation of the M1 is unlikely to occur prior to movement onset. The ipsilateral motor cortex (resting side) is in an inhibited state during motor preparation and execution (Leocani et al., 2000). In a study based on the dual TMS paradigm, Marinovic et al. (2015) found that MEPs on the resting side were significantly facilitated only after movement initiation of the acting side. There is robust evidence that the ipsilateral M1 is significantly suppressed

during this period. This inhibition of M1 activity ipsilateral to the movement side may involve cortico-cortical and subcortico-cortical circuits.

The interhemispheric inhibition of the two sides of the M1 or from the motor-related cortex in the contralateral hemisphere has been well explored in previous studies (Ni et al., 2009; Perez and Cohen, 2009). It is generally believed that the involvement of transcallosal glutamatergic pathways links the pyramidal tract with GABAergic interneurons (Reis et al., 2008). It has also been noted that dysgenesis of the corpus callosum significantly affects the function of the FPN (Hearne et al., 2019). Therefore, it can be inferred that there is a potential connection between the FPN and the corpus callosum. Since the corpus callosum plays a key role in interhemispheric inhibition, the FPN may be indirectly involved in this inhibitory regulation of the contralateral motor cortex. However, the exact mechanism remains unclear.

In addition, the FPN may play a facilitating role in the motor cortex responsible for the current movement. In some sequential motor-learning tasks, the FPN and M1 contralateral to the movement side exhibit simultaneous activation during the preparation phase (Maruyama et al., 2021). This is explained as internal reproduction and learning during the motor preparation phase. After the hypothetical motor commands were generated in one side of the M1, a well-timed activation signal from the PMRF-ARAS triggered its early release, which was quickly output to the periphery *via* the RST descending pathway (Marinovic and Tresilian, 2016; Carlsen and Maslovat, 2019). This activation *via* the ARAS is likely to induce a signal that ascends bilaterally but may be ineffective for the contralateral M1, where no motor commands are generated.

The inhibition of the excitability of the ipsilateral M1 in this study may be attributable to our modification of the testing paradigm. In those TMS tests (Marinovic et al., 2015; Chen et al., 2019, 2022), all trials with loud startle stimuli were involved, but our study suggested that approximately half of the startle stimuli did not induce the SE. The occurrence of SE has been confirmed to be highly related to the level of preparation (Leow et al., 2018). Therefore, the absence of a clear definition of successful induction of the SE may dilute the positive trials and thus cause underestimation of this effect in the analyses. In addition, this cortical activity might be task specific. The finger or arm movements used in their tests may evoke lower cortical activation when compared with the reaching tasks, which involve substantial trunk and proximal joint movements. Since the measurement channel for the M1 had low specificity in this study, further confirmation is still needed. Furthermore, as suggested by other researchers (Carlsen et al., 2003; Carlsen and Maslovat, 2019; Maslovat et al., 2021), using SCM^{+} as a marker of successful induction of the SE should be considered in future studies.

In addition, the SN, which is in the same triple-network model as the FPN, may also influence activation. It is mainly responsible for detecting salient events and initiating appropriate control signals to other cortices or networks (Menon and Uddin, 2010; Menon, 2011). In the present study, it seemed to produce a stronger facilitation effect than control or SCM^{-} trials on the right FPN during RST facilitation. Since the regions of interest designated in the present study did not include the anterior insula and anterior cingulate cortex, regions in the SN, further verification is needed.

Interpretation of the negative fluctuation in HbO/HbR signals

From previous studies, we know that the frontal cortex plays an important role in premotor information processing and motor task preparation (Sahyoun et al., 2004; Koechlin and Hyafil, 2007). Activation of the frontal cortex occurs before task execution and decreases with the advent of movement (Suzuki et al., 2008). Moreover, our ASP paradigm clearly required a long preparation period for the task, which was not limited to the time period starting with the warning cue but also the period after receiving the task information. During these tasks, the subjects need to get into a highly prepared state before movement execution, which is closely related to the delay of motion initiation (Leow et al., 2018). That is, a spike in HbO/HbR changes for the block-averaged figures generated in this study occurred in or near the baseline (time window −5∼0 s), indicating high activation of the frontal cortex as well as increased blood flow. As a result, HbO changes across the channel exhibited task-related negative fluctuations, as Suzuki et al. (2008) reported. The lagged negative fluctuations in HbO signals may reflect different activation levels in the frontal cortex among trials during the motor preparation period. Therefore, a larger negative fluctuation after baseline may represent more cortical activation during the period of motor preparation. We interpreted the HbR fluctuation in channel 11, which had the same negative trend as HbO, as a manifestation of blood flow fluctuations. The effect of blood flow may be greater than that of pure HbR fluctuations. Since the baseline from which the graph (**Figure 2**) was generated was not highly consistent with the β value calculation (resting state before and after the test), the results may have included some variability.

Limitations

This study also has some limitations. First, not all signal noise caused by vascular or blood pressure (Scholkmann et al., 2022) was removed, but the current filter parameter settings cover most physiological signals. Moreover, we performed within-subject comparisons that may be able to circumvent the decreased test power due to interindividual differences. In addition, there were significant individual differences in HbO/HbR fluctuations; thus, the contrast map of brain activation in a single subject may not be a good way to explain our results. The subject whose brain activation signatures best represented our findings was selected and presented. Taking into account the reliability and presentability of the findings, we retained the results before correction for multiple comparisons in the SPM figures.

Furthermore, fNIRS itself has some inherent limitations. First, the low sampling rate makes the final data unable to accurately reflect the entire process and temporal order of cortical HbO/HbR fluctuations. Cortical activity, motor initiation, and feedback adjustment in the ASP reaching tasks are completed within tens of milliseconds. EEG, which has a higher sampling rate may be a better method to investigate the coherence between cortical signals and muscular performance. Second, in setting the fNIRS data collection channels, we failed to focus on the ipsilateral motor areas. The setting channels displayed low specificity (31.56%) for the M1.

An improved paradigm with short-separation channels may bring better results (Yucel et al., 2021). Moreover, we initially explored the feasibility of using fNIRS to analyze ASP in healthy people; further exploration is needed to determine its application in patients with brain injury. Some preliminary research has suggested that RST facilitation under startle stimuli in patients with cortical injury may be more pronounced and differ from that in healthy individuals (DeLuca et al., 2022; Swann et al., 2022). More ASP movement paradigms with greater sample sizes are needed.

Conclusion

In summary, this study found that activation of prefrontal regions was significantly associated with the SE and RST facilitation during ASP reaching tasks. Additional activation was most pronounced in the right dlPFC in SCM^{+} trials during this process. Moreover, enhanced inhibition of the ipsilateral M1 was also observed. The above findings suggest a PMRF-ARAS-FPN modulation system for motor output during RST facilitation. The right dlPFC may play an important role in this process. These results can inform future studies on RST facilitation from the perspective of brain networks and support the development of neuromodulation technology to support RST function *via* non-invasive stimulation. Such novel rehabilitation strategies may provide stroke survivors with additional benefits.

Data availability statement

The raw data supporting the conclusions of this article will be made available by the authors, without undue reservation.

Ethics statement

The studies involving human participants were reviewed and approved by the Ethics Committee of Tongji Hospital. The patients/participants provided their written informed consent to participate in this study.

Author contributions

XH, XH, and NX designed this research. NX, CH, Y-AL, MG, ZC, XW, JX, and WL participated into the participants recruitment, research implementation, and data collection. NX and CH did the data analysis and wrote the draft. YL participated the modification of this manuscript. All authors had full access to the data and have reviewed this research and approved the submitted version.

Funding

This work supported by the National Natural Science Foundation of China (grant nos. U 1913601 and 91648203).

Acknowledgments

We thank all volunteers who participated in this study for their support.

Conflict of interest

The authors declare that the research was conducted in the absence of any commercial or financial relationships that could be construed as a potential conflict of interest.

Publisher's note

All claims expressed in this article are solely those of the authors and do not necessarily represent those of their affiliated organizations, or those of the publisher, the editors and the reviewers. Any product that may be evaluated in this article, or claim that may be made by its manufacturer, is not guaranteed or endorsed by the publisher.

Supplementary material

The Supplementary Material for this article can be found online at: https://www.frontiersin.org/articles/10.3389/fnins.2023.1112046/full#supplementary-material

References

Alagona, G., Delvaux, V., Gerard, P., De Pasqua, V., Pennisi, G., Delwaide, P. J., et al. (2001). Ipsilateral motor responses to focal transcranial magnetic stimulation in healthy subjects and acute-stroke patients. *Stroke* 32, 1304–1309. doi: 10.1161/01.str.32.6.1304

Atkinson, E., Skarabot, J., Ansdell, P., Goodall, S., Howatson, G., and Thomas, K. (2022). Does the reticulospinal tract mediate adaptation to resistance training in humans? *J. Appl. Physiol.* 133, 689–696. doi: 10.1152/japplphysiol.00264.2021

Baker, S. N. (2011). The primate reticulospinal tract, hand function and functional recovery. *J. Physiol.* 589(Pt. 23), 5603–5612. doi: 10.1113/jphysiol.2011.215160

Bawa, P., Hamm, J. D., Dhillon, P., and Gross, P. A. (2004). Bilateral responses of upper limb muscles to transcranial magnetic stimulation in human subjects. *Exp. Brain Res.* 158, 385–390. doi: 10.1007/s00221-004-2031-x

Boyne, P., DiFrancesco, M., Awosika, O. O., Williamson, B., and Vannest, J. (2021). Mapping the human corticoreticular pathway with multimodal delineation of the gigantocellular reticular nucleus and high-resolution diffusion tractography. *J. Neurol. Sci.* 434:120091. doi: 10.1016/j.jns.2021.120091

Brass, M., Zysset, S., and von Cramon, D. Y. (2001). The inhibition of imitative response tendencies. *Neuroimage* 14, 1416–1423. doi: 10.1006/nimg.2001.0944

Brown, E. N., Purdon, P. L., and Van Dort, C. J. (2011). General anesthesia and altered states of arousal: a systems neuroscience analysis. *Annu. Rev. Neurosci.* 34, 601–628. doi: 10.1146/annurev-neuro-060909-153200

Brownstone, R. M., and Chopek, J. W. (2018). Reticulospinal systems for tuning motor commands. *Front. Neural Circuits* 12:30. doi: 10.3389/fncir.2018.00030

Buckner, R. L. (2013). The brain's default network: origins and implications for the study of psychosis. *Dialogues Clin. Neurosci.* 15, 351–358. doi: 10.31887/DCNS.2013.15.3/rbuckner

Cano, J. C., Huang, W., and Fenelon, K. (2021). The amygdala modulates prepulse inhibition of the auditory startle reflex through excitatory inputs to the caudal pontine reticular nucleus. *BMC Biol.* 19:116. doi: 10.1186/s12915-021-01050-z

Carlsen, A. N., and Maslovat, D. (2019). Startle and the StartReact effect: physiological mechanisms. *J. Clin. Neurophysiol.* 36, 452–459. doi: 10.1097/WNP.0000000000000582

Carlsen, A. N., Chua, R., Inglis, J. T., Sanderson, D. J., and Franks, I. M. (2003). Startle response is dishabituated during a reaction time task. *Exp. Brain Res.* 152, 510–518. doi: 10.1007/s00221-003-1575-5

Carlsen, A. N., Maslovat, D., and Franks, I. M. (2012). Preparation for voluntary movement in healthy and clinical populations: evidence from startle. *Clin. Neurophysiol.* 123, 21–33. doi: 10.1016/j.clinph.2011.04.028

Carlsen, A. N., Maslovat, D., Lam, M. Y., Chua, R., and Franks, I. M. (2011). Considerations for the use of a startling acoustic stimulus in studies of motor preparation in humans. *Neurosci. Biobehav. Rev.* 35, 366–376. doi: 10.1016/j.neubiorev.2010.04.009

Chen, W. L., Wagner, J., Heugel, N., Sugar, J., Lee, Y. W., Conant, L., et al. (2020). Functional near-infrared spectroscopy and its clinical application in the field of neuroscience: advances and future directions. *Front. Neurosci.* 14:724. doi: 10.3389/fnins.2020.00724

Chen, Y. T., Li, S., Zhang, Y., Zhou, P., and Li, S. (2022). Startling acoustic stimulation has task-specific effects on intracortical facilitation and inhibition at rest and during visually guided isometric elbow flexion in healthy individuals. *Motor Control* 27, 96–111. doi: 10.1123/mc.2022-0014

Chen, Y. T., Li, S., Zhou, P., and Li, S. (2019). A startling acoustic stimulation (SAS)-TMS approach to assess the reticulospinal system in healthy and stroke subjects. *J. Neurol. Sci.* 399, 82–88. doi: 10.1016/j.jns.2019.02.018

Choudhury, S., Shobhana, A., Singh, R., Sen, D., Anand, S. S., Shubham, S., et al. (2019). The relationship between enhanced reticulospinal outflow and upper limb function in chronic stroke patients. *Neurorehabil. Neural Repair* 33, 375–383. doi: 10.1177/1545968319836233

Cope, M., and Delpy, D. T. (1988). System for long-term measurement of cerebral blood and tissue oxygenation on newborn infants by near infra-red transillumination. *Med. Biol. Eng. Comput.* 26, 289–294. doi: 10.1007/BF02447083

DeLuca, M., Low, D., Kumari, V., Parton, A., Davis, J., and Mohagheghi, A. A. (2022). A systematic review with meta-analysis of the StartReact effect on motor responses in stroke survivors and healthy individuals. *J. Neurophysiol.* 127, 938–945. doi: 10.1152/jn.00392.2021

Fernandez-Del-Olmo, M., Rio-Rodriguez, D., Iglesias-Soler, E., and Acero, R. M. (2014). Startle auditory stimuli enhance the performance of fast dynamic contractions. *PLoS One* 9:e87805. doi: 10.1371/journal.pone.0087805

Fisher, K. M., Zaaimi, B., and Baker, S. N. (2012). Reticular formation responses to magnetic brain stimulation of primary motor cortex. *J. Physiol.* 590, 4045–4060. doi: 10.1113/jphysiol.2011.226209

Fisher, K. M., Zaaimi, B., Edgley, S. A., and Baker, S. N. (2021). Extensive cortical convergence to primate reticulospinal pathways. *J. Neurosci.* 41, 1005–1018. doi: 10.1523/jneurosci.1379-20.2020

Fisher, R. J., Sharott, A., Kuhn, A. A., and Brown, P. (2004). Effects of combined cortical and acoustic stimuli on muscle activity. *Exp. Brain Res.* 157, 1–9. doi: 10.1007/s00221-003-1809-6

Furubayashi, T., Ugawa, Y., Terao, Y., Hanajima, R., Sakai, K., Machii, K., et al. (2000). The human hand motor area is transiently suppressed by an unexpected auditory stimulus. *Clin. Neurophysiol.* 111, 178–183. doi: 10.1016/s1388-2457(99)00200-x

Glover, I. S., and Baker, S. N. (2020). Cortical, corticospinal, and reticulospinal contributions to strength training. *J. Neurosci.* 40, 5820–5832. doi: 10.1523/JNEUROSCI.1923-19.2020

Glover, I. S., and Baker, S. N. (2022). Both corticospinal and reticulospinal tracts control force of contraction. *J. Neurosci.* 42, 3150–3164. doi: 10.1523/jneurosci.0627-21.2022

Hearne, L. J., Dean, R. J., Robinson, G. A., Richards, L. J., Mattingley, J. B., and Cocchi, L. (2019). Increased cognitive complexity reveals abnormal brain network activity in individuals with corpus callosum dysgenesis. *Neuroimage Clin.* 21:101595. doi: 10.1016/j.nicl.2018.11.005

Huo, C., Xu, G., Li, W., Xie, H., Zhang, T., Liu, Y., et al. (2021). A review on functional near-infrared spectroscopy and application in stroke rehabilitation. *Med. Novel Technol. Dev.* 11:100064. doi: 10.1016/j.medntd.2021.100064

Jang, S. H., Choi, B. Y., Kim, S. H., Chang, C. H., Jung, Y. J., and Yeo, S. S. (2015). Injury of the corticoreticular pathway in subarachnoid haemorrhage after rupture of a cerebral artery aneurysm. *J. Rehabil. Med.* 47, 133–137. doi: 10.2340/16501977-1896

Jang, S. H., Kim, S. H., Kim, J. W., Lee, H. D., and Cho, M. K. (2021). Difference in the ascending reticular activating system between vegetative and minimally conscious states following traumatic brain injury. *Neuroreport* 32, 1423–1427. doi: 10.1097/WNR.0000000000001747

Kaller, C. P., Rahm, B., Spreer, J., Weiller, C., and Unterrainer, J. M. (2011). Dissociable contributions of left and right dorsolateral prefrontal cortex in planning. *Cereb. Cortex* 21, 307–317. doi: 10.1093/cercor/bhq096

Kaplan, J. T., Gimbel, S. I., and Harris, S. (2016). Neural correlates of maintaining one's political beliefs in the face of counterevidence. *Sci. Rep.* 6:39589. doi: 10.1038/srep39589

Ko, S. H., Kim, T., Min, J. H., Kim, M., Ko, H. Y., and Shin, Y. I. (2021). Corticoreticular pathway in post-stroke spasticity: a diffusion tensor imaging study. *J. Pers. Med.* 11:1151. doi: 10.3390/jpm11111151

Koechlin, E., and Hyafil, A. (2007). Anterior prefrontal function and the limits of human decision-making. *Science* 318, 594–598. doi: 10.1126/science.1142995

Kuhn, A. A., Sharott, A., Trottenberg, T., Kupsch, A., and Brown, P. (2004). Motor cortex inhibition induced by acoustic stimulation. *Exp. Brain Res.* 158, 120–124. doi: 10.1007/s00221-004-1883-4

Leocani, L., Cohen, L. G., Wassermann, E. M., Ikoma, K., and Hallett, M. (2000). Human corticospinal excitability evaluated with transcranial magnetic stimulation during different reaction time paradigms. *Brain* 123(Pt. 6), 1161–1173. doi: 10.1093/brain/123.6.1161

Leow, L. A., Tresilian, J. R., Uchida, A., Koester, D., Spingler, T., Riek, S., et al. (2021). Acoustic stimulation increases implicit adaptation in sensorimotor adaptation. *Eur. J. Neurosci.* 54, 5047–5062. doi: 10.1111/ejn.15317

Leow, L. A., Uchida, A., Egberts, J. L., Riek, S., Lipp, O. V., Tresilian, J., et al. (2018). Triggering mechanisms for motor actions: the effects of expectation on reaction times to intense acoustic stimuli. *Neuroscience* 393, 226–235. doi: 10.1016/j.neuroscience.2018.10.008

Lofberg, O., Julkunen, P., Paakkonen, A., and Karhu, J. (2014). The auditory-evoked arousal modulates motor cortex excitability. *Neuroscience* 274, 403–408. doi: 10.1016/j.neuroscience.2014.05.060

Maitland, S., and Baker, S. N. (2021). Ipsilateral motor evoked potentials as a measure of the reticulospinal tract in age-related strength changes. *Front. Aging Neurosci.* 13:612352. doi: 10.3389/fnagi.2021.612352

Marek, S., and Dosenbach, N. U. F. (2018). The frontoparietal network: function, electrophysiology, and importance of individual precision mapping. *Dialogues Clin. Neurosci.* 20, 133–140. doi: 10.31887/DCNS.2018.20.2/smarek

Marinovic, W., and Tresilian, J. R. (2016). Triggering prepared actions by sudden sounds: reassessing the evidence for a single mechanism. *Acta Physiol.* 217, 13–32. doi: 10.1111/apha.12627

Marinovic, W., Flannery, V., and Riek, S. (2015). The effects of preparation and acoustic stimulation on contralateral and ipsilateral corticospinal excitability. *Hum. Mov. Sci.* 42, 81–88. doi: 10.1016/j.humov.2015.05.003

Marinovic, W., Tresilian, J. R., de Rugy, A., Sidhu, S., and Riek, S. (2014). Corticospinal modulation induced by sounds depends on action preparedness. *J. Physiol.* 592, 153–169. doi: 10.1113/jphysiol.2013.254581

Maruyama, S., Fukunaga, M., Sugawara, S. K., Hamano, Y. H., Yamamoto, T., and Sadato, N. (2021). *Sequential finger-tapping learning mediated by the primary motor cortex and fronto-parietal network: a combined MRI-MRS study*. [preprint]. doi: 10.21203/rs.3.rs-197014/v1

Maslovat, D., Sadler, C. M., Smith, V., Bui, A., and Carlsen, A. N. (2021). Response triggering by an acoustic stimulus increases with stimulus intensity and is best predicted by startle reflex activation. *Sci. Rep.* 11:23612. doi: 10.1038/s41598-021-02825-8

Matsuyama, K., and Drew, T. (2000). Vestibulospinal and reticulospinal neuronal activity during locomotion in the intact cat. I. Walking on a level surface. *J. Neurophysiol.* 84, 2237–2256. doi: 10.1152/jn.2000.84.5.2237

McInnes, A. N., Corti, E. J., Tresilian, J. R., Lipp, O. V., and Marinovic, W. (2020). Neural gain induced by startling acoustic stimuli is additive to preparatory activation. *Psychophysiology* 57:e13493. doi: 10.1111/psyp.13493

Menon, V. (2011). Large-scale brain networks and psychopathology: a unifying triple network model. *Trends Cogn. Sci.* 15, 483–506. doi: 10.1016/j.tics.2011.08.003

Menon, V., and Uddin, L. Q. (2010). Saliency, switching, attention and control: a network model of insula function. *Brain Struct. Funct.* 214, 655–667. doi: 10.1007/s00429-010-0262-0

Mueller-Pfeiffer, C., Zeffiro, T., O'Gorman, R., Michels, L., Baumann, P., Wood, N., et al. (2014). Cortical and cerebellar modulation of autonomic responses to loud sounds. *Psychophysiology* 51, 60–69. doi: 10.1111/psyp.12142

Ni, Z., Gunraj, C., Nelson, A. J., Yeh, I. J., Castillo, G., Hoque, T., et al. (2009). Two phases of interhemispheric inhibition between motor related cortical areas and the

primary motor cortex in human. *Cereb. Cortex* 19, 1654–1665. doi: 10.1093/cercor/bhn201

Perez, M. A., and Cohen, L. G. (2009). Interhemispheric inhibition between primary motor cortices: what have we learned? *J Physiol* 587(Pt. 4), 725–726. doi: 10.1113/jphysiol.2008.166926

Pinti, P., Scholkmann, F., Hamilton, A., Burgess, P., and Tachtsidis, I. (2018). Current status and issues regarding pre-processing of fNIRS neuroimaging data: an investigation of diverse signal filtering methods within a general linear model framework. *Front. Hum. Neurosci.* 12:505. doi: 10.3389/fnhum.2018.00505

Rahimi, M., and Honeycutt, C. F. (2020). StartReact increases the probability of muscle activity and distance in severe/moderate stroke survivors during two-dimensional reaching task. *Exp. Brain Res.* 238, 1219–1227. doi: 10.1007/s00221-020-05797-9

Ramnani, N., and Owen, A. M. (2004). Anterior prefrontal cortex: insights into function from anatomy and neuroimaging. *Nat. Rev. Neurosci.* 5, 184–194. doi: 10.1038/nrn1343

Rangarajan, V., Schreiber, J. J., Barragan, B., Schaefer, S. Y., and Honeycutt, C. F. (2022). Delays in the reticulospinal system are associated with a reduced capacity to learn a simulated feeding task in older adults. *Front. Neural Circ.* 15:681706. doi: 10.3389/fncir.2021.681706

Reis, J., Swayne, O. B., Vandermeeren, Y., Camus, M., Dimyan, M. A., Harris-Love, M., et al. (2008). Contribution of transcranial magnetic stimulation to the understanding of cortical mechanisms involved in motor control. *J. Physiol.* 586, 325–351. doi: 10.1113/jphysiol.2007.144824

Sahyoun, C., Floyer-Lea, A., Johansen-Berg, H., and Matthews, P. M. (2004). Towards an understanding of gait control: brain activation during the anticipation, preparation and execution of foot movements. *Neuroimage* 21, 568–575. doi: 10.1016/j.neuroimage.2003.09.065

Saper, C. B., Scammell, T. E., and Lu, J. (2005). Hypothalamic regulation of sleep and circadian rhythms. *Nature* 437, 1257–1263. doi: 10.1038/nature04284

Schepens, B., and Drew, T. (2004). Independent and convergent signals from the pontomedullary reticular formation contribute to the control of posture and movement during reaching in the cat. *J. Neurophysiol.* 92, 2217–2238. doi: 10.1152/jn.01189.2003

Scholkmann, F., Tachtsidis, I., Wolf, M., and Wolf, U. (2022). Systemic physiology augmented functional near-infrared spectroscopy: a powerful approach to study the embodied human brain. *Neurophotonics* 9:030801. doi: 10.1117/1.NPh.9.3.030801

Shackman, A. J., McMenamin, B. W., Maxwell, J. S., Greischar, L. L., and Davidson, R. J. (2009). Right dorsolateral prefrontal cortical activity and behavioral inhibition. *Psychol. Sci.* 20, 1500–1506. doi: 10.1111/j.1467-9280.2009.02476.x

Skarabot, J., Folland, J. P., Holobar, A., Baker, S. N., and Del Vecchio, A. (2022). Startling stimuli increase maximal motor unit discharge rate and rate of force development in humans. *J. Neurophysiol.* 128, 455–469. doi: 10.1152/jn.00115.2022

Smith, S. M., Fox, P. T., Miller, K. L., Glahn, D. C., Fox, P. M., Mackay, C. E., et al. (2009). Correspondence of the brain's functional architecture during activation and rest. *Proc. Natl. Acad. Sci. U.S.A.* 106, 13040–13045. doi: 10.1073/pnas.0905267106

Smith, V., Maslovat, D., Drummond, N. M., Hajj, J., Leguerrier, A., and Carlsen, A. N. (2019). High-intensity transcranial magnetic stimulation reveals differential cortical contributions to prepared responses. *J Neurophysiol* 121, 1809–1821. doi: 10.1152/jn.00510.2018

Solnik, S., Rider, P., Steinweg, K., DeVita, P., and Hortobagyi, T. (2010). Teager-Kaiser energy operator signal conditioning improves EMG onset detection. *Eur. J. Appl. Physiol.* 110, 489–498. doi: 10.1007/s00421-010-1521-8

Suzuki, M., Miyai, I., Ono, T., and Kubota, K. (2008). Activities in the frontal cortex and gait performance are modulated by preparation. An fNIRS study. *Neuroimage* 39, 600–607. doi: 10.1016/j.neuroimage.2007.08.044

Swann, Z., Daliri, A., and Honeycutt, C. F. (2022). Impact of startling acoustic stimuli on word repetition in individuals with aphasia and apraxia of speech following stroke. *J. Speech Lang. Hear. Res.* 65, 1671–1685. doi: 10.1044/2022_JSLHR-21-00486

Uddin, L. Q., Yeo, B. T. T., and Spreng, R. N. (2019). Towards a universal taxonomy of macro-scale functional human brain networks. *Brain Topogr.* 32, 926–942. doi: 10.1007/s10548-019-00744-6

van Belle, J., Vink, M., Durston, S., and Zandbelt, B. B. (2014). Common and unique neural networks for proactive and reactive response inhibition revealed by independent component analysis of functional MRI data. *Neuroimage* 103, 65–74. doi: 10.1016/j.neuroimage.2014.09.014

van Lith, B. J. H., Coppens, M. J. M., Nonnekes, J., van de Warrenburg, B. P. C., Geurts, A. C., and Weerdesteyn, V. (2018). StartReact during gait initiation reveals differential control of muscle activation and inhibition in patients with corticospinal degeneration. *J. Neurol.* 265, 2531–2539. doi: 10.1007/s00415-018-9027-0

Wassermann, E. M., Pascual-Leone, A., and Hallett, M. (1994). Cortical motor representation of the ipsilateral hand and arm. *Exp. Brain Res.* 100, 121–132. doi: 10.1007/BF00227284

Weng, L., Xie, Q., Zhao, L., Zhang, R., Ma, Q., Wang, J., et al. (2017). Abnormal structural connectivity between the basal ganglia, thalamus, and frontal cortex in patients with disorders of consciousness. *Cortex* 90, 71–87. doi: 10.1016/j.cortex.2017.02.011

Wijdicks, E. F. M. (2019). The ascending reticular activating system. *Neurocrit. Care* 31, 419–422. doi: 10.1007/s12028-019-00687-7

Xia, N., He, C., Li, Y. A., Gu, M., Chen, Z., Wei, X., et al. (2021). Startle increases the incidence of anticipatory muscle activations but does not change the task-specific muscle onset for patients after subacute stroke. *Front. Neurol.* 12:789176. doi: 10.3389/fneur.2021.789176

Yeo, B. T., Krienen, F. M., Sepulcre, J., Sabuncu, M. R., Lashkari, D., Hollinshead, M., et al. (2011). The organization of the human cerebral cortex estimated by intrinsic functional connectivity. *J. Neurophysiol.* 106, 1125–1165. doi: 10.1152/jn.00338.2011

Yucel, M. A., Luhmann, A. V., Scholkmann, F., Gervain, J., Dan, I., Ayaz, H., et al. (2021). Best practices for fNIRS publications. *Neurophotonics* 8:012101. doi: 10.1117/1.NPh.8.1.012101

Zaaimi, B., Edgley, S. A., Soteropoulos, D. S., and Baker, S. N. (2012). Changes in descending motor pathway connectivity after corticospinal tract lesion in macaque monkey. *Brain* 135(Pt. 7), 2277–2289. doi: 10.1093/brain/aws115

Zhang, D., Zhou, Y., and Yuan, J. (2018). Speech prosodies of different emotional categories activate different brain regions in adult cortex: an fNIRS study. *Sci. Rep.* 8:218. doi: 10.1038/s41598-017-18683-2

Zhang, J., Wang, M., Wei, B., Shi, J., and Yu, T. (2022). Research progress in the study of startle reflex to disease states. *Neuropsychiatr. Dis. Treat.* 18, 427–435. doi: 10.2147/ndt.S351667

frontiers | Frontiers in Neuroscience

TYPE Original Research
PUBLISHED 24 February 2023
DOI 10.3389/fnins.2023.1099843

OPEN ACCESS

EDITED BY
Feng Zhang,
Third Hospital of Hebei Medical University, China

REVIEWED BY
Xiafeng Shen,
Shanghai Pudong Hospital, China
Jun Li Cui,
Shanghai Jiao Tong University, China
Zhang Pengyue,
Yunnan University of Traditional Chinese Medicine, China

*CORRESPONDENCE
Huixian Yu
✉ huixianyu@126.com

SPECIALTY SECTION
This article was submitted to Translational Neuroscience, a section of the journal Frontiers in Neuroscience

RECEIVED 16 November 2022
ACCEPTED 13 February 2023
PUBLISHED 24 February 2023

CITATION
Liu S, Yu H, Wang Z and Dai P (2023) Correlation analysis of balance function with plantar pressure distribution and gait parameters in patients with cerebral infarction in the basal ganglia region. *Front. Neurosci.* 17:1099843. doi: 10.3389/fnins.2023.1099843

Correlation analysis of balance function with plantar pressure distribution and gait parameters in patients with cerebral infarction in the basal ganglia region

Sihao Liu, Huixian Yu*, Zhaoxia Wang and Pei Dai

Department of Rehabilitation Medicine, Beijing Tiantan Hospital, Capital Medical University, Beijing, China

Objective: To analyze the correlation between balance function and gait parameters of patients with basal ganglia infarction. And to observe the influence of balance function on plantar pressure and hemiplegia gait based on the Berg Balance Scale (BBS) score.

Methods: One hundred and forty patients with cerebral infarction hemiplegia in the basal ganglia region (a study group, n = 140) and healthy people (a control group, n = 140) were enrolled. The study group was evaluated with the BBS, the 10 m walking test (10MWT), and the timed up-and-go test (TUGT). The gait parameters and the peak plantar pressure were measured in both groups while walking, and the differences between the groups were compared. In addition, the characteristics of the plantar pressure curve of the hemiplegic and non-hemiplegic sides during walking and the correlation between the 10MWT, the TUGT, the plantar pressure peak, the gait parameters,and the BBS score were analyzed in the study group.

Results: The peak plantar pressure of the forefoot and heel, stride length, lateral symmetry, stand phase, swing phase, and dual stand phase of both sides in the study group were significantly lower than those in the control group ($P < 0.05$). The BBS score negatively correlated with the 10MWT, the TUGT, the peak plantar pressure of the hemiplegic forefoot, midfoot, and the non-hemiplegic midfoot, the anterior to posterior position (ant/post position), hemiplegic stand phase, and the dual stand phase ($P < 0.05$). The BBS score positively correlated with the hemiplegic swing phase and stride length ($P < 0.05$).

Conclusion: A correlation was found between the forefoot plantar pressure and the stand phase of the hemiplegic limbs, the ant/post position, and the balance function after basal ganglion cerebral infarction. This association can be used in walking and balance assessment for stroke rehabilitation. Correcting forefoot pressure or the front and ant/post position can improve balance function.

KEYWORDS

stroke, walking function, balance function, plantar pressure, gait feature

1. Introduction

Motor dysfunction often occurs after a stroke (Wang, 2022). About 70% of stroke-affected patients have a walking dysfunction that limits their daily life. Restoring walking ability is one of the main demands of stroke-affected patients and their families, and it is the most important and most commonly shared rehabilitation goal (Mehrholz et al., 2018).

Balance dysfunction is one of the main factors influencing walking in stroke-affected patients (Rahimzadeh Khiabani et al., 2017). Due to the decline in sensory, exercise, or information-processing ability, and muscle spasticity, decreased muscle strength, and excessive energy consumption, patients experience balance dysfunction and have a high risk of falling after a stroke (Li, 2022). Reportedly, 65% of stroke-affected patients have a history of falling, which causes muscle tissue damage and ankle sprains and affects their recovery process (Lee and Lee, 2019).

Abnormal gait in stroke-affected patients, including walking parameters, transfer ability, and plantar pressure, differs from healthy people and affects the recovery process (You et al., 2016). However, clinically evaluating the balance function after stroke is limited to dynamic and static assessment, and the balance function is an indicator of patients' ability to walk independently (Lee et al., 2013). Most scholars characterize walking as a rhythmic movement, and few studies have focused on the effect of balance function on the dynamic plantar pressure and gait characteristics of hemiplegia after stroke (Lee et al., 2020). Lewek et al. (2014) studied the relationship between gait symmetry and balance function in stroke-affected patients but only measured the correlation between the walking weight distribution and stance time asymmetry and did not further evaluate the gravity distribution and symmetry of patients when walking. Obembe et al. (2014) suggested that balance function during walking is associated with gait speed and cadence in stroke-affected patients but did not explore the effect of balance function on plantar pressure distribution during walking.

The balance characteristics of infarcts in different brain regions are not identical, and failure to distinguish between stroke sites may affect the results of the study. Cerebral infarction in the basal ganglia area is common, and hemiplegia has a prominent gait (Alexander et al., 2009). In the present study, evaluating the balance function of patients with cerebral infarction in the basal ganglia area reduced the disturbance of balance function from other intracranial injuries. Gait analysis and plantar pressure analysis were used to evaluate the patients' walking function. Based on previous research, the correlation between balance function and plantar pressure during walking was explored, and the effect of balance function after stroke in the basal ganglion area on the characteristics of hemiplegic gait was further examined.

2. Materials and methods

2.1. Patients

One hundred and forty patients with cerebral infarction treated in the Department of Rehabilitation Medicine of Beijing Tiantan Hospital between January 2021 and August 2022 were enrolled as a study group. Another one hundred and forty healthy people were collected as a control group. There were no significant differences in age, gender, height, or weight (**Table 1**). This study was approved by the ethics committee of Beijing Tiantan Hospital, Capital Medical University (KY2021-040-02).

The inclusion criteria were: (1) age 40–70 years old, (2) primary basal ganglia area cerebral infarction diagnosed by magnetic resonance imaging or computed tomography, (3) the onset of the disease was >1 month ago, (4) no sensory impairments, (5) no serious cognitive dysfunction (Mini-Mental State Examination score >26), (6) could walk 10 m or more independently, and (7) provided a signed informed consent form.

The exclusion criteria were: (1) cerebrovascular disease progression and unstable vital signs; (2) other neurological or mental diseases, such as stroke, brain trauma, or Parkinson's disease; (3) severe heart, lung, liver, or kidney dysfunction; (4) sensory aphasia, cognitive impairment, or unable to cooperate with the evaluation and examination; (5) fractures and arthritis affecting the walking function of patients; or (6) proprioception disorders.

The suspension criteria were: (1) severe adverse reactions or inability to continue, (2) deterioration of the condition or serious complications, (3) failure to cooperate and to receive required treatment, or (4) patients and their families requesting withdrawal from the study.

2.2. Measurement

2.2.1. The 10-m walking test

The 10-m walking test (10MWT) measures the walking ability of stroke-affected patients (Yeung et al., 2018). Patients were asked to walk 16 m forward at their fastest speed in a state of natural relaxation, after which the time they spent walking between the 3-m and the 13-m points was recorded.

2.2.2. The timed up-and-go test

The timed up-and-go test (TUGT) measures metastatic ability and postural control in stroke-affected patients (Dong et al., 2021). The patients were seated in a chair, lean against the chair back, and put their hands on the armrests, after which the researcher recorded with the stopwatch from the moment the patient got up, walked for 3 m, turned around a cone, and returned to the chair. When the patient sat back on the chair, the researcher stopped recording.

2.2.3. Berg Balance Scale

The Berg Balance Scale (BBS) measures the balance ability of stroke-affected patients (Blum and Korner-Bitensky, 2008). It has 14 actions, each recorded with 0–4 points according to the degree of completion, with a total score of 56 points. The higher the score, the better the balance function. Patients were guided to complete 14 actions, such as independent sitting, from sitting to standing, independent standing, and from standing to sitting.

2.2.4. Dynamic plantar pressure assessment and gait analysis

The Zebris plantar pressure measurement system (Zebris FDM 1.12) was used to complete the evaluation. The participants had to take off their shoes, stand on the running platform, and hold their hands on the railings on both sides of the runway while a safety

device was clamped on their chest. The runway was open, and the participant was instructed to follow it. The speed of the running platform gradually increased, and when it reached the speed at which the participant was comfortable, the participant was asked to release the railings, turn on the evaluation device, and then stop the device after walking for 30 s. The device mainly recorded the data of both lower limbs while walking, including the peak plantar pressure (N/cm^2) of the forefoot, midfoot, and heel, and the gait parameters. The gait parameters included the proportions of the stand, swing, and dual stand phases (%), and the step width (cm), stride length (cm), and the center of plantar (COP) included the anterior to posterior (ant/post) position (mm) and lateral symmetry (mm).

2.3. Statistical analysis

Graph Pad Prism 9.0 (Graph Pad Software, Inc.) was used for the statistical analysis and graphing. Standard deviations and means were used to describe measurement data that followed a normal distribution. Baseline data analysis of mean ± standard deviation or median and quartile were used for quantitative data. The spacing was described, and the *t* test (or Wilcoxon test) was used to compare this between the groups. The paired *t* test was used for intra-group comparisons, the unpaired *t* test was used for comparisons between the groups, and the chi-squared test was used for gender comparisons between the groups. The Pearson correlation coefficient was used to analyze the correlation between the BBS, the TUGT, and the 10MWT in stroke-affected patients and the correlation between the BBS score and the peak plantar pressure and gait parameters of the bilateral limbs. Any *P* values < 0.05 were considered statistically significant.

3. Results

3.1. Comparison of peak plantar pressure and gait parameters in both groups

In the control group, there was no significant difference in bilateral peak plantar pressure and gait cycle ($P > 0.05$). There were no significant differences in step width and ant/post position between the two groups ($P > 0.05$). In addition, the peak plantar pressure of the forefoot and heel, stride length, swing phase in the study group were significantly lower than those in the control group ($P < 0.05$), while the stand phase, dual stand phase and the lateral symmetry in the study group were higher than those in the control group ($P < 0.05$) (Table 2 and Figures 1–3). The dynamic plantar pressure model diagram like Figure 4. The model diagram of COP just like Figures 5, 6.

3.2. Comparison of peak plantar pressure and gait parameters between the non-hemiplegic side and the hemiplegic side in the study group

There was no significant difference in the peak plantar pressure of the midfoot between the non-hemiplegic side and the hemiplegic side ($P > 0.05$). However, the peak plantar pressure of the forefoot and heel on the non-hemiplegic side and the non-hemiplegic swing and stand phase were significantly higher than in the hemiplegic side in the study group ($P < 0.05$) (Table 2 and Figures 1–3).

TABLE 1 General situation of both groups.

Group	Sex (*n*) male/female	Age (years)	Height (cm)	Weight (kg)
Control group	96/44	58.5 ± 9.3	168.8 ± 7.5	65.2 ± 8.7
Study group	82/58	57.6 ± 10.2	168.5 ± 8.1	66.8 ± 8.6
P	0.082	0.463	0.691	0.116

TABLE 2 Comparison of peak plantar pressure and gait parameters in both groups.

Project	Control group		Study group	
	Left	Right	Non-hemiplegic	Hemiplegic
Forefoot (N/m^2)	36.86 ± 11.07	36.93 ± 10.28	23.83 ± 6.85*	20.17 ± 6.91*#
Midfoot (N/m^2)	14.80 ± 4.03	15.04 ± 5.33	14.6 ± 6.52	15.74 ± 8.68
Heel (N/m^2)	29.75 ± 16.07	29.53 ± 15.94	22.62 ± 7.14*	20.11 ± 7.45*#
Swing phase (%)	30.79 ± 6.26	30.99 ± 6.17	21.42 ± 6.41*	25.2 ± 6.05*#
Stand phase (%)	69.12 ± 6.85	69.25 ± 6.46	79.36 ± 6.68*	75.13 ± 6.39*#
Dual stance phase (%)	39.22 ± 12.71		57.41 ± 11.66*	
Step width (cm)	14.03 ± 2.37		14.55 ± 3.94	
Stride length (cm)	68.94 ± 18.34		36.52 ± 14.84*	
Lateral symmetry (mm)	5.89 ± 3.72		14.49 ± 11.49*	
Anterior to posterior position (mm)	150.6 ± 9.52		150.6 ± 28.15	

Compared with the the control group, *indicates $P < 0.05$. Compared with the non-hemiplegic limb, #indicates $P < 0.05$.

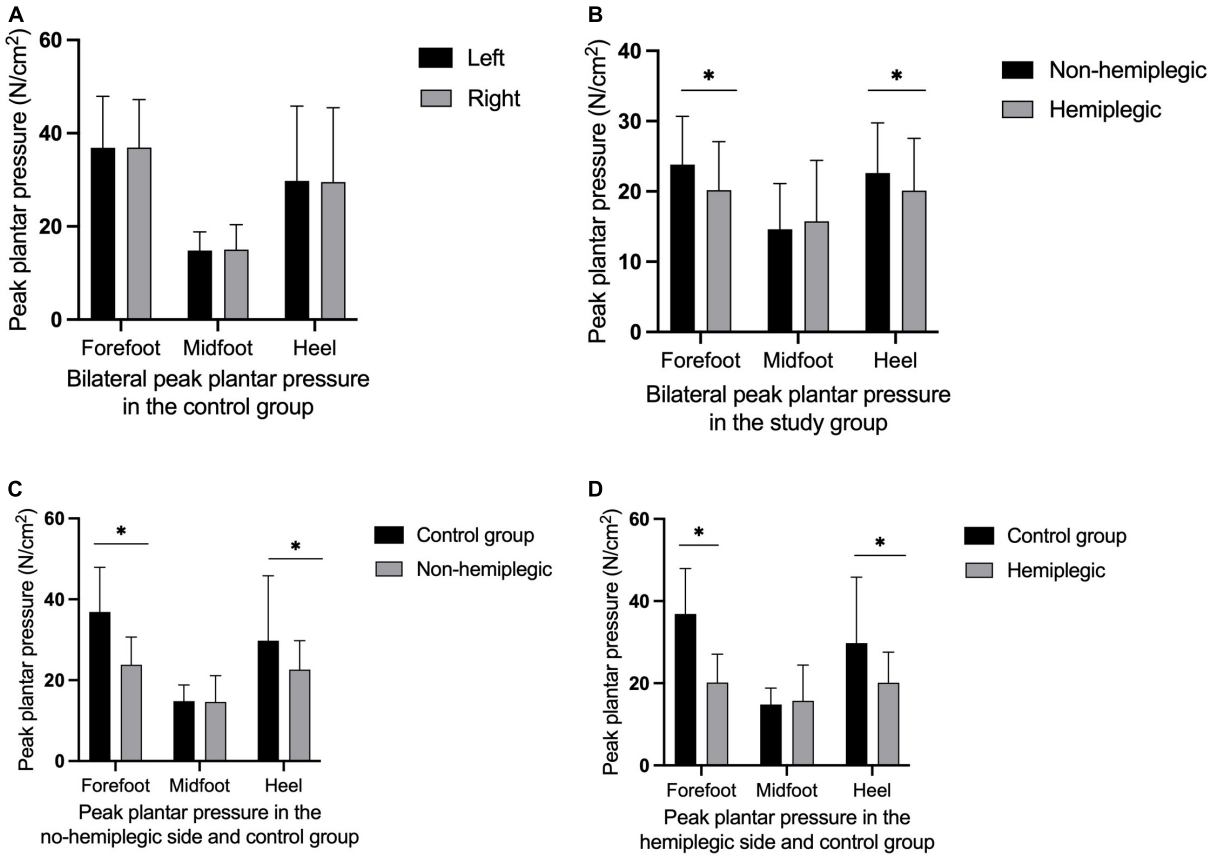

FIGURE 1
Peak plantar pressure in both group. There was no significant difference in bilateral peak plantar pressure in the control group **(A)** ($P > 0.05$). The peak plantar pressure of the forefoot and heel on the non-hemiplegic side were significantly higher than in the hemiplegic side in the study group **(B)** ($P < 0.001$). The peak plantar pressure of the forefoot and heel on the non-hemiplegic side of the study group was significantly lower than that in the control group **(C)** ($P < 0.05$). The peak plantar pressure of the forefoot and heel on the hemiplegic side of the study group was significantly lower than that in the control group **(D)** ($P < 0.05$). *Indicates significantly different.

3.3. Correlation analysis between the Berg Balance Scale score and peak plantar pressure and gait parameters in the study group

The BBS and the 10MWT had a negative correlation ($r = -0.727$, $P < 0.001$), as did the BBS and the TUGT ($r = -0.738$, $P < 0.001$). The BBS score was not correlated with step width, or lateral symmetry ($P > 0.05$), but it was negatively correlated with the ant/post position ($r = -0.444$, $P < 0.001$) and positively correlated with the stride length ($r = 0.286$, $P < 0.001$). The BBS score was not correlated with the peak plantar pressure of the non-hemiplegic forefoot, non-hemiplegic heel, or hemiplegic heel ($P > 0.05$), but it was negatively correlated with the peak plantar pressure of the hemiplegic forefoot ($r = -0.398$, $P < 0.001$), hemiplegic midfoot ($r = -0.353$, $P < 0.001$), and the non-hemiplegic midfoot ($r = -0.502$, $P < 0.001$). The BBS score was not correlated with the non-hemiplegic stand phase, non-hemiplegic swing phase ($P > 0.05$), but it was negatively correlated with the hemiplegic stand phase ($r = -0.36$, $P = 0.023$), hemiplegic swing phase ($r = 0.338$, $P < 0.001$) and the dual stand phase ($r = -0.366$, $P < 0.001$) (Table 3 and Figures 7–9).

4. Discussion

The gait patterns caused by cerebral infarction in different regions are dissimilar (Bhatt et al., 2018). This study mainly observed the relation between balance function and gait after cerebral infarction in the basal ganglia region.

Stroke-affected patients have abnormal gait, weakened physical control, swaying trunk, asymmetrical weight-bearing of both lower limbs, and reduced ability to shift their center of gravity, resulting in unstable walking and an increased risk of falling (Saleh et al., 2019).

This study compared the plantar pressures in both groups. The plantar pressure of the forefoot and heel of the hemiplegic side of the study group was significantly lower than that of the non-hemiplegic side. The bilateral plantar pressure of the study group was significantly lower than that of the control group. The plantar pressure of the midfoot in both groups did not change significantly. These results indicate that the plantar pressure of patients with basal ganglia cerebral infarction was abnormal, and the non-hemiplegic side also showed abnormal plantar pressure distribution due to the influence of the hemiplegic side.

This trial also compared the gait cycles of the two groups. In the study group, the hemiplegic side swing phase was higher than that of the non-hemiplegic side, while the hemiplegic side

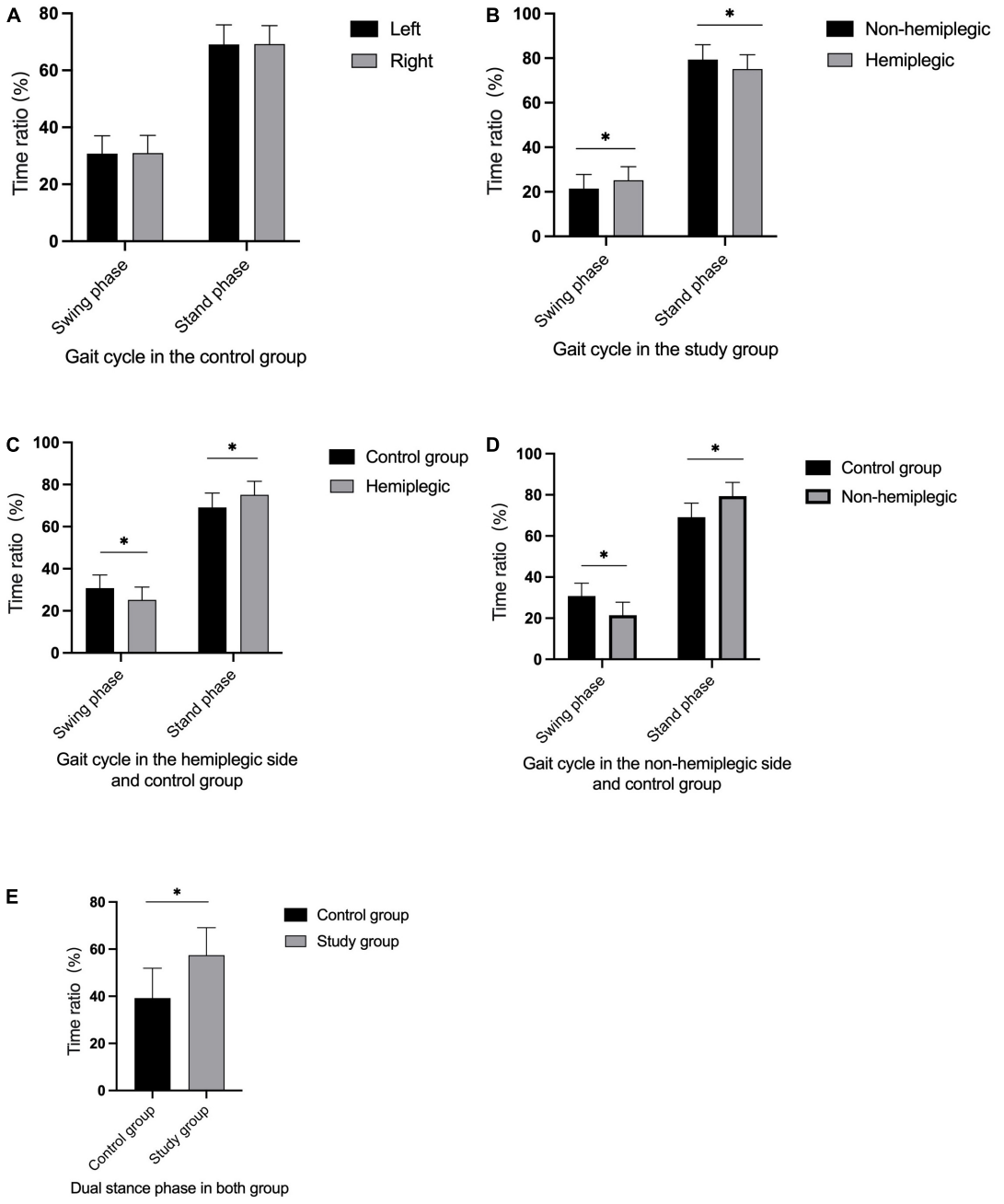

FIGURE 2
Gait cycle in both group. There was no significant difference in bilateral gait cycle in the control group **(A)** ($P > 0.05$). The non-hemiplegic swing and stand phase were significantly higher than in the hemiplegic side in the study group **(B)** ($P < 0.001$). The swing phase in the hemiplegic side in the study group was significantly lower than in the control group, while the stand phase in the hemiplegic side was higher than in the control group **(C)** ($P < 0.05$). The swing phase in the non-hemiplegic side in the study group was significantly lower than in the control group, while the stand phase in the non-hemiplegic side was higher than in the control group **(D)** ($P < 0.05$). The dual stand phase in the study group was higher than in the control group **(E)** ($P < 0.001$). *Indicates significantly different.

stand phase was lower than that on the non-hemiplegic side. In the study group, the swing phase was significantly lower while the stand and dual stance phases were significantly higher than those in the control group, indicating that the basal ganglia region stroke-affected patients had abnormal gait and poor walking stability. To avoid falls, the time taken for the forefoot to leave the ground to the heel to land is shortened, resulting in prolonged unilateral support. This study showed that the stride length of the patients in the study group was significantly reduced compared with that of the control group, and the lateral symmetry was significantly increased. This indicates that stroke-affected patients have a short stride length and a gait with poor left–right symmetry, and therefore suggests a high risk of falling, even if they could walk independently.

In a meta-analysis, van Duijnhoven et al. (2016) reported that giving patients balance training and exercise therapy, such as the center-of-gravity metastasis, could improve their balance function

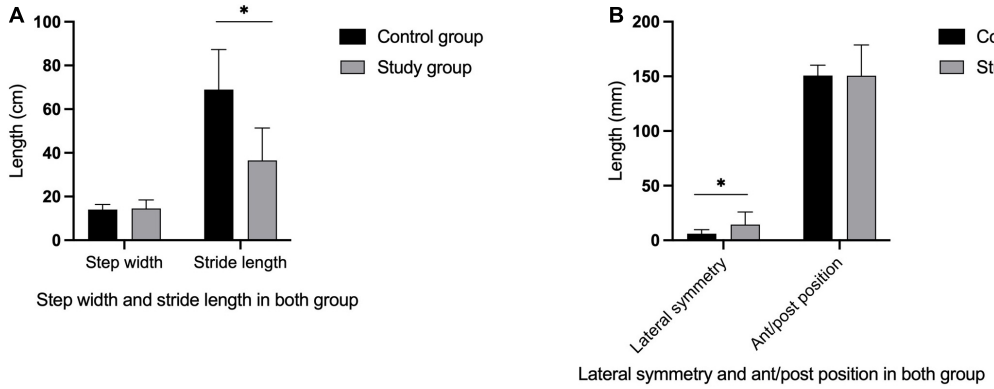

FIGURE 3
Gait parameters in both group. The stride length in the study group was significantly lower than in the control group **(A)** ($P < 0.05$), while there was no significant differences in step width between two groups **(A)** ($P > 0.05$). The lateral symmetry in the study group were higher than in the control group **(B)** ($P < 0.05$), while there was no significant differences in ant/post position between the two groups **(B)** ($P > 0.05$). *Indicates significantly different.

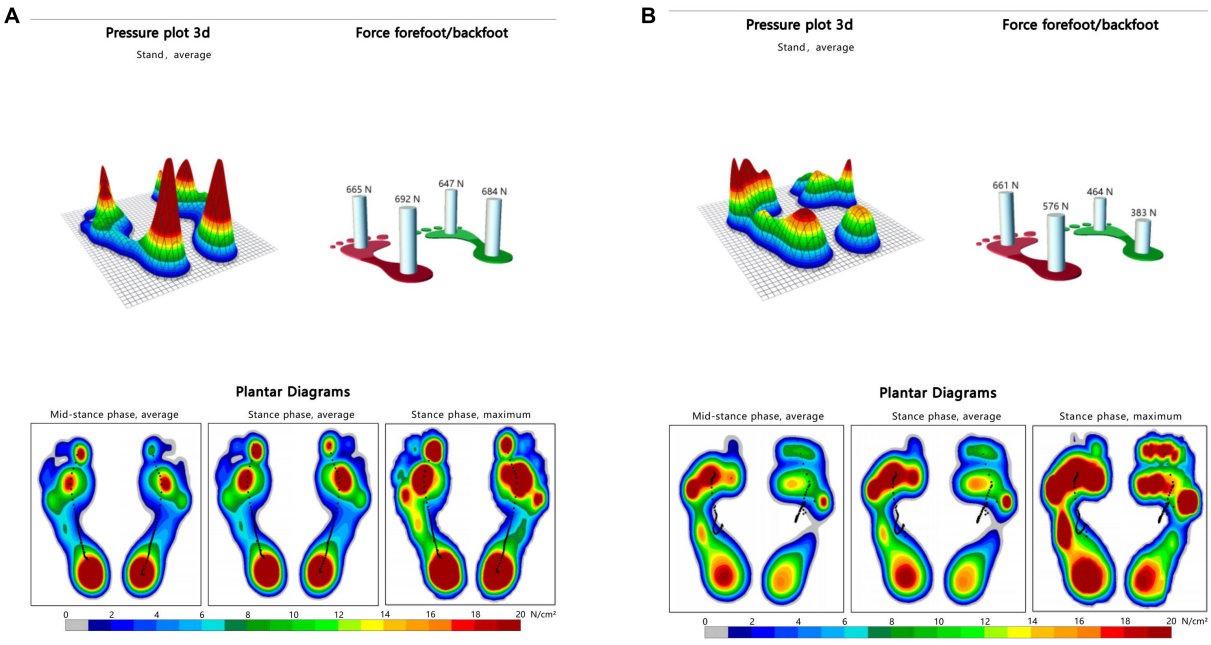

FIGURE 4
Dynamic plantar pressure model diagrams in both group. When healthy people walking, the plantar pressure on both sides were evenly distributed, showing obvious symmetry **(A)**. While stroke patients walking, bilateral plantar pressure were unevenly distributed, showing significant asymmetry **(B)**. Right side is the hemiplegic side in panel **(B)**, and the peak plantar pressure of the forefoot and heel in the hemiplegic side were lower than those in the non-hemiplegic side.

and walking ability. The current study showed that the BBS score was negatively correlated with the 10MWT and the TUGT. This indicated that the patient's balance function was related to their walking function, which follows previous studies. Chen et al. (2005) argued that patients with hemiplegia have weak limbs during the swing of the lower limbs on the hemiplegic side and need to provide compensation from the non-hemiplegic side, which reduces the speed; also, the 10MWT could reflect the dynamic changes in the pace of patients with hemiplegia during walking. The present study showed that better balance function of stroke-affected patients was associated with the shorter time and faster pace required to complete the 10MWT. The TUGT can assess the risk of falling during walking in stroke-affected patients and the ability of sit to stand transfer and posture control (Pérez-de la Cruz, 2021). The better the balance function of patients, the stronger the posture control ability, the higher the walking stability, and the lower the risk of falling.

The results revealed no significant correlation between the BBS score and step width, but revealed positive correlation between the BBS score and stride length in stroke-affected patients. Koch et al. conducted a gait analysis of stroke-affected patients, finding these patients had balance disorders and unstable walking. Still, they

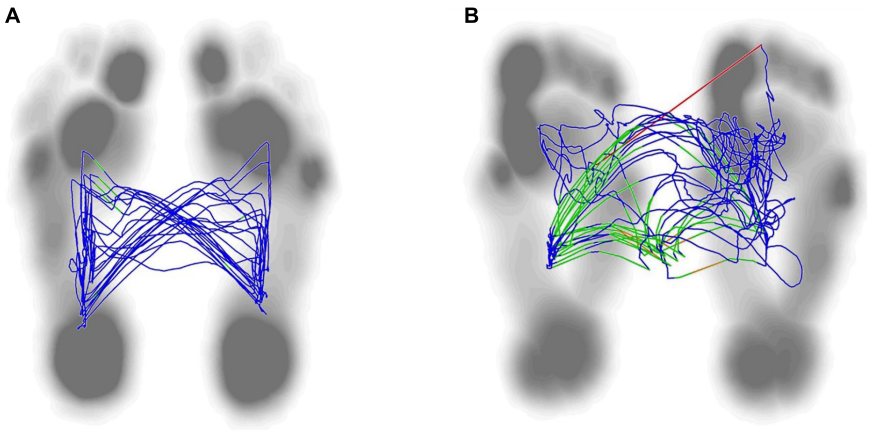

FIGURE 5
Lateral symmetry of center of plantar in both group. The normal center pressure trajectories distributed in a butterfly shape, with left-right symmetry **(A)**. The center pressure trajectory distribution of stroke patient was asymmetrical and shifting toward the hemiplegic side **(B)**.

did not analyze the correlation between the balance function and stride length and step width (Koch et al., 2019). This may suggest that the gait characteristics of sensory and non-sensory disorder balance dysfunction are different. Hong et al. (2020) reported that the motor function of the hemiplegic lateral limbs in stroke-affected patients was impaired, and to maintain better gait stability during walking, the patient's step width was significantly increased and the stride length was reduced. However, the effect of non-sensory balance function on stroke-affected patients was not ruled out. Lewek et al. (2014) argued that the BBS score was correlated with stride length, and walking step width could indicate the balance ability in stroke-affected patients.

After a stroke, the asymmetric gait during walking activates a compensation mode through muscle movement, posture, and gait training, which is conducive to the emergence of normal gait (Beyaert et al., 2015). Yang et al. (2018) reported that improving

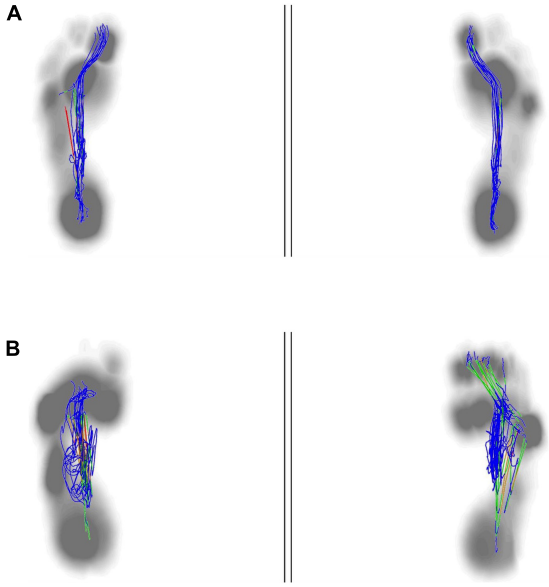

FIGURE 6
Anterior to posterior position of center of plantar. The anterior to posterior pressure line start from the heel to the big toe. The normal plantar pressure trajectory from anterior to posterior was almost overlapped **(A)**. The plantar pressure trajectory from anterior to posterior in stroke patient was not exactly overlapping, mainly concentrated in the midfoot, and was shorter than the healthy people **(B)**.

TABLE 3 Correlations between the Berg Balance Scale score and peak plantar pressure and gait parameters in the study group.

Project	Berg Balance Scale score	
	r	*P*
10-m walk test	−0.727	<0.001
Timed up-and-go test	−0.738	<0.001
Peak plantar pressure of hemiplegic forefoot	−0.398	<0.001
Peak plantar pressure of hemiplegic midfoot	−0.353	<0.001
Peak plantar pressure of hemiplegic heel	−0.012	0.887
Peak plantar pressure of non-hemiplegic forefoot	−0.073	0.392
Peak plantar pressure of non-hemiplegic midfoot	−0.502	<0.001
Peak plantar pressure of non-hemiplegic heel	0.057	0.501
Step width	−0.105	0.219
Stride length	0.286	0.0006
Lateral symmetry	−0.054	0.525
Anterior to posterior position	−0.444	<0.001
Hemiplegic stand phase	−0.36	0.023
Hemiplegic swing phase	0.338	<0.001
Non-hemiplegic stand phase	0.089	0.298
Non-hemiplegic swing phase	−0.11	0.197
Dual stance phase	−0.366	<0.001

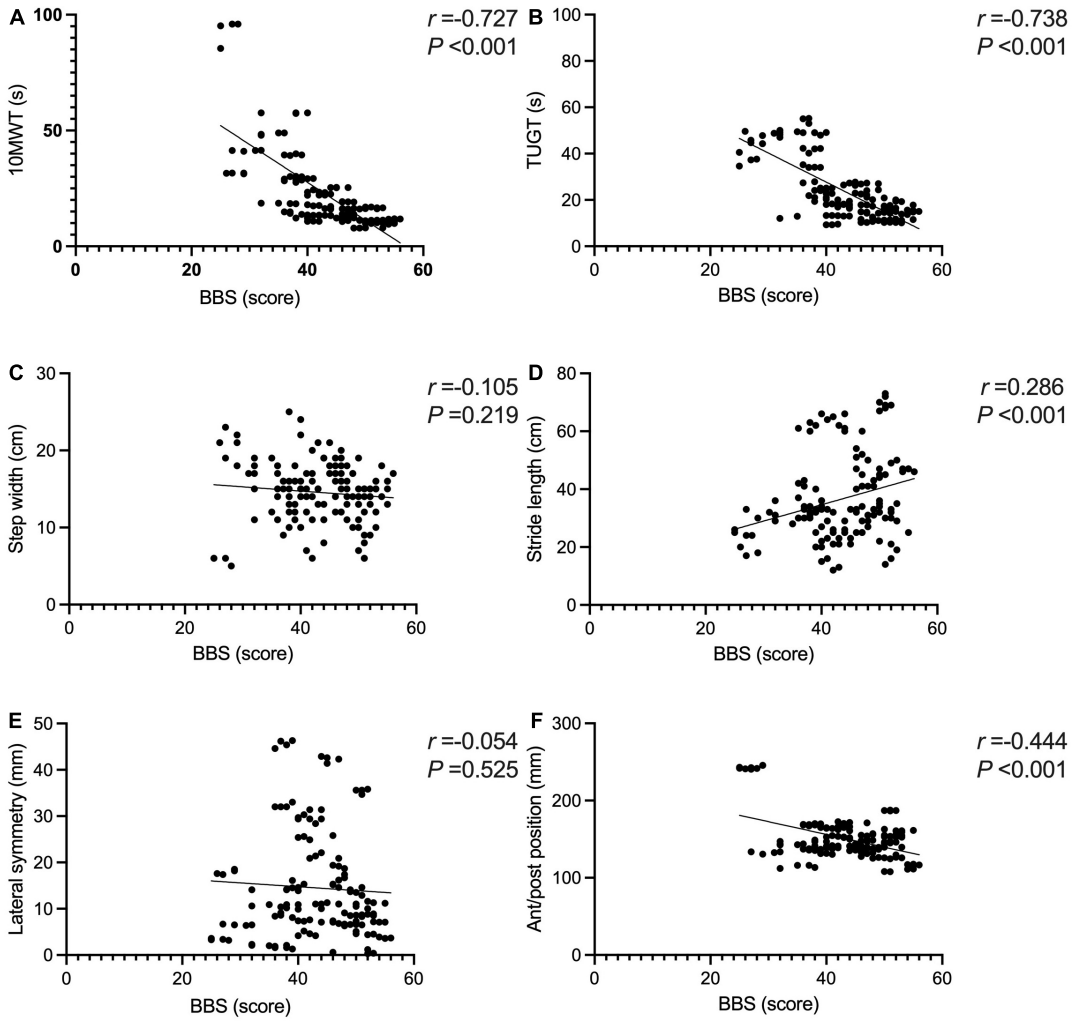

FIGURE 7
Correlations between the Berg Balance Scale score and gait parameters in the study group. The BBS and the 10MWT had a negative correlation **(A)** ($r = -0.727$, $P < 0.001$). The BBS and the TUGT had a negative correlation **(B)** ($r = -0.738$, $P < 0.001$). The BBS score was not correlated with step width **(C)** ($P > 0.05$). The BBS score was positively correlated with the stride length **(D)** ($r = 0.286$, $P < 0.001$). The BBS score was not correlated with lateral symmetry **(E)** ($P > 0.05$). The BBS score was negatively correlated with the ant/post position **(F)** ($r = -0.444$, $P < 0.001$). *Indicates significantly different.

the gait symmetry of stroke-affected patients can advance their walking ability. Forghany reported that stroke-affected patients acquired a pattern of bipedal asymmetry when walking, which was related to limited walking. Hornby et al. (2019) believed that improving the walking ability of stroke-affected patients made it possible to improve gait symmetry, especially patients' confidence in obtaining balance.

The present study suggested that the balance function of stroke-affected patients affects their gait symmetry. The balance function mainly affects the support line of the ant/post position. Better balance function of the patient may be associated with a stronger ability to support the front and back positions and better front–back symmetry, eventually resulting in a shorter length of the support line in the front and back positions. No significant correlation was found between equilibrium function and lateral symmetry, which needs to be explored further.

The present study analyzed the correlation between the BBS score and dynamic peaked plantar pressure. The results showed there was no obvious correlation between the BBS score and non-paralytic forefoot and heel, and hemiplegic midfoot and heel, but a negative correlation with hemiplegic forefoot and midfoot and non-paralytic midfoot was found. Rogers et al. (2020) suggested the changes in plantar pressure during walking in patients to improve walking ability should be explored. Forghany et al. (2015) reported that the plantar pressure distribution of stroke-affected patients is asymmetric. In the support phase, the lateral forefoot and heel are under greater pressure, while the hemiplegic heel is under the most pressure, and the midfoot and forefoot are under less pressure (Forghany et al., 2015). Lou et al. (2020) found that, after the patient's walking ability improved, the peak plantar pressure in the hemiplegic forefoot increased and the peak plantar pressure on the non-hemiplegic heel was lower than before.

Few reports exist about the changes in balance function and plantar pressure during walking. This study further explored the changes in plantar pressure in patients with stroke balance function during walking. It is believed that the balance function after stroke

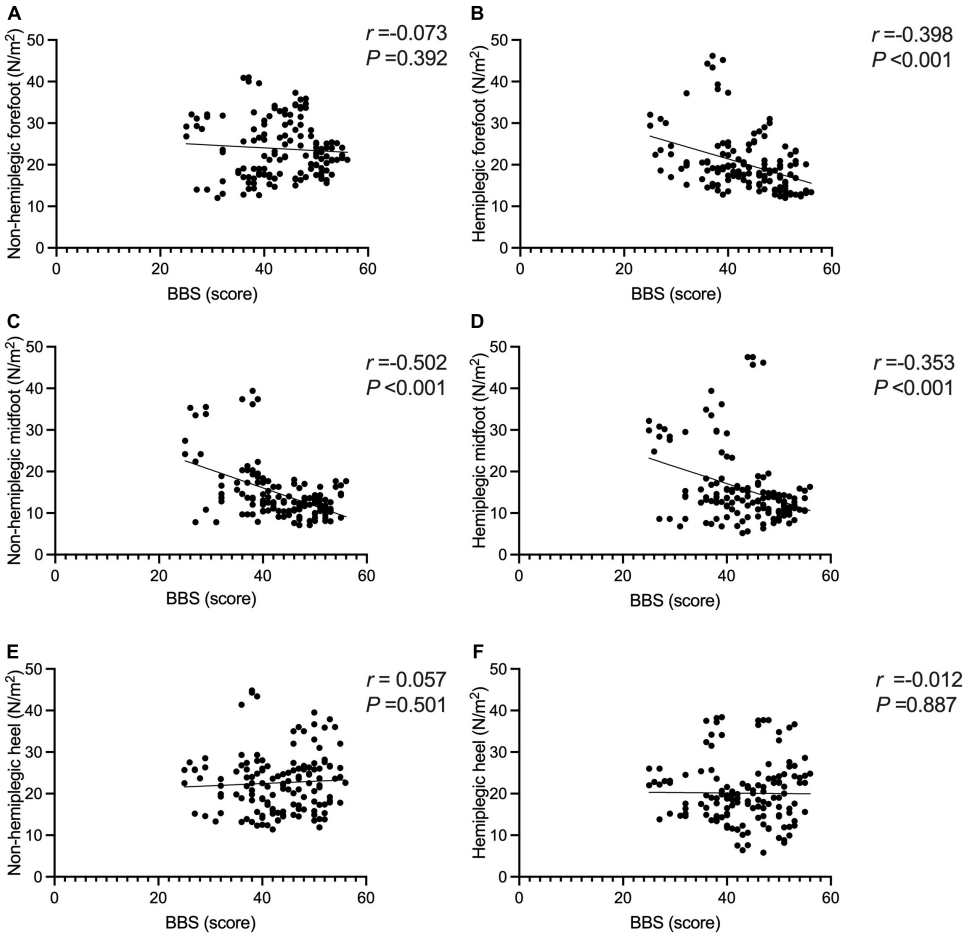

FIGURE 8
Correlations between the Berg Balance Scale score and peak plantar pressure in the study group. The BBS score was not correlated with the peak plantar pressure of the non-hemiplegic forefoot **(A)** ($P > 0.05$), but it was negatively correlated with the peak plantar pressure of the hemiplegic forefoot **(B)** ($r = -0.398$, $P < 0.001$). The BBS score was negatively correlated with the peak plantar pressure of the non-hemiplegic midfoot **(C)** ($r = -0.502$, $P < 0.001$) and the hemiplegic midfoot **(D)** ($r = -0.353$, $P < 0.001$). The BBS score was not correlated with the peak plantar pressure of the non-hemiplegic heel **(E)** ($P > 0.05$) and hemiplegic heel **(F)** ($P > 0.05$).

is closely related to the hemiplegic forefoot and midfoot and non-paralyzed midfoot. When stroke-affected patients walk, due to hemiplegic lateral foot inversion and toe flexion (Park et al., 2021), the plantar pressure cannot be transferred to the inner side of the forefoot in the support phase, the pressure is concentrated on the outside of the forefoot, and the peak pressure on the forefoot is higher. Patients with a better balance function can relieve the foot-inverted mode. In the support phase, the contact area between the forefoot and the ground becomes larger, resulting in a decrease in the peak pressure of the forefoot. The higher the balance function, the lower the peak pressure of the forefoot in the support phase.

In the present study, there was no obvious correlation between the BBS score and the stance phase, swing phase of the non-hemiplegic limbs, while the BBS score was negatively correlated with the stance and swing phases of the hemiplegic limbs and dual stance phase. Wang et al. (2021) reported that as the pressure of hemiplegic forefoot in stroke-affected patients improved, the active dorsiflexion of the hemiplegic foot was promoted, the center of gravity was easier to move forward, the walking ability improved, and the balance ability improved. In et al. (2017) improved the patient's knee extension ability, strengthened the contact area of the feet in the stance phase, and strengthened the dorsiflexion to reduce the time of the hemiplegic stance and swing phases, improve the patient's balance function, and improve their walking ability. The present study's findings are consistent with those of previous studies. The better the balance function, the more sufficient the center of gravity shift and the more adequate the ankle dorsiflexion during the foot landing (Persson et al., 2011).

The characteristics of gait under balance dysfunction caused by different reasons are dissimilar. The mature research is mostly about gait characteristics under proprioception impairment, and the effect of hemiplegic gait or balance function under abnormal postural control on gait is unclear (Luque-Moreno et al., 2019). The plantar pressure distribution during walking reflects the abnormal gait of patients with walking dysfunction, the uneven distribution of body weight, and the process of pressure changes in both limbs (Lund et al., 2018). Abnormal distribution of plantar pressure increases the risk of injury to the patient's waist, knees, calves, ankles, and feet, further increasing the risk of falls during walking

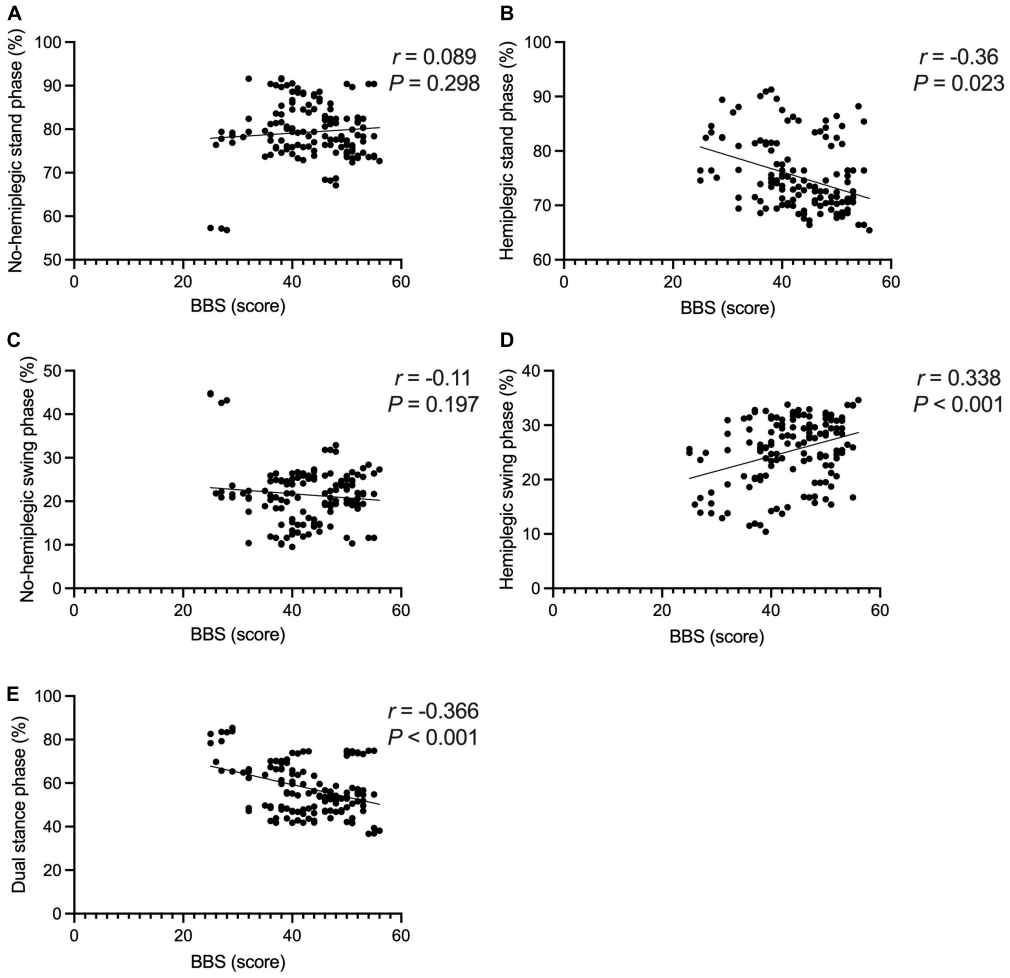

FIGURE 9
Correlations between the Berg Balance Scale score and gait cycle in the study group. The BBS score was not correlated with the non-hemiplegic stand phase **(A)** ($P > 0.05$), non-hemiplegic swing phase **(B)** ($P > 0.05$). The BBS score was negatively correlated with the hemiplegic stand phase **(C)** ($r = -0.36$, $P = 0.023$), hemiplegic swing phase **(D)** ($r = -0.338$, $P < 0.001$). The BBS score was negatively correlated with dual stand phase **(E)** ($r = -0.366$, $P < 0.001$).

training and affecting the recovery of the patient's walking ability (Yang et al., 2014).

Existing studies have shown that balance function affects walking in stroke-affected patients (An and Shaughnessy, 2011), and the plantar pressure distribution reflects the patient's ability to walk (Kimura et al., 2022). However, there are few studies exploring balance function and plantar pressure, and the distribution of balance ability and plantar pressure during walking in stroke-affected patients is unclear (Bower et al., 2019). When stroke-affected patients with balance dysfunction perform walking training, their balance function affects their posture control, transfer ability, and the length of the limb support and double support phases of the hemiplegic side during walking, increasing the asymmetry of their hemiplegic gait. This affects their gait pace and stability and increases the risk of falling. Walking training should pay attention to the plantar pressure distribution of the forefoot and midfoot on the hemiplegic side and improve the symmetry of the ant/post positions to progress the patient's walking ability. This provides a new direction for subsequent rehabilitation treatment.

This study has certain limitations: (1) the small sample size may mean the changes in different variables may have been too small to be significant, impacting the final result and (2) there is a difference between the running platform and a normal walking mode, and the measurement of the plantar pressure may have caused errors and affected the test results. In future research, the sample size should be increased, the authority of the research should be enhanced, and the patient's walking ability should be improved through the patient's plantar pressure and front–back position symmetry to provide a new direction to treat stroke-affected patients.

5. Conclusion

After cerebral infarction in the basal ganglia, there is typically asymmetry in the pressure of the forefoot and the ant/post position, which significantly affects the balance function. It is necessary to pay attention to the distribution of hemiplegic forefoot plantar pressure, the control of gait phase,

and the processing of the ant/post position to better improve balance and posture control, reducing the risk of falling.

Data availability statement

The original contributions presented in this study are included in the article/supplementary material, further inquiries can be directed to the corresponding author.

Ethics statement

The study was approved by the Ethics Committee of Beijing Tiantan Hospital Affiliated with Capital Medical University (Approval No. KY2021-040-02). The patients/participants provided their written informed consent to participate in this study.

Author contributions

SL: methodology, validation, formal analysis, and writing—original draft preparation. HY: conceptualization, writing—review and editing, supervision, and project administration. ZW: software and data curation. PD: resources and visualization. All authors contributed to manuscript revision, read, and approved the submitted version.

Funding

This work was supported by grants from the National Natural Science Foundation of China (grant numbers: 82000723, 81974357, and 81772438) and the National Natural Science Foundation of Capital Medical University (grant number: XZR2021-114).

Acknowledgments

Thanks to the experts and colleagues who provided guidance and assistance in this study and all enrolled patients.

Conflict of interest

The authors declare that the research was conducted in the absence of any commercial or financial relationships that could be construed as a potential conflict of interest.

Publisher's note

References

Alexander, L., Black, S., Patterson, K., Gao, F., Danells, C., and McIlroy, W. (2009). Association between gait asymmetry and brain lesion location in stroke patients. *Stroke* 40, 537–544. doi: 10.1161/STROKEAHA.108.527374

An, M., and Shaughnessy, M. (2011). The effects of exercise-based rehabilitation on balance and gait for stroke patients: A systematic review. *J. Neurosci. Nurs.* 43, 298–307. doi: 10.1097/JNN.0b013e318234ea24

Beyaert, C., Vasa, R., and Frykberg, G. (2015). Gait post-stroke: Pathophysiology and rehabilitation strategies. *Neurophysiol. Clin.* 45, 335–355.

Bhatt, A., Brucker, J., and Almast, J. (2018). Beyond stroke-uncommon causes of diffusion restriction in the basal ganglia. *Emerg. Radiol.* 25, 87–92. doi: 10.1007/s10140-017-1550-2

Blum, L., and Korner-Bitensky, N. (2008). Usefulness of the berg balance scale in stroke rehabilitation: A systematic review. *Phys. Ther.* 88, 559–566.

Bower, K., Thilarajah, S., Pua, Y., Williams, G., Tan, D., Mentiplay, B., et al. (2019). Dynamic balance and instrumented gait variables are independent predictors of falls following stroke. *J. Neuroeng. Rehabil.* 16:3. doi: 10.1186/s12984-018-0478-4

Chen, G., Patten, C., Kothari, D., and Zajac, F. (2005). Gait differences between individuals with post-stroke hemiparesis and non-disabled controls at matched speeds. *Gait Posture* 22, 51–56.

Dong, K., Meng, S., Guo, Z., Zhang, R., Xu, P., Yuan, E., et al. (2021). The effects of transcranial direct current stimulation on balance and gait in stroke patients: A systematic review and meta-analysis. *Front. Neurol.* 12:650925. doi: 10.3389/fneur.2021.650925

Forghany, S., Nester, C., Tyson, S., Preece, S., and Jones, R. (2015). Plantar pressure distribution in people with stroke and association with functional consequences. *Physiotherapy* 101, e399–e400.

Hong, S., Jung, S., Oh, H., Lee, S., and Woo, Y. (2020). Effects of the immobilization of the upper extremities on spatiotemporal gait parameters during walking in stroke patients: A preliminary study. *Biomed. Res. Int.* 2020:6157231. doi: 10.1155/2020/6157231

Hornby, T., Henderson, C., Plawecki, A., Lucas, E., Lotter, J., Holthus, M., et al. (2019). Contributions of Stepping Intensity and Variability to mobility in individuals poststroke. *Stroke* 50, 2492–2499.

In, T., Jin, Y., Jung, K., and Cho, H. (2017). Treadmill training with thera-band improves motor function, gait and balance in stroke patients. *NeuroRehabilitation* 40, 109–114. doi: 10.3233/NRE-161395

Kimura, N., Kawasaki, S., Tsuruda, A., Nogi, S., and Ohata, K. (2022). The centre of pressure position determined by capacity of weight-shifting in stride stances in individuals with post-stroke. *Clin. Biomech. (Bristol, Avon)* 91:105534. doi: 10.1016/j.clinbiomech.2021.105534

Koch, G., Bonní, S., Casula, E., Iosa, M., Paolucci, S., Pellicciari, M., et al. (2019). Effect of cerebellar stimulation on gait and balance recovery in patients with hemiparetic stroke: A randomized clinical trial. *JAMA Neurol.* 76, 170–178. doi: 10.1001/jamaneurol.2018.3639

Lee, D., and Lee, G. (2019). Effect of afferent electrical stimulation with mirror therapy on motor function, balance, and gait in chronic stroke survivors: A randomized controlled trial. *Eur. J. Phys. Rehabil. Med.* 55, 442–449. doi: 10.23736/S1973-9087.19.05334-6

Lee, N., Kwon, J., Son, S., Nam, S., Choi, Y., and Kim, C. (2013). Changes of plantar pressure distributions following open and closed kinetic chain exercise in patients with stroke. *NeuroRehabilitation* 32, 385–390. doi: 10.3233/NRE-130859

Lee, P., Huang, J., Tseng, H., Yang, Y., and Lin, S. (2020). Effects of trunk exercise on unstable surfaces in persons with stroke: A randomized controlled trial. *Int. J. Environ. Res. Public Health* 17:9135.

Lewek, M., Bradley, C., Wutzke, C., and Zinder, S. (2014). The relationship between spatiotemporal gait asymmetry and balance in individuals with chronic stroke. *J. Appl. Biomech.* 30, 31–36.

Li, Y. (2022). Effectiveness of proprioceptive neuromuscular facilitation techniques in improving balance in poststroke patients: A systematic review. *Brain Netw. Modul.* 1, 9–12. doi: 10.1177/0269215519830159

Lou, Y., Yang, J., Ma, Y., and Zhen, X. (2020). Effects of different acupuncture methods combined with routine rehabilitation on gait of stroke patients. *World J. Clin. Cases* 8, 6282–6295.

Lund, C., Dalgas, U., Grønborg, T., Andersen, H., Severinsen, K., Riemenschneider, M., et al. (2018). Balance and walking performance are improved after resistance and aerobic training in persons with chronic stroke. *Disabil. Rehabil.* 40, 2408–2415.

Luque-Moreno, C., Cano-Bravo, F., Kiper, P., Solís-Marcos, I., Moral-Munoz, J., Agostini, M., et al. (2019). Reinforced feedback in virtual environment for plantar flexor poststroke spasticity reduction and gait function improvement. *Biomed. Res. Int.* 2019:6295263. doi: 10.1155/2019/6295263

Mehrholz, J., Pohl, M., Kugler, J., and Elsner, B. (2018). The improvement of walking ability following stroke. *Dtsch. Arztebl. Int.* 115, 639–645.

Obembe, A., Olaogun, M., and Adedoyin, R. (2014). Gait and balance performance of stroke survivors in South-Western Nigeria–a cross-sectional study. *Pan Afr. Med. J.* 17:6. doi: 10.11694/pamj.supp.2014.17.1.3001

Park, C., Son, H., and Yeo, B. (2021). The effects of lower extremity cross-training on gait and balance in stroke patients: A double-blinded randomized controlled trial. *Eur. J. Phys. Rehabil. Med.* 57, 4–12. doi: 10.23736/S1973-9087.20.06183-3

Pérez-de la Cruz, S. (2021). Comparison between three therapeutic options for the treatment of balance and gait in stroke: A randomized controlled trial. *Int. J. Environ. Res. Public Health* 18:426. doi: 10.3390/ijerph18020426

Persson, C., Hansson, P., and Sunnerhagen, K. (2011). Clinical tests performed in acute stroke identify the risk of falling during the first year: Postural stroke study in Gothenburg (POSTGOT). *J. Rehabil. Med.* 43, 348–353. doi: 10.2340/16501977-0677

Rahimzadeh Khiabani, R., Mochizuki, G., Ismail, F., Boulias, C., Phadke, C., and Gage, W. (2017). Impact of spasticity on balance control during quiet standing in persons after stroke. *Stroke Res. Treat.* 2017:6153714. doi: 10.1155/2017/6153714

Rogers, A., Morrison, S., Gorst, T., Paton, J., Freeman, J., Marsden, J., et al. (2020). Repeatability of plantar pressure assessment during barefoot walking in people with stroke. *J. Foot Ankle Res.* 13:39. doi: 10.1186/s13047-020-00407-x

Saleh, M., Rehab, N., and Aly, S. (2019). Effect of aquatic versus land motor dual task training on balance and gait of patients with chronic stroke: A randomized controlled trial. *NeuroRehabilitation* 44, 485–492. doi: 10.3233/NRE-182636

van Duijnhoven, H., Heeren, A., Peters, M., Veerbeek, J., Kwakkel, G., Geurts, A., et al. (2016). Effects of exercise therapy on balance capacity in chronic stroke: Systematic review and meta-analysis. *Stroke* 47, 2603–2610.

Wang, C. (2022). The role of neuromodulation to drive neural plasticity in stroke recovery: A narrative review. *Brain Netw. Modul.* 1, 2–8.

Wang, J., Qiao, L., Yu, L., Wang, Y., Taiar, R., Zhang, Y., et al. (2021). Effect of customized Insoles on gait in post-stroke hemiparetic individuals: A randomized controlled trial. *Biology (Basel)* 10:1187. doi: 10.3390/biology10111187

Yang, J., Ahn, N., Kim, D., and Kim, D. (2014). Plantar pressure distribution during robotic-assisted gait in post-stroke hemiplegic patients. *Ann. Rehabil. Med.* 38, 145–152. doi: 10.5535/arm.2014.38.2.145

Yang, Y., Mi, P., Huang, S., Chiu, S., Liu, Y., and Wang, R. (2018). Effects of neuromuscular electrical stimulation on gait performance in chronic stroke with inadequate ankle control—A randomized controlled trial. *PLoS One* 13:e0208609. doi: 10.1371/journal.pone.0208609

Yeung, L., Ockenfeld, C., Pang, M., Wai, H., Soo, O., Li, S., et al. (2018). Randomized controlled trial of robot-assisted gait training with dorsiflexion assistance on chronic stroke patients wearing ankle-foot-orthosis. *J. Neuroeng. Rehabil.* 15:51. doi: 10.1186/s12984-018-0394-7

You, Y., Chung, S., and Lee, H. (2016). Impact of the difference in the plantar flexor strength of the ankle joint in the affected side among hemiplegic patients on the plantar pressure and walking asymmetry. *J. Phys .Ther. Sci.* 28, 3015–3019. doi: 10.1589/jpts.28.3015

frontiers | Frontiers in Neuroscience

TYPE Original Research
PUBLISHED 27 February 2023
DOI 10.3389/fnins.2023.1125418

OPEN ACCESS

EDITED BY
Feng Zhang,
The Third Hospital of Hebei Medical University, China

REVIEWED BY
Lai Wang,
Henan University, China
Xiaodong Liu,
The Chinese University of Hong Kong, China

*CORRESPONDENCE
Lidian Chen
✉ cld@fjtcm.edu.cn

†These authors have contributed equally to this work

SPECIALTY SECTION
This article was submitted to Translational Neuroscience, a section of the journal Frontiers in Neuroscience

RECEIVED 16 December 2022
ACCEPTED 02 February 2023
PUBLISHED 27 February 2023

CITATION
Yang N, Chen S, Liu S, Ling S and Chen L (2023) Increased low frequency fluctuation in the brain after acupuncture treatment in CSVDCI patients: A randomized control trial study.
Front. Neurosci. 17:1125418.
doi: 10.3389/fnins.2023.1125418

Increased low frequency fluctuation in the brain after acupuncture treatment in CSVDCI patients: A randomized control trial study

Nan Yang[1,2†], Sina Chen[2†], Shuxue Liu[2], Shuiqiao Ling[2] and Lidian Chen[1*]

[1]Fujian University of Traditional Chinese Medicine, Fuzhou, Fujian, China, [2]Zhongshan Hospital of Traditional Chinese Medicine, Zhongshan, Guangdong, China

Background: Cerebral small vessel disease (CSVD) is one of two cognition-impairing diseases. Acupuncture (Acu) is a flexible treatment with few adverse effects and is thus widely used to treat neurological problems.

Methods: We recruited a total of 60 patients and assigned them to two groups (n = 30 each group). During the study, some participants were excluded by quality control, and a total of 44 subjects (25 Acu and 19 controls) were completed to investigate the therapeutic efficacy of acupuncture on CSVD cognitive impairment (CSVDCI). The following demographic and clinical variables were compared between the two groups: gender, age, education, smoking, alcohol, Montreal cognitive assessment (MoCA), symbol digit modalities test (SDMT), verbal fluency test (VFT), digit span task (DST), Boston naming test (BNT) scores, and amplitude of low-frequency fluctuation (ALFF) under the typical band (0.01–0.08 Hz). Mixed effect analysis was utilized to test for differences between the two groups before and after the treatment.

Results: Following acupuncture treatment, the Acu group scored higher on MoCA, SDMT, VFT, DST, and BNT compared to controls ($P < 0.05$). The brain regions showing substantially greater ALFF values in the Acu group were the right inferior temporal gyrus, left middle occipital gyrus, left superior occipital gyrus, left insula, bilateral postcentral gyrus, right superior parietal gyrus, right cerebellum, right precuneus, and right precentral gyrus ($P < 0.005$, no correction). The ALFF values in the right inferior temporal gyrus ($P = 0.027$), left middle occipital gyrus ($P = 0.005$), left superior occipital gyrus ($P = 0.011$), and right superior parietal gyrus ($P = 0.043$) were positively associated with MoCA.

Conclusion: We found that acupuncture modulates the functional activity of temporal, occipital, and parietal regions of the brain in CSVDCI patients.

KEYWORDS

cognitive function, acupuncture, small vessel disease, fMRI, brain activity

1. Introduction

CSVDCI is the most common cause of vascular cognitive impairment (VCI), accounting for approximately 74% of all occurrences (Rao et al., 2009). It is not commonly known that CSVDCI is an important subtype of VCI due to its quiet onset and lack of prominent clinical features (Brookes et al., 2014), also representing the primary clinical manifestation of CSVD. CSVDCI shows a similar pattern of cognitive decompensation to the VCI, which is characterized by reduced executive function, attention, and information processing speed, with relatively intact memory function in the early stages and gradual development of dementia (Chen et al., 2019). In addition, cognitive impairment worsens with the development of the disease, which severely impacts patient quality of life.

Early management of CSVDCI can enhance cognitive performance and patient quality of life, while partially slowing the course of cognitive decline. Several conservative treatments, including the use of an acetylcholinesterase inhibitor and N-methyl-d-aspartate (NMDA) receptor antagonist were proposed for the symptomatic treatment of dementia (Arvanitakis et al., 2019). However, a limited number of targeted drugs effectively improved cognitive function in CSVDCI patients (Pantoni, 2010), with minimal efficacy for dementia (Bath and Wardlaw, 2015). Interestingly, acupuncture has been widely used in China as a complementary alternative treatment for dementia, and also been accepted for VCI treatment in Western medicine (Ji et al., 2021). The main advantage of acupuncture is the lower incidence of adverse effects that characterize pharmaceutical approaches (NIH Consensus Conference, 1998; Kim et al., 2019). Importantly, clinical randomized trials demonstrated the short-term impact of acupuncture on cognitive function in VCI patients (Yang et al., 2014; Yang et al., 2019; Huang et al., 2021).

With an increasing understanding of the etiological basis of CSVD in the elderly population, inflammatory responses have been associated with its development and progression (Li et al., 2020). Wang et al. demonstrated that acupuncture attenuates inflammation-related cognitive impairment in experimental vascular dementia (VD) by inhibiting the miR-93-mediated TLR4/MyD88/NF-κB signaling pathway (Wang et al., 2020). In addition, acupuncture reduces oxidative stress and inflammation associated with TXNIP, plays a neuroprotective role in VD rats (Du et al., 2018), enhances cognitive function and induces neuroprotective effects against inflammation in CCH rats by activating α7nAChR and the JAK2-STAT3 pathway (Cao et al., 2021).

Various ancient and modern acupuncture publications showed the Shenting (GV24) and Baihui (GV20) are vital distal acupoints associated with the cure of dementia, dizziness, headache, among other brain diseases. Huang et al. (2015) conducted a meta-analysis study that included 1,637 subjects with post-stroke cognitive impairment (PSCI), and found that integrating Shenting and Baihui acupuncture with computer-assisted cognitive training significantly improves attention deficits in stroke patients. Similar results were found in a randomized controlled trial of 2 × 2 factorial design conducted by Yang S. et al. (2014).

Resting-state functional magnetic resonance imaging (MRI) has been extensively employed to investigate the functional mechanisms underlying a variety of neurological diseases, and may also provide insights on the ability of acupuncture to improve cognitive performance (Cai et al., 2018). Measurements such as functional connectivity (FC) and degree centrality (DC) were created to mimic the brain network (Park and Friston, 2013). Zang et al. (2007) suggested ALFF to estimate regional brain activity and found it could represent the activity of different brain regions at the resting state. In addition, abnormal ALFF levels were found in people with cognitive problems and abnormal brain function, a powerful determinant of cognitive decline (Li et al., 2021; Wang et al., 2021; Zhang J. et al., 2021), and different brain regions, including the parietal, insular and cingulate regions. This is significantly correlated with cognitive function in patients with subcortical vascular cognitive dysfunction, which may lead to decreased cortical activation (Li et al., 2015). CSVDCI patients with cerebral microbleeds (CMBs) have altered spontaneous brain activity of the default, sensorimotor, and fronto-parietal lobe networks, that may impact potential neurophysiological mechanisms of intrinsic brain activity (Feng et al., 2021).

Since 1990, an increasing number of studies used imaging to explore the physio-pathological mechanisms of acupuncture for the treatment of disease (Dhond et al., 2007). Acupuncture improves cognitive function in patients with Parkinson and increases ALFF values of the default network, visual network, and insular lobe. This has led to the hypothesis that acupuncture can activate the cerebellum-thalamus-cortex loop by regulating the spontaneous activity of the brain in key regions, a neurophysiological mechanism to improve cognitive dysfunction (Li Z. et al., 2018). Moxibustion therapy can improve the cognitive function of patients with mild cognitive impairment by adjusting the ALFF values of the default, visual and subcortical networks (Lai et al., 2022), and might thus reveal the brain regions involved in cognitive function improvement through acupuncture.

Here, we examined the differences in ALFF values between the Shenting/Baihui acupoints and conventional drug treatment in CSVDCI patients, before and after treatment (in 12 weeks), to uncover the associated neural mechanisms.

2. Materials and methods

2.1. Participants

CSVDCI patients were enrolled at the Zhongshan Hospital of Traditional Chinese Medicine from July 1st 2017 to July 30th 2019. The protocol was approved by the research ethics committee of the Zhongshan Hospital of Traditional Chinese Medicine (reference: 2017ZSZY-LLK-219). We recruited CSVDCI patients at the neurology outpatient and inpatient departments. All participants signed an informed consent form prior to enrollment.

Patients with the following conditions were considered eligible: (i) age between 40 and 80 years, (ii) comply with diagnostic imaging criteria for cerebral small vessel disease and vascular cognitive impairment, (iii) MoCA score between 10 and 26, (iv) not receiving regular acupuncture treatment for the recent six months.

Patients with the following conditions were excluded: (i) cognitive dysfunction caused by macrovascular, cardiogenic cerebral embolism, (ii) patients with severe speech, vision,

or hearing impairments or mental disorders that impact cognitive examinations, (iii) cognitive dysfunction caused by neuropsychological disorders (e.g., depression), (iv) illiterates that could not cooperate with cognitive examinations, (v) prior alcohol and drug abuse experience, (vi) combination of serious diseases, including of the cardiovascular, hepatic, nephrology, endocrine system and hematopoietic systems, (vii) participating in other clinical trials.

The CSVD patients were diagnosed according to the Neuroimaging Standards for Research into Small Vessel Disease (Wardlaw et al., 2013). Specifically, the diagnostic standard for imaging of CSVD included: (i) Recent small subcortical infarct: Axial views showing an infarct diameter smaller than 20 mm, which could be larger than 20 mm in the coronal or sagittal views, (ii) Lacunes of presumed vascular origin: round or ovoid, 3–15 mm in diameter, distributed in subcortical regions, filled with the same signals as cerebrospinal fluid (CSF), (iii) white matter hyperintensity (WMH) of presumed vascular origin: abnormal brain white matter (WM) signals, lesions of variable size, showing a high signal on the T2-weighted or T2-weighted FLAIR images. (iv) Perivascular space: the signal of perivascular space was the same as that of the CSF in all MRI sequences. The shape was linear when the image plane ran parallel to the blood vessels and round or oval when running perpendicular to the vessels, usually smaller than 3 mm in diameter, (v) Cerebral microbleeds, which were defined as the following changes in the images obtained with T2*-weighted gradient-echo sensitive to magnetizing effects. For example: (1) small round or oval, clear boundary, homogeneity, lack of signal focus; (2) diameter of 2–5 mm (maximum 10 mm) and lesion surrounded by the brain parenchyma; (3) brain atrophy: reduced brain volume not associated with specific focal lesions, such as trauma and cerebral infarction.

The sample size was estimated using the Gpower3.1 software. The MoCA total score was used as the main impact indicator. Based on previous studies (Wang et al., 2016), which estimated the MoCA difference for VCI patients treated with acupuncture as 5.5 ± 2.2, and the MoCA difference for the control group as 3.1 ± 1.8. The Gpower3.1 software estimated the effect value for acupuncture to improve cognitive function in VCI patients to be 1.194045, whereby we set the α value to 0.01, the Power (1-β) value to 0.9, and the effect value to 1.194045, which was calculated using a sample size of 23 cases per group. With a shedding rate of 20%, we predicted a total sample size of 56, with 28 cases per group.

A total of sixty patients were enrolled after screening for eligibility, and were randomly allocated to either the acupuncture or conventional treatment groups. At the baseline, all patients underwent fMRI. We removed 11 and 5 patients from the conventional and acupuncture groups, respectively, due to excessive head motion or rejection of the second fMRI scan.

2.2. Protocol

This study represents a randomized controlled trial using fMRI scans to assess the effect and mechanisms of acupuncture treatment on CSVDCI. Participants completed fMRI scans and cognitive function assessments at the baseline. We randomly divided the participants into two groups, one receiving acupuncture at the Shenting and Baihui acupoints combined with conventional treatment, and the other receiving conventional treatment only. After treatment, fMRI scans and cognitive function assessments were performed again (Figure 1). The acupuncture treatment lasted for approximately 40 min.

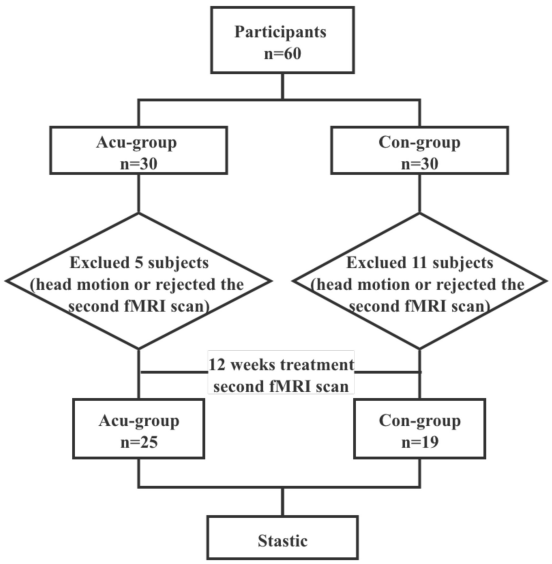

FIGURE 1
Workflow and group inclusion/exclusion criteria.

2.3. Blind

A random number generator with SPSS 22.0 statistical software was used by a researcher specializing in random assignment to derive 60 random numbers and generate a random assignment sequence. The cards with the random numbers, groupings, and interventions were then concealed in airtight, opaque envelopes and kept securely by this researcher. This person was not allowed to participate in the recruitment screening, outcome assessment and statistical analysis of this study.

2.4. Treatment program

2.4.1. Acupuncture treatment

With the thumb and forefinger holding the needle handle, the doctor alternately twists the needle body clockwise and counterclockwise to make it rotate quickly (180–300 times/min), and continues twisting for 2–3 min. After this, twist once every 10 min (following Deqi), and keep the needle for 40 min. Participants received acupuncture treatment once a day, for five days a week over a total of 12 weeks of intervention. Our selected points are Shenting and Baihui. Shenting is on the head, 0.5 inch straight up from the middle of the front hairline. The Baihui point is located at the intersection of the median line at the top of the head and the line connecting the tips of the two ears. The acupuncture treatments were performed by Yang Xiaoyan, an associate chief physician who practices acupuncture for more than 10 years.

TABLE 1 Demographics at the baseline.

Characteristics	Acu-group (n = 25)	Con-group (n = 19)	P-value
Gender (M/F)[a]	13/12	9/10	0.761
Age (in years)[b]	61.9 ± 4.56	62.94 ± 2.83	0.375
Education (in years)[b]	9.48 ± 2.94	8.68 ± 2.05	0.321
Smoking (often/sometimes/never)[c]	4/3/18	3/3/13	0.836
Alcohol (often/sometimes/never)[c]	4/3/18	3/5/11	0.429

Values are presented as the mean ± SD. M, male; F, female; SD, standard deviation. [a]p-values for the Pearson chi-square test. [b]p-values for two-sample independent t-test. [c]p-values for the Mann–Whitney U test.

2.4.2. Conventional treatment

Conventional treatment included donepezil tablets to improve cognition, aspirin to anti-platelet aggregation, atorvastatin calcium tablets to regulate lipid levels, in addition to blood pressure and blood glucose control according to the patient's underlying disease, and each patient participated in modern cognitive rehabilitation training.

2.5. Cognitive assessment

Before and after the treatment, all participants completed a cognitive assessment. (i) The MoCA includes eight cognitive domains: visual-spatial and executive functions, naming, memory, attention, language, abstraction, delayed recall, and orientation. The total score and the score of each cognitive domain were recorded following previous studies (O'Driscoll and Shaikh, 2017). For education levels lower than 12 years, we added 1 point to the total score. (ii) SDMT (Silva et al., 2018): participants were asked to convert nonsensical symbols into numbers within 90 s, while we recorded the number of correct answers, which were given one point each. (iii) VFT (Sutin et al., 2019) consisted of three parts, including semantic, phonetic, and motor fluency. Participants were asked to say the corresponding words within one minute as required, and the sum of the three groups of correct numbers was the total score. (iv) DST (Leung et al., 2011) consisted of two parts, digit forward and digit backward. During the test, participants were asked to simultaneously remember two numbers read by the researcher, with one digit per second starting with the first set. (v) The BNT (Durant et al., 2021) test provided 30 graphs, with the number of correctly named graphs representing the total score. We also collected information on sociodemographic background, medication, and disease history. The cognitive assessors were Huang Xiaohuang and Ling Shuiqiao, both physicians are at the level of attending physician or higher and have at least 5 years of training in cognitive aspects of therapy.

TABLE 2 Cognitive assessments at the baseline.

Characteristics	Acu-group (n = 25)	Con-group (n = 19)	P-value
MoCA[a]	22.00 (6.00)	22.00 (6.00)	0.319
SDMT[a]	52.00 (14.00)	51.00 (10.00)	0.859
VFT[a]	21.00 (8.00)	20.00 (5.00)	0.243
DST[b]	7.36 ± 1.97	6.47 ± 1.39	0.103
BNT[b]	17.96 ± 2.49	17.36 ± 2.38	0.431

MoCA, SDMT, and VFT values are presented as M(IQR); DST and BNT values are presented as the mean ± SD. M, median; IQR, interquartile range; SD, standard deviation. [a]p-values for the Mann–Whitney U test. [b]p-values for two-sample independent t-test.

2.6. Imaging data acquisition

All images were obtained using a GE 3T MRI scanner with an 8-channel phased-array head coil. The participants were requested to keep their eyes closed, relax but not fall asleep, and minimize head movement during the scanning. Functional images were collected with a gradient echo-planar imaging (EPI) sequence with the following parameters: repetition time (TR) = 2,000 ms, echo time (TE) = 30 ms, flip angle (FA) = 90°, field of view (FOV) = 240 mm × 240 mm, slice thickness = 3.5 mm, inter-slice gap = 0.7 mm, data matrix = 64 × 64, 33 interleaved axial slices coving the whole brain, and 240 volumes acquired in about 8 min. In addition, high resolution brain structural images were acquired using a T1-weighed 3D BRAVO sequence with the following parameters: TR = 8.0 ms, TE = 3.0 ms, FA = 12°, data matrix = 256 × 256, FOV = 256 mm × 256 mm, slice thickness = 1 mm, and 188 sagittal slices covering the whole brain. The conventional T1-weighted and T2-weighted FLAIR images were acquired for clinical assessment. All MRI images for each participant were acquired in the same session.

2.7. Data pre-processing

The fMRI data were preprocessed using the DPARSF toolbox[1] based on MATLAB. Before pre-processing the data, we visually inspected both brain functional and structural images, and excluded the datasets with significant signal dropouts, distortion, and other quality problems. The pre-processing procedure included: (1) removing the first 10 volumes to keep the magnetization equilibrium; (2) performing slice-timing and head-movement correction to remove effects caused by these factors; (3) conducting a linear co-registration between functional and structural images for each participant; (4) regressing the signals of the WM and CSF, and head-movement parameters (Friston-24 model); (5) performing a non-linear transformation between structural and template brain images of the Montreal Neurological Institute (MNI) space; normalizing functional images into the MNI space with a 3 mm^3 × 3 mm^3 × 3 mm^3 voxel size; and smoothing with a Gaussian kernel of 5 mm full width at half maximum (FWHM), and (6) performing temporal band-pass filtering for the typical band (0.01–0.08 Hz). This study discarded the fMRI data for subjects with head motion displacement > 3 mm or rotation > 3° in any axis (x, y, and z-axis). Data pre-processing was performed by Chen Sina.

1 http://rfmri.org/dpabi

TABLE 3 Group differences before and after treatment.

Characteristics	Acu-group (n = 25)		Con-group (n = 19)		P-value
	Rank	Percentage	Rank	Percentage	
MoCA	2.0 (2.0)	10.53%	1.0 (2.0)	6.55%	**0.015**
SDMT	4.0 (2.0)	8.15	2.0 (1.0)	2.23	**0.000**
VFT	3.0 (1.5)	15.56	2.0 (2.0)	9.72	**0.009**
DST	2.0 (1.0)	35.52	1.0 (2.0)	32.85	**0.005**
BNT	2.0 (2.0)	10.86	1.0 (2.0)	7.90	**0.015**

Values are presented as M(IQR); P-values for the Mann–Whitney U test. Percentage means "Pre- and post-treatment difference/Pre-treatment value". M, median; IQR, interquartile range.

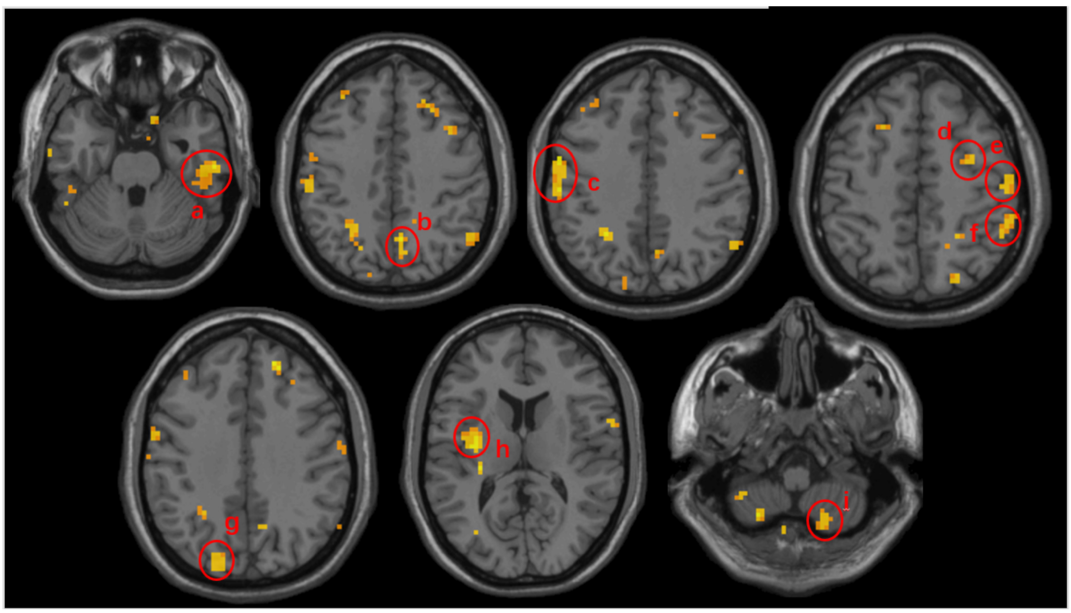

FIGURE 2
Volumetric results of the subtracted ALFF values mix effect analysis between the acupuncture and control groups. Subtracted ALFF values before and after the intervention was extracted separately from ACU and CON groups and mix effect analysis was performed to compute the difference for the treatment effect. Warmer colors represent higher ALFF changes in the acu-group compared to the con-group. Peak coordinates refer to the Montreal Neurological Institute (MNI) atlas. a, the right inferior temporal gyrus; b, the right precuneus; c, the left postcentral gyrus; d, the left precentral gyrus; e, the right postcentral gyrus; f, the right superior parietal gyrus; g, the left middle occipital gyrus; h, the left insula; i, the right cerebellum.

2.8. ALFF analysis

We first performed voxel-wise Fast Fourier Transform (FFT) for each participant to convert the filtered time series into the frequency domain to obtain the power spectrum. Since the power at a given frequency is proportional to the square of the magnitude of that frequency component, we calculated the square root of the power spectrum at each frequency and the average square root in the typical frequency band (0.01–0.08 Hz) at each voxel. This averaged square root was taken as ALFF (Zang et al., 2007), which was assumed to reflect the absolute intensity of spontaneous brain activity.

2.9. Statistical analysis

2.9.1. Demographic and cognitive assessment

A χ^2-test was used to test between-group differences in gender. A t-test was used to test between-group differences in age. The Mann–Whitney U test was used to evaluate the education level, smoking, and alcohol consumption history between groups. The statistical significance level was set at $p < 0.05$. Statistical analysis was conducted using SPSS (version 22.0). Continuous variables of MoCA without normal distributions were analyzed using the Mann-Whitney U test. VFT, SDMT, BNT, and DST with normal distribution were analyzed using an independent t-test.

2.9.2. ALFF and brain-cognitive correlation

The between-group differences test in ALFF was conducted using PALM and implemented in the DPARSF toolbox (see text footnote 1). In the calculations, a general linear model (GLM) was applied, and gender, education, and age factors were regressed. The significance level was set at $P < 0.005$. Permutation tests and multiple comparison corrections were applied to all statistics. Mixed effect analysis with a whole brain mask was utilized while examining group differences, which involved a comparison of the ALFF maps.

TABLE 4 Comparison of the difference between the before and after ALFF values of the two groups.

Conditions	Cluster size	Brain region	Peak *t*-values	MNI		
				X	*Y*	*Z*
Con>Acu	None cluster					
Acu>Con	86	Temporal_Inf_R	4.00158	57	−21	−27
	81	Occipital_Mid/Sup_L	4.14463	−33	−72	15
	65	Insula_L	4.08554	−33	−9	12
	48	Postcentral_L	3.94765	−57	0	39
	45	Parietal_Sup_R	3.78277	27	−51	54
	39	Cerebellum_R	3.35485	18	−63	−57
	34	Precuneus_R	3.83540	6	−60	42
	31	Precentral_R	3.88859	54	3	27
	31	Postcentral_R	3.53786	66	−12	27

The significance threshold was set at $P < 0.005$ with no correction. Con-group ($n = 19$), acu-group ($n = 25$). Coordinates of the peak voxel are shown in the Montreal Neurological Institute (MNI) space. The *t*-value corresponds to the peak voxel with a significant between-group difference in ALFF. Inf, inferior; Mid, middle; Sup, superior; L(R), left (right) hemisphere.

TABLE 5 Comparison of ALFF values before and after treatment in acu-group.

Group	Conditions	Cluster size	Brain region	Peak *t*-values	MNI		
					X	*Y*	*Z*
Acu-group	Post>Pre	2010	Frontal_Mid_R/L Frontal_Sup_R/L Frontal_Inf_R/L	6.3066	0	48	45
		231	Caudate_L/ Putamen_L	4.3959	−21	3	9

This result was achieved by comparing the ALFF maps before and after treatment. L, left; R, right; Mid, middle; Sup, superior; Inf, inferior.

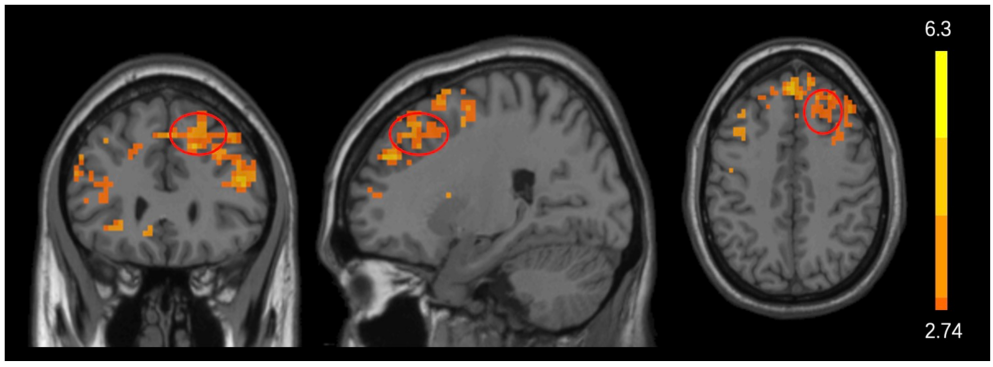

FIGURE 3
Acupuncture effects before and after treatment. Significant changes in ALFF values before and after acupuncture treatment in the acu-group. Significantly increased (marked in warmer colors) ALFF values were found in the frontal cortex after acupuncture treatment. The red circle represents the frontal lobe.

For each group, the ALFF maps were assessed using paired *t*-test. The significance level was set at a corrected two-tailed *P* value <0.05. Corrections for multiple testing were done using the threshold free cluster enhancement (TFCE) and family wise error (FWE) methods with the DPABI package.

Mean ALFF values of the obtained regions with significant group differences were extracted. Pearson's correlation analysis was performed to examine the association between ALFF values and MoCA changes. All statistical analyses were performed using SPSS and a statistical significance level of $P < 0.05$.

3. Results

3.1. Demographics and acupuncture effects on cognition

Table 1 shows the demographic characteristics of all participants in each group. There were no significant differences in demographic variables between the two groups ($P > 0.05$). After statistical analysis, the results also showed no statistically significant differences in MoCA, SDMT, VFT, DST, and BNT

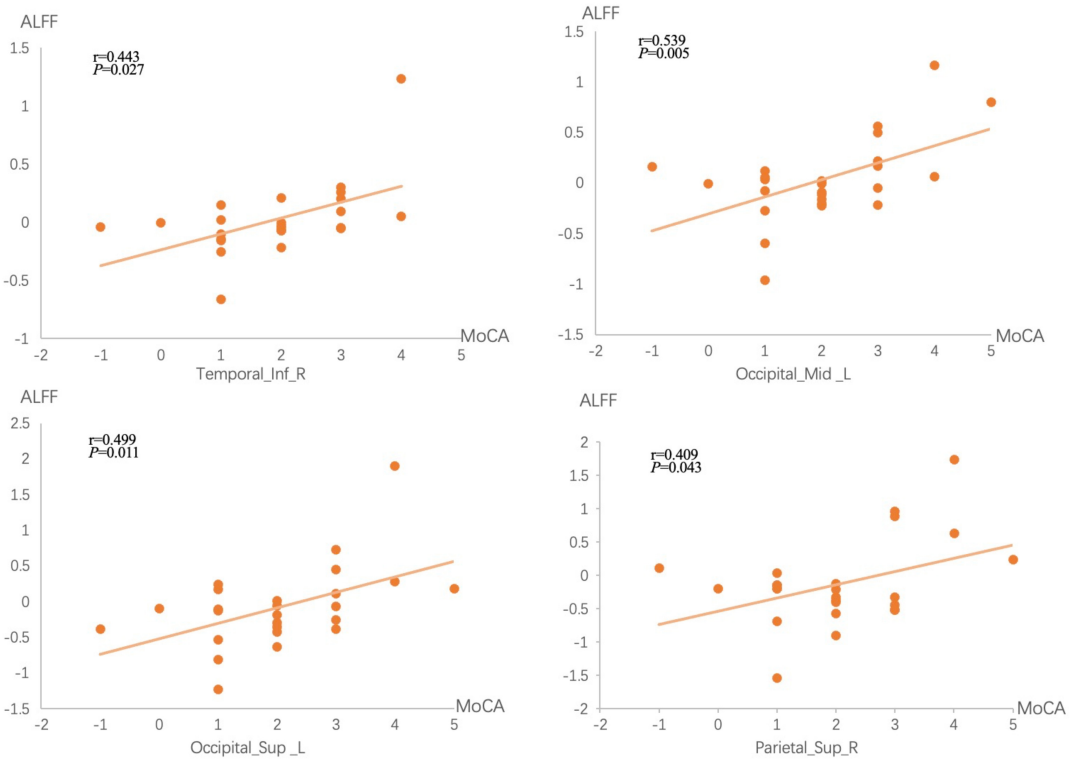

FIGURE 4
Correlations between brain measures and treatment performances. The *x*-axis represents the difference in MoCA scores before and after treatment, while the *y*-axis represents ALFF values differences before and after treatment.

scores between the two groups of subjects at the baseline level ($P > 0.05$). Further details are shown in Table 2. Compared with pre-intervention, the acupunture group showed better improved than the control group as measured by the MoCA, SDMT, VFT, DST, and BNT scores after intervention (Table 3).

3.2. Acupuncture effects on regional functional activity

3.2.1. Between-group analysis

Comparing the ALFF differences before and after the intervention in the two groups, we found several brain regions with significantly higher ALFF values in the treatment group compared to controls, including the right inferior temporal gyrus, the left middle occipital gyrus, the left superior occipital gyrus, the left insula, the bilateral postcentral gyrus, the right superior parietal gyrus, the right cerebellum, the right precuneus, and the right precentral gyrus ($P < 0.005$). Details are shown in Figure 2 and Table 4.

3.2.2. Longitudinal analysis

Paired *t*-test results (TFCE and FWE multiple comparisons corrected $P < 0.05$ and cluster size > 200 voxels) showed that, when compared with pre-treatment, acupuncture at Shenting and Baihui showed increased ALFF values in the bilateral middle/superior/inferior frontal gyrus and the left caudate and putamen (Table 5 and Figure 3). In the control group, we found no significant differences before or after treatment.

3.3. Association between the changes in ALFF and MoCA after acupuncture

Correlation analysis showed differences in ALFF values in the right inferior temporal gyrus, left middle occipital gyrus, left superior occipital gyrus, and right superior parietal gyrus in the acupuncture group were significantly positively correlated with change of MoCA ($P < 0.05$; Figure 4).

4. Discussion

We investigated cognitive function alterations (including MoCA, DST, VFT, SDMT, and BNT) in CSVDCI patients before and after acupuncture treatment, and performed neurology mechanisms voxel-based analysis of MRI-derived ALFF maps. According to our findings, and in contrast to conventional treatments, acupuncture at Shenting and Baihui significantly improved the cognitive function of patients. Importantly, we found an increase in spontaneous activity in regional brain areas, such as the right inferior temporal gyrus, left middle occipital gyrus, left superior occipital gyrus, and right superior parietal gyrus.

By comparing ALFF changes with those observed in the control group, we found that acupuncture combined with conventional treatment increased ALFF values of the right inferior temporal gyrus, left middle occipital gyrus, left superior occipital gyrus, left insula, bilateral postcentral gyrus, right superior parietal gyrus, right cerebellum, right precuneus, and right precentral gyrus in

CSVDCI patients. This suggests that acupuncture at Shenting and Baihui may improve cognitive function by enhancing neuronal excitability in some brain regions of CSVDCI patients.

The inferior temporal gyrus is located in the temporal lobe. The structures in the medial temporal lobe, including the hippocampus, the internal olfactory and perirhinal cortex, and parietal hippocampal cortex, are important elements of long-term memory processing (Lech and Suchan, 2013). Wu et al. (2017) found that the combination of acupuncture and conventional treatment significantly improves motor and cognitive functions in stroke patients, and increased Reho values in the middle temporal gyrus. According to the authors, acupuncture may have a specific mechanism of action. PET technology showed that acupuncture points, such as Baihui, significantly increased glucose metabolism in the temporal and frontal lobes, improving cognitive function (Huang et al., 2007). Combined with our findings, the evidence supports that acupuncture of Shenting and Baihui significantly improve temporal lobe glucose metabolism levels, enhance energy supply, and increase local neuronal activity in CSVDCI patients, thus improving temporal lobe related cognitive functions.

Both the middle and superior occipital gyrus are part of the occipital lobe, an essential component of the visual center that transmits spatial information to the parietal lobe, which conveys the integrated spatial information to the prefrontal lobe, eventually forming spatial memory in the prefrontal area (Andersson et al., 2019). Previous studies found that the size of the white matter lesion volume in the occipital lobe in MCI patients is negatively correlated with cerebral blood flow, suggesting that decreased cerebral blood flow in the occipital lobe may lead to lesions in occipital lobe structures and to a decrease in cognitive function (Kim et al., 2020). According brain neuroimaging studies meta-analysis (Cao et al., 2020), the occipital lobe plays a role in the pathophysiology of dementia, suggesting it should be a target region for scalp acupuncture for treating dementia. Acupuncture of Shenting and Baihui improved executive function and visuospatial localization in CSVDCI patients, and their improvement was also correlated with improved spontaneous activity in the occipital lobe region.

The parietal cortex is an interesting part of the association cortex. Throughout modern neuroscience research, this region has been associated with a wide range of sensory, motor, and cognitive functions (Freedman and Ibos, 2018). Functional magnetic resonance imaging has been widely used to study the effects of acupuncture on neural activity. A study on functional MRI in MCI patients suggested that acupuncture increases functional connectivity between the parietal lobe and other cognitively relevant areas (Tan et al., 2017). Conversely, acupuncture increased Reho values of the parietal lobe in MCI patients. Hence, it is possible that that acupuncture also improves the regional homogeneity of different delicate structures in the parietal gyrus and increases spontaneous brain activity (Liu et al., 2014). Zhang J. et al. (2021) found that acupuncture reorganizes cognition-related brain areas, including the inferior frontal gyrus, and the temporal, parietal, and occipital lobes, and modulates post-stroke function and structural plasticity.

Acupuncture is widely used to cure post-stroke hemiplegia, cognitive dysfunction, anxiety, depression, among others (Wang et al., 2018; Du et al., 2020; Zhang et al., 2021). Li A. et al. (2018) explored the activating effects of acupuncture on the brain of healthy individuals using fMRI techniques and found it activates the postcentral gyrus, the precuneus, and the temporal and occipital lobes. Our results further validate these findings and reinforce the fact that acupuncture positively impacts spontaneous activity in various brain regions of CSDVDCI patients. Specifically, significant brain responses were observed after acupuncture stimulation at Shenting and Baihui, as well as improved ALFF values of the right inferior temporal gyrus, left middle occipital gyrus, superior occipital gyrus, and right superior parietal gyrus, which were positively correlated with an improvement in cognitive function.

5. Limitations

(1) The sample size was limited because this was a single-center study and screening for contraindications to MRI scanning was inadequate, resulting in some patients being unable to participate in the examination due to e.g., the presence of dentures, excessive head movement, and other factors. (2) In addition to cognitive dysfunction, CSVDCI patients also present with limb dysfunction, such as movement delays and mild hemiparesis, but our study did not evaluate such patients.

6. Conclusion

Acupuncture of Shenting and Baihui effectively improves cognitive brain function in CSVDCI patients. This may be related to an increase in spontaneous activity in local brain regions and changes in ALFF values at the right inferior temporal gyrus, left middle occipital gyrus, left inferior occipital gyrus, and left superior parietal gyrus.

Data availability statement

The raw data supporting the conclusions of this article will be made available by the authors, without undue reservation.

Ethics statement

The studies involving human participants were reviewed and approved by the Institutional Review Board of Zhongshan TCM hospital (ClinicalTrials.gov identifier: 2017ZSZY-LLK-219). The patients/participants provided their written informed consent to participate in this study. Written informed consent was obtained from the individual(s) for the publication of any potentially identifiable images or data included in this article.

Author contributions

NY and LC designed the study. NY, SC, LC, SXL, and SQL collected the data. NY and SC analyzed the data and prepared the

manuscript. All authors contributed to the article and approved the submitted version.

Funding

This work was supported by a grant from Zhongshan Municipal Bureau of Science and Technology (2019B1005).

Acknowledgments

We thank Xiaohuang Huang for her assistance in assessing cognitive function.

Conflict of interest

The authors declare that the research was conducted in the absence of any commercial or financial relationships that could be construed as a potential conflict of interest.

Publisher's note

All claims expressed in this article are solely those of the authors and do not necessarily represent those of their affiliated organizations, or those of the publisher, the editors and the reviewers. Any product that may be evaluated in this article, or claim that may be made by its manufacturer, is not guaranteed or endorsed by the publisher.

References

Andersson, P., Ragni, F., and Lingnau, A. (2019). Visual imagery during real-time fMRI neurofeedback from occipital and superior parietal cortex. *Neuroimage* 200, 332–343. doi: 10.1016/j.neuroimage.2019.06.057

Arvanitakis, Z., Shah, R. C., and Bennett, D. A. (2019). Diagnosis and management of dementia: Review. *JAMA* 322, 1589–1599.

Bath, P. M., and Wardlaw, J. M. (2015). Pharmacological treatment and prevention of cerebral small vessel disease: A review of potential interventions. *Int. J. Stroke* 10, 469–478. doi: 10.1001/jama.2019.4782

Brookes, R. L., Herbert, V., Paul, S., Hannesdottir, K., Markus, H. S., and Morris, R. G. (2014). Executive dysfunction, awareness deficits and quality of life in patients with cerebral small vessel disease: A structural equation model. *Neuropsychology* 28, 247–253. doi: 10.1037/neu0000015

Cai, R. L., Shen, G. M., Wang, H., and Guan, Y. Y. (2018). Brain functional connectivity network studies of acupuncture: A systematic review on resting-state fMRI. *J. Integr. Med.* 16, 26–33. doi: 10.1016/j.joim.2017.12.002

Cao, J., Huang, Y., Meshberg, N., Hodges, S. A., and Kong, J. (2020). Neuroimaging-based scalp acupuncture locations for dementia. *J. Clin. Med.* 9:2477. doi: 10.3390/jcm9082477

Cao, Y., Wang, L., Lin, L. T., Wang, X. R., Ma, S. M., Yang, N. N., et al. (2021). Acupuncture attenuates cognitive deficits through α7nAChR mediated anti-inflammatory pathway in chronic cerebral hypoperfusion rats. *Life Sci.* 266:118732. doi: 10.1016/j.lfs.2020.118732

Chen, X., Wang, J., Shan, Y., Cai, W., Liu, S., Hu, M., et al. (2019). Cerebral small vessel disease: Neuroimaging markers and clinical implication. *J. Neurol.* 266, 2347–2362.

Dhond, R. P., Kettner, N., and Napadow, V. (2007). Neuroimaging acupuncture effects in the human brain. *J. Altern. Complement. Med.* 13, 603–616.

Du, S. Q., Wang, X. R., Zhu, W., Ye, Y., Yang, J. W., Ma, S. M., et al. (2018). Acupuncture inhibits TXNIP-associated oxidative stress and inflammation to attenuate cognitive impairment in vascular dementia rats. *CNS Neurosci. Ther.* 24, 39–46. doi: 10.1111/cns.12773

Du, Y., Zhang, L., Liu, W., Rao, C., Li, B., Nan, X., et al. (2020). Effect of acupuncture treatment on post-stroke cognitive impairment: A randomized controlled trial. *Medicine* 99:e23803.

Durant, J., Berg, J. L., Banks, S. J., Kaylegian, J., and Miller, J. B. (2021). Comparing the boston naming test with the neuropsychological assessment battery-naming subtest in a neurodegenerative disease clinic population. *Assessment* 28, 1256–1266. doi: 10.1177/1073191119872253

Feng, M., Wen, H., Xin, H., Zhang, N., Liang, C., and Guo, L. (2021). Altered spontaneous brain activity related to neurologic dysfunction in patients with cerebral small vessel disease. *Front. Aging Neurosci.* 13:731585. doi: 10.3389/fnagi.2021.731585

Freedman, D. J., and Ibos, G. (2018). An integrative framework for sensory, motor, and cognitive functions of the posterior parietal cortex. *Neuron* 97, 1219–1234.

Huang, J., McCaskey, M. A., Yang, S., Ye, H., Tao, J., Jiang, C., et al. (2015). Effects of acupuncture and computer-assisted cognitive training for post-stroke attention deficits: Study protocol for a randomized controlled trial. *Trials* 16:546. doi: 10.1186/s13063-015-1054-x

Huang, L., Yin, X., Li, W., Cao, Y., Chen, Y., Lao, L., et al. (2021). Effects of acupuncture on vascular cognitive impairment with no dementia: A randomized controlled trial. *J. Alzheimers Dis.* 81, 1391–1401.

Huang, Y., Chen, J., Htut, W. M., Lai, X., and Wik, G. (2007). Acupuncture increases cerebral glucose metabolism in human vascular dementia. *Int. J. Neurosci.* 117, 1029–1037. doi: 10.1080/00207450600936825

Ji, S., Duan, J., Hou, X., Zhou, L., Qin, W., Niu, H., et al. (2021). The role of acupuncture improving cognitive deficits due to alzheimer's disease or vascular diseases through regulating neuroplasticity. *Neural Plast.* 2021:8868447.

Kim, C. M., Alvarado, R. L., Stephens, K., Wey, H. Y., Wang, D. J. J., Leritz, E. C., et al. (2020). Associations between cerebral blood flow and structural and functional brain imaging measures in individuals with neuropsychologically defined mild cognitive impairment. *Neurobiol. Aging* 86, 64–74. doi: 10.1016/j.neurobiolaging.2019.10.023

Kim, H., Kim, H. K., Kim, S. Y., Kim, Y. I., Yoo, H. R., and Jung, I. C. (2019). Cognitive improvement effects of electro-acupuncture for the treatment of MCI compared with Western medications: A systematic review and meta-analysis. *BMC Complement. Altern. Med.* 19:13. doi: 10.1186/s12906-018-2407-2

Lai, Z., Zhang, Q., Liang, L., Wei, Y., Duan, G., Mai, W., et al. (2022). Efficacy and mechanism of moxibustion treatment on mild cognitive impairment patients: An fMRI study using ALFF. *Front. Mol. Neurosci.* 15:852882. doi: 10.3389/fnmol.2022.852882

Lech, R. K., and Suchan, B. (2013). The medial temporal lobe: Memory and beyond. *Behav. Brain Res.* 254, 45–49. doi: 10.1016/j.bbr.2013.06.009

Leung, J. L., Lee, G. T., Lam, Y. H., Chan, R. C., and Wu, J. Y. (2011). The use of the Digit Span Test in screening for cognitive impairment in acute medical inpatients. *Int. Psychogeriatr.* 23, 1569–1574. doi: 10.1017/S1041610211000792

Li, A., Wang, Y. H., Zhang, F., Wang, F., Zeng, X. X., Yue, J. H., et al. (2018). Acupuncture for gender differences and similarities in cerebral activity of health volunteers: A pilot fMRI study. *Medicine* 97:e13655. doi: 10.1097/MD.0000000000013655

Li, C., Yang, J., Yin, X., Liu, C., Zhang, L., Zhang, X., et al. (2015). Abnormal intrinsic brain activity patterns in leukoaraiosis with and without cognitive impairment. *Behav. Brain Res.* 292, 409–413. doi: 10.1016/j.bbr.2015.06.033

Li, T., Huang, Y., Cai, W., Chen, X., Men, X., Lu, T., et al. (2020). Age-related cerebral small vessel disease and inflammaging. *Cell Death Dis.* 11:932.

Li, Y., Li, M., Feng, Y., Ma, X., Tan, X., Chen, Y., et al. (2021). Aberrant brain spontaneous activity and synchronization in type 2 diabetes mellitus subjects without mild cognitive impairment. *Front. Neurosci.* 15:749730. doi: 10.3389/fnins.2021.749730

Li, Z., Chen, J., Cheng, J., Huang, S., Hu, Y., Wu, Y., et al. (2018). Acupuncture modulates the cerebello-thalamo-cortical circuit and cognitive brain regions in

patients of Parkinson's disease with tremor. *Front. Aging Neurosci.* 10:206. doi: 10.3389/fnagi.2018.00206

Liu, Z., Wei, W., Bai, L., Dai, R., You, Y., Chen, S., et al. (2014). Exploring the patterns of acupuncture on mild cognitive impairment patients using regional homogeneity. *PLoS One* 9:e99335. doi: 10.1371/journal.pone.0099335

NIH Consensus Conference (1998). Acupuncture. *JAMA* 280, 1518–1524.

O'Driscoll, C., and Shaikh, M. (2017). Cross-cultural applicability of the montreal cognitive assessment (MoCA): A systematic review. *J. Alzheimers Dis.* 58, 789–801. doi: 10.3233/JAD-161042

Pantoni, L. (2010). Cerebral small vessel disease: From pathogenesis and clinical characteristics to therapeutic challenges. *Lancet Neurol.* 9, 689–701.

Park, H. J., and Friston, K. (2013). Structural and functional brain networks: From connections to cognition. *Science* 342:1238411.

Rao, R., Tah, V., Casas, J. P., Hingorani, A., Whittaker, J., Smeeth, L., et al. (2009). Ischaemic stroke subtypes and their genetic basis: A comprehensive meta-analysis of small and large vessel stroke. *Eur. Neurol.* 61, 76–86. doi: 10.1159/000177939

Silva, P. H. R., Spedo, C. T., Barreira, A. A., and Leoni, R. F. (2018). Symbol digit modalities test adaptation for magnetic resonance imaging environment: A systematic review and meta-analysis. *Mult. Scler. Relat. Disord.* 20, 136–143. doi: 10.1016/j.msard.2018.01.014

Sutin, A. R., Stephan, Y., and Terracciano, A. (2019). Verbal fluency and risk of dementia. *Int. J. Geriatr. Psychiatry* 34, 863–867.

Tan, T. T., Wang, D., Huang, J. K., Zhou, X. M., Yuan, X., Liang, J. P., et al. (2017). Modulatory effects of acupuncture on brain networks in mild cognitive impairment patients. *Neural. Regen. Res.* 12, 250–258.

Wang, L., Feng, Q., Wang, M., Zhu, T., Yu, E., Niu, J., et al. (2021). An effective brain imaging biomarker for AD and aMCI: ALFF in slow-5 frequency band. *Curr. Alzheimer Res.*. 18, 45–55. doi: 10.2174/1567205018666210324130502

Wang, L., Yang, J. W., Lin, L. T., Huang, J., Wang, X. R., Su, X. T., et al. (2020). Acupuncture attenuates inflammation in microglia of vascular dementia rats by inhibiting miR-93-mediated TLR4/MyD88/NF-κB signaling pathway. *Oxid. Med. Cell Longev.* 2020:8253904. doi: 10.1155/2020/8253904

Wang, S., Yang, H., Zhang, J., Zhang, B., Liu, T., Gan, L., et al. (2016). Efficacy and safety assessment of acupuncture and nimodipine to treat mild cognitive impairment after cerebral infarction: A randomized controlled trial. *BMC Complement. Altern. Med.* 16:361. doi: 10.1186/s12906-016-1337-0

Wang, X., Zhang, Q., Cui, B., Huang, L., Wang, D., Ye, L., et al. (2018). Scalp-cluster acupuncture with electrical stimulation can improve motor and living ability in convalescent patients with post-stroke hemiplegia. *J. Tradit. Chin. Med.* 38, 452–456.

Wardlaw, J. M., Smith, E. E., Biessels, G. J., Cordonnier, C., Fazekas, F., Frayne, R., et al. (2013). Neuroimaging standards for research into small vessel disease and its contribution to ageing and neurodegeneration. *Lancet Neurol.* 12, 822–838.

Wu, P., Zeng, F., Yin, C., Xiong, Y., Bai, Y., Wang, D., et al. (2017). Effect of acupuncture plus conventional treatment on brain activity in ischemic stroke patients: A regional homogeneity analysis. *J. Tradit. Chin. Med.* 37, 650–658.

Yang, B. F., Zeng, X. H., Liu, Y., Fu, Q. N., He, T., Li, F., et al. (2014). Effect of acupuncture treatment on vascular cognitive impairment without dementia: Study protocol for a randomized controlled trial. *Trials* 15:442. doi: 10.1186/1745-6215-15-442

Yang, J. W., Shi, G. X., Zhang, S., Tu, J. F., Wang, L. Q., Yan, C. Q., et al. (2019). Effectiveness of acupuncture for vascular cognitive impairment no dementia: A randomized controlled trial. *Clin. Rehabil.* 33, 642–652.

Yang, S., Ye, H., Huang, J., Tao, J., Jiang, C., Lin, Z., et al. (2014). The synergistic effect of acupuncture and computer-based cognitive training on post-stroke cognitive dysfunction: A study protocol for a randomized controlled trial of 2 × 2 factorial design. *BMC Complement. Altern. Med.* 14:290. doi: 10.1186/1472-6882-14-290

Zang, Y. F., He, Y., Zhu, C. Z., Cao, Q. J., Sui, M. Q., Liang, M., et al. (2007). Altered baseline brain activity in children with ADHD revealed by resting-state functional MRI. *Brain Dev.* 29, 83–91.

Zhang, J., Lu, C., Wu, X., Nie, D., and Yu, H. (2021). Neuroplasticity of acupuncture for stroke: An evidence-based review of MRI. *Neural Plast.* 2021:2662585. doi: 10.1155/2021/2662585

Zhang, S. H., Wang, Y. L., Zhang, C. X., Zhang, C. P., Xiao, P., Li, Q. F., et al. (2021). Effect of interactive dynamic scalp acupuncture on post-stroke cognitive function, depression, and anxiety: A multicenter, randomized, controlled trial. *Chin. J. Integr. Med.* 28, 106–115. doi: 10.1007/s11655-021-3338-1

Zhang, X., Xue, C., Cao, X., Yuan, Q., Qi, W., Xu, W., et al. (2021). Altered patterns of amplitude of low-frequency fluctuations and fractional amplitude of low-frequency fluctuations between amnestic and vascular mild cognitive impairment: An ALE-based comparative meta-analysis. *Front. Aging Neurosci.* 13:711023. doi: 10.3389/fnagi.2021.711023

frontiers | Frontiers in Neuroscience

TYPE Original Research
PUBLISHED 01 March 2023
DOI 10.3389/fnins.2023.1131862

OPEN ACCESS

EDITED BY
Feng Zhang,
Third Hospital of Hebei Medical University, China

REVIEWED BY
Yiji Su,
The First Affiliated Hospital of Guangxi Medical University, China
Liying Zhang,
Third Affiliated Hospital of Sun Yat-sen University, China

*CORRESPONDENCE
Hongxiang Zhu
✉ 13632414410@163.com
Yue Lan
✉ bluemooning@163.com

SPECIALTY SECTION
This article was submitted to Translational Neuroscience, a section of the journal Frontiers in Neuroscience

RECEIVED 26 December 2022
ACCEPTED 14 February 2023
PUBLISHED 01 March 2023

CITATION
Ding Q, Lin T, Cai G, Ou Z, Yao S, Zhu H and Lan Y (2023) Individual differences in beta-band oscillations predict motor-inhibitory control. *Front. Neurosci.* 17:1131862. doi: 10.3389/fnins.2023.1131862

Individual differences in beta-band oscillations predict motor-inhibitory control

Qian Ding[1,2,3], Tuo Lin[1], Guiyuan Cai[1], Zitong Ou[2], Shantong Yao[2], Hongxiang Zhu[2]* and Yue Lan[1,3]*

[1]Department of Rehabilitation Medicine, Guangzhou First People's Hospital, South China University of Technology, Guangzhou, Guangdong, China, [2]Department of Rehabilitation Medicine, Guangdong Provincial People's Hospital (Guangdong Academy of Medical Sciences), Southern Medical University, Guangzhou, Guangdong, China, [3]Guangzhou Key Laboratory of Aging Frailty and Neurorehabilitation, Guangzhou, Guangdong, China

Objective: The ability of motor-inhibitory control is critical in daily life. The physiological mechanisms underlying motor inhibitory control deficits remain to be elucidated. Beta band oscillations have been suggested to be related to motor performance, but whether they relate to motor-inhibitory control remains unclear. This study is aimed at systematically investigating the relationship between beta band oscillations and motor-inhibitory control to determine whether beta band oscillations were related to the ability of motor-inhibitory control.

Methods: We studied 30 healthy young adults (age: 21.6 ± 1.5 years). Stop-signal reaction time (SSRT) was derived from stop signal task, indicating the ability of motor-inhibitory control. Resting-state electroencephalography (EEG) was recorded for 12 min. Beta band power and functional connectivity (including global efficiency) were calculated. Correlations between beta band oscillations and SSRT were performed.

Results: Beta band EEG power in left and right motor cortex (MC), right somatosensory cortex (SC), and right inferior frontal cortex (IFC) was positively correlated with SSRT (P's = 0.031, 0.021, 0.045, and 0.015, respectively). Beta band coherence between bilateral MC, SC, and IFC was also positively correlated with SSRT (P's < 0.05). Beta band global efficiency was positively correlated with SSRT ($P = 0.01$).

Conclusion: This is the first study to investigate the relationship between resting-state cortical beta oscillations and response inhibition. Our findings revealed that individuals with better ability of motor inhibitory control tend to have less cortical beta band power and functional connectivity. This study has clinical significance on the underlying mechanisms of motor inhibitory control deficits.

KEYWORDS

EEG, motor inhibitory control, beta-band oscillations, functional connectivity, global efficiency

1. Introduction

Motor-inhibitory control refers to the ability that inhibits inappropriate motor responses and expresses more appropriate responses, which is considered as an important ability in daily life (Chowdhury et al., 2017). The ability of motor-inhibitory control can be measured by stop signal task (SST) (Aron, 2011; Bari and Robbins, 2013; Schall et al., 2017), in which participants are instructed to inhibit an already initiated action. Stop-signal reaction time (SSRT) can be estimated based on the latency to inhibit a prepotent response (i.e., stopping efficiency). Prolonged SSRT suggests poor ability of motor-inhibitory control (Chowdhury et al., 2017). It has been reported that SSRT tend to be prolonged in conditions such as Parkinson's disease (PD) (Jenkinson and Brown, 2011), attention deficit/hyperactivity disorder (Lijffijt et al., 2005) and schizophrenia (Badcock et al., 2002). The physiological mechanisms underlying the motor inhibitory control deficits remain less clear (Bari and Robbins, 2013).

As a common neuroimaging approach, electroencephalography (EEG) has been widely applied in the field of neurophysiological research. Ongoing spontaneous EEG oscillations are usually categorized into five frequency bands, including delta, theta, alpha, beta, and gamma bands. In particular, rhythmic activity in the beta band (i.e., 15–30 Hz) is classically considered as being related to sensorimotor functions (Pfurtscheller et al., 1996), but the functional role of beta-band activity has not been fully elucidated. Beta-band activity (i.e., EEG power) has been suggested as a signature of an active process that promotes the existing motor set whilst compromising neuronal processing of new movements (specifically related to maintain the status quo). Excessive beta-band activity has been associated with worse motor performance (Gilbertson et al., 2005; Androulidakis et al., 2006, 2007). Although some studies have reported positive correlations between beta band activity and impulsivity (Threadgill and Gable, 2018; Wendel et al., 2021), whether beta-band activity is related to the ability of motor inhibitory control remains unclear. Based on the theoretical link between motor inhibitory control and impulsivity, we speculate that beta band activity is less in individuals with worse ability of motor inhibitory control.

Functional connectivity stands for the synchrony of cortical activity in anatomically distinct but functionally collaborating brain regions (Vecchio et al., 2019). Unlike EEG power reflecting oscillatory synchronization within local cortical neuronal populations, functional connectivity represents neuronal synchronization between distributed cortical regions (Silberstein et al., 2005). Graph theory analysis is an approach that characterizes functional brain network based on functional connectivity (Park et al., 2014). Global efficiency refers to the average of interregional efficiency between each pair of brain region over the whole brain. As one of the most common metrics in graph theory analysis, global efficiency represents the efficiency in transporting information at a global scale (Park et al., 2014). Some studies investigated the relationship between beta band functional connectivity and motor performance, reporting that individuals with greater beta band functional connectivity tend to have worse motor performance (Gilbertson et al., 2005; Silberstein et al., 2005). However, whether there is a relationship between beta band functional connectivity and motor inhibitory control remains unclear. Investigating the relationship between beta band functional connectivity and global efficiency would provide valuable information on understanding the neural mechanisms of motor inhibitory control deficits.

In present study, we investigated the relationship between beta-band oscillations and motor inhibitory control (i.e., SSRT). We anticipated that beta band power, functional connectivity, and global efficiency would be positively correlated with SSRT. Our findings will have implications on understanding physiological mechanisms of motor inhibitory control deficits and possibly inform the development of new treatment for inhibitory control deficits.

Abbreviations: SST, stop signal task; SSRT, stop-signal reaction time; PD, Parkinson's disease; EEG, electroencephalography; IFC, inferior frontal cortex; MC, motor cortex; SC, somatosensory cortex; AUC, area under the curve; SD, standard deviation.

2. Materials and methods

2.1. Participants

A total of 30 healthy adults [8 males; mean age: 21.6 (SD = 1.5) years] participated in this study. Written informed consent was obtained prior to enrollment. All procedures were approved by the Guangzhou First People's Hospital Human Research Ethics Committee.

2.2. Stop signal task

Stop signal task was used to assess the ability of motor-inhibitory control (Verbruggen and Logan, 2008). A 13.5-inch Dell laptop running E-Prime v.3.0 (Psychological Software Tools Inc., Pittsburgh, PA, USA) was used to present stimuli and record keypresses. At the beginning, participants were asked to read instructions on the computer screen. On "Go" trials, a black arrow was presented on the screen, and participants were instructed to press the left-arrow key for a leftward pointing arrow with the left index finger, and to press the right-arrow key for a rightward pointing arrow with the right index finger. On "Nogo" trials, a red arrow was presented on the screen, and participants were instructed not to press any key. On "Stop" trials, a "Stop" signal (red arrow) would occur after the "Go" signal (i.e., the black arrow turned red after a delay). Participants were asked to stop their initial response when the "Stop" signal occurred. Participants were instructed to respond as quickly and accurately as possible to black arrows, and not to delay their response to wait in case the "Stop" signal occurred (Ding et al., 2021a).

On each trial, a fixation cross was presented for 300 ms, followed by the "Go" or "Nogo" signal. The maximum response time was set at 1,000 ms, and the intertrial interval was set at 500 ms. On "Stop" trials, the "Stop" signal was presented after the onset of the "Go" signal. At the beginning of the session, the "Stop" signal occurred 250 ms after the "Go" signal. In the trials where response inhibition was successful, the stop signal delay (SSD) was increased by 50 ms on the next "Stop" trial. In the trials where inhibition failed, SSD was decreased by 50 ms on the next "Stop" trial. This

ensured an overall successful rate of inhibition [i.e., *P* (respond| signal)] close to 50%. The experiment included 24 practice trials and 400 experimental trials, consisting of 70% "Go" trials, 10% "Nogo" trials, and 20% "Stop" trials, administered in a completely random sequence. The details of SST were described in a previous paper (Ding et al., 2021a).

The SSRT was estimated using the integration method with Go omission replacement (Verbruggen et al., 2019; Ding et al., 2021a), which has been suggested to be more accurate and have higher test-retest reliability than other methods (especially the mean method) for SSRT calculation (Ding et al., 2021a). With the integration method, SSRT was calculated by the mean SSD subtracted from the nth Go reaction time. Here, n stands for a point on the Go reaction time distribution where the integral of the reaction time curve is equivalent to *P* (respond| signal). Go omissions refers to Go trials on which the participants did not respond before the response deadline. In the cases of Go omissions, the SSRT was assigned with the maximum reaction time (RT) (1,000 ms) to compensate for the lack of responses (Verbruggen et al., 2019).

2.3. Electroencephalography (EEG)

2.3.1. EEG acquisition

Electroencephalography acquisition was performed after the completion of SST. The participants were seated comfortably in a sound-shielded, dimly lit room for resting-state EEG recording, which lasted 13 min: 6 min with eyes closed, followed by 1 min with eyes open, and 6 min with eyes closed. Scalp EEG signals were recorded using a 128-channel HydroCel Geodesic Sensor Net (Electrical Geodesics, Inc., Eugene, OR, USA) in a geodesic pattern over the surface of the head with a vertex reference. It included 19 contacts at the equivalent 10–20 system locations. The EEG data were digitized and amplified at a 2,000 Hz sampling rate with a Geodesic EEG system 400 (Electrical Geodesics, Inc., Eugene, OR, USA). An online bandpass filter (0.1–100 Hz) was applied and the impedance for the whole net was kept below 10 kΩ throughout data collection (Cai et al., 2021). The 12 min EEG recording with eyes closed was exported after data collection for further analysis.

2.3.2. EEG analysis

Acquired EEG signal were analyzed off-line using MATLAB2019b (Mathworks, Inc., Natick, USA). EEGLAB toolbox (version 14.1.2b) was used for EEG data preprocessing (Delorme and Makeig, 2004). After the EEG data were imported in EEGLAB, the signal was sampled down to 1,000 Hz. Afterward, the EEG data were filtered with a band-pass filter with cut-off values ranging from 0.1 to 40 Hz and segmented in epochs lasting 1,000 ms. The independent component analysis was subsequently performed to exclude components endowing eye (blink and movement), cardiac, and muscular artifacts. The resulting data were further visually inspected to exclude remaining "bad trials" (i.e., amplitudes > 80 μV) and re-referenced using the average signal of every scalp electrode as reference (Cai et al., 2021).

Power and functional connectivity analyses were conducted using customed MATLAB scripts. Absolute power was calculated by fast Fourier transform and averaged in 13–30 Hz for beta band. As we were interested in assessing cortical activities in brain areas including inferior frontal cortex (IFC), motor cortex (MC), and somatosensory cortex (SC), six clusters of electrodes (three clusters for each hemisphere) were selected according to 10–20 system nomenclature (Ding et al., 2022). The averaged power of all electrodes in each cluster was calculated for statistical analysis.

Coherence was calculated using customed MATLAB scripts to reflect functional connectivity between different cortical regions. The Welch's averaged, modified periodogram method (Welch, 1967), was performed to calculate the squared coherence between each pair of electrodes in four frequency bands. All connectivity matrices were Fisher's z-transformed (Arun et al., 2020) to the set of Gaussian distributed values and the z-scores were used for further analysis. The averaged z-scores of each pair of electrodes between brain regions of interest were calculated for statistical analysis (Ding et al., 2021b).

GRaph thEoretical Network Analysis (GRETNA) toolbox was used for graph theory analysis (Wang et al., 2015). A graph is based on a set of nodes, and the connections between nodes are edges. Nodes and edges together form the brain network. In the current study, weighted and undirected networks were built based on coherence (Vecchio et al., 2019). As there was no definite method for selecting a single threshold, we integrated the metrics over the entire threshold range (i.e., 0.1–0.4, with an interval of 0.05) to obtain the area under the curve (AUC) to characterize the brain network (Wang et al., 2015; Yan et al., 2017; Ding et al., 2021b). Global efficiency characterizes information transferring ability in the entire brain network (G) (Park et al., 2014). Global efficiency was computed as the average of nodal efficiency across all nodes in the brain network:

$$E_{global}(G) = \frac{1}{N(N-1)} \sum_{j \neq i \in G} \frac{1}{D(i,j)} \quad (1)$$

where *D(i, j)* is the shortest path length between node *i* and node *j*, and *N* is the number of nodes in the network.

2.4. Statistical analysis

Statistical analysis was performed in Graphpad Prism (version 8.3.0). Data were found to meet the normality assumption using the Kolmogorov–Smirnov test. Pearson correlations were performed to investigate the relationship between physiological data and behavioral data (i.e., SST measures). False discovery rate corrections were applied for multiple correlations. All *P*-values presented in

TABLE 1 Behavioral data of SST measures.

Go accuracy (%)	Nogo accuracy (%)	*P* (Go omissions) (%)	Go RT (ms)	RT unsuccessful stop (ms)	*P* (respond| signal) (%)	SSD (ms)	SSRT (ms)
96.88 (3.96)	95.00 (7.30)	1.51 (3.21)	458.92 (97.55)	411.91 (94.34)	46.25 (6.50)	203.81 (126.60)	240.14 (28.76)

Data are presented as mean (standard deviation). SST, stop signal task; RT, reaction time; SSD, stop signal delay; SSRT, stop signal reaction time.

current study are those after the false discovery rate correction. For all analyses, the statistical significance was set at $P < 0.05$.

3. Results

3.1. Behavioral data

Behavioral data of SST measures are summarized in **Table 1**.

3.2. Physiological data

3.2.1. Power analysis

Figure 1A shows the beta band power spectrum. Our data revealed significant positive correlations between SSRT and cortical beta power in left and right MC, right SC, and right IFC (r's = 0.49, 0.52, 0.45, and 0.55, P's = 0.031, 0.021, 0.045, and 0.015, respectively) (**Figures 1B–E**), indicating individuals with poor ability of response inhibition tended to have greater EEG power in those brain regions. There was no significant correlation between other SST measures and cortical beta power in any brain region (P's > 0.05).

3.2.2. Coherence

Figure 2A shows the matrix for beta band coherence between pairs of electrodes in bilateral MC, SC, and IFC. Our data revealed significant correlations between SSRT and coherence of each pair of brain regions (P's < 0.05) (**Figures 2B**, **3**). There was no significant correlation between other SST measures and beta coherence (P's > 0.05).

3.2.3. Graph theory analysis

Our data revealed significant positive correlation between beta band global efficiency and SSRT ($r = 0.59$, $P = 0.01$) (**Figure 4**). There was no significant correlation between other SST measures and beta band global efficiency (P's > 0.05).

4. Discussion

This study investigated the relationship between resting state cortical beta activity and response inhibition. Our primary findings are (1) beta band EEG power in bilateral sensorimotor cortices and right inferior prefrontal cortex was positively correlated with SSRT; (2) beta band coherence between bilateral sensorimotor and inferior prefrontal cortices was positively correlated with SSRT; (3) beta band global efficiency was positively correlated with SSRT.

4.1. Beta band activity

Beta band power in bilateral sensorimotor cortices and right IFC was positively correlated with SSRT, suggesting that individuals with better ability of response inhibition tend to have less resting beta power. To our knowledge, no previous study has investigated the relationship between resting beta power and response inhibition. Prolonged SSRT has been observed in many psychiatric conditions with impaired urge control (i.e., impulsivity), such as attention deficit/hyperactivity disorder (Lijffijt et al., 2005) and schizophrenia (Badcock et al., 2002), suggesting a theoretical link between motor-inhibitory control deficits and impulsivity (Bari and Robbins, 2013; Skippen et al., 2019). Some studies investigated the relationship between resting beta power and trait impulsivity (assessed by questionnaires) and reported that individuals with higher level of trait impulsivity tend to have greater resting beta power (Threadgill and Gable, 2018; Wendel et al., 2021). Our study for the first time investigated the relationship between resting band power and the ability of inhibitory control rather than impulsivity. In line with previous studies (Threadgill and Gable, 2018; Wendel et al., 2021), our results revealed positive correlations between resting beta power and response inhibition and extended the relationship to another aspect of impulsivity.

The neural mechanisms underlying the relationship between beta band oscillatory activity and response inhibition remains unclear. Beta power has been suggested as a signature of an active process promoting the existing motor set whereas compromising neuronal processing of new movements (Androulidakis et al., 2006, 2007; Pogosyan et al., 2009; Engel and Fries, 2010). It has been reported that voluntary movements are slowed if they are triggered during the period of enhanced spontaneous beta band activity (Androulidakis et al., 2006, 2007), suggesting spontaneous enhancement of beta band oscillatory activity relates to impaired motor performance. Previous studies applied transcranial alternating-current stimulation on MC and observed increased resting beta activity accompanied by slowed hand and finger movements (Pogosyan et al., 2009; Wach et al., 2013). Taken together, these evidence suggest that beta band activity possibly signals the tendency of the sensorimotor system to maintain the status quo, and excessive beta band activity would slow down motor performance (Engel and Fries, 2010).

Unlike previous studies investigating the relationship between resting beta activity and velocity of voluntary movement (e.g., visuomotor tracking task) (Pogosyan et al., 2009; Wach et al., 2013), our current study for the first time investigated the relationship between resting beta activity and the ability of response inhibition. Results from previous studies and the current study suggest that excessive beta band activity slows down the velocity of both motor tasks and response inhibition, even though the neural substrates for motor execution and motor inhibitory control are different. This indicates that excessive beta band activity may relate to an overall slowdown of motor performance regardless of the type of movement.

Interestingly, we observed a significant correlation between SSRT and beta band power in bilateral sensorimotor cortex and right IFC, but not in the left IFC. Our results are in line with previous studies reporting that right IFC is an important structure for motor inhibitory control (Aron, 2007; Cunillera et al., 2014, 2016; Chowdhury et al., 2019). As most previous studies (including our current study) included only right-handed participants (Cunillera et al., 2014, 2016), how handedness influences the laterality of motor inhibitory control has not been systematically investigated. Therefore, cautions are needed when generalizing the conclusion that the right IFC, rather than the left IFC, is a critical area in the motor inhibitory network to left-handed individuals.

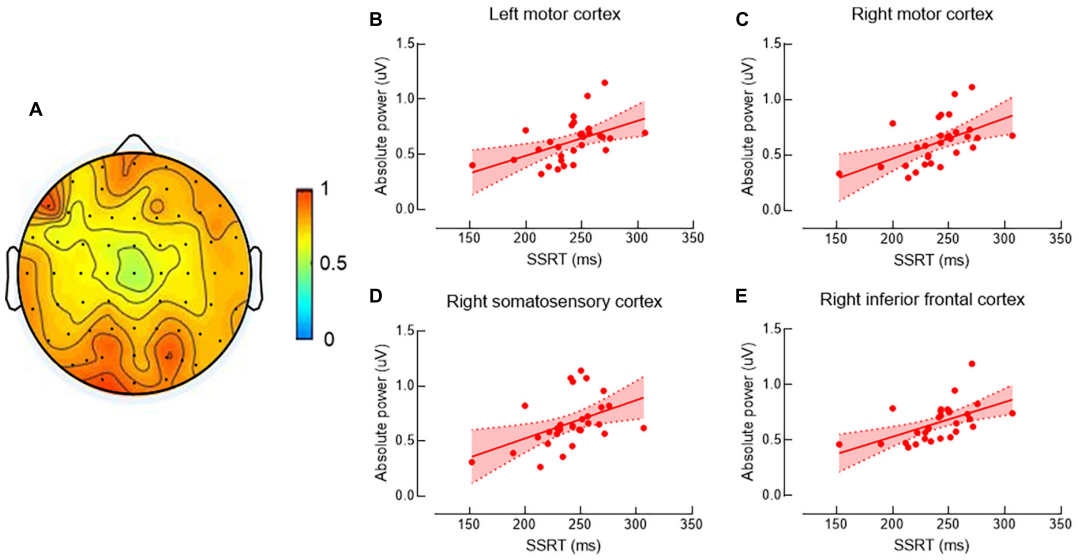

FIGURE 1
Correlations between beta band power and stop-signal reaction time (SSRT). The topographic map shows beta band power **(A)**. Data are presented as raw values of power. Scatter plots show the significant positive correlations between SSRT and beta band power in left motor cortex (MC) **(B)**, right MC **(C)**, right motor somatosensory cortex (SC) **(D)**, and right inferior frontal cortex (IFC) **(E)**. As longer SSRT is associated with more poor ability of response inhibition, individuals with poor ability of response inhibition tended to have greater electroencephalography (EEG) power in the above brain regions.

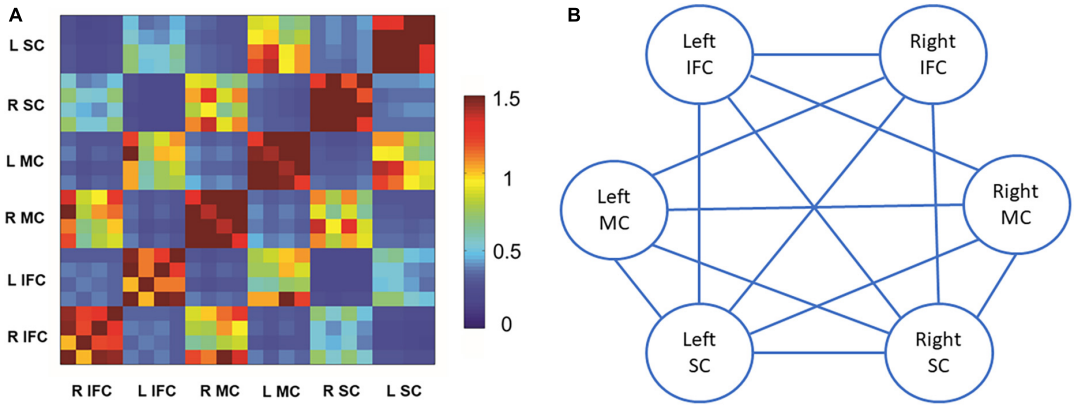

FIGURE 2
Beta band coherence in each pair of brain regions of interest and the correlations with stop-signal reaction time (SSRT). **(A)** Beta band coherence between bilateral motor cortex, somatosensory cortex, and inferior frontal cortex. Data are presented as z-scores of coherences. There were four electroencephalography (EEG) channels included for each brain region of interest. **(B)** Illustration of correlations between SSRT and beta band coherence in each pair of brain regions of interest. Solid lines stand for significant positive correlations between SSRT and beta band coherence in the pair of brain regions. L stands for left, and R stands for right. SC refers to somatosensory cortex. MC refers to motor cortex. IFC refers to inferior frontal cortex.

4.2. Beta band functional connectivity

Both beta band global efficiency and coherence between bilateral sensorimotor cortices and IFC were positively correlated with SSRT. Our findings suggest that in addition to beta band oscillatory activity, beta band functional connectivity also associates with response inhibition.

Unlike EEG power reflecting oscillatory synchronization within local cortical neuronal populations, functional connectivity represents neuronal synchronization between distributed cortical regions (Silberstein et al., 2005). Oscillatory synchronization between cortical areas has been increasingly recognized as a critical mechanism in motor organization (Serrien and Brown, 2003; Serrien et al., 2003). Although the relationship between local beta cortical oscillatory activity and impaired motor performance has been extensively investigated (Androulidakis et al., 2006, 2007; Engel and Fries, 2010), fewer studies investigated the relationship between beta band functional connectivity and motor performance (Gilbertson et al., 2005; Silberstein et al., 2005). Silberstein et al. (2005) reported a positive correlation between beta band functional connectivity over distributed cortical regions and motor impairment in PD patients. Gilbertson et al. (2005)

10.3389/fnins.2023.1131862

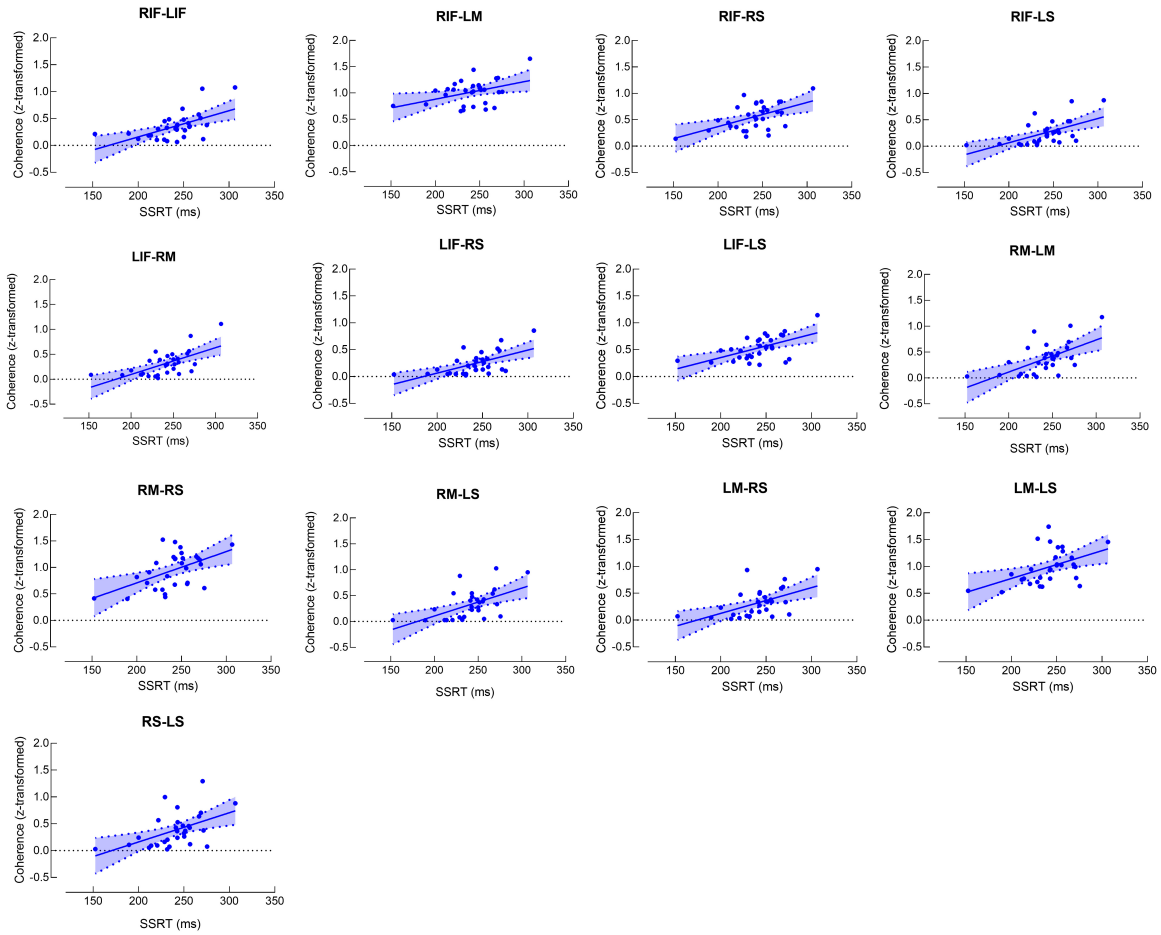

FIGURE 3
Scatter plots for correlations between stop-signal reaction time (SSRT) and beta band coherence. Each scatter plot represents significant positive correlation between SSRT and beta band coherence in the pair of brain regions. RS and LS refer to right and left somatosensory cortex, respectively. RM and LM refer to right and left motor cortex, respectively. RIF and LIF refer to right and left inferior frontal cortex, respectively.

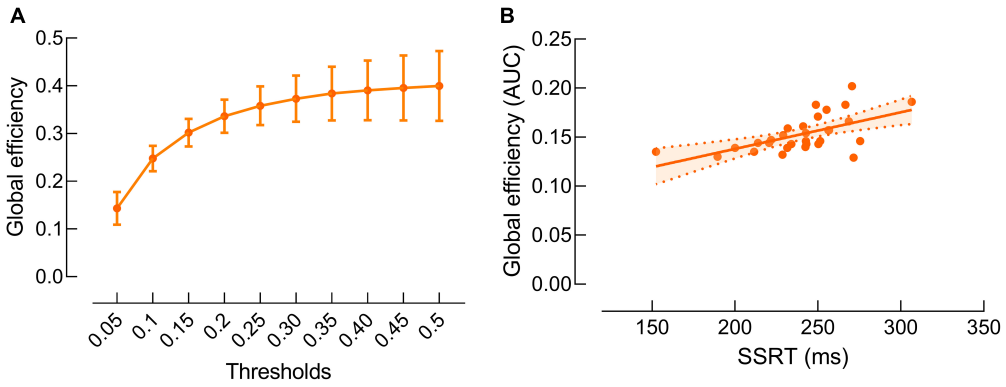

FIGURE 4
Correlations between beta band global efficiency and stop-signal reaction time (SSRT). **(A)** Beta band global efficiency at each threshold. Data are presented as mean and standard error. **(B)** Significant positive correlation between beta band global efficiency and SSRT. Data are presented as areas under the curves of global efficiency at all thresholds.

reported that the greater beta band corticomuscular coherence was related to the worse motor performance in healthy adults. Although response inhibition is different from other movement type, similar correlations between beta band functional connectivity and motor performance were observed (Gilbertson et al., 2005; Silberstein et al., 2005), suggesting individuals with worse motor performance, regardless of the movement type, tend to have excessive beta band functional connectivity.

We also observed the relationship between beta band global efficiency and the ability of response inhibition. Global efficiency exhibits the efficiency in transporting information at a global scale between genetic brain areas, and greater global efficiency reflects higher information transferring efficiency over the entire brain (Vecchio et al., 2019). Our results suggest that individuals with lower efficiency in transporting information in the brain tend to have worse ability of response inhibition.

4.3. Clinical implications

Our current study is the first study to investigate the relationship between resting-state cortical beta band activity and response inhibition. We observed positive correlations between beta band power, coherence and global efficiency and SSRT, indicating individuals with stronger cortical beta band activity tend to have worse ability of inhibitory motor control.

Cortical beta band activity has been reported to be elevated in PD, and PD patients with greater beta band activity tend to have worse motor performance (Silberstein et al., 2005; Jenkinson and Brown, 2011). As PD is characterized as a loss of dopaminergic neurons in basal ganglia, excessive beta band activity has been associated with reduced cortical dopaminergic tone (Jenkinson and Brown, 2011). Silberstein et al. (2005) reported a reduction in cortical beta band activity after dopaminergic therapy accompanied by motor improvement in PD patients, further supporting the existence of a direct relationship between cortical beta activity and dopaminergic tone. Based on this premise, the correlations between beta band activity and response inhibition observed in the current study suggest that dopaminergic neurons possibly play a role in response inhibition.

Despite the extensive existing literature, there is still lack of solid evidence indicating the involvement of dopaminergic neurons in motor inhibitory control (Stinear et al., 2009; Swann et al., 2011; Haynes and Haber, 2013; Benis et al., 2014; Aron et al., 2016; Duque et al., 2017). Suppression an initiated motor output requires both an increase in intracortical inhibition and a reduction in excitatory input from thalamus to primary MC (Duque et al., 2017). Efficient inhibitory control relies on a "hyper-direct" pathway from the frontal cortex to the subthalamus nucleus in basal ganglia, providing a mechanism for rapidly inhibiting the motor system in a global manner (Nambu et al., 2002; Wessel et al., 2016; Wessel and Aron, 2017). As an important neurotransmitter in the cortico-basal ganglia network, dopamine possibly plays a critical role in response inhibition (Lindenbach and Bishop, 2013; Schall et al., 2017). Therefore, the current study provides additional evidence suggesting that dopaminergic neurons are possibly involved in motor inhibitory control.

4.4. Limitations

As a pilot study, the sample size of current study is small (N = 30). In addition, our sample includes only young adults, which is another limitation of current study. Cautions are needed when generalizing our findings to other populations, such as aging population and PD patients. Future studies are needed to test our results in other populations with larger sample sizes.

5. Conclusion

This is the first study to investigate the relationship between resting state cortical beta activity and response inhibition. This study revealed positive correlations between cortical beta band activity, coherence and global efficiency and SSRT, indicating individuals with less cortical beta band activity and functional connectivity tend to have better ability of motor inhibitory control. Our findings have implications on development of new treatment for the diseases with impaired motor inhibitory control.

Data availability statement

The raw data supporting the conclusions of this article will be made available by the authors, without undue reservation.

Ethics statement

The studies involving human participants were reviewed and approved by the Guangzhou First People's Hospital Human Research Ethics Committee. The patients/participants provided their written informed consent to participate in this study.

Author contributions

YL, HZ, and QD designed the experiment and wrote the manuscript. QD and TL recruited the participants. QD, GC, ZO, and SY conducted the experiments. QD and GC reduced, analyzed, and interpreted the data. All authors contributed to the article and approved the submitted version.

Funding

This study was supported by the National Natural Science Foundation of China [81974357 (YL) and 82102678 (QD)], the Guangzhou Municipal Science and Technology Program [202206010197 (YL)], and the Guangdong Basic and Applied Basic Research Foundation [2020A1515110761 (QD)].

Acknowledgments

We thank all our participants for their interest and time investment.

Conflict of interest

The authors declare that the research was conducted in the absence of any commercial or financial relationships that could be construed as a potential conflict of interest.

Publisher's note

References

Androulidakis, A. G., Doyle, L. M., Gilbertson, T. P., and Brown, P. (2006). Corrective movements in response to displacements in visual feedback are more effective during periods of 13-35 Hz oscillatory synchrony in the human corticospinal system. *Eur. J. Neurosci.* 24, 3299–3304. doi: 10.1111/j.1460-9568.2006.05201.x

Androulidakis, A. G., Doyle, L. M., Yarrow, K., Litvak, V., Gilbertson, T. P., and Brown, P. (2007). Anticipatory changes in beta synchrony in the human corticospinal system and associated improvements in task performance. *Eur. J. Neurosci.* 25, 3758–3765. doi: 10.1111/j.1460-9568.2007.05620.x

Aron, A. R. (2007). The neural basis of inhibition in cognitive control. *Neuroscientist* 13, 214–228.

Aron, A. R. (2011). From reactive to proactive and selective control: Developing a richer model for stopping inappropriate responses. *Biol. Psychiatry* 69, e55–e68. doi: 10.1016/j.biopsych.2010.07.024

Aron, A. R., Herz, D. M., Brown, P., Forstmann, B. U., and Zaghloul, K. (2016). Frontosubthalamic circuits for control of action and cognition. *J. Neurosci.* 36, 11489–11495. doi: 10.1523/JNEUROSCI.2348-16.2016

Arun, K. M., Smitha, K. A., Sylaja, P. N., and Kesavadas, C. (2020). Identifying resting-state functional connectivity changes in the motor cortex using fNIRS during recovery from stroke. *Brain Topogr.* 33, 710–719. doi: 10.1007/s10548-020-00785-2

Badcock, J. C., Michie, P. T., Johnson, L., and Combrinck, J. (2002). Acts of control in schizophrenia: Dissociating the components of inhibition. *Psychol. Med.* 32, 287–297.

Bari, A., and Robbins, T. W. (2013). Inhibition and impulsivity: Behavioral and neural basis of response control. *Prog. Neurobiol.* 108, 44–79.

Benis, D., David, O., Lachaux, J. P., Seigneuret, E., Krack, P., Fraix, V., et al. (2014). Subthalamic nucleus activity dissociates proactive and reactive inhibition in patients with Parkinson's disease. *Neuroimage* 91, 273–281. doi: 10.1016/j.neuroimage.2013.10.070

Cai, G., Wu, M., Ding, Q., Lin, T., Li, W., Jing, Y., et al. (2021). The corticospinal excitability can be predicted by spontaneous electroencephalography oscillations. *Front. Neurosci.* 15:722231. doi: 10.3389/fnins.2021.722231

Chowdhury, N. S., Livesey, E. J., Blaszczynski, A., and Harris, J. A. (2017). Pathological gambling and motor impulsivity: A systematic review with meta-analysis. *J. Gambl. Stud.* 33, 1213–1239.

Chowdhury, N. S., Livesey, E. J., and Harris, J. A. (2019). Contralateral and ipsilateral relationships between intracortical inhibition and stopping efficiency. *Neuroscience* 415, 10–17. doi: 10.1016/j.neuroscience.2019.07.013

Cunillera, T., Brignani, D., Cucurell, D., Fuentemilla, L., and Miniussi, C. (2016). The right inferior frontal cortex in response inhibition: A tDCS-ERP co-registration study. *Neuroimage* 140, 66–75. doi: 10.1016/j.neuroimage.2015.11.044

Cunillera, T., Fuentemilla, L., Brignani, D., Cucurell, D., and Miniussi, C. (2014). A simultaneous modulation of reactive and proactive inhibition processes by anodal tDCS on the right inferior frontal cortex. *PLoS One* 9:e113537. doi: 10.1371/journal.pone.0113537

Delorme, A., and Makeig, S. (2004). EEGLAB: An open source toolbox for analysis of single-trial EEG dynamics including independent component analysis. *J. Neurosci. Methods* 134, 9–21.

Ding, Q., Cai, H., Wu, M., Cai, G., Chen, H., Li, W., et al. (2021a). Short intracortical facilitation associates with motor-inhibitory control. *Behav. Brain Res.* 407:113266.

Ding, Q., Zhang, S., Chen, S., Chen, J., Li, X., Chen, J., et al. (2021b). The effects of intermittent theta burst stimulation on functional brain network following stroke: An electroencephalography study. *Front. Neurosci.* 15:755709. doi: 10.3389/fnins.2021.755709

Ding, Q., Chen, S., Chen, J., Zhang, S., Peng, Y., Chen, Y., et al. (2022). Intermittent Theta burst stimulation increases natural oscillatory frequency in ipsilesional motor cortex post-stroke: A transcranial magnetic stimulation and electroencephalography study. *Front. Aging Neurosci.* 14:818340. doi: 10.3389/fnagi.2022.818340

Duque, J., Greenhouse, I., Labruna, L., and Ivry, R. B. (2017). Physiological markers of motor inhibition during human behavior. *Trends Neurosci.* 40, 219–236.

Engel, A. K., and Fries, P. (2010). Beta-band oscillations–signalling the status quo? *Curr. Opin. Neurobiol.* 20, 156–165. doi: 10.1016/j.conb.2010.02.015

Gilbertson, T., Lalo, E., Doyle, L., Di Lazzaro, V., Cioni, B., and Brown, P. (2005). Existing motor state is favored at the expense of new movement during 13-35 Hz oscillatory synchrony in the human corticospinal system. *J. Neurosci.* 25, 7771–7779. doi: 10.1523/JNEUROSCI.1762-05.2005

Haynes, W. I., and Haber, S. N. (2013). The organization of prefrontal-subthalamic inputs in primates provides an anatomical substrate for both functional specificity and integration: Implications for Basal Ganglia models and deep brain stimulation. *J. Neurosci.* 33, 4804–4814. doi: 10.1523/JNEUROSCI.4674-12.2013

Jenkinson, N., and Brown, P. (2011). New insights into the relationship between dopamine, beta oscillations and motor function. *Trends Neurosci.* 34, 611–618. doi: 10.1016/j.tins.2011.09.003

Lijffijt, M., Kenemans, J. L., Verbaten, M. N., and Van Engeland, H. (2005). A meta-analytic review of stopping performance in attention-deficit/hyperactivity disorder: Deficient inhibitory motor control? *J. Abnorm. Psychol.* 114, 216–222. doi: 10.1037/0021-843X.114.2.216

Lindenbach, D., and Bishop, C. (2013). Critical involvement of the motor cortex in the pathophysiology and treatment of Parkinson's disease. *Neurosci. Biobehav. Rev.* 37, 2737–2750.

Nambu, A., Tokuno, H., and Takada, M. (2002). Functional significance of the cortico-subthalamo-pallidal 'hyperdirect' pathway. *Neurosci. Res.* 43, 111–117.

Park, C. H., Chang, W. H., Yoo, W. K., Shin, Y. I., Kim, S. T., and Kim, Y. H. (2014). Brain topological correlates of motor performance changes after repetitive transcranial magnetic stimulation. *Brain Connect.* 4, 265–272.

Pfurtscheller, G., Stancak, A. Jr., and Neuper, C. (1996). Post-movement beta synchronization. A correlate of an idling motor area? *Electroencephalogr. Clin. Neurophysiol.* 98, 281–293.

Pogosyan, A., Gaynor, L. D., Eusebio, A., and Brown, P. (2009). Boosting cortical activity at Beta-band frequencies slows movement in humans. *Curr. Biol.* 19, 1637–1641. doi: 10.1016/j.cub.2009.07.074

Schall, J. D., Palmeri, T. J., and Logan, G. D. (2017). Models of inhibitory control. *Philos. Trans. R. Soc. Lond. B Biol. Sci.* 372:20160193. doi: 10.1098/rstb.2016.0193

Serrien, D. J., and Brown, P. (2003). The integration of cortical and behavioural dynamics during initial learning of a motor task. *Eur. J. Neurosci.* 17, 1098–1104.

Serrien, D. J., Fisher, R. J., and Brown, P. (2003). Transient increases of synchronized neural activity during movement preparation: Influence of cognitive constraints. *Exp. Brain Res.* 153, 27–34. doi: 10.1007/s00221-003-1578-2

Silberstein, P., Pogosyan, A., Kuhn, A. A., Hotton, G., Tisch, S., Kupsch, A., et al. (2005). Cortico-cortical coupling in Parkinson's disease and its modulation by therapy. *Brain* 128, 1277–1291.

Skippen, P., Matzke, D., Heathcote, A., Fulham, W. R., Michie, P., and Karayanidis, F. (2019). Reliability of triggering inhibitory process is a better predictor of impulsivity than SSRT. *Acta Psychol. (Amst.)* 192, 104–117. doi: 10.1016/j.actpsy.2018.10.016

Stinear, C. M., Coxon, J. P., and Byblow, W. D. (2009). Primary motor cortex and movement prevention: Where Stop meets Go. *Neurosci. Biobehav. Rev.* 33, 662–673. doi: 10.1016/j.neubiorev.2008.08.013

Swann, N., Poizner, H., Houser, M., Gould, S., Greenhouse, I., Cai, W., et al. (2011). Deep brain stimulation of the subthalamic nucleus alters the cortical profile of response inhibition in the beta frequency band: A scalp EEG study in Parkinson's disease. *J. Neurosci.* 31, 5721–5729. doi: 10.1523/JNEUROSCI.6135-10.2011

Threadgill, A. H., and Gable, P. A. (2018). Resting beta activation and trait motivation: Neurophysiological markers of motivated motor-action preparation. *Int. J. Psychophysiol.* 127, 46–51. doi: 10.1016/j.ijpsycho.2018.03.002

Vecchio, F., Tomino, C., Miraglia, F., Iodice, F., Erra, C., Di Iorio, R., et al. (2019). Cortical connectivity from EEG data in acute stroke: A study via graph theory as a potential biomarker for functional recovery. *Int. J. Psychophysiol.* 146, 133–138. doi: 10.1016/j.ijpsycho.2019.09.012

Verbruggen, F., Aron, A. R., Band, G. P., Beste, C., Bissett, P. G., Brockett, A. T., et al. (2019). A consensus guide to capturing the ability to inhibit actions and impulsive behaviors in the stop-signal task. *Elife* 8:e46323. doi: 10.7554/eLife.46323

Verbruggen, F., and Logan, G. D. (2008). Long-term aftereffects of response inhibition: Memory retrieval, task goals, and cognitive control. *J. Exp. Psychol. Hum. Percept. Perform.* 34, 1229–1235. doi: 10.1037/0096-1523.34.5.1229

Wach, C., Krause, V., Moliadze, V., Paulus, W., Schnitzler, A., and Pollok, B. (2013). Effects of 10 Hz and 20 Hz transcranial alternating current stimulation (tACS) on motor functions and motor cortical excitability. *Behav. Brain Res.* 241, 1–6.

Wang, J., Wang, X., Xia, M., Liao, X., Evans, A., and He, Y. (2015). GRETNA: A graph theoretical network analysis toolbox for imaging connectomics. *Front. Hum. Neurosci.* 9:386. doi: 10.3389/fnhum.2015.00386

Welch, P. D. (1967). "Use of fast fourier transform for estimation of power spectra - a method based on time averaging over short modified periodograms," in *Proceeding of the IEEE Transactions on Audio and Electroacoustics*. Vol. 15. (Piscataway, NJ: IEEE), 70–73.

Wendel, C. J., Wilhelm, R. A., and Gable, P. A. (2021). Individual differences in motivation and impulsivity link resting frontal alpha asymmetry and motor beta activation. *Biol. Psychol.* 162:108088. doi: 10.1016/j.biopsycho.2021.108088

Wessel, J. R., and Aron, A. R. (2017). On the globality of motor suppression: Unexpected events and their influence on behavior and cognition. *Neuron* 93, 259–280. doi: 10.1016/j.neuron.2016.12.013

Wessel, J. R., Ghahremani, A., Udupa, K., Saha, U., Kalia, S. K., Hodaie, M., et al. (2016). Stop-related subthalamic beta activity indexes global motor suppression in Parkinson's disease. *Mov. Disord.* 31, 1846–1853. doi: 10.1002/mds.26732

Yan, T., Wang, W., Liu, T., Chen, D., Wang, C., Li, Y., et al. (2017). Increased local connectivity of brain functional networks during facial processing in schizophrenia: Evidence from EEG data. *Oncotarget* 8, 107312–107322. doi: 10.18632/oncotarget.20598

frontiers | Frontiers in Neuroscience

TYPE Original Research
PUBLISHED 08 March 2023
DOI 10.3389/fnins.2023.1146620

OPEN ACCESS

EDITED BY
Guang-Qing Xu,
The First Affiliated Hospital of Sun Yat-sen University, China

REVIEWED BY
Xiaomin Cai,
University of Miami, United States
Zenglin Cai,
Affiliated Suzhou Science and Technology Town Hospital of Nanjing Medical University, China

*CORRESPONDENCE
Yini Dang
✉ yeani_hi@126.com
Yu Zheng
✉ zhengyu8710@163.com
Binbin Yu
✉ coldrain24@163.com
Risheng Cao
✉ rishengcao@njmu.edu.cn

†These authors have contributed equally to this work

SPECIALTY SECTION
This article was submitted to Translational Neuroscience, a section of the journal Frontiers in Neuroscience

RECEIVED 17 January 2023
ACCEPTED 22 February 2023
PUBLISHED 08 March 2023

CITATION
Zhang X, Wang X, Wang S, Zhang Y, Wang Z, Yang Q, Wang S, Cao R, Yu B, Zheng Y and Dang Y (2023) Machine learning algorithms assisted identification of post-stroke depression associated biological features. *Front. Neurosci.* 17:1146620. doi: 10.3389/fnins.2023.1146620

Machine learning algorithms assisted identification of post-stroke depression associated biological features

Xintong Zhang[1†], Xiangyu Wang[2†], Shuwei Wang[3†], Yingjie Zhang[1†], Zeyu Wang[4†], Qingyan Yang[1], Song Wang[5], Risheng Cao[6*], Binbin Yu[1*], Yu Zheng[1*] and Yini Dang[7*]

[1]Department of Rehabilitation Medicine, The First Affiliated Hospital of Nanjing Medical University, Nanjing, Jiangsu, China, [2]Department of Rehabilitation Medicine, The Affiliated Lianyungang Oriental Hospital of Kangda College of Nanjing Medical University, Lianyungang, Jiangsu, China, [3]Department of Critical Care Medicine, Taizhou Hospital of Zhejiang Province Affiliated to Wenzhou Medical University, Taizhou, Zhejiang, China, [4]Department of Rehabilitation Medicine, Shanghai Ruijin Rehabilitation Hospital, Shanghai, China, [5]Department of Neurological Rehabilitation, Wuxi Yihe Rehabilitation Hospital, Wuxi, Jiangsu, China, [6]Department of Science and Technology, The First Affiliated Hospital of Nanjing Medical University, Nanjing, Jiangsu, China, [7]Department of Gastroenterology, The First Affiliated Hospital of Nanjing Medical University, Nanjing, Jiangsu, China

Objectives: Post-stroke depression (PSD) is a common and serious psychiatric complication which hinders functional recovery and social participation of stroke patients. Stroke is characterized by dynamic changes in metabolism and hemodynamics, however, there is still a lack of metabolism-associated effective and reliable diagnostic markers and therapeutic targets for PSD. Our study was dedicated to the discovery of metabolism related diagnostic and therapeutic biomarkers for PSD.

Methods: Expression profiles of GSE140275, GSE122709, and GSE180470 were obtained from GEO database. Differentially expressed genes (DEGs) were detected in GSE140275 and GSE122709. Functional enrichment analysis was performed for DEGs in GSE140275. Weighted gene co-expression network analysis (WGCNA) was constructed in GSE122709 to identify key module genes. Moreover, correlation analysis was performed to obtain metabolism related genes. Interaction analysis of key module genes, metabolism related genes, and DEGs in GSE122709 was performed to obtain candidate hub genes. Two machine learning algorithms, least absolute shrinkage and selection operator (LASSO) and random forest, were used to identify signature genes. Expression of signature genes was validated in GSE140275, GSE122709, and GSE180470. Gene set enrichment analysis (GSEA) was applied on signature genes. Based on signature genes, a nomogram model was constructed in our PSD cohort (27 PSD patients vs. 54 controls). ROC curves were performed for the estimation of its diagnostic value. Finally, correlation analysis between expression of signature genes and several clinical traits was performed.

Results: Functional enrichment analysis indicated that DEGs in GSE140275 enriched in metabolism pathway. A total of 8,188 metabolism associated genes were identified by correlation analysis. WGCNA analysis was constructed to obtain 3,471 key module genes. A total of 557 candidate hub genes were identified by interaction analysis. Furthermore, two signature genes (SDHD and FERMT3)

were selected using LASSO and random forest analysis. GSEA analysis found that two signature genes had major roles in depression. Subsequently, PSD cohort was collected for constructing a PSD diagnosis. Nomogram model showed good reliability and validity. AUC values of receiver operating characteristic (ROC) curve of SDHD and FERMT3 were 0.896 and 0.964. ROC curves showed that two signature genes played a significant role in diagnosis of PSD. Correlation analysis found that SDHD (r = 0.653, $P < 0.001$) and FERM3 (r = 0.728, $P < 0.001$) were positively related to the Hamilton Depression Rating Scale 17-item (HAMD) score.

Conclusion: A total of 557 metabolism associated candidate hub genes were obtained by interaction with DEGs in GSE122709, key modules genes, and metabolism related genes. Based on machine learning algorithms, two signature genes (SDHD and FERMT3) were identified, they were proved to be valuable therapeutic and diagnostic biomarkers for PSD. Early diagnosis and prevention of PSD were made possible by our findings.

KEYWORDS

post-stroke depression, metabolism, WGCNA, machine learning algorithms, GEO

Introduction

Stroke remains the second leading cause of death and may lead to long-term disability in adults (GBD 2019 Stroke Collaborators, 2021; Sun et al., 2021). After the acute stage, most of stroke patients suffer from physical and mental disabilities of varying degrees, including hemiplegia, reduced energy, and disturbed sleep (Zhang et al., 2013; Dong et al., 2021). Previous studies have shown that about 30–40% of stroke patients develop post-stroke depression (PSD) which is a mood disorder characterized by depression and anhedonia, and is associated with decreased rehabilitation motivation, reduced quality of life, poor functional outcome, as well as increased cost of treatment and burden of family caregiver (Li et al., 2020). One meta-analysis concluded that a hazard ratio for post-stroke depression and all-cause mortality was 1.59 (Cai et al., 2019). However, PSD is often concealed due to unrecognized depressive symptoms and their decreased willingness of treatment attendance (Klinedinst et al., 2012). Diagnosis of PSD is currently based on clinical symptoms, and there is no reliable objective parameter. Therefore, it is necessary to explore the new diagnostic and therapeutic biomarkers for PSD in subacute period of stroke.

There is accumulating evidence that PSD and metabolism are intimately related. Compared with non-PSD, stroke patients with PSD have higher glutamate levels in the frontal lobe (Wang et al., 2012). Previous studies found that a high level of homocysteine has been identified as the qualifiable risk factor for ischemic stroke, and elevated serum level of homocysteine is also significantly associated with depression (Li et al., 2017; Zhou et al., 2018). Jiang et al. (2021) demonstrated that gut microbiome may participate in the development of PSD, the discriminating fecal metabolites were mainly involved in lipid metabolism, amino acid metabolism, carbohydrate metabolism and nucleotide metabolism. These results indicated that metabolism plays an important role in the pathological process of PSD.

Recently with the assistant of advanced sequencing technologies and machine learning algorithms, intelligent hub gene and signaling pathway detection becomes realistic. Several studies based on weighted gene co-expression network analysis (WGCNA) have reported changes in relevant key pathways and differential expression of key related genes in post-stroke patients (Li et al., 2020; Wang et al., 2020; Lin et al., 2021). Furthermore, Liu et al. (2022) used WGCNA combined with the random forest model and the least absolute shrinkage and selection operator (LASSO) analysis to identify 10 key genes in patients with Alzheimer's Disease. However, these techniques have not been widely applied in the investigation of metabolism biomarkers of PSD.

Upon the above concerns, this study employed multiple bioinformatic approaches to find possible biomarkers. Firstly, three gene expression profiles of stroke were obtained from GEO database. Differentially expressed genes (DEGs) were detected. WGCNA was constructed to identify disease related module genes. Then, correlation analysis was performed to obtain metabolism related genes. Interaction analysis was performed to obtain candidate hub genes. Subsequently, signature genes were identified by LASSO and random forest analysis. Gene set enrichment analysis was applied on signature genes. Finally, a diagnosis model was built in PSD cohort. In general, the findings of this research may assist in the diagnosis and treatment of PSD as well as increase our understanding of etiology of PSD.

Materials and methods

Data sources and processing

Three datasets (GSE140275, GSE122709, GSE180470) were downloaded from Gene Expression Omnibus (GEO).[1] The GSE140275 dataset contained six patients, including three healthy controls (HC) and three stroke patients. The GSE122709 dataset

1 http://www.ncbi.nlm.nih.gov/geo/

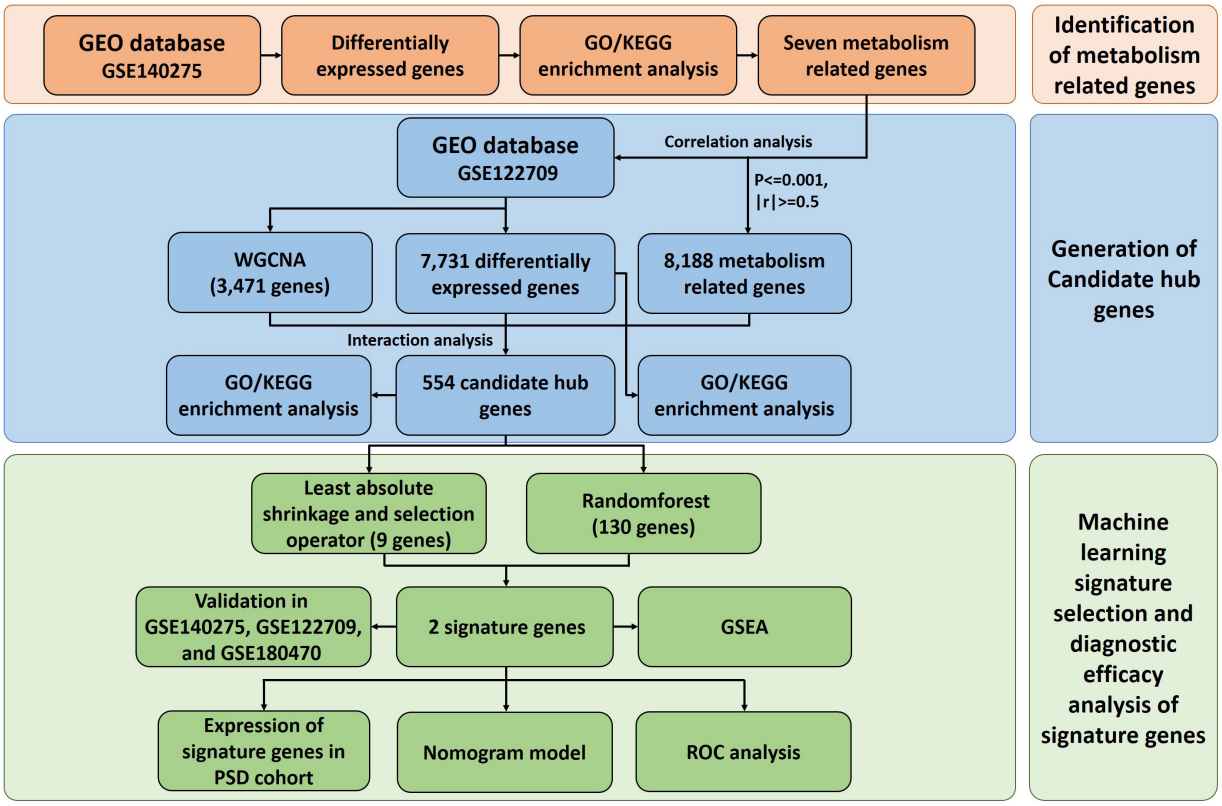

FIGURE 1
Flow chart. GEO, Gene Expression Omnibus; WGCNA, weighted gene co-expression network analysis; PSD, post-stroke depression; ROC, receiver operating characteristic; GO, gene ontology; KEGG, Kyoto Encyclopedia of Genes and Genomes; GSEA, gene set enrichment analysis.

included five HC and ten stroke patients. GSE180470 dataset included three HC and three stroke patients. Expressions of three datasets were all derived from human blood tissue. "Limma" and "edgeR" package in R software was used to investigate differentially expressed genes (DEGs) (Robinson et al., 2010; Ritchie et al., 2015), which was specified as "P-value < 0.05 and $\log_2$ (fold change) > 1 or $\log_2$ (fold change) < -1." For visualization, the volcano plots were generated to show DEGs, while the top 25 upregulated and the top 25 downregulated DEGs were displayed by heatmaps.

Functional enrichment analysis

Functional enrichment analysis was conducted to evaluate major biological attributes of DEGs, specifically including Gene Ontology (GO) and Kyoto Encyclopedia of Genes and Genomes (KEGG) pathway analysis using "ClusterProfiler" package in R software. Threshold was set at P-value < 0.05. GO categories comprised biological processes (BP), molecular functions (MF), and cellular components (CC) (Zhu et al., 2022).

Weighted gene co-expression network analysis (WGCNA)

Based on scale-free topology criterion, co-expression network in GSE122709 dataset was constructed using "WGCNA" package in R software to identify co-expression gene modules (Langfelder and Horvath, 2008). Briefly, genes with read counts less than 10 and "NA" were filtered out, top 5,000 variant genes were selected. Pearson's correlations between each gene pair were calculated to build an adjacency matrix. Afterward, a "soft" threshold power (β) was estimated according to the criteria of scale-free topology to construct a biologically important scale-free network. Dynamic Tree Cut algorithm was then used to identify gene modules (Lin et al., 2021). Module membership (MM) and gene significance (GS) were estimated to connect modules with clinical characteristics. Hub gene modules were designated as those with the highest Pearson module membership correlation and P-value < 0.05 (Liu et al., 2021).

Screening for candidate hub genes

Based on R software, "WGCNA" package was used for correlation analysis for genes in GSE122709 and seven genes associated with metabolism with the following parameters: $|R| > 0.5$, $P < 0.001$. Then, we identified candidate hub genes by the intersection of DEGs, key module genes and metabolism related genes. Finally, results were visualized by Venn diagram *via* online tool Venny 2.1.0[2] (He et al., 2021).

2 https://bioinfogp.cnb.csic.es/tools/venny/index.html

Identification for signature genes in patients with stroke

We screened candidate hub genes by the intersection of DEGs, key module genes and metabolism related genes. Subsequently, two machine learning algorithms, least absolute shrinkage and selection operator (LASSO) and random forest, were used to identify hub gene. LASSO, a dimension reduction approach, shows superiority in evaluating high-dimensional data in comparison to regression analysis (Kang et al., 2021). The "glmnet" package was used to implement LASSO analysis with a turning/penalty parameter utilizing a 10-fold cross-validation. Furthermore, the "random forest" package was used for performing the random forest analysis which determined the optimal number of variables by computing average error rate of candidate hub genes (Mantero and Ishwaran, 2021). A random forest tree model was built and the importance scores of each candidate hub genes were identified. Genes with importance value >0.25 were determined. The intersection genes of LASSO and random forest analysis were used to pick signature genes of patients with stroke.

Establishment of nomogram

The "rms" package was applied for incorporating signature genes to establish a nomogram. The "score" is the score of the relevant item below, and the "total score" is the sum of all the elements above. Calibration curves were used for assessing the predictive power of the model. Clinical usefulness of nomogram was evaluated by decision curve analysis, which determines clinical practicability of nomogram by quantifying the net benefits under different threshold probabilities in the validation set. Furthermore, we performed clinical impact curves to evaluate clinical utility of the model (Xu et al., 2021).

Curve analysis of receiver operating characteristics (ROC)

The "pROC" package was applied to create Receiver Operating Characteristic (ROC) curves to determine the area under the curve (AUC) for screening signature genes and evaluating their diagnostic value (Robin et al., 2011). AUCs of 0.5–0.7 were considered with low diagnostic accuracy, 0.7–0.9 were considered with moderate accuracy, and >0.9 indicates high accuracy.

Gene set enrichment analysis (GSEA)

To functionally investigate the biological significance of signature genes, GSEA (version 4.1.0) was performed in different subgroups. KEGG gene sets were chosen as the gene set database (Subramanian et al., 2005). Normalized enrichment score (NES) and false discovery rate (FDR) were used to determine if differences were statistically significant and cut-off values were FDR < 0.25, $P < 0.05$, and $|\text{NES}| > 1$.

PSD validation cohort

This was a cohort study enrolled at the First Affiliated Hospital of Nanjing Medical University from September 2020 to April 2022. It was approved by the Committee of Institutional Ethics (Institutional Review Board, 2018-SR-339) and all participants provided written informed consent prior to participation. Patients eligible for inclusion in the study were: (1) aged older than 18 years; (2) diagnosed with ischemic stroke on brain MRI; (3) with stable vital signs (Luft et al., 2004; Upreti et al., 2019). Patients were excluded if (1) presence of severe cognitive impairment; (2) participated in other clinical trials within 6 months (Shi et al., 2021; Yu et al., 2022).

All participants underwent an initial clinical assessment, including the collection of clinical and demographic information. Depression symptoms in post-stroke patients were evaluated by the Hamilton Depression Rating Scale 17-item (HAMD) at 1 month after stroke by a trained neurologist (Lin et al., 2020; Qiao et al., 2020). A score of 0–7 was considered normal, while a HAMD score ≥8 is indicative of depression. Stroke severity was measured using the National Institute of Health Stroke Scale (NIHSS) (He et al., 2020). Modified Rankin Scale (mRS) was used to estimate the functional disability (Liu et al., 2018). Independence and level of activities of daily life (ADL) were evaluated with the Barthel index (Kamal et al., 2020). For research purposes, a blood sample (10 ml) was taken from each subject for further ELISA assessment when they completed the HAMD assessment.

ELISA analysis

Concentration of signature genes in serum of stroke patients were measured using ELISA kit (antibodies-online, Philadelphia, PA, USA). Briefly, 100 μL standard or sample were added to each well and incubated for 90 min at 37°C. After washing two times, 100 μL Biotin-labeled antibody working solution was added and incubated for 60 min for 37°C. After plates were washed three times. A total of 100 μL SABC Working Solution was added and incubated for 30 min at 37°C. Subsequently, 90 μL TMB Substrate Solution was added and incubated 20 min at 37°C. After the incubation, 50 μL stop solution was added into each well to stop the reaction. Finally, Absorbance value at 450 nm was read immediately and calculation (Kaida et al., 2013; Zhou et al., 2015).

Statistical analysis

All statistical analyses in our study were implemented using R software (version 4.1.2). The difference between the two groups was analyzed by Student's *t*-test. The correlation between genes in GSE122709 and metabolism related genes was determined using Pearson's correlation test. All statistical *P*-values were two-sided, and statistical significance was considered with P-value < 0.05.

Results

Detailed procedure of our study is shown in **Figure 1**.

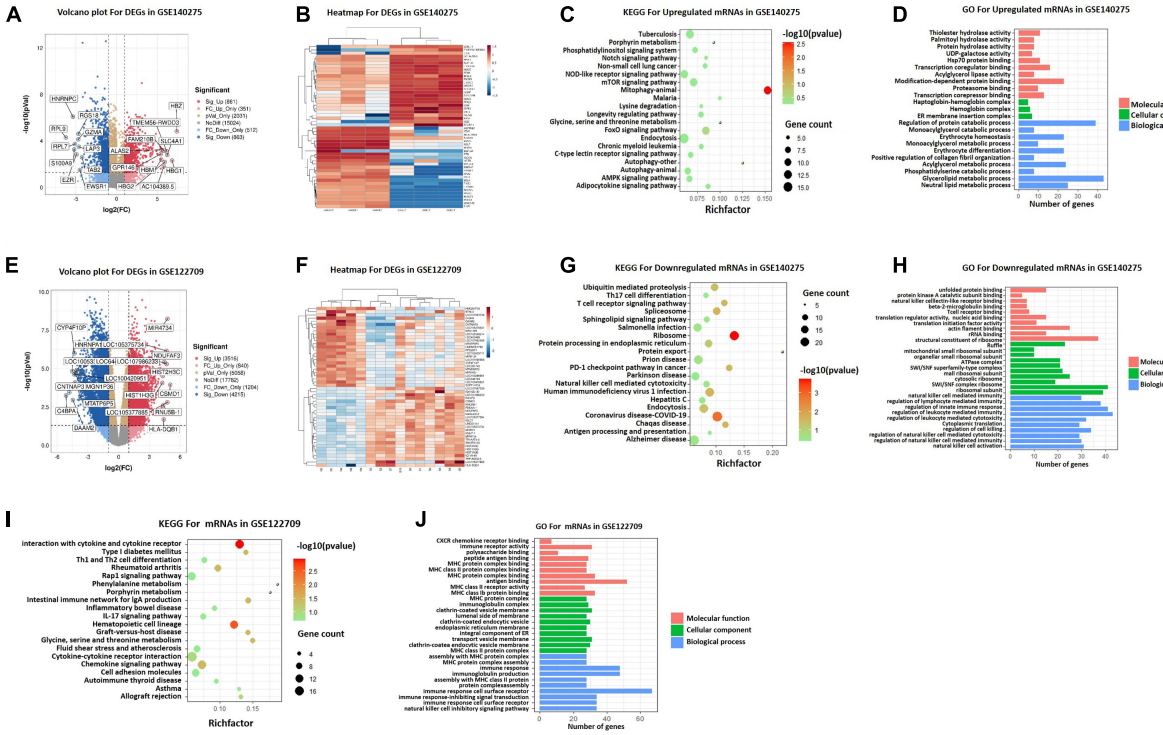

FIGURE 2
DEGs screening and functional enrichment analysis. **(A)** Volcano plot of differentially expressed genes in GSE140275. **(B)** Heatmap of differentially expressed genes in GSE140275. **(C)** KEGG pathway analyses of upregulated mRNAs in GSE140275. **(D)** GO functional analyses of upregulated mRNAs in GSE140275. **(E)** Volcano plot of differentially expressed genes in GSE122709. **(F)** Heatmap of differentially expressed genes in GSE122709. **(G)** KEGG pathway analyses of downregulated mRNAs in GSE140275. **(H)** GO functional analyses of downregulated mRNAs in GSE140275. **(I)** KEGG pathway analyses of mRNAs in GSE122709. **(J)** GO functional analyses of mRNAs in GSE122709. GO, Gene Ontology; KEGG, Kyoto Encyclopedia of Genes and Genomes; DEGs, differentially expressed genes.

Identification of DEGs between HC and stroke patients

To identify potential DEGs, expression profiles of GSE140275 and GSE122709 in GEO database were performed using "Limma" package with $P < 0.05$ and $|\log FC| > 1$ as threshold. A total of 1,724 DEGs were screened in GSE140275 including 861 upregulated genes and 863 downregulated genes (Supplementary Table 1). A total of 7,731 DEGs were obtained, of which 3,516 genes presented upregulation and 4,215 genes presented downregulation in GSE122709 (Supplementary Table 2). The volcano plots were demonstrated in Figures 2A, E. The heatmap showed the top 25 upregulated and top 25 downregulated DEGs between healthy control and stroke patients (Figures 2B, F).

Functional enrichment analysis of DEGs in GSE140275

Functional enrichment analysis was carried out to investigate the biological functions of DEGs in GSE140275. Among upregulated DEGs, KEGG enrichment analysis demonstrated that "autophagy," "porphyrin metabolism," and "glycine, serine and threonine metabolism" were highly enriched (Figure 2C); GO analysis showed that multiple metabolic pathways were also significantly enriched in biological processes, such as "monoacylglycerol metabolic process," "acylglycerol metabolic process," and "glycerolipid metabolic process" (Figure 2D). The results of KEGG showed downregulated DEGs were especially enriched in "ribosome," "protein export," and "T cell receptor signaling pathway" (Figure 2G). Additional GO analysis suggested downregulated DEGs were significantly enriched in "structural constituent of ribosome" in MFs, "ribosome" in CCs, and "regulation of leukocyte mediated immunity" in BPs (Figure 2H). Similarly, KEGG pathways analysis of GSE122709 showed that "porphyrin metabolism", and "glycine, serine and threonine metabolism" were significantly enriched (Figures 2I, J), indicating that metabolism played an important role in stroke.

Construction of the weighted gene co-expression network

The GSE122709 dataset (five HC and 10 stroke patients) was obtained for WGCNA analysis to identify modules of highly correlated genes. A scale-free co-expression network was constructed with the soft threshold to 20 and the mean connectivity is relatively favorable (Figures 3A, B). We selected 0.25 as clustering height limit to merge the strongly associated modules (Figure 3C). Subsequently, 24 signature modules were identified and labeled with different colors (Figure 3D). The correlation between modules was computed, and the results were showed

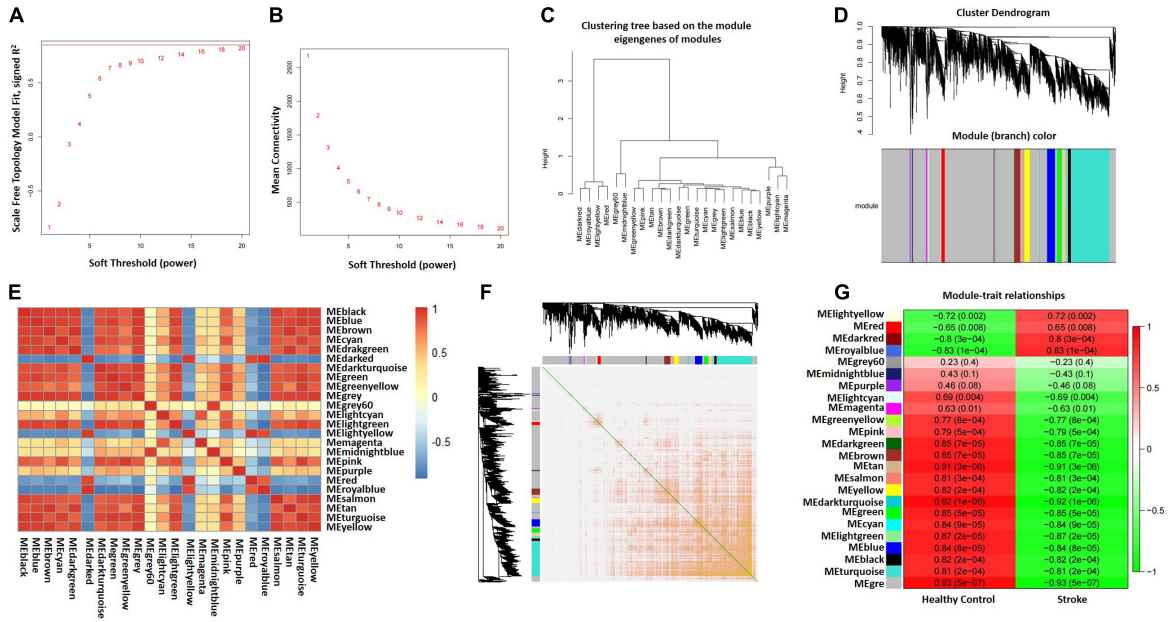

FIGURE 3
Construction of WGCNA co−expression network. **(A)** Scale-free fit index. **(B)** Mean connectivity. **(C)** Clustered dendrograms. **(D)** Clustering dendrogram of genes, various colors represent different modules. **(E)** Correlation heatmap between modules. Red and blue represent positive and negative correlations, respectively. **(F)** Clustering dendrogram of module feature genes. **(G)** Heatmap of module−trait correlations. Red and green represent positive and negative correlations, respectively. HC, healthy control; WGCNA, weighted gene co-expression network analysis.

in Figure 3E. In addition, transcription correlation analysis was performed and demonstrated that there was no substantive connection between modules (Figure 3F). Finally, we calculated the correlation between each module and clinical features. Results indicated that the MEroyalblue module was negatively correlated with HC (r = –0.83, P = 1e–04) and positively correlated with stroke (r = 0.83, P = 1e–04), while the Megrey module was negatively correlated with stroke (r = –0.93, P =5e–07) and positively correlated with healthy control (r = 0.93, P = 5e–07) (Figure 3G and Supplementary Table 3). Therefore, Meroyalblue and Megrey modules were identified as clinically meaningful modules.

Identification of metabolism related candidate hub genes

Based on KEGG pathway analysis in GSE140275, we extracted porphyrin metabolism and glycine, serine and threonine metabolism related genes (ALAS2, FECH, COX10, GCAT, HMBS, PGAM2, and AOC2). Correlation analysis between seven genes and all genes in GSE122709 dataset was conducted. A total of 8,188 metabolism related genes were identified ($|r| \geq 0.5$, $P \leq 0.001$). The heatmap of correlation analysis were shown in Figure 4A. Subsequently, we interacted DEGs in GSE122709, genes in Meroyalblue and Megrey modules, and metabolism related genes, 554 common genes were obtained as metabolism related candidate hub genes (Figure 4B). Functional enrichment analysis revealed that metabolism related candidate hub genes were enriched in "oxidative phosphorylation," "ATP synthesis coupled electron transport," "cell-substrate junction," and "carbohydrate transmembrane transporter activity" (Figures 4C, D).

Selection of signature genes *via* machine learning algorithms

Least absolute shrinkage and selection operator and random forest algorithms were applied to identify signature genes from 554 metabolism related candidate hub genes. For LASSO analysis, nine signature genes were selected from statistically significant univariate variables (Figures 5A, B and Supplementary Table 4). For random forest analysis, we set importance value to 0.25 as the threshold and 130 signature genes were determined (Figures 5C, D and Supplementary Table 5). The interaction analysis of LASSO and random forest indicated that two signature genes were finally screened out, including succinate dehydrogenase complex subunit D (SDHD) and fermitin family member 3 (FERMT3) (Figure 5E). Finally, correlation analysis of two signature genes and metabolism related genes (ALAS2, FECH, COX10, GCAT, HMBS, PGAM2, and AOC2) demonstrated that SDHD and FERMT3 were significantly correlated with metabolism (Figure 5F).

Validation of signature genes

We further investigated the role of SDHD and FERMT3. The expression of SDHD and FERMT3 was verified in GSE140275 and GSE122709. The results showed that SDHD was substantially upregulated in the stroke group, while the same trend was seen in expression of FERMT3 (Figures 6A, B). To further confirm the reliability of our results, validation dataset (GSE180470) was used to validate expression of SDHD and FERMT3. SDHD and FERMT3 were highly expressed in the stroke group (Figure 6C), suggesting that these genes may play a significant role in stroke.

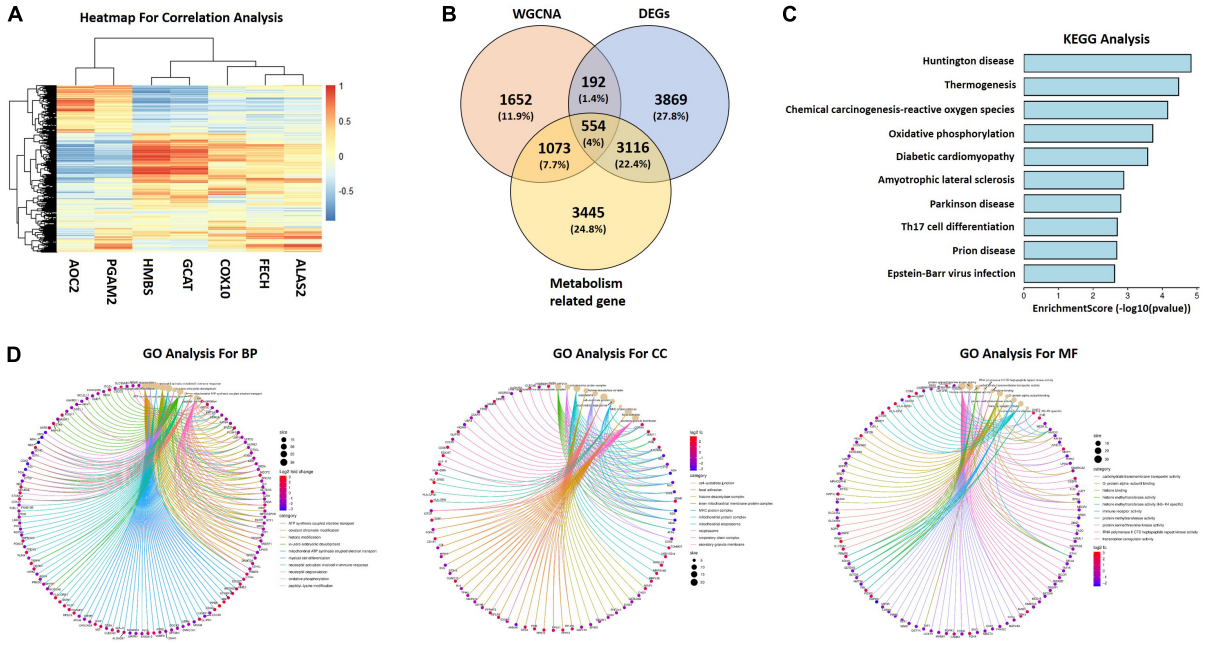

FIGURE 4
Generation of metabolism related candidate hub genes. **(A)** Correlation heatmap between seven metabolism related genes and DEGs in GSE122709. Red represents positive correlations, and blue represents negative correlations. **(B)** Venn diagram to identify candidate hub genes between metabolism related genes, key modules genes and DEGs. **(C)** KEGG analysis of candidate hub genes. **(D)** GO analysis of candidate hub genes. WGCNA, weighted gene co-expression network analysis; DEGs, differentially expressed genes; KEGG, Kyoto Encyclopedia of Genes and Genomes; GO, Gene Ontology; BP, biological processes; CC, cellular components; MF, molecular functions.

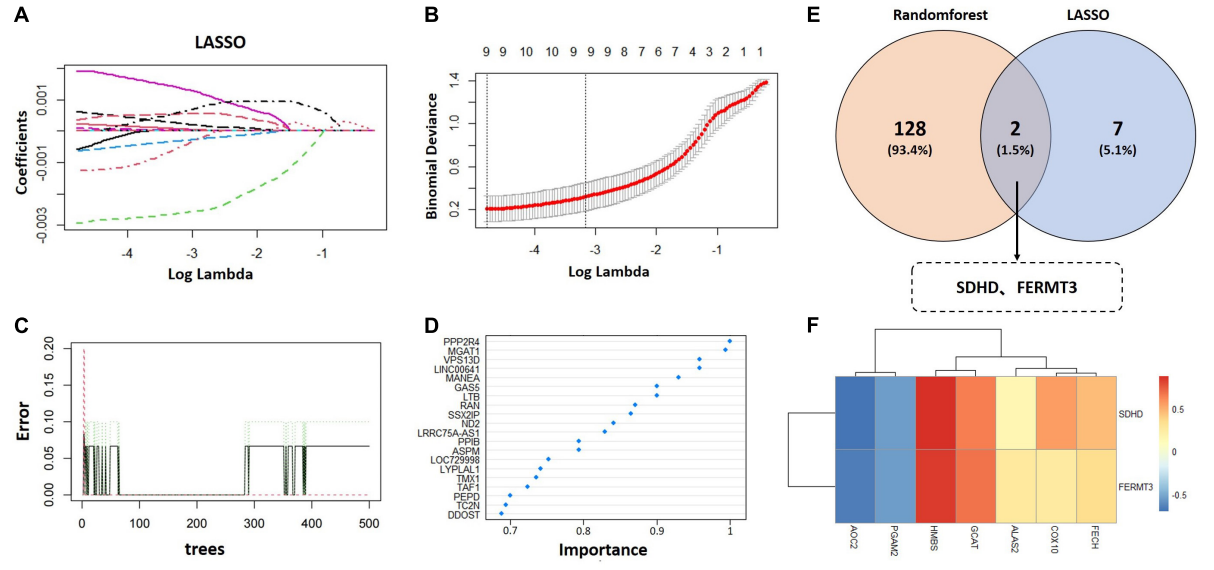

FIGURE 5
Selection of signature genes. **(A)** Parameter selection was performed through LASSO regression. **(B)** Elucidation of LASSO coefficient profiles for selected factors. **(C)** Random forest error rate versus the number of classification trees. **(D)** The top 20 relatively important genes. **(E)** Venn diagram to identify signature genes between LASSO and random forest. **(F)** Heatmap of correlation analysis between two signature genes and metabolism related genes (ALAS2, FECH, COX10, GCAT, HMBS, PGAM2, and AOC2). LASSO, the least absolute shrinkage and selection operator.

GSEA analysis of signature genes

Gene set enrichment analysis was performed for evaluating signaling pathways involved in the signature genes. The results showed that SDHD was significantly correlated with "emotional lability," "depression," and "abnormal fear anxiety related behavior" (Figure 6D). Meanwhile, "depression," "emotional blunting," and "abnormal fear anxiety related behavior" were detected for FERMT3 (Figure 6E). The results indicated that SDHD and FERMT3

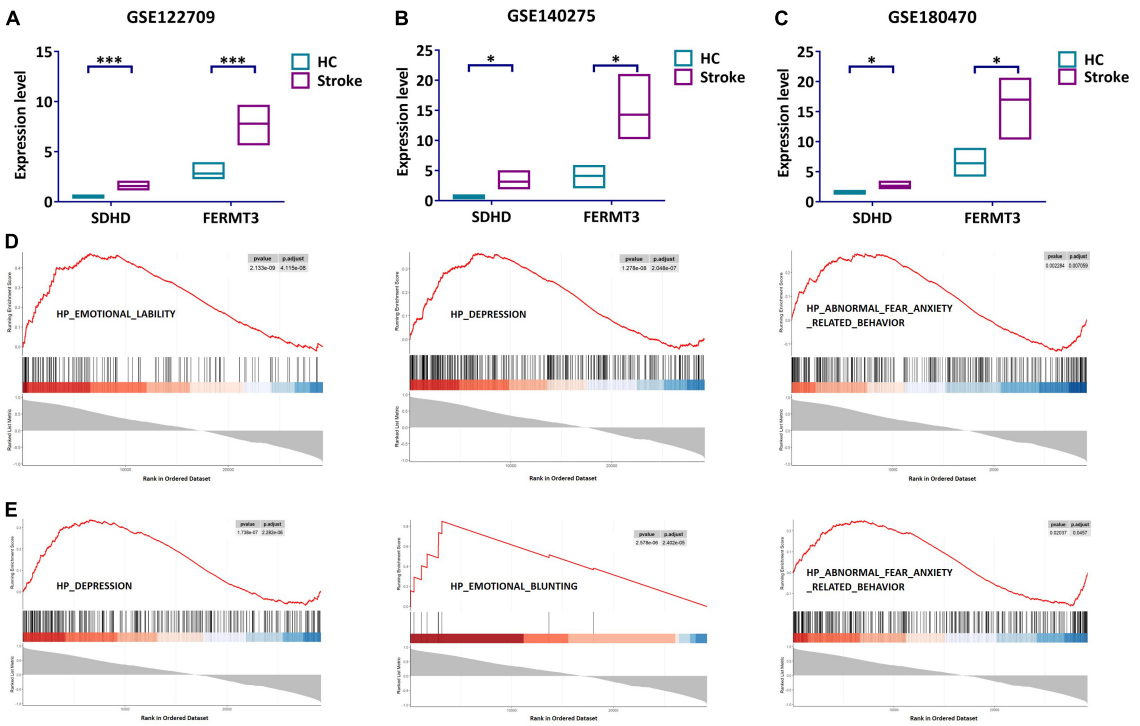

FIGURE 6
Validation and GSEA analysis of signature genes. **(A)** Expression level of SDHD and FERMT3 in GSE122709. **(B)** Expression level of SDHD and FERMT3 in GSE140275. **(C)** Expression level of SDHD and FERMT3 in GSE180470. **(D)** GSEA analysis of SDHD. **(E)** GSEA analysis of FERMT3. $^{*}P < 0.05$; $^{***}P < 0.001$. HC, healthy control; GSEA, gene set enrichment analysis.

played a key role for diagnosis of psychosocial state in stroke patients.

Diagnostic efficacy of signature genes in PSD patients

Based on GSEA analysis of two signature genes (SDHD and FERMT3), we found that they have a significant correlation with depression. Therefore, we collected 81 stroke patients who were assigned into the PSD group (mean HAMD score = 14.74) and non-PSD group (mean HAMD score = 3.41). There was no difference in baseline clinical features between groups (**Supplementary Table 6**). Meanwhile, expression of serum SDHD and FERMT3 in all patients were detected by ELISA kit. SDHD and FERMT3 presented higher expression in the PSD group than the non-PSD group (**Figures 7A, B**), indicating their potential roles in diagnosis of depression in stroke patients. To predict diagnostic performance of signature genes in stroke patients with depression, the nomogram model for the signature genes (SDHD and FERMT3) was built using "rms" package (**Figure 7C**). Calibration curves demonstrated that the difference between the real and predicted depression risks was very minimal, indicating the nomogram model enabled an accurate estimation (**Figure 7D**). In addition, decision curves analysis demonstrated that the nomogram provided a greater clinical benefit (**Figure 7E**). The ROC curve also showed that the model was able to help clinicians accurately diagnose depression of stroke patients (**Figure 7F**). Additionally, correlation analysis between two signature genes and several clinical traits (HAMD, NIHSS, BI, and mRS) indicated that SDHD ($r = 0.653$, $P < 0.001$) and FERM3 ($r = 0.728$, $P < 0.001$) were positively related HAMD, while SDHD also displayed a negative association with Barthel index ($r = -0.224$, $P = 0.044$) (**Figures 7G, H**).

Discussion

In this study, we included three datasets (GSE140275, GSE122709, GSE180470) with 27 patients for data analysis. We first screened 1,724 DEGs in GSE140275 including 861 upregulated genes and 863 downregulated genes. Subsequent KEGG enrichment analysis showed "porphyrin metabolism" and "glycine, serine and threonine metabolism" were highly enriched. Recent research reveals that stroke causes systemic complications, including hyperlipemia, high blood viscosity, dysfunctional gut microbiota, and a leaky gut (Yamashiro et al., 2017; Chen et al., 2019a). Chen et al. (2019b) demonstrated that stroke would cause gut microbiota dysbiosis, translocation of gut microbiota, and disruption to the gut barrier. And supplementation of short chain fatty acids (SCFAs), especially butyric acid, could remodel the gut microbiota and treat stroke (Chen et al., 2019a). Moreover, with the development of biology, metabolomics was applied to explore biomarkers and mechanisms of stroke by identifying metabolic alterations. Several studies reported the increase in ketone bodies levels in rats with stroke compared with sham group (Chen et al., 2019c; Wang et al., 2019). Fu et al. (2019) reported a decrease in β-hydroxybutyric acid level in serum but an increase in brain tissue in stroke rats, providing more energy for brain. These

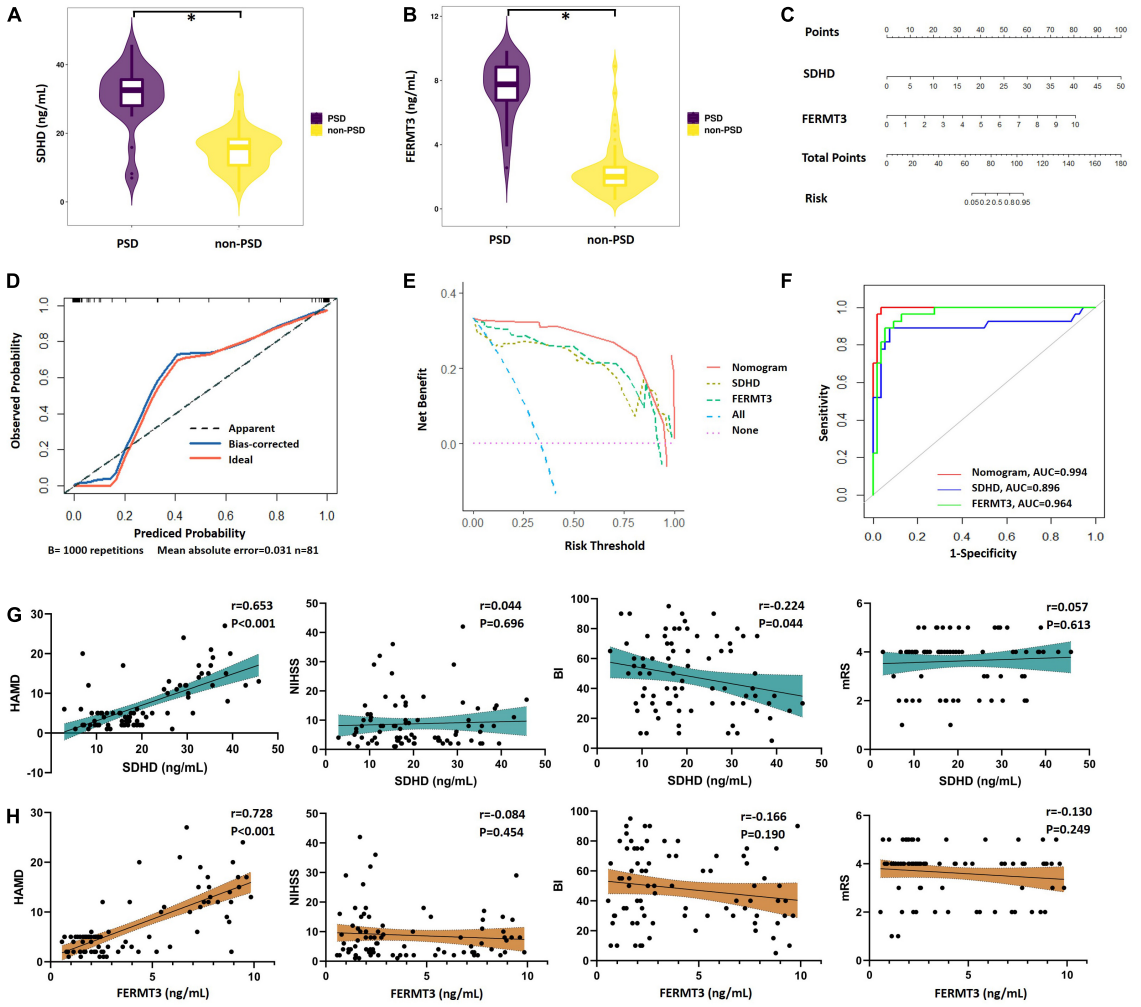

FIGURE 7
Performance of signature genes in PSD patients. **(A)** Expression level of SDHD in PSD and non-PSD groups. **(B)** Expression level of FERMT3 in PSD and non-PSD groups. **(C)** Nomograms for the prediction of the PSD risk. **(D)** Scatter diagram of calibration plot for internal verification of the nomogram model. **(F)** DCA curves of the nomogram model. **(E)** ROC curves of the nomogram model. **(G)** Correlation between expression of SDHD and four clinical traits (HAMD, NIHSS, BI, and mRS). **(H)** Correlation between expression of FERMT3 and four clinical traits (HAMD, NIHSS, BI, and mRS). PSD, post-stroke depression; DCA, decision curve analysis; ROC, receiver operating characteristic; AUC, area under the curve; HAMD, Hamilton Depression Rating Scale 17-item; NIHSS, National Institute of Health Stroke Scale; BI, Barthel index; mRS, Modified Rankin Scale. $^{*}P < 0.05$.

studies suggest that metabolism features strongly correlate with prevention, diagnosis and treatment of stroke. Based on the role of metabolism in stroke, we extracted seven genes related to the "porphyrin metabolism" and "glycine, serine and threonine metabolism" pathways, including ALAS2, FECH, COX10, GCAT, HMBS, PGAM2, and AOC2. We then performed correlation analysis between these genes enriched in these two pathways in GSE140275 and all genes in GSE122709 to identify metabolism related genes. A total of 8,188 metabolism related genes were identified. Nevertheless, with the help of advanced bioinformatic approaches genetic information could be further derived.

Weighted gene co-expression network analysis (WGCNA) is a frequently applied method to identify co-expression pattern at whole transcriptome level. Wang et al. (2019) performed WGCNA analysis to investigate co-expression modules related with osteosarcoma and found genes in brown module might be related with carcinogenesis of osteosarcoma. In addition, there were several studies screened key module genes related to stroke by WGCNA analysis (Fan et al., 2022; Zheng et al., 2022). However, metabolism related pathways and key genes in stroke are seldomly identified. Therefore, we performed WGCNA analysis of GSE122709 to identify 24 gene modules. No significant correlation between dividing modules was found. Module-traits relationship analysis indicated that Meroyalblue and Megrey modules were significantly associated with stroke disease. After this step, we interacted DEGs in GSE122709, genes in Meroyalblue and MEgrey modules, and metabolism related gene and showed 554 metabolism related candidate hub genes. Nonetheless, a single WGCNA analysis had significant limitations and inaccuracies (Tzimas et al., 2019). Currently, studies applied WGCNA were normally combined with multiple machine learning algorithms to identify biomarkers for disease prognosis and diagnosis. Zhao et al. (2022) identified four core genes (BTN3A2, CYFIP2, ST8SIA1, and TYMS) as biomarker for diagnosis of rheumatoid arthritis *via* comprehensive analysis of WGCNA, LASSO, random forest, and support vector machine analysis. By WGCNA, LASSO, and random forest algorithms,

Fan et al. (2022) obtained five signature genes (UPP1, S100A9, KIF1B, S100A12, SLC26A8) and emerged remarkable diagnostic performance in pediatric septic shock. In the current study, LASSO regression analysis and random forest algorithms found two signature genes, then three validation datasets, including GSE140275, GSE122709, and GSE180470, confirmed that SDHD and FERMT3 were highly expressed in the stroke group.

SDHD, one subunit of succinate dehydrogenase (SDH), dual roles in respiration by transferring electrons from succinate to ubiquinone in the mitochondrial electron transport chain (ETC) and catalyzing oxidation of succinate to fumarate in the mitochondrial Krebs cycle (Cecchini, 2003; Sun et al., 2005). Researchers reported mutations of SDHD in patients with hereditary pheochromocytomas and hereditary paragangliomas (Baysal et al., 2000). *In vitro* experiment performed by Bandara et al. (2021) demonstrated that mutation of SDHD *via* CRISPR/Cas9 approach could suppress glycolysis and overall ATP synthesis in HEK293. Overexpression of SDHD could significantly suppressed cell proliferation *in vitro* and tumor growth of HCC cells *in vivo* (Yuan et al., 2022). FERMT3 is a member of the kindlin family of binding proteins containing the FERM domain (Rognoni et al., 2016). FERMT3 mediates integrin activation and integrin-ligand binding. Therefore, FERMT3 is closely related to various biological activities, including cell adhesion, spreading, cell survival, proliferation and differentiation (Rognoni et al., 2016). Mutations of FERMT3 gene could cause leukocyte adhesion deficiency type III (LAD III) (Kuijpers et al., 2009). Liu et al. (2021) performed RNA sequencing in patients with triple-negative breast cancer and identified FERMT3 as protective gene in compound kushen injection treatment. Nonetheless, correlations of FERMT3 and SDHD with stroke have not been previously reported.

Post-stroke depression (PSD), the most common psychiatric problem after stroke, is an independent risk factor of stroke mortality (D'Anci et al., 2019). PSD is closely associated with worse outcomes of physical and cognitive recovery, functioning, and health related quality of life (Villa et al., 2018). It is worth noting that PSD might halt or impede rehabilitation treatments. However, the complex pathophysiology of PSD is still only partly known till now. The current evidence indicates genetic factors as major aetiopathological predictors for PSD. Yang et al. (2010) reported that IL-18 level in serum on day 7 after admission might predict the risk of PSD. Plasma levels of glutamate and glutamate oxaloacetate transaminase at admission were also reported to be closely related PSD within 3 months (Cheng et al., 2014). To further probe the role of hub genes in stroke, we performed a GSEA analysis of signature genes. The results demonstrated that SDHD and FERMT3 were significantly enriched in depression. Then we validated our findings in stroke patients with and without depression. We found increase expression levels of SDHD and FERMT3 in stroke patients with depression, compatible with our previous research inferences. In addition, based on the two signature genes (SDHD and FERMT3) that we identified, we successfully established a PSD diagnosis for evaluating diagnosis value of SDHD and FERMT3 in our PSD cohort. Nomogram model showed great predictive ability and clinical usefulness. Meanwhile, AUC values of SDHD and FERMT3 were 0.896 and 0.964. Our results suggested that SDHD and FERMT3 might play essential roles in diagnosis of PSD. Finally, we performed correlation analysis of two signature genes and several clinical traits. We found that the SDHD and FERM3 were positively correlated with depression, which suggested that SDHD and FERMT3 had certain therapeutic predictive value in PSD. Moreover, SDHD was also found a negative correlation with activities of daily living in this study. Considering the feature of this parameters, it suggested that these two signature genes may also serve as biomarkers to monitor the mental functional prognosis in patients with PSD (van Hulsteijn et al., 2013).

The present study also has certain shortcomings. Firstly, we collected data from public databases with small samples. There could have been a selection bias. Large datasets of stroke patients are limited, so we tried to minimize the bias of our results by validating signature genes across multiple datasets. Secondly, the metabolism related-pathways and -hub genes in stroke lack literature support and required further confirmation. Thirdly, although two metabolism related signature genes were identified as potential predictors for PSD, larger patient cohorts should be examined in the future to validate the correlation between two signature genes (SDHD and FERMT3) with PSD. Then further *in vivo* or *in vitro* studies should be carried out to validate diagnostic value and potential therapeutic value.

Conclusion

In conclusion, we identified two signature genes (SDHD and FERMT3) in peripheral blood of stroke patients by machine learning. SDHD and FERMT3 were found to be significantly associated with depression, and were identified as diagnostic and therapeutic signatures by our stroke cohorts with and without PSD, which could be a valuable reference for future clinical practice.

Data availability statement

The original contributions presented in this study are included in the article/**Supplementary material**, further inquiries can be directed to the corresponding authors.

Ethics statement

The studies involving human participants were reviewed and approved by the Committee of Institutional Ethics of the First Affiliated Hospital of Nanjing Medical University. The patients/participants provided their written informed consent to participate in this study.

Author contributions

YD, YZhe, BY, and RC designed the current study. XZ, XW, and ShuweiW collected the clinical information. YZha and SongW completed data downloading and processing. XZ, ZW, and YZha performed bioinformatics analysis. QY performed ELISA testing. YZhe, XZ, and YZha drafted the manuscript. YD supervised and modified the drafting process. All authors contributed to the article and approved the submitted version.

Funding

This study was funded by the National Natural Science Foundation of China (82000529 and 82272595), the Natural Science Foundation of Jiangsu Province (SBK2020042595), and the National Key Research & Development Program of the Ministry of Science and Technology of the People's Republic of China (2018YFC2002300 and 2018YFC2002301).

Conflict of interest

The authors declare that the research was conducted in the absence of any commercial or financial relationships that could be construed as a potential conflict of interest.

Publisher's note

All claims expressed in this article are solely those of the authors and do not necessarily represent those of their affiliated organizations, or those of the publisher, the editors and the reviewers. Any product that may be evaluated in this article, or claim that may be made by its manufacturer, is not guaranteed or endorsed by the publisher.

Supplementary material

The Supplementary Material for this article can be found online at: https://www.frontiersin.org/articles/10.3389/fnins.2023.1146620/full#supplementary-material

SUPPLEMENTARY TABLE 1
Differentially expressed genes in GSE140275.

SUPPLEMENTARY TABLE 2
Differentially expressed genes in GSE122709.

SUPPLEMENTARY TABLE 3
Correlation analysis results of modules and clinical features.

SUPPLEMENTARY TABLE 4
Signature genes selected by least absolute shrinkage and selection operator (LASSO) analysis.

SUPPLEMENTARY TABLE 5
Signature genes determined by random forest analysis.

References

Bandara, A., Drake, J., and Brown, D. (2021). Complex II subunit SDHD is critical for cell growth and metabolism, which can be partially restored with a synthetic ubiquinone analog. *BMC Mol. Cell Biol.* 22:35. doi: 10.1186/s12860-021-00370-w

Baysal, B., Ferrell, R., Willett-Brozick, J., Lawrence, E., Myssiorek, D., Bosch, A., et al. (2000). Mutations in SDHD, a mitochondrial complex II gene, in hereditary paraganglioma. *Science* 287, 848–851.

Cai, W., Mueller, C., Li, Y., Shen, W., and Stewart, R. (2019). Post stroke depression and risk of stroke recurrence and mortality: A systematic review and meta-analysis. *Ageing Res. Rev.* 50, 102–109.

Cecchini, G. (2003). Function and structure of complex II of the respiratory chain. *Annu. Rev. Biochem.* 72, 77–109.

Chen, R., Wu, P., Cai, Z., Fang, Y., Zhou, H., Lasanajak, Y., et al. (2019a). Puerariae lobatae radix with Chuanxiong rhizoma for treatment of cerebral ischemic stroke by remodeling gut microbiota to regulate the brain-gut barriers. *J. Nutr. Biochem.* 65, 101–114. doi: 10.1016/j.jnutbio.2018.12.004

Chen, R., Xu, Y., Wu, P., Zhou, H., Lasanajak, Y., Fang, Y., et al. (2019b). Transplantation of fecal microbiota rich in short chain fatty acids and butyric acid treat cerebral ischemic stroke by regulating gut microbiota. *Pharmacol. Res.* 148:104403. doi: 10.1016/j.phrs.2019.104403

Chen, S., Sun, M., Zhao, X., Yang, Z., Liu, W., Cao, J., et al. (2019c). Neuroprotection of hydroxysafflor yellow A in experimental cerebral ischemia/reperfusion injury via metabolic inhibition of phenylalanine and mitochondrial biogenesis. *Mol. Med. Rep.* 19, 3009–3020. doi: 10.3892/mmr.2019.9959

Cheng, S., Zhao, Y., Li, J., Chen, X., Wang, R., and Zeng, J. (2014). Plasma levels of glutamate during stroke is associated with development of post-stroke depression. *Psychoneuroendocrinology* 47, 126–135. doi: 10.1016/j.psyneuen.2014.05.006

D'Anci, K., Uhl, S., Oristaglio, J., Sullivan, N., and Tsou, A. (2019). Treatments for post-stroke motor deficits and mood disorders: A systematic review for the 2019 U.S. department of Veterans affairs and U.S. department of defense guidelines for stroke rehabilitation. *Ann. Intern. Med.* 171, 906–915. doi: 10.7326/M19-2414

Dong, L., Brown, D., Chervin, R., Case, E., Morgenstern, L., and Lisabeth, L. (2021). Pre-stroke sleep duration and post-stroke depression. *Sleep Med.* 77, 325–329. doi: 10.1016/j.sleep.2020.04.025

Fan, J., Shi, S., Qiu, Y., Liu, M., and Shu, Q. (2022). Analysis of signature genes and association with immune cells infiltration in pediatric septic shock. *Front. Immunol.* 13:1056750. doi: 10.3389/fimmu.2022.1056750

Fan, X., Chen, H., Xu, C., Wang, Y., Yin, P., Li, M., et al. (2022). S1PR3, as a core protein related to ischemic stroke, is involved in the regulation of blood-brain barrier damage. *Front. Pharmacol.* 13:834948. doi: 10.3389/fphar.2022.834948

Fu, X., Wang, J., Liao, S., Lv, Y., Xu, D., Yang, M., et al. (2019). (1)H NMR-based metabolomics reveals refined-Huang-Lian-Jie-Du-decoction (BBG) as a potential ischemic stroke treatment drug with efficacy and a favorable therapeutic window. *Front. Pharmacol.* 10:337. doi: 10.3389/fphar.2019.00337

GBD 2019 Stroke Collaborators (2021). Global, regional, and national burden of stroke and its risk factors, 1990-2019: A systematic analysis for the Global Burden of Disease Study 2019. *Lancet Neurol.* 20, 795–820.

He, D., Li, Q., Du, G., Meng, G., Sun, J., and Chen, S. (2021). An integration of network pharmacology and experimental verification to investigate the mechanism of guizhi to treat nephrotic syndrome. *Front. Pharmacol.* 12:755421. doi: 10.3389/fphar.2021.755421

He, L., Wang, J., Zhang, L., Wang, F., Dong, W., and Yang, H. (2020). Admission heart rate variability is associated with poststroke depression in patients with acute mild-moderate ischemic stroke. *Front. Psychiatry* 11:696. doi: 10.3389/fpsyt.2020.00696

Jiang, W., Gong, L., Liu, F., Ren, Y., and Mu, J. (2021). Alteration of gut microbiome and correlated lipid metabolism in post-stroke depression. *Front. Cell. Infect. Microbiol.* 11:663967. doi: 10.3389/fcimb.2021.663967

Kaida, Y., Fukami, K., Matsui, T., Higashimoto, Y., Nishino, Y., Obara, N., et al. (2013). DNA aptamer raised against AGEs blocks the progression of experimental diabetic nephropathy. *Diabetes* 62, 3241–3250.

Kamal, A., Khoja, A., Usmani, B., Magsi, S., Malani, A., Peera, Z., et al. (2020). Effect of 5-minute movies shown via a mobile phone app on risk factors and mortality after stroke in a low- to middle-income country: Randomized controlled trial for the stroke caregiver dyad education intervention (Movies4Stroke). *JMIR mHealth uHealth* 8:e12113. doi: 10.2196/12113

Kang, J., Choi, Y., Kim, I., Lee, H., Kim, H., Baik, S., et al. (2021). LASSO-based machine learning algorithm for prediction of lymph node metastasis in T1 colorectal cancer. *Cancer Res. Treat.* 53, 773–783. doi: 10.4143/crt.2020.974

Klinedinst, N., Dunbar, S., and Clark, P. (2012). Stroke survivor and informal caregiver perceptions of poststroke depressive symptoms. *J. Neurosci. Nurs.* 44, 72–81.

Kuijpers, T., van de Vijver, E., Weterman, M., de Boer, M., Tool, A., van den Berg, T., et al. (2009). LAD-1/variant syndrome is caused by mutations in FERMT3. *Blood* 113, 4740–4746. doi: 10.1182/blood-2008-10-182154

Langfelder, P., and Horvath, S. (2008). WGCNA: An R package for weighted correlation network analysis. *BMC Bioinformatics* 9:559. doi: 10.1186/1471-2105-9-559

Li, G., Miao, J., Sun, W., Song, X., Lan, Y., Zhao, X., et al. (2020). Lower serum uric acid is associated with post-stroke depression at discharge. *Front. Psychiatry* 11:52. doi: 10.3389/fpsyt.2020.00052

Li, Y., Cao, L., Liu, L., and Qi, Q. (2017). Serum levels of homocysteine at admission are associated with post-stroke depression in acute ischemic stroke. *Neurol. Sci.* 38, 811–817. doi: 10.1007/s10072-017-2848-2

Li, Z., Cui, Y., Feng, J., and Guo, Y. (2020). Identifying the pattern of immune related cells and genes in the peripheral blood of ischemic stroke. *J. Transl. Med.* 18:296.

Lin, S., Luan, X., He, W., Ruan, Y., Yuan, C., Fan, A., et al. (2020). Post-stroke depression and estimated glomerular filtration rate: A prospective stroke cohort. *Neuropsychiatr. Dis. Treat.* 16, 201–208. doi: 10.2147/NDT.S225905

Lin, W., Wang, Y., Chen, Y., Wang, Q., Gu, Z., and Zhu, Y. (2021). Role of calcium signaling pathway-related gene regulatory networks in ischemic stroke based on multiple WGCNA and single-cell analysis. *Oxid. Med. Cell Longev.* 2021:8060477. doi: 10.1155/2021/8060477

Liu, C., Zhang, X., Chai, H., Xu, S., Liu, Q., Luo, Y., et al. (2022). Identification of immune cells and key genes associated with Alzheimer's disease. *Int. J. Med. Sci.* 19, 112–125.

Liu, K., Chen, S., and Lu, R. (2021). Identification of important genes related to ferroptosis and hypoxia in acute myocardial infarction based on WGCNA. *Bioengineered* 12, 7950–7963. doi: 10.1080/21655979.2021.1984004

Liu, M., Li, G., Tang, J., Liao, Y., Li, L., Zheng, Y., et al. (2018). The influence of sex in stroke thrombolysis: A systematic review and meta-analysis. *J. Clin. Neurol.* 14, 141–152.

Liu, X., Wu, Y., Zhang, Y., Bu, D., Wu, C., Lu, S., et al. (2021). High throughput transcriptome data analysis and computational verification reveal immunotherapy biomarkers of compound Kushen injection for treating triple-negative breast cancer. *Front. Oncol.* 11:747300. doi: 10.3389/fonc.2021.747300

Luft, A., McCombe-Waller, S., Whitall, J., Forrester, L., Macko, R., Sorkin, J., et al. (2004). Repetitive bilateral arm training and motor cortex activation in chronic stroke: A randomized controlled trial. *JAMA* 292, 1853–1861.

Mantero, A., and Ishwaran, H. (2021). Unsupervised random forests. *Stat. Anal. Data Min.* 14, 144–167.

Qiao, J., Sui, R., Zhang, L., and Wang, J. (2020). Construction of a risk model associated with prognosis of post-stroke depression based on magnetic resonance spectroscopy. *Neuropsychiatr. Dis. Treat.* 16, 1171–1180. doi: 10.2147/NDT.S245129

Ritchie, M., Phipson, B., Wu, D., Hu, Y., Law, C., Shi, W., et al. (2015). limma powers differential expression analyses for RNA-sequencing and microarray studies. *Nucleic Acids Res.* 43, e47. doi: 10.1093/nar/gkv007

Robin, X., Turck, N., Hainard, A., Tiberti, N., Lisacek, F., Sanchez, J., et al. (2011). pROC: An open-source package for R and S+ to analyze and compare ROC curves. *BMC Bioinformatics* 12:77. doi: 10.1186/1471-2105-12-77

Robinson, M., McCarthy, D., and Smyth, G. (2010). edgeR: A bioconductor package for differential expression analysis of digital gene expression data. *Bioinformatics* 26, 139–140.

Rognoni, E., Ruppert, R., and Fässler, R. (2016). The kindlin family: Functions, signaling properties and implications for human disease. *J. Cell Sci.* 129, 17–27. doi: 10.1242/jcs.161190

Shi, Y., Guo, L., Chen, Y., Xie, Q., Yan, Z., Liu, Y., et al. (2021). Risk factors for ischemic stroke: Differences between cerebral small vessel and large artery atherosclerosis aetiologies. *Folia Neuropathol.* 59, 378–385.

Subramanian, A., Tamayo, P., Mootha, V., Mukherjee, S., Ebert, B., Gillette, M., et al. (2005). Gene set enrichment analysis: A knowledge-based approach for interpreting genome-wide expression profiles. *Proc. Natl. Acad. Sci. U.S.A.* 102, 15545–15550.

Sun, F., Huo, X., Zhai, Y., Wang, A., Xu, J., Su, D., et al. (2005). Crystal structure of mitochondrial respiratory membrane protein complex II. *Cell* 121, 1043–1057.

Sun, P., Ma, F., Xu, Y., Zhou, C., Stetler, R., and Yin, K. (2021). Genetic deletion of endothelial microRNA-15a/16-1 promotes cerebral angiogenesis and neurological recovery in ischemic stroke through Src signaling pathway. *J. Cereb. Blood Flow Metab.* 41, 2725–2742. doi: 10.1177/0271678X211010351

Tzimas, C., Rau, C., Buergisser, P., Jean-Louis, G. Jr., Lee, K., Chukwuneke, J., et al. (2019). WIPI1 is a conserved mediator of right ventricular failure. *JCI Insight* 5:e122929. doi: 10.1172/jci.insight.122929

Upreti, H., Kasmani, J., Dane, K., Braunstein, E., Streiff, M., Shanbhag, S., et al. (2019). Reduced ADAMTS13 activity during TTP remission is associated with stroke in TTP survivors. *Blood* 134, 1037–1045. doi: 10.1182/blood.2019001056

van Hulsteijn, L., Louisse, A., Havekes, B., Kaptein, A., Jansen, J., Hes, F., et al. (2013). Quality of life is decreased in patients with paragangliomas. *Eur. J. Endocrinol.* 168, 689–697.

Villa, R., Ferrari, F., and Moretti, A. (2018). Post-stroke depression: Mechanisms and pharmacological treatment. *Pharmacol. Ther.* 184, 131–144.

Wang, D., Wang, Q., Chen, R., Yang, S., Li, Z., and Feng, Y. (2019). Exploring the effects of Gastrodia elata Blume on the treatment of cerebral ischemia-reperfusion injury using UPLC-Q/TOF-MS-based plasma metabolomics. *Food Funct.* 10, 7204–7215. doi: 10.1039/c9fo01729a

Wang, J., Wang, Y., Zhong, Y., Li, X., Du, S., Xie, P., et al. (2019). Identification of co-expression modules and pathways correlated with osteosarcoma and its metastasis. *World J. Surg. Oncol.* 17:46.

Wang, M., Wang, L., Pu, L., Li, K., Feng, T., Zheng, P., et al. (2020). LncRNAs related key pathways and genes in ischemic stroke by weighted gene co-expression network analysis (WGCNA). *Genomics* 112, 2302–2308. doi: 10.1016/j.ygeno.2020.01.001

Wang, X., Li, Y., Li, M., Lu, J., Zhao, J., Sun, X., et al. (2012). Glutamate level detection by magnetic resonance spectroscopy in patients with post-stroke depression. *Eur. Arch. Psychiatry Clin. Neurosci.* 262, 33–38. doi: 10.1007/s00406-011-0209-3

Xu, D., Wang, Y., Liu, X., Zhou, K., Wu, J., Chen, J., et al. (2021). Development and clinical validation of a novel 9-gene prognostic model based on multi-omics in pancreatic adenocarcinoma. *Pharmacol. Res.* 164:105370. doi: 10.1016/j.phrs.2020.105370

Yamashiro, K., Tanaka, R., Urabe, T., Ueno, Y., Yamashiro, Y., Nomoto, K., et al. (2017). Gut dysbiosis is associated with metabolism and systemic inflammation in patients with ischemic stroke. *PLoS One* 12:e0171521. doi: 10.1371/journal.pone.0171521

Yang, L., Zhang, Z., Sun, D., Xu, Z., Zhang, X., and Li, L. (2010). The serum interleukin-18 is a potential marker for development of post-stroke depression. *Neurol. Res.* 32, 340–346. doi: 10.1179/016164110X12656393665080

Yu, B., Zhang, X., Cheng, Y., Liu, L., YanJiang, Wang, J., et al. (2022). The effects of the biceps brachii and brachioradialis on elbow flexor muscle strength and spasticity in stroke patients. *Neural Plast.* 2022:1295908. doi: 10.1155/2022/1295908

Yuan, T., Zhou, T., Qian, M., Du, J., Liu, Y., Wang, J., et al. (2022). SDHA/B reduction promotes hepatocellular carcinoma by facilitating the deNEDDylation of cullin1 and stabilizing YAP/TAZ. *Hepatology* doi: 10.1002/hep.32621

Zhang, Y., Zhang, P., Shen, X., Tian, S., Wu, Y., Zhu, Y., et al. (2013). Early exercise protects the blood-brain barrier from ischemic brain injury via the regulation of MMP-9 and occludin in rats. *Int. J. Mol. Sci.* 14, 11096–11112. doi: 10.3390/ijms140611096

Zhao, Z., He, S., Yu, X., Lai, X., Tang, S., Mariya, M., et al. (2022). Analysis and experimental validation of rheumatoid arthritis innate immunity gene CYFIP2 and pan-cancer. *Front. Immunol.* 13:954848. doi: 10.3389/fimmu.2022.954848

Zheng, P., Chen, L., Liu, P., Pan, H., Fan, W., and Liu, Z. (2022). Identification of immune-related key genes in the peripheral blood of ischaemic stroke patients using a weighted gene coexpression network analysis and machine learning. *J. Transl. Med.* 20:361. doi: 10.1186/s12967-022-03562-w

Zhou, Y., Wu, W., Lindholt, J., Sukhova, G., Libby, P., Yu, X., et al. (2015). Regulatory T cells in human and angiotensin II-induced mouse abdominal aortic aneurysms. *Cardiovasc. Res.* 107, 98–107.

Zhou, Z., Liang, Y., Qu, H., Zhao, M., Guo, F., Zhao, C., et al. (2018). Plasma homocysteine concentrations and risk of intracerebral hemorrhage: A systematic review and meta-analysis. *Sci. Rep.* 8:2568. doi: 10.1038/s41598-018-21019-3

Zhu, M., Zeng, Q., Fan, T., Lei, Y., Wang, F., Zheng, S., et al. (2022). Clinical significance and immunometabolism landscapes of a novel recurrence-associated lipid metabolism signature in early-stage lung adenocarcinoma: A comprehensive analysis. *Front. Immunol.* 13:783495. doi: 10.3389/fimmu.2022.783495

frontiers | Frontiers in Neuroscience

TYPE Systematic Review
PUBLISHED 11 April 2023
DOI 10.3389/fnins.2023.1157920

OPEN ACCESS

EDITED BY
Feng Zhang,
Third Hospital of Hebei Medical University,
China

REVIEWED BY
Shanggui Su,
Guangxi Medical University,
China
Dongxu Chen,
Nanxishan Hospital of Guangxi Zhuang
Autonomous Region,
China

*CORRESPONDENCE
Lian Duan
✉ Duanlian202210@163.com
Lei Yang
✉ leon_yang30@163.com

†These authors have contributed equally to this study

SPECIALTY SECTION
This article was submitted to Translational Neuroscience, a section of the journal Frontiers in Neuroscience

RECEIVED 03 February 2023
ACCEPTED 20 March 2023
PUBLISHED 11 April 2023

CITATION
Lin X, Zhang Y, Chen X, Wen L, Duan L and Yang L (2023) Effects of noninvasive brain stimulation on dual-task performance in different populations: A systematic review. *Front. Neurosci.* 17:1157920. doi: 10.3389/fnins.2023.1157920

Effects of noninvasive brain stimulation on dual-task performance in different populations: A systematic review

Xiaoying Lin[1,2†], Yanming Zhang[3†], Xi Chen[1], Lifen Wen[1], Lian Duan[4*] and Lei Yang[1*]

[1]Department of Rehabilitation Medicine, The Second People's Hospital of Kunming, Yunnan Province, China, [2]School of Rehabilitation, Kunming Medical University, Yunnan Province, China, [3]Department of Rehabilitation Medicine, Xuanwu Hospital, Capital Medical University, Beijing, China, [4]Department of Manipulation, Yuxi Hospital of Traditional Chinese Medicine, Yunnan Province, China

Background: Increasing research has investigated the use of noninvasive brain stimulation (NIBS) on augmenting dual-task (DT) performance.

Objective: To investigate the effects of NIBS on DT performance in different populations.

Methods: Extensive electronic database search (from inception to November 20, 2022) was conducted in PubMed, Medline, Cochrane Library, Web of Science and CINAHL to identify randomized controlled trials (RCTs) that investigated the effects of NIBS on DT performance. Main outcomes were balance/mobility and cognitive function under both single-task (ST) and DT conditions.

Results: Fifteen RCTs were included, involving two types of intervention techniques: transcranial direct current stimulation (tDCS) (twelve RCTs) and repetitive transcranial magnetic stimulation (rTMS) (three RCTs); and four different population groups: healthy young adults, older adults, Parkinson's disease (PD), and stroke. For tDCS, under DT condition, significant improvement in speed was only observed in one PD and one stroke RCT, and stride time variability in one older adults RCT. Reduction in DTC in some gait parameters was demonstrated in one RCT. Only one RCT showed significant reduction in postural sway speed and area during standing under DT condition in young adults. For rTMS, significant improvements in fastest walking speed and time taken to Timed-up-and-go test under both ST and DT conditions were observed at follow-up in one PD RCT only. No significant effect on cognitive function in any RCT was observed.

Conclusion: Both tDCS and rTMS showed promising effects in improving DT walking and balance performance in different populations, however, due to the large heterogeneity of included studies and insufficient data, any firm conclusion cannot be drawn at present.

KEYWORDS

noninvasive brain stimulation, transcranial direct current stimulation, transcranial magnetic stimulation, dual-task, systematic review

Introduction

Performing two tasks simultaneously (i.e., dual-task (DT) conditions) are common scenarios in many activities of daily living, for example, walking while talking, or while negotiating obstacles (Hillel et al., 2019). Therefore, how to improve the DT function is a topic of significance. Although a few systematic reviews have examined the efficacy of DT training on DT performance in different population (Delong and Wichmann, 2015; Yang et al., 2018; De Freitas et al., 2020), the optimal strategy of improving DT function in different population is yet to be developed.

Performing DT activities is the result of interplay of different structures of the central nervous system: the dorsolateral prefrontal cortex (DLPFC), supplementary motor area (SMA), primary motor cortex (M1), and cerebellum (Vitorio et al., 2017). As compared to walking alone, additional attention and cognitive resources are required in these challenging conditions, thus making the two tasks compete for the limited cognitive resources (Tombu and Jolicoeur, 2003), which will lead to DT "costs" (i.e., decrements) in motor and/or cognitive task performance (Lundin-Olsson et al., 1997; Yang et al., 2018). Among them, the DLPFC, a brain region that plays a critical role in executive functions, mainly mediates the cognitive process involved in dual-tasking (Weiss et al., 2015).

At present, there are two types of non-invasive brain stimulation (NIBS): transcranial magnetic stimulation (TMS) and transcranial direct current stimulation (tDCS), which uses electricity or magnetic flux to stimulate the intracranial neural tissues in a non-invasive way to regulate the excitability of central nerves and may induce lasting changes in neural plasticity, thus improving the function of subjects (Hara et al., 2021). Recent NIBS studies have shown their promising potential in the rehabilitation of neurological diseases. For example, it has been found that TMS was effective when combined with conventional training in improving depression, cognitive function, upper limb motor function, balance and gait after stroke (Zhang et al., 2017; Begemann et al., 2020; Behrangrad et al., 2021; Hara et al., 2021; Xie et al., 2021). tDCS has also demonstrated its effects on enhancing learning, working memory, executive planning, picture naming, and motor recovery in healthy young adults (Nitsche et al., 2003; Fregni et al., 2005; Dockery et al., 2009), as well as in the treatment of bipolar depression patients (D'Urso et al., 2023). Nevertheless, current studies that investigated the effects of NIBS on DT performance in different populations are scarce. Only several studies suggested that the NIBS may reduce the cost of performing a cognitive task when combined with a ambulation or postural control task in different populations (Wrightson et al., 2015; Zhou et al., 2015; Manor et al., 2018).

To sum up, since the NIBS has demonstrated facilitating motor and cognitive process separately in different populations, it was postulated that NIBS would be potentially useful in performing motor and cognitive tasks simultaneously, i.e., improving DT performance. However, whether using NIBS can address motor-cognitive interference in different populations is yet to be explored. Therefore, the aim of this systematic review was to investigate the effects of NIBS on DT performance in different populations.

Methods

This systematic review was conducted according to the PRISMA guidelines (Page et al., 2021).

Search strategy

Two independent investigators performed extensively searches using the following databases: PubMed, Medline, Cochrane Library, Web of Science and CINAHL. The literature search was performed using the keyword combination: [(NIBS) OR (TMS) OR (tDCS)] AND [(dual-task) OR (cognitive-motor)] AND [(walking) OR (gait) OR (balance)]. In addition, we also performed forward searches with Web of Science, and screened the reference list of each included publication so as not to miss any potential literature that met our criteria. The last search was conducted on December 20, 2022. Details of search strategy for the PubMed were provided in Appendix 1. Similar strategies were adapted to other databases.

Eligibility criteria

The inclusion criteria were constructed as follows: (1) Both groups received the same intervention, except that the experimental group received TMS or tDCS intervention, while the control group received sham stimulation or no stimulation; (2) The outcomes involved the measures of motor or cognitive performance under DT condition; (3) The study design was randomized controlled RCT (RCT). The exclusion criteria were: (1) Case reports, non-experimental results, letters to the editor, conference reports, dissertations and reviews; (2) The full text of the publication was unavailable, despite contacted the authors.

Assessment of methodological quality

The methodological quality of each included publication was assessed by using the Cochrane risk of bias tool (The Cochrane Collaboration), which is rated by the five dimensions: selection bias, performance bias, detection bias, attrition bias and reporting bias, with a full score of 12[1]. A study that does not meet the six criteria items or has a fatal defect is considered to have a high risk of bias. For example, if the drop-out rate is greater than 50%, it is considered as a fatal defect.

Two independent investigators (LXY, ZYM) jointly analyzed and determined the risk of bias for each publications, any disagreement between them was discussed and resolved with the principal investigator (YL).

Data extraction and synthesis

Two independent investigators (LXY, ZYM) firstly screened the title and abstract of the searched publications. Then, the eligibility was

1 https://training.cochrane.org/handbook/current

further identified through full-text reading. If there was any disagreement, discussed and resolved with the third investigator (YL).

For the eligible publications, the first author extracted the general information about the study, e.g., participants' characteristics, intervention protocols, and outcome measures. The primary outcomes extracted were walking (speed, step length, cadence, etc) and balance (center of pressure-related parameters) measures under both single - task (ST) and DT condition, as well as the corresponding DT-cost (DTC), while the secondary outcomes were cognitive performance under both ST and DT conditions, and other functions.

Due to the large heterogeneity of the included studies (different populations, different measures and small number of eligible studies), meta-analysis for each outcome was not performed. However, if the between-group comparison was significant, in order to facilitate the comparison across RCTs, we calculated the effect size (Hedges' g) of gait, balance, cognition and other parameters under ST and DT conditions based on the original data given in the publications. For the follow-up results, we calculated the Hedges' g between the follow-up value and the pre-intervention value, in order to check whether the treatment effect still exists at the follow-up.

Result

Article selection and methodology assessment

The literature search process is shown in Figure 1, 1,023 publications were generated from the electronic search. After screening, 1,008 articles did not meet the inclusion criteria, thus were removed. Finally, 15 randomized controlled RCTs (RCTs) were identified in this review. The methodological quality of included RCTs was summarized in Table 1. The total risk of bias assessment score of the 15 included RCTs ranged from 7 to 10, indicating "low risks" (Table 1).

Participants' characteristics and intervention protocols

The demographics were summarized in Table 2, involving two types of intervention techniques: repetitive TMS (rTMS) (three RCTs) and tDCS (twelve RCTs); and four different population groups: healthy young adults (four RCTs, $N = 73$), older adults (four RCTs, $N = 100$), PD (five RCTs, $N = 132$), and stroke (two RCTs, $N = 63$). The average age of participants ranged from 21.1 (1) to 82 (4) years.

rTMS protocols

Three RCTs investigated the effects of rTMS in healthy young adults, individuals with stroke and individuals with PD respectively, with different stimulation protocols. Goh et al. (2019, 2020) applied one single-session 5 Hz rTMS to healthy young adults and individuals with stroke. The stimulation targets of the experimental group were in the left DLPFC or SMA, while the control group was in the M1 (Goh et al., 2019, 2020). Chung et al. (2020) set the target over the leg area of bilateral M1 with three different groups (1 Hz, 25 Hz and sham stimulation) for 12 sessions.

tDCS protocols

The effects of tDCS were examined in 12 RCTs, involving four different populations, namely, healthy young adults, older adults,

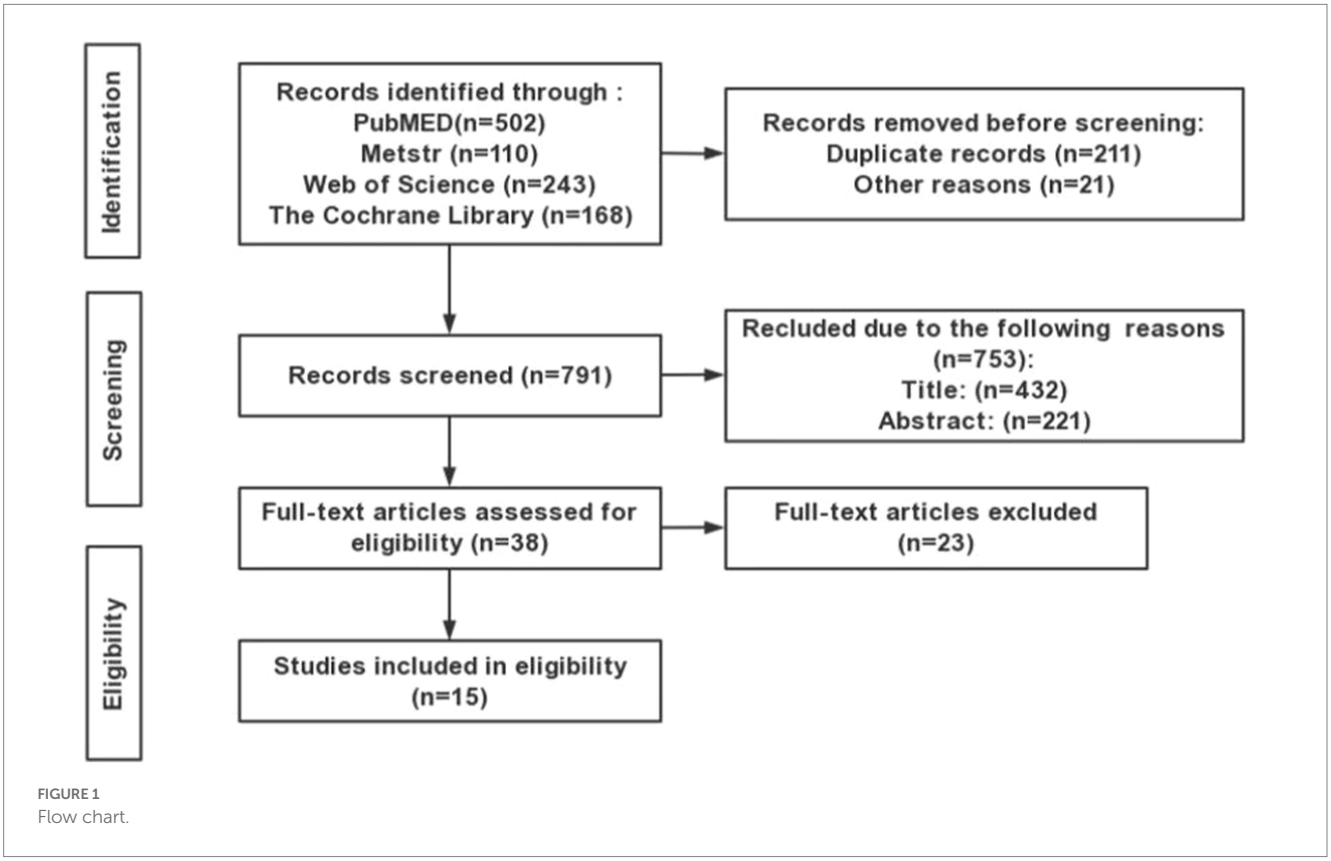

FIGURE 1
Flow chart.

TABLE 1 Risk of bias.

Study	Randomization adequate	Concealed allocation	Blind subjects	Blind therapists	Blind assessors	Was the drop-out rate described and acceptable?	Were all randomized participants analyzed in the group to which they were allocated?	Free of selective outcome reporting?	Similarity of baseline characteristics	Cointerventions avoided or similar	Compliance acceptable	Timing of the outcome assessments similar	Total risk of bias score
rTMS trials ($N = 3$)													
Goh et al. (2020)	✓	–	–	?	–	✓	✓	✓	✓	?	✓	✓	7
Goh et al. (2019)	✓	–	–	?	?	✓	✓	✓	✓	?	✓	✓	7
Chung et al. (2020)	✓	✓	✓	?	✓	✓	✓	✓	✓	?	✓	✓	10
tDCS trials													
Zhou et al. (2014)	✓	✓	✓	?	✓	✓	✓	✓	✓	?	✓	✓	10
Wrightson et al. (2015)	✓	✓	✓	?	✓	✓	✓	✓	✓	?	✓	✓	10
Pineau et al. (2021)	✓	–	✓	?	✓	✓	✓	✓	✓	?	✓	✓	9
Zhou et al. (2015)	✓	✓	✓	?	✓	✓	✓	✓	✓	?	✓	✓	10
Manor et al. (2016)	✓	✓	✓	?	✓	✓	✓	✓	✓	?	✓	✓	10
Manor et al. (2018)	✓	✓	✓	?	✓	✓	✓	✓	✓	?	✓	✓	10
Schneider et al. (2021)	✓	✓	✓	?	✓	✓	✓	✓	✓	?	✓	✓	10
Schabrun et al. (2016)	✓	✓	✓	?	✓	✓	✓	✓	✓	?	✓	✓	10
Swank et al. (2016)	✓	✓	✓	?	✓	✓	✓	✓	✓	?	✓	✓	10
Mishra and Thrasher (2021)	✓	✓	✓	?	✓	✓	✓	✓	✓	?	✓	✓	10
Wong et al. (2022a,b)	✓	✓	✓	?	✓	✓	✓	✓	✓	?	✓	✓	10
Wong et al. (2022a,b)	✓	✓	✓	?	✓	✓	✓	✓	✓	?	✓	✓	10

✓ = yes; – = no; ? = unclear.

10.3389/fnins.2023.1157920

TABLE 2 Characteristics of participants and intervention protocols.

Study	Characteristics of participants			Intervention protocols			
	Population and sample size (ratio of female)	Age (y) [Mean (SD)]	Disease onset duration (y)	EG	CG	Intervention period	Additional therapy
rTMS ($N = 3$)							
Goh et al. (2019)	Young EG1: 9 (55.6%) EG2: 10 (60%)	29.3 (5.8)	--	Site: EG1: DLPFC; EG2: SMA Parameters: 90% RMT, 5 Hz, ITI of 30s, 1,200 pulses	Site: the left M1 Parameters: 90% RMT, 5 Hz, ITI of 30s, 1,200 pulses	1 session	NR
Goh et al. (2020)	Stroke 15 (33%)	57.7 (9.7)	22.8 (16.7)	Site: EG1: DLPFC; EG2: SMA Parameters: 90% RMT, 5 Hz, ITI of 30s, 1,200 pulses	Site: the left M1 Parameters: 90% RMT, 5 Hz, ITI of 30s, 1,200 pulses	1 session	NR
Chung et al. (2020)	PD EG1: 17 (41%) EG2: 17 (47%) CG: 16 (56%)	EG1: 62.7 (6.8) EG2: 62.1 (5.7) CG: 62.1 (5.7)	EG: 5.2 (3.4) EG2: 7.5 (4.9) CG: 6.9 (3.3)	Site: the leg area of bilateral M1 Parameters: EG1: 25 Hz; EG2: 1 Hz; 80% RMT, ITI of 50s, 1,200 pulses	Site: the leg area of bilateral M1 Parameters: sham	4 days/week, for 3 weeks (12 sessions)	30 min of treadmill training.
tDCS ($N = 12$)							
Zhou et al. (2014)	Young 20 (50%)	22 (2)	--	Site: Anode: L-DLPFC; Cathoda: R- supraorbital region Parameters: 1.1 ± 0.3 mA, 20 min	Site: Anode: L-DLPFC; Cathoda: R- supraorbital region Parameters: 0 mA, 20 min	1 session	NR
Wrightson et al. (2015)	Young 10 (NR)	23 (3.2)	--	Site: EG1: Anode: PFC; EG2: Cathoda: PFC Parameters: 1.5 mA, 15 min	Site: PFC Parameters: 0 mA, 0.5 min	1 session	NR
Pineau et al. (2021)	Young EG: 12 (25%) CG: 12 (25%)	EG: 21.6 (1.6) CG: 21.1 (1.0)	--	Site: Anode:L-DLPFC; Cathoda:R- supraorbital region Parameters: 2 mA/ 30 min	Site: Anode:L-DLPFC; Cathoda:R- supraorbital region Parameters: 2 mA/ 1 min	1 session	NR
Zhou et al. (2015)	Older 20 (45%)	63 (3.6)	--	Site: Anode: L-DLPFC; Cathoda: R- supraorbital region Parameters: 1.4 ± 0.4 mA/ 20 min	Site: Anode:L-DLPFC; Cathoda:R- supraorbital region Parameters: 2 mA/ 1 min	1 session	NR
Manor et al. (2016)	Older 37 (67.6%)	61 (5.0)	--	Site: Anode:L-DLPFC; Cathoda:R- supraorbital region Parameters: 1.4 ± 0.4 mA/ 20 min	Site: Anode:L-DLPFC; Cathoda:R- supraorbital region Parameters: 2 mA/ 1 min	1 session	NR
Manor et al. (2018)	Older EG: 9 (55.6%) CG: 9 (55.6%)	EG: 82 (4.0) CG: 79 (4.0)	--	Site: Anode:L-DLPFC; Cathoda:R- supraorbital region Parameters: 1.9 ± 0.3 mA/ 20 min	Site: Anode:L-DLPFC; Cathoda:R- supraorbital region Parameters: 2.0 ± 0.1 mA/ 1 min	5 days/week, for 2 weeks (10 sessions)	NR
Schneider et al. (2021)	Older 25 (80%)	73.9 (5.2)	--	Site: M1 + LDLPFC Parameters: 20 min	Site: M1 + LDLPFC Parameters: sham	1 session	EG: tDCS+walking; CG: sham+walking

(Continued)

TABLE 2 (Continued)

Study	Characteristics of participants			Intervention protocols			
	Population and sample size (ratio of female)	Age (y) [Mean (SD)]	Disease onset duration (y)	EG	CG	Intervention period	Additional therapy
Schabrun et al. (2016)	PD EG: 8 (NR) CG: 8 (NR)	EG: 72 (4.9) CG: 63 (11.0)	EG: 6.9 (4.4) CG: 4.6 (3.9)	Site: Anode:L-M1; Cathoda:R- supraorbital region Parameters: 2 mA/ 20 min	Site: Anode:L-M1; Cathoda:R- supraorbital region Parameters: 2 mA/ 0 min	3 days/week, for 3 weeks (9 sessions)	20 min of gait training
Swank et al. (2016)	PD 10 (NR)	68.7 (10.2)	7.9 (7.1)	Site: Anode:L-DLPFC; Cathoda:R- supraorbital region Parameters: 2 mA/ 20 min	Site: Anode: L-DLPFC; Cathoda: R- supraorbital region Parameters: 1 mA/ 0.5 min	1 session	NR
Mishra and Thrasher (2021)	PD 20 (NR)	67.8(8.3)	4.8 (3.8)	Site: Anode:L-DLPFC; Cathoda:R- supraorbital region Parameters: 2 mA/ 30 min	Site: Anode: L-DLPFC; Cathoda: R- supraorbital region Parameters: 2 mA/ 1 min	1 session	NR
Wong et al. (2022a,b)	PD EG1: 9 EG2: 9 EG3: 9 CG: 9	EG1: 54.20 (4.1) EG2: 50.09 (2.4) EG3: 61.30 (7.9) CG: 58.30 (8.0)	EG1: 7.8 (5.7) EG2: 6.2 (3.3) EG3: 4.1 (3.3) CG: 8.3 (0.12)	Site: Anode: EG1: L- M1; EG2: L-DLPFC; EG3: L-Cerebellum; Cathode: R- supraorbital region Parameters: 2 mA/ 20 min	Site: Anode: L- M1; Cathode: Contralateral supraorbital ridge Parameters: 2 mA/ 1 min	1 session	30 min of gait training
Wong et al. (2022a,b)	Stroke EG1: 12 EG2: 12 EG3: 12 CG: 12	EG1:54.3 (16.1) EG2: 53.3 (19.0) EG3: 59.2 (12.7) CG: 55.2 (14.0)	EG1:59.9 (57.3) EG2: 63.0 (40.8) EG3: 57.8 (71.3) CG: 57.4 (58.2)	Site: EG1: Anode: ipsilesional M1; Cathode: contralateral supraorbital ridge; EG2: Anode: ipsilesional M1; Cathoda:contralesional M1; EG3: Anode: contralateral supraorbital ridge; Cathode: contralesional M1 Parameters: 2 mA/ 20 min	Site: Anode: ipsilesional M1; Cathode: contralateral supraorbital ridge Parameters: 2 mA/ 1 min	1 session	NR

CG: control group; EG: experimental group; L: left; NR: not reported; PD: Parkinson's Disease; R: right.

individuals with PD, and individuals with stroke. The anode was placed over the left DLPFC, left-M1, M1-LDLPFC, left cerebellum, or PFC, while the cathode were generally on the right supraorbital cortex (Zhou et al., 2014, 2015; Wrightson et al., 2015; Manor et al., 2016, 2018; Schabrun et al., 2016; Swank et al., 2016; Mishra and Thrasher, 2021; Pineau et al., 2021; Schneider et al., 2021; Wong et al., 2022a,b). Participants in most studies received only one session stimulation (Zhou et al., 2014, 2015; Wrightson et al., 2015; Manor et al., 2016; Swank et al., 2016; Mishra and Thrasher, 2021; Pineau et al., 2021; Schneider et al., 2021; Wong et al., 2022a,b). The intensities and duration of stimulation ranged from 1.1 to 2 mA, and 15 to 30 min, respectively.

Effects of rTMS on walking ability

Healthy young adults and individuals with stroke

No significant improvement in speed was observed in healthy young adults and individual with stroke under either ST or DT condition (Goh et al., 2019, 2020; Table 3).

Individuals with PD

Compared with the control group, significant improvements in fastest walking speed and time taken to TUG under both ST and DT conditions were only observed at follow-up in one RCT (Chung et al., 2020; Table 3).

Effects of tDCS on walking ability

Healthy young adults

No significant improvements in speed or stride time variability under either ST or DT condition, DTC in speed, or in stride time variability was observed (Zhou et al., 2014; Wrightson et al., 2015; Table 3).

Older adults

Except the stride time variability under DT condition, none of gait parameters (speed, TUG, stride time) showed better improvement under ST or DT condition (Manor et al., 2018). On the contrary, some

DTC measures, such as DTC in stride time, stride time variability, swing time variability, and step regularity demonstrated significant better improvement (Schneider et al., 2021; Table 3).

Individuals with PD

Except significant improvement in speed under DT condition was reported in one RCT only (Wong et al., 2022a,b), no significant improvement in any gait parameter was identified in other RCTs (Schabrun et al., 2016; Swank et al., 2016; Mishra and Thrasher, 2021; Table 3).

Individuals with stroke

Only one RCT demonstrated the significant improvement in speed under both ST and DT condition, and cadence in ST condition (Wong et al., 2022a,b; Table 3).

Effects of tDCS on balance function

In five RCTs that investigated the balance function in healthy young adults and older adults, only one RCT showed significant reduction in postural sway speed and area during standing under DT condition (Zhou et al., 2014; Table 3).

Effects of NIBS on cognitive function

No significant effect on cognitive function was observed in healthy young adults or older adults (Goh et al., 2019, 2020; Table 3).

Effects of NIBS on other functions

Individuals with PD

Only one RCT reported that the rTMS could significantly improve the score of Movement Disorders Society-Unified Parkinson's Disease Rating Scale part III (MDS-UPDRS III) at post-intervention and one-month follow-up, cortical silent period (CSP) at post-intervention, and short-interval intracortical inhibition (SICI) at one-month follow-up (Chung et al., 2020). No significant improvement in quality of life scores-39 was identified in the tDCS RCT (Swank et al., 2016). Only one trail demonstrated the tDCS could significantly lengthen CSP in DLPFC group (Wong et al., 2022a,b; Table 4).

Individuals with stroke

Significant improvement of CSP was demonstrated by one tDCS RCT only (Wong et al., 2022a,b; Table 4).

Discussion

Findings of this review

A total of 15 RCTs were included in this review, comparing the effects of NIBS with sham-stimulation in different populations. Significant improvements in DT walking (speed, time taken to TUG, cadence) and balance (postural sway speed and area) performance were only observed in 3 (Chung et al., 2020; Wong et al., 2022a,b) and 1 (Zhou et al., 2014) RCTs, respectively. Similarly, reduction in DTC in some gait parameters (stride time, stride time variability, swing time variability, step regularity) was demonstrated in one RCT only (Schneider et al., 2021). In addition, due to the limited number and large heterogeneity of included RCTs, there was no evidence to suggest that NIBS was superior to sham-stimulation in improving DT walking and balance function.

rTMS effects on mobility function

Chung et al. showed that rTMS (25 Hz, 1 Hz, or sham) applying to the leg area of bilateral M1 in individuals with PD followed by treadmill training could significantly improve the time taken to TUG and fastest walking speed under both ST and DT conditions, and MDS-UPDRS III scores at post-intervention and follow-up. This was similar to the results of Yang et al. (2018) study. The meta-analysis by Yang et al. (2018) investigated the optimal therapeutic effects of rTMS parameters on mobility dysfunction and provided evidence supporting that rTMS could be effective in improving mobility function in individuals with PD. Chung et al. (2020) and Yang et al. (2018) both concluded that high-frequency (25 Hz) rTMS could significantly improve cortical excitability in individuals with PD, this behavioral changes could be associated with increased cortical excitability. On one hand, rTMS can improve the neurological plasticity through the regulation of central nervous system (King and Tang, 2022); on the other hand, rTMS-primed treadmill training could strengthen synaptic connections in M1, which participates in the processing and storage of new information for motor consolidation, thereafter, leading to more stable and longer duration effect.

By contrast, in Goh et al. study, no significant improvement was identified in either healthy young adults or stroke under either ST or DT condition. This could be attributed to the only one-single session of stimulation was applied in their RCT, making no stimulation effect accumulated.

tDCS effects on mobility function

Significant improvements in gait parameters were demonstrated by only one RCT, respectively, in stroke (ST condition: speed, cadence; DT condition: speed) (Wong et al., 2022a,b) and PD (DT condition: speed) (Wong et al., 2022a,b). Only one RCT reported the significant findings in DT postural sway speed and area (Zhou et al., 2014). Therefore, there is insufficient data on the effect of tDCS on mobility in the four studied populations at present. Future research should further investigate the effects of tDCS on DT mobility function in different population with larger sample size and longer intervention period.

The DTC in gait parameters, such as, stride time variability, swing time variability and step regularity, were significantly reduced (Schneider et al., 2021) in healthy young adults and older adults. Theoretically, under DT condition, cognitive resources would be divided, leading one or both tasks deteriorated (Sigman and Dehaene, 2006). However, the DT interference in walking was improved after tDCS intervention, this phenomenon could be mainly due to the activation of DLPFC by tDCS, which promotes the speed of task processing in the brain (Filmer et al., 2013), i.e., improving the executive function, thereby reducing the DTC. The assumption was

TABLE 3 NIBS: Effects on mobility outcomes.

Outcomes	tDCS (*N*=10)		TMS (N=3)	
	Under ST condition	Under DT condition	Under ST condition	Under DT condition
Walking function				
Healthy young adults (*N* = 3)	Speed[a] (Pineau et al., 2021), Stride time variability (Wrightson et al., 2015): (NS)	Speed[a] (Zhou et al., 2014), DTC in speed (Zhou et al., 2014), DTC in stride time variability (Wrightson et al., 2015): (NS)	Speed[a] (Goh et al., 2019): (NS)	Speed[a] (Goh et al., 2019): (NS)
Older adults (*N* = 3)	Speed (Manor et al., 2016, 2018), TUG (Manor et al., 2018), 4-m walking time (Manor et al., 2018), Stride time (Manor et al., 2018), Stride time variability and 2-week-FU (Manor et al., 2018): (NS)	Speed (Manor et al., 2016, 2018), Stride time (Manor et al., 2018), and their corresponding DTC: (NS) DTC in Stride time variability (Manor et al., 2018) and Double support time (Schneider et al., 2021): (NS) Stride time variability (Manor et al., 2018): −0.61*; DTC in Stride time (Schneider et al., 2021): 1.14*; Stride time variability (Schneider et al., 2021): 4.04*; Swing time variability (Schneider et al., 2021): 0.87*; Step regularity (Schneider et al., 2021): 0.46*		
Stroke (*N* = 2)	Step time (Wong et al., 2022a,b), Step length (Wong et al., 2022a,b), DTC in Speed (Wong et al., 2022a,b): (NS) Speed (Wong et al., 2022a,b): 0.37* Cadence (Wong et al., 2022a,b): 0.5*	Cadence (Wong et al., 2022a,b), Step time: (NS) (Wong et al., 2022a,b), Step length (Wong et al., 2022a,b), DTC in Speed (Wong et al., 2022a,b): (NS) Speed (Wong et al., 2022a,b): 0.27 ~ 0.34*	Speed[a] (Goh et al., 2020): (NS)	Speed[a] (Goh et al., 2020): (NS)
Parkinson's disease (*N* = 4)	Speed (Schabrun et al., 2016; Mishra and Thrasher, 2021; Wong et al., 2022a,b), TUG (Schabrun et al., 2016; Swank et al., 2016; Wong et al., 2022a,b), Cadence (Schabrun et al., 2016; Wong et al., 2022a,b), Stride time (Wong et al., 2022a,b), Step length (Schabrun et al., 2016; Wong et al., 2022a,b), Double support time and 12-week FU(Schabrun et al., 2016): (NS)	Speed (Schabrun et al., 2016; Mishra and Thrasher, 2021), DTC in speed (Mishra and Thrasher, 2021; Wong et al., 2022a,b), TUG[a] (Schabrun et al., 2016; Swank et al., 2016), Cadence: (NS) (Schabrun et al., 2016; Wong et al. 2022a,b), Stride time (Wong et al., 2022a,b), Step length (Schabrun et al., 2016; Wong et al., 2022a,b), Double support time and 12-week FU (Schabrun et al., 2016): (NS) Speed (Zhou et al., 2014): 0.65*	Fastest walking speed and 1-month FU (Chung et al., 2020): (NS) month FU (Chung et al., 2020): 0.51* TUG and 1-month FU (Chung et al., 2020): (NS) 3-month FU (Chung et al., 2020): −0.64*	TUG (Chung et al., 2020): (NS) 1-month FU (Chung et al., 2020): −0.67* 3-month FU (Chung et al., 2020): −0.59*
Balance function (laboratory-based measures)				
Healthy young adults (*N* = 3)	Postural sway speed and area[a] (Zhou et al., 2014), Range AP and ML (Eyes open/closed) (Pineau et al., 2021), Mean velocity (Eyes open/closed) (Pineau et al., 2021): (NS)	ML/AP trunk RoM and their corresponding DTC (Wrightson et al., 2015; Pineau et al., 2021), DTC in postural sway speed and area[a] (Zhou et al., 2014), Mean velocity (open/closed): (NS) (Pineau et al., 2021) Postural sway area and speed[a]* (Zhou et al., 2014)		
Older adults (*N* = 2)	COP complexity index[a] (Zhou et al., 2015), Standing postural sway area, speed and 2-week-FU (Manor et al., 2016, 2018): (NS)	COP complexity index and its DTC[a] (Zhou et al., 2015), Standing postural sway area, speed and their corresponding DTC (Manor et al., 2018; Mishra and Thrasher, 2021): (NS)		

[a]: Original data not reported.
*: Significant improvement in experimental group compared with control group, values are standardized effect sizes for significant results (Hedges' g: 0.2 = small, 0.5 = medium, 0.8 = large).
AP: anterior–posterior; DTC: dual-task costs; ML: medio-lateral; NS: not significant; RoM: range of motion; TUG: timed up and go test.

TABLE 4 NIBS: Effects on cognition and other outcomes.

Outcomes	tDCS (*N*=10)		TMS (*N*=3)	
	Under ST condition	Under DT condition	Under ST condition	Under DT condition
Cognitive function				
Healthy young adults (*N* = 3)	Serial subtraction[a] (Pineau et al., 2021), Error ratio: (NS) (Wrightson et al., 2015)	Serial subtraction[a] (Pineau et al., 2021), DTC in Error ratio: (NS) (Wrightson et al., 2015)	Serial subtraction[a] (Goh et al., 2020): (NS)	Serial subtraction[a] (Goh et al., 2020): (NS)
Older adults (*N* = 4)	MoCA (Manor et al., 2018), TMT (Part B – Part A) (Manor et al., 2018), Stroop[a] (Manor et al., 2016), Serial subtraction[a] (Manor et al., 2016): (NS)	Serial subtraction error rate (Zhou et al., 2015), DTC in Serial subtraction[a] (Mishra and Thrasher, 2021): (NS)		
Stroke (*N* = 1)			Serial subtraction[a] (https://training.cochrane.org/handbook/current, see footnote 1): (NS)	Serial subtraction[a] (https://training.cochrane.org/handbook/current, see footnote 1): (NS)
Parkinson's disease (*N* = 3)	Words generated[a] (Wong et al., 2022a,b): (NS)	Words generated (Swank et al., 2016), DTC in Words generated (Wong et al., 2022a,b), Serial subtraction (Swank et al., 2016; Schneider et al., 2021), DTC in Serial subtraction[a] (Schneider et al., 2021): (NS)		
Other functions				
Parkinson's disease (*N* = 3)	PDQ-39[a] (Swank et al., 2016), Resting motor threshold (Zhou et al., 2014), Motor evoked potentials (Zhou et al., 2014): (NS) CSP (Zhou et al., 2014): 0.19*		Slope of RC (Goh et al., 2019), SICI (Goh et al., 2019): (NS) CSP: 0.55* (Goh et al., 2019) MDS-UPDRS III (Goh et al., 2019):-0.62* ~ −0.32* 1-mon follow-up (Goh et al., 2019): −0.51* SICI: 1-mon FU (Goh et al., 2019): −0.33* 3-mon FU (Goh et al., 2019): (NS)	
Stroke (*n* = 1)	Resting motor threshold (Schabrun et al., 2016), SICI (Schabrun et al., 2016): (NS) CSP (Schabrun et al., 2016): 0.39 ~ 0.48*			

[a]: Original data not reported.
*: Significant improvement in experimental group compared with control group; values are standardized effect sizes for significant results (Hedges' g: 0.2 = small, 0.5 = medium, 0.8 = large).
CSP: cortical silent period; DTC:Dual-task costs; MDS-UPDRS III: Movement Disorders Society–Unified Parkinson's Disease Rating Scale part III; MoCA: Montreal Cognitive Assessment; NS: not significant; PDQ-39: quality of life scores-39; RC: recruitment curve; SICI: short-interval intracortical inhibition; TMT (Part B – Part A): Trail Making Test Part B minus Part A.

supported by the fact that the stimulation site of the 7 included RCTs in this review was all on the PFC (DLPFC) (Healthy young adults: 3 studies; Older adults: 4 studies). Previous literature suggested that the DLPFC, particularly the left DLPFC, plays a critical role in regulating the execution of mobility-cognitive task, possibly due to its role in executive function (Beurskens et al., 2014; Liu et al., 2018). Alternatively, DLPFC is closely related to DT function. To sum up, tDCS applied to DLPFC seems to be able to decrease the DTC in gait parameters of healthy young adults and older adults.

Although the improvements in walking, balance, or cognition were generally not significant, many studies in recent years have shown that there was a tendency for NIBS to improve the modulating cortical efficiency in healthy young adults, older adults, individuals with stroke and individuals with PD (Cosentino et al., 2017; Ghosh et al., 2019; Bai et al., 2022). Theoretically, the behavioral or functional changes would occur after the plasticity changes. Since most RCTs in our review applied only one single-session stimulation (Zhou et al., 2014, 2015; Wrightson et al., 2015; Manor et al., 2016; Swank et al., 2016; Mishra and Thrasher, 2021; Pineau et al., 2021; Schneider et al., 2021; Wong et al., 2022a,b) or short intervention period (2–3 weeks) (Schabrun et al., 2016; Manor et al., 2018), the plasticity changes could have not occurred. In addition, the basal ganglia, central to movement

disorders pathophysiology, could not be reached directly by tDCS or rTMS, but stimulation of appropriate cortical areas may affect activity in these circuits and may produce clinical benefit (Delong and Wichmann, 2015; Latorre et al., 2019).

NIBS effects on cognitive function

Overall, the effect of NIBS on cognitive function was not significant under either ST or DT condition in any population studied. This is quite different from the results of previous systematic review and meta-analysis, despite the populations were different. In their review, tDCS could significantly improve attention/vigilance in different brain disorders (schizophrenia, depression, dementia, PD, MS, stroke, and TBI) (Begemann et al., 2020), and both tDCS and rTMS shows promising positive effects in attention, memory, and working memory for post-stroke patients with deficits in cognitive function (Hara et al., 2021). The inconsistency in findings may be mainly attributed to that only one single-session intervention (short period) adopted by most RCTs (Zhou et al., 2014, 2015; Wrightson et al., 2015; Manor et al., 2016; Swank et al., 2016; Goh et al., 2019, 2020; Mishra and Thrasher, 2021; Schneider et al., 2021), leading to no intervention effect could be accumulated. However, since there is lack of data, the effects of NIBS on DT cognitive function need to be further explored.

Comparison of tDCS and rTMS effects on DT performance

Although tDCS showed significant improvement in DT walking speed in stroke (Wong et al., 2022a,b) and PD (Wong et al., 2022a,b) respectively in one RCT, while rTMS did not show any significant changes after intervention, the treatment effects of tDCS and rTMS were not comparable in different populations, due to the limited number of studies included in this review, different stimulation target, and the different intervention protocol adopted in each trail.

Limitations

Limitations of studies reviewed

Small sample size (9 ~ 20) (Zhou et al., 2014, 2015; Wrightson et al., 2015; Schabrun et al., 2016; Swank et al., 2016; Manor et al., 2018; Goh et al., 2019, 2020; Mishra and Thrasher, 2021) and short intervention period (only one-single session) (Zhou et al., 2014, 2015; Wrightson et al., 2015; Manor et al., 2016; Swank et al., 2016; Goh et al., 2019, 2020; Mishra and Thrasher, 2021; Pineau et al., 2021; Schneider et al., 2021; Wong et al., 2022a,b) were adopted by most RCTs, making the results should be interpreted with caution.

Limitations of this systematic review

There are several limitations in our review. The publications were only screened in the English databases and may ignore potential publications in other languages. In addition, the meta-analysis was not performed due to the heterogeneity in stimulation parameters and populations studied of the included publications.

Conclusion

Both tDCS and rTMS showed promising effects in improving DT walking and balance performance in different populations, however, due to the large heterogeneity of included studies and insufficient data, any firm conclusion cannot be drawn at present. More well-designed studies with longer intervention period and larger sample size are needed.

Data availability statement

The raw data supporting the conclusions of this article will be made available by the authors, without undue reservation.

Author contributions

All authors listed have made a substantial, direct, and intellectual contribution to the work and approved it for publication. XL, YZ, LD, and LY provided concept/idea/research design. XL and LY provided writing. XL, XC, and LW. provided data collection and quality assessment of the study. LW and LD provided data analysis. LY provided project management. All authors provided consultation (including review of manuscript before submission).

Funding

This study was supported by the funding of Kunming Health Science and Technology Talent Training Project, Training Plan for Medical Science and Technology Descipline Leaders, No. 2022-SW (Leaders)-27.

Conflict of interest

The authors declare that the research was conducted in the absence of any commercial or financial relationships that could be construed as a potential conflict of interest.

Publisher's note

All claims expressed in this article are solely those of the authors and do not necessarily represent those of their affiliated organizations, or those of the publisher, the editors and the reviewers. Any product that may be evaluated in this article, or claim that may be made by its manufacturer, is not guaranteed or endorsed by the publisher.

Supplementary material

The Supplementary material for this article can be found online at: https://www.frontiersin.org/articles/10.3389/fnins.2023.1157920/full#supplementary-material

References

Bai, Z., Zhang, J., and Fong, K. (2022). Effects of transcranial magnetic stimulation in modulating cortical excitability in patients with stroke: a systematic review and meta-analysis. *J. Neuroeng. Rehabil.* 19:24. doi: 10.1186/s12984-022-00999-4

Begemann, M. J., Brand, B. A., Curcic-Blake, B., Aleman, A., and Sommer, I. E. (2020). Efficacy of non-invasive brain stimulation on cognitive functioning in brain disorders: a meta-analysis. *Psychol. Med.* 50, 2465–2486. doi: 10.1017/S0033291720003670

Behrangrad, S., Zoghi, M., Kidgell, D., and Jaberzadeh, S. (2021). The effect of a single session of non-invasive brain stimulation on balance in healthy individuals: a systematic review and best evidence synthesis. *Brain Connect.* 11, 695–716. doi: 10.1089/brain.2020.0872

Beurskens, R., Helmich, I., Rein, R., and Bock, O. (2014). Age-related changes in prefrontal activity during walking in dual-task situations: a fNIRS study. *Int. J. Psychophysiol.* 92, 122–128. doi: 10.1016/j.ijpsycho.2014.03.005

Chung, C. L. H., Mak, M. K. Y., and Hallett, M. (2020). Transcranial magnetic stimulation promotes gait training in Parkinson's disease. *Ann. Neurol.* 88, 933–945. doi: 10.1002/ana.25881

Cosentino, G., Valentino, F., Todisco, M., Alfonsi, E., Davì, R., Savettieri, G., et al. (2017). Effects of more-affected vs. less-affected motor cortex TDCS in Parkinson's disease. *Front. Hum. Neurosci.* 11:309. doi: 10.3389/fnhum.2017.00309

De Freitas, T. B., Leite, P. H. W., Doná, F., Pompeu, J. E., Swarowsky, A., and Torriani-Pasin, C. (2020). The effects of dual task gait and balance training in Parkinson's disease: a systematic review. *Physiother. Theory Pract.* 36, 1088–1096. doi: 10.1080/09593985.2018.1551455

Delong, M. R., and Wichmann, T. (2015). Basal ganglia circuits as targets for neuromodulation in Parkinson disease. *JAMA Neurol.* 72, 1354–1360. doi: 10.1001/jamaneurol.2015.2397

Dockery, C. A., Hueckel-Weng, R., Birbaumer, N., and Plewnia, C. (2009). Enhancement of planning ability by transcranial direct current stimulation. *J. Neurosci.* 29, 7271–7277. doi: 10.1523/JNEUROSCI.0065-09.2009

D'Urso, G., Toscano, E., Barone, A., Palermo, M., Dell'Osso, B., di Lorenzo, G., et al. (2023). Transcranial direct current stimulation for bipolar depression: systematic reviews of clinical evidence and biological underpinnings. *Prog. Neuro-Psychopharmacol. Biol. Psychiatry* 121:110672. doi: 10.1016/j.pnpbp.2022.110672

Filmer, H. L., Mattingley, J. B., and Dux, P. E. (2013). Improved multitasking following prefrontal tdcs. *Cortex* 49, 2845–2852. doi: 10.1016/j.cortex.2013.08.015

Fregni, F., Boggio, P. S., Nitsche, M., Bermpohl, F., Antal, A., Feredoes, E., et al. (2005). Anodal transcranial direct current stimulation of prefrontal cortex enhances working memory. *Exp. Brain Res.* 166, 23–30. doi: 10.1007/s00221-005-2334-6

Ghosh, S., Hathorn, D., Eisenhauer, J., Dixon, J., and Cooper, I. D. (2019). Anodal transcranial direct current stimulation over the vertex enhances leg motor cortex excitability bilaterally. *Brain Sci.* 9:98. doi: 10.3390/brainsci9050098

Goh, H., Connolly, K., Hardy, J., McCain, K., and Walker-Batson, D. (2020). Single session of repetitive transcranial magnetic stimulation to left dorsolateral prefrontal cortex increased dual-task gait speed in chronic stroke: a pilot study. *Gait Posture* 78, 1–5. doi: 10.1016/j.gaitpost.2020.02.020

Goh, H., Ewing, S., Marchuk, D., Newton, A., and Nyangani, I. (2019). Facilitation of supplementary motor area excitability improves dual-task walking in young adults. *Neurosci. Lett.* 698, 1–6. doi: 10.1016/j.neulet.2019.01.004

Hara, T., Shanmugalingam, A., Mcintyre, A., and Burhan, A. M. (2021). The effect of non-invasive brain stimulation (nibs) on attention and memory function in stroke rehabilitation patients: a systematic review and meta-analysis. *Diagnostics (Basel)* 11:227. doi: 10.3390/diagnostics11020227

Hillel, I., Gazit, E., Nieuwboer, A., Avanzino, L., Rochester, L., Cereatti, A., et al. (2019). Is every-day walking in older adults more analogous to dual-task walking or to usual walking? Elucidating the gaps between gait performance in the lab and during 24/7 monitoring. *Eur. Rev. Aging Phys. Act.* 16:6. doi: 10.1186/s11556-019-0214-5

King, E. S., and Tang, A. D. (2022). Intrinsic plasticity mechanisms of repetitive transcranial magnetic stimulation. *Neuroscientist* 5:2044981046. doi: 10.1177/10738584221118262

Latorre, A., Rocchi, L., Berardelli, A., Bhatia, K. P., and Rothwell, J. C. (2019). The use of transcranial magnetic stimulation as a treatment for movement disorders: a critical review. *Mov. Disord.* 34, 769–782. doi: 10.1002/mds.27705

Liu, Y. C., Yang, Y. R., Tsai, Y. A., Wang, R. Y., and Lu, C. F. (2018). Brain activation and gait alteration during cognitive and motor dual task walking in stroke-a functional near-infrared spectroscopy study. *IEEE Trans. Neural Syst. Rehabil. Eng.* 26, 2416–2423. doi: 10.1109/TNSRE.2018.2878045

Lundin-Olsson, L., Nyberg, L., and Gustafson, Y. (1997). "Stops walking when talking" as a predictor of falls in elderly people. *Lancet* 349:617. doi: 10.1016/S0140-6736(97)24009-2

Manor, B., Zhou, J., Harrison, R., Lo, O. Y., Travison, T. G., Hausdorff, J. M., et al. (2018). Transcranial direct current stimulation may improve cognitive-motor function in functionally limited older adults. *Neurorehabil. Neural Repair* 32, 788–798. doi: 10.1177/1545968318792616

Manor, B., Zhou, J., Jor'Dan, A., Zhang, J., Fang, J., and Pascual-Leone, A. (2016). Reduction of dual-task costs by noninvasive modulation of prefrontal activity in healthy elders. *J. Cogn. Neurosci.* 28, 275–281. doi: 10.1162/jocn_a_00897

Mishra, R. K., and Thrasher, A. T. (2021). Transcranial direct current stimulation of dorsolateral prefrontal cortex improves dual-task gait performance in patients with Parkinson's disease: a double blind, sham-controlled study. *Gait Posture* 84, 11–16. doi: 10.1016/j.gaitpost.2020.11.012

Nitsche, M. A., Schauenburg, A., Lang, N., Liebetanz, D., Exner, C., Paulus, W., et al. (2003). Facilitation of implicit motor learning by weak transcranial direct current stimulation of the primary motor cortex in the human. *J. Cogn. Neurosci.* 15, 619–626. doi: 10.1162/089892903321662994

Page, M. J., Mckenzie, J. E., Bossuyt, P. M., Boutron, I., Hoffmann, T. C., Mulrow, C. D., et al. (2021). The PRISMA 2020 statement: an updated guideline for reporting systematic reviews. *BMJ* 372:n71. doi: 10.1136/bmj.n71

Pineau, N., Robin, A., Bulteau, S., Thomas-Ollivier, V., Sauvaget, A., and Deschamps, T. (2021). Does the transcranial direct current stimulation improve dual-task postural control in young healthy adults? *Cogn. Process.* 22, 291–298. doi: 10.1007/s10339-020-01000-7

Schabrun, S. M., Lamont, R. M., and Brauer, S. G. (2016). Transcranial direct current stimulation to enhance dual-task gait training in Parkinson's disease: a pilot rct. *PLoS One* 11:e158497. doi: 10.1371/journal.pone.0158497

Schneider, N., Dagan, M., Katz, R., Thumm, P. C., Brozgol, M., Giladi, N., et al. (2021). Combining transcranial direct current stimulation with a motor-cognitive task: the impact on dual-task walking costs in older adults. *J. Neuroeng. Rehabil.* 18:23. doi: 10.1186/s12984-021-00826-2

Sigman, M., and Dehaene, S. (2006). Dynamics of the central bottleneck: dual-task and task uncertainty. *PLoS Biol.* 4:e220. doi: 10.1371/journal.pbio.0040220

Swank, C., Mehta, J., and Criminger, C. (2016). Transcranial direct current stimulation lessens dual task cost in people with Parkinson's disease. *Neurosci. Lett.* 626, 1–5. doi: 10.1016/j.neulet.2016.05.010

Tombu, M., and Jolicoeur, P. (2003). A central capacity sharing model of dual-task performance. *J. Exp. Psychol. Hum. Percept. Perform.* 29, 3–18. doi: 10.1037/0096-1523.29.1.3

Vitorio, R., Stuart, S., Rochester, L., Alcock, L., and Pantall, A. (2017). Fnirs response during walking - artefact or cortical activity? A systematic review. *Neurosci. Biobehav. Rev.* 83, 160–172. doi: 10.1016/j.neubiorev.2017.10.002

Weiss, A., Herman, T., Giladi, N., and Hausdorff, J. M. (2015). Association between community ambulation walking patterns and cognitive function in patients with Parkinson's disease: further insights into motor-cognitive links. *Parkinsons Dis.* 2015:547065, 1–11. doi: 10.1155/2015/547065

Wong, P. L., Yang, Y. R., Huang, S. F., Fuh, J. L., Chiang, H. L., and Wang, R. Y. (2022a). Transcranial direct current stimulation on different targets to modulate cortical activity and dual-task walking in individuals with Parkinson's disease: a double blinded randomized controlled RCT. *Front. Aging Neurosci.* 14:807151. doi: 10.3389/fnagi.2022.807151

Wong, P. L., Yang, Y., Tang, S., Huang, S. F., and Wang, R. Y. (2022b). Comparing different montages of transcranial direct current stimulation on dual-task walking and cortical activity in chronic stroke: double-blinded randomized controlled RCT. *BMC Neurol.* 22:119. doi: 10.1186/s12883-022-02644-y

Wrightson, J. G., Twomey, R., Ross, E. Z., and Smeeton, N. J. (2015). The effect of transcranial direct current stimulation on task processing and prioritisation during dual-task gait. *Exp. Brain Res.* 233, 1575–1583. doi: 10.1007/s00221-015-4232-x

Xie, Y. J., Chen, Y., Tan, H. X., Guo, Q. F., Lau, B. W., and Gao, Q. (2021). Repetitive transcranial magnetic stimulation for lower extremity motor function in patients with stroke: a systematic review and network meta-analysis. *Neural Regen. Res.* 16, 1168–1176. doi: 10.4103/1673-5374.300341

Yang, C., Guo, Z., Peng, H., Xing, G., Chen, H., McClure, M. A., et al. (2018). Repetitive transcranial magnetic stimulation therapy for motor recovery in Parkinson's disease: a meta-analysis. *Brain Behav.* 8:e1132. doi: 10.1002/brb3.1132

Zhang, L., Xing, G., Fan, Y., Guo, Z., Chen, H., and Mu, Q. (2017). Short- and long-term effects of repetitive transcranial magnetic stimulation on upper limb motor function after stroke: a systematic review and meta-analysis. *Clin. Rehabil.* 31, 1137–1153. doi: 10.1177/0269215517692386

Zhou, J., Hao, Y., Wang, Y., Jor'dan, A., Pascual-Leone, A., Zhang, J., et al. (2014). Transcranial direct current stimulation reduces the cost of performing a cognitive task on gait and postural control. *Eur. J. Neurosci.* 39, 1343–1348. doi: 10.1111/ejn.12492

Zhou, D., Zhou, J., Chen, H., Manor, B., Lin, J., and Zhang, J. (2015). Effects of transcranial direct current stimulation (TDCS) on multiscale complexity of dual-task postural control in older adults. *Exp. Brain Res.* 233, 2401–2409. doi: 10.1007/s00221-015-4310-0

frontiers | Frontiers in Neuroscience

TYPE Original Research
PUBLISHED 17 April 2023
DOI 10.3389/fnins.2023.1129590

OPEN ACCESS

EDITED BY
Feng Zhang,
Third Hospital of Hebei Medical University,
China

REVIEWED BY
Jian Li,
Beijing University of Posts and Telecommunications,
China
Dongke Yu,
Sichuan Academy of Medical Sciences and Sichuan Provincial People's Hospital,
China

*CORRESPONDENCE
Yi Wu
✉ wuyi@fudan.edu.cn
Xiao Xiao
✉ xiaoxiao@fudan.edu.cn
Qun Zhang
✉ zqun_888@163.com

†These authors have contributed equally to this work and share first authorship

‡These authors have contributed equally to this work and share last authorship

SPECIALTY SECTION
This article was submitted to Translational Neuroscience, a section of the journal Frontiers in Neuroscience

RECEIVED 22 December 2022
ACCEPTED 30 March 2023
PUBLISHED 17 April 2023

CITATION
Liu L, Ding M, Wu J, Zhang Y, Guo S, Wang N, Wang H, Yu K, Weng Y, Luo L, Zhang J, Zhang Q, Qiu K, Wu Y, Xiao X and Zhang Q (2023) Design and evaluation of a rodent-specific focal transcranial magnetic stimulation coil with the custom shielding application in rats.
Front. Neurosci. 17:1129590.
doi: 10.3389/fnins.2023.1129590

Design and evaluation of a rodent-specific focal transcranial magnetic stimulation coil with the custom shielding application in rats

Li Liu[1†], Ming Ding[2†], Junfa Wu[1†], Yuwen Zhang[3], Shaoqian Guo[4], Nianhong Wang[1], He Wang[3], Kewei Yu[1], Yuanfeng Weng[2], Lu Luo[1], Jingjun Zhang[1], Quan Zhang[4], Kai Qiu[4], Yi Wu[1*‡], Xiao Xiao[2*‡] and Qun Zhang[1*‡]

[1]Department of Rehabilitation Medicine, Huashan Hospital, Fudan University, Shanghai, China, [2]Behavioral and Cognitive Neuroscience Center, Institute of Science and Technology for Brain-Inspired Intelligence, Fudan University, Shanghai, China, [3]Institute of Science and Technology for Brain-Inspired Intelligence, Fudan University, Shanghai, China, [4]Nanjing Vishee Medical Technology Co., Ltd., Nanjing, China

Repetitive TMS has been used as an alternative treatment for various neurological disorders. However, most TMS mechanism studies in rodents have been based on the whole brain stimulation, the lack of rodent-specific focal TMS coils restricts the proper translation of human TMS protocols to animal models. In this study, we designed a new shielding device, which was made of high magnetic permeability material, to enhance the spatial focus of animal-use TMS coils. With the finite element method, we analyzed the electromagnetic field of the coil with and without the shielding device. Furthermore, to assess the shielding effect in rodents, we compared the c-fos expression, the ALFF and ReHo values in different groups following a 15min 5Hz rTMS paradigm. We found that a smaller focality with an identical core stimulation intensity was achieved in the shielding device. The 1T magnetic field was reduced from 19.1mm to 13mm in diameter, and 7.5 to 5.6mm in depth. However, the core magnetic field over 1.5T was almost the same. Meanwhile, the area of electric field was reduced from 4.68cm^2 to 4.19cm^2, and 3.8mm to 2.6mm in depth. Similar to this biomimetic data, the c-fos expression, the ALFF and ReHo values showed more limited cortex activation with the use of the shielding device. However, compared to the rTMS group without the shielding application, more subcortical regions, like the striatum (CPu), the hippocampus, the thalamus, and the hypothalamus were also activated in the shielding group. This indicated that more deep stimulation may be achieved by the shielding device. Generally, compared with the commercial rodents' TMS coil (15mm in diameter), TMS coils with the shielding device achieved a better focality (~6mm in diameter) by reducing at least 30% of the magnetic and electric field. This shielding device may provide a useful tool for further TMS studies in rodents, especially for more specific brain area stimulation.

KEYWORDS

rTMS, high magnetic permeability material, electromagnetic shielding, finite element method, fluorescence imaging, fMRI

Introduction

Transcranial magnetic stimulation (TMS) is a non-invasive procedure that uses a magnetic field to modulate neuronal activity (Salinas et al., 2016; Toledo et al., 2021). Repetitive TMS (rTMS) has been used as an alternative treatment for various neurological disorders, usually when other treatments are ineffective (Lefaucheur et al., 2020). Although, the molecular mechanisms underlying TMS-induced neurorecovery have been systematically studied in rodent models (Xing et al., 2022), most TMS studies in rodents were based on the whole brain stimulation with the commercial coils (Roth et al., 2007; Vahabzadeh-Hagh et al., 2012; Guerra et al., 2020). The lack of rodent-specific focal TMS coils restricts the proper translation of human TMS protocols to animal models. However, neither intensity reduction nor miniature coil construction to increase the coil focality is perfect, because low-intensity is not sufficient to mimic the human stimulation conditions, while the miniature coil could not bear long-term stimulation (Cohen and Cuffin, 1991; Rodger et al., 2012; Tang et al., 2016). Therefore, given the three important TMS parameters, i.e., pulse capacitor(C), high-voltage power (U) and inductance coil (Ls) are mutually interacted, it is not easy to make a TMS coil that is localized and with a high-magnetic and high-electric field.

Previous studies have reported that shielding device with high permeability material (silicon) may be useful to increase the coil focality approximately 50% without changing the coil type (Boonzaier et al., 2020). However, the above shielding material was not able to withstand prolonged TMS stimulation due to overheating. Accumulating evidence suggests that "thin, light, wide and strong" absorbing materials were more suitable for the TMS electromagnetic shielding (Kim et al., 2006). Meanwhile, other studies have shown that using highly permeable soft magnetic ferrite could improve focalization of the coil, whereas they only simulated the distribution of the electric field, and no *in vivo* data have been available to reveal the real neuron activation in TMS stimulation with or without the shielding device (Zhang et al., 2013; Zhao et al., 2015). As there is large discrepancies between *in vivo* and bionic simulation data, more work needs to be done to reveal the actual changes in the brain.

Therefore, in this study, in addition to the magnetic and electric field distribution analysis with the Finite element method (FEM), we further used the immunofluorescence (IF) and functional magnetic resonance imaging (fMRI) to assess the aftereffects of a 15 min 5 Hz rTMS paradigm in rats with or without the shielding device.

Materials and methods

The shielding device

Absorbing material, a sort of electromagnetic (EM) shielding material, is thin coating with light weight. It has a strong absorbing performance (Wen et al., 2014; Huang et al., 2021; Nuhiji et al., 2021; Du, 2022). Through magnetic loss, dielectric loss, or resistive loss, the absorbing material can reduce the EM field as required (Zhang et al., 2020). The magnetic loss material (the ferrite, magnetic metal, alloys, etc.) and the conductive loss material (the carbon material, graphene, MXene, *SiC*, etc.) can convert the electromagnetic force into heat directly (Gao et al., 2020), while the dielectric loss of material, like the TiO2, MnO2, etc. will consume the electromagnetic and further convert it into heat (Qin et al., 2022). In this study, we used a composite absorbing material made by mixing magnetic powder and epoxy resin to make the custom-made shielding device. Furthermore, a 15 mm diameter hole was designed in the center of the shielding device to realize the focal stimulation. Specifically, the shielding device is circle with a 45 mm outer diameter and a 2 mm thickness (Figures 1A,B). The TMS coil center was tangentially attached above the right brain with the shielding device pasted on the back (Figures 1C–F).

Animals

Female Sprague–Dawley rats of clean grade (230–250 g) from Shanghai JSJ Company were used in this study. All the animals were housed in an environment with a temperature of 22–25°C, relative humidity of 65 ± 5%, and a light/dark cycle of 12/12 h and had free access to food and water. All animal studies (including the rats euthanasia procedure) were reviewed and approved by Fudan University Animal Welfare and Ethics committee (Ethical permit numbers: 2020 Huashan hospital JS-151).

rTMS treatment

The rats were randomly divided into three groups: the rTMS with the custom shielding group (rTMS+shileding), the rTMS with a plastic board group (rTMS), and the sham stimulation group (Sham). Before the rTMS stimulation, the rats were anesthetized with 1% isoflurane in oxygen air and then fixed in the stereotaxic apparatus. The magnetic stimulator (VISHEE-TMS-013, Nanjing VISHEE Medical Technology, Nanjing, China) with a circular coil (inner diameter: 15 mm, outer diameter: 45 mm) was used to deliver the rTMS. In this study, the coil material was the 38-turns oxygen-free copper used in many studies which generates a vertical electric field. When TMS stimulation was performed, the TMS coil was fixed to the stereotaxic apparatus, and the center of the coil was attached tangentially to the rat's right lateral parietal association (LPtA) cortex (coordinates: ~3 mm lateral to the midline and ~ 3.36 mm caudal to Bregma). In addition, the center of the coil was hollowed, we could accurately locate the target coordinates to avoid displacement. For the rTMS+shileding group, the coil was attached with the custom shielding device which the inner radius was 7.5 mm. Therefore about 4.5 mm of the left hemisphere was exposed under the device hole. Meanwhile in the rTMS group, the coil was attached with a plastic board of the same weight. For the sham group, the rats were administered with an identical manipulation without real TMS stimulation (instead, they received an auditory stimulus) (Figure 2). In our study, 5 Hz rTMS protocol consisted of stimulation for 2 s followed by rest for 13 s and was repeated 60 times, at 35% maximum stimulator output of 15 min (600 pulses).

Immunofluorescence staining

Approximately 1.5 h after the rTMS paradigm, the rats were perfused with 0.9% sodium chloride followed by 4% paraformaldehyde. The brain tissues were fixed with 4% paraformaldehyde for 12 h before transferring into a 30% sucrose solution. Coronal sections were cut on a freezing microtome. The sections (30 μm) were washed with PBS three times, followed by 0.3% Triton X-100 incubation for 10 min and

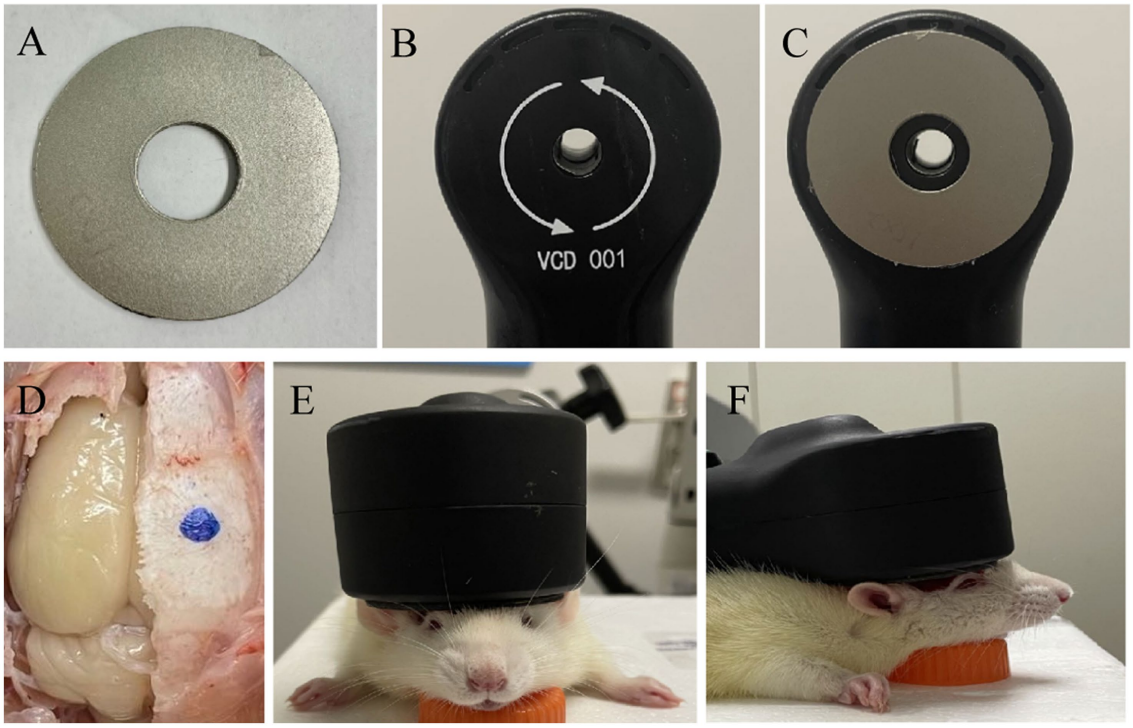

FIGURE 1
Schematic of TMS stimulation and shielding material. **(A)** Shielding device. **(B)** TMS coil. **(C)** The TMS coil with high magnetic permeability material. **(D)** The center of TMS stimulation at the blue dot. **(E,F)** Images of TMS stimulation on anesthetic rats.

1% BSA for 1 h at room temperature. Samples were then incubated with rabbit anti-c-fos antibody (1:1000, 226003, synaptic system) at 4°C overnight and then with donkey anti-rabbit IgG H&L (Alexa Fluor® 594) (1:1000, Abcam, USA) for 1 h at room temperature. A confocal laser-scanning microscope (Olympus, FV3000) was used to assess the c-fos expression in different groups.

MRI assessment

All the rats were further anesthetized with 1% isoflurane in oxygen air. The breathing and heart rate were monitored. The body temperature was kept by a water circulation system set at 37°C. *In vivo* whole-brain MRI images were acquired immediately after the rTMS ($n = 5$ per group) with an 11.7 T MRI scanner (Bruker, Ettlingen, Germany). A 4-channel surface array coil (Bruker BioSpin, Billerica, MA) was adopted to receive the magnetic resonance signals. The resting state functional MRI (rsfMRI) was acquired with a spin-echo echo-planer (SE-EPI) sequence: repetition time (TR) = 2000 ms, echo time (TE) = 12.8 ms, the field of view (FOV) = 30 × 30 mm, and slice thickness = 0.5 mm. The anatomical image (T2 image) was acquired by a spin echo (Turbo-RARE) sequence. The T2 image sequence parameters were: TR = 5,000 ms, TE = 25 ms, FOV = 30 × 30 mm, and slice thickness = 0.5 mm.

MRI data analysis

The MRI data were analyzed by the Statistical Parametric Mapping software (SPM12, University College London, U.K.), FMRIB Software Library (FSL), ANTs, and DPABI (a toolbox for Data Processing & Analysis for Brain Imaging). All the raw images were enlarged by a factor of ten to correlate the image dimensions to human images by SPM12. The rat brain mask was obtained by the ITK-SNAP (a toolbox for Data Processing & Analysis for Brain Imaging) and FSL. The slice timing, realignment, and normalization were processed by the *in vivo* functional template (SIGMA) using ANTs. After normalization, all images were smoothed using a Gaussian Kernel of 4 mm (FWHM).

The amplitude of low-frequency fluctuation (ALFF) and regional homogeneity (ReHo) was calculated for the traditional low-frequency band (0.01–0.08 Hz) by DPABI. One-way ANOVA (two-tailed) multiple comparisons test was used to analyze the ALFF and ReHo values among the sham group, the rTMS group, and the rTMS+shielding group. The resulting statistical map was set at $p < 0.05$ (with correct).

Statistical analysis

GraphPad Prism 8 and Image-J software were used to analyze the c-fos staining data. Data were presented as mean ± SEM using unpaired two-tailed Student's *t*-test. A value of $p < 0.05$ was considered significantly different.

Results

The shielding device increases the TMS coil focality

In order to validate the high magnetic permeability material shielding effect, we analyzed the electromagnetic field of the coil by

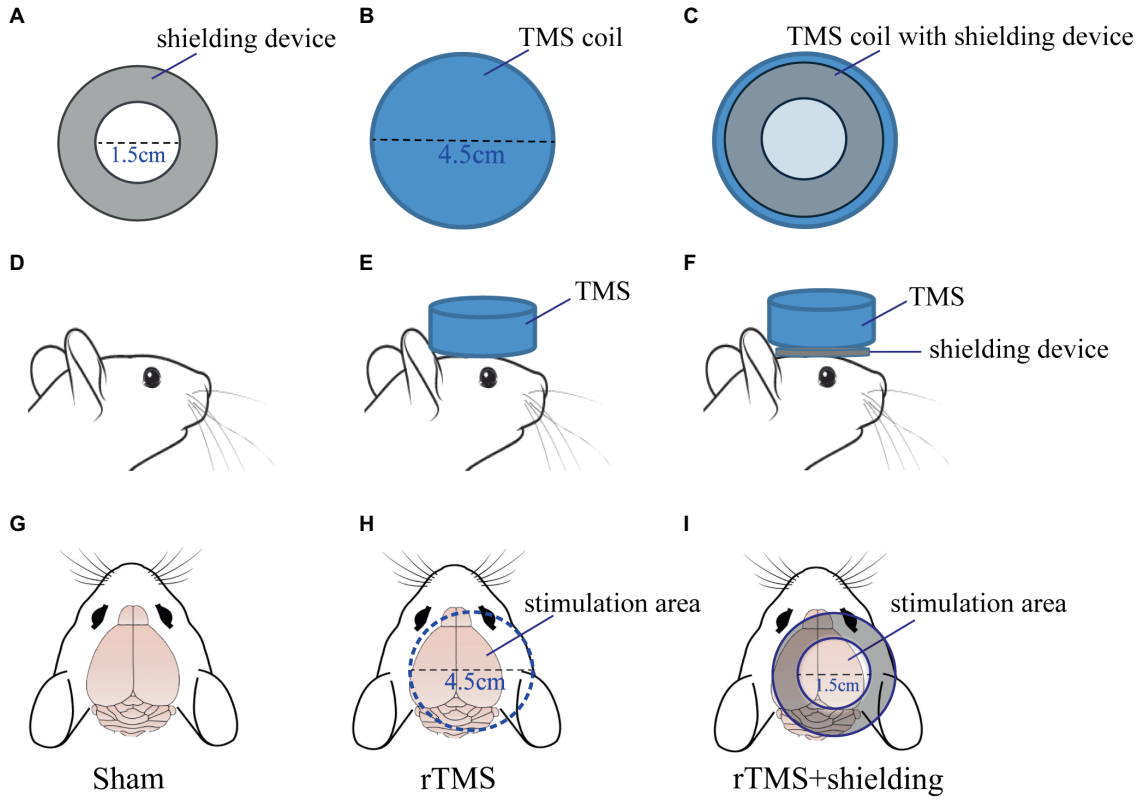

FIGURE 2
The TMS coil and shielding device. **(A)** The shielding device. **(B)** The TMS circular coil. **(C)** The TMS coil with the shielding device. **(D,G)** The sham group. **(E,H)** the rTMS group. **(F,I)** The rTMS +shielding group.

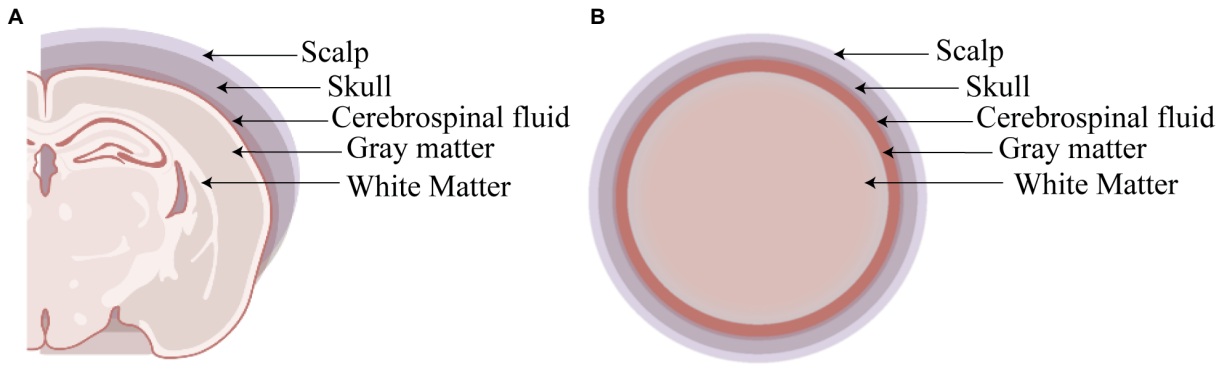

FIGURE 3
The rat head model. **(A)** Coronal section of rat head model. **(B)** The sphere shape of head model.

the finite element method (FEM) software ANSYS. As shown in Figures 3A,B, a concentric sphere model was established to mimic the rat head model. The model consisted of 5 parts, including the scalp, the skull, the cerebrospinal fluid (CSF), the gray matter (GM), and the white matter (WM). The specific parameters are shown in Table 1, including the radius, the conductivity, and the relative permittivity. With the shielding device, the TMS magnetic field was more focused. As shown in Figures 4A,B, the whole magnetic field distribution was smaller than the non-shielding group. Figures 4C,D shown that the 1 T magnetic field (green area), which is small enough to induce the neuron activity (Boyer et al., 2022), is 19.1 mm vs. 13 mm in diameter

TABLE 1 Tissue permittivity and conductivity.

Tissue name	Radius (mm)	Conductivity	Relative permittivity
Scalp	10	0.31061	25,809
Skull	9.7	0.02038	30,382
CSF	8.9	2	109
GM	8.8	0.10696	26,640
WM	7.4	0.65578	57,359

CSF, Cerebrospinal Fluid GM, Gray Matter WM, White Matter.

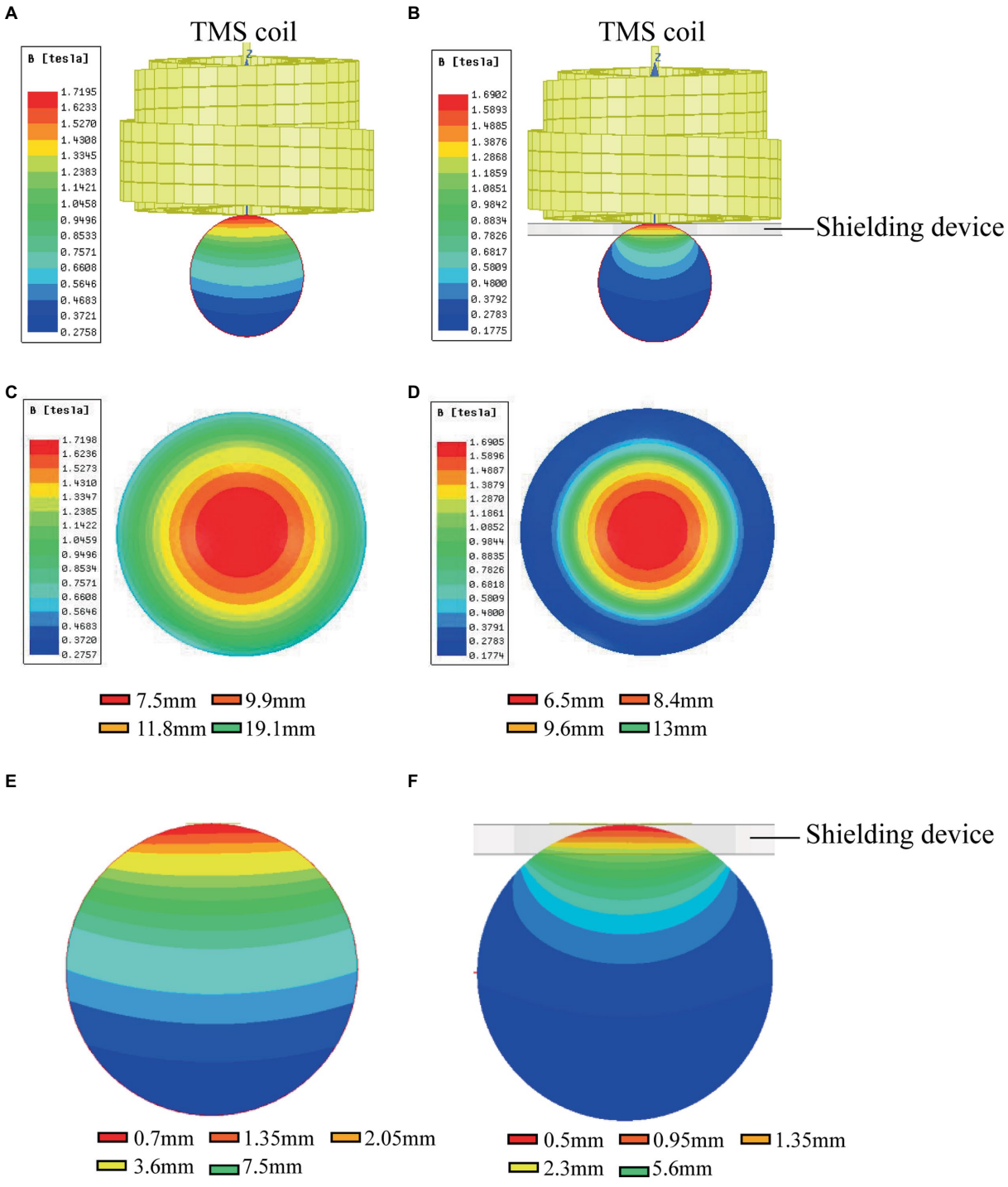

FIGURE 4
The magnetic fields of TMS coil with or without shielding device. **(A)** The sketch of the TMS coil without shielding device. **(B)** The sketch of the TMS coil with shielding device. **(C)** An overhead view of the magnetic field without the shielding device. **(D)** An overhead view of the magnetic field with the shielding device. **(E)** A coronal view of the magnetic field without the shielding device. **(F)** A coronal view of the magnetic field with the shielding device.

(rTMS vs. rTMS+shielding), while the magnetic field over 1.5 T (red area) is 7.5 mm vs. 6.5 mm (rTMS vs. rTMS+shielding). Furthermore, compared with the rTMS group, the depth of 1 T magnetic field (green area) was reduced from 7.5 to 5.6 mm, while the magnetic field over 1.5 T (red area) was reduced from 0.7 to 0.5 mm with the shielding device (Figures 4E,F). The electric field distributions of TMS coil with or without shielding device were significant differences, the results shown better focal stimulation in coil with shielding. Compare with the rTMS group, the area of electric field (read area) was reduced from 4.68cm^2 to 4.19cm^2, while the maximum E values in the center was reduced 30%, from 83 V/m to 58 V/m with the shielding device (Figures 5A–D). In addition, the depth (red arrow) of electric field was

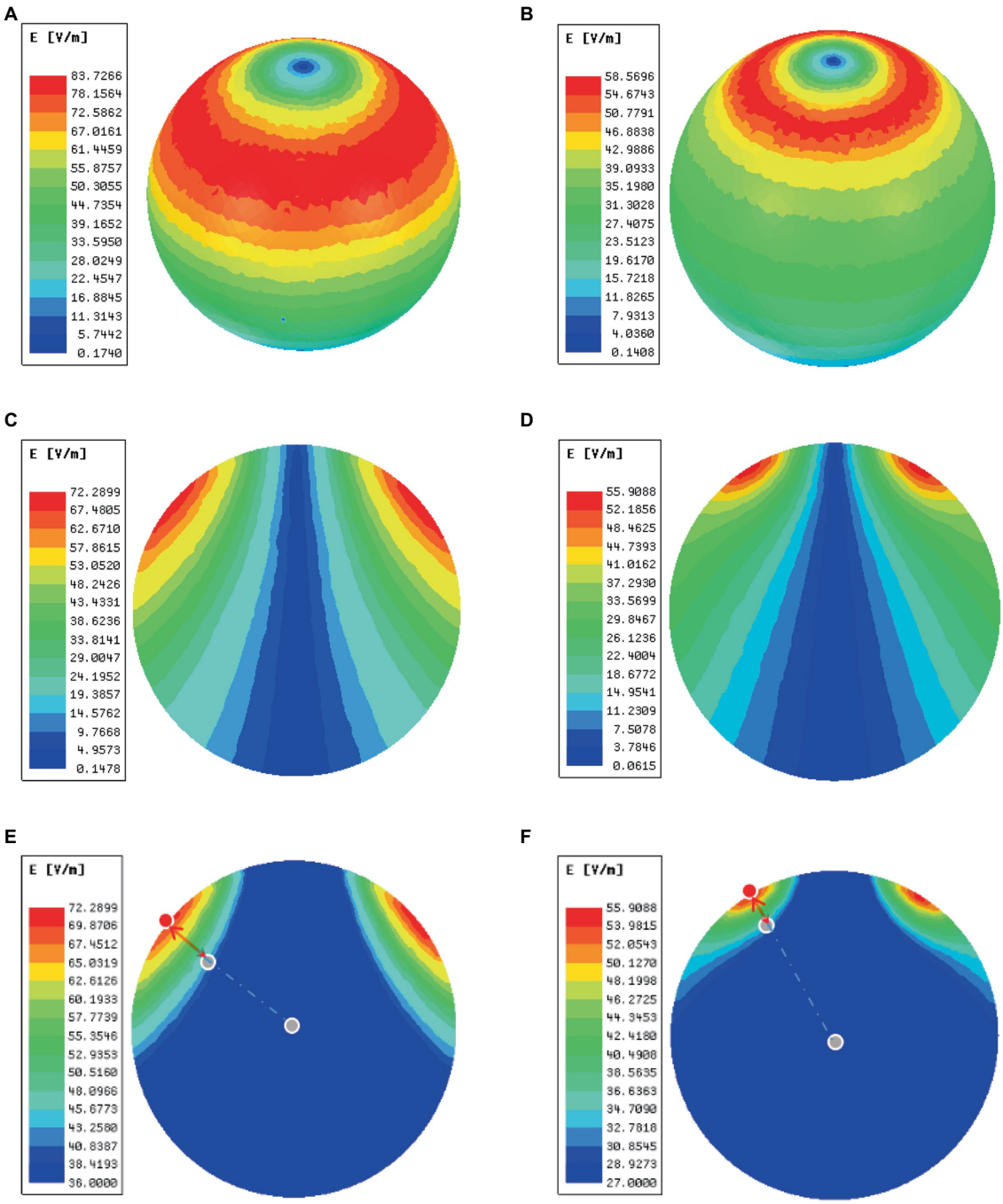

FIGURE 5
The electric fields of TMS coil with or without the shielding device. **(A)** An overhead view of the electric field without the shielding device. **(B)** An overhead view of the electric field with the shielding device. **(C)** A coronal view of the electric field without the shielding device. **(D)** A coronal view of the electric field with the shielding device. **(E)** The area (green area) and depth (red arrow) of electric field distribution without the shielding device. **(F)** The area (read area) and depth (red arrow) of electric field distribution with the shielding device. The red dots represent the electric field (E=E_max) of the cortical surface, and the gray dots in the center of the sphere represents the electric field (E=E_max/2) of the brain.

reduced from 3.8 mm to 2.6 mm, as well as the volume reduced from 1.78 cm^3 to 1.09 cm^3 (rTMS vs. rTMS+shielding; Figures 5E,F). The results indicated that a smaller focality with an identical core stimulation intensity was achieved in the shielding device. However, we should note that a different magnetic and electric field distribution occurred under the shielding material. A more vertical magnetic and electric field was produced by the device.

The shielding device reduces the rTMS-induced c-fos activation in the RSD, PtA, and S1 cortex

To further test the neuronal activity effect of TMS with shielding device *in vivo*, we assessed the c-fos expression, an indicator of neuronal activity that peaks 1–3 h post-stimulus exposure (Olsen

10.3389/fnins.2023.1129590

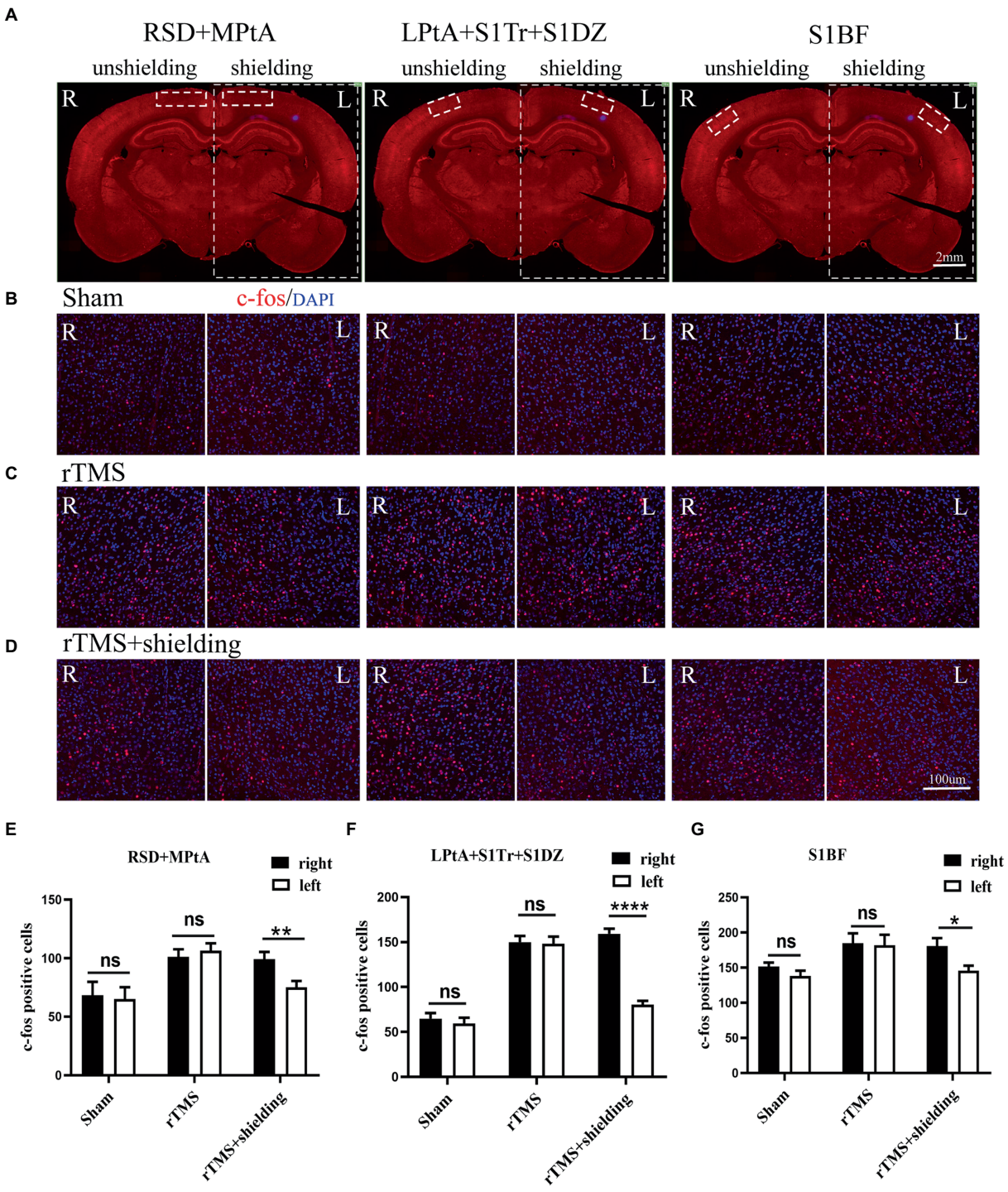

FIGURE 6
The c-fos expression in the cortex. **(A)** A schematic illustration of three different regions in the left and right cortex on a brain slice; the left cortex is under the shielding material, while the right cortex is exposed to the magnetic field. The scale bar is 2mm. **(B–D)** Representative fluorescent images of three different regions in the left and right cortex of the sham group **(B)**, the rTMS group **(C)** and the rTMS+shielding group **(D)**. The scale bar is 100μm. **(E–G)** Quantitative analyses of the c-fos expression in each group. Data are shown as the mean±SEM (n=3). *p< 0.05, **p< 0.01, ****p< 0.0001. RSD: retrosplenial dysgranular cortex; MPtA: medial parietal association cortex; LPtA:lateral parietal association cortex; S1Tr: primary somatosensory cortex, trunk region; S1DZ: primary somatosensory cortex, dysgranular region; S1BF: primary somatosensory cortex, barrel field.

et al., 2022). Compared with the sham group (Figure 6B), 1.5 h after one session (600 pulse) of rTMS increased the relative c-fos expression in the rTMS group (Figure 6C) in three regions (Figure 6A), i.e., the right RSD + MPtA (Sham vs. rTMS, p = 0.018), the right LPtA+S1Tr + S1DZ (Sham vs. rTMS, p < 0.0001) and the right S1BF (Sham vs. rTMS, p = 0.026). Moreover, the left RSD + MPtA, LPtA+S1Tr + S1DZ and S1BF also showed higher expression than the sham group. (Sham vs. rTMS, value of p is p = 0.004, p < 0.0001,

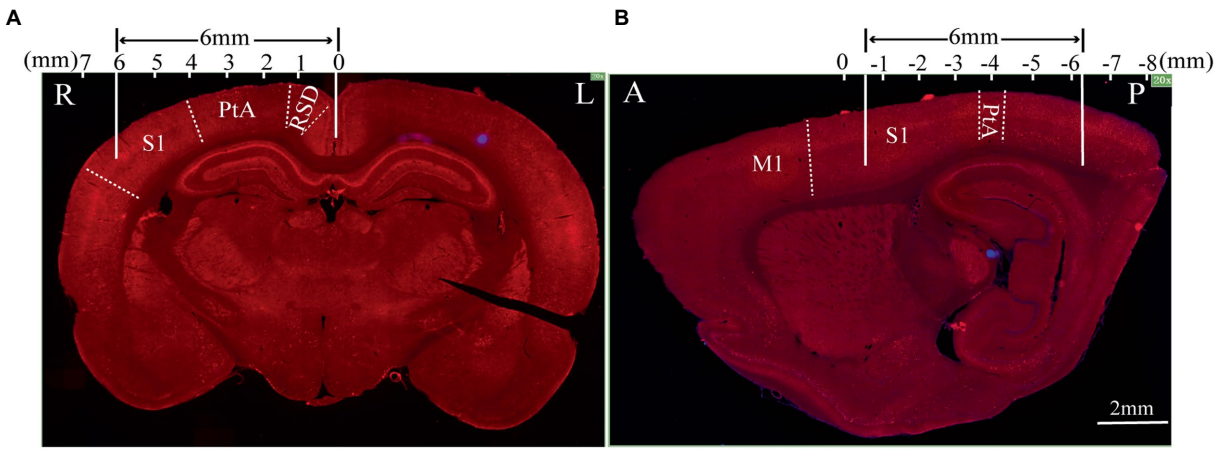

FIGURE 7
The effective stimulation area of the TMS coil with the shielding device. **(A)** Coronal section; **(B)** sagittal section.The scale bar is 2mm. S1: primary somatosensory cortex; PtA: parietal association cortex; RSD: retrosplenial dysgranular cortex; M1: primary motor cortex.

$p = 0.023$, respectively). Since the TMS coil was attached to the right hemisphere, in the rTMS+shielding group, the right cortex (unshielded region) was found to have a higher c-fos expression compared to the left cortex (shielded region), including the RSD + MPtA (right vs. left, $p = 0.009$), the LPtA+S1Tr + S1DZ (right vs. left, $p < 0.0001$) and the S1BF (right vs. left, $p = 0.011$; Figure 6D), while no difference was found between the two hemispheres in the sham group and rTMS group ($p > 0.05$; Figures 6E–G). The c-fos was the most expressed in the right RSD, PtA and S1 on the coronal section, and S1 and PtA on the sagittal section, while a low c-fos expression was detected around the area. This indicated that the effective stimulation area was approximately 6 mm in diameter with a shielding material (Figures 7A,B).

The shielded region shows less aftereffects following rTMS in brain structure and function

For assessment of the aftereffect of rTMS stimulation, fMRI was used to acquire high-spatial-resolution data. We measured the rsfMRI signals among the sham group, rTMS group, and rTMS+shielding groups. Compared to the sham group, the ALFF and ReHo values of the rTMS group showed that both the left and right hemispheres were activated by the rTMS, including the primary somatosensory cortex (S1), the secondary somatosensory cortex (S2), the striatum (CPu), the insular, the hippocampus, the thalamus and the hypothalamus (Figure 8A). However, compared to the sham group, the ALFF and ReHo values were significantly higher in the right cerebral hemisphere in the rTMS+shielding group. Different from the rTMS group, more right hemispherical area showed higher values in the rTMS+shielding group, like the retrosplenial dysgranular cortex (RSD) and parietal association cortex (PtA; Figure 8B). In addition, in comparison to the rTMS group, the ALFF and ReHo values in the right hemispheres were higher in the shielding group, including the piriform cortex (Pir) and S1, while in the left hemisphere, the values were obviously lower, like the S1 (Figure 8C).

Discussion

In the present study, we have developed a new TMS shielding device capable of enhancing the spatial focus of the TMS circular coils for rodents use. The new application was verified in the rat cortex, including the RSD, PtA, and S1. The electromagnetic field distribution and the neuronal activation results indicated a significant decrease in rTMS stimulation area in the anesthesia rats with the shielding device. In view of these findings, we provided a useful tool for further accurate TMS studies in rodents.

Compared with the previous shielding materials like silicon, we used a much thinner, lighter, and stronger absorbing material to shield the electromagnetic of the TMS coil. The material has better adhesion and anti-corrosion with low eddy current and good thermal conductivity. The material produces little heat after long-term TMS. Moreover, the material is flexible, which allows us to customize the shape to meet the needs of different stimulation paradigm. Furthermore, although previous studies have reported the highly permeable soft magnetic ferrite could improve the figure-eight coil focalization, the electric fields distribution of TMS coil has not been further validated on humans or animals (Zhang et al., 2013; Zhao et al., 2015). In our study, besides the magnetic and electric field distribution with the FEM, we also further validated the shielding effect *in vivo* with the fMRI and c-fos staining.

The inner diameter of the hole in the shielding device was 15 mm, the effective stimulation area was only approximately ~6 mm in diameter. Compared with the commercial rodents' TMS coil (15 mm in diameter), TMS coils with shielding devices achieved a better focality (~6 mm in diameter). With the center of the TMS coil aligned with the following coordinates: ~3 mm lateral to the midline and ~ 3.36 mm caudal to Bregma, only the RSD, PtA, and S1 were activated. This indicated that more specific brain area stimulation may be achieved by the shielding device, especially for those diseases involving the above brain areas, like stroke or other neurodegenerative diseases. Although the previous study reported a stimulation with 1 mm diameter (Meng et al.,

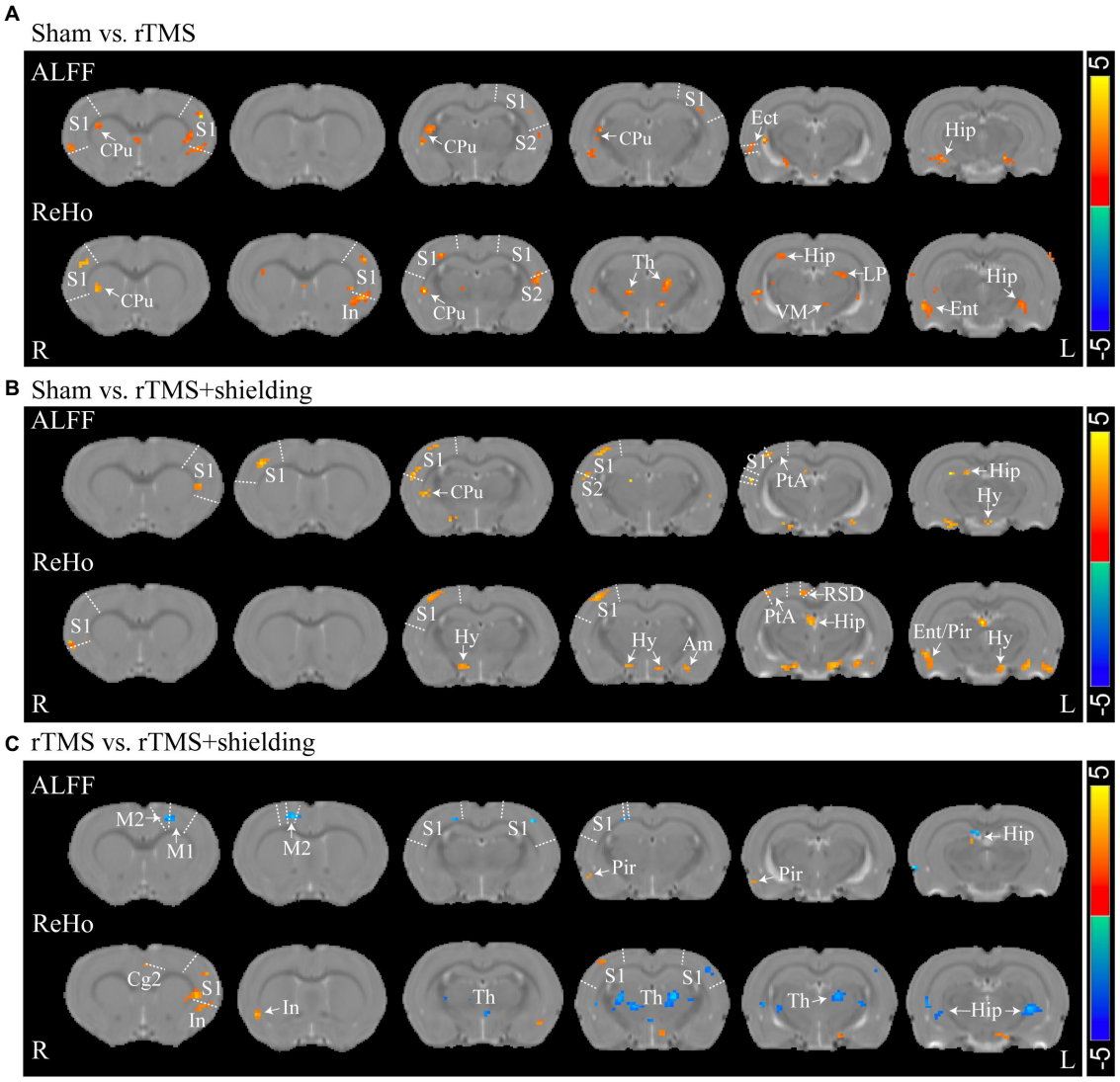

FIGURE 8
Statistical maps of a voxel of ALFF and ReHo analysis. **(A)** The ALFF and ReHo analysis between Sham (n=5) and rTMS groups (n=5). **(B)** Comparison of the ALFF and ReHo analysis between Sham and rTMS+shielding groups (n=5). **(C)** Comparison the ALFF and ReHo analysis between rTMS and rTMS+shielding groups. S1: primary somatosensory cortex; S2: secondary somatosensory cortex; CPu: Striatum; Th: thalamus; Hy: hypothalamus; Am: amygdaloid; Ect: ectorhinal cortex; LP: lateral posterior thalamic nucleus; PtA: parietal association cortex; Hip: hippocampus; RSD: retrosplenial dysgranular cortex; M2: secondary motor cortex; Ent: entorhinal cortex; Pir: piriform cortex; VM: ventromedial thalamic nucleus. In: insular; Cg2: cingulate cortex, area 2.

2022), the electromagnetic field may not be enough to provide continuous stimulation because of heating. As shown in Figures 4C–D, the 1 T magnetic field, which is enough to induce the neuron activity, was 19.1 mm vs. 13 mm in diameter (rTMS vs. rTMS+shielding), thus indicating a lower focality that was achieved with our shielding device. Moreover, without excessively changing the core stimulation, the magnetic field over 1.5 T (red area) was just 7.5 mm vs. 6.5 mm (rTMS vs. rTMS+shielding). Similarly, the area of electric field was reduced from 4.68cm^2 to 4.19cm^2, and the depth reduced from 3.8 mm to 2.6 mm (rTMS vs. rTMS+shielding). However, we should note that a different magnetic and electric field distribution occurred under the shielding material with a more vertical magnetic and electric field into the brain tissue. This may well explain the fMRI data showing more hemispherical region activation in the shielding group, such as S1.

Furthermore, different from the c-fos results, we also observed multiple neuron activation in the subcortical regions and S2 besides the cortical activation, like the striatum (CPu), the hippocampus, the thalamus, and the hypothalamus, which may be due to brain interconnection activation *via* transsynaptic way (Eldaief et al., 2011; Halko et al., 2014; Chen et al., 2020) since the primary somatosensory cortex (S1) sends a massive, topographically organized projection directly to the S2, striatum (CPu; Hur and Zaborszky, 2005; Aronoff et al., 2010; Sun et al., 2021; Whilden et al., 2021), while parietal association cortex (PtA) and retrosplenial dysgranular cortex (RSD) are also connected with the thalamus and hypothalamus (van Groen and Wyss, 1992). The activation of CPu and the deep nuclei of the

thalamus and hypothalamus may be due to the TMS stimulation in the S1 and other cortex.

The present study has several limitations. First, the ratio of the magnetic powder and epoxy resin, the TMS intensity and the frequency, the brain dielectric constants are all important variables that may affect the shielding effect, different models and TMS parameters may need accordingly adjustments. Secondly, we only explored the shielding effect by analyzing the neuronal activity and the BOLD response signals. However, motor evoked potential (MEP), a widely used tool to assess corticospinal conduction (Bestmann and Krakauer, 2015; Jiang et al., 2021; Wilson et al., 2021; Meng et al., 2022), may be another way to assess the shielding effect. Although the shielding was applied, we could locate more accurate M1 hotpots; yet, as noted above, attention should be paid to the effective neuron activity in the human head with our material parameters. Different kinds of head models may probably need a different but specific shielding material.

In summary, this study reported a novel TMS shielding device. Compared to the conventional animal TMS coil, this new tool provides a more focal and effective electric field induced in the rat hemisphere and may be used for future human translational TMS studies.

Data availability statement

The datasets presented in this article are not readily available because the original contributions presented in this study are included in the article/supplementary material, further inquiries can be directed to the corresponding author. Requests to access the datasets should be directed to QunZ, zqun_888@163.com.

Ethics statement

The animal study was reviewed and approved by Fudan University Animal Welfare and Ethics committee (Ethical permit numbers: 2020 Huashan hospital JS-151).

Author contributions

LiL, YZ, YFW, LuL, and JZ performed experiments. MD analyzed the fMRI data. SG, QuanZ, and KQ designed the shielding device and analysis data. QunZ, XX, YW, KY, NW, and HW designed the study and reviewed the manuscript. LiL and JW prepared manuscript. All authors contributed to the article and approved the submitted version.

Funding

This study was supported by the National Key R&D Program of China (2021ZD0202805 and 2019YFA0709504), the Natural Science Foundation of China (NSFC, nos. 81972141, 81972140, 82002392, 82172544 and 31900719), Shanghai Municipal Key Clinical Specialty (nos. SHSLCZDZK02702), and Shanghai Sailing Program (20YF1403500), the Innovative Research Team of High-level Local Universities in Shanghai, 111 Project (B18015), Shanghai Municipal Science and Technology Major Project (2018SHZDZX01), and Shanghai Center for Brain Science and Brain-Inspired Technology.

Conflict of interest

SG, QuanZ, and KQ were employed by Nanjing Vishee Medical Technology Co., Ltd.

The remaining authors declare that the research was conducted in the absence of any commercial or financial relationships that could be construed as a potential conflict of interest.

Publisher's note

References

Aronoff, R., Matyas, F., Mateo, C., Ciron, C., Schneider, B., and Petersen, C. C. (2010). Long-range connectivity of mouse primary somatosensory barrel cortex. *Eur. J. Neurosci.* 31, 2221–2233. doi: 10.1111/j.1460-9568.2010.07264.x

Bestmann, S., and Krakauer, J. W. (2015). The uses and interpretations of the motor-evoked potential for understanding behaviour. *Exp. Brain Res.* 233, 679–689. doi: 10.1007/s00221-014-4183-7

Boonzaier, J., Petrov, P. I., Otte, W. M., Smirnov, N., Neggers, S., and Dijkhuizen, R. M. (2020). Design and evaluation of a rodent-specific transcranial magnetic stimulation coil: an in silico and in vivo validation study. *Neuromodulation* 23, 324–334. doi: 10.1111/ner.13025

Boyer, M., Baudin, P., Stengel, C., Valero-Cabré, A., Lohof, A. M., Charpier, S., et al. (2022). In vivo low-intensity magnetic pulses durably alter neocortical neuron excitability and spontaneous activity. *J. Physiol.* 600, 4019–4037. doi: 10.1113/JP283244

Chen, J., Ma, N., Hu, G., Nousayhah, A., Xue, C., Qi, W., et al. (2020). rTMS modulates precuneus-hippocampal subregion circuit in patients with subjective cognitive decline. *Aging (Albany NY)* 13, 1314–1331. doi: 10.18632/aging.202313

Cohen, D., and Cuffin, B. N. (1991). Developing a more focal magnetic stimulator. Part i: some basic principles. *J. Clin. Neurophysiol.* 8, 102–111. doi: 10.1097/00004691-199101000-00013

Du, Y. (2022). Advances in carbon-based microwave absorbing materials. *Materials* 15:1359. doi: 10.3390/ma15041359

Eldaief, M. C., Halko, M. A., Buckner, R. L., and Pascual-Leone, A. (2011). Transcranial magnetic stimulation modulates the brain's intrinsic activity in a frequency-dependent manner. *Proc. Natl. Acad. Sci. U. S. A.* 108, 21229–21234. doi: 10.1073/pnas.1113103109

Gao, N., Li, W. P., Wang, W. S., Liu, D. P., Cui, Y. M., Guo, L., et al. (2020). Balancing dielectric loss and magnetic loss in fe-nis2/nis/pvdf composites toward strong microwave reflection loss. *ACS Appl. Mater. Interfaces* 12, 14416–14424. doi: 10.1021/acsami.9b23379

Guerra, A., Ranieri, F., Falato, E., Musumeci, G., di Santo, A., Asci, F., et al. (2020). Detecting cortical circuits resonant to high-frequency oscillations in the human primary motor cortex: a tms-tacs study. *Sci. Rep.* 10:7695. doi: 10.1038/s41598-020-64717-7

Halko, M. A., Farzan, F., Eldaief, M. C., Schmahmann, J. D., and Pascual-Leone, A. (2014). Intermittent theta-burst stimulation of the lateral cerebellum increases functional connectivity of the default network. *J. Neurosci.* 34, 12049–12056. doi: 10.1523/JNEUROSCI.1776-14.2014

Huang, Y., Chen, M., Xie, A., Wang, Y., and Xu, X. (2021). Recent advances in design and fabrication of nanocomposites for electromagnetic wave shielding and absorbing. *Materials* 14:4148. doi: 10.3390/ma14154148

Hur, E. E., and Zaborszky, L. (2005). Vglut2 afferents to the medial prefrontal and primary somatosensory cortices: a combined retrograde tracing in situ hybridization study [corrected]. *J. Comp. Neurol.* 483, 351–373. doi: 10.1002/cne.20444

Jiang, N., Wang, L., Huang, Z., and Li, G. (2021). Mapping responses of lumbar paravertebral muscles to single-pulse cortical tms using high-density surface electromyography. *IEEE Trans. Neural Syst. Rehabil. Eng.* 29, 831–840. doi: 10.1109/TNSRE.2021.3076095

Kim, D. H., Georghiou, G. E., and Won, C. (2006). Improved field localization in transcranial magnetic stimulation of the brain with the utilization of a conductive shield plate in the stimulator. *I.E.E.E. Trans. Biomed. Eng.* 53, 720–725. doi: 10.1109/TBME.2006.870244

Lefaucheur, J. P., Aleman, A., Baeken, C., Benninger, D. H., Brunelin, J., di Lazzaro, V., et al. (2020). Evidence-based guidelines on the therapeutic use of repetitive transcranial magnetic stimulation (rTMS): an update (2014–2018). *Clin. Neurophysiol.* 131, 474–528. doi: 10.1016/j.clinph.2019.11.002

Meng, Q., Nguyen, H., Vrana, A., Baldwin, S., Li, C. Q., Giles, A., et al. (2022). A high-density theta burst paradigm enhances the aftereffects of transcranial magnetic stimulation: evidence from focal stimulation of rat motor cortex. *Brain Stimul.* 15, 833–842. doi: 10.1016/j.brs.2022.05.017

Nuhiji, B., Bower, M. P., Proud, W., Burpo, S. J., Day, R. J., Scaife, R. J., et al. (2021). The effects of absorbing materials on the homogeneity of composite heating by microwave radiation. *Materials* 14:7362. doi: 10.3390/ma14237362

Olsen, L. K., Moore, R. J., Bechmann, N. A., Ethridge, V. T., Gargas, N. M., Cunningham, S. D., et al. (2022). Vagus nerve stimulation-induced cognitive enhancement: hippocampal neuroplasticity in healthy male rats. *Brain Stimul.* 15, 1101–1110. doi: 10.1016/j.brs.2022.08.001

Qin, M., Zhang, L., and Wu, H. (2022). Dielectric loss mechanism in electromagnetic wave absorbing materials. *Adv. Sci.* 9:e2105553. doi: 10.1002/advs.202105553

Rodger, J., Mo, C., Wilks, T., Dunlop, S. A., and Sherrard, R. M. (2012). Transcranial pulsed magnetic field stimulation facilitates reorganization of abnormal neural circuits and corrects behavioral deficits without disrupting normal connectivity. *FASEB J.* 26, 1593–1606. doi: 10.1096/fj.11-194878

Roth, Y., Amir, A., Levkovitz, Y., and Zangen, A. (2007). Three-dimensional distribution of the electric field induced in the brain by transcranial magnetic stimulation using figure-8 and deep h-coils. *J. Clin. Neurophysiol.* 24, 31–38. doi: 10.1097/WNP.0b013e31802fa393

Salinas, F. S., Franklin, C., Narayana, S., Szabo, C. A., and Fox, P. T. (2016). Repetitive transcranial magnetic stimulation educes frequency-specific causal relationships in the motor network. *Brain Stimul.* 9, 406–414. doi: 10.1016/j.brs.2016.02.006

Sun, Z., Schneider, A., Alyahyay, M., Karvat, G., and Diester, I. (2021). Effects of optogenetic stimulation of primary somatosensory cortex and its projections to striatum on vibrotactile perception in freely moving rats. *eNeuro* 8, ENEURO.0453–ENEU20.2021. doi: 10.1523/ENEURO.0453-20.2021

Tang, A. D., Lowe, A. S., Garrett, A. R., Woodward, R., Bennett, W., Canty, A. J., et al. (2016). Construction and evaluation of rodent-specific rTMS coils. *Front. Neural Circuits* 10:47. doi: 10.3389/fncir.2016.00047

Toledo, R. S., Stein, D. J., Sanches, P., Da, S. L., Medeiros, H. R., Fregni, F., et al. (2021). rTMS induces analgesia and modulates neuroinflammation and neuroplasticity in neuropathic pain model rats. *Brain Res.* 1762:147427. doi: 10.1016/j.brainres.2021.147427

Vahabzadeh-Hagh, A. M., Muller, P. A., Gersner, R., Zangen, A., and Rotenberg, A. (2012). Translational neuromodulation: approximating human transcranial magnetic stimulation protocols in rats. *Neuromodulation* 15, 296–305. doi: 10.1111/j.1525-1403.2012.00482.x

van Groen, T., and Wyss, J. M. (1992). Connections of the retrosplenial dysgranular cortex in the rat. *J. Comp. Neurol.* 315, 200–216. doi: 10.1002/cne.903150207

Wen, B., Cao, M., Lu, M., Cao, W., Shi, H., Liu, J., et al. (2014). Reduced graphene oxides: light-weight and high-efficiency electromagnetic interference shielding at elevated temperatures. *Adv. Mater.* 26, 3484–3489. doi: 10.1002/adma.201400108

Whilden, C. M., Chevee, M., An, S. Y., and Brown, S. P. (2021). The synaptic inputs and thalamic projections of two classes of layer 6 corticothalamic neurons in primary somatosensory cortex of the mouse. *J. Comp. Neurol.* 529, 3751–3771. doi: 10.1002/cne.25163

Wilson, M. T., Moezzi, B., and Rogasch, N. C. (2021). Modeling motor-evoked potentials from neural field simulations of transcranial magnetic stimulation. *Clin. Neurophysiol.* 132, 412–428. doi: 10.1016/j.clinph.2020.10.032

Xing, Y., Zhang, Y., Li, C., Luo, L., Hua, Y., Hu, J., et al. (2022). Repetitive transcranial magnetic stimulation of the brain after ischemic stroke: mechanisms from animal models. *Cell. Mol. Neurobiol.* doi: 10.1007/s10571-022-01264-x

Zhang, S., Yin, T., Liu, Z., Li, Y., Jin, J., and Ma, R. (2013). Experimental study to improve the focalization of a figure-eight coil of rTMS by using a highly conductive and highly permeable medium. *IEEE Trans. Neural Syst. Rehabil. Eng.* 21, 364–369. doi: 10.1109/TNSRE.2012.2194723

Zhang, C., Zhao, K., Li, X., Dong, W., Wang, S., Zhou, Y., et al. (2020). Natural iron embedded hierarchically porous carbon with thin-thickness and high-efficiency microwave absorption properties. *RSC Adv.* 10, 38989–38999. doi: 10.1039/d0ra07963d

Zhao, C., Zhang, S., Liu, Z., and Yin, T. (2015). Simulation study to improve focalization of a figure eight coil by using a conductive shield plate and a ferromagnetic block. *IEEE Trans. Neural Syst. Rehabil. Eng.* 23, 529–537. doi: 10.1109/TNSRE.2015.2389263

frontiers | Frontiers in Neuroscience

TYPE Original Research
PUBLISHED 05 May 2023
DOI 10.3389/fnins.2023.1168773

OPEN ACCESS

EDITED BY
Ying Shen,
The First Affiliated Hospital of Nanjing Medical University, China

REVIEWED BY
Nan Yan,
Chinese Academy of Sciences (CAS), China
Xiaokuo He,
Xiamen Fifth Hospital, China
Chuan Guo,
Nanjing Medical University, China

*CORRESPONDENCE
Yulai Gong
✉ 38146686@qq.com

RECEIVED 18 February 2023
ACCEPTED 18 April 2023
PUBLISHED 05 May 2023

CITATION
Zou J, Yin Y, Lin Z and Gong Y (2023) The analysis of brain functional connectivity of post-stroke cognitive impairment patients: an fNIRS study.
Front. Neurosci. 17:1168773.
doi: 10.3389/fnins.2023.1168773

The analysis of brain functional connectivity of post-stroke cognitive impairment patients: an fNIRS study

Jiahuan Zou[1], Yongyan Yin[1], Zhenfang Lin[2] and Yulai Gong[2]*

[1]School of Medical and Life Sciences, Chengdu University of Traditional Chinese Medicine, Chengdu, Sichuan, China, [2]Department of Neurology, Sichuan Bayi Rehabilitation Center (Sichuan Provincial Rehabilitation Hospital), Chengdu, Sichuan, China

Background: Post-stroke cognitive impairment (PSCI) is a considerable risk factor for developing dementia and reoccurrence of stroke. Understanding the neural mechanisms of cognitive impairment after stroke can facilitate early identification and intervention.

Objectives: Using functional near-infrared spectroscopy (fNRIS), the present study aimed to examine whether resting-state functional connectivity (FC) of brain networks differs in patients with PSCI, patients with Non-PSCI (NPSCI), and healthy controls (HCs), and whether these features could be used for clinical diagnosis of PSCI.

Methods: The present study recruited 16 HCs and 32 post-stroke patients. Based on the diagnostic criteria of PSCI, post-stroke patients were divided to the PSCI or NPSCI group. All participants underwent a 6-min resting-state fNRIS test to measure the hemodynamic responses from regions of interests (ROIs) that were primarily distributed in the prefrontal, somatosensory, and motor cortices.

Results: The results showed that, when compared to the HC group, the PSCI group exhibited significantly decreased interhemispheric FC and intra-right hemispheric FC. ROI analyses showed significantly decreased FC among the regions of somatosensory cortex, dorsolateral prefrontal cortex, and medial prefrontal cortex for the PSCI group than for the HC group. However, no significant difference was found in the FC between the PSCI and the NPSCI groups.

Conclusion: Our findings provide evidence for compromised interhemispheric and intra-right hemispheric functional connectivity in patients with PSCI, suggesting that fNIRS is a promising approach to investigate the effects of stroke on functional connectivity of brain networks.

KEYWORDS

stroke, post-stroke cognitive impairment, functional connectivity, functional near-infrared spectroscopy, assessment

Introduction

Stroke, the third leading cause of mortality globally, continues to be a significant contributor to long-term disability and cognitive impairment (Feigin et al., 2021). Stroke-induced structural damage can have widespread effects on brain function beyond the focal lesion site (Griffis et al., 2020). The risk of cognitive impairment after stroke is estimated to be five to eight times higher

than in the general population (Kulesh et al., 2018). A previous study found that, despite minimal or no physical impairment, nearly half of patients with a lacunar infarct had cognitive impairment after stroke (Jacova et al., 2012). Moreover, post-stroke cognitive impairment (PSCI) is associated with an increased risk of recurrent stroke (Rostamian et al., 2014).

The assessment of cognitive function after stroke is challenging, as there is no agreed-upon gold standard for measuring PSCI. Several neuropsychological tests are commonly used, such as the Informant Questionnaire for Cognitive Decline in the Elderly (IQCODE), Oxford Cognitive Screen (OCS), Mini-Mental State Examination (MMSE), and Montreal Cognitive Assessment (MoCA) (Zhang and Bi, 2020). However, these tests may be influenced by post-stroke complications (e.g., language impairment, mood disorders) and the timing of testing (Huang et al., 2022), which could limit their validity and reliability for diagnosing and predicting PSCI. Moreover, although various biomarkers for PSCI have been proposed in recent years, such as genetic polymorphisms, inflammatory markers, growth factors, oxidative damage markers, and metabolic markers (Mijajlovic et al., 2017; Zhang and Bi, 2020), none of them have been widely accepted or validated.

Non-invasive neuroimaging techniques such as functional magnetic resonance imaging (fMRI) and functional near-infrared spectroscopy (fNIRS) have emerged as effective tools to explore the intrinsic functional organization of the human brain. Previous studies have shown a significant correlation between the hemodynamic responses measured by fNIRS and the blood oxygen level dependent (BOLD) responses obtained by fMRI, suggesting a close analogy between the two methods (Cui et al., 2011; Sato et al., 2013). However, fMRI may not be feasible for some patients due to the severity of their illness or various contraindications (Pendlebury et al., 2015). Furthermore, the noise of the MRI scanner and the discomfort of immobilization may confound the natural frequency or quality of stimulus-independent thoughts (Pinti et al., 2020), which could affect the accurate assessment of cognitive impairment. fNIRS, on the other hand, has advantages over other neuroimaging techniques, such as higher spatial resolution than EEG/MEG, higher temporal resolution than fMRI, and lower sensitivity to body movement (Huo et al., 2021). Therefore, fNIRS may be a suitable alternative for investigating the neural mechanisms of cognitive impairment related to stroke.

Functional connectivity (FC) analysis is a common method to assess brain function (Zhang et al., 2022). The human brain is a complex and dynamic system that can be modeled as a network of structural or functional connections (Niu and He, 2014). FC quantifies the temporal correlation of neurophysiological events in spatially distinct brain regions and reveals functional interactions of specific brain areas and local networks (Auer, 2008). Previous studies have shown that FC disruptions caused by lesions are strongly related to clinical impairments in various cognitive and behavioral domains (Baldassarre et al., 2016b). In the present study, we used fNIRS to examine the changes in resting-state FC among certain brain regions involved in cognitive functions in stroke patients with and without cognitive impairment and healthy controls. We aimed to improve the screening methods for PSCI risk and to elucidate the neural mechanisms of PSCI.

Materials and methods

Participants

Thirty-two stroke patients were recruited from Sichuan Bayi Rehabilitation Center in the present study. The inclusion criteria for stroke patients were as follows: (1) stroke that occurred 1–6 months prior to the first assessment (Dong et al., 2021), confirmed by clinical CT or MRI scanning during hospitalization; (2) age between 30 and 70 years; (3) no history of previous clinical stroke, dementia, untreated psychiatric illness, uncorrected hearing or visual impairment, aphasia or neglect; and (4) able to follow instructions and consent to participate. Also, 16 age-matched healthy participants were included as a control group. The inclusion criteria for HC were: (1) no history of neurological or psychiatric diseases; (2) normal cognitive function. All participants were right-handed and provided written informed consent in accordance with the Declaration of Helsinki. The experimental protocol was approved by the ethics committee of the Sichuan Bayi Rehabilitation Center (CKLL-20220010).

Clinical assessment and diagnosis of PSCI

The stroke patients were divided to two groups: PSCI group and NPSCI group. The diagnostic criteria of PSCI were defined as follows: (1) the patient or a reliable informant reported cognitive impairment after stroke, or a clinician observed cognitive impairment after stroke; (2) the patient scored below the education-adjusted cutoffs on the MoCA test: ≤13 for illiterate individuals, ≤19 for those with 1–6 years of education, and ≤24 for those with 7 or more years of education (Lu et al., 2011). An experienced therapist from the Department of Rehabilitation Medicine in Sichuan Bayi Rehabilitation Center administered the Chinese version of MMSE and MoCA (Jia et al., 2021) to assess the cognitive function of all participants. Participants' demographic and clinical characteristics are presented in Table 1.

Data acquisition

A multi-channel fNIRS system (NIRSport, NIRx Medical Technologies LLC) was used to measure the concentration change of oxyhemoglobin (HbO), deoxyhemoglobin (HbR), and total hemoglobin (HbT). The system recorded the absorption of near-infrared light at the wavelengths of 760 and 850 nm with a sampling frequency of 7.8 Hz. The Modified Beer–Lambert law (MBLL) (Cui et al., 2011) was used to calculate the changes in chromophore concentrations from the attenuation of light entering the head at multiple wavelengths. We placed 16 emitters and 15 detectors alternately in each location according to the international 10–20 electroencephalography (EEG) placement system, resulting in a total of 31 probes with 40 measurement channels (see Figure 1). The distance between an emitter and a detector pair was 3 cm. The area between the detector probe and emitter probe pair was defined as a "channel." The middle optrode was placed on the FPz, and the lowest probes were positioned along the Fp1-Fp2 line. The emitters and detectors were symmetrically located in the prefrontal cortex (PFC), sensorimotor cortex (SMC), and premotor and supplementary motor

TABLE 1 The demographic and clinical characteristics of all subjects.

Characteristics	PSCI (*n*=16)	NPSCI (*n*=16)	HC (*n*=16)	*p*-value
Age (years) [median (IQR)]	62.0 (7.75)	54.5 (11.75)	54.0 (6.5)	0.060
Gender [*N* (%)]				0.135
Male	12 (75)	15 (94)	10 (63)	
Female	4 (25)	1 (6)	6 (37)	
Education (years) [median (IQR)]	7.5 (6.00)	9 (9.75)	9 (5.25)	0.447
Stroke type [*N* (%)]				0.156
Ischemic stroke	11 (69)	6 (38)	—	
Hemorrhage stroke	5 (31)	10 (62)	—	
Disease duration (days) [median (IQR)]	60 (76.75)	90 (108)	—	0.416
Hemisphere of lesion [*N* (%)]				1.000
Left	6 (38)	6 (38)	—	
Right	9 (56)	9 (56)	—	
Bilateral	1 (6)	1 (6)	—	
Lesion location [*N* (%)]				0.452
Frontoparietal lobe	4 (25)	4 (25)	—	
Brain stem	3 (19)	1 (6)	—	
Thalamus	2 (12)	0 (0)		
Basal ganglia	6 (38)	8 (50)	—	
Multiple sites	1 (6)	3 (19)		
MMSE [median (IQR)]	23.5 (5.75)	28.0 (1.00)	29.0 (1.75)	<0.001
MoCA [median (IQR)]	16 (4.25)	24 (2.00)	26 (3.00)	<0.001

PSCI, post-stroke cognitive impairment; NPSCI, post-stroke without cognitive impairment; HC, healthy controls; S, ischemic stroke; H, hemorrhagic stroke; MMSE, Mini-Mental State Examination; MoCA, Montreal Cognitive Assessment.

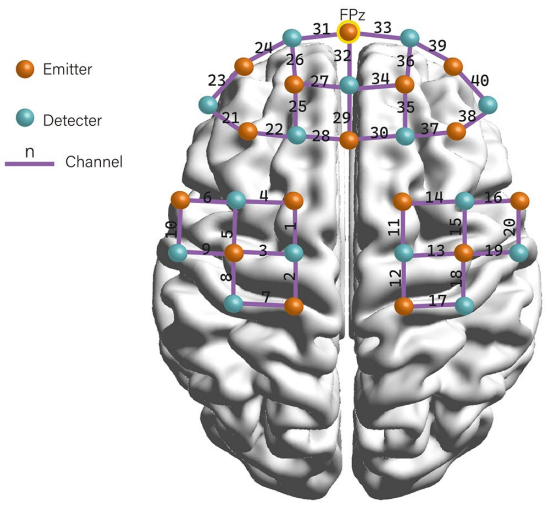

FIGURE 1
Configuration of fNIRS channels.

cortex (PMC/SMA) regions on both hemispheres. Participants wore the fNIRS detection cap and sat in a chair. They were instructed to keep still with their eyes closed, relax their mind, and minimize their movement for at least 6 min for the resting-state recording (Guo et al., 2022).

Data preprocessing

Preprocessing of fNIRS data was performed using Homer2 toolbox in Matlab 2013a (MathWorks Inc.). Noisy channels and unrelated time periods were manually identified and removed prior to converting the data into optical density data. Channels with motion artifacts were identified and corrected (Scholkmann et al., 2010), and removed by performing cubic spline interpolation. A 3th order Butterworth band-pass filter with cut-off frequencies of 0.01–0.1 Hz was then applied to remove artifacts, including cardiac interference (~1.3 Hz) and respiration (~0.25 Hz) (Pinti et al., 2018). Finally, the modified Beer–Lambert equation was used to convert the optical density data into HbO and HbR concentrations.

Functional connectivity

According to the standard Brodmann brain localization, the 40 channels were divided into 13 regions of interests (ROIs), including the left/right dorsolateral PFC (DLPFC), ventrolateral PFC (VLPFC), orbital PFC (OFC), primary somatosensory cortex (S1), primary motor cortex (M1), premotor cortex and supplementary motor area (PMC/SMA), and the medial PFC (MPFC). We averaged the HbO, HbR, and HbT of all channels in each ROI and then calculated the Phase-Locking Value (PLV) as the FC value to describe the linear correlation relationship of two-time domain signals. The formula used is as follows: $PLV_t = \frac{1}{n}\left|\Sigma_{t=1}^{n} e^{i(\phi_{xt}-\phi_{yt})}\right|$, where n is the number of timepoints, ϕ_{xt} represents the phase value of the signal X at time t, and ϕ_{yt} is the phase value of the signal Y at time t. The value range of PLV is [0,1].

Data analyses

Demographic and clinical differences between PSCI patients, N-PSCI patients, and healthy subjects were analyzed using SPSS Statistics 26.0. The Shapiro–Wilk test confirmed that all variables were not normally distributed. The Mann–Whitney *U*-test was used to compare disease duration and the Kruskal-Wallis H test was used to compare age, education, MMSE and MoCA. Sex, stroke types, hemisphere of lesion, and lesion location were compared using Fisher's exact probability method.

The fNIRS data were analyzed using MATLAB (2020a, MathWorks Inc.). One-way ANOVA was performed on the hemisphere-based FC and the ROI-based FC separately. False discovery rate (FDR) was used to correct the *p*-value. Bonferroni correction was used for the multiple comparisons. A difference with $p < 0.05$ was considered statistically significant.

Results

Demographic and physiological characteristics

The present study recruited 33 stroke patients in total. One PSCI patient was excluded from the analysis due to his poor channel signal quality. Therefore, the final sample consisted of 16 PSCI patients, 16 NPSCI patients, and 16 HCs. Table 1 shows the demographic and clinical characteristics of the three groups. There were no significant differences in age, gender, education, stroke type, disease duration, hemisphere of lesion, and lesion location among the groups ($p > 0.05$). The PSCI group had lower MMSE and MoCA scores than the NPSCI group ($p < 0.001$). The NPSCI and HC groups did not differ significantly in MMSE and MoCA scores ($p > 0.05$, Bonferroni corrected).

Hemisphere-based functional connectivity

To examine the differences in connectivity patterns across hemispheres, we analyzed the FC based on three hemoglobin concentrations: HbO, HbR, and HbT. The results showed that FCs based on HbO and HbT were not significantly different across the three groups ($p > 0.05$, FDR corrected). Figure 2 shows the main changes in FC between interhemispheric and intrahemispheric regions based on HbR. The results showed that the NPSCI and PSCI groups had significantly lower interhemispheric FC than the HC group ($p = 0.005$ and $p = 0.013$, respectively, Bonferroni corrected; Figure 2A). Additionally, the PSCI group had significantly lower FC within the right hemisphere than the HC group ($p = 0.008$, Bonferroni corrected; Figure 2B). There was no significant difference in FC within the left hemisphere among the three groups ($p > 0.05$, FDR corrected; Figure 2C).

Region-of-interest-based functional connectivity

Figure 3A displays the correlation matrix maps of HbR-based FC within the HC, NPSCI, and PSCI groups. There were significant differences among the three groups in S1.L-DLPFC.R ($F = 7.48$, $p = 0.031$, FDR corrected), S1.R-DLPFC.R ($F = 14.04$, $p = 0.001$, FDR corrected), S1.R-MPFC ($F = 9.83$, $p = 0.011$, FDR corrected), PMC/SMA.L-DLPFC.R ($F = 8.00$, $p = 0.028$, FDR corrected), and PMC/SMA.L-DLPFC.R ($F = 8.00$, $p = 0.028$, FDR corrected; Figure 3B). *Post-hoc* Bonferroni comparisons showed that NPSCI and PSCI groups had significantly lower FC in S1.L-DLPFC, S1.R-DLPFC.R, S1.R-MPFC ($p < 0.05$) than the HC group. In addition, as shown in Figure 3C, the NPSCI group showed significantly decreased FC in PMC/SMA.L-DLPFC, and the PSCI group showed significantly decreased FC in S1.L-S1.R. However, there was no significant difference between the NPSCI and PSCI groups in any region. Similarly, the FC based on HbO and HbT were not significantly different across the three groups.

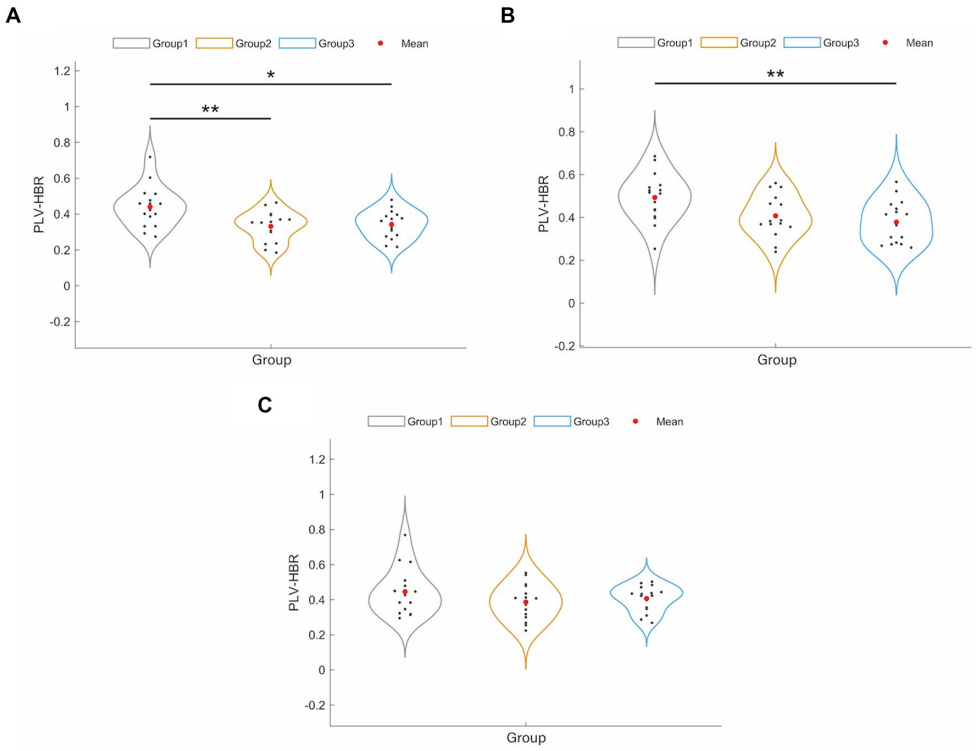

FIGURE 2
The results of significant changes of hemisphere-based FC value between HC, PSCI and NPSCI groups based on HbR. **(A)** Interhemispheric FC. **(B)** Intra-right hemispheric FC. **(C)** Intra-left hemispheric FC. Group 1: HC group; group 2: NPSCI group; group 3: PSCI group. $*p<0.05$, $**p<0.01$.

Discussion

In the present study, we used fNIRS-based resting-state FC to investigate the changes in brain network patterns in PSCI patients compared to HCs. Our main finding was that the PSCI group showed a significant reduction of interhemispheric FC relative to HCs, which was in line with previous fMRI studies. Siegel et al. (2016) proposed the "network phenotype of stroke injury," based on resting-state fMRI data from 100 sub-acute stroke patients, which was characterized by decreased interhemispheric FC and increased intrahemispheric FC between normally anticorrelated networks. Similar decreases in interhemispheric FC have been reported in various behavioral domains after stroke, such as attention, language, motor function, memory, and vision (Baldassarre et al., 2014, 2016a; Tang et al., 2016; Tao and Rapp, 2020; Tao et al., 2022). Our finding adds more evidence to the notion that impaired interhemispheric communication may be a key feature of stroke.

The neural mechanism underlying the reduced interhemispheric FC after stroke remains unclear. One possible explanation is that the structural connections or mechanisms that facilitate the transfer of signals between the hemispheres may be damaged or dysfunctional (Siegel et al., 2016). An animal stroke model study showed that reduced interhemispheric FC was related to decreased transcallosal manganese transport from contralesional M1 to ipsilesional SMC (van Meer et al., 2010). However, Siegel et al. (2016) found that lesion load only partially predicted the global average reduction in interhemispheric FC ($r = 0.46$), and that lesion location information did not improve the prediction. This finding suggests that interhemispheric FC disruption is a general consequence of stroke rather than a result of specific structural damage to the corpus callosum or thalamus. Tao and Rapp (2020) found that the interhemispheric FC of chronic post-stroke dysgraphia was significantly and positively correlated with spelling performance. Another study examined the predictive value of resting-state FC measured by fMRI on the third post-stroke day for the 90-day functional outcome of patients. They found that patients with better functional outcome had higher interhemispheric FC than patients with worse outcome. These findings indicate that interhemispheric FC could be a potential biomarker for the functional prognosis of stroke patients.

We also found that the PSCI group had lower FC within the right hemisphere than the HCs. There is abundant but inconsistent evidence for intra-hemispheric connectivity. Siegel et al. (2016) proposed the second stroke phenotype feature as increased FC between ipsilesional dorsal attentional network (DAN) and default mode network (DMN). They also found that this increased FC between ipsilesional functional networks was correlated with the decrease in interhemispheric FC. Similarly, increased correlations between regions within each hemisphere have been observed in monkeys after corpus callosum and anterior commissure separation (O'Reilly et al., 2013). Puig et al. (2018) suggested that structural neural adaptations may occur in more severe brain damage, with reduced interhemispheric connectivity leading to compensatory increase in ipsilateral connectivity, which may not be needed in patients with good prognosis. Tao and Rapp (2020) found that patients with chronic post-stroke dysgraphia had higher intrahemispheric connectivity in both the ipsilesional and contralesional hemispheres. However, several studies have reported lower than normal intrahemispheric FC in post-stroke aphasia (van Hees et al., 2014; Zhu et al., 2014; Nair et al., 2015). These results suggest that the effects of lesions on FC may differ across different functional networks within each hemisphere, and that the intrahemispheric FC patterns cannot be simply described as being overall higher or lower than normal. Therefore, we need to interpret this result with caution.

The analysis of ROIs showed that PSCI group had decreased FC in S1.L- S1.R, S1.L-DLPFC.R, S1.R-DLPFC.R, and S1.R-MPFC compared to HCs. Several fMRI studies have linked cognitive impairment to disruption of the default mode network (DMN) and the frontoparietal network (FPN) in stroke (Ding et al., 2014; Jiang et al., 2018; Rao et al., 2022). The DMN and FPN systems are both involved in spontaneous thought (Smallwood et al., 2012). The DMN is associated with stimulus-independent cognition and has two main hubs: the posterior cingulate cortex (PCC) and MPFC (Buckner and DiNicola, 2019). Jiang et al. (2018) found reduced connectivity within the DMN (especially the right MPFC and precuneus) in patients with acute brainstem ischemic stroke. The FPN is involved in cognitive control and mainly includes the middle frontal gyrus, dorsal anterior cingulate cortex, precuneus, caudate nucleus, and DLPFC (Andrews-Hanna, 2012). The functional integration of the FPN and overall cognitive ability have a significant positive correlation, suggesting that the strength of functional integration of the FPN and the rest of the brain is crucial for supporting superior cognitive functioning (Marek and Dosenbach, 2018). A study of dynamic functional network connectivity analysis suggested that cognitive impairment after stroke may result from a functional disconnection between the primary and FPN-centered high-order cognitive control networks. Increased FPN-centered functional network connectivity might compensate for maintaining cognitive function (Rao et al., 2022). The decreased functional connectivity of these regions may reflect functional and structural changes caused by stroke, which may impair the brain network integration and affect multiple cognitive domains.

Interestingly, the present study only found a significant difference in the connectivity derived from HbR during the resting state, and no significant results in the FC based on HbO and HbT. Nguyen et al. (2019) suggested that HbR might be more specific to the brain functional connectivity during resting state because it is more closely related to the amount of oxygen consumed by the tissues. HbO, on the other hand, is mainly related to the oxygen inflow of the brain tissue and generally considered to be the most reliable indicator for functional brain activation since it has a higher amplitude and is less affected by noise (Wolf et al., 2011). Previous studies on functional activation have shown that the BOLD signal has a stronger temporal and spatial correlation with HbR than with HbO (Huppert et al., 2006; Alderliesten et al., 2014). However, many studies have found either a slightly better correlation or a consistent correlation with HbO (Wolf et al., 2011; Duan et al., 2012; Sasai et al., 2012). Several resting-state FC studies based on fNIRS have reported that, compared to HbO, the more locally focused RSFC pattern of HbR, along with weaker RSFC strength, resulted in lower reliability (Lu et al., 2010; Zhang et al., 2010; Wolf et al., 2011), although the difference in reliability between the fNIRS parameters was small. These conflicting results indicate that more research is needed to clarify the relationship between the fNIRS parameters and their impact on RSFC.

Our work offers a new insight into the mechanisms of cognitive deficits in stroke patients, but it has some limitations. First and foremost, we recruited a relatively small number of individuals from a single institution. This ensured the quality of the data, but limited the statistical power and generalizability of the results. Moreover, the clinical characteristics of patients are quite

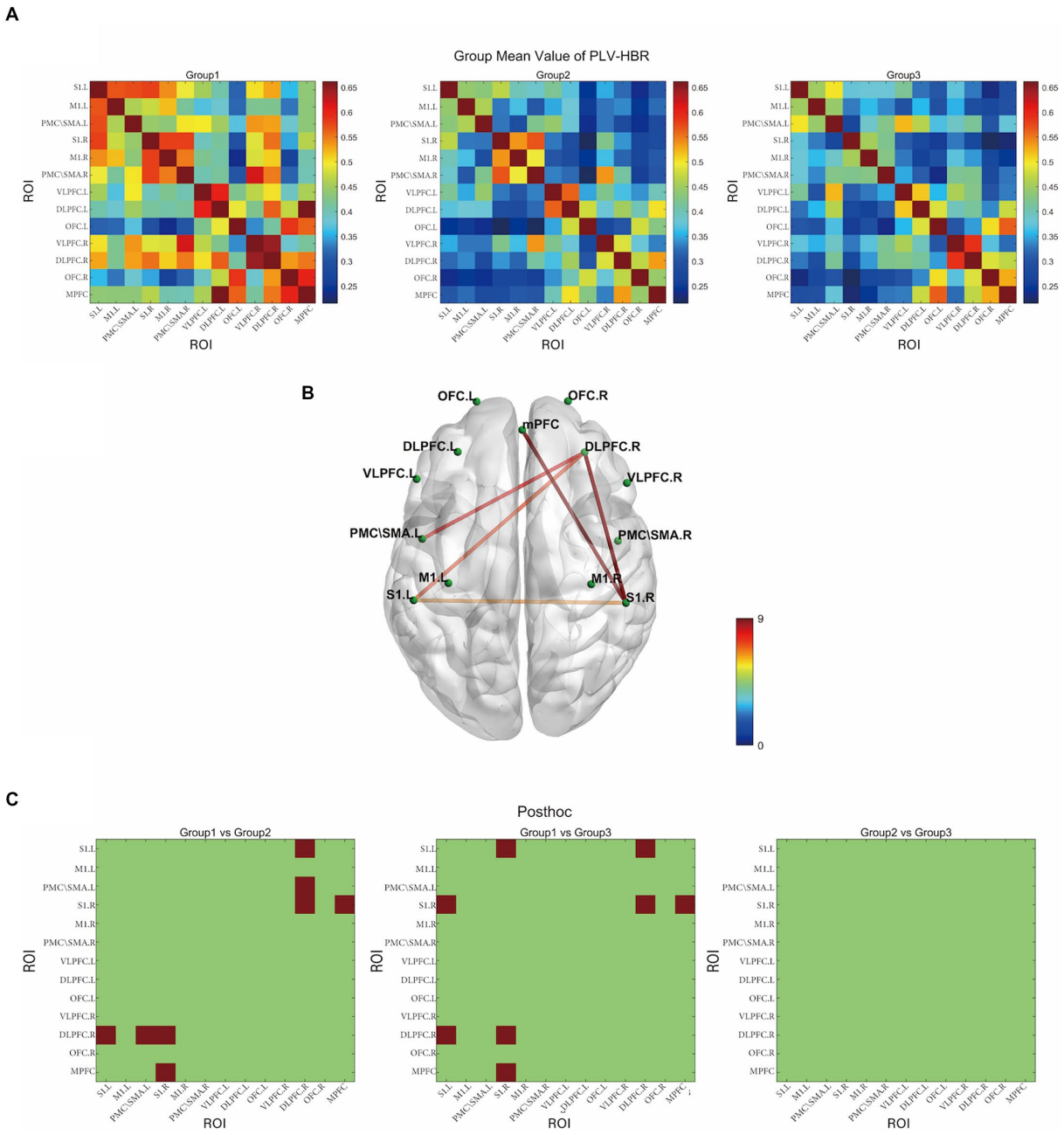

FIGURE 3
The resting-state functional connectivity in deoxyhemoglobin. **(A)** Group-averaged resting-state functional connectivity matrix diagram. **(B)** ROI-based connections with significant inter-group differences ($p<0.05$, FDR corrected). **(C)** The results of *post-hoc* comparisons ($p<0.05$, Bonferroni corrected). Group 1: HC group; group 2: NPSCI group; group 3: PSCI group. The color bar indicates the statistical significance threshold.

heterogeneous depending on stroke characteristics such as type, volume, number, location (cortical or subcortical), and severity. These variables could have certain effects on characterizing neurological outcomes. In addition, we did not find a significant difference between the PSCI and NPSCI groups, which may be due to the above limitations. Therefore, a large-sample multicenter longitudinal study is needed to further investigate the pathophysiology of PSCI, which could facilitate the prevention, diagnosis and treatment of PSCI.

Conclusion

We found reductions in interhemispheric and intra-right hemispheric FC, especially in S1.L-S1.R, S1.L-DLPFC.R, S1.R-DLPFC.R, and S1.R-MPFC, in PSCI patients. These FC changes may be involved in the pathogenic mechanism of PSCI. Therefore, resting-state fNIRS could be a promising technique to identify patients at risk of PSCI, to establish effective prevention strategies, and to guide clinical treatment.

Data availability statement

The raw data supporting the conclusions of this article will be made available by the authors, without undue reservation.

Ethics statement

The studies involving human participants were reviewed and approved by The Ethics Committee of the Sichuan Bayi Rehabilitation Center. The patients/participants provided their written informed consent to participate in this study.

Author contributions

JZ, YY, and YG contributed to the conception and design of the study. JZ and YY carried out the experiments. JZ performed the data analyses and wrote the manuscript. YG and ZL provided input on grammar and rhetoric. All authors contributed to the revision of the manuscript and read and approved the submitted version.

Conflict of interest

The authors declare that the research was conducted in the absence of any commercial or financial relationships that could be construed as a potential conflict of interest.

Publisher's note

All claims expressed in this article are solely those of the authors and do not necessarily represent those of their affiliated organizations, or those of the publisher, the editors and the reviewers. Any product that may be evaluated in this article, or claim that may be made by its manufacturer, is not guaranteed or endorsed by the publisher.

References

Alderliesten, T., De Vis, J. B., Lemmers, P. M., van Bel, F., Benders, M. J., Hendrikse, J., et al. (2014). Simultaneous quantitative assessment of cerebral physiology using respiratory-calibrated MRI and near-infrared spectroscopy in healthy adults. *NeuroImage* 85, 255–263. doi: 10.1016/j.neuroimage.2013.07.015

Andrews-Hanna, J. R. (2012). The brain's default network and its adaptive role in internal mentation. *Neuroscientist* 18, 251–270. doi: 10.1177/1073858411403316

Auer, D. P. (2008). Spontaneous low-frequency blood oxygenation level-dependent fluctuations and functional connectivity analysis of the 'resting' brain. *Magn. Reson. Imaging* 26, 1055–1064. doi: 10.1016/j.mri.2008.05.008

Baldassarre, A., Ramsey, L., Hacker, C. L., Callejas, A., Astafiev, S. V., Metcalf, N. V., et al. (2014). Large-scale changes in network interactions as a physiological signature of spatial neglect. *Brain* 137, 3267–3283. doi: 10.1093/brain/awu297

Baldassarre, A., Ramsey, L., Rengachary, J., Zinn, K., Siegel, J. S., Metcalf, N. V., et al. (2016a). Dissociated functional connectivity profiles for motor and attention deficits in acute right-hemisphere stroke. *Brain* 139, 2024–2038. doi: 10.1093/brain/aww107

Baldassarre, A., Ramsey, L. E., Siegel, J. S., Shulman, G. L., and Corbetta, M. (2016b). Brain connectivity and neurological disorders after stroke. *Curr. Opin. Neurol.* 29, 706–713. doi: 10.1097/WCO.0000000000000396

Buckner, R. L., and DiNicola, L. M. (2019). The brain's default network: updated anatomy, physiology and evolving insights. *Nat. Rev. Neurosci.* 20, 593–608. doi: 10.1038/s41583-019-0212-7

Cui, X., Bray, S., Bryant, D. M., Glover, G. H., and Reiss, A. L. (2011). A quantitative comparison of NIRS and fMRI across multiple cognitive tasks. *NeuroImage* 54, 2808–2821. doi: 10.1016/j.neuroimage.2010.10.069

Ding, X., Li, C. Y., Wang, Q. S., Du, F. Z., Ke, Z. W., Peng, F., et al. (2014). Patterns in default-mode network connectivity for determining outcomes in cognitive function in acute stroke patients. *Neuroscience* 277, 637–646. doi: 10.1016/j.neuroscience.2014.07.060

Dong, Y., Ding, M., Cui, M., Fang, M., Gong, L., Xu, Z., et al. (2021). Development and validation of a clinical model (DREAM-LDL) for post-stroke cognitive impairment at 6 months. *Aging (Albany NY)* 13, 21628–21641. doi: 10.18632/aging.203507

Duan, L., Zhang, Y. J., and Zhu, C. Z. (2012). Quantitative comparison of resting-state functional connectivity derived from fNIRS and fMRI: a simultaneous recording study. *NeuroImage* 60, 2008–2018. doi: 10.1016/j.neuroimage.2012.02.014

Feigin, V. L., Stark, B. A., Johnson, C. O., Roth, G. A., Bisignano, C., Abady, G. G., et al. (2021). Global, regional, and national burden of stroke and its risk factors, 1990–2019: a systematic analysis for the global burden of disease study 2019. *Lancet Neurol.* 20, 795–820. doi: 10.1016/S1474-4422(21)00252-0

Griffis, J. C., Metcalf, N. V., Corbetta, M., and Shulman, G. L. (2020). Damage to the shortest structural paths between brain regions is associated with disruptions of resting-state functional connectivity after stroke. *NeuroImage* 210:116589. doi: 10.1016/j.neuroimage.2020.116589

Guo, C., Sui, Y., Xu, S., Zhuang, R., Zhang, M., Zhu, S., et al. (2022). Contralaterally controlled neuromuscular electrical stimulation-induced changes in functional connectivity in patients with stroke assessed using functional near-infrared spectroscopy. *Front. Neural. Circuits* 16:955728. doi: 10.3389/fncir.2022.955728

Huang, Y. Y., Chen, S. D., Leng, X. Y., Kuo, K., Wang, Z. T., Cui, M., et al. (2022). Post-stroke cognitive impairment: epidemiology, risk factors, and management. *J. Alzheimers Dis.* 86, 983–999. doi: 10.3233/JAD-215644

Huo, C., Xu, G., Li, W., Xie, H., Zhang, T., Liu, Y., et al. (2021). A review on functional near-infrared spectroscopy and application in stroke rehabilitation. *Medicine Novel Technol. Devices* 11:100064. doi: 10.1016/j.medntd.2021.100064

Huppert, T. J., Hoge, R. D., Diamond, S. G., Franceschini, M. A., and Boas, D. A. (2006). A temporal comparison of BOLD, ASL, and NIRS hemodynamic responses to motor stimuli in adult humans. *NeuroImage* 29, 368–382. doi: 10.1016/j.neuroimage.2005.08.065

Jacova, C., Pearce, L. A., Costello, R., McClure, L. A., Holliday, S. L., Hart, R. G., et al. (2012). Cognitive impairment in lacunar strokes: the SPS3 trial. *Ann. Neurol.* 72, 351–362. doi: 10.1002/ana.23733

Jia, X., Wang, Z., Huang, F., Su, C., Du, W., Jiang, H., et al. (2021). A comparison of the Mini-mental state examination (MMSE) with the Montreal cognitive assessment (MoCA) for mild cognitive impairment screening in Chinese middle-aged and older population: a cross-sectional study. *BMC Psychiatry* 21:485. doi: 10.1186/s12888-021-03495-6

Jiang, L., Geng, W., Chen, H., Zhang, H., Bo, F., Mao, C. N., et al. (2018). Decreased functional connectivity within the default-mode network in acute brainstem ischemic stroke. *Eur. J. Radiol.* 105, 221–226. doi: 10.1016/j.ejrad.2018.06.018

Kulesh, A., Drobakha, V., Kuklina, E., Nekrasova, I., and Shestakov, V. (2018). Cytokine response, tract-specific fractional anisotropy, and brain morphometry in post-stroke cognitive impairment. *J. Stroke Cerebrovasc. Dis.* 27, 1752–1759. doi: 10.1016/j.jstrokecerebrovasdis.2018.02.004

Lu, J., Li, D., Li, F., Zhou, A., Wang, F., Zuo, X., et al. (2011). Montreal cognitive assessment in detecting cognitive impairment in Chinese elderly individuals: a population-based study. *J. Geriatr. Psychiatry Neurol.* 24, 184–190. doi: 10.1177/0891988711422528

Lu, C. M., Zhang, Y. J., Biswal, B. B., Zang, Y. F., Peng, D. L., and Zhu, C. Z. (2010). Use of fNIRS to assess resting state functional connectivity. *J. Neurosci. Methods* 186, 242–249. doi: 10.1016/j.jneumeth.2009.11.010

Marek, S., and Dosenbach, N. U. F. (2018). The frontoparietal network: function, electrophysiology, and importance of individual precision mapping. *Dialogues Clin. Neurosci.* 20, 133–140. doi: 10.31887/DCNS.2018.20.2/smarek

Mijajlovic, M. D., Pavlovic, A., Brainin, M., Heiss, W. D., Quinn, T. J., Ihle-Hansen, H. B., et al. (2017). Post-stroke dementia – a comprehensive review. *BMC Med.* 15:11. doi: 10.1186/s12916-017-0779-7

Nair, V. A., Young, B. M., La, C., Reiter, P., Nadkarni, T. N., Song, J., et al. (2015). Functional connectivity changes in the language network during stroke recovery. *Ann. Clin. Transl. Neurol.* 2, 185–195. doi: 10.1002/acn3.165

Nguyen, T., Kim, M., Gwak, J., Lee, J. J., Choi, K. Y., Lee, K. H., et al. (2019). Investigation of brain functional connectivity in patients with mild cognitive impairment: a functional near-infrared spectroscopy (fNIRS) study. *J. Biophotonics* 12:e201800298. doi: 10.1002/jbio.201800298

Niu, H., and He, Y. (2014). Resting-state functional brain connectivity: lessons from functional near-infrared spectroscopy. *Neuroscientist* 20, 173–188. doi: 10.1177/1073858413502707

O'Reilly, J. X., Croxson, P. L., Jbabdi, S., Sallet, J., Noonan, M. P., Mars, R. B., et al. (2013). Causal effect of disconnection lesions on interhemispheric functional connectivity in rhesus monkeys. *Proc. Natl. Acad. Sci. U. S. A.* 110, 13982–13987. doi: 10.1073/pnas.1305062110

Pendlebury, S. T., Klaus, S. P., Thomson, R. J., Mehta, Z., Wharton, R. M., Rothwell, P. M., et al. (2015). Methodological factors in determining risk of dementia after transient ischemic attack and stroke: (III) applicability of cognitive tests. *Stroke* 46, 3067–3073. doi: 10.1161/STROKEAHA.115.010290

Pinti, P., Scholkmann, F., Hamilton, A., Burgess, P., and Tachtsidis, I. (2018). Current status and issues regarding pre-processing of fNIRS neuroimaging data: an investigation of diverse signal filtering methods within a general linear model framework. *Front. Hum. Neurosci.* 12:505. doi: 10.3389/fnhum.2018.00505

Pinti, P., Tachtsidis, I., Hamilton, A., Hirsch, J., Aichelburg, C., Gilbert, S., et al. (2020). The present and future use of functional near-infrared spectroscopy (fNIRS) for cognitive neuroscience. *Ann. N. Y. Acad. Sci.* 1464, 5–29. doi: 10.1111/nyas.13948

Puig, J., Blasco, G., Alberich-Bayarri, A., Schlaug, G., Deco, G., Biarnes, C., et al. (2018). Resting-state functional connectivity magnetic resonance imaging and outcome after acute stroke. *Stroke* 49, 2353–2360. doi: 10.1161/STROKEAHA.118.021319

Rao, B., Wang, S., Yu, M., Chen, L., Miao, G., Zhou, X., et al. (2022). Suboptimal states and frontoparietal network-centered incomplete compensation revealed by dynamic functional network connectivity in patients with post-stroke cognitive impairment. *Front. Aging Neurosci.* 14:893297. doi: 10.3389/fnagi.2022.893297

Rostamian, S., Mahinrad, S., Stijnen, T., Sabayan, B., and de Craen, A. J. (2014). Cognitive impairment and risk of stroke: a systematic review and meta-analysis of prospective cohort studies. *Stroke* 45, 1342–1348. doi: 10.1161/STROKEAHA.114.004658

Sasai, S., Homae, F., Watanabe, H., Sasaki, A. T., Tanabe, H. C., Sadato, N., et al. (2012). A NIRS-fMRI study of resting state network. *NeuroImage* 63, 179–193. doi: 10.1016/j.neuroimage.2012.06.011

Sato, H., Yahata, N., Funane, T., Takizawa, R., Katura, T., Atsumori, H., et al. (2013). A NIRS-fMRI investigation of prefrontal cortex activity during a working memory task. *NeuroImage* 83, 158–173. doi: 10.1016/j.neuroimage.2013.06.043

Scholkmann, F., Spichtig, S., Muehlemann, T., and Wolf, M. (2010). How to detect and reduce movement artifacts in near-infrared imaging using moving standard deviation and spline interpolation. *Physiol. Meas.* 31, 649–662. doi: 10.1088/0967-3334/31/5/004

Siegel, J. S., Ramsey, L. E., Snyder, A. Z., Metcalf, N. V., Chacko, R. V., Weinberger, K., et al. (2016). Disruptions of network connectivity predict impairment in multiple behavioral domains after stroke. *Proc. Natl. Acad. Sci. U. S. A.* 113, E4367–E4376. doi: 10.1073/pnas.1521083113

Smallwood, J., Brown, K., Baird, B., and Schooler, J. W. (2012). Cooperation between the default mode network and the frontal-parietal network in the production of an internal train of thought. *Brain Res.* 1428, 60–70. doi: 10.1016/j.brainres.2011.03.072

Tang, C., Zhao, Z., Chen, C., Zheng, X., Sun, F., Zhang, X., et al. (2016). Decreased functional connectivity of homotopic brain regions in chronic stroke patients: a resting state fMRI study. *PLoS One* 11:e0152875. doi: 10.1371/journal.pone.0152875

Tao, Y., and Rapp, B. (2020). How functional network connectivity changes as a result of lesion and recovery: an investigation of the network phenotype of stroke. *Cortex* 131, 17–41. doi: 10.1016/j.cortex.2020.06.011

Tao, Y., Tsapkini, K., and Rapp, B. (2022). Inter-hemispheric synchronicity and symmetry: the functional connectivity consequences of stroke and neurodegenerative disease. *Neuroimage Clin* 36:103263. doi: 10.1016/j.nicl.2022.103263

van Hees, S., McMahon, K., Angwin, A., de Zubicaray, G., Read, S., and Copland, D. A. (2014). A functional MRI study of the relationship between naming treatment outcomes and resting state functional connectivity in post-stroke aphasia. *Hum. Brain Mapp.* 35, 3919–3931. doi: 10.1002/hbm.22448

van Meer, M. P., van der Marel, K., Otte, W. M., Berkelbach van der Sprenkel, J. W., and Dijkhuizen, R. M. (2010). Correspondence between altered functional and structural connectivity in the contralesional sensorimotor cortex after unilateral stroke in rats: a combined resting-state functional MRI and manganese-enhanced MRI study. *J. Cereb. Blood Flow Metab.* 30, 1707–1711. doi: 10.1038/jcbfm.2010.124

Wolf, U., Toronov, V., Choi, J. H., Gupta, R., Michalos, A., Gratton, E., et al. (2011). Correlation of functional and resting state connectivity of cerebral oxy-, deoxy-, and total hemoglobin concentration changes measured by near-infrared spectrophotometry. *J. Biomed. Opt.* 16:087013. doi: 10.1117/1.3615249

Zhang, X., and Bi, X. (2020). Post-stroke cognitive impairment: a review focusing on molecular biomarkers. *J. Mol. Neurosci.* 70, 1244–1254. doi: 10.1007/s12031-020-01533-8

Zhang, H., Zhang, Y. J., Lu, C. M., Ma, S. Y., Zang, Y. F., and Zhu, C. Z. (2010). Functional connectivity as revealed by independent component analysis of resting-state fNIRS measurements. *NeuroImage* 51, 1150–1161. doi: 10.1016/j.neuroimage.2010.02.080

Zhang, S., Zhu, T., Tian, Y., Jiang, W., Li, D., and Wang, D. (2022). Early screening model for mild cognitive impairment based on resting-state functional connectivity: a functional near-infrared spectroscopy study. *Neurophotonics* 9:045010. doi: 10.1117/1.NPh.9.4.045010

Zhu, D., Chang, J., Freeman, S., Tan, Z., Xiao, J., Gao, Y., et al. (2014). Changes of functional connectivity in the left frontoparietal network following aphasic stroke. *Front. Behav. Neurosci.* 8:167. doi: 10.3389/fnbeh.2014.00167

frontiers | Frontiers in Neuroscience

TYPE Original Research
PUBLISHED 09 May 2023
DOI 10.3389/fnins.2023.1166010

OPEN ACCESS

EDITED BY
Feng Zhang,
Third Hospital of Hebei Medical University, China

REVIEWED BY
Yuefei Liu,
University of Ulm, Germany
Yongshuai Han,
New York Blood Center, United States
Ruslan Rust,
University of Zurich, Switzerland

*CORRESPONDENCE
Bingquan Ma
✉ bqm@zzu.edu.cn
Bo Yang
✉ fccyangb@163.com

†These authors have contributed equally to this work

RECEIVED 14 February 2023
ACCEPTED 06 April 2023
PUBLISHED 09 May 2023

CITATION
Zhou Q, Dong Y, Wang K, Wang Z, Ma B and Yang B (2023) A comprehensive analysis of the hub genes for oxidative stress in ischemic stroke. *Front. Neurosci.* 17:1166010. doi: 10.3389/fnins.2023.1166010

A comprehensive analysis of the hub genes for oxidative stress in ischemic stroke

Qing Zhou[1†], Yang Dong[2†], Kun Wang[3†], Ziyan Wang[2], Bingquan Ma[1*] and Bo Yang[2*]

[1]Rehabilitation Medicine, The First Affiliated Hospital of Zhengzhou University, Zhengzhou, China, [2]Department of Neurosurgery, The First Affiliated Hospital of Zhengzhou University, Zhengzhou, China, [3]Department of Anesthesiology, The First Affiliated Hospital of Zhengzhou University, Zhengzhou, China

Ischemic stroke (IS), resulting from the occlusion of the cerebral artery and subsequent interruption of blood flow, represents a major and critical threat to public health. Oxidative stress (OS) has been confirmed to play a role in the IS pathological process and neural death. Understanding the essential role of OS-related genes in ischemic stroke is critical to understanding the current perception of the pathophysiological process in IS. Herein, by integrating three IS datasets (GSE16561, GSE22255, and GSE58294), we divided IS samples into the low- and high-OS groups by calculating the OS score identified by the oxidative stress gene set. The functional enrichment analysis of differentially expressed genes (DEGs) between the low- and high-OS groups indicated that DEGs were associated with hypoxia, the inflammatory response, and oxidative phosphorylation pathways. Furthermore, nine hub genes (namely TLR1, CXCL1, MMP9, TLR4, IL1R2, EGR1, FOS, CXCL10, and DUSP1) were identified through the Girvan–Newman algorithm and cytoHubba algorithms. Nine hub genes were highly expressed in IS samples and positively related to neutrophils and macrophages. Drug-sensitive analysis targeting hub genes defined allopurinol and nickel sulfate as potential candidates for impairing the neural death caused by oxidative stress in IS. Finally, we employed five machine learning methods to check the efficacy of the predictive model identified by nine hub genes. The results showed that our model had superior power for predicting the OS activity of IS patients. TLR4 was found to have excellent diagnostic value and a wide-spectrum interaction with other hub genes. Our research emphasized the impact of oxidative stress on ischemic stroke, which supports the idea that antioxidants hold great promise in ischemic stroke therapy.

KEYWORDS

oxidative stress, ischemic stroke, antioxidant, therapy, prognosis, hub genes

1. Introduction

Stroke is the main cause of death and long-term disability worldwide. Ischemic stroke (IS) is the primary type of stroke, accounting for more than 80% of all types of strokes (Cui et al., 2021; Jolugbo and Ariëns, 2021). Ephemeral or prolonged cerebral artery occlusion, followed by hypoxia, can lead to neuronal apoptosis and death, resulting in focal brain damage and functional defects, which are the major contributors to stroke-related morbidity and mortality (Campbell and Khatri, 2020; Tao et al., 2020). IS blocks the blood and oxygen supply to the brain, which induces a series of downstream metabolism events in the oxygen-rich tissues and neural cells (An et al., 2021), of which neuronal apoptosis, inflammatory response, angiogenic edema, and increased intracranial pressure occur. Recent studies have shown that chronic inflammation and blood–brain barrier leakage damage brain tissues

(Spychala et al., 2018). At present, the effective treatment of ischemic stroke, including the intravenous injection of recombinant tissue plasminogen activator and intravascular thrombectomy, shows good therapeutic effects in recanalization (Paul and Candelario-Jalil, 2021). However, two rapid reperfusion methods are limited by extremely narrow treatment time windows, and only a minority of patients obtain timely treatment due to the strict contraindications (An et al., 2021). The pathophysiological mechanism underlying IS remains poorly defined. Therefore, there is an urgent need to delineate the mechanistic aspects and develop new treatment methods for improving the clinical outcome of IS.

A growing body of evidence has found that there is a continuum of intricate processes that play a role in neuronal death, such as neuroinflammation, oxidative stress, excitotoxicity, and apoptosis, in IS development (Li et al., 2017; Xiong et al., 2018; Qin et al., 2022). Oxidative stress (OS) is defined as a dysfunction between the generation of oxidants, reactive oxygen free radicals (ROS), and their abolishing system, antioxidants, under the harmful stimulation of internal and external environments (Ornatowski et al., 2020). Numerous reports have discovered that OS is associated with multiple diseases, as it produces excessive ROS that overwhelms the antioxidant system's maximum capacity (Zhang et al., 2020; Forman and Zhang, 2021). The overwhelming ROS levels hasten the oxidation of macromolecules, including nucleic acids, membrane lipids, and proteins, which is a damaging signal that leads to cellular dysfunction. Oxidative stress plays a crucial role in the pathogenesis of stroke by triggering a cascade of events, such as oxidative damage to lipids, proteins, and nucleic acids, leading to cytotoxicity (ref PMID 23011809).

Additionally, it induces an inflammatory response and causes neuronal apoptosis, leading to neurodegeneration, and cell death. Moreover, it activates the autophagic pathway and damages the blood–brain barrier, further exacerbating the severity of the stroke (Ref PMID 29087944 and 36439687). Given the devastating effects of oxidative stress in stroke, antioxidants have been proposed as a potential therapeutic approach to alleviate the pathological processes associated with this condition. The macrophage-mimicking MnO_2 nanoparticles can scavenge the surplus ROS by recognizing adhesion molecules that interact with the macrophage membrane protein. The reduced oxidative stress signal modifies the inflammatory phenotypes by increasing the M2-macrophage amount, which facilitates the survival of injured neurons (Li et al., 2021). These findings have revealed that oxidative stress exerts an overarching influence on IS initiation, and antioxidant therapy could be a novel therapeutic approach for treating the reperfusion injury associated with IS.

The current study investigated the crosstalk between oxidative stress and IS progression and therapy. Three IS-associated GEO datasets (GSE16561, GSE22255, and GSE58294) and the oxidative stress gene set derived from the gene ontology website (http://geneontology.org/) were enrolled in our analysis work. We dissected the OS-related hub genes that play a crucial role in IS development. Similarly, the immune cell features of hub genes were also investigated, and we constructed a prognosis model for evaluating the OS level. Furthermore, the potential drugs that target OS hub genes were also identified. Multiple machine-learning methods were used to check the efficacy of the prognostic model created by the hub genes. Our research highlighted the major influence of oxidative stress on ischemic stroke, providing novel therapeutic opportunities for the treatment of IS.

2. Materials and methods

2.1. Data collection

Three IS GEO datasets, GSE16561 (24 control samples and 39 IS samples), GSE22255 (20 control samples and 20 IS samples), and GSE58294 (23 control samples and 69 IS samples), were selected for our analysis. The whole blood mRNA expression data in ischemic stroke patients and survival data were downloaded from the GEO website (https://www.ncbi.nlm.nih.gov/geo/). All the data processing and analysis were implemented in the R project. The original expression data were transformed into log2 format after background correction. Finally, three datasets were combined, and batch effects were eliminated by applying the "Combat" algorithm. In addition, the OS-related gene set was collected from the gene ontology database (http://geneontology.org/).

2.2. Identification of high- and low-OS groups

The single sample gene set enrichment analysis (ssGSEA) was employed to calculate the normalized enrichment score (NES), which represents the relative degree of OS level in each IS patient (Zhuang et al., 2021). Then, the total IS samples were divided into the high- and low-OS groups using hierarchical clustering based on the median OS score.

2.3. Function enrichment analysis

The DEGs between the high- and low-OS groups were acquired using the limma package in R with the significant criteria: |Log FC| of >0.5 and a P-value of <0.05. Subsequently, the hallmark pathway set and the Kyoto Encyclopedia of Genes and Genomes (KEGG) pathway set were obtained from the online website (http://gsea-msigdb.org/) for the subsequent function enrichment analysis. The Clue GO tool in the Cystoscape software was introduced to visualize the pathway enrichment results. We selected the gene set enrichment analysis (GSEA) to explore the differential pathways between the high- and low-OS groups.

2.4. Immune infiltration cell analysis

CIBERSORT was developed to calculate the content of each immune cell subgroup by collecting the gene expression features of 22 human immune cell subtypes via the deconvolution method according to the principle of linear support vector regression (Newman et al., 2015). CIBERSORT is a superior method for the deconvolution analysis of complex mixtures and expression matrices containing similar cell types. The

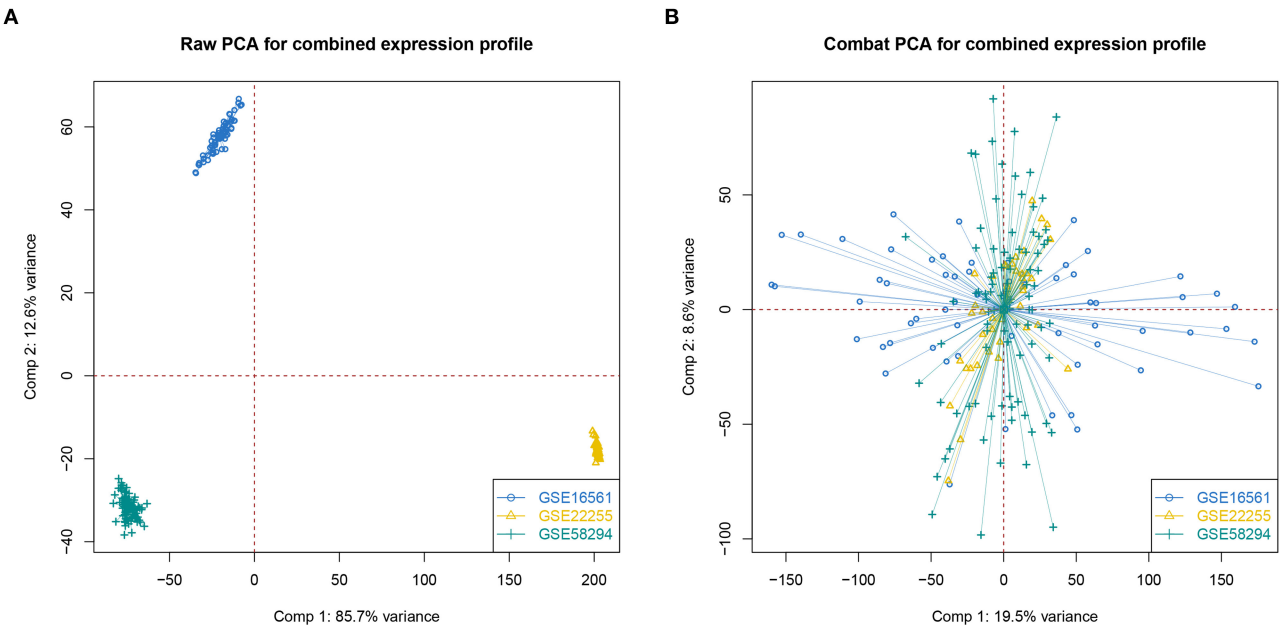

FIGURE 1
The PCA analysis of data merging. **(A, B)** PCA analysis without or with correcting batch effect.

immune cell content of IS patients was evaluated by applying the CIBERSORT algorithm. Moreover, the differences in immune cells between the high- and low-OS groups were analyzed.

2.5. Establishment of hub genes

The protein-protein interaction (PPI) network of the aforementioned DEGs was obtained from the string website, and the key node genes were analyzed. Subsequently, the significant gene communities were identified using the Girvan–Newman algorithm (Newman and Girvan, 2004). A total of 12 genes in 18 significant gene communities were found. Furthermore, we acquired the top 10 genes calculated by three cytoHubba algorithms (MCC, MNC, and degree) (Han et al., 2021). The overlapping genes between the 12 community genes and the top 10 genes were identified as the hub genes. Nine hub genes were acquired for the following analysis.

2.6. Correlation analysis of hub genes and immune cells

Based on our metadata generated by three GEO datasets, we investigated the expression differences of nine hub genes in the normal group and IS samples. Subsequently, the correlation between the gene expression of 9 hub genes and 22 immune cells was analyzed using CIBERSORT.

2.7. Sensitive drug analysis of hub genes

The sensitive drug candidates of nine hub genes were investigated using the DSigDB database in Enrichr (https://maayanlab.cloud/Enrichr/).

2.8. Prognostic value analysis of hub genes

Five machine learning methods, including logistic, Bayesian logistic, decision tree, random forest, and boosting, were used to evaluate the predictive accuracy of the hub gene model in diagnosing the IS samples with different OS statuses. The predominant hub genes were screened out by boosting. Furthermore, the receiver operating curves were used to examine the predictive value of nine hub genes in estimating the OS level. Finally, the correlation analysis between the nine hub genes and each other was conducted to determine the key node hub genes.

3. Results

3.1. Identification of the high- and low-OS groups in IS

First, we merged three IS-associated GEO datasets (GSE16561, GSE22255, and GSE58294) into the metadata for the following comparable analysis. The sample distribution pattern is shown in Figure 1A before data merging, while Figure 1B displays the PCA result after discharging the batch effect, suggesting that the samples were mixed thoroughly. Single sample Gene Set Enrichment Analysis (ssGSEA) indicated that 128 IS samples

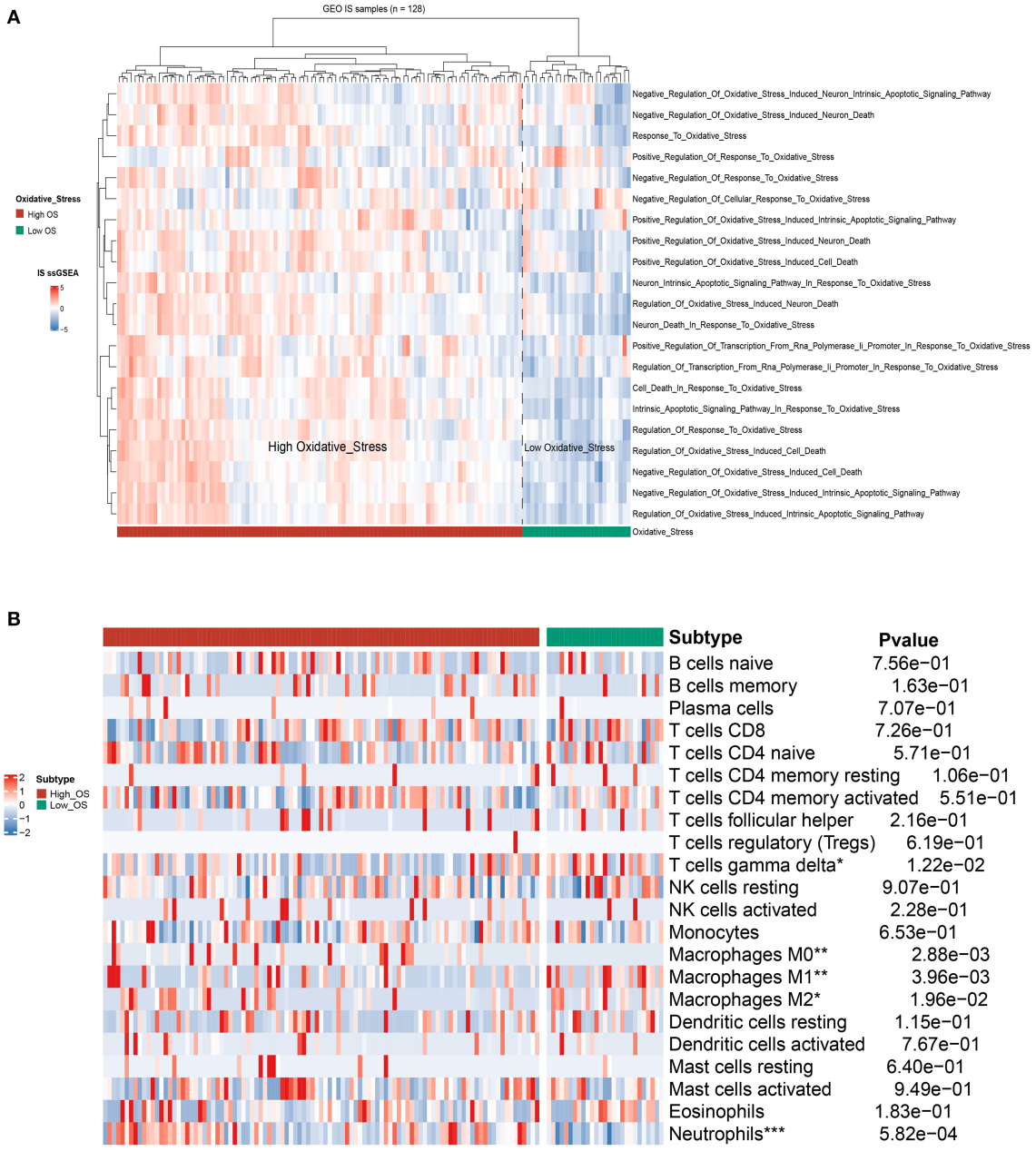

FIGURE 2
The identification of OS subtypes based on ssGSEA. **(A)** The hierarchical clustering heat map of the high- and low-OS groups. **(B)** The heatmap of immune cell flirtation in two OS subgroups. *$p < 0.05$, **$p < 0.01$, and ***$p < 0.001$ indicated the statistical significance of data.

were divided into the high- and low-OS groups (Figure 2A). The contents of neutrophils and macrophages in the high-OS group were significantly increased, indicating that oxidative stress influenced the neutrophils and macrophages in IS (Figure 2B).

3.2. GSEA and KEGG analysis between low- and high-OS groups

We examined the differentially expressed pathways between the high- and low-OS groups using GSEA. The investigation from the hallmark gene sets showed that hypoxia, TNF signaling through the NF-κB pathways, epithelial-mesenchymal transition, and inflammatory response were significantly concentrated in the high-OS group, while the oxidative phosphorylation and interferon-γ response pathways were augmented considerably in the low-OS group (Figure 3A). The KEGG pathway analysis demonstrated that focal adhesion, regulation of the actin cytoskeleton, the neurotrophic signaling pathway, apoptosis, and leukocyte migration through endothelial cells, and the chemokine signal transduction pathway were substantially enriched in the high-OS group, suggesting that the high oxidative stress activity was associated with inflammatory response (Figure 3B). The low-OS

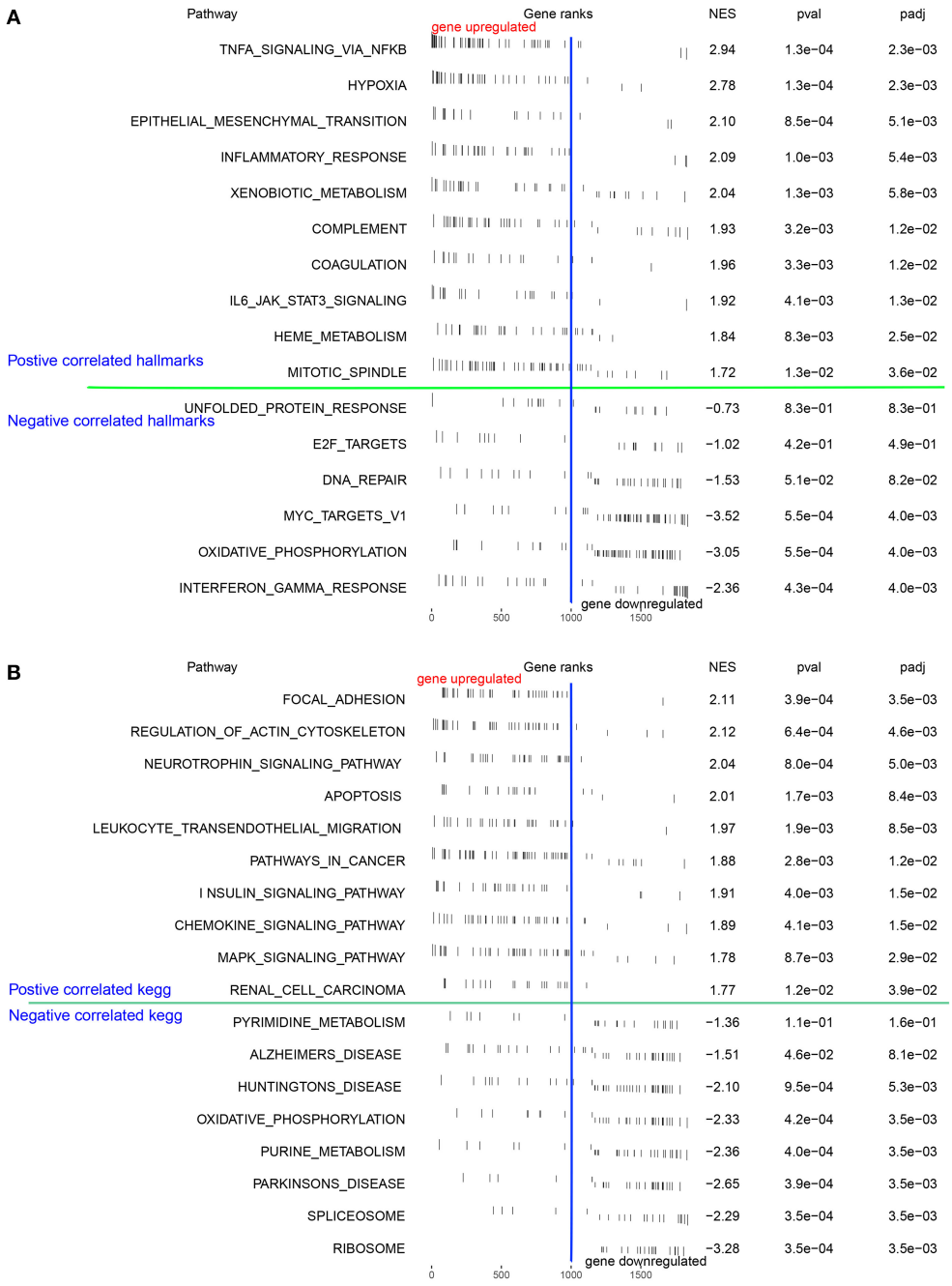

FIGURE 3
Function enrichment analysis. **(A, B)** The GSEA and the KEGG analysis of DEGs between the high- and low-OS groups.

group was characterized by the RNA processing pathways such as spliceosomes and ribosomes (Figure 3B). As the level of oxidative stress increased, the levels of hypoxia and inflammation in patients with IS also increased.

3.3. Identification of hub genes

A total of 85 DEGs between the high- and low-OS groups were collected (Figure 4A). The Clue GO enrichment analysis indicated that these DEGs were significantly associated with NAD+ nucleosidase activity and the CXCR chemokine receptor binding signaling pathways (Figure 4B). The genes of significant communities were obtained using the Girvan–Newman algorithm and 18 gene communities, among which 12 vital genes were found (Figure 4C). We also acquired the top 10 genes identified by the three cytoHubba algorithms (MCC, MNC, and Degree). Taking the section between 12 community genes and 10 top genes, nine overlapping genes (namely TLR1, CXCL1, MMP9, TLR4, IL1R2, EGR1, FOS, CXCL10, and DUSP1) were regarded as hub genes for the following analysis (Figure 4D).

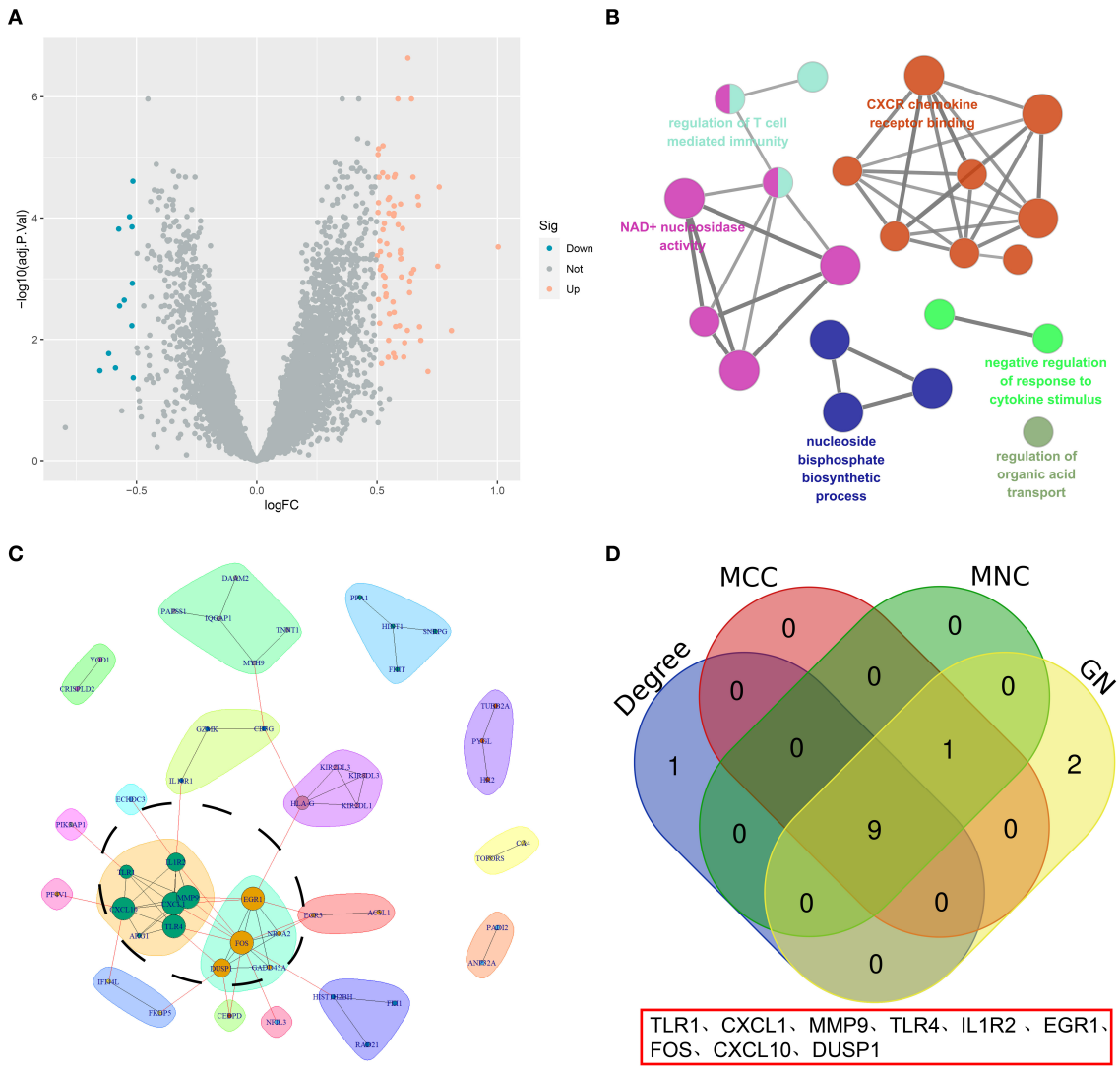

FIGURE 4
The screening of hub genes. **(A)** A volcano map of DEGs between the high- and low-OS groups. **(B)** The KEGG analysis of DEGs. **(C)** The significant gene community identified by GN. **(D)** The Venn diagram of hub genes.

3.4. Correlation of hub genes and immune infiltration cells

First, we surveyed the overall gene expression pattern of nine hub genes in IS samples and matched the normal groups. The results showed that all hub genes other than CXCL10 were enhanced in IS patients, suggesting that these hub genes played a prompting role in IS initiation (Figure 5A). Most hub genes were positively correlated with neutrophils, M0-macrophages, and activated mast cells, representing a severe inflammatory response. However, there was an overall inverse correlation between most hub genes and T cells with distinct functional phenotypes (Figure 5B).

3.5. The potential sensitive drug prediction of hub genes

The top 10 sensitive drugs were found to be allopurinol, nickel sulfate, phencyclidine, beta-escin, vanoxerine curcumin, azacyclonol, benzene, trimipramine, and arsenenous acid (Figures 6A, B). It was found that allopurinol and nickel sulfate were sensitive to nearly all hub genes. Developing a novel strategy based on allopurinol and nickel sulfate could improve the clinical outcome of IS patients with the genetic hub gene features. Notably, FOS, EGR1, DUSP1, and CXCL1 were discovered to have a strong interactive relationship with the sensitive drugs compared with other hub genes.

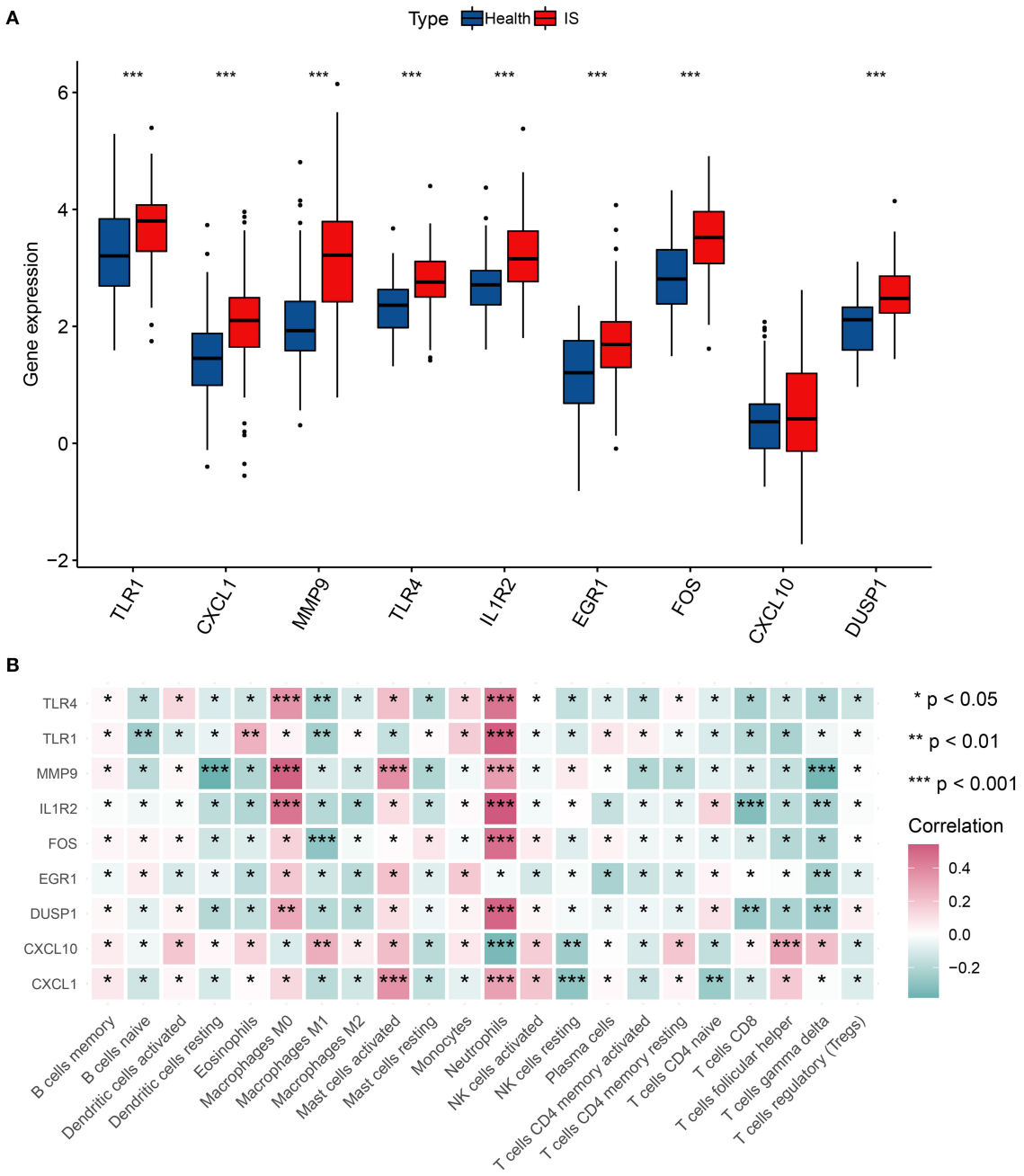

FIGURE 5
Correlation analysis of hub genes and immune cells. **(A)** The gene expression of nine hub genes in IS. **(B)** Correlation matrix of nine hub genes and immune infiltration cell amount. *$p < 0.05$, **$p < 0.01$, and ***$p < 0.001$ indicated the statistical significance of data.

3.6. Prognostic effect validation of hub genes

Multiple machine-learning methods were employed to evaluate the predictive accuracy of hub genes in distinguishing the IS subtypes with different OS levels. The results from five machine learning methods showed that the model composed of nine hub genes could distinguish the high-OS group from the low-OS group (Figure 7A). The prognostic model generated by nine hub genes performed excellently in evaluating the OS status. Boosting results showed that EGR1, TLR4, and TLR1 were three important factors in the prognostic signature (Figure 7B). Among the nine hub genes, TLR4 had the highest AUC value (Figure 7C). At the same time, there was a good positive correlation between TLR4 and the other eight hub genes (Figure 7D).

4. Discussion

The current study divided the IS samples into the low- and high-OS groups according to the median oxidative stress score

A

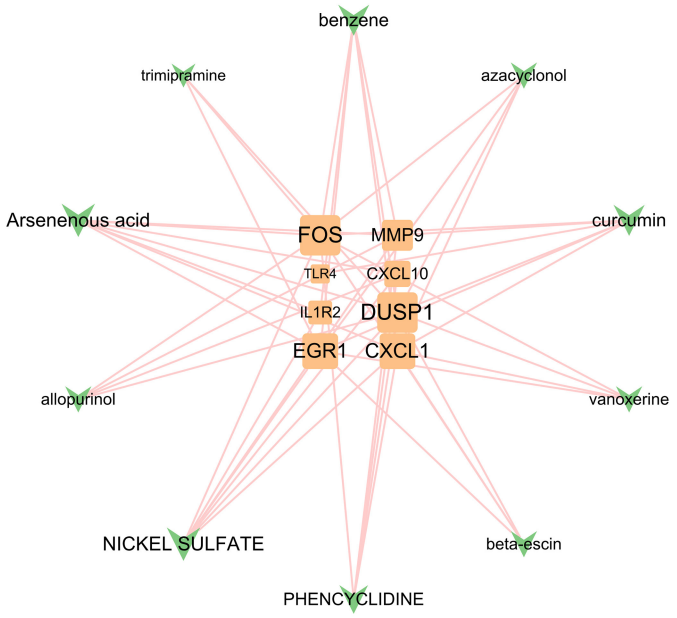

B

Term	P-value	Adjusted P-value	Odds Ratio	Combined Score
allopurinol CTD 00005353	4.49E-11	4.85E-08	1229.415385	29293.68712
NICKEL SULFATE CTD 00001417	5.49E-10	2.97E-07	119.2517544	2542.711469
PHENCYCLIDINE CTD 00005881	2.19E-08	4.71E-06	111.3119369	1963.272157
beta-escin PC3 UP	2.39E-08	4.71E-06	221.3222222	3884.025949
vanoxerine PC3 UP	2.52E-08	4.71E-06	218.2794521	3819.027044
curcumin CTD 00000663	2.61E-08	4.71E-06	74.44741874	1299.853954
azacyclonol PC3 UP	4.75E-08	7.34E-06	185.1627907	3122.408099
benzene CTD 00005481	6.47E-08	8.60E-06	63.5442623	1051.904508
trimipramine MCF7 UP	7.15E-08	8.60E-06	587.4705882	9665.600052
Arsenenous acid CTD 00000922	1.42E-07	1.42E-05	51.29130775	808.7186054

FIGURE 6
Top 10 sensitive drugs targeting hub genes. **(A)** The hub gene-drug network. **(B)** Top 10 sensitive drugs with the highest combined scores.

calculated using the ssGSEA method. In this study, we found that hypoxia signaling was mainly enriched in the high oxidative stress group compared with the low oxidative stress activity group, suggesting the intricate interaction between hypoxia and the OS response. A previous study reported that hypoxia is a predominant driving factor in inducing oxidative stress (Pialoux and Mounier, 2012). For example, hypoxia exposure mediates oxidative stress in the brain region by reducing the biochemical activity of antioxidant enzymes such as SOD, CAT, and GSH while elevating oxidative stress markers such as MDA and TAC in the hippocampus (Mohamed et al., 2019). The periodic aggregation of HIF-1α induced by hypoxia promotes NADPH oxidase activation, intensifying ROS export (Prabhakar and Semenza, 2012; Wang et al., 2020).

Conversely, oxidative stress governs the hypoxia process. The latest proceedings have certified that high-ROS concentration stimulation increases HIF's expression (You et al., 2021). As previously described, OS swells the retinal cell inflammation by activating the cGAS-STING signaling provoked by inflating DNA damage and cytosolic leakage (Zou et al., 2022). We also found that the inflammation signal pathway was augmented in the high-OS group of IS patients, highlighting the prevailing function of oxidative stress in controlling inflammation. Consistent with our findings, the KEGG analysis revealed that leukocyte transendothelial migration, the chemokine signaling pathway, and chemokine receptor binding were augmented in the high-OS group, demonstrating the active inflammatory response in the context of high oxidative stress.

By performing the Girvan–Newman analysis, we identified 12 key genes in 18 predominant gene communities. We further identified nine overlapping hub genes, including TLR1, CXCL1, MMP9, TLR4, IL1R2, EGR1, FOS, CXCL10, and DUSP1, by taking the intersection between the 12 community genes and the top 10 genes defined by three cytoHubba algorithms. Our analysis revealed that these hub genes play crucial roles in the oxidative stress process, which is often associated with inflammation and thrombosis.

For instance, a previous study has shown that an excess concentration of hepatic CXCL1 leads to an oxidative stress response, as indicated by the increased activation of stress kinases such as apoptosis signal-regulating kinase 1, which accelerates the nonalcoholic steatohepatitis progression (Hwang et al., 2020).

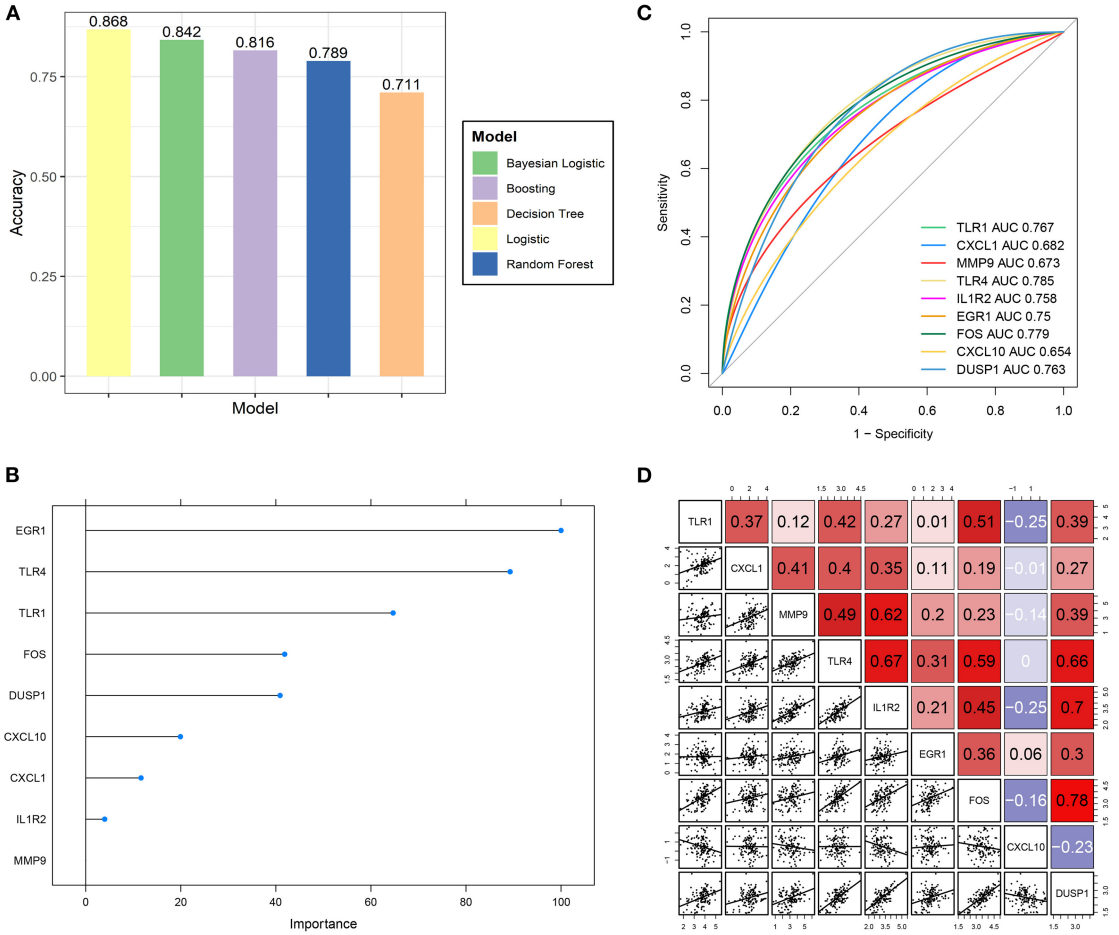

FIGURE 7
Predictive ability validation of hub genes. **(A)** The predictive accuracy of the prognostic model by five machine learning methods for the IS OS subgroups. **(B)** The importance ranking of nine hub genes by boosting analysis. **(C)** The ROC curve of nine hub genes predicts the high- and low-OS groups. **(D)** Correlation analysis of nine hub genes with each other.

TLR4 activation can increase the oxidative stress response and enhance ROS generation in the activated macrophage cells in thrombosis, while nattokinase treatment can reduce inflammation and oxidative stress (Wu et al., 2020).

Additionally, our correlation analysis indicated that hub gene expression levels were positively associated with the numbers of neutrophils and macrophages, which are the major infiltration cells in the inflammatory response (Martini et al., 2019). There was a complex crosstalk between oxidative stress and inflammation in ischemic stroke. We also found evidence that the deficiency of S-adenosylhomocysteine hydrolase (SAHH) urges the EGR1 to recruit in the promoter region of the thioredoxin-interacting protein (TXNIP), which increases TXNIP expression (Dai et al., 2021). The excessive TXNIP signal promotes oxidative stress and follows NLRP3 inflammasome motivation, contributing to diabetic nephropathy progression (Dai et al., 2021). Our analysis demonstrated that these hub genes are involved in the oxidative stress process, with nearly all hub genes being upregulated in IS samples relative to the normal groups. Taken together, our findings suggest that developing anti-thrombotic drugs with anti-inflammatory and antioxidative stress effects could be a promising therapeutic strategy for ischemic stroke.

The management of acute ischemic stroke at present involves the crucial process of mitigating the harmful effects of excessive ROS during ischemia/reperfusion. One protective microglia subtype in stroke-associated microglia is characterized by the upregulation of an antioxidant enzyme, Peroxiredoxin-1 (Prdx1), which induces the expression of stroke-protective molecules, such as osteopontin and ferritin (Kim et al., 2022). Inhibiting Prdx1 expression significantly intensifies the infarction and inflammatory responses by suppressing the antioxidant gene, such as Txn1 and Mt2 expression (Kim et al., 2022). With antioxidants being a part of current IS treatment, we sought to identify potential drugs targeting hub genes. Among the 10 drugs found to be sensitive, allopurinol and nickel sulfate were discovered to be sensitive to almost all hub genes. Finally, we constructed a predictive model depending on nine hub genes to evaluate oxidative stress activity in ischemic stroke. The analysis from five machine learning methods (logistic, Bayesian logistic, decision tree, random forest, and boosting) showed that the predictive model consisting of nine hub genes exhibited excellent performance. EGR1, TLR4, and TLR1 were identified as the three key factors in determining the oxidative stress subgroups, which is consistent with the results of previous studies (Wu et al., 2020; Dai et al., 2021). We discovered

that TLR4 had the highest AUC value and the strongest positive correlation with the other eight hub genes. Increasing TLR4/NOX2 signaling activity triggers a severe oxidative stress response in polystyrene microplastics-mediated uterine fibrosis (Wu et al., 2022). Suppressing the TLR4/NOX2 signaling pathway significantly decreases ROS export in cells and curbs the expression of fibrotic and collagen-associated genes (Wu et al., 2022). Antioxidant therapy targeting TLR4/NOX2 signaling could be an innovative option for alleviating uterine fibrosis. Together with our data, these findings highlight the critical role of TLR4 in oxidative stress and antioxidant therapy.

5. Conclusion

In summary, our study provides valuable insights into the role of oxidative stress in the pathological process of ischemic stroke. Two IS subgroups were formed based on the high- and low-OS levels. Significant differences were observed in the expression levels of genes related to hypoxia and inflammation between the two groups. Notably, nine hub genes which are primarily associated with neutrophils and macrophages were found to be significantly upregulated in the IS samples. Using machine learning algorithms, we developed a predictive model based on nine hub genes. It can potentially facilitate the development of novel therapeutic targets for improving the clinical outcome of ischemic stroke. Our findings contribute to a better understanding of the underlying mechanisms of ischemic stroke and may lead to the development of more effective interventions for this clinically important condition.

Data availability statement

The datasets presented in this study can be found in online repositories. The names of the repository/repositories and accession number(s) can be found in the article/supplementary material.

Author contributions

QZ, YD, and KW contributed to the design and implementation of the research and wrote the manuscript. ZW contributed to the analyses of the results. QZ wrote the article and provided critical comments. BM and BY designed and supported the study and edited the manuscript. All the authors substantially contributed to the work presented in this article. All authors reviewed and approved the final manuscript.

Funding

This study was supported by the 2022 joint construction project of the Henan Medical Science and Technology Breakthrough Plan (Grant No.: LHGJ20220347).

Conflict of interest

The authors declare that the research was conducted in the absence of any commercial or financial relationships that could be construed as a potential conflict of interest.

Publisher's note

References

An, H., Zhou, B., and Ji, X. (2021). Mitochondrial quality control in acute ischemic stroke. *J. Cerebr. Blood Flow Metabol.* 41, 3157–3170. doi: 10.1177/0271678X211046992

Campbell, B. C. V., and Khatri, P. (2020). Stroke. *Lancet* 396, 129–142. doi: 10.1016/S0140-6736(20)31179-X

Cui, Y., Zhang, Y., Zhao, X., Shao, L., Liu, G., Sun, C., et al. (2021). ACSL4 exacerbates ischemic stroke by promoting ferroptosis-induced brain injury and neuroinflammation. *Brain Behav. Immun.* 93, 312–321. doi: 10.1016/j.bbi.2021.01.003

Dai, X., Liao, R., Liu, C., Liu, S., Huang, H., Liu, J., et al. (2021). Epigenetic regulation of TXNIP-mediated oxidative stress and NLRP3 inflammasome activation contributes to SAHH inhibition-aggravated diabetic nephropathy. *Redox Biol.* 45, 102033. doi: 10.1016/j.redox.2021.102033

Forman, H. J., and Zhang, H. (2021). Targeting oxidative stress in disease: promise and limitations of antioxidant therapy. *Nat. Rev. Drug Discov.* 20, 689–709. doi: 10.1038/s41573-021-00233-1

Han, Y., Wu, J., Gong, Z., Zhou, Y., Li, H., Wang, B., et al. (2021). Identification and development of a novel 5-gene diagnostic model based on immune infiltration analysis of osteoarthritis. *J. Transl. Med.* 19, 522. doi: 10.1186/s12967-021-03183-9

Hwang, S., He, Y., Xiang, X., Seo, W., Kim, S.-J., Ma, J., et al. (2020). Interleukin-22 ameliorates neutrophil-driven nonalcoholic steatohepatitis through multiple targets. *Hepatology* 72, 412–429. doi: 10.1002/hep.31031

Jolugbo, P., and Ariëns, R. A. S. (2021). Thrombus composition and efficacy of thrombolysis and thrombectomy in acute ischemic stroke. *Stroke* 52, 1131–1142. doi: 10.1161/STROKEAHA.120.032810

Kim, S., Lee, W., Jo, H., Sonn, S.-K., Jeong, S.-J., Seo, S., et al. (2022). The antioxidant enzyme Peroxiredoxin-1 controls stroke-associated microglia against acute ischemic stroke. *Redox Biol.* 54, 102347. doi: 10.1016/j.redox.2022.102347

Li, C., Zhao, Z., Luo, Y., Ning, T., Liu, P., Chen, Q., et al. (2021). Macrophage-disguised manganese dioxide nanoparticles for neuroprotection by reducing oxidative stress and modulating inflammatory microenvironment in acute ischemic stroke. *Adv. Sci. (Weinh)* 8, e2101526. doi: 10.1002/advs.202101526

Li, T., Qin, J.-J., Yang, X., Ji, Y.-X., Guo, F., Cheng, W.-L., et al. (2017). The ubiquitin E3 Ligase TRAF6 exacerbates ischemic stroke by ubiquitinating and activating Rac1. *J. Neurosci.* 37, 12123–12140. doi: 10.1523/JNEUROSCI.1751-17.2017

Martini, E., Kunderfranco, P., Peano, C., Carullo, P., Cremonesi, M., Schorn, T., et al. (2019). Single-cell sequencing of mouse heart immune infiltrate in pressure overload-driven heart failure reveals extent of immune activation. *Circulation* 140, 2089–2107. doi: 10.1161/CIRCULATIONAHA.119.041694

Mohamed, A. A. R., Metwally, M. M., Khalil, S. R., Salem, G. A., and Ali, H. A. (2019). Moringa oleifera extract attenuates the CoCl induced hypoxia of rat's brain: Expression pattern of HIF-1α, NF-kB, MAO and EPO. *Biomed. Pharm.* 109, 1688–1697. doi: 10.1016/j.biopha.2018.11.019

Newman, A. M., Liu, C. L., Green, M. R., Gentles, A. J., Feng, W., Xu, Y., et al. (2015). Robust enumeration of cell subsets from tissue expression profiles. *Nat. Methods* 12, 453–457. doi: 10.1038/nmeth.3337

Newman, M. E. J., and Girvan, M. (2004). Finding and evaluating community structure in networks. *Phys. Rev. E Stat. Nonlin Soft Matter Phys.* 69, 026113. doi: 10.1103/PhysRevE.69.026113

Ornatowski, W., Lu, Q., Yegambaram, M., Garcia, A. E., Zemskov, E. A., Maltepe, E., et al. (2020). Complex interplay between autophagy and oxidative stress in the development of pulmonary disease. *Redox Biol.* 36, 101679. doi: 10.1016/j.redox.2020.101679

Paul, S., and Candelario-Jalil, E. (2021). Emerging neuroprotective strategies for the treatment of ischemic stroke: An overview of clinical and preclinical studies. *Exper. Neurol.* 335, 113518. doi: 10.1016/j.expneurol.2020.113518

Pialoux, V., and Mounier, R. (2012). Hypoxia-induced oxidative stress in health disorders. *Oxid. Med. Cell. Long.* 2012, 940121. doi: 10.1155/2012/940121

Prabhakar, N. R., and Semenza, G. L. (2012). Adaptive and maladaptive cardiorespiratory responses to continuous and intermittent hypoxia mediated by hypoxia-inducible factors 1 and 2. *Physiol. Rev.* 92, 967–1003. doi: 10.1152/physrev.00030.2011

Qin, C., Yang, S., Chu, Y.-H., Zhang, H., Pang, X.-W., Chen, L., et al. (2022). Signaling pathways involved in ischemic stroke: molecular mechanisms and therapeutic interventions. *Signal Transduct. Target Ther.* 7, 215. doi: 10.1038/s41392-022-01064-1

Spychala, M. S., Venna, V. R., Jandzinski, M., Doran, S. J., Durgan, D. J., Ganesh, B. P., et al. (2018). Age-related changes in the gut microbiota influence systemic inflammation and stroke outcome. *Ann. Neurol.* 84, 23–36. doi: 10.1002/ana.25250

Tao, T., Liu, M., Chen, M., Luo, Y., Wang, C., Xu, T., et al. (2020). Natural medicine in neuroprotection for ischemic stroke: Challenges and prospective. *Pharmacol. Ther.* 216, 107695. doi: 10.1016/j.pharmthera.2020.107695

Wang, N., Shi, X.-F., Khan, S. A., Wang, B., Semenza, G. L., Prabhakar, N. R., et al. (2020). Hypoxia-inducible factor-1 mediates pancreatic β-cell dysfunction by intermittent hypoxia. *Am. J. Physiol. Cell Physiol.* 319, C922–C932. doi: 10.1152/ajpcell.00309.2020

Wu, H., Wang, Y., Zhang, Y., Xu, F., Chen, J., Duan, L., et al. (2020). Breaking the vicious loop between inflammation, oxidative stress and coagulation, a novel anti-thrombus insight of nattokinase by inhibiting LPS-induced inflammation and oxidative stress. *Redox Biol.* 32, 101500. doi: 10.1016/j.redox.2020.101500

Wu, H., Xu, T., Chen, T., Liu, J., and Xu, S. (2022). Oxidative stress mediated by the TLR4/NOX2 signalling axis is involved in polystyrene microplastic-induced uterine fibrosis in mice. *Sci. Total Environ.* 838, 155825. doi: 10.1016/j.scitotenv.2022.155825

Xiong, X. -Y., Liu, L., and Yang, Q-. W. (2018). Refocusing Neuroprotection in Cerebral Reperfusion Era: New Challenges and Strategies. *Front. Neurol.* 9, 249. doi: 10.3389/fneur.2018.00249

You, L., Zhao, Y., Kuca, K., Wang, X., Oleksak, P., Chrienova, Z., et al. (2021). Hypoxia, oxidative stress, and immune evasion: a trinity of the trichothecenes T-2 toxin and deoxynivalenol (DON). *Arch. Toxicol.* 95, 1899–1915. doi: 10.1007/s00204-021-03030-2

Zhang, P., Li, T., Wu, X., Nice, E. C., Huang, C., and Zhang, Y. (2020). Oxidative stress and diabetes: antioxidative strategies. *Front. Med.* 14, 583–600. doi: 10.1007/s11684-019-0729-1

Zhuang, W., Sun, H., Zhang, S., Zhou, Y., Weng, W., Wu, B., et al. (2021). An immunogenomic signature for molecular classification in hepatocellular carcinoma. *Mol. Ther. Nucleic. Acids* 25, 105–115. doi: 10.1016/j.omtn.2021.06.024

Zou, M., Ke, Q., Nie, Q., Qi, R., Zhu, X., Liu, W., et al. (2022). Inhibition of cGAS-STING by JQ1 alleviates oxidative stress-induced retina inflammation and degeneration. *Cell Death Differ.* 29, 1816–1833. doi: 10.1038/s41418-022-00967-4

frontiers | Frontiers in Neuroscience

TYPE Original Research
PUBLISHED 12 May 2023
DOI 10.3389/fnins.2023.1182181

OPEN ACCESS

EDITED BY
Guang-qing Xu,
The First Affiliated Hospital of Sun Yat-sen University, China

REVIEWED BY
Jianghong He,
Capital Medical University, China
Bin Hu,
University of Calgary, Canada

*CORRESPONDENCE
Xiaoying Zhang
✉ 389608661@qq.com

†These authors have contributed equally to this work and share first authorship

RECEIVED 08 March 2023
ACCEPTED 13 April 2023
PUBLISHED 12 May 2023

CITATION
Xiao X, Chen W and Zhang X (2023) The effect and mechanisms of music therapy on the autonomic nervous system and brain networks of patients of minimal conscious states: a randomized controlled trial.
Front. Neurosci. 17:1182181.
doi: 10.3389/fnins.2023.1182181

The effect and mechanisms of music therapy on the autonomic nervous system and brain networks of patients of minimal conscious states: a randomized controlled trial

Xiang Xiao[1,2,3†], Wenyi Chen[2,4,5†] and Xiaoying Zhang[2,3,4,5*†]

[1]School of Music and Dance, Hunan First Normal University, Changsha, Hunan, China, [2]School of Rehabilitation Medicine, Capital Medical University, Beijing, China, [3]Department of Neurorehabilitation, China Rehabilitation Research Center, Beijing, China, [4]Department of Music Artificial Intelligence and Music Information Technology, Central Conservatory of Music, Beijing, China, [5]Music Therapy Center, China Rehabilitation Research Center, Beijing, China

Introduction: Music therapy has been employed as an alternative treatment modality for the arousal therapy of patients with disorders of consciousness (DOC) in clinical settings. However, due to the absence of continuous quantitative measurements and the lack of a non-musical sound control group in most studies, the identification of the specific impact of music on DOC patients remains challenging. In this study, 20 patients diagnosed with minimally consciousness state (MCS) were selected, and a total of 15 patients completed the experiment.

Methods: All patients were randomly assigned to three groups: an intervention group (music therapy group, n=5), a control group (familial auditory stimulation group, n=5), and a standard care group (no sound stimulation group, n=5). All three groups received 30min of therapy five times a week for a total of 4weeks (20 times per group, 60 times in total). Autonomic nervous system (ANS) measurements, Glasgow Coma Scale (GCS), and functional magnetic resonance—diffusion tensor imaging (fMRI-DTI) were used to measure the peripheral nervous system indicators and brain networks, and to evaluate patients' behavior levels.

Results: The results reveal that PNN50 (p=0.0004**), TP (p=0.0003**), VLF (p=0.0428**), and LF/HF (p=0.0001**) in the music group were significantly improved compared with the other two groups. Such findings suggest that the ANS of patients with MCS exhibits higher activity levels during music exposure compared to those exposed to family conversation or no auditory stimulation. In fMRI-DTI detection, due to the relative activity of ANS in the music group, the ascending reticular activation system (ARAS) in the brain network also exhibited significant nerve fiber bundle reconstruction, superior temporal gyrus (STG), transverse temporal gyrus (TTG), inferior temporal gyrus (ITG), limbic system, corpus callosum, subcorticospinal trace, thalamus and brainstem regions. In the music group, the reconstructed network topology was directed rostrally to the diencephalon's dorsal nucleus, with the brainstem's medial region serving as the hub. This network was found to be linked with the caudal corticospinal tract and the ascending lateral branch of the sensory nerve within the medulla.

Conclusion: Music therapy, as an emerging treatment for DOC, appears to be integral to the awakening of the peripheral nervous system-central nervous system based on the hypothalamic-brainstem-autonomic nervous system (HBA) axis, and is worthy of clinical promotion. The research was supported by the Beijing Science and

Technology Project Foundation of China, No. Z181100001718066, and the National Key R&D Program of China No. 2022YFC3600300, No. 2022YFC3600305.

KEYWORDS

disorders of consciousness, minimally consciousness state, music therapy, music auditory stimulation, autonomic nervous system, fMRI-DTI

Introduction

Minimal consciousness state (MCS) is a serious disorder of consciousness (DOC), which is different from vegetative state (*VS*) (Eapen et al., 2017). MCS is primarily characterized by a patient's capacity to exhibit limited yet distinct self-awareness and environmental perception (Rasmus et al., 2019). In 2022, the International Society of Disorders of Consciousness defined MCS as "a state with small and clear behavioral evidence of severe conscious changes in the perception of the self and the environment"(Bodien et al., 2022; Bower et al., 2022). Studies have shown that patients with MCS have a relatively complete neural network under severe brain damage, which differs from persistent *VS* (Fischer et al., 2022; Fitzpatrick-DeSalme et al., 2022; Kondziella and Stevens, 2022). Neurobehavioral and imaging studies have revealed that there are significant differences in clinical manifestations and neurological symptoms between MCS and *VS* (Istace, 2022). However, owing to the variability of arousal levels and the dysfunction of sensory, motor, and language systems in patients with DOC, communication between patients and examiners is restricted, leading to a high incidence of misdiagnosis in clinical practice (Bellon et al., 2022; Ismail et al., 2022). At the same time, MCS has greater neurological rehabilitation potential than *VS* patients in terms of prognosis, and thus, is of great clinical value for multiple wake-promoting treatments for MCS patients (Bagnato, 2022).

The DOC patient assessment determines the level of awareness of a patient by identifying whether the response to the stimulus is reflexive, or comes from an active action in which part of the perceptual capacity is engaged (Young and Peterson, 2022). The current clinical assessment scales for early disturbance of consciousness include Glasgow Coma Scale (GCS) (Mehta and Chinthapalli, 2019), Coma Recovery Scale-revised (CRS-R) and other scales, which are used to differentiate *VS* from MCS (Giacino et al., 2004). Moreover, neuroimaging assessment is also a significant tool for the diagnosis of DOC. Structural imaging techniques, including T1 and T2 weighted magnetic resonance imaging (MRI) and functional MRI (fMRI) (Sanz et al., 2021), can facilitate the quantification of brain atrophy in patients with DOC (Fins, 2011). Such methods can also effectively identify the precise location of brain injuries, hypoxic–ischemic lesions, and diffuse axonal injuries (Humble et al., 2018). Fractional anisotropy (FA) of key regions detected by diffusion tensor imaging (DTI) is a reference index for predicting the prognosis of DOC (Li et al., 2022). In general, CRS-R is used as the preferred tool for prognosis evaluation in clinical practice, and GOS-E is used as an auxiliary scale for prognosis evaluation (Annen et al., 2019).

At present, DOC lacks exact and effective treatment methods. Despite the lack of systematic research and sufficient evidence-based medical evidence, clinical research and attempts to treat DOC have been conducted in consideration of the large number of DOC patients and the considerable treatment demand. The main treatment methods include surgery, medication, hyperbaric oxygen therapy, neuromodulation therapy (invasive, non-invasive, etc.), physical therapy, and others. As an emerging rehabilitation modality in recent years, music therapy has shown significantly positive effects in promoting recovery for patients with consciousness disorders (Grimm and Kreutz, 2018; Bower et al., 2022; Liu et al., 2022). Music has a wide range of activation effects on the cerebral cortex, such as the bilateral frontal lobe, temporal lobe, parietal lobe and cerebellum, and the emotion-related frontal lobe, cingulate gyrus, amygdala and hippocampus are particularly responsive (Rollnik and Altenmüller, 2014). The use of a patient's favorite music for auditory stimulation is conducive to the recovery of consciousness (Magee et al., 2015).

Music, particularly songs that patients find appealing, frequently elicit emotional resonance (Hu et al., 2021). One vital strategy in accomplishing music therapy is to select songs that patients enjoy and have them performed live by music therapists (Magee et al., 2014). The songs sung by the music therapist in the present study were chosen accurately based on the patients' preferences and emotional engagement (Pool et al., 2020). The effects of music intervention, including both active and receptive music therapy, had a positive impact on patients with DOC (Zhang et al., 2021). In the field of rehabilitation medicine, awakening treatment of DOC combined with music therapy, as a different treatment strategy, can effectively improve the consciousness state of patients with cerebral MCS (Arroyo-Anlló et al., 2013). Evidence has shown that music can activate the function of the default mode affective network in patients with DOC (Janelli et al., 2004; Riganello et al., 2015; De Luca et al., 2022). Despite such findings, there are difficulties in terms of drawing conclusions due to the few studies that did not use continuous quantitative measures and the lack of control groups to show the distinctive effects of music on patients with DOC. Three groups were used to compare the activation of autonomic nervous system and brain network in patients with MCS over 4 weeks: music therapy group (played by music therapist), the voices of family members (recorded), and a standard care group, to clarify the specific role of music therapy.

Subjects and methods

Twenty patients were recruited from China Rehabilitation Research Center, and the inclusion criteria were as follows: (1) MCS diagnosed by CRS-R and GOS-E (Giacino et al., 2004); (2) inpatients with a disease duration of at least 3 months; (3) aged 18–60 years old; (4) can tolerate the treatment in the supine position for more than half an hour; (5) no previous music education background; (6) informed consent was obtained from patients and their families. The exclusion criteria consisted of: (1) severe arrhythmia, malignant arrhythmia or other diseases, or

history of cardiac surgery; (2) orthostatic hypotension; (3) severe hearing impairment. The withdrawal and termination criteria were as follows: termination of treatment can occur if the patient's condition changes due to discharge or voluntary withdrawal. A total of 15 subjects completed the experiment. Five subjects ($n=5$) withdrew from the experiment due to transfer to another hospital or personal reasons. The characteristic data are presented in Table 1.

Patient recruitment was conducted from December 2019 to September 2022, the data of participants' characteristics are shown in Table 1. Fifteen patients were randomly divided into three groups: the intervention group was the music therapy group ($n=5$), the control group was the familial auditory stimulation group ($n=5$), and the standard care group was the no auditory stimulation intervention group ($n=5$). There were no significant differences in the ratio of male to female, age, time of injury and education among the three groups ($p>0.05$).

Table 1 presents the distribution of group differences, gender, age, injury time and education background of the three groups of patients. The remaining data were expressed as standard deviation + mean and analyzed by paired t test. Experimental group: music therapy group; Control group: familial auditory stimulation group; standard care: standard care group. $p>0.05$ indicates that there was no significant difference among the three groups.

Study design

The present study constituted a randomized controlled trial with a pre-and post-test experimental design that featured three separate groups, namely the experimental ($n=5$), control ($n=5$), and standard care group ($n=5$). The study was conducted using a single-blind design, in which participants only knew they were participating in a clinical trial after signing an informed consent form, and a masking design was used for grouping information and data analysis. The study was conducted at CRRC from December 2019 to November 2022. This study was supported by the Beijing Science and Technology Project Foundation of China, No. Z181100001718066; and the National Key R&D Program of China No. 2022YFC3600300, No. 2022YFC3600305. This research proposal has been approved by the Ethics Committee of CRRC (approval No. 2018–022-1) on March 12, 2018 (Supplementary material), and informed consent (Supplementary material) was obtained from the participants, relatives or guardians before commencing the study. The study trial was registered with the Clinical Trial Registry (Registration No. ChiCTR1800017809) on August 15, 2018.

Procedure

After approval by the CRRC Ethics Committee and registration for clinical trials, subjects were initially screened by neurosurgeons. Patients who initially received a score on the GCS indicating moderate to severe impairment of consciousness were referred to the music therapy department following consultation. Potential participants were identified by music therapy investigators according to predetermined inclusion and exclusion criteria. Subsequently, the investigators confirmed the eligibility of the patients and invited their family members to participate in the study after obtaining their signed informed consent forms. Topics included study purpose, procedure, risks, benefits, confidentiality, and subjects' rights. Upon enlistment, GCS scores were used to determine whether patients had impaired hearing function and computer-generated sequences (Excel 2013, Microsoft Office, Seattle, WA, USA) were used to randomly assign patients to one of the three groups. Participants in the intervention group received music therapy from a music therapist for 4 weeks, while participants in the control group received familial auditory stimulation for 4 weeks, with no acoustic stimulation in the standard care group. The enrollment and assignment of participants is shown in Figure 1.

Figure 1 illustrates that 20 participants were enrolled in the study, 15 participates completed the trial, and 5 participants withdrew: COVID-19 ($n=3$), midway transfers ($n=1$) or other personal reasons ($n=1$). The experimental group ($n=5$) received music therapy administered by a music therapist, whereas the control group ($n=5$) was subjected to auditory stimulation provided by their respective family members. Meanwhile, the standard care group was given no auditory stimulation. Two rounds of evaluation were conducted during the whole period, namely T0 (baseline) and T1 (after 4 weeks). The data analysis included a sample of 15 patients who were in a minimally conscious state.

TABLE 1 Baseline characteristics of participants included in the present study.

	Intervention group	Control group	Standard care	Value of *p*
	Mean±SD	Mean±SD	Mean±SD	
Minimally consciousness state (MCS)	5	5	5	>0.05
Gender				
Male	2	3	4	>0.05
Female	3	2	1	>0.05
Age	26.8 ± 11.21	50.8 ± 10.13	38.8 ± 15.07	
Time since injury	7.53 ± 5.04	5.79 ± 4.41	8.15 ± 1.33	
Education background				
primary school	1	3	0	>0.05
junior high school	0	1	2	>0.05
Bachelor degree or above	4	1	3	>0.05

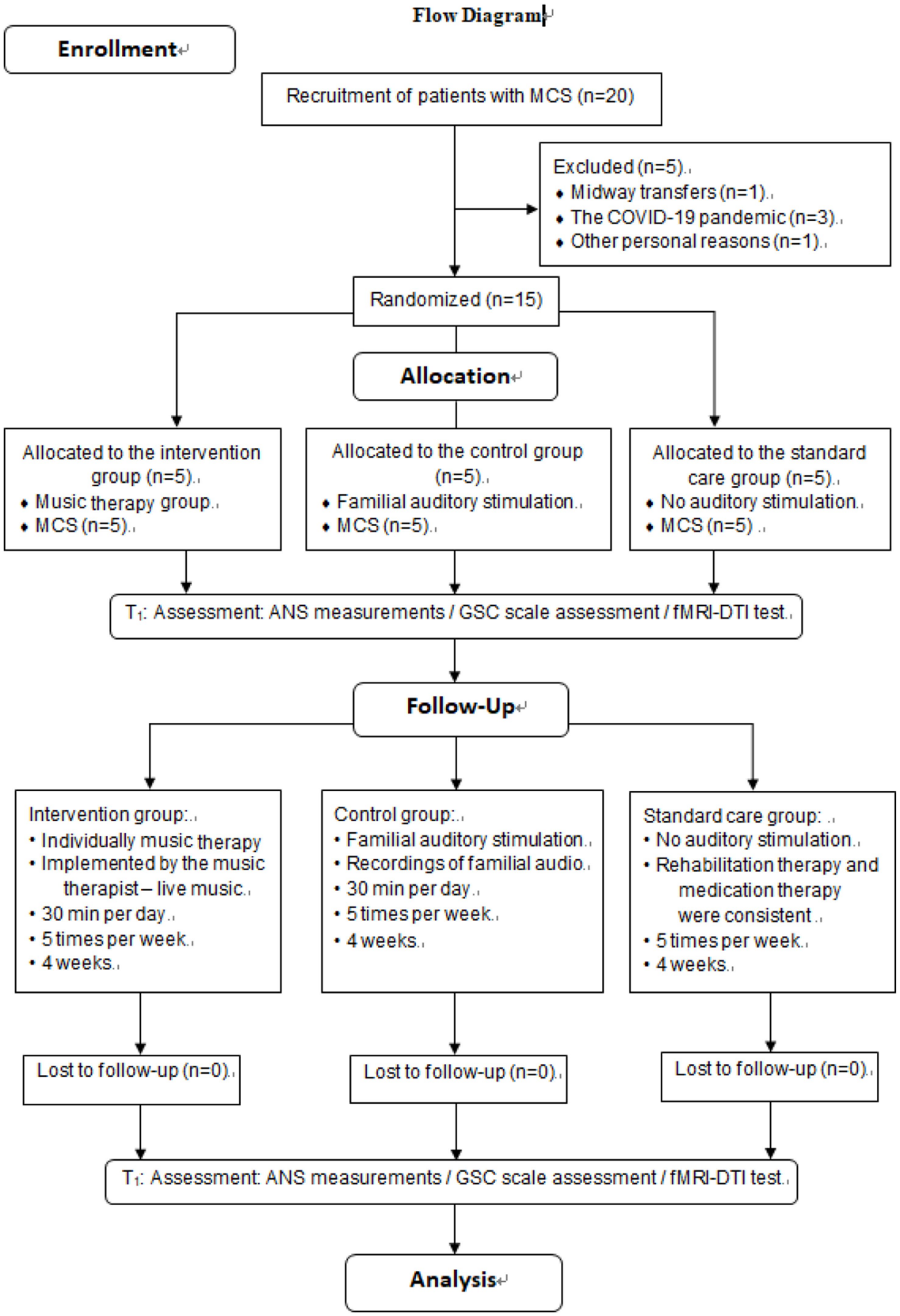

FIGURE 1
Flow diagram, consort flowchart for participants' recruitment and allocation.

Interventions

The treatment intervention began after the subjects were enrolled. All patients in the experimental group received live music therapy the control group received sound auditory stimulation recorded by family members, and standard care group did not receive auditory stimulation. Each patient received 30 min of training five times a week for 4 weeks. Music therapy was performed by registered music therapists who were licensed to ensure the professionalism of the intervention. The familial stimuli were generated through recordings of family member voices, with the family members engaging in conversation pertaining to the patient's past personal life experiences, and expressing such content directly to the patient.

The live music therapy supported by music therapist

In the intervention group, a music therapist performed a fixed program of musical therapy session (a set of songs edited in a fixed order). The song selection was based on the patient's musical preferences. Sources of songs are: (1) Songs that are played most frequently in the mobile phone music app of patients; (2) The family members informed the music therapist of the patient's favorite singer, and the music therapist selected the most famous songs of the singer for intervention. The standardized procedure for music therapy consisted of a fixed pattern lasting for a duration of 30 min, comprising (1) an opening piece, specifically the "Hello song" composed by the therapist with a duration of 2.5 min, followed by (2) a song content component that involved the selection of music with emotional significance to the subjects and their significant relationships (for example, parents, couples/lovers, children, grandparents, friends) from their past life experiences, with a total duration of 25 min. For instance, one subject had previously viewed the film "Hello, Li Huanying" with their mother before experiencing injury, and had a powerful emotional response to the theme song "Daylily Flower" played at the end of the movie. As a result, during the music sessions, the music therapist performed the song live for the patient, while simultaneously incorporating a section of lyrics that were thematically related to the mother based on the film's premise. The music therapy procedure concluded (3) with the "Goodbye Song" (2.5 min), which featured lyrics composed by the therapist (Supplementary material).

Familial auditory stimulation supported by patients' family members

The researchers communicated with the patients' families to confirm the content and duration of the recordings. The recording content was related to the patients' personal life experiences. The patients' loved ones had a daily conversation around the theme of each "patient's personal life," and the conversation content was recorded in WMA or MP3 format for 30 min (Supplementary material).

Standard care group

The standard care group did not receive auditory stimulation, but the rehabilitation therapy and medication therapy were consistent with the experimental group and the control group.

Measurements

Before the intervention, all the participants were assessed at baseline by the researcher, using (1) automatic nerve system (ANS) testing for physiological examination of the peripheral nervous system; (2) the Glasgow Coma Scale (GCS) (Mehta and Chinthapalli, 2019) for behavioral assessment; and (3) Functional Magnetic Resonance Imaging-Diffusion Tensor Imaging (fMRI-DTI) (Gould et al., 2021). Behavioral and radiological changes were observed at a second assessment 4 weeks later.

Automatic nerve system test

The ANS Bodyguard device (Version 3.1, Meiyang Limited, Beijing, China) was used to record the sympathetic and parasympathetic nervous system indicators as follows: (1) Percentage of the number of adjacent sinus beats with difference > 50 ms in total sinus beats, PNN50; (2) Total Power, TP; (3) Low Frequency, LF; (4) High Frequency, HF; (5) LF norm/HF norm = LF/(LF + HF) × 100; (6) Very low frequency band, VLF. Low frequency and high frequency were obtained in the ranges of 0.04–0.15 Hz and 0.15–0.40 Hz, respectively (Gitler et al., 2022). The magnitude of high frequency and the ratio of low frequency to high frequency (LF/HF) corresponded to the intensity of vagal activity and sympathetic vagal balance, respectively. Specifically, the size of LF is involved in vagus and sympathetic nerve activity (Lee and Shields, 2022). The natural logarithms of powers (lnLF and lnHF) were used to evaluate the magnitude of each spectral component. The ratio of LF component to HF component (LF/HF ratio) was calculated by dividing lnLF by lnHF (lnLF/lnHF).

Glasgow coma scale (GCS)

GCS is a behavioral assessment method for assessing the degree of consciousness of patients (Eapen et al., 2017). The level of consciousness was assessed by evaluating eye opening, language, and movement. A higher score indicated a better state of consciousness. Specifically (1) the blink reflex was graded on a scale of self-opening (4′), opening eyes upon hearing one's name (3′), opening eyes in response to a painful stimulus (2′), or no reaction (1′); (2) the language reflex was graded on a scale of accurate orientation and correct responses (5′), correct orientation but incorrect responses (4′), ability to speak but unable to answer (3′), ability to produce only sounds (2′), and inability to produce any sounds (1′); and (3) the motor reflex was graded on a scale of ability to follow commands (6′), ability to point to the site of pain (5′), retraction of limbs in response to a painful stimulus (4′), flexion of both upper limbs (3′), extension of limbs (2′), and complete relaxation of limbs (1′) (Mehta and Chinthapalli, 2019).

Functional magnetic resonance imaging-diffusion tensor imaging

Functional Magnetic Resonance Imaging (fMRI) uses magnetic resonance imaging to measure the hemodynamic changes caused by neuronal activity. Generally, fMRI has the scanning characteristics of high spatial resolution (2-3 mm) and high temporal resolution (within 1 s, rapid imaging time is 30-100 mm). Such method can reveal the functional reorganization of different regions of the brain. Diffusion

tensor imaging (DTI), a type of fMRI technique that examines the connectivity and integrity of living tissue, is designed to visualize the direction of nerve fiber bundles in the white matter of the brain, resulting in a detailed tensor image of the central nervous system fibers.

The DTI index adopted in the present study was a parameter of fractional anisotropy (FA) of the reaction part. The value ranged from 0 to 1, where 0 represents the maximum anisotropic dispersion and 1 represents the maximum anisotropic dispersion. The method involved sensitive gradients applied in six different non-collinear directions with a slice thickness of 1 mm, using a 256 matrix scanning protocol and a 256×256 isotropic resolution of 1 square mm. Scans were performed at T1 and T2 to visualize the fiber tracts of water molecules in the X, Y, and Z directions of the brain.

Statistical analysis

Measurements of the three groups were collected at 2 time points before intervention (baseline, T0) and after intervention (4 weeks later, T2), being expressed in the form of mean ± standard deviation. Two-factor analysis of variance was used to observe the differences between differences groups, time effects, and the interaction effects between time and groups. SPSS 23.0 (SPSS Inc., Chicago, IL, USA, IBM Lenovo, BJIBM Lenovo, BJ, USA) was used for statistical analysis of the three sets of data to determine the specific effects of the intervention.

Results

The ANS index in the intervention group was significantly improved compared with the control group and the standard care group

The excitability of the ANS system in MCS patients was evaluated in respect of six aspects: (1) PNN50; (2) TP; (3) LF; (4) HF; (5) VLF; and (6) LF/HF. After 4 weeks of treatment, PNN50 was significantly higher in the intervention group (a) than in the control group (b) and the standard care group (c) ($p = 0.0004$, a > b > c, Figure 2A). TP in the intervention group was significantly higher than those in the control group and the standard care group ($p = 0.0003$, a > b > c, Figure 2B). For LF, there were no obvious differences between the three groups ($p = 0.2401$, a≒b≒c, Figure 2C), which was the same for HF ($p = 0.1685$, a≒b≒c, Figure 2D). VLF in the intervention group was significantly higher than those in the control group and the standard care group ($p = 0.0428$, a > b > c, Figure 2E). However, for the ratio of LF/HF, the intervention group showed considerably significant improvement over the control group and the standard care group ($p = 0.0001$, a > b > c, Figure 2F). The results are shown in Table 2 and Figure 2.

The GCS scores in the intervention group were significantly improved compared with the control group and the standard care group

The degree of consciousness of MCS patients was scored using the GCS. GCS can be evaluated in four domains: (1) blink reflex; (2) speech reflex; (3) limb reflexes, and (4) total GCS score. After 4 weeks of treatment, the blink reflex frequencies in the intervention group (a) and control group (b) were significantly higher than that in standard care group (c), and the score in the intervention group was higher than that in the control group ($p = 0.0071$, a > b > c, Figure 3A). The speech reflex frequencies of the intervention group and the control group were significantly higher than that of the standard care group (c), and the score of the intervention group was higher than that of the control group ($p = 0.0063$, a > b > c, Figure 3B). The limb reflex frequencies were significantly higher in the intervention and control groups than in the standard care group (c), where the intervention group scored higher than the control group ($p = 0.0001$ a > b > c, Figure 3C). The total GCS scores of the intervention and control groups were higher than that of the standard care group (c), where the intervention group had a higher score than the control group ($p = 0.0001$, a > b > c, Figure 3D). The results are shown in Table 3 and Figure 3.

Visualization effect of music therapy on brain network in the patients with MCS

After performing Pipeline for Analyzing braiN Diffusion imAges (PANDA) analysis using MATLAB and considering the 246 brain regions (Fan et al., 2016), it was observed that compared with the control group, the dorsolateral area of the superior frontal gyrus (SFG), middle frontal gyrus (MFG), ventrolateral of middle frontal gyrus, orbitofrontal cortex, precentral gyrus, superior temporal gyrus, transverse temporal gyrus, inferior temporal gyrus, corpus callosum, parahippocampal, inferior parietal lobule, postcentral gyrus, insular gyrus, cingulate gyrus, basal ganglia and other regions exhibited a significant increase in Fractional Anisotropy (FA), Fiber Number (FN), and Path Length (Length). Table 3 shows the highlighted regions of interest (ROIs) of FA, FN, and length enhancement trends after music-based MIT intervention (Figure 4; Supplementary material).

Positive effects of music therapy on hypothalamic-brainstem-autonomic nervous system axis of autonomic nervous system-central nervous system in patients with MCS

After PANDA analysis using MATLAB and considering the accuracy of white matter fiber bundle shape tracking by DTI (Fan et al., 2016), it was identified that compared with the control group and the standard care group, neural fiber traces in the superior frontal gyrus (SFG), middle frontal gyrus (MFG), precentral gyrus (PrG), postcentral gyrus (PoG), superior temporal gyrus (STG), transverse temporal gyrus (TTG), inferior temporal gyrus (ITG), limbic system, corpus callosum, subcorticospinal trace, thalamus and brainstem regions were significantly increased in the experimental group. Figure 4 shows the results of the experimental group after music therapy compared with the control group and the standard care group. The results of the three groups are shown in Figure 4.

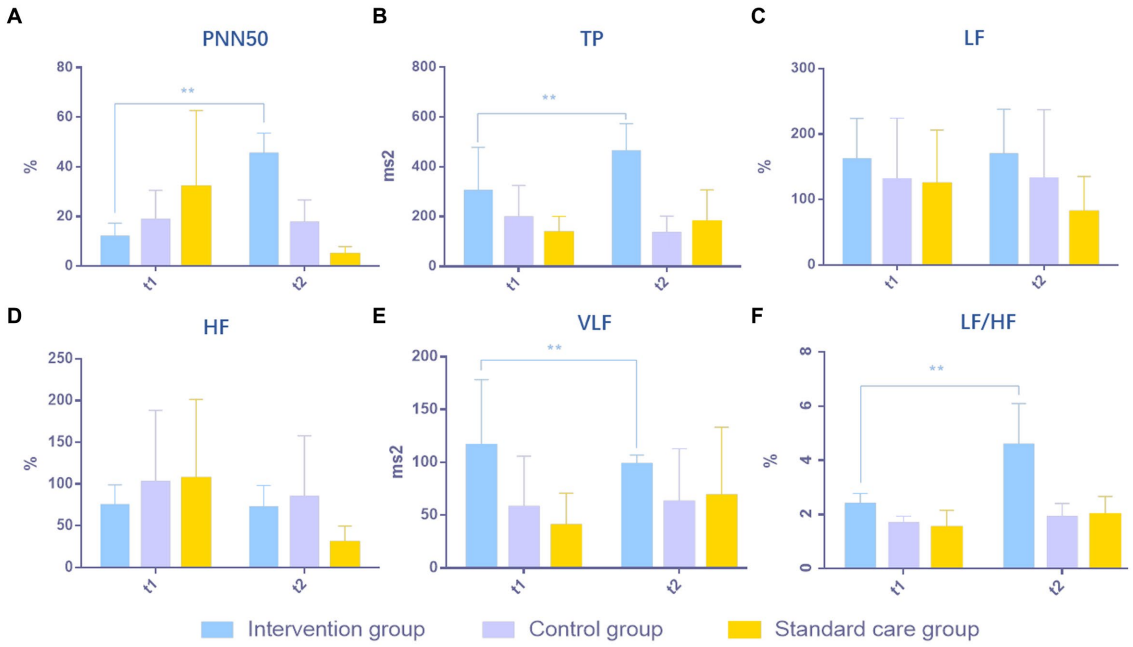

FIGURE 2
Comparison of results of ANS in MCS patients in three groups. **(A)** PNN50, **(B)** TP, **(C)** LF, **(D)** HF, **(E)** VLF, **(F)** LF/HF. $^{**}p$ <0.01, significant difference; $^{*}p$ <0.05, difference.

TABLE 2 The results of the ANS tests in patients with minimally conscious states across the study period for the intervention group (a), the control group (b), and the standard care group (c).

		Intervention group (a) (n=5) Mean±SD	Control group (b) (n=5) Mean±SD	Standard care (c) (n=5) Mean±SD	p	Intergroup comparison
PNN50 (%)	t_1	11.92 ± 5.40	18.68 ± 11.91	31.89 ± 30.78	0.7475	a>b>c **
	t_2	45.39 ± 8.25	17.58 ± 9.10	4.73 ± 3.15	0.0004**	
TP (ms^2)	t_1	303.01 ± 175.37	196.74 ± 128.15	135.62 ± 65.06	0.2903	a>b>c **
	t_2	462.61 ± 110.49	134.07 ± 68.07	179.38 ± 128.13	0.0003**	
LF (%)	t_1	161.67 ± 62.15	130.79 ± 93.49	123.92 ± 82.53	0.7436	a≒b≒c
	t_2	169.20 ± 68.99	132.45 ± 105.01	80.95 ± 54.33	0.2401	
HF (%)	t_1	74.73 ± 24.38	102.59 ± 85.88	106.75 ± 94.90	0.3901	a≒b≒c
	t_2	72.18 ± 26.17	84.63 ± 73.11	30.15 ± 19.48	0.1685	
VLF (%)	t_1	116.14 ± 62.27	57.36 ± 48.62	40.04 ± 30.91	0.5712	a>b>c *
	t_2	98.04 ± 8.99	62.44 ± 50.52	68.28 ± 64.92	0.0428*	
LF/HF (%)	t_1	2.39 ± 0.39	1.68 ± 0.26	1.52 ± 0.64	0.0191	a>b>c **
	t_2	4.58 ± 1.52	1.91 ± 0.50	1.99 ± 0.68	0.0001**	

Data were expressed as mean ± SD (n = 15), and two-way ANOVA was used to analysis the data. $^{**}p$ < 0.01, significant difference; $^{*}p$ < 0.05, difference. >, greater than or equal to; ≒, approximately equal to.

Discussion

By autonomously regulating the nervous system according to the different auditory stimuli given, music can widely activate the brain network (Zatorre et al., 2007; Alluri et al., 2012; Särkämö et al., 2013; Koelsch, 2014; Fan et al., 2016) and increase the blood flow of intracerebral arteries, thereby providing a favorable environment for the overall recovery of the brain. The auditory complexity of music has an environmental enrichment effect (Engineer et al., 2004; Teppo et al., 2008) in patients with MCS, which has a behavioral and neurobiological level of facilitation in autonomic nervous system arousal in patients with DOC. Several prior studies have reported on neural reorganization of brain networks in patients with MCS following music-supported therapy. Additionally, other studies have provided further evidence of music therapy on central neural plasticity related to

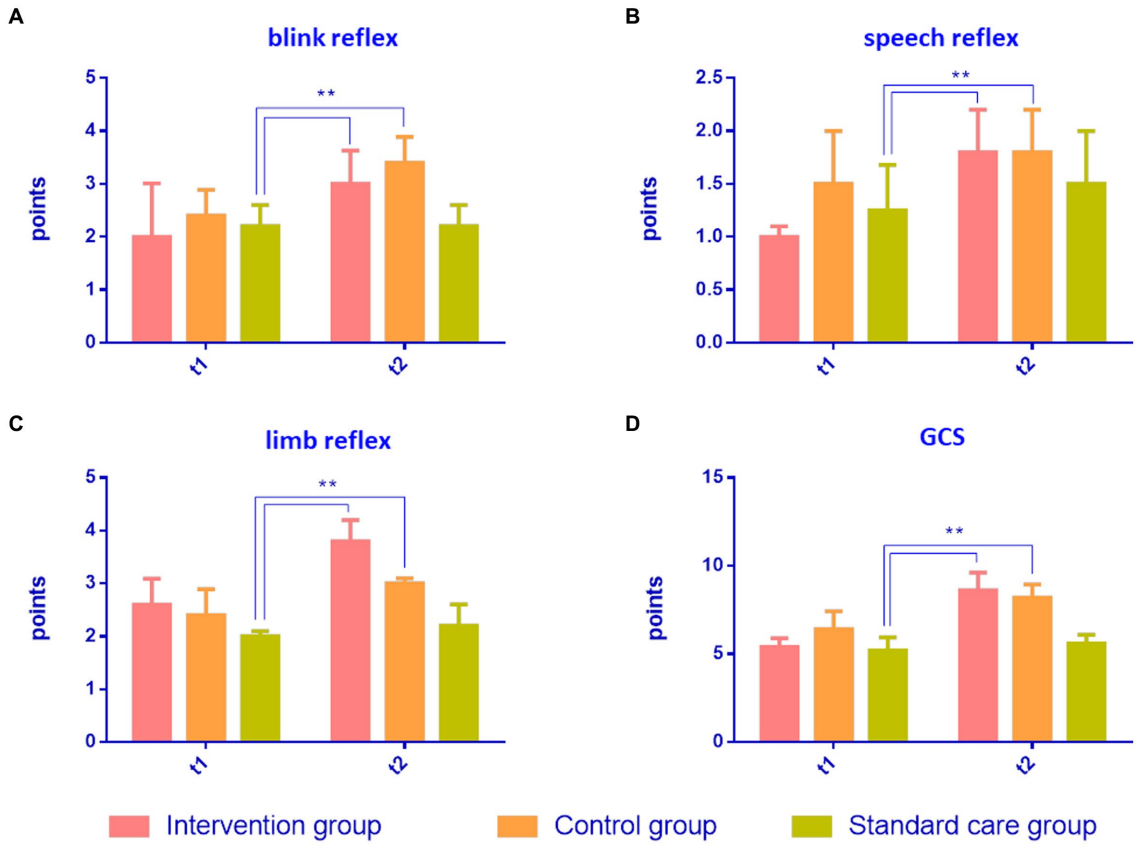

FIGURE 3
Comparison of results of GCS scores in MCS patients in three groups. **(A)** Blink reflex, **(B)** speech reflex, **(C)** limb reflex, and **(D)** GCS score. $^{**}p < 0.01$, significant difference; $^{*}p < 0.05$, difference.

TABLE 3 The results of GCS scores in patients with minimally consciousness states across the study period for the intervention group (a), the control group (b), and the standard care group (c).

		Intervention group (a)	Control group (b)	Standard care (c)	*p*	Intergroup comparison
		(*n*=5)	(*n*=5)	(*n*=5)		
		Mean±SD	Mean±SD	Mean±SD		
Blink	t_1	2.02±0.01	2.40±0.49	2.20±0.40	0.3084	
	t_2	3.01±0.63	3.40±0.49	2.20±0.40	0.0071**	a>b>c**
Speech	t_1	1.01±0.01	1.05±0.50	1.25±0.43	0.274	
	t_2	1.80±0.40	1.80±0.40	1.50±0.50	0.0063**	a>b>c**
Motor	t_1	2.60±0.49	2.40±0.49	2.01±0.01	0.784	
	t_2	3.80±0.40	1.50±0.50	2.20±0.40	0.0001**	a>b>c**
Total	t_1	5.40±0.49	6.40±1.02	5.20±0.75	0.2379	
	t_2	8.60±1.02	8.20±0.75	5.60±0.49	0.0001**	a>b>c**

Data were expressed as mean±SD ($n=15$), and two-way ANOVA was used to analysis the data. $^{**}p < 0.01$, significant difference; $^{*}p < 0.05$, difference. >, greater than or equal to.

auditory and motion (Amengual et al., 2013; Grau-Sanchez et al., 2013; Ripollés et al., 2016). The aim of the present study was to focus on two key points: firstly, investigating the activity of the autonomic nervous system based on the hypothalamus-pituitary–adrenal axis in MCS patients stimulated by music. Secondly, observing the structural remodeling outcomes of neural networks in the brain when the peripheral nervous system is activated.

The ANS activity of MCS patients was increased in music therapy—based on the theory of hypothalamic brainstem autonomic nervous system

Music produces measurable cardiovascular and endocrine responses, indicated by reduced serum cortisol levels and inhibition of

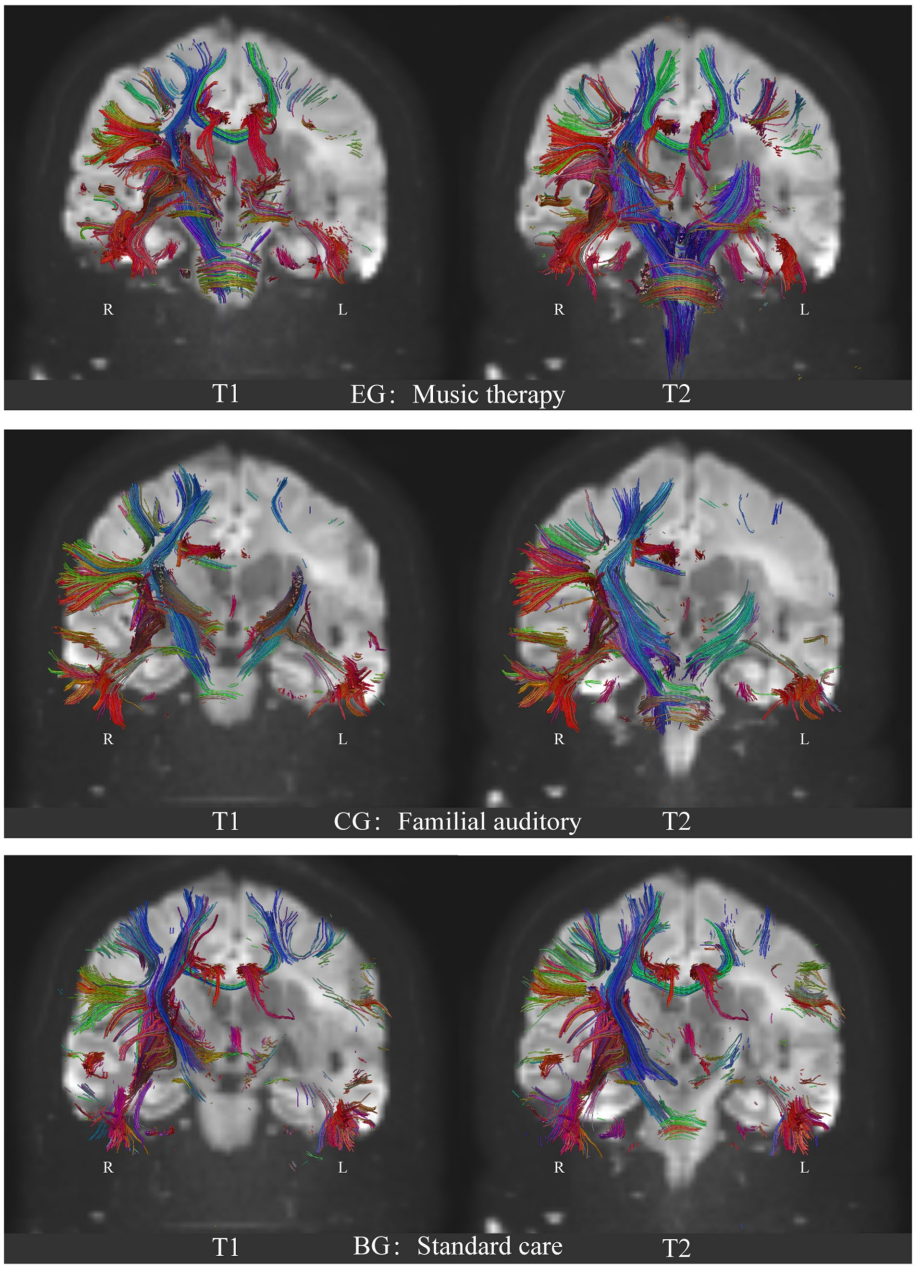

FIGURE 4
Comparison of the neural fibers trace results of DTI on brain network of the three groups. EG: experimental group, music auditory stimulation group; CG: control group, familial auditory stimulation group, BG: standard care group, no auditory stimulation group. T1: baseline, before intervention; T2: 1month after intervention. R: right hemisphere; L: Left hemisphere. Blue: Superior–Inferior direction of the nerve fiber bundle; Red: Anterior–Posterior direction of the nerve fiber bundle; Green: Left–Right direction of nerve fiber bundles.

cardiovascular stress reactions (Sihvonen et al., 2017). This theory relies on the musical effectiveness on the hypothalamic brainstem autonomic (HBA) axis, which is proposed in 2017, which states that music-induced activation of the parasympathetic nervous system and inhibition of the sympathetic nervous system, and induce improvement of arousal might therefore enhance recovery of cognitive functions in patients (Sihvonen et al., 2017). In the regulation of the autonomic nervous system (ANS), external stimuli are received through bodily receptors, serving as a crucial source for the modulation of the sympathetic and parasympathetic nervous systems. The autonomic nervous system is often referred to as the involuntary nervous system due to its lack of control by conscious awareness. In the control of ANS, signals from the outside world are received through body receptors, which is a significant stimulus source for the antagonism or inhibition of ANS sympathetic and parasympathetic nerves. In the present study, patients in the experimental group received music therapy through auditory means. The song selection was based on the patients' personal life experiences and included their favorite songs prior to the onset of illness. The input form was auditory stimulation in the form of live singing of the songs by a music therapist. Patients in the music group received more varied sound signals than those in the control group who listened to family voices and the standard care group who received no auditory stimuli. Compared with the abstract content of familial conversation (better brain function is needed to recognize sound properties and understand

the meaning of the conversation), the emotional experience brought by the melodic and harmonic richness of music is more concentrated in the thalamus and hypothalamus, which are the central starting point of the HBA axis. As such, after receiving auditory input from music, PNN50 and TP in the ANS in the music group were significantly increased. Decreased PNN50 indicates decreased parasympathetic excitability (Tak et al., 2010). Since patients in the standard care group were not treated with auditory stimulation other than standard care and nutritional neuro-medications, parasympathetic PNN50 decreased compared with patients in the other two groups who received auditory interventions, suggesting the possibility of autonomic nervous system disorders. Such findings indicate that while listening to the familiar music that made patients feel present, the experimental group exhibited an increase in sinus heart rate, myocardial sympathetic and vagal tone, as well as a decrease in balance. When the experimental group listened to familiar music, significant changes in VLF, LF/HF and other values of ANS showed that the experience generated during listening to music could induce immediate cardiovascular and endocrine responses, and such positive experiences were related to the fast reward circuit. According to the upward circulation of the HBA axis, after stimulation by music, ANS excitation could further result in activity of the brain stem and hypothalamus, thereby promoting the activity of the MCS brain network.

Music therapy activates the brain network or spare neural networks more broadly in MCS patients—based on the results of DTI analysis

According to the results of FA (anisotropy) in the analysis of fMRI-DTI, the FA showed a significant increase in the macro structure of the right temporal lobe after music therapy intervention in the experimental group. Particularly, there was a noticeable trend of fiber bundle reconstruction in the internal sac and corpus callosum. In the experimental group, the increase in the FA value in the knee and pressure area of the corpus callosum was significantly correlated with the improvement in the GSC score. In addition, FA increased significantly in the posterior corpus callosum, corticospinal tract, cingulate tract, posterior branch of internal capsule, inferior fronto-occipital tract and superior longitudinal tract. Such findings positively correlated with increased blinking and motor reflex in the experimental group. In the speech reflex of GCS between the music group and the familial group, the difference between the two groups was not significant, but it was significantly different from the standard care group. This behavior result is also verified in the results of DTI imaging. It is well known that auditory semantic understanding is in the ventral pathway of the left temporal lobe, while speech output is in the temporoparietal and frontal lobe regions that transmit auditory-motor signals. Songs expressing emotion can be understood as an emotional language to some extent. When the vocal music is sung live, the right middle and front of the superior temporal gyrus, and amygdala of the subjects were involved in the activity at the same time. Therefore, in the experimental group, both the bilateral temporal lobe and the ventral frontal parietal cortex based on semantic understanding and melody perception responded simultaneously, forming an automatic processing of auditory integrity-verbal motor output, hence inducing the occasional verbal phonological behavior. However, in the familial group, because the conversational communication is more integrated the semantic understanding area of the left superior temporal gyrus and the verbal motor output area of the frontal parietal lobe, the relative voice behavior feedback was also seen in the GCS score.

Because MCS patients are consistently characterized by abnormal white matter signals, after 4 weeks of quantitative stimulation with two different sounds, music and family conversation, definite changes in nerve fiber bundles in the ascending reticular activating system (ARAS) were evident in the music group (Figure 4; EG: T2). The musical stimuli given had the following characteristics: (1) the patient was familiar with the past and had emotional involvement; (2) music therapists sang live and helped patients to feel present. ANS HRV response increment through the connectivity of up and down neural fiber bundles. Compared with the other two groups, the bulbar, pons, and midbrain of the experimental group showed an obvious thickening trend. It is suggested that under the input signal of vocal activity, the enhancement of important physiological activities such as cardiovascular and respiratory strengthens the lateral branches of sensory nerves connecting the lower corticospinal tract and the ascending medulla in the brainstem and diencephalon (dorsal encephalon nucleus), which enhances the Brownian motion trajectory of water molecules, and thus remodels the nerve fiber bundle in the brainstem and the distal sub cerebral. (DTI 3D Video in Supplementary material).

For patients with MCS, the challenge of awakening consciousness is a widespread issue. Live music therapy, a non-invasive treatment primarily utilizing auditory input to the receptors and created by a music therapist, promotes physiological arousal of the HPA axis and ARAS activation in MCS patients. Such innovative treatment approach aligns with the growing trend of heart-brain integrated prevention strategies and offers a new avenue for the clinical treatment of consciousness disorders.

Limitations

The small sample size is one of the limitations of the present study. If a larger sample size can be included in future studies, so as to expand the number of subjects under three different conditions for comparison, there will be more evidence for clinical research.

Implications for clinical practice

In the present study, the clinical significance of live music therapy administered by music therapists for patients with MCS was demonstrated, and the potential therapeutic mechanisms were tentatively revealed. In the future, the hope is that an increasing number of music therapists will participate in clinical practice as part of a multidisciplinary team, under the guidance of medical professionals, with the aim of aiding in the awakening of DOC patients.

Conclusion

Live music therapy, administered by a professional music therapist, is more effective for MCS patients than listening to familial auditory stimulation, and is worth promoting in clinical practice in the future.

Data availability statement

The original contributions presented in the study are included in the article/Supplementary material, further inquiries can be directed to the corresponding author.

Ethics statement

The studies involving human participants were reviewed and approved by the Ethics Committee of China Rehabilitation Research Center (approval No. 2018–022-1) on March 12, 2018, and informed consent was obtained from the participants, relatives or guardians before commencing the study. The study trial was registered with the Clinical Trial Registry (Registration No. ChiCTR1800017809) on August 15, 2018. The patients/participants provided their written informed consent to participate in this study. Written informed consent was obtained from the individual (s) for the publication of any potentially identifiable images or data included in this article.

Declaration of patient consent

The authors certify that they obtained consent forms from patients. In the form, patients gave their consent for their images and other clinical information to be reported in the journal. The patients understood that their names and initials would not be published.

Reporting statement

The writing and editing of the article were performed in accordance with the Consolidated Standards Of Reporting Trials (CONSORT) Statement.

Biostatistics statement

The statistical methods of this study were reviewed by the epidemiologist of Capital Medical University, China.

Data availability statement

Deidentified participant data, along with corresponding data dictionaries, will be made available for sharing. Furthermore, related documents such as the study protocol and statistical analysis plan will also be accessible. The data will become available in the next 5 years. Research colleagues can access the data through the China Clinical Trials Registry, the Resman clinical trials public administration platform.

Author contributions

XX was in charge of manuscript writing. XZ was responsible for study design, patient allocation, protocol development, data statistics, result description, statistical chart drawing, clinical analysis and discussion description, and is the corresponding author. WC implemented the assessment, evaluation, original data collection and supported music therapy. All authors contributed to the article and approved the submitted version.

Funding

This work was supported by the Beijing Science and Technology Project Foundation of China, No. Z181100001718066, and the National Key R&D Program of China Nos. 2022YFC3600300 and 2022YFC3600305.

Acknowledgments

This research was supported by the China Rehabilitation Research Center (CRRC). We thank Yinan Li to support music therapy as assistance. We thank our colleagues from Music Therapy Center, CRRC; Department of Neurosurgery, CRRC; Capital Medical University, Central Conservatory of Music; who provided technical support and greatly assisted the research.

Conflict of interest

The authors declare that the research was conducted in the absence of any commercial or financial relationships that could be construed as a potential conflict of interest.

Publisher's note

Supplementary material

The Supplementary material for this article can be found online at: https://www.frontiersin.org/articles/10.3389/fnins.2023.1182181/full#supplementary-material

References

Alluri, V., Toiviainen, P., Jääskeläinen, I. P., Glerean, E., Sams, M., and Brattico, E. (2012). Large-scale brain networks emerge from dynamic processing of musical timbre, key and rhythm. *NeuroImage* 59, 3677–3689. doi: 10.1016/j.neuroimage.2011.11.019

Amengual, J. L., Rojo, N., Veciana de Las Heras, M., Marco-Pallarés, J., Grau-Sánchez, J., et al. (2013). Sensorimotor plasticity after music-supported therapy in chronic stroke patients revealed by transcranial magnetic stimulation. *PLoS One* 8:e61883. doi: 10.1371/journal.pone.0061883

Annen, J., Filippini, M. M., Bonin, E., Cassol, H., Aubinet, C., Carrière, M., et al. (2019). Diagnostic accuracy of the CRS-R index in patients with disorders of consciousness. *Brain Inj.* 33, 1409–1412. doi: 10.1080/02699052.2019.1644376

Arroyo-Anlló, E. M., Díaz, J. P., and Gil, R. (2013). Familiar music as an enhancer of self-consciousness in patients with Alzheimer's disease. *Bio Med Res. Int.* 2013:752965, 1–10. doi: 10.1155/2013/752965

Bagnato, S. (2022). The role of plasticity in the recovery of consciousness. *Handb. Clin. Neurol.* 184, 375–395. doi: 10.1016/B978-0-12-819410-2.00020-5

Bellon, P. A., Bosso, M. J., Echegaray, J. E. C., Larocca, F., Gagliardi, J., Primosich, W. A., et al. (2022). Tracheostomy Decannulation and disorders of consciousness evolution. *Respir. Care* 67, 209–215. doi: 10.4187/respcare.08301

Bodien, Y. G., Katz, D. I., Schiff, N. D., and Giacino, J. T. (2022). Behavioral assessment of patients with disorders of consciousness. *Semin. Neurol.* 42, 249–258. doi: 10.1055/s-0042-1756298

Bower, J., Magee, W. L., Catroppa, C., and Baker, F. A. (2022). Content validity and inter-rater reliability of the music interventions in pediatric DoC behavior observation record. *J. Music. Ther.* doi: 10.1093/jmt/thac013

De Luca, R., Bonanno, M., Vermiglio, G., Trombetta, G., Andidero, E., Caminiti, A., et al. (2022). Robotic Verticalization plus music therapy in chronic disorders of consciousness: promising results from a pilot study. *Brain Sci.* 12:1045. doi: 10.3390/brainsci12081045

Eapen, B. C., Georgekutty, J., Subbarao, B., Bavishi, S., and Cifu, D. X. (2017). Disorders of consciousness. *Phys. Med. Rehabil. Clin. N. Am.* 28, 245–258. doi: 10.1016/j.pmr.2016.12.003

Engineer, N. D., Percaccio, C. R., Pandya, P. K., Raluca, M., Rathbun, D. L., and Kilgard, M. P. (2004). Environmental enrichment improves response strength, threshold, selectivity, and latency of auditory cortex neurons. *J. Neurophysiol.* 92, 73–82. doi: 10.1152/jn.00059.2004

Fan, L., Li, H., Zhuo, J., Zhang, Y., Wang, J., Chen, L., et al. (2016). The human Brainnetome atlas: a new brain atlas based on connectional architecture. *Cereb. Cortex* 26, 3508–3526. doi: 10.1093/cercor/bhw157

Fins, J. J. (2011). Neuroethics, neuroimaging, and disorders of consciousness: promise or peril? *Trans. Am. Clin. Climatol. Assoc.* 122, 336–346.

Fischer, D., Newcombe, V., Fernandez-Espejo, D., and Snider, S. B. (2022). Applications of advanced MRI to disorders of consciousness. *Semin. Neurol.* 42, 325–334. doi: 10.1055/a-1892-1894

Fitzpatrick-DeSalme, E., Long, A., Patel, F., and Whyte, J. (2022). Behavioral assessment of patients with disorders of consciousness. *J Clin. Neurophysiol.* 39, 4–11. doi: 10.1097/WNP.0000000000000666

Giacino, J. T., Kalmar, K., and Whyte, J. (2004). The JFK coma recovery scale-revised: measurement characteristics and diagnostic utility. *Arch. Phys. Med. Rehabil.* 85, 2020–2029. doi: 10.1016/j.apmr.2004.02.033

Gitler, A., Vanacker, L., De Couck, M., De Leeuw, I., and Gidron, Y. (2022). Neuromodulation applied to diseases: the case of HRV biofeedback. *J. Clin. Med.* 11:5927. doi: 10.3390/jcm11195927

Gould, L., Kress, S., Neudorf, J., Gibb, K., Persad, A., Meguro, K., et al. (2021). An fMRI, DTI and neurophysiological examination of atypical Organization of Motor Cortex in Ipsilesional hemisphere following post-stroke recovery. *J. Stroke Cerebrovasc. Dis.* 30:105593. doi: 10.1016/j.jstrokecerebrovasdis.2020.105593

Grau-Sanchez, J., Amengual, J. L., Rojo, N., Veciana de Las Heras, M., Montero, J., et al. (2013). Plasticity in the sensorimotor cortex induced by music-supported therapy in stroke patients: a TMS study. *Front. Hum. Neurosci.* 7:494. doi: 10.3389/fnhum.2013.00494

Grimm, T., and Kreutz, G. (2018). Music interventions in disorders of consciousness (DOC) - a systematic review. *Brain Inj.* 32, 704–714. doi: 10.1080/02699052.2018.1451657

Hu, Y., Yu, F., Wang, C., Yan, X., and Wang, K. (2021). Can music influence patients with disorders of consciousness? An event-related potential study. *Front. Neurosci.* 15:596636. doi: 10.3389/fnins.2021.596636

Humble, S. S., Wilson, L. D., Wang, L., Long, D. A., Smith, M. A., Siktberg, J. C., et al. (2018). Prognosis of diffuse axonal injury with traumatic brain injury. *J. Trauma Acute Care Surg.* 85, 155–159. doi: 10.1097/TA.0000000000001852

Ismail, F. Y., Saleem, G. T., and Ljubisavljevic, M. R. (2022). Brain data in pediatric disorders of consciousness: special considerations. *J Clin. Neurophysiol.* 39, 49–58. doi: 10.1097/WNP.0000000000000772

Istace, T. (2022). Empowering the voiceless. Disorders of consciousness, neuroimaging and supported decision-making. *Front. Psych.* 13:923488. doi: 10.3389/fpsyt.2022.923488

Janelli, L. M., Kanski, G. W., and Wu, Y. W. (2004). The influence of individualized music on patients in physical restraints: a pilot study. *J. N. Y. State Nurses Assoc.* 35, 22–27.

Koelsch, S. (2014). Brain correlates of music-evoked emotions. *Nat. Rev. Neurosci.* 15, 170–180. doi: 10.1038/nrn3666

Kondziella, D., and Stevens, R. D. (2022). Classifying disorders of consciousness: past, present, and future. *Semin. Neurol.* 42, 239–248. doi: 10.1055/a-1883-1021

Lee, J., and Shields, R. K. (2022). Sympathetic vagal balance and cognitive performance in Young adults during the NIH cognitive test. *J. Funct. Morphol. Kinesiol.* 7:59. doi: 10.3390/jfmk7030059

Li, X., Sawamura, D., Hamaguchi, H., Urushibata, Y., Feiweier, T., Ogawa, K., et al. (2022). Microscopic fractional anisotropy detects cognitive training-induced microstructural brain changes. *Tomography (Ann Arbor, Mich.)* 8, 33–44. doi: 10.3390/tomography8010004

Liu, Z. B., Liu, Y. S., Zhao, L., Li, M. Y., Liu, C. H., Zhang, C. X., et al. (2022). Short-term efficacy of music therapy combined with α binaural beat therapy in disorders of consciousness. *Front. Psychol.* 13:947861. doi: 10.3389/fpsyg.2022.947861

Magee, W. L., Ghetti, C. M., and Moyer, A. (2015). Feasibility of the music therapy assessment tool for awareness in disorders of consciousness (MATADOC) for use with pediatric populations. *Front. Psychol.* 6:698. doi: 10.3389/fpsyg.2015.00698

Magee, W. L., Siegert, R. J., Daveson, B. A., Lenton-Smith, G., and Taylor, S. M. (2014). Music therapy assessment tool for awareness in disorders of consciousness (MATADOC): standardisation of the principal subscale to assess awareness in patients with disorders of consciousness. *Neuropsychol. Rehabil.* 24, 101–124. doi: 10.1080/09602011.2013.844174

Mehta, R., and Chinthapalli, K. (2019). *Glasgow coma scale explained*, BMJ, 365:l 1296. doi: 10.1136/bmj.l1296

Pool, J. W., Siegert, R. J., Taylor, S., Dunford, C., and Magee, W. (2020). Evaluating the validity, reliability and clinical utility of the music therapy sensory instrument for cognition, consciousness and awareness (MuSICCA): protocol of a validation study. *BMJ Open* 10:e039713. doi: 10.1136/bmjopen-2020-039713

Rasmus, A., Góral-Półrola, J., Orłowska, E., Wiłkość-Dębczyńska, M., and Grzywniak, C. (2019). Nonverbal communication of trauma patients in a state of minimal consciousness. *Ann. Agric. Environ. Med.* 26, 304–308. doi: 10.26444/aaem/91911

Riganello, F., Cortese, M. D., Arcuri, F., Quintieri, M., and Dolce, G. (2015). How can music influence the autonomic nervous system response in patients with severe disorder of consciousness? *Front. Neurosci.* 9:461. doi: 10.3389/fnins.2015.00461

Ripollés, P., Rojo, N., Grau-Sanchez, J., Amengual, J. L., Càmara, E., et al. (2016). Music supported therapy promotes motor plasticity in individuals with chronic stroke. *Brain Imaging Behav.* 10, 1289–1307. doi: 10.1007/s11682-015-9498-x

Rollnik, J. D., and Altenmüller, E. (2014). Music in disorders of consciousness. *Front. Neurosci.* 8:190. doi: 10.3389/fnins.2014.00190

Sanz, L. R. D., Thibaut, A., Edlow, B. L., Laureys, S., and Gosseries, O. (2021). Update on neuroimaging in disorders of consciousness. *Curr. Opin. Neurol.* 34, 488–496. doi: 10.1097/WCO.0000000000000951

Särkämö, T., Tervaniemi, M., and Huotilainen, M. (2013). Music perception and cognition: development, neural basis, and rehabilitative use of music. *Wiley Interdiscip. Rev. Cogn. Sci.* 4, 441–451. doi: 10.1002/wcs.1237

Sihvonen, A. J., Teppo, S., Vera, L., Mari, T., Eckart, A., and Seppo, S. (2017). Music-based interventions in neurological rehabilitation. *Lancet Neurol.* 16, 648–660. doi: 10.1016/S1474-4422(17)30168-0

Tak, L. M., Janssens Karin, A. M., Andrea, D., Slaets Joris, P. J., and Rosmalen Judith, G. M. (2010). Age-specific associations between cardiac vagal activity and functional somatic symptoms: a population-based study. *Psychother. Psychosom.* 79, 179–187. doi: 10.1159/000296136

Teppo, S., Mari, T., Sari, L., Anita, F., Seppo, S., Mikko, M., et al. (2008). Music listening enhances cognitive recovery and mood after middle cerebral artery stroke. *Brain* 131, 866–876. doi: 10.1093/brain/awn013

Young, M. J., and Peterson, A. (2022). Neuroethics across the disorders of consciousness care continuum. *Semin. Neurol.* 42, 375–392. doi: 10.1055/a-1883-0701

Zatorre, R. J., Chen, J. L., and Penhune, V. B. (2007). When the brain plays music: auditory-motor interactions in music perception and production. *Nat. Rev. Neurosci.* 8, 547–558. doi: 10.1038/nrn2152

Zhang, X. Y., Li, J. J., Lu, H. T., Teng, W. J., and Liu, S. H. (2021). Positive effects of music therapist's selected auditory stimulation on the autonomic nervous system of patients with disorder of consciousness: a randomized controlled trial. *Neural Regen. Res.* 16, 1266–1272. doi: 10.4103/1673-5374.301021

frontiers | Frontiers in Neuroscience

TYPE Review
PUBLISHED 10 July 2023
DOI 10.3389/fnins.2023.1216215

OPEN ACCESS

EDITED BY
Feng Zhang,
Third Hospital of Hebei Medical University, China

REVIEWED BY
Shurong Duan,
First Affiliated Hospital of Harbin Medical University, China
Huayan Liu,
First Affiliated Hospital of China Medical University, China

*CORRESPONDENCE
Zhuo Xu
✉ xuzhuo@jlu.edu.cn

RECEIVED 03 May 2023
ACCEPTED 15 June 2023
PUBLISHED 10 July 2023

CITATION
Zhao Q, Du X, Chen W, Zhang T and Xu Z (2023) Advances in diagnosing mild cognitive impairment and Alzheimer's disease using ^{11}C-PIB- PET/CT and common neuropsychological tests.
Front. Neurosci. 17:1216215.
doi: 10.3389/fnins.2023.1216215

Advances in diagnosing mild cognitive impairment and Alzheimer's disease using ^{11}C-PIB-PET/CT and common neuropsychological tests

Qing Zhao[1], Xinxin Du[1], Wenhong Chen[2], Ting Zhang[3,4] and Zhuo Xu[3]*

[1]Department of Neurology, China-Japan Union Hospital of Jilin University, Changchun, Jilin, China, [2]Department of Sleep Medicine, Guangxi Zhuang Autonomous Region People's Hospital, Nanning, Guangxi, China, [3]Department of Rehabilitation, China-Japan Union Hospital of Jilin University, Changchun, Jilin, China, [4]Rehabilitation Therapeutics, School of Nursing of Jilin University, Changchun, Jilin, China

Alzheimer's disease (AD) is a critical health issue worldwide that has a negative impact on patients' quality of life, as well as on caregivers, society, and the environment. Positron emission tomography (PET)/computed tomography (CT) and neuropsychological scales can be used to identify AD and mild cognitive impairment (MCI) early, provide a differential diagnosis, and offer early therapies to impede the course of the illness. However, there are few reports of large-scale ^{11}C-PIB-PET/CT investigations that focus on the pathology of AD and MCI. Therefore, further research is needed to determine how neuropsychological test scales and PET/CT measurements of disease progression interact.

KEYWORDS

Alzheimer's disease, PET/CT, mild cognitive impairment, neuropsychological test scale, amyloid

1. Introduction

Diagnosis and treatment of dementia is challenging and has an impact on both social care and global health. Dementia affects more than 50 million people worldwide and according to the most recent estimates, as the population ages, this number is predicted to quadruple (GBD 2016 Dementia Collaborators, 2019). According to The World Alzheimer's Disease Report, dementia is the third most serious health issue, with enormous financial expenses, after cancer and cardiovascular disease globally (Prince et al., 2015).

Alzheimer's disease (AD) is a neurodegenerative disease that is the leading cause of dementia and accounts for 60–80% of dementia cases (Scheltens et al., 2021). The main pathological features include the formation of senile plaques by intracerebral Aβ protein deposition and intracellular neurogenic fiber tangles by tau protein hyper-phosphorylation (Carreiras et al., 2013; Hansson, 2021; Tzioras et al., 2023). It has been shown that the prevalence of AD doubles approximately every 5 years after the age of 65 years (Hane et al., 2017). According to the latest global burden of Disease study, AD remains the fifth leading cause of death worldwide (GBD 2016 Neurology Collaborators, 2019; 2022 Alzheimer's disease facts and…, 2022).

Mild cognitive impairment (MCI) is a transition stage between normal cognitive aging and dementia. Recent studies have shown that the prevalence of MCI in the global community exceeds 15% and that the prevalence of MCI increases with age (Bai et al., 2022). The conversion rate from MCI to AD is approximately 15% per year (Hojjati et al., 2018). Intervention and treatment of patients at the MCI stage can benefit patients by slowing the progression of the disease and reducing the conversion rate of AD.

The current clinical diagnosis of AD is usually based on the patient's medical history, symptoms, neuropsychological test scales, blood tests, cerebrospinal fluid tests, and imaging (Hane et al., 2017; Teunissen et al., 2022). Neuropsychological scales have been widely used in clinical settings (Espinosa et al., 2017). Moreover, with the development of computer and neuroimaging technologies, it is possible to identify AD early and noninvasively. In recent years, researchers have widely used amyloid and tau imaging using positron emission tomography (PET) for the differential diagnosis of dementia, especially for the diagnosis of AD (Jack et al., 2018). Nevertheless, there are few reports on the diagnosis of AD using ^{11}C-PIB-PET/computed tomography (CT) and the relevance of ^{11}C-PIB-PET/CT combined with neuropsychological testing scales in AD and MCI disease progression and condition assessment. Currently, there is no established cure for dementia; however, there are treatments to impede cognitive decline or reduce dementia-related behavioral and psychiatric symptoms (Sharma, 2019). The application of PET/CT and neuropsychological examinations can improve the precision of early diagnosis of dementia and give patients the opportunity to intervene early, which is clinically important to prevent the onset of dementia and delay the progression of the disease (Oddo et al., 2004). This article reviews the progress of PIB-PET/CT with commonly used neuropsychological scales in MCI and AD.

2. Diagnosis of Alzheimer's disease and mild cognitive impairment

Alzheimer's disease is a progressive neurodegenerative disease characterized by cognitive impairment and affects activities of daily living (Rowe and Villemagne, 2011). Although the pathogenesis of AD has not been clearly elucidated, the most common mechanisms suggested include Aβ protein deposition, tau protein hyper phosphorylation, and processes involving inflammatory mechanisms, oxidative stress, mitochondrial mechanisms, and cerebrovascular mechanisms (Ferrari and Sorbi, 2021). These neuropathological changes are believed to start 15–20 years before the appearance of clinical symptoms of dementia (Trejo-Lopez et al., 2022). Their transcendental pathophysiological characteristics can be detected using cerebrospinal fluid evaluation or imaging techniques (Scheltens et al., 2021). The primary clinical symptoms include decreased cognitive function, decreased brain function, progressive memory loss, and progressive loss of self-care and psychiatric symptoms as the disease worsens, causing a great burden on the family and society (Livingston et al., 2017; Lane et al., 2018). Estimations of AD prevalence suggest that biologically defined AD is three times more prevalent than clinically defined AD (Scheltens et al., 2021). Over the past 30 years, mortality rates for AD and other dementias in China have been on the rise and have increased significantly with age (Bai and Dong, 2021). Current medications for AD only temporarily alleviate memory symptoms and other cognitive changes, but do not stop or reverse AD progression (Dong et al., 2019).

MCI, which is the prodromal stage of AD, is an intermediate stage between normal cognitive aging and overt dementia, characterized by marked cognitive decline beyond normal aging, but not meeting clinical diagnostic criteria for AD, with relative maintenance of activities of daily living (Petersen, 2004). It is believed that MCI represents a significant step in the aging process and MCI may represent an early stage of dementia with a tendency to progress to clinically diagnosed dementia. Approximately, 10–15% of patients with MCI progress to AD annually (Petersen, 2000; Gauthier et al., 2011) with a lifetime prevalence of 60–90% (Anderson, 2019). Some patients then remain stable (Diniz et al., 2008). Recent studies have shown that 12.2% of people over 55 years of age in China have MCI, and the prevalence of MCI increases with age (Lu et al., 2021).

New diagnostic criteria for AD and AD-derived MCI (Albert et al., 2011; McKhann et al., 2011) include biomarkers based on neuroimaging or cerebrospinal fluid tests that can increase the sensitivity or specificity of the diagnosis (Zhang et al., 2014). The definitive diagnosis of AD can only be made by neuropathological examination, although neuropsychological and imaging examinations are still preferred methods for clinical diagnosis of AD (Tiwari et al., 2019). The Mini Mental State Examination (MMSE) and Montreal Cognitive Assessment (MoCA) scores have substantial specificity and sensitivity in clinically diagnosing AD (Nasreddine et al., 2005; Chen et al., 2016). Physicians now widely use PET/CT examinations for early diagnosis and assessment of AD. PET/CT helps to accurately identify patients with MCI who may transition to AD or other forms of dementia.

3. PET/CT in Alzheimer's disease and mild cognitive impairment

Some studies suggest that onset of AD is initiated with deposition of Aβ in the brain, followed by pathological changes in peripheral nerve cells and glial cells (Selkoe and Hardy, 2016). Aβ deposition begins before the onset of clinical symptoms, such as cognitive decline and behavioral changes (Jack et al., 2013; Zetterberg and Blennow, 2013). Identifying and quantifying amyloid deposition *in vivo* is valuable in AD research, has been used in large synergistic studies, and has value in clinical settings (Brown et al., 2019). According to the 2011 recommendations of the European and US National Aging and Alzheimer's Societies to revise the diagnostic criteria for AD (Dubois et al., 2007, 2010; McKhann et al., 2011), the detection of Aβ deposits at the MCI stage may provide a basis for the early diagnosis of AD and timely intervention.

Molecular imaging methods are based on a visual depiction of functional or pathological changes in the brain for the clinical diagnosis of neurodegenerative diseases, and recently, amyloid and tau imaging techniques using PET have been widely used for the differential diagnosis of dementia and are important for the diagnosis of AD (Jack et al., 2018), PET imaging is to measure glucose metabolism, β-amyloid plaques, and neurogenic fiber tangles in the framework of amyloid-tau-neurodegeneration (Jack et al., 2018). Using radiotracers specific to β-amyloid plaques, PET imaging provides a useful tool for quantifying β-amyloid deposition in various brain regions.

3.1. Amyloid study

There is growing evidence that amyloid-PET is a valuable support for clinicians, leading to changes in diagnosis and treatment planning based on traditional workups and increasing confidence in etiologic diagnosis. Commonly used tracers for Aβ-PET include ^{11}C-Pittsburgh compound B (PIB) and ^{18}F labeled tracers (^{18}F-Flutemetamol, ^{18}F-florbetapir and ^{18}F-forbetaben) (Villemagne et al., 2012; Landau et al., 2013). A multicenter study in 2019 involving 18,295 patients demonstrated that implementing PET scan led to higher diagnostic certainty (Rabinovici et al., 2019). In 2004, the first study was conducted. ^{11}C-PIB-PET/CT was first performed in 2004, and ^{11}C-PIB was the first PET radioactive tracer capable of *in vivo* specific quantification of brain amyloid (Klunk et al., 2004; Cohen and Klunk, 2014). It is currently the most widely used PET Aβ ligand for the early identification and diagnosis of AD. It can visualize the deposition of Aβ in the brain before the onset of clinical symptoms (Bateman et al., 2012). Several studies have confirmed the correlation between PET/CT measurements and histological evidence of deposited Aβ (Ikonomovic et al., 2008; Choi et al., 2012; Okazawa et al., 2020). Quantitative metrics such as the standardized uptake ratio (SUVR) and the distribution volume ratio (DVR) have been used to effectively differentiate healthy individuals from those with AD. Previous studies have shown that in patients with MCI and AD, ^{11}C-PIB binding in the cerebellum is negligible and that the cerebellum is a better choice as a comparison region for PET quantification. SUVR of each brain region can be obtained by dividing the standard ^{11}C-PIB uptake values in each brain region by the cerebellar uptake values (Herholz, 2003). However, the total scan and wait time for SUVR/DVR would add up to at least 1 h. Recent studies have found that the amyloid quantification index (AQI) can differentiate MCI from AD and predict the progression of MCI. AQI was calculated linearly by combining AQI_roi of the featured brain regions, and its coefficients were determined by linear regression. AQI measured the difference between PiB retention and brain tracer clearance with higher accuracy and sensitivity than SUVR and DVR (Shen et al., 2022). A combination of AQI with magnetic resonance imaging (MRI) can be used to predict the progression of MCI with higher accuracy than that with AQI alone (Patel et al., 2020). Most patients with AD's ^{11}C-PIB are positive and have an elevated cortical distribution volume ratio. Aβ imaging enables the study of the relationship between amyloid deposition and brain structure in patients with AD. Furthermore, it also aids in understanding the function of Aβ through normal aging and the changes that occur during the progression to AD. In addition, it aids in monitoring of the biological effects of anti-Aβ drugs on neurodegeneration and cognitive decline (Cohen et al., 2012). Previous studies have shown that significant differences in PIB retention are observed in regions known to contain amyloid deposits, such as the frontal and parietal cortices and the striatum (Tryputsen et al., 2015). Studies on ^{11}C-PIB PET have shown strong cortical retention in almost all patients with AD (Rabinovici et al., 2007). Furthermore, ^{11}C-PIB PET cortical preservation is associated with brain atrophy as measured using MRI (Chételat et al., 2010).

In MCI, ^{11}C-PIB positivity is an important predictor of progression to AD, and Aβ-positive individuals are more likely to progress to AD. Presence of amyloid deposists can also predict eventual progression to MCI or AD in individuals with normal cognitive function. Therefore, it aids in early detection, early diagnosis, and interventions (Jansen et al., 2015; Brown et al., 2019). To date, the pathological relevance of large-scale ^{11}C-PIB-PET/CT studies to detect MCI has been less explored. The conversion rate of MCI to AD has been reported to be between 8 and 16% per year (Mitchell and Shiri-Feshki, 2009). 50–60% of the subjects with MCI are positive for ^{11}C-PiB-PET/CT, and 10 to 15% of Aβ-positive MCI eventually convert to AD each year (Rowe and Villemagne, 2011). A longitudinal study with a 3-year follow-up showed that 70% of ^{11}C-PIB-positive patients with MCI eventually developed dementia (Okello et al., 2009). A systematic review that included 9 study cohorts with 300 patients with MCI found that the estimated sensitivity of ^{11}C-PIB-PET/CT to identify patients with MCI who convert to AD was 96% (95% CI 87 to 99%) (Zhang et al., 2014). Ciarmiello et al. (2019) found a linear relationship between increased amyloid deposition and memory dysfunction, and proposed a SUVR threshold of 1.3 to identify MCI populations at risk of progression to AD. ^{11}C-PIB uptake increases early in the progression to AD and then plateaus, with an S-shaped increase in Aβ load during the transition from normal aging to MCI and AD (Koivunen et al., 2011). Additionally, numerous studies have shown that patients with AD have significant bilateral retention of ^{11}C-PIB in the precuneus, temporal lobe, superior limbic gyrus, and cingulate gyrus, as well as in the right insula and nucleus accumbens (Cohen and Klunk, 2014; He et al., 2015; Byun et al., 2017; Wenjun et al., 2017).

Furthermore, previous studies have confirmed that ^{11}C-PIB-PET/CT has a sensitivity of 83.3–100% and a specificity of 41.1–100% to predict the transformation of MCI to AD (López-de-Eguileta et al., 2020). Therefore, ^{11}C-PIB-PET/CT is an important neuroimaging tool for the clinical diagnosis of AD, with high sensitivity. The ability to accurately quantify Aβ protein deposition at different stages of AD provides important imaging evidence for the early identification and diagnosis of AD and provides an important basis for early anti-Aβ therapy and efficacy testing. However, the short radioactive half-life has been a major limitation of ^{11}C-PiB PET, preventing its widespread use, and therefore, other ^{18}F-labeled PET tracers have been developed (Byun et al., 2017). Recent studies have shown that the three ^{18}F-labeled tracers are also highly consistent in terms of diagnostic accuracy, and have 89–97% sensitivity and 63–93% specificity in differentiating AD from MCI with similar results in visual and quantitative analysis (Landau et al., 2014; Prestia et al., 2015). A meta-analysis (Morris et al., 2016) found that the three ^{18}F labeled tracers had better diagnostic accuracy in distinguishing patients with AD from healthy individuals. Recent studies have shown that ^{18}F-flutemetamol uptake is negatively correlated with scores on neuropsychological test scales, with higher tracer uptake associated with lower scores (Heurling et al., 2016).

Previous studies have found that the sites of Aβ deposition that are significantly different between AD and MCI are the inferior frontal gyrus (left), the superior frontal gyrus (left), the parahippocampal and perirhinal gyrus (left and right), the syrinx (left and right), the postcentral gyrus (left), the cuneus (right), the nucleus accumbens (left and right) and pallidum (right) (Klunk et al., 2004; Jack et al., 2009; Koivunen et al., 2011; He et al., 2015). A recent study showed that in patients with MCI, visuospatial function is usually correlated with the degree of Aβ burden in the frontal regions, while in patients with AD, the Rey Complex Figure Test scores negatively correlated with SUVR in the frontal, temporal, parietal, occipital, anterior cingulate, posterior cingulate, and posterior cingulate gyri (Park et al.,

2020). The frontal lobe is an important brain region for situational memory extraction and is closely related to memory function in humans, and the deposition of Aβ may lead to neuronal damage in the frontal areas, further leading to impaired memory function in patients with AD (Jiménez-Bonilla et al., 2019). Roh et al. (2011) showed that the basal ganglia regulate motor neural pathways in the brain and are involved in higher cognitive functions such as emotional expression and associative memory, while the nucleus accumbens is in the basal ganglia and can be altered in the early stages of AD, leading to an overall decrease in cognitive function. In addition, a recent study has shown that the cortical nucleus is involved in higher cognitive functions, such as emotional expression and memory. Furthermore, a recent study (Park et al., 2020) found significant hemispheric asymmetries in these brain regions that correlate with neuropsychological scale scores, with a higher concentration on the left side, which can be associated with major cognitive deficits in patients. In conclusion, Aβ deposition may cause neuronal cell damage in the above brain regions, leading to cognitive impairment, but further pathological and neuroanatomical exploration of the specific disease mechanism is needed.

3.2. Synaptic vesicle glycoprotein 2A PET/CT

Synapses are critical for cognitive function, and cognitive impairment is strongly associated with loss of synaptic density, which is observed in the early stages of clinical AD, accompanied by loss several presynaptic proteins (Robinson et al., 2014). Therefore, evaluation of synaptic density is valuable in AD research and enhancing treatment efficacy. A new approach to imaging synaptic density using synaptic vesicle protein 2A (SV2A) has recently emerged, and several SV2A ligands have been developed and translated for human use. SV2A PET can directly display synaptic density in AD. ^{11}C-UCB-J is a recently developed PET tracer (Carson et al., 2022) it was demonstrated that SV2A binding was extensively reduced in the medial temporal and neocortical regions of the brain of patients with early AD (Mecca et al., 2020). Chen et al. (2021) also obtained similar results, with ^{11}C-UCB-J binding showing a similar reduction in the medial temporal lobe of patients with AD compared to healthy participants. Recent studies have found that patients with AD have higher tau deposition and lower hippocampal SV2A binding (Mecca et al., 2022). O'Dell et al. (2021) measured the volumetric ratio of the ^{11}C-UCB-J distribution and Aβ deposition in ^{11}C-PiB and observed a significant negative correlation between overall Aβ deposition and hippocampal SV2A binding in patients with MCI. Furthermore, low MMSE scores in patients with MCI are also reported to be associated with lower SV2A binding in structures such as the hippocampus, parahippocampal gyrus, and inferior and superior temporal gyri (Vanhaute et al., 2020). Studies have shown that a deposition of Aβ in the parahippocampal and peripheral gyrus of the left hippocampal is associated with impaired cognitive function, and that the parahippocampal and peripheral gyrus of the hippocampal is an important component of the medial temporal lobe, responsible for the extraction, encoding, and highly correlated with situational memory function (Burgess et al., 2002). The sinohypothalamic gyrus is a cortex associated with the encoding of visual signals and is related to working memory processing and spatial localization. Impaired working memory processing and spatial localization in AD are also correlated with Aβ protein deposition in this region of the brain. Higher uptake of ^{18}F-florbetapir is associated with a lower uptake of ^{11}C-UCB-J, and both are associated with altered synaptic function in the occipital lobe (Coomans et al., 2021). However, due to their small sample size, these studies are limited in their ability to investigate the effects of important demographic variables. Future studies with larger sample sizes and greater educational attainment may help better understand the interaction of these variables with AD.

3.3. FDG-PET

FDG-PET is used to reflect regional glucose depletion directly related to the local intensity of brain glutamatergic synaptic and astrocytic activity (Reivich et al., 1977). Regional changes in neuronal activity caused by neurodegeneration can be sensitively reflected by regional depletion of brain glucose (Drzezga et al., 2005). The decrease in brain metabolism detected with FDG-PET is a hallmark of neurodegeneration, and FDG-PET is useful for early diagnosis, as it can reveal the characteristic pattern of AD neurodegeneration in individuals with MCI who will transition to AD earlier. Normal FDG-PET can predict clinical stability over several years of follow-up (Iaccarino et al., 2019) and abnormal FDG-PET is associated with an increased risk of progressive cognitive deterioration (Caroli et al., 2015). Several studies have shown that ^{18}F-FDG PET is strongly correlated with patient symptoms and clinical severity, and it could be an ideal tool for disease staging and follow-up (Herholz, 2012). Studies have shown the added value of FDG-PET in predicting conversion to AD dementia in patients with MCI compared with conventional cerebrospinal fluid or MRI scans, especially for short-term progression (Blazhenets et al., 2020). Shaffer et al. (2013) found that combining MRI, FDG-PET and cerebrospinal fluid testing significantly improved the accuracy of predicting AD transformation compared to clinical testing alone. A recent study found that ^{18}F-FDG metabolism showed a similar degree of reduction in the medial temporal lobe of patients with AD (Chen et al., 2021). Ottoy et al. (2019) found that hypometabolism of the hippocampal volume based on NMR flattening and the posterior cingulate gyrus based on ^{18}F-FDG-PET was an accurate indicator of short-term conversion to AD dementia in patients with MCI at 80 and 83%, respectively, while the combination of neuropsychological tests (visuospatial construction skills), the hippocampal volume based on NMR flattening and ^{18}F-FDG-PET had a specificity of 96% and sensitivity was 92%. In summary, PET/CT studies combined with other neuroimaging, blood, cerebrospinal fluid, and neuropsychological tests can provide a deeper understanding of the pathogenesis and progression of AD.

4. Neuropsychological test scales in Alzheimer's disease and mild cognitive impairment

Neuropsychological tests are currently an important and cost-effective tool for diagnosing AD and MCI and differentiating subtypes of MCI (Espinosa et al., 2017). The most common neuropsychological tests used in clinical practice are the Clinical Dementia Rating (CDR),

MoCA, MMSE, Activity of Daily Living Scale (ADL) (Lim and Loo, 2018). Hughes et al. (1982) developed CDR in 1982 and Morris (1993) published a revised version in 1993. The CDR provides a simple clinical assessment tool to grade the degree of cognitive impairment and activities of daily living clinically. The test takes approximately 40 min to perform and assesses six items separately—memory, orientation, judgment and problem solving, social interaction, family life and hobbies, and independent living; the severity scale is graded as healthy, suspected dementia, mild dementia, moderate dementia, and severe dementia, with scores based on a decrease in a specific area because of impaired intelligence, and no scores based on other causes such as disability (Morris, 1993). CDR values of 0.5, 1, 2, 3 are considered suspected, mild, moderate, and severe dementia, respectively (Julayanont and DeToledo, 2022). CDR has important clinical applications in differentiating dementia from MCI. MoCA (Hoops et al., 2009) is a rating scale primarily used for rapid screening of MCI (O'Driscoll and Shaikh, 2017). The cognitive domains assessed include visual space, execution, naming, memory, attention, language, abstraction, and orientation, and the scale is more comprehensive than the MMSE. Nasreddine et al. (2005) proposed a threshold of 26-point scale in 2005. They suspected patients with scores below 25 had MCI and O'Driscoll and Shaikh (2017) adjusted the score with 1 point for individuals with 12 years of education or less to account for educational effects. The MoCa test task is more complex but more sensitive than MMSE and takes approximately 10 min to detect patients with MCI and mild AD (Nasreddine et al., 2005; Hoops et al., 2009; Horton et al., 2015).

MMSE (Nieuwenhuis-Mark, 2010) is a widely used clinical cognitive screening scale that includes items for orientation, memory, recall, naming, attention, executive and visuospatial items. It has a total score of 30, with higher scores showing better cognitive function. The MMSE is a simple 5–10-min test that assesses cognitive deficits due to lesions in the left hemisphere (Jia et al., 2021). However, the MMSE is limited by the fact that the scores are influenced by age, education, and cultural background (Anderson, 2019). At older ages (>75–80 years), MMSE scores are lower and can overestimate the severity of cognitive impairment. Furthermore, clinicians should interpret MMSE results with caution in patients with very low levels of education (for example, those who cannot read), as their total MMSE score may be lower for this reason. Despite their cognitive impairment, patients with higher education may obtain a higher MMSE score (Piersma et al., 2018). The Chinese MMSE stratifies the diagnosis of AD based on educational attainment: ≤19 points for the illiterate group, ≤22 points for the elementary school group, ≤23 points for the middle and high school groups, and ≤26 points for the higher education group, with an average of ≤23 points (Jia et al., 2021). Most studies in China and abroad set the MMSE scores of patients with MCI at 25–27, and the census scores are commonly set at 24–28 (Sachdev et al., 2015). Additionally, the MMSE is a brief screening test that only superficially assesses the cognitive domains of visuospatial and executive functions (Tombaugh and McIntyre, 1992; Nieuwenhuis-Mark, 2010). The MMSE is more appropriate than the MoCA for patients with AD with more severe functional impairment (Nasreddine et al., 2005). The MMSE memory assessment is simple and shows a high sensitivity in those with severe cognitive dysfunction compared to patients with early stage of the condition and those who show only situational memory impairment. The MoCA scale is better than the MMSE in assessing various cognitive functions and evaluating memory (Pinto et al., 2019). Several previous studies have found lower MMSE and MoCa scores in AD than in MCI, suggesting that cognitive impairment is more severe in patients with AD than in patients with MCI (McKhann et al., 2011; Lim and Loo, 2018).

Other neuropsychological scales commonly used in clinical practice include the Alzheimer's Disease Assessment Scale (ADAS-cog), the Revised Hasegawa's Dementia Scale (HDS-R), the Memory Alteration Test (M@T) (Rami et al., 2007), and Quick Screen for Mild Cognitive Impairment (Qmci) (O'Caoimh et al., 2012). In addition, we have used the Hachinski Inchemic Score (HIS); the clock drawing test (CDT), and the global deterioration scale (GDS). A variety of cognitive tests have good diagnostic precision and MMSE, MoCA, and CDR are commonly used to assess the degree of dementia in patients. The HIS is often used to distinguish vascular dementia and mixed dementia. The M@T and Qmci tests are brief tests developed for the diagnosis of MCI and have high sensitivity (Breton et al., 2019). The Hamilton Depression Scale (HAMD) and Hamilton Anxiety Scale (HAMA) were used to identifying and exclude patients with depression and anxiety, respectively. Park et al. showed that patients with early-onset AD had poor performance on the anterior and posterior finger, visual breadth, visual counts, Rey complex map tests, suggesting poorer attention and visuospatial function and specific cognitive dysfunction in patients with AD (Park et al., 2020). Each of the scales have specific strengths and limitations; Hence, using a combination of these scales can help improve the detection rate of AD and MCI, assess the efficacy of AD treatment, and guide rehabilitation. Combining neuropsychological testing scales with clinical history, symptoms, signs, imaging, and laboratory tests is essential for comprehensive and holistic clinical assessment.

5. Vignette and outlook

With the aging of the population, neurodegenerative diseases, primarily Alzheimer's disease, have become a serious health risk among older individuals and a major global health problem, affecting the quality of life of patients and imposing a heavy burden on caregivers and society. Early diagnosis and treatment can slow cognitive decline and reduce the appearance of behavioral and psychiatric symptoms associated with AD. PET/CT provides certain imaging evidence to identify MCI that may progress to AD, and in combination with neuropsychological examination, can improve the accuracy of the early diagnosis of AD and give patients the opportunity to intervene early. Few large-scale ^{11}C-PIB-PET/CT studies have been conducted to explore the pathology of AD and MCI, and researchers need to further explore the correlation between PET/CT combined with neuropsychological test scales in disease progression and assessment of AD and MCI.

Author contributions

All authors listed have made a substantial, direct, and intellectual contribution to the work and approved it for publication.

Funding

This study was supported by Jilin Provincial Science and Technology Development Program Project (20230402012GH), Jilin Provincial Engineering Laboratory of Memory and Cognitive Disorders (2020C054), and Jilin Province Science and Technology Development Plan Project (20200404076YY).

Acknowledgments

We thank all our colleagues in the institute for their assistance and propose throughout the research.

Conflict of interest

The authors declare that the research was conducted in the absence of any commercial or financial relationships that could be construed as a potential conflict of interest.

Publisher's note

All claims expressed in this article are solely those of the authors and do not necessarily represent those of their affiliated organizations, or those of the publisher, the editors and the reviewers. Any product that may be evaluated in this article, or claim that may be made by its manufacturer, is not guaranteed or endorsed by the publisher.

References

(2022). 2022 Alzheimer's disease facts and figures. *Alzheimers Dement.* 18, 700–789. doi: 10.1002/alz.12638

Albert, M. S., Dekosky, S. T., Dickson, D., Dubois, B., Feldman, H. H., Fox, N. C., et al. (2011). The diagnosis of mild cognitive impairment due to Alzheimer's disease: recommendations from the national institute on aging-Alzheimer's association workgroups on diagnostic guidelines for Alzheimer's disease. *Alzheimers Dement* 7, 270–279. doi: 10.1016/j.jalz.2011.03.008

Anderson, N. D. (2019). State of the science on mild cognitive impairment (MCI). *CNS Spectr.* 24, 78–87. doi: 10.1017/S1092852918001347

Bai, W., Chen, P., Cai, H., Zhang, Q., Su, Z., Cheung, T., et al. (2022). Worldwide prevalence of mild cognitive impairment among community dwellers aged 50 years and older: a meta-analysis and systematic review of epidemiology studies. Age. *Age Ageing* 51. doi: 10.1093/ageing/afac173

Bai, R., and Dong, W. (2021). Trends in mortality rates for Alzheimer's disease and other dementias over 30 years in China. *Am. J. Alzheimers Dis. Other Dement.* 36. doi: 10.1177/15333175211044884

Bateman, R. J., Xiong, C., Benzinger, T. L., Fagan, A. M., Goate, A., Fox, N. C., et al. (2012). Clinical and biomarker changes in dominantly inherited Alzheimer's disease. *N. Engl. J. Med.* 367, 795–804. doi: 10.1056/NEJMoa1202753

Blazhenets, G., Ma, Y., Sörensen, A., Schiller, F., Rücker, G., Eidelberg, D., et al. (2020). Predictive value of (18)F-Florbetapir and (18)F-Fdg pet for conversion from mild cognitive impairment to Alzheimer dementia. *J. Nucl. Med.* 61, 597–603. doi: 10.2967/jnumed.119.230797

Breton, A., Casey, D., and Arnaoutoglou, N. A. (2019). Cognitive tests for the detection of mild cognitive impairment (MCI), the prodromal stage of dementia: meta-analysis of diagnostic accuracy studies. *Int. J. Geriatr. Psychiatry* 34, 233–242. doi: 10.1002/gps.5016

Brown, E. E., Rashidi-Ranjbar, N., Caravaggio, F., Gerretsen, P., Pollock, B. G., Mulsant, B. H., et al. (2019). Brain amyloid pet tracer delivery is related to white matter integrity in patients with mild cognitive impairment. *J. Neuroimaging* 29, 721–729. doi: 10.1111/jon.12646

Burgess, N., Maguire, E. A., and O'keefe, J. (2002). The human hippocampus and spatial and episodic memory. *Neuron* 35, 625–641. doi: 10.1016/S0896-6273(02)00830-9

Byun, B. H., Kim, B. I., Park, S. Y., Ko, I. O., Lee, K. C., Kim, K. M., et al. (2017). Head-to-head comparison of 11c-Pib and 18f-Fc119s for Aβ imaging in healthy subjects, mild cognitive impairment patients, and Alzheimer's disease patients. *Medicine (Baltimore)* 96:E6441. doi: 10.1097/MD.0000000000006441

Caroli, A., Prestia, A., Galluzzi, S., Ferrari, C., Van Der Flier, W. M., Ossenkoppele, R., et al. (2015). Mild cognitive impairment with suspected nonamyloid pathology (snap): prediction of progression. *Neurology* 84, 508–515. doi: 10.1212/WNL.0000000000001209

Carreiras, M. C., Mendes, E., Perry, M. J., Francisco, A. P., and Marco-Contelles, J. (2013). The multifactorial nature of Alzheimer's disease for developing potential therapeutics. *Curr. Top. Med. Chem.* 13, 1745–1770. doi: 10.2174/15680266113139990135

Carson, R. E., Naganawa, M., Toyonaga, T., Koohsari, S., Yang, Y., Chen, M. K., et al. (2022). Imaging of synaptic density in neurodegenerative disorders. *J. Nucl. Med.* 63, 60s–67s. doi: 10.2967/jnumed.121.263201

Chen, M. K., Mecca, A. P., Naganawa, M., Gallezot, J. D., Toyonaga, T., Mondal, J., et al. (2021). Comparison of [(11)C]Ucb-J and [(18)F]Fdg pet in Alzheimer's disease: a tracer kinetic modeling study. *J. Cereb. Blood Flow Metab.* 41, 2395–2409. doi: 10.1177/0271678X211004312

Chen, X., Zhou, Y., Wang, R., Cao, H., Reid, S., Gao, R., et al. (2016). Potential clinical value of multiparametric pet in the prediction of Alzheimer's disease progression. *PLoS One* 11:E0154406. doi: 10.1371/journal.pone.0154406

Chételat, G., Villemagne, V. L., Bourgeat, P., Pike, K. E., Jones, G., Ames, D., et al. (2010). Relationship between atrophy and beta-amyloid deposition in Alzheimer disease. *Ann. Neurol.* 67, 317–324. doi: 10.1002/ana.21955

Choi, S. R., Schneider, J. A., Bennett, D. A., Beach, T. G., Bedell, B. J., Zehntner, S. P., et al. (2012). Amp correlation of amyloid pet ligand florbetapir F 18 binding with Aβ aggregation and neuritic plaque deposition in postmortem brain tissue. *Alzheimer Dis. Assoc. Disord.* 26, 8–16.

Ciarmiello, A., Tartaglione, A., Giovannini, E., Riondato, M., Giovacchini, G., Ferrando, O., et al. (2019). Amyloid burden identifies neuropsychological phenotypes at increased risk of progression to Alzheimer's disease in mild cognitive impairment patients. *Eur. J. Nucl. Med. Mol. Imaging* 46, 288–296. doi: 10.1007/s00259-018-4149-2

Cohen, A. D., and Klunk, W. E. (2014). Early detection of Alzheimer's disease using PiB and FDG PET. *Neurobiol. Dis.* 72, 117–122. doi: 10.1016/j.nbd.2014.05.001

Cohen, A. D., Rabinovici, G. D., Mathis, C. A., Jagust, W. J., Klunk, W. E., and Ikonomovic, M. D. (2012). Using Pittsburgh compound B for in vivo pet imaging of fibrillar amyloid-beta. *Adv. Pharmacol.* 64, 27–81. doi: 10.1016/B978-0-12-394816-8.00002-7

Coomans, E. M., Schoonhoven, D. N., Tuncel, H., Verfaillie, S. C. J., Wolters, E. E., Boellaard, R., et al. (2021). In vivo tau pathology is associated with synaptic loss and altered synaptic function. *Alzheimers Res. Ther.* 13:35. doi: 10.1186/s13195-021-00772-0

Diniz, B. S., Nunes, P. V., Yassuda, M. S., Pereira, F. S., Flaks, M. K., Viola, L. F., et al. (2008). Mild cognitive impairment: cognitive screening or neuropsychological assessment? *Braz. J. Psychiatry* 30, 316–321. doi: 10.1590/S1516-44462008000400003

Dong, Y., Li, X., Cheng, J., and Hou, L. (2019). Drug development for Alzheimer's disease: microglia induced neuroinflammation as a target? *Int. J. Mol. Sci.* 20:558. doi: 10.3390/ijms20030558

Drzezga, A., Grimmer, T., Riemenschneider, M., Lautenschlager, N., Siebner, H., Alexopoulus, P., et al. (2005). Prediction of individual clinical outcome in mci by means of genetic assessment and (18)F-FDG PET. *J. Nucl. Med.* 46, 1625–1632.

Dubois, B., Feldman, H. H., Jacova, C., Cummings, J. L., Dekosky, S. T., Barberger-Gateau, P., et al. (2010). Revising the definition of Alzheimer's disease: a new lexicon. *Lancet Neurol.* 9, 1118–1127. doi: 10.1016/S1474-4422(10)70223-4

Dubois, B., Feldman, H. H., Jacova, C., Dekosky, S. T., Barberger-Gateau, P., Cummings, J., et al. (2007). Research criteria for the diagnosis of Alzheimer's disease: revising the Nincds-Adrda criteria. *Lancet Neurol.* 6, 734–746. doi: 10.1016/S1474-4422(07)70178-3

Espinosa, A., Alegret, M., Pesini, P., Valero, S., Lafuente, A., Buendía, M., et al. (2017). Cognitive composites domain scores related to neuroimaging biomarkers within probable-amnestic mild cognitive impairment-storage subtype. *J. Alzheimers Dis.* 57, 447–459. doi: 10.3233/JAD-161223

Ferrari, C., and Sorbi, S. (2021). The complexity of Alzheimer's disease: an evolving puzzle. *Physiol. Rev.* 101, 1047–1081. doi: 10.1152/physrev.00015.2020

Gauthier, S., Patterson, C., Gordon, M., Soucy, J. P., Schubert, F., and Leuzy, A. (2011). Commentary on "recommendations from the National Institute on Aging-Alzheimer's association workgroups on diagnostic guidelines for Alzheimer's disease." a Canadian perspective. *Alzheimers Dement* 7, 330–332. doi: 10.1016/j.jalz.2011.03.006

GBD 2016 Dementia Collaborators (2019). Global, regional, and national burden of Alzheimer's disease and other dementias, 1990–2016: a systematic analysis for the Global Burden of Disease Study 2016. *Lancet Neurol.* 18, 88–106. doi: 10.1016/S1474-4422(18)30403-4

GBD 2016 Neurology Collaborators (2019). Global, regional, and national burden of neurological disorders, 1990–2016: a systematic analysis for the Global Burden of Disease Study 2016. *Lancet Neurol.* 18, 459–480. doi: 10.1016/S1474-4422(18)30499-X

Hane, F. T., Robinson, M., Lee, B. Y., Bai, O., Leonenko, Z., and Albert, M. S. (2017). Recent progress in Alzheimer's disease research, part 3: diagnosis and treatment. *J. Alzheimers Dis.* 57, 645–665. doi: 10.3233/JAD-160907

Hansson, O. (2021). Biomarkers for neurodegenerative diseases. *Nat. Med.* 27, 954–963. doi: 10.1038/s41591-021-01382-x

He, W., Liu, D., Radua, J., Li, G., Han, B., and Sun, Z. (2015). Meta-analytic comparison between PIB-PET and FDG-PET results in Alzheimer's disease and MCI. *Cell Biochem. Biophys.* 71, 17–26. doi: 10.1007/s12013-014-0138-7

Herholz, K. (2003). Pet studies In Dementia. *Ann. Nucl. Med.* 17, 79–89. doi: 10.1007/BF02988444

Herholz, K. (2012). Use of FDG PET as an imaging biomarker in clinical trials of Alzheimer's disease. *Biomark. Med* 6, 431–439. doi: 10.2217/bmm.12.51

Heurling, K., Leuzy, A., Zimmer, E. R., Lubberink, M., and Nordberg, A. (2016). Imaging B-amyloid using [(18)F]flutemetamol positron emission tomography: from dosimetry to clinical diagnosis. *Eur. J. Nucl. Med. Mol. Imaging* 43, 362–373. doi: 10.1007/s00259-015-3208-1

Hojjati, S. H., Ebrahimzadeh, A., Khazaee, A., and Babajani-Feremi, A. (2018). Predicting conversion from MCI to AD by integrating rs-fMRI and structural MRI. *Comput. Biol. Med.* 102, 30–39. doi: 10.1016/j.compbiomed.2018.09.004

Hoops, S., Nazem, S., Siderowf, A. D., Duda, J. E., Xie, S. X., Stern, M. B., et al. (2009). Validity of the MoCA and MMSE in the detection of MCI and dementia in Parkinson disease 73, 1738–1745. doi: 10.1212/WNL.0b013e3181c34b47

Horton, D. K., Hynan, L. S., Lacritz, L. H., Rossetti, H. C., Weiner, M. F., and Cullum, C. M. (2015). An abbreviated Montreal Cognitive Assessment (MOCA) for dementia screening. *Clin. Neuropsychol.* 29, 413–425. doi: 10.1080/13854046.2015.1043349

Hughes, C. P., Berg, L., Danziger, W. L., Coben, L. A., and Martin, R. L. (1982). A new clinical scale for the staging of dementia. *Br. J. Psychiatry* 140, 566–572. doi: 10.1192/bjp.140.6.566

Iaccarino, L., Sala, A., and Perani, D. (2019). Predicting long-term clinical stability in amyloid-positive subjects by FDG-PET. *Ann. Clin. Transl. Neurol.* 6, 1113–1120. doi: 10.1002/acn3.782

Ikonomovic, M. D., Klunk, W. E., Abrahamson, E. E., Mathis, C. A., Price, J. C., Tsopelas, N. D., et al. (2008). Post-mortem correlates of in vivo PiB-PET amyloid imaging in a typical case of Alzheimer's disease. *Brain* 131, 1630–1645. doi: 10.1093/brain/awn016

Jack, C. R. Jr., Bennett, D. A., Blennow, K., Carrillo, M. C., Dunn, B., Haeberlein, S. B., et al. (2018). NIA-AA research framework: toward a biological definition of Alzheimer's disease. *Alzheimers Dement.* 14, 535–562. doi: 10.1016/j.jalz.2018.02.018

Jack, C. R. Jr., Lowe, V. J., Weigand, S. D., Wiste, H. J., Senjem, M. L., Knopman, D. S., et al. (2009). Serial PIB and MRI in normal, mild cognitive impairment and Alzheimer's disease: implications for sequence of pathological events in Alzheimer's disease. *Brain* 132, 1355–1365. doi: 10.1093/brain/awp062

Jack, C. R. Jr., Wiste, H. J., Weigand, S. D., Knopman, D. S., Lowe, V., Vemuri, P., et al. (2013). Amyloid-first and neurodegeneration-first profiles characterize incident amyloid pet positivity. *Neurology* 81, 1732–1740. doi: 10.1212/01.wnl.0000435556.21319.e4

Jansen, W. J., Ossenkoppele, R., Knol, D. L., Tijms, B. M., Scheltens, P., Verhey, F. R., et al. (2015). Prevalence of cerebral amyloid pathology in persons without dementia: a meta-analysis. *JAMA* 313, 1924–1938. doi: 10.1001/jama.2015.4668

Jia, X., Wang, Z., Huang, F., Su, C., Du, W., Jiang, H., et al. (2021). A comparison of the Mini- Mental State Examination (MMSE) with the Montreal Cognitive Assessment (MoCA) for mild cognitive impairment screening in Chinese middle-aged and older population: a cross-sectional study. *BMC Psychiatry* 21:485. doi: 10.1186/s12888-021-03495-6

Jiménez-Bonilla, J. F., Quirce, R., De Arcocha-Torres, M., Martínez-Rodríguez, I., Martínez-Amador, N., Sánchez-Salmón, A., et al. (2019). A 5-year longitudinal evaluation in patients with mild cognitive impairment by 11c-PIB PET/CT: a visual analysis. *Nucl. Med. Commun.* 40, 525–531. doi: 10.1097/MNM.0000000000001004

Julayanont, P., and Detoledo, J. C. (2022). Validity of the clinical dementia rating scale sum of boxes in staging and detection of cognitive impairment in Mexican Americans. *J. Geriatr. Psychiatry Neurol.* 35, 128–134. doi: 10.1177/0891988720973755

Klunk, W. E., Engler, H., Nordberg, A., Wang, Y., Blomqvist, G., Holt, D. P., et al. (2004). Imaging brain amyloid in Alzheimer's disease with Pittsburgh compound-B. *Ann. Neurol.* 55, 306–319. doi: 10.1002/ana.20009

Koivunen, J., Scheinin, N., Virta, J. R., Aalto, S., Vahlberg, T., Någren, K., et al. (2011). Amyloid PET imaging in patients with mild cognitive impairment: a 2-year follow-up study. *Neurology* 76, 1085–1090. doi: 10.1212/WNL.0b013e318212015e

Landau, S. M., Breault, C., Joshi, A. D., Pontecorvo, M., Mathis, C. A., Jagust, W. J., et al. (2013). Amyloid-B imaging with Pittsburgh compound B and Florbetapir: comparing radiotracers and quantification methods. *J. Nucl. Med.* 54, 70–77. doi: 10.2967/jnumed.112.109009

Landau, S. M., Thomas, B. A., Thurfjell, L., Schmidt, M., Margolin, R., Mintun, M., et al. (2014). Amyloid pet imaging in Alzheimer's disease: a comparison of three radiotracers. *Eur. J. Nucl. Med. Mol. Imaging* 41, 1398–1407. doi: 10.1007/s00259-014-2753-3

Lane, C. A., Hardy, J., and Schott, J. M. (2018). Alzheimer's disease. *Eur. J. Neurol.* 25, 59–70. doi: 10.1111/ene.13439

Lim, M. Y. L., and Loo, J. H. Y. (2018). Screening an elderly hearing impaired population for mild cognitive impairment using Mini-Mental State Examination (MMSE) and Montreal Cognitive Assessment (MoCA). *Int. J. Geriatr. Psychiatry* 33, 972–979. doi: 10.1002/gps.4880

Livingston, G., Sommerlad, A., Orgeta, V., Costafreda, S. G., Huntley, J., Ames, D., et al. (2017). Dementia prevention, intervention, and care. *Lancet* 390, 2673–2734. doi: 10.1016/S0140-6736(17)31363-6

López-De-Eguileta, A., Lage, C., López-García, S., Pozueta, A., García-Martínez, M., Kazimierczak, M., et al. (2020). Evaluation of choroidal thickness in prodromal Alzheimer's disease defined by amyloid PET. *PLoS One* 15:E0239484. doi: 10.1371/journal.pone.0239484

Lu, Y., Liu, C., Yu, D., Fawkes, S., Ma, J., Zhang, M., et al. (2021). Prevalence of mild cognitive impairment in community-dwelling Chinese populations aged over 55 years: a meta-analysis and systematic review. *BMC Geriatr.* 21:10. doi: 10.1186/s12877-020-01948-3

Mckhann, G. M., Knopman, D. S., Chertkow, H., Hyman, B. T., Jack, C. R. Jr., Kawas, C. H., et al. (2011). The diagnosis of dementia due to Alzheimer's disease: recommendations from the National Institute on aging-Alzheimer's Association workgroups on diagnostic guidelines for Alzheimer's disease. *Alzheimers Dement.* 7, 263–269. doi: 10.1016/j.jalz.2011.03.005

Mecca, A. P., Chen, M. K., O'dell, R. S., Naganawa, M., Toyonaga, T., Godek, T. A., et al. (2022). Association of entorhinal cortical tau deposition and hippocampal synaptic density in older individuals with normal cognition and early Alzheimer's. *Neurobiol. Aging* 111, 44–53. doi: 10.1016/j.neurobiolaging.2021.11.004

Mecca, A. P., Chen, M. K., O'dell, R. S., Naganawa, M., Toyonaga, T., Godek, T. A., et al. (2020). In vivo measurement of widespread synaptic loss in Alzheimer's disease with Sv2A PET. *Alzheimers Dement.* 16, 974–982. doi: 10.1002/alz.12097

Mitchell, A. J., and Shiri-Feshki, M. (2009). Rate of progression of mild cognitive impairment to dementia - meta-analysis of 41 robust inception cohort studies. *Acta Psychiatr. Scand.* 119, 252–265. doi: 10.1111/j.1600-0447.2008.01326.x

Morris, J. C. (1993). The Clinical Dementia Rating (CDR): current version and scoring rules. *Neurology* 43, 2412–2414. doi: 10.1212/WNL.43.11.2412-a

Morris, E., Chalkidou, A., Hammers, A., Peacock, J., Summers, J., and Keevil, S. (2016). Diagnostic accuracy of (18)F amyloid pet tracers for the diagnosis of Alzheimer's disease: a systematic review and meta-analysis. *Eur. J. Nucl. Med. Mol. Imaging* 43, 374–385. doi: 10.1007/s00259-015-3228-x

Nasreddine, Z. S., Phillips, N. A., Bédirian, V., Charbonneau, S., Whitehead, V., Collin, I., et al. (2005). The Montreal Cognitive Assessment, MoCA: a brief screening tool for mild cognitive impairment. *J. Am. Geriatr. Soc.* 53, 695–699. doi: 10.1111/j.1532-5415.2005.53221.x

Nieuwenhuis-Mark, R. E. (2010). The death knoll for the MMSE: has it outlived its purpose? *J. Geriatr. Psychiatry Neurol.* 23, 151–157. doi: 10.1177/0891988710363714

O'caoimh, R., Gao, Y., Mcglade, C., Healy, L., Gallagher, P., Timmons, S., et al. (2012). Comparison of the quick mild cognitive impairment (Qmci) screen and the SMMSE in screening for mild cognitive impairment. *Age Age Ageing* 41, 624–629. doi: 10.1093/ageing/afs059

Oddo, S., Billings, L., Kesslak, J. P., Cribbs, D. H., and Laferla, F. M. (2004). Abeta immunotherapy leads to clearance of early, but not late, hyperphosphorylated tau aggregates via the proteasome. *Neuron* 43, 321–332. doi: 10.1016/j.neuron.2004.07.003

O'dell, R. S., Mecca, A. P., Chen, M. K., Naganawa, M., Toyonaga, T., Lu, Y., et al. (2021). Association of Aβ deposition and regional synaptic density in early Alzheimer's disease: a pet imaging study with [(11)C]Ucb-J. *Alzheimers Res. Ther.* 13:11. doi: 10.1186/s13195-020-00742-y

O'driscoll, C., and Shaikh, M. (2017). Cross-cultural applicability of the Montreal Cognitive Assessment (MoCA): a systematic review. *J. Alzheimers Dis.* 58, 789–801. doi: 10.3233/JAD-161042

Okazawa, H., Ikawa, M., Tsujikawa, T., Makino, A., Mori, T., Kiyono, Y., et al. (2020). Noninvasive measurement of [(11)C]PiB distribution volume using integrated PET/MRI. *Diagnostics* 10:993. doi: 10.3390/diagnostics10120993

Okello, A., Koivunen, J., Edison, P., Archer, H. A., Turkheimer, F. E., Någren, K., et al. (2009). Conversion of amyloid positive and negative mci to ad over 3 years: an 11c-PIB PET study. *Neurology* 73, 754–760. doi: 10.1212/WNL.0b013e3181b23564

Ottoy, J., Niemantsverdriet, E., Verhaeghe, J., De Roeck, E., Struyfs, H., Somers, C., et al. (2019). Association of short-term cognitive decline and MCI-to-AD dementia and MCI-to-AD dementia conversion with CSF, MRI, amyloid- and (18)F-FDG-PET imaging. *Neuroimage Clin.* 22:101771. doi: 10.1016/j.nicl.2019.101771

Park, S. Y., Byun, B. H., Kim, B. I., Lim, S. M., Ko, I. O., Lee, K. C., et al. (2020). The correlation of neuropsychological evaluation with 11c-PiB and 18f-Fc119s amyloid PET in mild cognitive impairment and Alzheimer disease. *Medicine* 99:E19620. doi: 10.1097/MD.0000000000019620

Patel, K. P., Wymer, D. T., Bhatia, V. K., Duara, R., and Rajadhyaksha, C. D. (2020). Multimodality imaging of dementia: clinical importance and role of integrated anatomic and molecular imaging. *Radiographics* 40, 200–222. doi: 10.1148/rg.2020190070

Petersen, R. C. (2000). Mild cognitive impairment: transition between aging and Alzheimer's disease. *Neurologia* 15, 93–101.

Petersen, R. C. (2004). Mild cognitive impairment as a diagnostic entity. *J. Intern. Med.* 256, 183–194. doi: 10.1111/j.1365-2796.2004.01388.x

Piersma, D., Fuermaier, A. B. M., De Waard, D., De Deyn, P. P., Davidse, R. J., De Groot, J., et al. (2018). The MMSE should not be the sole Indicator of fitness to drive in mild Alzheimer's dementia. *Acta Neurol. Belg.* 118, 637–642. doi: 10.1007/s13760-018-1036-3

Pinto, T. C. C., Machado, L., Bulgacov, T. M., Rodrigues-Júnior, A. L., Costa, M. L. G., Ximenes, R. C. C., et al. (2019). Is the Montreal Cognitive Assessment (MoCA) screening superior to the Mini-Mental State Examination (MMSE) in the detection of mild cognitive impairment (MCI) and Alzheimer's disease (AD) in the elderly? *Int. Psychogeriatr.* 31, 491–504. doi: 10.1017/S1041610218001370

Prestia, A., Caroli, A., Wade, S. K., Van Der Flier, W. M., Ossenkoppele, R., Van Berckel, B., et al. (2015). Prediction of ad dementia by biomarkers following the NIA-AA and IWG diagnostic criteria in MCI patients from three European memory clinics. *Alzheimers Dement.* 11, 1191–1201. doi: 10.1016/j.jalz.2014.12.001

Prince, M., Wimo, A., Guerchet, M., and Wu, Y.-T. (2015). *World Alzheimer Report 2015: the global impact of dementia: an analysis of prevalence, incidence, cost and trends*. London Alzheimer's Disease International (ADI)

Rabinovici, G. D., Furst, A. J., O'neil, J. P., Racine, C. A., Mormino, E. C., Baker, S. L., et al. (2007). 11C-PIB PET imaging in Alzheimer disease and frontotemporal lobar degeneration. *Neurology* 68, 1205–1212. doi: 10.1212/01.wnl.0000259035.98480.ed

Rabinovici, G. D., Gatsonis, C., Apgar, C., Chaudhary, K., Gareen, I., Hanna, L., et al. (2019). Association of amyloid positron emission tomography with subsequent change in clinical management among medicare beneficiaries with mild cognitive impairment or dementia. *JAMA* 321, 1286–1294. doi: 10.1001/jama.2019.2000

Rami, L., Molinuevo, J. L., Sanchez-Valle, R., Bosch, B., and Villar, A. (2007). Screening for amnestic mild cognitive impairment and early Alzheimer's disease with M@T (memory alteration test). *Int. J. Geriatr. Psychiatry* 22, 294–304. doi: 10.1002/gps.1672

Reivich, M., Kuhl, D., Wolf, A., Greenberg, J., Phelps, M., Ido, T., et al. (1977). Measurement of local cerebral glucose metabolism in man with 18f-2-Fluoro-2-Deoxy-D-Glucose. *Acta Neurol. Scand. Suppl.* 64, 190–191.

Robinson, J. L., Molina-Porcel, L., Corrada, M. M., Raible, K., Lee, E. B., Lee, V. M., et al. (2014). Perforant path synaptic loss correlates with cognitive impairment and Alzheimer's disease in the oldest-old. *Brain* 137, 2578–2587. doi: 10.1093/brain/awu190

Roh, J. H., Qiu, A., Seo, S. W., Soon, H. W., Kim, J. H., Kim, G. H., et al. (2011). Volume reduction in subcortical regions according to severity of Alzheimer's disease. *J. Neurol.* 258, 1013–1020. doi: 10.1007/s00415-010-5872-1

Rowe, C. C., and Villemagne, V. L. (2011). Brain amyloid imaging. *J. Nucl. Med.* 52, 1733–1740. doi: 10.2967/jnumed.110.076315

Sachdev, P. S., Lipnicki, D. M., Kochan, N. A., Crawford, J. D., Thalamuthu, A., Andrews, G., et al. (2015). The prevalence of mild cognitive impairment in diverse geographical and ethnocultural regions: the cosmic collaboration. *PLoS One* 10:E0142388. doi: 10.1371/journal.pone.0142388

Scheltens, P., De Strooper, B., Kivipelto, M., Holstege, H., Chételat, G., Teunissen, C. E., et al. (2021). Alzheimer's disease. *Lancet* 397, 1577–1590. doi: 10.1016/S0140-6736(20)32205-4

Selkoe, D. J., and Hardy, J. (2016). The amyloid hypothesis of Alzheimer's disease at 25 years. *EMBO Mol. Med.* 8, 595–608. doi: 10.15252/emmm.201606210

Shaffer, J. L., Petrella, J. R., Sheldon, F. C., Choudhury, K. R., Calhoun, V. D., Coleman, R. E., et al. (2013). Predicting cognitive decline in subjects at risk for Alzheimer disease by using combined cerebrospinal fluid, MR imaging, and PET biomarkers. *Radiology* 266, 583–591. doi: 10.1148/radiol.12120010

Sharma, K. (2019). Cholinesterase inhibitors as Alzheimer's therapeutics (review). *Mol. Med. Rep.* 20, 1479–1487. doi: 10.3892/mmr.2019.10374

Shen, C., Wang, Z., Chen, H., Bai, Y., Li, X., Liang, D., et al. (2022). Identifying mild Alzheimer's disease with first 30-min (11)C-PiB PET scan. *Front. Aging Neurosci.* 14:785495. doi: 10.3389/fnagi.2022.785495

Teunissen, C. E., Verberk, I. M. W., Thijssen, E. H., Vermunt, L., Hansson, O., Zetterberg, H., et al. (2022). Blood-based biomarkers for Alzheimer's disease: towards clinical implementation. *Lancet Neurol.* 21, 66–77. doi: 10.1016/S1474-4422(21)00361-6

Tiwari, S., Atluri, V., Kaushik, A., Yndart, A., and Nair, M. (2019). Alzheimer's disease: pathogenesis, diagnostics, and therapeutics. *Int. J. Nanomedicine* 14, 5541–5554. doi: 10.2147/IJN.S200490

Tombaugh, T. N., and Mcintyre, N. J. (1992). The mini-mental state examination: a comprehensive review. *J. Am. Geriatr. Soc.* 40, 922–935. doi: 10.1111/j.1532-5415.1992.tb01992.x

Trejo-Lopez, J. A., Yachnis, A. T., and Prokop, S. (2022). Neuropathology of Alzheimer's disease. *Neurotherapeutics* 19, 173–185. doi: 10.1007/s13311-021-01146-y

Tryputsen, V., Dibernardo, A., Samtani, M., Novak, G. P., Narayan, V. A., and Raghavan, N. (2015). Optimizing regions-of-interest composites for capturing treatment effects on brain amyloid in clinical trials. *J. Alzheimers Dis.* 43, 809–821. doi: 10.3233/JAD-131979

Tzioras, M., Mcgeachan, R. I., Durrant, C. S., and Spires-Jones, T. L. (2023). Synaptic degeneration in Alzheimer disease. *Nat. Rev. Neurol.* 19, 19–38. doi: 10.1038/s41582-022-00749-z

Vanhaute, H., Ceccarini, J., Michiels, L., Koole, M., Sunaert, S., Lemmens, R., et al. (2020). In vivo synaptic density loss is related to tau deposition in amnestic mild cognitive impairment. *Neurology* 95, E545–E553. doi: 10.1212/WNL.0000000000009818

Villemagne, V. L., Mulligan, R. S., Pejoska, S., Ong, K., Jones, G., O'keefe, G., et al. (2012). Comparison of 11c-PiB and 18F-florbetaben for Aβ imaging in ageing and Alzheimer's disease. *Eur. J. Nucl. Med. Mol. Imaging* 39, 983–989. doi: 10.1007/s00259-012-2088-x

Wenjun, W., Venugopalan, J., and Wang, M. D. (2017). 11c-PIB PET image analysis for Alzheimer's diagnosis using weighted voting ensembles. *Annu. Int. Conf. IEEE Eng. Med. Biol. Soc.* 2017, 3914–3917. doi: 10.1109/EMBC.2017.8037712

Zetterberg, H., and Blennow, K. (2013). Biomarker evidence for uncoupling of amyloid build-up and toxicity in Alzheimer's disease. *Alzheimers Dement.* 9, 459–462. doi: 10.1016/j.jalz.2012.07.002

Zhang, S., Smailagic, N., Hyde, C., Noel-Storr, A. H., Takwoingi, Y., Mcshane, R., et al. (2014). (11) C-PIB-PET for the early diagnosis of Alzheimer's disease dementia and other dementias in people with mild cognitive impairment (MCI). *Cochrane Database Syst. Rev.*:Cd010386. doi: 10.1002/14651858.CD010386.pub2

frontiers | Frontiers in Neuroscience

TYPE Original Research
PUBLISHED 27 July 2023
DOI 10.3389/fnins.2023.1222541

OPEN ACCESS

EDITED BY
Guang-qing Xu,
The First Affiliated Hospital of Sun Yat-sen University, China

REVIEWED BY
Lihua Sun,
Shanghai Jiao Tong University, China
Zong Zhuang,
Nanjing Drum Tower Hospital, China
Wenhua Fan,
Capital Medical University, China

*CORRESPONDENCE
Yi Sun
✉ sunyigood2021@163.com
Lixin Li
✉ lilixin2@hotmail.com

†These authors have contributed equally to this work and share first authorship

RECEIVED 14 May 2023
ACCEPTED 03 July 2023
PUBLISHED 27 July 2023

CITATION
Wang X, Hui X, Wang X, Huang B, Gan X, Liu X, Shen Z, Sun Y and Li L (2023) Utilization of clinical and radiological parameters to predict cognitive prognosis in patients with mild-to-moderate traumatic brain injury. *Front. Neurosci.* 17:1222541. doi: 10.3389/fnins.2023.1222541

Utilization of clinical and radiological parameters to predict cognitive prognosis in patients with mild-to-moderate traumatic brain injury

Xi Wang[1†], Xiaobo Hui[1,2†], Xiangyu Wang[3†], Baosheng Huang[4], Xiaokui Gan[4], Xingdong Liu[1], Zhiyan Shen[1], Yi Sun[1*] and Lixin Li[1*]

[1]Department of Neurosurgery, The First Affiliated Hospital of Nanjing Medical University, Nanjing, China, [2]Department of Neurosurgery, The Affiliated Huaian No. 1 People's Hospital of Nanjing Medical University, Huaian, Jiangsu, China, [3]Department of Rehabilitation Medicine, The Affiliated Lianyungang Oriental Hospital of Kangda College of Nanjing Medical University, Lianyungang, Jiangsu, China, [4]Department of Neurosurgery, Sir Run Run Hospital, Nanjing Medical University, Nanjing, China

Background: Cognitive impairment is a common sequela following traumatic brain injury (TBI). This study aimed to identify risk factors for cognitive impairment after 3 and 12 months of TBI and to create nomograms to predict them.

Methods: A total of 305 mild-to-moderate TBI patients admitted to the First Affiliated Hospital with Nanjing Medical University from January 2018 to January 2022 were retrospectively recruited. Risk factors for cognitive impairment after 3 and 12 months of TBI were identified by univariable and multivariable logistic regression analyses. Based on these factors, we created two nomograms to predict cognitive impairment after 3 and 12 months of TBI, the discrimination and calibration of which were validated by plotting the receiver operating characteristic (ROC) curve and calibration curve, respectively.

Results: Cognitive impairment was detected in 125/305 and 52/305 mild-to-moderate TBI patients after 3 and 12 months of injury, respectively. Age, the Glasgow Coma Scale (GCS) score, >12 years of education, hyperlipidemia, temporal lobe contusion, traumatic subarachnoid hemorrhage (tSAH), very early rehabilitation (VER), and intensive care unit (ICU) admission were independent risk factors for cognitive impairment after 3 months of mild-to-moderate TBI. Meanwhile, age, GCS score, diabetes mellitus, tSAH, and surgical treatment were independent risk factors for cognitive impairment after 12 months of mild-to-moderate TBI. Two nomograms were created based on the risk factors identified using logistic regression analyses. The areas under the curve (AUCs) of the two nomograms to predict cognitive impairment after 3 and 12 months of mild-to-moderate TBI were 0.852 (95% CI [0.810, 0.895]) and 0.817 (95% CI [0.762, 0.873]), respectively.

Conclusion: Two nomograms are created to predict cognitive impairment after 3 and 12 months of TBI. Age, GCS score, >12 years of education, hyperlipidemia, temporal lobe contusion, tSAH, VER, and ICU admission are independent risk factors for cognitive impairment after 3 months of TBI; meanwhile, age, the GCS scores, diabetes mellitus, tSAH, and surgical treatment are independent risk factors of cognitive impairment after 12 months of TBI. Two nomograms, based on both groups of factors, respectively, show strong discriminative abilities.

KEYWORDS

traumatic brain injury, cognitive impairment, predictive factor, nomogram, radiological parameters

Introduction

New cases of traumatic brain injury (TBI) are estimated to be 20 million per year, posing a heavy global burden of disease (Injury and Spinal Cord Injury, 2019). Based on the Glasgow Coma Scale (GCS) scores, TBI is classified as mild-to-moderate (GCS, 9–15 points) and severe (GCS, ≤8 points). The incidence of mild-to-moderate TBI is much higher than that of severe TBI. Despite its low mortality, mild-to-moderate TBI still causes multiple neurological deficits in survivors (Pavlovic et al., 2019).

Cognitive impairment, a common type of neurological dysfunction after mild-to-moderate TBI, markedly worsens the quality of life and the long-term neurological outcomes in survivors (McHugh et al., 2006). Cognitive impairment after mild-to-moderate TBI is usually manifested as the impairment of executive function, memory, attention, speech, and naming (Miotto et al., 2010; Panwar et al., 2019). Cognitive function can be recovered in some TBI patients within 1–3 months post-TBI, but cognitive impairment may stay for a long term in some cases (McHugh et al., 2006). A previous study has reported that 19.2% of mild TBI patients and 39.3% of moderate TBI patients still experience cognitive impairment after 3 months of injury (Othman et al., 2022). Draper and Ponsford (2008) have revealed that cognitive impairment may persist in some patients even after 10 years of TBI, the degree of which is positively correlated with the severity of the injury.

Post-TBI cognitive impairment has been well-studied. At present, therapeutic strategies mainly include medications, rehabilitation exercises, and transcranial magnetic stimulation (TMS) (Neville et al., 2015; Jenkins et al., 2019; Martinez-Molina et al., 2022). However, efficient predictive factors for identifying high-risk populations are scant, so intervention strategies are not started promptly. In the present retrospective study, we analyzed risk factors for cognitive impairment after 3 and 12 months of mild-to-moderate TBI. Based on these factors, two nomograms were created to predict cognitive impairment in mild-to-moderate TBI patients after 3 and 12 months of injury.

Methods

Subjects

Mild-to-moderate TBI patients admitted to the Neurosurgery Department, the First Affiliated Hospital with Nanjing Medical University from January 2018 to January 2022 were retrospectively recruited. The inclusion criteria were as follows: (*i*) aged over 16 years old and under 90 years old; (*ii*) an interval time <24 h from TBI to admission; (*iii*) the lowest score of GCS at admission, 3 h after admission, and 6 h after admission was ≥9; and (*iv*) computed tomography (CT) of the head performed within 6 h of admission and 48 h before discharge. The exclusion criteria were as follows: (*i*) death during hospitalization; (*ii*) severe compound injuries; (*iii*) history of mental illnesses or cognitive impairments; (*iv*) hormonal disorders during the course of disease; and (*v*) status epilepticus during the course of the disease. Written informed consent was obtained from all subjects or their guardians. This study was approved by the Ethics Committee of the First Affiliated Hospital of Nanjing Medical University (No. 2022-SR-354).

Data collection

The following data were recorded: (*i*) baseline characteristics, including sex, age, and years of education; (*ii*) medical history, including the history of hypertension, diabetes mellitus, and hyperlipidemia; (*iii*) clinical characteristics of TBI, including the GCS score and causes of injury; (*iv*) imaging features of TBI, including injury site (right, left, and both); contusions in the temporal, frontal, parietal, and occipital lobes; epidural, subdural, or traumatic subarachnoid hemorrhage (tSAH); and subdural effusion on discharge; and (*v*) treatment, including surgical treatment, ICU admission, and very early rehabilitation (VER). VER was defined as rehabilitation exercises that commenced within 3 days after admission or immediately after postoperative vital signs were stable. The GCS score was selected and recorded as the lowest score of GCS at admission, 3 h after admission, and 6 h after admission. The computed tomography (CT) examination of the TBI patient showed the presence of high-density shadow in the subarachnoid space, which was defined as tSAH. Subdural effusion was defined as effusion that appeared within 10 days of TBI with a similar uniform low-density area, width >3 mm, and CT value <20 Hu. ICU admission was defined as treatment in the intensive care unit during hospitalization regardless of the length of stay in the ICU.

Assessment of cognitive impairment

The survivors of mild-to-moderate TBI patients were followed up for 12 months after the injury. A widely used tool to detect cognitive impairment with high sensitivity and specificity, the Montreal Cognitive Assessment (MoCA), was performed at 3 and 12 months post-TBI. The MoCA score increased by 1 point when traumatic brain injury patients had <12 years of education. Ranging from 0 to 30 points, a lower MoCA score indicated a worse cognitive function (Nasreddine et al., 2005). In the present study, cognitive impairment was defined as those with a maximal MoCA score of 26 points.

Statistical analysis

Categorical variables were expressed as number of cases (*n*) and percentage (%). Continuous variables in a normal distribution were expressed as mean ± standard deviation ($x \pm SD$); otherwise, they were expressed as median (M) and interquartile boundary values (P25, P75). Variables with a *p*-value of <0.10 in the univariable logistic regression model were introduced into the multivariable logistic regression model using the backward elimination method. The odds ratio (OR) and the corresponding 95% confidence interval (95% CI) and *p*-value were calculated. Nomograms were created using an R package by incorporating variables with a *p*-value of <0.05 identified using the multivariable logistic

regression analysis. The discriminative ability of the nomogram was assessed by plotting the receiver operating characteristic (ROC) curve and calculating the C-statistics, which was equal to the area under the curve (AUC). The C-statistics ranged from 0.5 to 1.0, and a higher C-statistics indicated better discrimination of the nomogram. Internal validation of the nomogram was performed within 1,000 bootstrap resampling. A linear calibration curve indicated an acceptable goodness-of-fit of the nomogram. Statistical analysis was performed using SPSS 23.0 and packages of rms, readr, pROC, formula, and ggplot2 in R, and figures were programmatically created using R 3.6.1. A p-value of <0.05 was considered statistically significant.

Results

Clinical characteristics of subjects

A total of 365 patients with mild-to-moderate TBI were recruited. After excluding 12 deaths and 48 subjects who were lost to follow-up, 305 eligible patients were finally included in this study, including 190 with mild TBI (GCS 13–15 points) and 115 with moderate TBI (GCS 9–12 points).

After 3 months of TBI, 125 (41.0%) patients developed cognitive impairment. The incidences of cognitive impairment in mild and moderate TBI patients after 3 months of injury were 28.9% and 60.9%, respectively. Later, 52 (17.0%) TBI patients still suffered from cognitive impairment after 12 months of injury, with incidences of cognitive impairment in mild and moderate TBI patients of 8.4% and 31.3%, respectively.

Independent risk factors for cognitive impairment after 3 and 12 months of mild-to-moderate TBI

The univariable logistic regression analysis revealed that age ($P < 0.001$), GCS scores ($P < 0.001$), >12 years of education ($P < 0.001$), hyperlipidemia ($P < 0.001$), injury side ($P = 0.005$), temporal lobe contusion ($P < 0.001$), subdural hematoma ($P < 0.001$), tSAH ($P < 0.001$), surgical treatment ($P = 0.016$), subdural effusion ($P = 0.035$), and ICU admission ($P < 0.001$) were significantly correlated with cognitive impairment after 3 months of mild-to-moderate TBI (Table 1). In addition, age ($P = 0.003$), GCS score ($P < 0.001$), >12 years of education ($P = 0.047$), diabetes mellitus ($P = 0.005$), hyperlipidemia ($P = 0.004$), injury side (bilateral sides vs. right side, $P = 0.045$), temporal lobe contusion ($P = 0.001$), subdural hematoma ($P = 0.003$), tSAH ($P < 0.001$), surgical treatment ($P = 0.001$), subdural effusion ($P = 0.015$), and ICU admission ($P < 0.001$) were significantly correlated with cognitive impairment after 12 months of mild-to-moderate TBI (Table 2).

We later introduced variables with a p-value of <0.10 identified using the univariable logistic regression analysis into the multivariable logistic regression analysis. Age (OR, 1.036; 95% CI [1.012,1.059]; $P = 0.003$), GCS scores (OR, 0.807; 95% CI [0.681, 0.957]; $P = 0.014$), >12 years of education (OR, 0.223; 95% CI [0.088, 0.566]; $P = 0.002$), hyperlipidemia (OR, 3.249; 95% CI [1.520, 6.941]; $P = 0.002$), temporal lobe contusions (OR, 2.606; 95% CI [1.422, 4.776]; $P = 0.002$), tSAH (OR, 2.837; 95% CI [1.506, 5.346]; $P = 0.001$), VER (OR, 0.166; 95% CI [0.060, 0.458]; $P = 0.001$), and ICU admission (OR, 2.285; 95% CI [1.070, 4.881]; $P = 0.033$) were independent risk factors for cognitive impairment after 3 months of mild-to-moderate TBI (Table 1). In addition, age (OR, 1.035; 95% CI [1.003, 1.068]; $P = 0.031$), GCS scores (OR, 0.777; 95% CI [0.637, 0.948]; $P = 0.013$), diabetes mellitus (OR, 4.443; 95% CI [1.259, 15.681]; $P = 0.020$), tSAH (OR, 2.449; 95% CI [1.046, 5.735]; $P = 0.039$), and surgical treatment (OR, 2.473; 95% CI [1.031, 5.932]; $P = 0.042$) were independent risk factors for cognitive impairment after 12 months of mild-to-moderate TBI (Table 2).

Two nomograms to predict cognitive impairment after 3 and 12 months of mild-to-moderate TBI

Two nomograms were then created based on risk factors identified using the multivariable logistic regression analysis to predict cognitive impairment after 3 and 12 months of mild-to-moderate TBI (Figures 1, 2). The total score was the sum of the points for each covariate in the nomogram and corresponded to the predicted probability of the outcome of interest. The AUCs of the nomogram to predict cognitive impairment after 3 and 12 months of mild-to-moderate TBI were 0.852 (95% CI [0.810, 0.895]) and 0.817 (95% CI [0.762, 0.873]), respectively, suggesting a good discriminative ability of the two nomograms (Figures 3, 4). The C-statistics of a nomogram to predict cognitive impairment after 3 months of mild-to-moderate TBI was 0.834 by internal validation using bootstrapping with 1,000 iterations. The C-statistics of a nomogram to predict cognitive impairment after 12 months of mild-to-moderate TBI was 0.799 after bootstrapping. The actual and predicted probabilities of cognitive impairment on the Y-axis and X-axis were plotted, respectively. The calibration curves showed an acceptable goodness-of-fit of the nomograms (Figures 5, 6).

Discussion

Cognitive impairment is a common complication following mild-to-moderate TBI, which may last for a long term. de Boussard et al. (2005) have reported that 26% of mild TBI patients develop cognitive impairment 3 months later. Consistently, Skandsen et al. (2010) have illustrated that 43% of moderate TBI patients have cognitive impairment at 3 months post-TBI. An observational study in Malaysia has shown that 19.2% of mild TBI patients and 39.3% of moderate TBI patients presented cognitive impairment after 3 months of injury (Othman et al., 2022). In the present study, the incidences of cognitive impairment after 3 months of mild and moderate TBI were 28.9% and 60.9%, respectively. Both higher incidences, compared to those previously reported, may be attributed to the differences in age, cause of injury, and injury site. Few previous studies have focused on cognitive impairment 1 year after mild-to-moderate TBI. Schneider et al. (2022) have reported

TABLE 1 Univariable and multivariable logistic regression analyses on cognitive impairment after 3 months of mild-to-moderate TBI ($n = 305$).

	TBI patients with cognitive impairment ($n = 125$)	TBI patients without cognitive impairment ($n = 180$)	Univariate analysis		Multivariate analysis	
			OR (95% CI)	*P*-value	OR (95% CI)	*P*-value
Age (years)	57.10 ± 12.43	49.69 ± 15.97	1.036 (1.019, 1.054)	<0.001	1.036 (1.012, 1.059)	0.003*
Male sex (*n*, %)	93 (74.4%)	127 (70.6%)	1.213 (0.725, 2.028)	0.462		
GCS scores (points)	12 (10,14)	14 (12.25,15)	0.725 (0.647, 0.812)	<0.001	0.807 (0.681, 0.957)	0.014*
Causes of injury (*n*, %)						
Falling injury	53 (42.4%)	75 (41.7%)		0.401		
Traffic accident	66 (52.8%)	89 (49.4%)	1.049 (0.653, 1.686)	0.842		
Blunt injury	6 (4.8%)	16 (8.9%)	0.531 (0.195, 1.445)	0.215		
Years of education>12 (*n*, %)	13 (10.4%)	55 (30.6%)	0.264 (0.137, 0.508)	<0.001	0.223 (0.088, 0.566)	0.002*
Diabetes mellitus (*n*, %)	13 (10.4%)	10 (5.6%)	1.973 (0.836, 4.655)	0.121		
Hypertension (*n*, %)	32 (25.6%)	36 (20.0%)	1.376 (0.800, 2.369)	0.249		
Hyperlipemia (*n*, %)	39 (31.2%)	21 (11.7%)	3.434 (1.900, 6.205)	<0.001	3.249 (1.520, 6.941)	0.002*
Injury side (*n*, %)						
Right side	23 (18.4%)	61 (33.9%)		0.005		0.372
Left side	39 (31.2%)	57 (31.7%)	1.815 (0.967, 3.404)	0.063	1.738 (0.763, 3.957)	0.188
Bilateral sides	63 (50.4%)	62 (34.4%)	2.695 (1.488, 4.882)	0.001	1.628 (0.732, 3.619)	0.232
Contusions (*n*, %)						
Temporal lobe	82 (65.6%)	60 (33.3%)	3.814 (2.356, 6.175)	<0.001	2.606 (1.422, 4.776)	0.002*
Frontal lobe	67 (53.6%)	90 (50.0%)	1.155 (0.731, 1.825)	0.536		
Parietal lobe	7 (5.6%)	22 (12.2%)	0.426 (0.176, 1.031)	0.058	0.468 (0.165, 1.329)	0.154
Occipital lobe	10 (8.0%)	9 (5.0%)	1.652 (0.651, 4.192)	0.291		
Hematoma (*n*, %)						
Epidural hematoma	21 (16.8%)	47 (26.1%)	0.571 (0.322, 1.015)	0.056	0.820 (0.359, 1.872)	0.637
Subdural hematoma	69 (55.2%)	60 (33.3%)	2.464 (1.541, 3.940)	<0.001	1.226 (0.658, 2.284)	0.522
tSAH	92 (73.6%)	69 (38.3%)	4.485 (2.724, 7.383)	<0.001	2.837 (1.506, 5.346)	0.001*
Surgical treatment (*n*, %)	71 (56.8%)	77 (42.8%)	1.759 (1.109, 2.789)	0.016	1.736 (0.848, 3.553)	0.131
VER (*n*, %)	12 (9.6%)	31 (17.2%)	0.510 (0.251, 1.038)	0.063	0.166 (0.060, 0.458)	0.001*
Subdural effusion (*n*, %)	24 (19.2%)	19 (10.6%)	2.014 (1.050, 3.862)	0.035	1.198 (0.519, 2.768)	0.672
ICU admission (*n*, %)	68 (54.4%)	53 (29.4%)	2.859 (1.776, 4.602)	<0.001	2.285 (1.070, 4.881)	0.033*

TBI, traumatic brain injury; OR, odds ratio; GCS, Glasgow Coma Scale; tSAH, traumatic subarachnoid hemorrhage; VER, very early rehabilitation; ICU, intensive care unit. *$p < 0.05$.

that 10.1% of mild TBI patients have cognitive impairment even after 1 year of injury. Similarly, our data revealed that the incidence of cognitive impairment after 12 months of mild-to-moderate TBI was 17.0%, i.e., 8.4% in mild and 31.3% in moderate TBI patients.

We later created two nomograms to predict cognitive impairment in mild-to-moderate TBI patients after 3 and 12 months of TBI, based on independent risk factors identified using the multivariable logistic regression analysis. Through a retrospective analysis of the clinical data of 305 mild-to-moderate TBI patients, we found that older age, low GCS score, hyperlipidemia, temporal lobe contusion, tSAH, and ICU admission were independent risk factors for cognitive impairment after 3 months of mild-to-moderate TBI, while >12 years of education and VER were protective factors. In addition, older age, low GCS score, diabetes mellitus, tSAH, and surgical treatment were independent risk factors for cognitive impairment after 12 months of mild-to-moderate TBI.

Age, GCS score, and tSAH were all closely linked with cognitive impairment at 3 and 12 months after mild-to-moderate TBI. Leukoaraiosis and poor neuroplasticity in elderly patients can increase the risk of cognitive impairment after TBI (Nguyen et al., 2019). Both aging and TBI cause the loss of brain volume and a decline of white matter integrity, and their additive effect,

TABLE 2 Univariable and multivariable logistic regression analyses on cognitive impairment after 12 months of mild-to-moderate TBI ($n = 305$).

	TBI patients with cognitive impairment ($n = 52$)	TBI patients without cognitive impairment ($n = 253$)	Univariate analysis		Multivariate analysis	
			OR (95% CI)	*P*-value	OR (95% CI)	*P*-value
Age (years)	58.40 ± 10.74	51.56 ± 15.55	1.034 (1.011, 1.057)	0.003	1.035 (1.003, 1.068)	0.031*
Male sex (*n*, %)	41 (78.8%)	179 (70.8%)	1.541 (0.751, 3.161)	0.238		
GCS scores (points)	11 (10.13)	14 (12.15)	0.701 (0.609, 0.808)	<0.001	0.777 (0.637, 0.948)	0.013*
Causes of injury (*n*, %)						
Falling injury	21 (40.4%)	107 (42.3%)		0.848		
Traffic accident	28 (53.8%)	127 (50.2%)	1.123 (0.603, 2.091)	0.714		
Blunt injury	3 (5.8%)	19 (7.5%)	0.805 (0.218, 2.965)	0.744		
Years of education>12 (*n*, %)	6 (11.5%)	62 (24.5%)	0.402 (0.164, 0.986)	0.047	0.367 (0.117, 1.156)	0.087
Diabetes mellitus (*n*, %)	9 (17.3%)	14 (5.5%)	3.573 (1.455, 8.772)	0.005	4.443 (1.259, 15.681)	0.020*
Hypertension (*n*, %)	17 (32.7%)	51 (20.2%)	1.924 (0.999, 3.707)	0.051	0.972 (0.405, 2.331)	0.949
Hyperlipemia (*n*, %)	18 (34.6%)	42 (16.6%)	2.660 (1.374, 5.148)	0.004	2.224 (0.945, 5.230)	0.067
Injury side (*n*, %)						
Right side	9 (17.3%)	75 (29.6%)		0.129		0.824
Left side	16 (30.8%)	80 (31.6%)	1.667 (0.695, 3.999)	0.253	1.376 (0.473, 4.004)	0.558
Bilateral sides	27 (51.9%)	98 (38.7%)	2.296 (1.019, 5.172)	0.045	1.121 (0.418, 3.009)	0.820
Contusions (*n*, %)						
Temporal lobe	35 (67.3%)	107 (42.3%)	2.809 (1.495, 5.279)	0.001	1.637 (0.757, 3.540)	0.211
Frontal lobe	30 (57.7%)	127 (50.2%)	1.353 (0.740, 2.472)	0.326		
Parietal lobe	1 (1.9%)	28 (11.1%)	0.158 (0.021, 1.185)	0.073	0.172 (0.021, 1.437)	0.104
Occipital lobe	6 (11.5%)	13 (5.1%)	2.408 (0.871, 6.661)	0.090		
Hematoma (*n*, %)						
Epidural hematoma	9 (17.3%)	59 (23.3%)	0.688 (0.317, 1.494)	0.345		
Subdural hematoma	32 (61.5%)	97 (38.3%)	2.573 (1.393, 4.752)	0.003	1.222 (0.576, 2.590)	0.602
tSAH	41 (78.8%)	120 (47.4%)	4.131 (2.031, 8.401)	<0.001	2.449 (1.046, 5.735)	0.039*
Surgical treatment (*n*, %)	36 (69.2%)	112 (44.3%)	2.833 (1.495, 5.367)	0.001	2.473 (1.031, 5.932)	0.042*
VER (*n*, %)	7 (13.5%)	36 (14.2%)	0.938 (0.392, 2.240)	0.885		
Subdural effusion (*n*, %)	13 (25.0%)	30 (11.9%)	2.478 (1.189, 5.164)	0.015	1.700 (0.668, 4.327)	0.266
ICU admission (*n*, %)	34 (65.4%)	87 (34.4%)	3.604 (1.924, 6.750)	<0.001	1.891 (0.791, 4.521)	0.152

TBI, traumatic brain injury; OR, odds ratio; GCS, Glasgow Coma Scale; tSAH, traumatic subarachnoid hemorrhage; VER, very early rehabilitation; ICU, intensive care unit. *$p < 0.05$.

notably, prolongs the negative influence of cognitive impairment on elderly patients with TBI (Farbota et al., 2012; Arenth et al., 2014; Kim et al., 2021). The hippocampus is a region responsible for cognitive function, especially memory function. Biological functions of the hippocampus can be largely impaired by subarachnoid hemorrhage, the subsequent middle cerebral artery spasm can reduce blood supply, block synaptic neurotransmission, and damage plasticity (Tariq et al., 2010; Regnier-Golanov et al., 2022). Neuroinflammation and oxidative stress in hippocampal neurons secondary to subarachnoid hemorrhage also contribute to cognitive impairment (Han et al., 2014; Hu et al., 2021). In patients with aneurysmal subarachnoid hemorrhage, abnormal changes in the microstructure of the white matter result in cognitive impairment 3 months after the onset (Reijmer et al., 2018).

Cognitive outcomes vary a lot after contusion and hemorrhage in different brain regions. Martin et al. (2017) have demonstrated that the volume of frontal lobe contusion is not linked with cognitive outcomes, while a larger volume of temporal lobe contusion predicts a worse cognitive function after 6 months of injury. A close correlation is identified between the hemorrhage site and the incidence of dementia within 6 months of cerebral hemorrhage rather than delayed dementia after 6 months (Biffi et al., 2016). Our results showed that mild-to-moderate TBI patients with temporal lobe contusions had a higher risk of cognitive

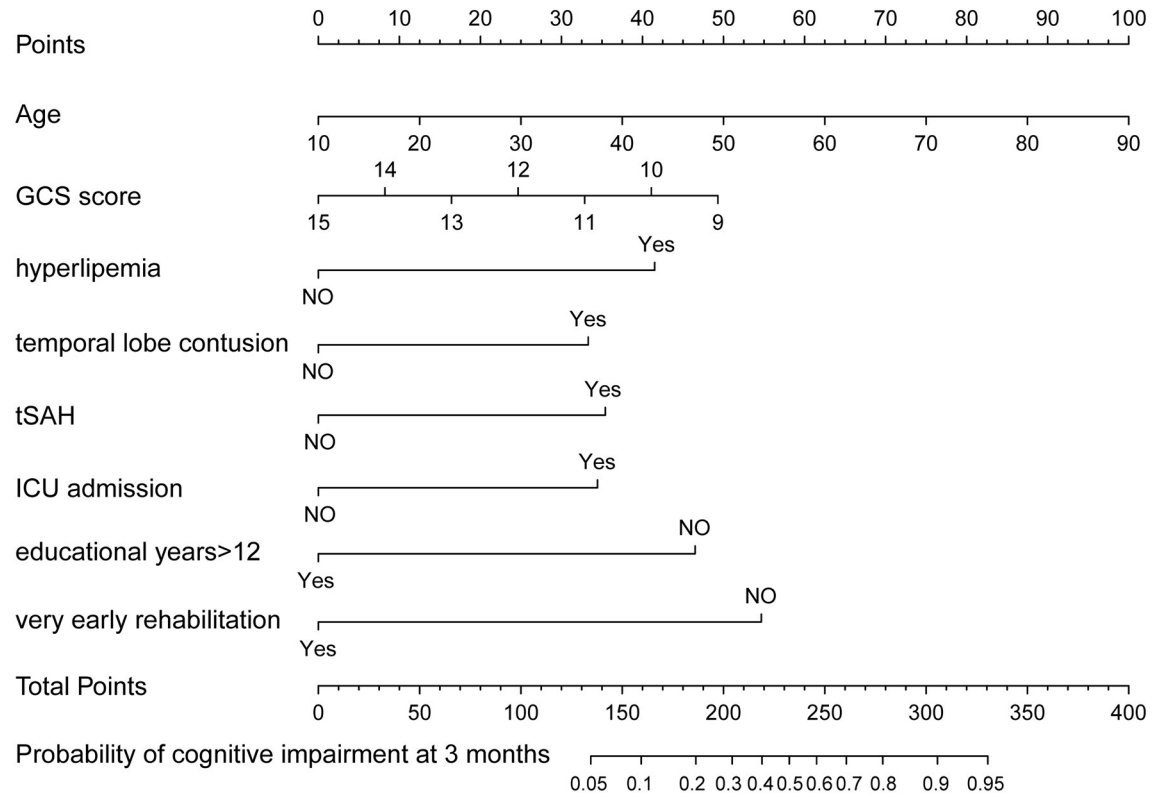

FIGURE 1
Nomogram predicting cognitive impairment at 3 months after mild-to-moderate TBI.

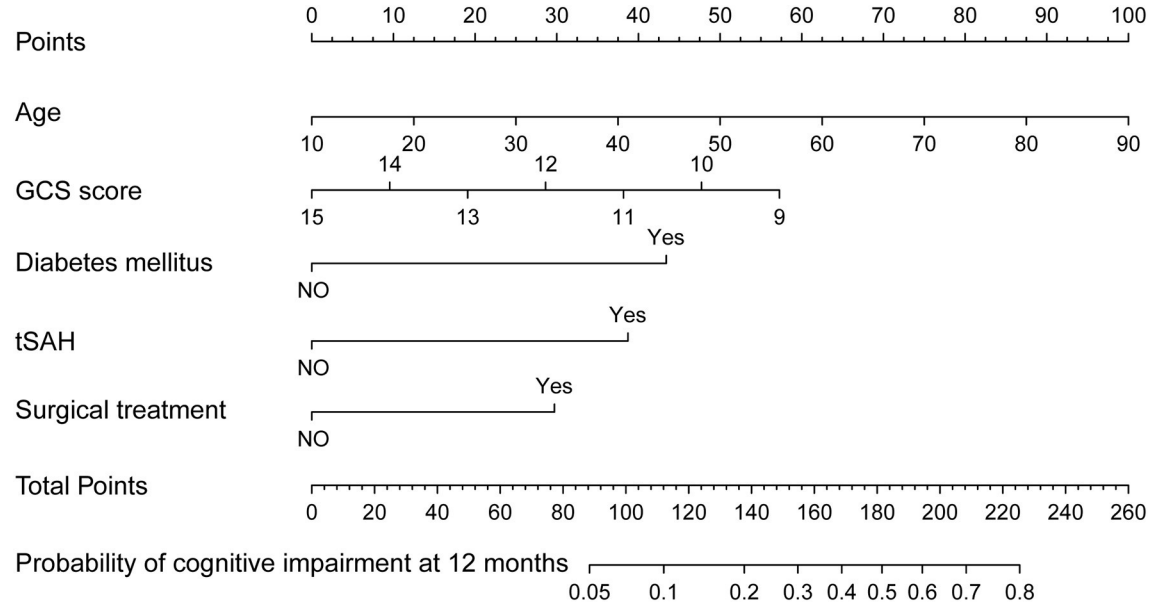

FIGURE 2
Nomogram predicting cognitive impairment at 12 months after mild-to-moderate TBI.

impairment at 3 months post-TBI, but cognitive impairment at 12 months was not significantly correlated with the site of contusion.

Hypertension, diabetes mellitus, and hyperlipidemia have not been the focus of research concerning cognitive impairment following TBI. Our data demonstrated that hyperlipidemia and

diabetes mellitus were independent risk factors of cognitive impairment 3 and 12 months after mild-to-moderate TBI, respectively. The risk of cognitive impairment in patients with diabetes mellitus is 1.5–2 times higher than that in patients without diabetes mellitus (Cukierman et al., 2005). Lachmann et al. (2018) have found that diabetes mellitus is linked with an increased risk of postoperative cognitive impairment rather than hypertension. The negative influence of diabetes mellitus on cognitive function can be attributed to hippocampal atrophy and cerebral microvascular damage (van Elderen et al., 2010; Hayashi et al., 2011; Vuletic et al., 2013). Hyperlipidemia increases the incidence of carotid intimal thickening, and meanwhile, TBI may accelerate the process of atherosclerosis (Wang et al., 2018). A synergic effect of hyperlipidemia and TBI causes carotid atherosclerosis, and the subsequent cerebrovascular insufficiency or cerebral microinfarct poses a long-term impact on cognitive function.

Mild-to-moderate TBI patients who were admitted to the ICU were more likely to have cognitive impairment 3 months after TBI than those without an ICU admission, which may be linked with ICU-acquired delirium. A much higher incidence of delirium is detected in patients admitted to the ICU, which in TBI patients, can be as high as 60% (Wilson et al., 2023). Delirium is one of the important causes of long-term cognitive decline (Goldberg et al., 2020).

We further found that >12 years of education and VER were identified as protective factors for cognitive impairment at 3 months after mild-to-moderate TBI, which, however, did not influence cognitive function at 12 months. A high level of education provides a strong cognitive reserve to cope with TBI-induced physical and psychological challenges (Almeida-Meza et al., 2022). Cognitive impairment following TBI is found to be associated with the level of apolipoprotein E ε4 (ApoE-ε4), which reduces brain metabolism in the medial temporal and prefrontal lobe of TBI patients (Hellstrøm et al., 2022). Interestingly, a high level of education is able to reverse the negative influence of ApoE-ε4 on brain metabolism (Arenaza-Urquijo et al., 2015). VER is an emerging concept of rehabilitation. Currently, clinical data supporting the role of VER in TBI are controversial. In a retrospective cohort study involving acute stroke patients in Japan, VER is validated to reduce the disability rate of stroke (Matsui et al., 2010). However, a multi-center randomized controlled trial (RCT) illustrates that VER does not significantly improve the quality of life and communication skills of stroke patients

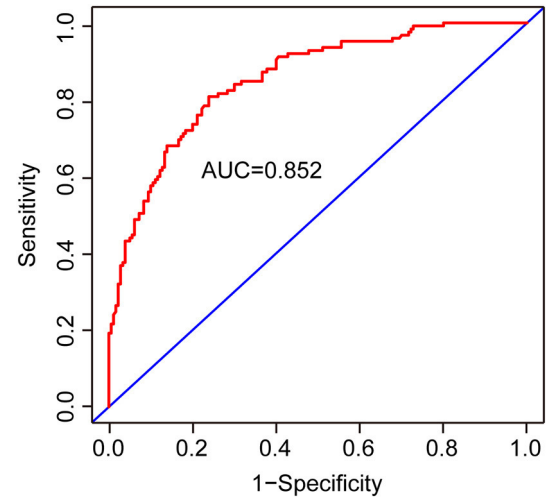

FIGURE 3
ROC curves to validate the discrimination of the nomogram predicting cognitive impairment 3 months after mild-to-moderate TBI.

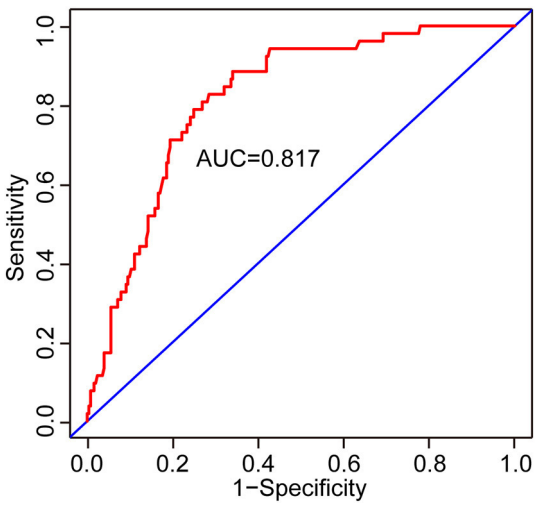

FIGURE 4
ROC curves to validate the discrimination of the nomogram predicting cognitive impairment at 12 months after mild-to-moderate TBI.

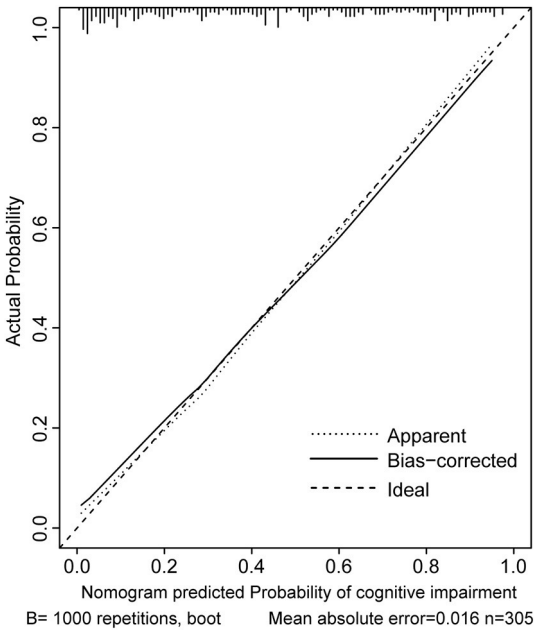

FIGURE 5
Calibration curves of the nomogram for predicting cognitive impairment at 3 months after mild-to-moderate TBI.

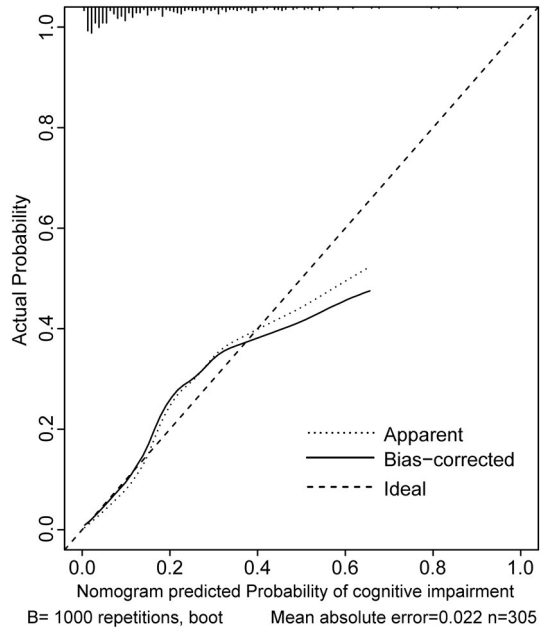

FIGURE 6
Calibration curves of the nomogram for predicting cognitive impairment at 12 months after mild-to-moderate TBI.

compared with conventional nursing care (Cumming et al., 2019; Godecke et al., 2021). In the present study, VER protected cognitive function in mild-to-moderate TBI patients possibly due to selection biases resulting from differences in comorbidities of other injuries, duration of disease stabilization, and the willingness to cooperate with rehabilitation exercises. Rigorous-designed RCTs are needed in future to analyze the clinical benefits of VER for mild-to-moderate TBI patients.

We finally created two nomograms to predict risk factors for cognitive impairment after 3 and 12 months of mild-to-moderate TBI, in which conventional demographic, clinical, and radiological data were incorporated. Both were accurate to predict cognitive impairment after TBI, thus making it possible to design an individualized and timely therapeutic strategy to prevent cognitive dysfunction. There are several limitations in the present study. First of all, we excluded TBI patients with severe combined injuries, which limited the application of the prediction models. Second, we did not retrospectively analyze electroencephalogram (EEG) data and laboratory testing data in TBI patients, which may influence the discriminative ability of the nomograms. Third, it was a single-center retrospective study that lacked external validation. Our findings should be further validated in multi-center clinical studies.

Conclusion

Age, GCS score, >12 years of education, hyperlipidemia, temporal lobe contusion, tSAH, VER, and ICU admission are independent risk factors for cognitive impairment after 3 months of TBI; meanwhile, age, the GCS scores, diabetes mellitus, tSAH, and surgical treatment are independent risk factors of cognitive impairment after 12 months of TBI. Two nomograms, based on both groups of factors, respectively, showed strong discriminative abilities for cognitive impairment, which may be used to assist clinical management of cognitive impairment following TBI.

Data availability statement

The original contributions presented in the study are included in the article/supplementary material, further inquiries can be directed to the corresponding authors.

Ethics statement

The studies involving human participants were reviewed and approved by Ethics Committee of the First Affiliated Hospital of Nanjing Medical University. The patients/participants provided their written informed consent to participate in this study.

Author contributions

XiW, XH, and XiaW conceived and designed the study. XiW, XG, XL, and YS collected the dates. BH and XH analyzed the results and wrote the manuscript. YS and LL reviewed and edited the manuscript. All authors contributed to the article and approved the submitted version.

Funding

This study was supported by grants from the Jiangsu Province Capability Improvement Project through Science, Technology and Education (grant number: ZDXK202225) and the National Natural Science Foundation of China (grant number: 81171147).

Conflict of interest

The authors declare that the research was conducted in the absence of any commercial or financial relationships that could be construed as a potential conflict of interest.

Publisher's note

References

Almeida-Meza, P., Richards, M., and Cadar, D. (2022). Moderating role of cognitive reserve markers between childhood cognition and cognitive aging: evidence from the 1946 British Birth Cohort. *Neurology* 99, e1239–e1250. doi: 10.1212/wnl.0000000000200928

Arenaza-Urquijo, E. M., Gonneaud, J., Fouquet, M., Perrotin, A., Mézenge, F., Landeau, B., et al. (2015). Interaction between years of education and APOE ε4 status on frontal and temporal metabolism. *Neurology* 85, 1392–1399. doi: 10.1212/wnl.0000000000002034

Arenth, P. M., Russell, K. C., Scanlon, J. M., Kessler, L. J., and Ricker, J. H. (2014). Corpus callosum integrity and neuropsychological performance after traumatic brain injury: a diffusion tensor imaging study. *J. Head Trauma Rehabil.* 29, E1–e10. doi: 10.1097/HTR.0b013e318289ede5

Biffi, A., Bailey, D., Anderson, C. D., Ayres, A. M., Gurol, E. M., Greenberg, S. M., et al. (2016). Risk factors associated with early vs. delayed dementia after intracerebral hemorrhage. *JAMA Neurol* 73, 969–976. doi: 10.1001/jamaneurol.2016.0955

Cukierman, T., Gerstein, H. C., and Williamson, J. D. (2005). Cognitive decline and dementia in diabetes–systematic overview of prospective observational studies. *Diabetologia* 48, 2460–2469. doi: 10.1007/s00125-005-0023-4

Cumming, T. B., Churilov, L., Collier, J., Donnan, G., Ellery, F., Dewey, H., et al. (2019). Early mobilization and quality of life after stroke: findings from AVERT. *Neurology* 93, e717–e728. doi: 10.1212/wnl.0000000000007937

de Boussard, Lundin, C. N., Karlstedt, A., Edman, D., and Bartfai, G. A., and Borg, J. (2005). S100 and cognitive impairment after mild traumatic brain injury. *J Rehabil Med* 37**,** 53-57. doi: 10.1080/16501970410015587

Draper, K., and Ponsford, J. (2008). Cognitive functioning 10 years following traumatic brain injury and rehabilitation. *Neuropsychology* 22, 618–625. doi: 10.1037/0894-4105.22.5.618

Farbota, K. D., Sodhi, A., Bendlin, B. B., McLaren, D. G., Xu, G., Rowley, H. A., et al. (2012). Longitudinal volumetric changes following traumatic brain injury: a tensor-based morphometry study. *J Int Neuropsychol Soc* 18, 1006–1018. doi: 10.1017/s1355617712000835

Godecke, E., Armstrong, E., Rai, T., Ciccone, N., Rose, M. L., Middleton, S., et al. (2021). A randomized control trial of intensive aphasia therapy after acute stroke: the very early rehabilitation for SpEech (VERSE) study. *Int. J. Stroke* 16, 556–572. doi: 10.1177/1747493020961926

Goldberg, T. E., Chen, C., Wang, Y., Jung, E., Swanson, A., Ing, C., et al. (2020). Association of delirium with long-term cognitive decline: a meta-analysis. *JAMA Neurol.* 77, 1373–1381. doi: 10.1001/jamaneurol.2020.2273

Han, S. M., Wan, H., Kudo, G., Foltz, W. D., Vines, D. C., Green, D. E., et al. (2014). Molecular alterations in the hippocampus after experimental subarachnoid hemorrhage. *J. Cereb. Blood Flow Metab.* 34, 108–117. doi: 10.1038/jcbfm.2013.170

Hayashi, K., Kurioka, S., Yamaguchi, T., Morita, M., Kanazawa, I., Takase, H., et al. (2011). (2011). Association of cognitive dysfunction with hippocampal atrophy in elderly Japanese people with type 2 diabetes. *Diabetes Res. Clin. Pract.* 94**,** 180–185. doi: 10.1016/j.diabres.07002

Hellstrøm, T., Andelic, N., Holthe, Ø., Helseth, E., Server, A., Eiklid, K., et al. (2022). APOE-ε4 is associated with reduced verbal memory performance and higher emotional, cognitive, and everyday executive function symptoms 2 months after mild traumatic brain injury. *Front. Neurol.* 13, 735206. doi: 10.3389/fneur.2022.735206

Hu, X., Yan, J., Huang, L., Araujo, C., Peng, J., Gao, L., et al. (2021). INT-777 attenuates NLRP3-ASC inflammasome-mediated neuroinflammation via TGR5/cAMP/PKA signaling pathway after subarachnoid hemorrhage in rats. *Brain Behav. Immun.* 91**,** 587-600. doi: 10.1016/j.bbi.09016

Injury, G. B. D. T. B., and Spinal Cord Injury, C. (2019). Global, regional, and national burden of traumatic brain injury and spinal cord injury, 1990-2016: a systematic analysis for the Global Burden of Disease Study 2016. *Lancet Neurol.* 18, 56–87. doi: 10.1016/S1474-4422(18)30415-0

Jenkins, P. O., Simoni, D. e., Bourke, S., Fleminger, N. J., Scott, J., Towey, G., et al. D.J., et al. (2019). Stratifying drug treatment of cognitive impairments after traumatic brain injury using neuroimaging. *Brain* 142, 2367–2379. doi: 10.1093/brain/awz149

Kim, E., Seo, H. G., Lee, H. H., Lee, S. H., Choi, S. H., Yoo, R. E., et al. (2021). Reduced brainstem volume after mild traumatic brain injury. *Am. J. Phys. Med. Rehabil.* 100, 473–482. doi: 10.1097/phm.0000000000001580

Lachmann, G., Feinkohl, I., Borchers, F., Ottens, T. H., Nathoe, H. M., Sauer, A. M., et al. (2018). Diabetes, but not hypertension and obesity, is associated with postoperative cognitive dysfunction. *Dement. Geriatr. Cogn. Disord.* 46, 193–206. doi: 10.1159/000492962

Martin, R. M., Wright, M. J., Lutkenhoff, E. S., Ellingson, B. M., Van Horn, J. D., Tubi, M., et al. (2017). Traumatic hemorrhagic brain injury: impact of location and resorption on cognitive outcome. *J. Neurosurg.* 126, 796–804. doi: 10.3171/2016.3.jns151781

Martinez-Molina, N., Siponkoski, S. T., and Sarkamo, T. (2022). Cognitive efficacy and neural mechanisms of music-based neurological rehabilitation for traumatic brain injury. *Ann. N. Y. Acad. Sci.* 1515, 20–32. doi: 10.1111/nyas.14800

Matsui, H., Hashimoto, H., Horiguchi, H., Yasunaga, H., and Matsuda, S. (2010). An exploration of the association between very early rehabilitation and outcome for the patients with acute ischaemic stroke in Japan: a nationwide retrospective cohort survey. *BMC Health Serv. Res.* 10, 213. doi: 10.1186/1472-6963-10-213

McHugh, T., and Laforce, R. Jr., Gallagher, P., Quinn, S., Diggle, P., and Buchanan, L. (2006). Natural history of the long-term cognitive, affective, and physical sequelae of mild traumatic brain injury. *Brain Cogn.* 60, 209–211.

Miotto, E. C., Cinalli, F. Z., Serrao, V. T., Benute, G. G., Lucia, M. C., Scaff, M., et al. (2010). Cognitive deficits in patients with mild to moderate traumatic brain injury. *Arq. Neuropsiquiatr.* 68, 862–868. doi: 10.1590/s0004-282x20100006000006

Nasreddine, Z. S., Phillips, N. A., Bédirian, V., Charbonneau, S., Whitehead, V., Collin, I., et al. (2005). The montreal cognitive assessment, MoCA: a brief screening tool for mild cognitive impairment. *J. Am. Geriatr. Soc.* 53, 695–699. doi: 10.1111/j.1532-5415.2005.53221.x

Neville, I. S., Hayashi, C. Y., El Hajj, S. A., Zaninotto, A. L., Sabino, J. P., Sousa, L. M., et al. Jr., et al. (2015). Repetitive transcranial magnetic stimulation (rTMS) for the cognitive rehabilitation of traumatic brain injury (TBI) victims: study protocol for a randomized controlled trial. *Trials* 16, 440. doi: 10.1186/s13063-015-0944-2

Nguyen, L., Murphy, K., and Andrews, G. (2019). Cognitive and neural plasticity in old age: a systematic review of evidence from executive functions cognitive training. *Ageing Res. Rev.* 53, 100912. doi: 10.1016/j.arr.2019.100912

Othman, A., Idris, Z., Rosman, A. K., Abdullah, J. M., Ghan, I. A., Zakaria, A. Z., et al. (2022). Cognitive impairment and neuropsychiatry manifestation following mild and moderate traumatic brain injury at 3 months and 6 months. *Malays. J. Med. Sci.* 29**,** 48–58. doi: 10.21315/mjms295.6

Panwar, N., Purohit, D., Deo Sinha, V., and Joshi, M. (2019). Evaluation of extent and pattern of neurocognitive functions in mild and moderate traumatic brain injury patients by using Montreal Cognitive Assessment (MoCA) score as a screening tool: an observational study from India. *Asian J. Psychiatr.* 41**,** 60–65. doi: 10.1016/j.ajp.08007

Pavlovic, D., Pekic, S., Stojanovic, M., and Popovic, V. (2019). Traumatic brain injury: neuropathological, neurocognitive and neurobehavioral sequelae. *Pituitary* 22, 270–282. doi: 10.1007/s11102-019-00957-9

Regnier-Golanov, A. S., Gulinello, M., Hernandez, M. S., Golanov, E. V., and Britz, G. W. (2022). Subarachnoid hemorrhage induces sub-acute and early chronic impairment in learning and memory in mice. *Transl. Stroke Res.* 13, 625–640. doi: 10.1007/s12975-022-00987-9

Reijmer, Y. D., van den Heerik, M. S., Heinen, R., Leemans, A., Hendrikse, J., Vis, d. e., et al. (2018). Microstructural white matter abnormalities and cognitive impairment after aneurysmal subarachnoid hemorrhage. *Stroke* 49, 2040–2045. doi: 10.1161/strokeaha.118.021622

Schneider, A. L. C., Huie, J. R., Boscardin, W. J., Nelson, L., Barber, J. K., Yaffe, K., et al. (2022). Cognitive outcome 1 year after mild traumatic brain injury: results from the TRACK-TBI study. *Neurology* 98, e1248–e1261. doi: 10.1212/wnl.0000000000200041

Skandsen, T., Finnanger, T. G., Andersson, S., Lydersen, S., Brunner, J. F., Vik, A., et al. (2010). (2010). Cognitive impairment 3 months after moderate and severe traumatic brain injury: a prospective follow-up study. *Arch. Phys. Med. Rehabil.* 91**,** 1904-1913. doi: 10.1016/j.apmr.0821

Tariq, A., Ai, J., Chen, G., Sabri, M., Jeon, H., Shang, X., et al. (2010). Loss of long-term potentiation in the hippocampus after experimental subarachnoid hemorrhage in rats. *Neuroscience* 165**,** 418-426. doi: 10.1016/j.neuroscience.10040

van Elderen, S. G., Roos, d. e., de Craen, A., Westendorp, A. J., Blauw, R. G., Jukema, G. J., et al. (2010). Progression of brain atrophy and cognitive decline in diabetes mellitus: a 3-year follow-up. *Neurology* 75, 997–1002. doi: 10.1212/WNL.0b013e3181f25f06

Vuletic, V., Drenjancevic, I., Rahelic, D., and Demarin, V. (2013). Effect of indomethacin on cerebrovascular reactivity in patients with type 2 diabetes mellitus. *Diabetes Res. Clin. Pract.* 101, 81–87. doi: 10.1016/j.diabres.04004

Wang, J., Su, E., Wang, H., Guo, C., Lawrence, D. A., Eitzman, D. T., et al. (2018). Traumatic brain injury leads to accelerated atherosclerosis in apolipoprotein E deficient mice. *Sci. Rep.* 8, 5639. doi: 10.1038/s41598-018-23959-2

Wilson, L. D., Maiga, A. W., Lombardo, S., Nordness, M. F., Haddad, D. N., Rakhit, S., et al. (2023). Prevalence and risk factors for intensive care unit delirium after traumatic brain injury: a retrospective cohort study. *Neurocrit. Care* 4, 1. doi: 10.1007./s12028-022-01666-1

frontiers | Frontiers in Neuroscience

TYPE Perspective
PUBLISHED 31 July 2023
DOI 10.3389/fnins.2023.1232308

OPEN ACCESS

EDITED BY
Ying Shen,
The First Affiliated Hospital of Nanjing Medical University, China

REVIEWED BY
Wen Wu,
Southern Medical University, China
Hua Yuan,
Fourth Military Medical University, China

*CORRESPONDENCE
Huijing Hu
✉ huhuijing@nwpu.edu.cn

†These authors have contributed equally to this work

RECEIVED 31 May 2023
ACCEPTED 12 July 2023
PUBLISHED 31 July 2023

CITATION
Song M, Zhang M, He S, Li L and Hu H (2023) Ultrasonic neuromodulation mediated by mechanosensitive ion channels: current and future.
Front. Neurosci. 17:1232308.
doi: 10.3389/fnins.2023.1232308

Ultrasonic neuromodulation mediated by mechanosensitive ion channels: current and future

Mengyao Song[1,2†], Mingxia Zhang[1,2†], Sixuan He[1,2], Le Li[1,2] and Huijing Hu[1,2*]

[1]Institute of Medical Research, Northwestern Polytechnical University, Xi'an, China, [2]Research and Development Institute of Northwestern Polytechnical University in Shenzhen, Shenzhen, China

Ultrasound neuromodulation technology is a promising neuromodulation approach, with the advantages of noninvasiveness, high-resolution, deep penetration and good targeting, which aid in circumventing the side effects of drugs and invasive therapeutic interventions. Ultrasound can cause mechanical effects, activate mechanosensitive ion channels and alter neuronal excitability, producing biological effects. The structural determination of mechanosensitive ion channels will greatly contribute to our understanding of the molecular mechanisms underlying mechanosensory transduction. However, the underlying biological mechanism of ultrasonic neuromodulation remains poorly understood. Hence, this review aims to provide an outline of the properties of ultrasound, the structures of specific mechanosensitive ion channels, and their role in ultrasound neuromodulation.

KEYWORDS

ultrasound, neuromodulation, Piezo ion channels, transient receptor potential channels, mechanosensitive ion channels

Introduction

Ultrasound refers to sound waves with frequencies above 20,000 Hertz (Hz), which exceeds the human hearing range of 20 Hz–20 kHz. With its high frequency and short wavelength, ultrasound has linear propagation capabilities within a finite distance, high beam focusing and excellent directionality features (Dell'Italia et al., 2022). Moreover, ultrasound is a noninvasive technique for neural regulation. It has high safety and can be employed in combination with magnetic resonance imaging. Exosomes produced by human astrocyte (HA) cells stimulated by ultrasound were comparable in terms of size distribution and morphology with those of untreated HA cells (Deng et al., 2021). Moreover, HE staining conducted after 4 weeks of ultrasound treatment showed no major organ damage, which further affirmed the safety of ultrasound therapy in human. Neuroregulatory technology, such as transcranial ultrasound stimulation, transcranial magnetic stimulation, transcranial electrical stimulation, deep brain stimulation, and optogenetics, is a kind of therapeutic approach that implements either implantable or nonimplantable devices to alleviate patients' symptoms. A comparison of these different neural regulation modes is shown in Table 1 below. It can effectively modulate the activity of the central, peripheral or autonomic nervous systems by either physical (e.g., light, sound, electricity, magnetism, etc.) or chemical (e.g., drugs) means (Jiang et al., 2019). Currently, ultrasound is frequently involved in treatment procedures as a physical factor. High-intensity ultrasound is typically recommended for tumor ablation, additionally, it has been applied to treat several

TABLE 1 Comparison of several neural regulation modes.

	Transcranial ultrasound stimulation (TUS)	Transcranial magnetic stimulation (TMS)	Transcranial electrical stimulation (TES)	Deep brain stimulation (DBS)	Optogenetics
Whether it is invasive or not	Noninvasive	Noninvasive	Noninvasive	Invasive	Invasive
Depth of action	Deep	Shallow, difficult to stimulate subcortical tissue	Shallow, difficult to stimulate subcortical tissue	Deep	The maximum stimulation depth of the two-photon optogenetic system is 400 μm.
Spatial resolution, precision	mm	>1 cm	cm	μm	Subcellular precision
The target/mode of action	Cortex (primary motor cortex (M1), somatosensory, primary visual cortex), deep brain (e.g., hippocampus, thalamus)	M1 area, SMA area, bilateral dorsolateral prefrontal cortex (DLPFC)	M1 area, DLPFC	Stereotactic implanted electrodes provide chronic electrical stimulation to specific targets in the brain	Specific neurons expressing the photosensitive protein can be induced via viral vector or transgenic means. When illuminated by different wavelengths and frequencies of light, these neurons become depolarized or hyperpolarized, leading to neuron excitation or inhibition.
Security	High and can be used in conjunction with magnetic resonance	rTMS has high safety, high frequency rTMS treatment may induce epilepsy (low probability).	Weak current do not induce action potential, will not induce seizures, high safety.	Batteries need to be replaced regularly, and there are surgical complications such as bleeding and infection.	Optical fiber implantation will still inevitably cause brain tissue damage and local bleeding to a certain extent, especially when large-diameter optical fibers are used for high-intensity light input.

neurological diseases including Parkinson's disease, essential tremor and obsessive–compulsive disorder (Sperling et al., 2018; Germann et al., 2021; Iorio-Morin et al., 2021). Low-intensity ultrasound is often used for neural regulation.

The effects of ultrasound mainly result from mechanical, cavitation and thermal effects (Darmani et al., 2022). Mechanical effects stem from ultrasound functioning as a mechanical wave, exerting radiation forces on biological tissues. Acoustic radiation force (ARF) can cause mechanical vibration and cell membrane deformation, and activate mechanosensitive ion channels in neurons, and discharge cells (Peng et al., 2020). On the other hand, thermal effects refer to biological tissue cells absorbing the energy of ultrasound, causing a subsequent temperature increase and mediating cell excitability. However, too high a temperature denatures enzymes and proteins, leading to decreased biological activity. Moreover, cavitation effects arise from the formation of small gas bubbles in tissue under positive and negative pressure phases of ultrasound oscillation stretching (Baek et al., 2017; Blackmore et al., 2019; Feng et al., 2019). Currently, it is commonly surmised that the biological impacts of ultrasound are primarily attributed to its mechanical influence rather than its thermal attributes.

Mechanosensitive (MS) ion channels refer to a group of transmembrane channel proteins that can convert mechanical stimuli signals into electrical or chemical signals. Mechanically-sensitive channels exist widely in bacterial, archaea, and eukaryotic organisms (Martinac, 2004). In bacteria and archaea, mechanosensitive channels serve as protection and survival mechanisms. Their primary function is to release intracellular substances as an emergency valve to lower osmotic pressure when the extracellular environment becomes hypotonic such as during heavy rain (Ajouz et al., 1998). The discovery of new families of mechanically activated ion channels, such as PIEZO, which have important *in vivo* physiological roles in mammals, opens new avenues for studying the role of mechanotransduction in human health and disease (Coste et al., 2010; Murthy et al., 2017; Kefauver et al., 2020). In 2016, Kubanek reported that ultrasound triggered a current via the heterologous expression of two pore domain potassium channels (K2P channels) including TREK-1, TREK-2, TRAAK and voltage-gated sodium channels (Nav1.5) in the *Xenopus* oocyte system (Kubanek et al., 2016). Heterologous expression of TRP-4 channels in *Caenorhabditis elegans* neurons revealed that their motion behavior was provoked by ultrasound. These discoveries suggest that the mechanical force generated by ultrasound could open mechanosensitive ion channels in the cell membrane and induce ion flow, which can alter neuronal excitability and eventually result in biological effects.

Despite substantial recent progress in the identification and characterization of mechanically activated ion channels, a variety of biological processes that depend on mechanotransduction remain poorly understood at the molecular level, and the identities of many mechanosensors remain elusive. Here, this article will first review the structures of several mechanosensitive ion channels and then outline the progress in their research related to ultrasound to help bolster our understanding of mechanotransduction at the molecular level.

Mechanosensitive ion channels of large conductance

Structure of mechanosensitive ion channels of large conductance

Sukharev et al. (1994) discovered two types of mechanosensitive ion channels in *E. coli*, which were named based on their pore size: the mechanosensitive channel of large conductance (MscL) and the mechanosensitive channel of small conductance (MscS). Perozo et al. (2002) demonstrated that the open state of MscL is highly dynamic, supporting a water-filled pore of at least 25 Å, lined mostly by the first transmembrane helix (TM1), allowing passage of large organic ions and small proteins. The patch-clamp electrical recording technique showed that when the patches were subjected to suction or solution bathing the patch was diluted, and voltage-controlled (−clamped) patches of *E. coli* membranes produced giant steps in unitary current (Martinac et al., 1987; Sukharev et al., 1993; Levina et al., 1999). MscS showed a single channel conductance of ~1 nS and demonstrated both pressure and voltage dependence, and selectivity for anions. While MscL with ~3 nS conductance when subjected to even stronger suction.

MscL is widely expressed in prokaryotic cells but is not present in eukaryotes. MscL has been extensively studied by scientists in recent years. Chang and colleagues indicated that the gating of MscL is primarily regulated by lipoprotein interactions (Chang et al., 1998). The composition of MscL comprises five identical subunits forming an ion channel, which is in turn regulated by membrane tension. The three-dimensional structure of the *Mycobacterium tuberculosis* MscL homolog was determined through X-ray crystallography, to a resolution of 3.5 angstroms. Each subunit consists of 136 amino acid residues, alongside two transmembrane α-helical regions (TM1 and TM2), and a loop region that links them on the extracellular side. The termini (N-terminal and C-terminal) are found on the cytoplasmic surface. The region responsible for pore formation by MscL results from TM1 of the five constituent subunits, and TM2 primarily associates with the cytoplasmic membrane lipid bilayer. MscL is a mechanically gated ion channel, featuring considerable conductance and no ion selectivity; physiologically, the protein structure resembles a cylinder. Additionally, MscL can be expressed stably in the cell membranes of eukaryotic cells.

Research on mechanosensitive ion channels of large conductance in ultrasonic neural modulation

The MscL channel is expressed in prokaryotes and its function in these cells has been extensively researched. However, the application and study of MscL in eukaryotes is just emerging. MscL channels can be expressed in eukaryotic cell lines including CHO and HEK293 cells (Doerner et al., 2012). Through electrophysiological experiments and dye release experiments, the authors demonstrated the mechanosensitive function of the MscL channels. Ye et al. (2018) also confirmed the channel activity of MscL in HEK293T cells and neurons through electrophysiological experiments. However, MscL channels expressed in eukaryotic systems have a lower opening threshold and smaller conductance than those in prokaryotes. Therefore, the authors expressed the functional mutant I92L MscL in neurons. Fluorescent localization and electrophysiological experiments proved that MscL I92L can be expressed and inserted into the neuronal membrane and has channel activity. Furthermore, MscL I92L demonstrated greater sensitivity to mechanical stimulation than the wild-type MscL channel. This is exemplified by only 30 mmHg of force leading to significant channel opening.

Piezo ion channels

Structure of Piezo ion channels

Piezo ion channels refer to a group of channels discovered and named by Coste et al. (2010). Piezo1 (Fam38A) was identified as the ion channel essential for generating mechanosensitive potentials in the Neuro2A cell line through expression profile and RNA interference knockdown of candidate genes techniques. Only two types of Piezo families have been discovered so far, Piezo1 (Fam38A) and Piezo2 (Fam38B). Piezo1 is a nonselective cationic channel that can be inhibited by GsMTx4 (tarantula venom), gadolinium (Gd), and ruthenium red (RR) (Copp et al., 2016). Piezo2, a mammalian cognate of Piezo1, records mechanically sensitive electrical currents in separated dorsal root ganglion (DRG)neurons. Piezo1 channels mainly exist in nonsensory tissues, including the skin, lungs, kidneys, and bladder. On the other hand, Piezo2 channels occur mainly in sensory tissues such as the trigeminal ganglion (TG), DRG sensory neurons, and Merkel cells.

Each subunit of Piezo proteins is made up of over 2000 amino acid residues, and their molecules are relatively large, having a molecular mass of $1.2 \times 10^{\wedge 6}$. Ge et al. determined that the full-length of the cryo-electron microscopy structure is 2,547 amino acids, with a resolution of 4.8 Å in mouse Piezo1 (Ge et al., 2015). The findings reveal that Piezo1 consists of a triple helix structure, with extracellular domains comprising three distal blades and a central cap. There are 14 apparently resolved segments per subunit in the transmembrane region that form three peripheral wings and a central pore module that encloses a potential ion-conducting pore. The carboxyl terminal is responsible for the pore section of the ion channel, while the amino terminal receives mechanical stimulation that opens the carboxyl terminal pore.

Research on Piezo ion channels in ultrasonic neural regulation

Piezo1 activation plays an essential role in mechanical transmission via ultrasonic stimulation. Qiu et al. (2019) conducted a study that revealed that the activation of heterologously expressed HEK293T cells and endogenous Piezo1 channels can be achieved through low-intensity and low-frequency ultrasound stimulation. This resulted in Ca^{2+} influx as well as increased nuclear c-Fos expression levels in primary neurons, although when pre-treated with a Piezo1 inhibitor the effect was inhibited in cells. Furthermore, the study demonstrated that ultrasonic stimulation significantly affected downstream Ca^{2+} signaling protein levels and induced the expression of important proteins such as phospho-CaMKII, phospho-CREB, and c-Fos in a neuronal cell line. These proteins are known to play significant roles in complex neuronal functions like learning, memory, and neuronal plasticity. Notably, the impact of ultrasonic stimulation on Ca^{2+} signaling protein levels was found to decrease with the loss of Piezo1 channel functions. In 2023, the authors also reported that Piezo1 knockout (P1KO) in the right motor cortex of mice significantly decreased ultrasound-induced neuronal calcium responses, limb movement, muscle electromyogram (EMG) signaling and C-Fos expression compared to the control. Central amygdala (CEA) neurons, having higher Piezo1 expression levels, displayed greater sensitivity to ultrasound than cortical neurons. Piezo1 is expressed in both neurons and astrocytes. The authors demonstrated that Piezo1 is expressed in different brain regions and that neuronal Piezo1 plays an important role in mediating ultrasound effects directly (Shen et al., 2021). The researchers also developed a Piezo1-targeted microbubble (PTMB) which can bind to the extracellular domains of the Piezo1 channel (Zhu et al., 2023).

Transient receptor potential channels

Structure of transient receptor potential

The discovery of the transient receptor potential (TRP) channel initially occurred within the visual system of *Drosophila melanogaster*, and was based upon the peculiar behavior of mutant Drosophila in response to sustained light exposure. This resulted in the production of transient potentials as opposed to sustained peak potentials. TRP channels have been found to be highly conserved genes across a broad spectrum of species, ranging from *Caenorhabditis elegans* to humans. They exhibit prominent distribution within sensory neurons and play crucial roles in the modulation of external mechanical stimuli, including pressure and sound waves. Additionally, these channels are implicated in the generation of senses associated with touch, pain, hearing, taste, and vision (Voolstra et al., 2010).

TRP channels are nonselective cationic channels that are highly permeable to Ca^{2+} and Na^{+}, with TRPM6 and TRPM7 being highly permeable to Mg^{2+}. Nilius and Owsianik (2011) classified TRP ion channels into seven subtypes and two categories based on amino acid sequences and three-dimensional structures. The first category includes TRPC (TRP-canonical), TRPV (TRP-vanilloid), TRPM (TRP-melastatin), TRPA (TRP-ankyrin) and TRPN (TRPNompC), whereas the second category includes TRPP (TRP-polycystin) and TRPML (TRP-mucolipin). The TRP channel family consists of nonselective cationic channels that are made up of four tetramer monomers. These monomers contain a hexaxial transmembrane (TM) domain with a pore ring structure located between TM5 and TM6.

Research on transient receptor potential channels in ultrasonic neural regulation

TRP-4 channels are primarily expressed in four CEPs including CEPDL, CEPDR, CEPVL and CEPVR dopaminergic neurons and in two ADEs consisting of ADEL and ADER dopaminergic neurons, and DVA and DVC interneurons in a few *C. elegans* neurons. Ibsen et al. (2015) conducted a study in which they observed the effect of defective TRP-4 mutation in nematodes with respect to their response to ultrasound-combined microbubbles. The mutant nematodes exhibited a reduction in large reversal responses compared to the wild type. Subsequently, researchers transferred the TRP-4 gene to amphid wing 'C' (AWC) neurons leading to its induction. This activation of TRP-4 gene expression in AWC neurons was found to result in the accumulation of calcium ions under specific peak negative pressures (0.41 and 0.47 MPa) of ultrasonic stimulation. This response was not observed in the wild-type AWC cells. Additionally, the decrease in contrarian motor behavior in *C. elegans* mutants with TRP-4 indicated that the induction of TRP-4 by ultrasonic stimulation (peak negative pressure < 0.5 MPa) might regulate the activity of neurons involved in reverse motor behavior, thereby leading to a reduction in reverse movement.

Two-pore-domain potassium channels

Structure of two-pore-domain potassium channels

The identification of the K2P channel first occurred in the human kidney, as its characteristic two pore regions prompted its labeling as a two-pore-domain potassium (K2P) channel. This particular form of channel is capable of activation along the entire range of physiological voltages, elucidating both the background potassium current and the baseline potassium current, and is not vulnerable to typical potassium channel blockers (Lesage et al., 1996).

Potassium channels are a diverse group of proteins that play a crucial role in regulating cellular activity and maintaining cellular homeostasis. These channels can be classified into three main types based on their structure and function: calcium-activated (KCa) potassium channels, two-pore-domain potassium channels (K2P) and inward-rectified potassium channels (Kir). Among these, K2P channels have gained particular attention in recent years due to their unique structure and function. Currently, K2P channels are categorized into six subgroups or "clades" each with distinct structural and functional characteristics. These six clades are: TWIK, TASK, TREK, TALK, THIK, and TRESK. Notably, only the TREK subgroup of K2P channels is known to be mechanically sensitive. Thus, understanding the distinct properties of each K2P channel subtype is critical for gaining insight into their role in physiological and pathological processes (Feliciangeli et al., 2015). Kv, KCa, and Kir are tetrameric channels, with each monomer having a single pore domain. However, K2P is a dimeric channel, and each monomer is composed of two pore regions. These channels consist of two pore domains (P1 and P2), two extracellular cap helices (C1 and C2), and four transmembrane domains (M1–M4) with both the amino and carboxyl terminus situated on the cytoplasmic side (Renigunta et al., 2015). K2P channels which are equipped with the capacity to perceive mechanical stimulation at the cellular membrane are classified as mechanically sensitive channels, namely TREK-1, TREK-2, and TRAAK. The high-resolution crystal structures of TWIK-1, TRAAK, and TREK-2 channels have been made available. These structures divulge the existence of multiple helices within the extracellular ring between TM1 and the P1, resulting in the formation of a physical obstruction that urges ions to exit via the side pore.

Research on two-pore-domain potassium channels in ultrasonic neuromodulation

Sorum et al. (2021) proposed that ultrasound has the potential to trigger the opening of mechanosensitive TRAAK channels through an increase in membrane tension. This study provides insight into the vital role of mechanosensitive channels in physiological responses to ultrasound and presents a promising avenue for gene targeting in the regulation of cellular auditory nerves. The authors observed that the application of short-pulsed, low-intensity ultrasound (10 ms, 5 MHz, 1.2 W/cm^2) led to a swift and robust activation of TRAAK channels in plaques of *Xenopus oocytes* expressing TRAAK as well as in cortical neurons of mice also expressing TRAAK. The K^{+} selective ultrasonic stimulation current featured a reversal potential that was proximal to the Nernst equilibrium potential for K+ ($EK^{+} = -59$ mV), comparable to the TRAAK currents for both base and pressure stimulation. In contrast, the study revealed that the non-mechanosensitive K2P ion channel TASK2 was not activated by ultrasound.

In addition to its role in neuromodulation, ultrasound also has various applications, such as reducing fracture healing time (especially in delayed healing and bone nonunion), preventing inflammatory loosening of prosthetics, and promoting tendon, ligament, and cartilage recovery. Furthermore, it can inhibit lipopolysaccharide-induced inflammation and reduce proinflammatory factors (Chan et al., 2010; Jeremias Júnior et al., 2011; Loyola-Sánchez et al., 2012; Ren et al., 2013; Zhao X et al., 2017;

TABLE 2 Studies on several mechanosensitive ion channels in ultrasonic neuromodulation.

Types of mechanosensitive ion channels	Author	Subject or site of ultrasonic stimulation	Main results	References
MscL	Ye et al.	Primary cultured rat hippocampal neurons and functional gain mutation I92L and HEK293T cells	MscL was expressed in primary cultured rat hippocampal neurons and demonstrated to be activated by low pressure ultrasonic pulses. I92L countersensitizes the MscL to ultrasound, triggering action potentials at a peak negative pressure as low as 0.25 MPa.	Ye et al. (2018)
	Qiu et al.	Neurons in the cerebral cortex or dorsomedial striatum of mice	Ultrasound triggered Ca^{2+} influx in 293T cells expressing MscL-G22S and activation of downstream neurons. Non-invasive ultrasound triggered neural activation in MscL-G22S expression regions, and c-Fos was significantly upregulated without widespread nonspecific activation. Rapid electromyographic response induced by ultrasound targeting MscL in M1 region of cortex; Ultrasound successfully activated MscL-expressing neurons in the deep DMS region.	Qiu et al. (2020)
	Heureaux et al.	Wild-type MscL and G22S mutant activated, retinal pigment epithelial cells (RPE)	Ultrasonic-driven integrin-bound microbubbles can cause MscL opening. The activation of MscL induced by acoustic tweezing cytometry (ATC) depends on the functional connection of microbubbles with the intact actin cytoskeleton.	Heureaux et al. (2014)
Piezo	Pan et al.	HEK293T cells, Jurkat T-cells and primary T cell (peripheral Blood mononuclear Cells, PBMCs)	Successful expression of the ion channel Piezo1 in HEK293T cells and subsequent Ca^{2+} influx triggered the downstream pathway for gene expression. The Piezo1 gene was transferred into Jurkat T cell lines and PBMCs to create chimeric antigen receptors, transactivated to open channels and stimulate ultrasound response. ReCoM is effective in controlling CAR expression in T cells to guide the recognition and eradication of tumor cells for controllable cancer immunotherapy.	Pan et al. (2018)
	Qiu et al.	HEK293T cells, mouse primary cortical neurons, mouse hippocampal cell line mHippoE-18 (CLU199), HeLa cells	The ultrasound alone activated both heterologous and endogenous Piezo1, initiating calcium influx and increased the expression of nuclear c-Fos in primary neurons, but not when pre-treated with Piezo1 inhibitor GsMTx-4. Ultrasound significantly augmented the expression of critical proteins including phospho-CaMKII, phospho-CREB, and c-Fos in neuronal cell lines. However, the downregulation of Piezo1 notably decreased this effect.	Qiu et al. (2019)
	Shen et al.	Neuro2A cell lines, rat hippocampal neurons	US energy can reach comparable levels of cytoplasmic Ca^{2+} transients at a peak negative pressure of 0.03 MPa in Piezo1-targeted microbubble (PTMB)-binding cells, whereas control cells typically require US intensity of 0.17 MPa. The cytoplasmic Ca^{2+} elevation was greatly reduced by chelating extracellular calcium ions or by using cationic ion channel inhibitors such as GsMTx-4, confirming that US-mediated calcium influx are dependent on the Piezo1 channels. Cavitation and heating effects of US hardly participate in the process of Ca^{2+} transients.	Shen et al. (2021)
	Zhu et al.	Conditional knockout mouse model, central amygdala (CEA) neurons, cortical neurons	Piezo1 knockout (P1KO) in the right motor cortex of mice significantly decreased ultrasound-induced neuronal calcium responses, limb movement, muscle electromyogram (EMG) signalings and C-Fos expression compared to the control. CEA neurons, having higher Piezo1 expression levels, displayed greater sensitivity to ultrasound than cortical neurons. Piezo1 expressed in both neurons and astrocytes. They demonstrated that Piezo1 expressed in different brain regions and neuronal Piezo1 played an important role in mediating ultrasound's effects directly.	Zhu et al. (2023)
	Zhang et al.	MC3T3-E1 cells	Piezo1 can transmit LIPUS-induced mechanical signals to intracellular calcium. Ca^{2+} influx acts as a second messenger to activate ERK1/2 phosphorylation and perinuclear F-actin filament polymerization, regulating MC3T3-E1 cells proliferation.	Zhang et al. (2021)

10.3389/fnins.2023.1232308

TABLE 2 (Continued)

Types of mechanosensitive ion channels	Author	Subject or site of ultrasonic stimulation	Main results	References
TRP	Ibsen et al.	*Caenorhabditis elegans*	Low-pressure ultrasound (with peak negative pressures of 0.4–0.6 MPa) specifically activated neurons expressing the TRP-4 channel. Misexpressing TRP-4 in ASH and AWC sensory neurons resulted in an increase in large reversals, while misexpressing it in PVD neurons suppressed this behavior, a novel role for this neuron.	Ibsen et al. (2015)
	Magaram et al.	*Caenorhabditis elegans*	Ultrasonic stimulation induced a reversal response in *C. elegans* by the pore-forming TRP-4 subunit and the DEG/ENaC/ASIC ion channel MEC-4. Under lower pressure (0.79 MPa), the expression of TRP-4 in AWC chemosensory neurons partially rescued the reversal of TRP-4 (ok1605) and Mec-4 (u253) mutants, in contrast to ASH, which only reversed at a higher pressure (>0.92 MPa).	Magaram et al. (2022)
	Oh et al.	Astrocyte, HEK293T, and HEK293T-piezo1 knockout (HEK-P1KO) cells	Low intensity low-frequency ultrasound (LILFU) induced neuromodulation by opening TRPA1 channels in astrocytes. The influx of Ca^{2+} caused a release of glial transmitters, including glutamate via Best1 channels. The released glutamate activated NMDA receptors in neighboring neurons and triggered action potential generation.	Oh et al. (2019)
	Duque et al.	C57BL/6J mice, Npr3-cre mice, Npr3-cre mice, Bl/6 male mice, Balb/c mice, TRPA1 knockout mice	Human transient receptor potential A1 (hs TRPA1) is ultrasonically sensitive to mammalian HEK cells and rodent neurons *in vitro* and *in vivo*. Ultrasound evoked gating of hsTRPA1 specifically requires its N-terminal tip region and cholesterol interactions. hs TRPA1 enhanced ultrasound-induced calcium transients and activated ultrasound-induced action potentials in primary neurons in rodents. Unilateral expression of hsTRPA1 in mouse layer V motor cortical neurons leads to c-fos expression and contralateral limb responses in response to ultrasound delivered through an intact skull.	Duque et al. (2022)
	Yoo et al.	Primary cortical neurons	Ultrasound stimulation triggers calcium entry across the plasma membrane. TRPP1/2, TRPC1, and Piezo1 as mechanosensitive ion channels involved the ultrasound response. Overexpression of TRPC1, TRPP2, and TRPM4 increased the sensitivity of cortical neurons to ultrasound with reduced pulse intensities and durations, in the case of TRPM4 greatly accelerated the response kinetics.	Yoo et al. (2022)
	Burks et al.	Female C3H, SV129 or TRPC1tm1Lbi/Mmjax (TRPC1 knockout) mice, C2C12 muscle cells or TCMK1 kidney cells	Inhibiting VGCC or TRPC1 *in vivo* prevented COX2 upregulation and the migration of MSCs to kidneys and muscle in response to PfUS. A TRPC1/VGCC complex was observed in plasma membranes. The inhibition of VGCC or TRPC1 blocked pFUS-induced Ca^{2+} transients in TCMK1 and C2C12 cells. The mechanical activation of the Na^{+} TRPC1 current upstream of VGCC was found to be caused by the pFUS acoustic radiation force, instead of direct opening VGCC.	Burks et al. (2019)

(Continued)

10.3389/fnins.2023.1232308

TABLE 2 (Continued)

Types of mechanosensitive ion channels	Author	Subject or site of ultrasonic stimulation	Main results	References
K2P	Zhao et al.	PC12 cells	Pre-treatment with LIPUS (1 MHz, 50 mW/cm^2, 20% duty cycle and 100-Hz pulse repetition frequency, 10 min) inhibited MPP1-induced neurotoxicity and mitochondrial dysfunction in PC12 cells. LIPUS regulated the expression of antioxidant proteins, specifically thioredoxin-1 and heme oxygenase-1, decreasing oxidative stress induced by MPP+. The prevention of neurocytotoxicity was observed through the activation of pathways that involved the phosphoinositide 3-kinase (PI3K)-Akt and extracellular signal-regulated kinase (ERK1/2). LIPUS protected neuronal cells from MPP + -induced cell death through the K2P channel- and stretch-activated ion channel-mediated downstream pathways.	Zhao L. et al. (2017)
	Kubanek et al.	*Xenopus* oocytes	Focused ultrasound (10 MHz, 0.3–4.9 W/cm^2) modulated the currents flowing through the ion channels averaged up to 23%, depending on channels and stimulus intensity. Repeated stimulation of the channel led to a reversible effect that decreased when the K2P channel was subjected to the blocking effect of $BaCl_2$. At the single cell level that focused US modulates the activity of specific ion channels to mediate transmembrane currents.	Kubanek et al. (2016)
	Sorum et al.	*Xenopus laevis* Oocytes, *Pichia pastoris* cells	Ultrasonic energy is transduced to TRAAK through the membrane in a manner analogous to canonical mechanical activation, likely increasing membrane tension to promote channel opening. Ultrasounic had an effect on modulation of neuronal expression TRAAK. These results suggest that mechanosensitive channels play a ctitical role in physiological responses to ultrasound and can be used as tools for acoustic neuromodulation of genetically targeted cells.	Sorum et al. (2021)
	Prieto et al.	CA1 pyramidal neurons in acute rodent hippocampal brain	Focused high-frequency (43 MHz) ultrasound inhibits or enhances firing in a spike frequency-dependent manner. Ultrasound increases the threshold current of action potential firing, the slope of the frequency input curve, and the maximum firing frequency. Ultrasound mildly hyperpolarizes the resting membrane potential, reduces action potential width, and increases the depth of after-hyperpolarization. Ultrasound activates thermosensitive and mechanosensitive two-pore-domain potassium (K2P) channels through acoustic radiation force-induced heating or mechanical effects. Finite element modeling shows that ultrasound affects the firing frequency of brain tissue by slightly raising the temperature (<2°C) and possibly through mechanical effects.	Prieto et al. (2020)

(Continued)

10.3389/fnins.2023.1232308

Jiang et al., 2019). Table 2 summarizes the research progress on the above mechanically sensitive ion channels related to ultrasonic neural regulation.

Summary

Mechanosensitive ion channels are mechanical force molecular sensors that are activated by mechanical stimuli and located on the cell membrane. These channels can quickly and efficiently convert mechanical stimuli into electrical and chemical signals. Stretching of mechanosensitive proteins can damage molecular binding sites, expose regulatory sites, and change the association or dissociation rates for protein binding (Ingham et al., 1997; Krammer et al., 2002; Cain et al., 2021). MS channel opening can result in ion influx. Additionally, numerous diseases such as muscular dystrophy, and cardiac arrhythmias and et al. have been related to defects in activating MS ion channels (Sukharev and Sachs, 2012). However, the gating mechanism and physiological effects of these channels differ. We also do not know the connection between the structure and the function of these MS ion channels. Ultrasound usually activates more than one MS ion channel, but it is unknown which one is working or how they work together. Our understanding of the mechanisms and functions of ultrasound activated mechanosensitive ion channels remains limited.

We need to develop innovative research methods and conduct more thorough research on the mechanism of these channels and explore screening of mechanically sensitive ion channels or their mutants that can be accurately controlled in the future. Addtionally, these MS ion channels should be expressed in various nerve cells. In future studies, researchers should clarify the expression profile of each ion channel in neuronal cells, and then study their sensitivity to ultrasound modulation, so as to summarize and compare the differences in the role of various ion channels in ultrasound modulation.

To date, previous studies have demonstrated the structure of some specific MS ion channels and their investigated their roles in ultrasonic neuromodulation. Ultrasound offers several advantages, including non-invasiveness, convenient *in vitro* regulation, intracranial multipoint focusing, spatiotemporal controllability and accuracy. Basic clinical trials have demonstrated that ultrasound can improve specific behaviors, such as increased responsiveness in patients with chronic disorders of consciousness (Cain et al., 2021) and improved mood (Reznik et al., 2020; Sanguinetti et al., 2020). However, further studies are needed to investigate how ultrasound acts on organisms, which mechanically sensitive channels it influences, and how different ultrasonic stimulation parameters produce varying effects. To gain a better understanding of ultrasonic neuromodulation efficacy, it is necessary to conduct these studies in various species and different disease models, and set different ultrasonic stimulation parameters to observe the applicability, persistence and timeliness of ultrasonic stimulation. It is also crucial to address the thermal and cavitation effects of ultrasonic stimulation and improve ultrasonic focusing resolution to increase the precision of ultrasonic regulation. Finally, innovative ultrasonic equipment should be developed to enhance the efficacy and applicability of wearable ultrasonic equipment.

Author contributions

HH: conceptualization. MS and MZ: writing—original draft preparation. MS, MZ, SH, LL, and HH: writing—review and editing. All authors contributed to the article and approved the submitted version.

Funding

This work was supported by the Natural Science Foundation of Shaanxi province (2022-JM482), Shenzhen Science and Technology Program (GJHZ20210705143401005), the Education and Teaching Reform Funds for the Central Universities (No. 23GZ230102), and the National Natural Science Foundation of China (No. 31771016).

Conflict of interest

The authors declare that the research was conducted in the absence of any commercial or financial relationships that could be construed as a potential conflict of interest.

Publisher's note

All claims expressed in this article are solely those of the authors and do not necessarily represent those of their affiliated organizations, or those of the publisher, the editors and the reviewers. Any product that may be evaluated in this article, or claim that may be made by its manufacturer, is not guaranteed or endorsed by the publisher.

References

Ajouz, B., Berrier, C., Garrigues, A., Besnard, M., and Ghazi, A. (1998). Release of thioredoxin via the mechanosensitive channel MscL during osmotic downshock of *Escherichia coli* cells. *J. Biol. Chem.* 273, 26670–26674. doi: 10.1074/jbc.273.41.26670

Baek, H., Pahk, K. J., and Kim, H. (2017). A review of low-intensity focused ultrasound for neuromodulation. *Biomed. Eng. Lett.* 7, 135–142. doi: 10.1007/s13534-016-0007-y

Blackmore, J., Shrivastava, S., Sallet, J., Butler, C. R., and Cleveland, R. O. (2019). Ultrasound neuromodulation: a review of results, mechanisms and safety. *Ultrasound. Med. Biol.* 45, 1509–1536. doi: 10.1016/j.ultrasmedbio.2018.12.015

Burks, S. R., Lorsung, R. M., Nagle, M. E., Tu, T. W., and Frank, J. A. (2019). Focused ultrasound activates voltage-gated calcium channels through depolarizing TRPC1 sodium currents in kidney and skeletal muscle. *Theranostics* 9, 5517–5531. doi: 10.7150/thno.33876

Cain, J. A., Spivak, N. M., Coetzee, J. P., Crone, J. S., Johnson, M. A., Lutkenhoff, E. S., et al. (2021). Ultrasonic thalamic stimulation in chronic disorders of consciousness. *Brain Stimul.* 14, 301–303. doi: 10.1016/j.brs.2021.01.008

Chan, Y. S., Hsu, K. Y., Kuo, C. H., Lee, S. D., Chen, S. C., Chen, W. J., et al. (2010). Using low-intensity pulsed ultrasound to improve muscle healing after laceration injury: an in vitro and in vivo study. *Ultrasound Med. Biol.* 36, 743–751. doi: 10.1016/j.ultrasmedbio.2010.02.010

Chang, G., Spencer, R. H., Lee, A. T., Barclay, M. T., and Rees, D. C. (1998). Structure of the MscL homolog from *Mycobacterium tuberculosis*: a gated mechanosensitive ion channel. *Science* 282, 2220–2226. doi: 10.1126/science.282.5397.2220

Copp, S. W., Kim, J. S., Ruiz-Velasco, V., and Kaufman, M. P. (2016). The mechano-gated channel inhibitor GsMTx4 reduces the exercise pressor reflex in decerebrate rats. *J. Physiol.* 594, 641–655. doi: 10.1113/jp271714

Coste, B., Mathur, J., Schmidt, M., Earley, T. J., Ranade, S., Petrus, M. J., et al. (2010). Piezo1 and Piezo2 are essential components of distinct mechanically activated cation channels. *Science* 330, 55–60. doi: 10.1126/science.1193270

Darmani, G., Bergmann, T. O., Butts Pauly, K., Caskey, C. F., de Lecea, L., Fomenko, A., et al. (2022). Non-invasive transcranial ultrasound stimulation for neuromodulation. *Clin. Neurophysiol.* 135, 51–73. doi: 10.1016/j.clinph.2021.12.010

Dell'Italia, J., Sanguinetti, J. L., Monti, M. M., Bystritsky, A., and Reggente, N. (2022). Current state of potential mechanisms supporting low intensity focused ultrasound for neuromodulation. *Front. Hum. Neurosci.* 16:872639. doi: 10.3389/fnhum.2022.872639

Deng, Z., Wang, J., Xiao, Y., Li, F., Niu, L., Liu, X., et al. (2021). Ultrasound-mediated augmented exosome release from astrocytes alleviates amyloid-β-induced neurotoxicity. *Theranostics* 11, 4351–4362. doi: 10.7150/thno.52436

Doerner, J. F., Febvay, S., and Clapham, D. E. (2012). Controlled delivery of bioactive molecules into live cells using the bacterial mechanosensitive channel MscL. *Nat. Commun.* 3:990. doi: 10.1038/ncomms1999

Duque, M., Lee-Kubli, C. A., Tufail, Y., Magaram, U., Patel, J., Chakraborty, A., et al. (2022). Sonogenetic control of mammalian cells using exogenous transient receptor potential A1 channels. *Nat. Commun.* 13:600. doi: 10.1038/s41467-022-28205-y

Feliciangeli, S., Chatelain, F. C., Bichet, D., and Lesage, F. (2015). The family of K2P channels: salient structural and functional properties. *J. Physiol.* 593, 2587–2603. doi: 10.1113/jphysiol.2014.287268

Feng, B., Chen, L., and Ilham, S. J. (2019). A review on ultrasonic neuromodulation of the peripheral nervous system: enhanced or suppressed activities? *Appl. Sci.* 9:1637. doi: 10.3390/app9081637

Ge, J., Li, W., Zhao, Q., Li, N., Chen, M., Zhi, P., et al. (2015). Architecture of the mammalian mechanosensitive Piezo1 channel. *Nature* 527, 64–69. doi: 10.1038/nature15247

Germann, J., Elias, G. J. B., Neudorfer, C., Boutet, A., Chow, C. T., Wong, E. H. Y., et al. (2021). Potential optimization of focused ultrasound capsulotomy for obsessive compulsive disorder. *Brain* 144, 3529–3540. doi: 10.1093/brain/awab232

Heureaux, J., Chen, D., Murray, V. L., Deng, C. X., and Liu, A. P. (2014). Activation of a bacterial mechanosensitive channel in mammalian cells by cytoskeletal stress. *Cell. Mol. Bioeng.* 7, 307–319. doi: 10.1007/s12195-014-0337-8

Ibsen, S., Tong, A., Schutt, C., Esener, S., and Chalasani, S. H. (2015). Sonogenetics is a non-invasive approach to activating neurons in *Caenorhabditis elegans*. *Nat. Commun.* 6:8264. doi: 10.1038/ncomms9264

Ingham, K. C., Brew, S. A., Huff, S., and Litvinovich, S. V. (1997). Cryptic self-association sites in type III modules of fibronectin. *J. Biol. Chem.* 272, 1718–1724. doi: 10.1074/jbc.272.3.1718

Iorio-Morin, C., Yamamoto, K., Sarica, C., Zemmar, A., Levesque, M., Brisebois, S., et al. (2021). Bilateral focused ultrasound thalamotomy for essential tremor (BEST-FUS phase 2 trial). *Mov. Disord.* 36, 2653–2662. doi: 10.1002/mds.28716

Jeremias Júnior, S. L., Camanho, G. L., Bassit, A. C., Forgas, A., Ingham, S. J., and Abdalla, R. J. (2011). Low-intensity pulsed ultrasound accelerates healing in rat calcaneus tendon injuries. *J. Orthop. Sports Phys. Ther.* 41, 526–531. doi: 10.2519/jospt.2011.3468

Jiang, X., Savchenko, O., Li, Y., Qi, S., Yang, T., Zhang, W., et al. (2019). A review of low-intensity pulsed ultrasound for therapeutic applications. *I.E.E.E. Trans. Biomed. Eng.* 66, 2704–2718. doi: 10.1109/tbme.2018.2889669

Kefauver, J. M., Ward, A. B., and Patapoutian, A. (2020). Discoveries in structure and physiology of mechanically activated ion channels. *Nature* 587, 567–576. doi: 10.1038/s41586-020-2933-1

Krammer, A., Craig, D., Thomas, W. E., Schulten, K., and Vogel, V. (2002). A structural model for force regulated integrin binding to fibronectin's RGD-synergy site. *Matrix Biol.* 21, 139–147. doi: 10.1016/s0945-053x(01)00197-4

Kubanek, J., Shi, J., Marsh, J., Chen, D., Deng, C., and Cui, J. (2016). Ultrasound modulates ion channel currents. *Sci. Rep.* 6:24170. doi: 10.1038/srep24170

Lesage, F., Guillemare, E., Fink, M., Duprat, F., Lazdunski, M., Romey, G., et al. (1996). TWIK-1, a ubiquitous human weakly inward rectifying K+ channel with a novel structure. *EMBO J.* 15, 1004–1011. doi: 10.1002/j.1460-2075.1996.tb00437.x

Levina, N., Tötemeyer, S., Stokes, N. R., Louis, P., Jones, M. A., and Booth, I. R. (1999). Protection of *Escherichia coli* cells against extreme turgor by activation of MscS and MscL mechanosensitive channels: identification of genes required for MscS activity. *EMBO J.* 18, 1730–1737. doi: 10.1093/emboj/18.7.1730

Loyola-Sánchez, A., Richardson, J., Beattie, K. A., Otero-Fuentes, C., Adachi, J. D., and MacIntyre, N. J. (2012). Effect of low-intensity pulsed ultrasound on the cartilage repair in people with mild to moderate knee osteoarthritis: a double-blinded, randomized, placebo-controlled pilot study. *Arch. Phys. Med. Rehabil.* 93, 35–42. doi: 10.1016/j.apmr.2011.07.196

Magaram, U., Weiss, C., Vasan, A., Reddy, K. C., Friend, J., and Chalasani, S. H. (2022). Two pathways are required for ultrasound-evoked behavioral changes in *Caenorhabditis elegans*. *PLoS One* 17:e0267698. doi: 10.1371/journal.pone.0267698

Martinac, B. (2004). Mechanosensitive ion channels: molecules of mechanotransduction. *J. Cell Sci.* 117, 2449–2460. doi: 10.1242/jcs.01232

Martinac, B., Buechner, M., Delcour, A. H., Adler, J., and Kung, C. (1987). Pressure-sensitive ion channel in *Escherichia coli*. *Proc. Natl. Acad. Sci. U. S. A.* 84, 2297–2301. doi: 10.1073/pnas.84.8.2297

Murthy, S. E., Dubin, A. E., and Patapoutian, A. (2017). Piezos thrive under pressure: mechanically activated ion channels in health and disease. *Nat. Rev. Mol. Cell Biol.* 18, 771–783. doi: 10.1038/nrm.2017.92

Nilius, B., and Owsianik, G. (2011). The transient receptor potential family of ion channels. *Genome Biol.* 12:218. doi: 10.1186/gb-2011-12-3-218

Oh, S. J., Lee, J. M., Kim, H. B., Lee, J., Han, S., Bae, J. Y., et al. (2019). Ultrasonic neuromodulation via astrocytic TRPA1. *Curr. Biol.* 29, 3386–3401.e8. doi: 10.1016/j.cub.2019.08.021

Pan, Y., Yoon, S., Sun, J., Huang, Z., Lee, C., Allen, M., et al. (2018). Mechanogenetics for the remote and noninvasive control of cancer immunotherapy. *Proc. Natl. Acad. Sci. U. S. A.* 115, 992–997. doi: 10.1073/pnas.1714900115

Peng, X., He, W., Xin, F., Genin, G. M., and Lu, T. J. (2020). The acoustic radiation force of a focused ultrasound beam on a suspended eukaryotic cell. *Ultrasonics* 108:106205. doi: 10.1016/j.ultras.2020.106205

Perozo, E., Cortes, D. M., Sompornpisut, P., Kloda, A., and Martinac, B. (2002). Open channel structure of MscL and the gating mechanism of mechanosensitive channels. *Nature* 418, 942–948. doi: 10.1038/nature00992

Prieto, M. L., Firouzi, K., Khuri-Yakub, B. T., Madison, D. V., and Maduke, M. (2020). Spike frequency-dependent inhibition and excitation of neural activity by high-frequency ultrasound. *J. Gen. Physiol.* 152:e202012672. doi: 10.1085/jgp.202012672

Qiu, Z., Guo, J., Kala, S., Zhu, J., Xian, Q., Qiu, W., et al. (2019). The mechanosensitive ion channel Piezo1 significantly mediates in vitro ultrasonic stimulation of neurons. *iScience* 21, 448–457. doi: 10.1016/j.isci.2019.10.037

Qiu, Z., Kala, S., Guo, J., Xian, Q., Zhu, J., Zhu, T., et al. (2020). Targeted neurostimulation in mouse brains with non-invasive ultrasound. *Cell Rep.* 32:108033. doi: 10.1016/j.celrep.2020.108033

Ren, L., Yang, Z., Song, J., Wang, Z., Deng, F., and Li, W. (2013). Involvement of p38 MAPK pathway in low intensity pulsed ultrasound induced osteogenic differentiation of human periodontal ligament cells. *Ultrasonics* 53, 686–690. doi: 10.1016/j.ultras.2012.10.008

Renigunta, V., Schlichthörl, G., and Daut, J. (2015). Much more than a leak: structure and function of K_2p-channels. *Pflugers Arch.* 467, 867–894. doi: 10.1007/s00424-015-1703-7

Reznik, S. J., Sanguinetti, J. L., Tyler, W. J., Daft, C., and Allen, J. J. B. (2020). A double-blind pilot study of transcranial ultrasound (TUS) as a five-day intervention: TUS mitigates worry among depressed participants. *Neurol. Psychiatry Brain Res.* 37, 60–66. doi: 10.1016/j.npbr.2020.06.004

Sanguinetti, J. L., Hameroff, S., Smith, E. E., Sato, T., Daft, C. M. W., Tyler, W. J., et al. (2020). Transcranial focused ultrasound to the right prefrontal cortex improves mood and alters functional connectivity in humans. *Front. Hum. Neurosci.* 14:52. doi: 10.3389/fnhum.2020.00052

Shen, X., Song, Z., Xu, E., Zhou, J., and Yan, F. (2021). Sensitization of nerve cells to ultrasound stimulation through Piezo1-targeted microbubbles. *Ultrason. Sonochem.* 73:105494. doi: 10.1016/j.ultsonch.2021.105494

Sorum, B., Rietmeijer, R. A., Gopakumar, K., Adesnik, H., and Brohawn, S. G. (2021). Ultrasound activates mechanosensitive TRAAK K(+) channels through the lipid membrane. *Proc. Natl. Acad. Sci. U. S. A.* 118:e2006980118. doi: 10.1073/pnas.2006980118

Sperling, S. A., Shah, B. B., Barrett, M. J., Bond, A. E., Huss, D. S., Gonzalez Mejia, J. A., et al. (2018). Focused ultrasound thalamotomy in Parkinson disease: nonmotor outcomes and quality of life. *Neurology* 91, e1275–e1284. doi: 10.1212/wnl.0000000000006279

Sukharev, S. I., Blount, P., Martinac, B., Blattner, F. R., and Kung, C. (1994). A large-conductance mechanosensitive channel in *E. coli* encoded by mscL alone. *Nature* 368, 265–268. doi: 10.1038/368265a0

Sukharev, S. I., Martinac, B., Arshavsky, V. Y., and Kung, C. (1993). Two types of mechanosensitive channels in the *Escherichia coli* cell envelope: solubilization and functional reconstitution. *Biophys. J.* 65, 177–183. doi: 10.1016/s0006-3495(93)81044-0

Sukharev, S., and Sachs, F. (2012). Molecular force transduction by ion channels: diversity and unifying principles. *J. Cell Sci.* 125, 3075–3083. doi: 10.1242/jcs.092353

Voolstra, O., Beck, K., Oberegelsbacher, C., Pfannstiel, J., and Huber, A. (2010). Light-dependent phosphorylation of the drosophila transient receptor potential ion channel. *J. Biol. Chem.* 285, 14275–14284. doi: 10.1074/jbc.M110.102053

Ye, J., Tang, S., Meng, L., Li, X., Wen, X., Chen, S., et al. (2018). Ultrasonic control of neural activity through activation of the mechanosensitive Channel MscL. *Nano Lett.* 18, 4148–4155. doi: 10.1021/acs.nanolett.8b00935

Yoo, S., Mittelstein, D. R., Hurt, R. C., Lacroix, J., and Shapiro, M. G. (2022). Focused ultrasound excites cortical neurons via mechanosensitive calcium accumulation and ion channel amplification. *Nat. Commun.* 13:493. doi: 10.1038/s41467-022-28040-1

Zhang, G., Li, X., Wu, L., and Qin, Y. X. (2021). Piezo1 channel activation in response to mechanobiological acoustic radiation force in osteoblastic cells. *Bone Res.* 9:16. doi: 10.1038/s41413-020-00124-y

Zhao, L., Feng, Y., Shi, A., Zhang, L., Guo, S., and Wan, M. (2017). Neuroprotective effect of low-intensity pulsed ultrasound against MPP(+)-induced neurotoxicity in PC12 cells: involvement of K2P channels and stretch-activated ion channels. *Ultrasound Med. Biol.* 43, 1986–1999. doi: 10.1016/j.ultrasmedbio.2017.04.020

Zhao, X., Zhao, G., Shi, Z., Zhou, C., Chen, Y., Hu, B., et al. (2017). Low-intensity pulsed ultrasound (LIPUS) prevents periprosthetic inflammatory loosening through FBXL2-TRAF6 ubiquitination pathway. *Sci. Rep.* 7:45779. doi: 10.1038/srep45779

Zhu, J., Xian, Q., Hou, X., Wong, K. F., Zhu, T., Chen, Z., et al. (2023). The mechanosensitive ion channel Piezo1 contributes to ultrasound neuromodulation. *Proc. Natl. Acad. Sci. U. S. A.* 120:e2300291120. doi: 10.1073/pnas.2300291120

frontiers | Frontiers in Neuroscience

TYPE Original Research
PUBLISHED 16 August 2023
DOI 10.3389/fnins.2023.1231693

OPEN ACCESS

EDITED BY
Feng Zhang,
Third Hospital of Hebei Medical University, China

REVIEWED BY
Xiaokuo He,
Xiamen Fifth Hospital, China
Hao Liu,
Weifang Medical University, China
Yue Lan,
Guangzhou First People's Hospital, China

*CORRESPONDENCE
Wanlong Lin
✉ 13162638165@163.com
Chunlei Shan
✉ shanclhappy@163.com

†These authors have contributed equally to this work

RECEIVED 30 May 2023
ACCEPTED 02 August 2023
PUBLISHED 16 August 2023

CITATION
Chen S, Zhang X, Chen X, Zhou Z, Cong W, Chong K, Xu Q, Wu J, Li Z, Lin W and Shan C (2023) The assessment of interhemispheric imbalance using functional near-infrared spectroscopic and transcranial magnetic stimulation for predicting motor outcome after stroke.
Front. Neurosci. 17:1231693.
doi: 10.3389/fnins.2023.1231693

The assessment of interhemispheric imbalance using functional near-infrared spectroscopic and transcranial magnetic stimulation for predicting motor outcome after stroke

Songmei Chen[1,2†], Xiaolin Zhang[1†], Xixi Chen[2†], Zhiqing Zhou[2], Weiqin Cong[1], KaYee Chong[2], Qing Xu[1], Jiali Wu[2], Zhaoyuan Li[1], Wanlong Lin[1*] and Chunlei Shan[2,3,4,5*]

[1]Department of Rehabilitation Medicine, Shanghai No.3 Rehabilitation Hospital, Shanghai, China, [2]School of Rehabilitation Science, Shanghai University of Traditional Chinese Medicine, Shanghai, China, [3]Center of Rehabilitation Medicine, Yueyang Hospital of Integrated Traditional Chinese and Western Medicine, Shanghai University of Traditional Chinese Medicine, Shanghai, China, [4]Engineering Research Center of Traditional Chinese Medicine Intelligent Rehabilitation, Ministry of Education, Shanghai, China, [5]Institute of rehabilitation, Shanghai Jiao Tong University School of Medicine, Shanghai, China

Objective: To investigate changes in interhemispheric imbalance of cortical excitability during motor recovery after stroke and to clarify the relationship between motor function recovery and alterations in interhemispheric imbalance, with the aim to establish more effective neuromodulation strategies.

Methods: Thirty-one patients underwent assessments of resting motor threshold (RMT) using transcranial magnetic stimulation (TMS); the cortical activity of the primary motor cortex (M1), premotor cortex (PMC), and supplementary motor area (SMA) using functional near-infrared spectroscopy (fNIRS); as well as motor function using upper extremity Fugl-Meyer (FMA-UE). The laterality index (LI) of RMT and fNIRS were also calculated. All indicators were measured at baseline(T_1) and 1 month later(T_2). Correlations between motor function outcome and TMS and fNIRS metrics at baseline were analyzed using bivariate correlation.

Results: All the motor function (FMA-UE_1, FMA-UE_2, FMA-d_2) and LI-RMT (LI-RMT_1 and LI-RMT_2) had a moderate negative correlation. The higher the corticospinal excitability of the affected hemisphere, the better the motor outcome of the upper extremity, especially in the distal upper extremity ($r = -0.366$, $p = 0.043$; $r = -0.393$, $p = 0.029$). The greater the activation of the SMA of the unaffected hemisphere, the better the motor outcome, especially in the distal upper extremity ($r = -0.356$, $p = 0.049$; $r = -0.367$, $p = 0.042$). There was a significant moderate positive correlation observed between LI-RMT_2 and LI-SMA_1 ($r = 0.422$, $p = 0.018$). The improvement in motor function was most significant when both LI-RMT_1 and LI-SMA_1 were lower. Besides, in patients dominated by unaffected hemisphere corticospinal excitability during motor recovery, LI-$(M1 + SMA + PMC)_2$ exhibited a significant moderate positive association with the proximal upper extremity function 1 month later ($r = 0.642$, $p = 0.007$).

Conclusion: The combination of both TMS and fNIRS can infer the prognosis of motor function to some extent. Which can infer the role of both hemispheres in recovery and may contribute to the development of effective individualized neuromodulation strategies.

KEYWORDS

stroke, transcranial magnetic stimulation, functional near-infrared spectroscopy, laterality index, interhemispheric imbalance

1. Introduction

Stroke has a high incidence and high disability rate worldwide (Bejot et al., 2016). More than half of strokes have impaired upper limb motor function, which seriously affects the quality of life and places a huge burden on families and society (Avan et al., 2019). Currently, the recovery of upper limb motor function remains one of the challenges of post-stroke rehabilitation (Bertani et al., 2017).

Recent years have seen the rapid development of non-invasive brain stimulation technologies. Repetitive transcranial magnetic stimulation (rTMS) is considered one of the effective methods to improve upper limb motor function after stroke (van Lieshout et al., 2019; Ni et al., 2022). At present, there are two theoretical models for the clinical application of rTMS in motor rehabilitation for stroke. They are the bilateral hemispheric competition model that advocates inhibition in the unaffected hemisphere (UH) or excitation in the affected hemisphere (AH) (Lefaucheur et al., 2020) and the vicariation model that advocates excitation in residual brain area of the AH or the UH (Di Pino et al., 2014). Given that these two theoretical models are inconsistent in guiding rTMS therapy, there is no consensus on the use of excitatory or inhibitory modulation in the UH (Long et al., 2018). Understanding the progression of interhemispheric imbalance in brain activation and its contribution to motor functional recovery is important for the development of effective neuromodulation strategies (Kinoshita et al., 2019). If we know which hemisphere plays a dominant role in the process of motor function recovery, we can adopt modulatory strategies to excite that hemisphere or inhibit the contralateral hemisphere. Therefore, it is clinically important to accurately determine the interhemispheric imbalance and to develop individualized neuromodulation strategies based on it.

On the other hand, there is no uniform standard regarding the target site of rTMS stimulation for stroke patients' motor function recovery. The most common site is the primary motor cortex (M1), because M1 is the major motor output pathway in humans (Lam et al., 2018; Lefaucheur et al., 2020). In addition, studies suggested that the secondary motor cortical areas, including the premotor cortex (PMC) and supplementary motor area (SMA), can also be used as modulatory targets. The PMC has fiber connections to M1 in both the ipsilateral and contralateral hemispheres. When the lesion is large over M1 area, the PMC can function instead of M1 (Buetefisch, 2015; Plow et al., 2015). Similarly, functional connections exist between SMA and M1 and SMA are also involved in corticospinal projections that may facilitate motor recovery after stroke (Matsunaga et al., 2005; Diao et al., 2017). Therefore, an in-depth understanding of the changes in the motor cortex during function improvement facilitates us to understand the mechanisms of functional recovery.

As a neuromodulation technique, transcranial magnetic stimulation (TMS) is not only a treatment therapy but also an assessment tool (Groppa et al., 2012). Single-pulse TMS assessment metrics such as resting motor threshold (RMT), and motor evoked potential (MEP) can evaluate the excitability of corticospinal motor neurons, and the functional integrity of the corticospinal tract (CST) (Andrews et al., 2022). It has been demonstrated indicators by TMS can be used as valid biomarkers to assess the recovery of neurological function (Kelley et al., 2014). Besides, another study measured RMT by TMS and calculated the laterality index (LI) of cortical excitability to confirm asymmetric functional changes in the cerebral hemispheres after stroke (Di Lazzaro et al., 2016). Studies have shown that the success of motor recovery after stroke is significantly determined by the direction and extent of cortical excitability changes in both hemispheres (Stinear et al., 2015; Veldema et al., 2021). Understanding the contribution of either cortical hemisphere to motor recovery may facilitate the development of effective individualized rehabilitation strategies (Kumar et al., 2016). So, the TMS assessment may identify the altered interhemispheric imbalance and guide selection of appropriate modulation protocol for stroke patients.

In addition to TMS, functional near-infrared spectroscopy (fNIRS) is a neuroimaging method for assessing brain function (Delorme et al., 2019). fNIRS can detect activation patterns in the cerebral motor cortex, reflecting changes in neural remodeling during the recovery of motor function after stroke (Huo et al., 2019). It has been shown that cerebral hemodynamic activity reflected by fNIRS can be a reliable neurobiomarker for the assessment of limb motor dysfunction in stroke patients (Wang et al., 2023). It is well known that stroke-induced motor deficits are associated with an interhemispheric imbalance of motor activation (Cunningham et al., 2015; Tang et al., 2015; Kinoshita et al., 2019). As motor function is restored, the balance of interhemispheric activation in the motor-related cortex changes (Tang et al., 2015). Then, a study showed that assessing cortical activation asymmetry by fNIRS can help predict the response to rehabilitation treatment (Tamashiro et al., 2019). Thus, fNIRS also promises to be a convenient technique for investigating the neural mechanisms underlying the dysfunction, which will deepen our understanding of stroke rehabilitation and potentially translate this knowledge to improve the effectiveness of rehabilitation interventions.

Although TMS and fNIRS assessment techniques have been used in clinical research, they also have certain limitations. fNIRS is able to detect a wide range of cortical areas, but it is limited by spatial resolution, which prevents it from detecting deep brain regions (Ni et al., 2022). In contrast, TMS measures the corticospinal excitability by evoking MEP in the primary motor cortical (M1). It only reflects the functional integrity of the cortical downstream pathways

emanating from M1, but compensates for the inability of fNIRS assessment to access deep brain motor pathways. The combined use of both methods will help us to gain insight into the changes in brain function during motor recovery after stroke. Therefore, we conducted a longitudinal, multimodal study using the clinical scale, TMS, and fNIRS measures to find the relationship between motor function recovery and interhemispheric imbalance changes.

2. Materials and methods

2.1. Participants

The present study was approved by the ethics committee at Shanghai No.3 Rehabilitation Hospital (ethics No. SH3RH-2021-EC-012), and was registered in the China Clinical Trial Registration Center (registration No. ChiCTR2200057378). All patients were informed about the nature of this study.

Thirty-one first-ever stroke patients (age 65.42 ± 10.15 years) participated in this study. The participants with stroke in this study were recruited from Shanghai No.3 Rehabilitation Hospital. The basic information of participants was presented in Table 1. Criteria for selecting the subjects were as follows: (1) first-ever stroke, (2) age of 30 and 80 years, (3) clear consciousness and stable vital signs, (4) no cognitive impairment (mini-mental state examination score ≥ 24 points). The exclusion criteria were: (1) contraindications to TMS (Najib and Horvath, 2014), (2) having visual and hearing impairment and cannot cooperate to complete the trials, (3) having severe heart, liver, or kidney dysfunction or malignancy, (4) other neurological diseases.

2.2. Experimental design

In this study, patients underwent clinical, neurophysiological, and neuroimaging assessments. The clinical assessment was performed using FMA-UE. The neurophysiological assessment was performed using RMT for corticospinal excitability. The neuroimaging assessment was performed using fNIRS to assess changes in motor cortical activation. The assessment metrics were labeled as 1 at baseline and 2 in 1 month later, such as FMA-UE$_1$ and FMA-UE$_2$. All participants received conventional medical treatments and rehabilitative therapies during participation. The conventional rehabilitative therapies include physiotherapy and occupational therapy.

2.3. Assessments and procedures

2.3.1. Clinical assessment

FMA-UE was used to quantify the initial deficit and to follow up on the recovery of voluntary movements of the paralyzed limb after 1 month. All clinical assessments were performed by a blinded specialized assessor at baseline and 1 month later. FMA-UE is a measure of upper extremity motor function for stroke patients with a total score of 66, which means that the lower the score, the more severe the degree of impairment (Gladstone et al., 2002). The distal portion of the tested upper limb in FMA-UE was recorded as FMA-d, while the proximal portion was recorded as FMA-p.

2.3.2. TMS assessment

All subjects were evaluated with TMS which was carried out by M-100 Ultimate Pulsed magnetic Stimulation Device (Shenzhen Yingchi Technology Co., Ltd., Shenzhen, China). The patients were asked to sit in a relaxed position, and the skin on which the electrodes were attached was defatted with 95% alcohol cotton balls. The recording electrode was located in the muscle belly of the first dorsal interosseous (FDI), the reference electrode was located in the tendon of FDI, and the ground electrode was located in the forearm. Detection was performed in a single-pulse stimulation mode. The evaluator held a figure-of-eight-shaped coil with BY90A model to deliver TMS to the motor cortex. The maximum magnetic field change rate on the coil surface was 16.09kT/s, the peak stimulus intensity was 1 T, the pulse rise time was 62.0 μs, and the bidirectional wave unilateral pulse width was 200 μs. The optimal location of the M1 was first found according to the international 10/20 EEG positioning system, and then the coil was moved in small steps in the hand region of M1 until the position where maximal MEPs were consistently obtained was found. The coil was placed on the scalp at this location with handles pointing backward and rotated approximately 45° from the midline. TMS intensity was expressed as a percentage of maximum stimulator output (%MSO). The minimum TMS intensity with MEP which was elicited in the contralateral FDI greater than 50 μV for at least 5 of 10 consecutive single-pulse stimuli was recorded as RMT. RMT was measured on both hemispheres separately, inducing MEP in the contralateral FDI (see Figure 1). For patients without evoked MEPs, RMT in the AH was defined as 110 %MSO (Kemlin et al., 2019).

2.3.3. fNIRS assessment

The fNIRS data acquisition was performed using the NirSmart system (Danyang Huichuang Medical Equipment Co., Ltd., China) with a sampling rate of 11 Hz. Optical signals of two different wavelengths (730 nm and 850 nm) can be recorded in the continuous waveform in this system. There are 14 light sources and 8 detectors on the acquisition cap, with a total of 26 channels. The region covered by the probe involves the sensorimotor areas of the bilateral cerebral cortex. We predefined the regions of interest (ROIs), including M1, SMA, and PMC (See Figure 2A).

In this study, fNIRS data in the task state were collected. All patients were asked to sit quietly and relaxed. The assessor would communicate the entire task flow with the patients in advance and ask them not to speak during the task. The task paradigm was block-designed, which consists of alternating 3 grasping tasks and 3 rests. Each task block lasted 25 s and each rest lasted 30s (See Figure 2B). During the task period, patients grasped actively or passively (if the patients were unable to grasp actively, the assessor helped the patients to grasp passively) (Du et al., 2019).

2.4. Data analysis

2.4.1. TMS data processing and analyses

To evaluate the hemispheric asymmetry of motor cortex excitability, we calculated the interhemispheric LI of the RMT. The LI of RMT was calculated as Formula (1).

TABLE 1 Demographic data and clinical history of the patients.

Patient	Sex	Age (years)	Stroke type	AH	Stroke duration (days)	BI	FMA-UE$_1$
1	F	59	Infarction	L	95	90	17
2	M	47	Infarction	L	26	90	54
3	M	69	Infarction	L	178	25	6
4	M	66	Infarction	L	47	45	10
5	M	66	Infarction	L	81	45	12
6	M	77	Infarction	L	441	55	41
7	M	66	Infarction	L	165	40	4
8	F	72	Infarction	L	32	45	37
9	M	38	Infarction	L	10	95	64
10	F	76	Infarction	L	209	75	10
11	M	66	Infarction	R	62	40	25
12	M	66	Infarction	R	96	40	27
13	M	66	Infarction	R	80	45	32
14	F	66	Infarction	R	35	40	0
15	M	57	Infarction	R	16	40	0
16	M	48	Hemorrhage	R	68	55	6
17	M	78	Infarction	R	59	90	44
18	M	64	Infarction	R	68	30	6
19	F	61	Infarction	R	9	35	8
20	F	74	Infarction	R	101	65	35
21	F	79	Infarction	L	102	30	16
22	M	73	Infarction	L	153	60	15
23	M	61	Infarction	L	182	45	26
24	M	66	Infarction	R	177	60	21
25	M	42	Hemorrhage	L	29	45	0
26	M	73	Infarction	L	32	60	19
27	F	72	Hemorrhage	R	88	45	9
28	M	72	Infarction	R	20	65	40
29	M	72	Hemorrhage	R	224	55	40
30	F	65	Infarction	R	51	70	22
31	M	71	Hemorrhage	R	63	60	36

M, male; F, female; L, left; R, right; AH, affected hemisphere; BI, Barthel index; FMA-UE$_1$, Fugl-Meyer assessment for the upper extremity score at baseline.

$$\mathrm{LI}(\mathrm{RMT}) = \frac{\mathrm{RMT_{AH}} - \mathrm{RMT_{UH}}}{\mathrm{RMT_{AH}} + \mathrm{RMT_{UH}}} \quad (1)$$

LI (RMT) represents the imbalance of corticospinal excitability in both hemispheres. Thus, a positive value indicates higher corticospinal excitability in the UH. The greater the difference from 0, the higher the degree of imbalance between the cerebral hemispheres (Di Lazzaro et al., 2016).

RMT was also expressed as a ratio ($R = \mathrm{RMT_{AH}}/\mathrm{RMT_{UH}}$) (Kemlin et al., 2019). The value after 1 month (recorded as R2) minus the baseline (recorded as R1) obtained the difference of R, i.e., d(R). d(R) > 0 indicates more changes in corticospinal excitability in the UH and d(R) < 0 indicates more changes in corticospinal excitability in the AH (Patel et al., 2020; de Freitas et al., 2022).

2.4.2. fNIRS data preprocessing and analyses

The fNIRS data were preprocessed using the Homer 2.0 toolkit under the MatlabR2013a operating environment. Data pre-processing includes conversion of the original signals, identification of artifacts and noise, as follows: data conversion to convert the raw signal into light intensity; identification of artifacts and correction; band-pass filtering of noise in the range of 0.01–0.1 Hz to eliminate possible respiratory and heart rate interference; conversion of the filtered light intensity into oxyhemoglobin (HBO) level according to the modified

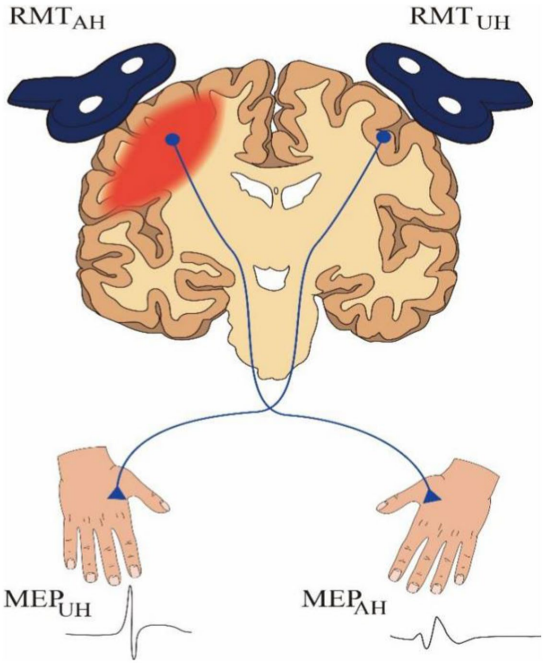

FIGURE 1
A schematic representation of TMS assessment. RMT, resting motor threshold; MEP, motor evoked potential; AH, affected hemisphere; UH, unaffected hemisphere.

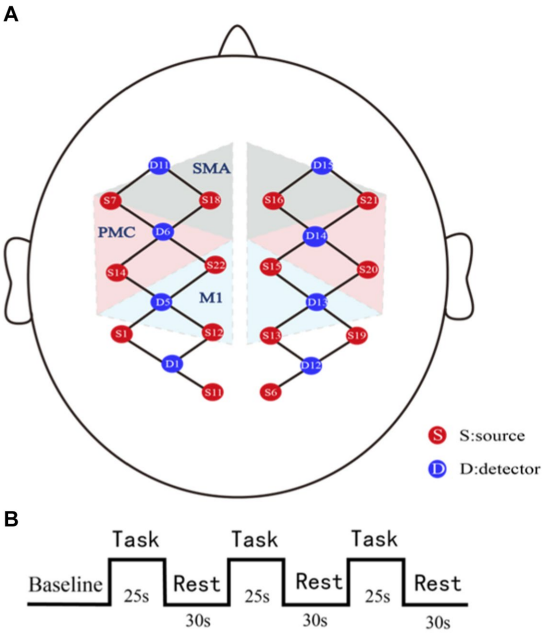

FIGURE 2
Schematic representations of fNIRS assessment. **(A)** fNIRS channels and region of interests (ROIs) map. SMA, supplementary motor area; PMC, premotor cortex; M1, the primary motor cortex. **(B)** Block design paradigm. Each task block lasted 25 s and each rest lasted 30s. The 10s pre-task period was used as the baseline.

Beer-Lamber law. We analyze the HBO level because it is reliable and sensitive to changes in cerebral blood flow (Kinoshita et al., 2019).

The preprocessed data are imported into NirSpark analysis software. Firstly, the three segment blocks of each data were averaged according to the mark to obtain accurate and stable data. The HBO concentration within 5 s before task onset was used as the baseline. The average HBO concentration during task performance minus the baseline concentration was the relative change in HBO concentration (ΔHBO). The ΔHBO on the corresponding channel of the ROI on each hemisphere was extracted and the LI was calculated to assess the hemispheric imbalance to determine the relative hemispheric dominance induced by the grasping task on the hemiplegic side (Borrell et al., 2023). The LI of ΔHBO was calculated as Formula (2). According to the following published literature in the previous manuscript (Borrell et al., 2023), the absolute value (ABS) in the denominator of the formula would prevent possible zero value.

$$\mathrm{LI}(\Delta\mathrm{HBO}) = \frac{\Delta\mathrm{HBO}_{\mathrm{AH}} - \Delta\mathrm{HBO}_{\mathrm{UH}}}{ABS(\Delta\mathrm{HBO}_{\mathrm{AH}}) + ABS(\Delta\mathrm{HBO}_{\mathrm{UH}})} \quad (2)$$

LI (ΔHBO) value ranges from −1 to 1, and it reveals which hemisphere experiences a larger change during the task. Negative LI (ΔHBO) values indicate UH dominant activity, while positive LI (ΔHBO) values indicate AH dominant activity (Borrell et al., 2023). Thus, the LI (ΔHBO) value of "−1" indicates complete UH dominance, and the LI (ΔHBO) value of "+1" indicates complete AH dominance. In this study, we calculated the LI of M1, SMA, PMC, and M1 + SMA + PMC.

2.5. Statistics analysis

Statistical analyses were performed with SPSS V.24.0 software. Behavioral data at baseline and 1 month later were tested using a paired *t*-test if they conformed to a normal distribution, otherwise, a nonparametric test was used. We evaluated the bivariate relation between the neuroimaging metrics and TMS metrics. To identify functionally relevant metrics, we calculated the correlation between FMA-UE and TMS (LI-RMT) and neuroimaging metrics (LI-M1, LI-SMA, LI-PMC). To explore the correlation between the indicators in the case of recovery dominated by different cerebral hemispheres (AH or UH), we additionally grouped the $d(R) > 0$ and $d(R) < 0$ groups according to $d(R)$ and performed correlation analyses. Pearson's correlation test was used if a normal distribution was consistent, and nonparametric Spearman's correlation test was used otherwise. Data conforming to the normal distribution are denoted by mean ± SD, otherwise, M (P25, P75). All data used a two-sided calibration with a test level of $\alpha = 0.05$. According to the previous study (Prion and Haerling, 2014), the interpretation of correlation coefficients are as follows: 0 to ±0.20 is negligible, ±0.21 to ±0.35 is weak, ±0.36 to ±0.67 is moderate, ±0.68 to 0.90 is strong, and ± 0.91 to ±1.00 is considered very strong.

3. Results

All 31 subjects completed two assessments at baseline and 1 month later. At the TMS assessment, a total of 20 subjects were

unable to induce the MEP at baseline and 19 subjects were unable to induce the MEP 1 month later. In addition, 23 subjects required assistance to complete the grasping task at the fNIRS assessment.

3.1. Metrics of interhemispheric imbalance and clinical assessment of motor function

3.1.1. Relationship between motor function and hemispheric asymmetry of corticospinal excitability

For all patients, motor function was significantly improved 1 month later compared to baseline ($p < 0.05$).

There was a significant moderate negative correlation between LI-RMT_1 and FMA-UE_2 as well as FMA-d_2 ($r = -0.366$, $p = 0.043$; $r = -0.393$, $p = 0.029$), which means the higher the corticospinal excitability of the AH, the better the motor outcome of the upper extremity, especially in the distal upper extremity. Additionally, a moderate negative correlation was observed between LI-RMT_2 and FMA-UE_1 ($r = -0.474$, $p = 0.007$) (see Figure 3).

3.1.2. Relationship between motor functional recovery and interhemispheric imbalance in motor cortical activity

For all patients, LI-SMA_1 exhibited a significant moderate negative association with both FMA-UE_2 and FMA-d_2 ($r = -0.356$, $p = 0.049$; $r = -0.367$, $p = 042$), which means the greater the activation of the SMA of the UH, the better the motor outcome, especially in the distal upper extremity (see Figure 4).

3.1.3. Relationship between motor function and combined fNIRS and TMS metrics

We calculated the mean value of LI-SMA_1 + LI-RMT_1. All patients were grouped according to the obtained mean, with one group being < mean (named g1) and the other group being > mean (named g2). There was a significant difference between g2 and g1. Compared with the g2 at the same time point, the function score of FMA-UE_2 and FMA-d_2 increased faster in g1 ($p = 0.023$ and $p = 0.029$, respectively), as shown in Table 2 and Figure 5. Both of these imply that the two states of SMA and M1 of the patient at baseline could predict future functional recovery.

3.2. Relationship between TMS and fNIRS measure of interhemispheric balance

For all patients, there was a significant moderate positive correlation observed between LI-RMT_2 and LI-SMA_1 ($r = 0.422$, $p = 0.018$). Additionally, LI-RMT_2 exhibited a negative association with LI-$M1_1$ ($r = -0.383$, $p = 0.034$) (see Figure 6).

3.3. Correlation of motor outcome based on interhemispheric asymmetry of corticospinal excitability

In the $d(R) > 0$ group, LI-PMC_2 exhibited a significant positive association with FMA-UE_2 ($r = 0.575$, $p = 0.020$). LI-$(M1 + SMA + PMC)_2$ exhibited a positive association with FMA-p_2 ($r = 0.642$, $p = 0.007$). There was a negative relation between LI-$M1_2$ and LI-PMC_2 ($r = -0.536$, $p = 0.031$) (see Figures 7A–C).

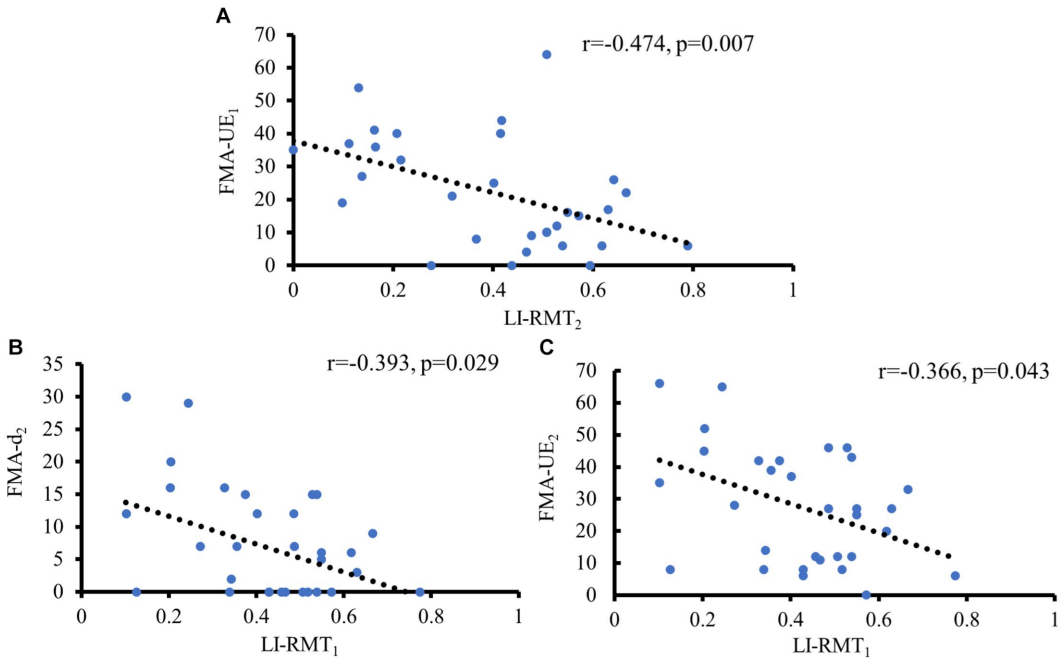

FIGURE 3
Significant correlations of motor function with LI- RMT. **(A)** Negative correlation between FMA-UE at baseline and LI-RMT at 1 month later; **(B)** Negative correlation between LI-RMT at baseline and FMA-UE at 1 month later; **(C)** Negative correlation between LI-RMT at baseline and FMA-d at 1 month later.

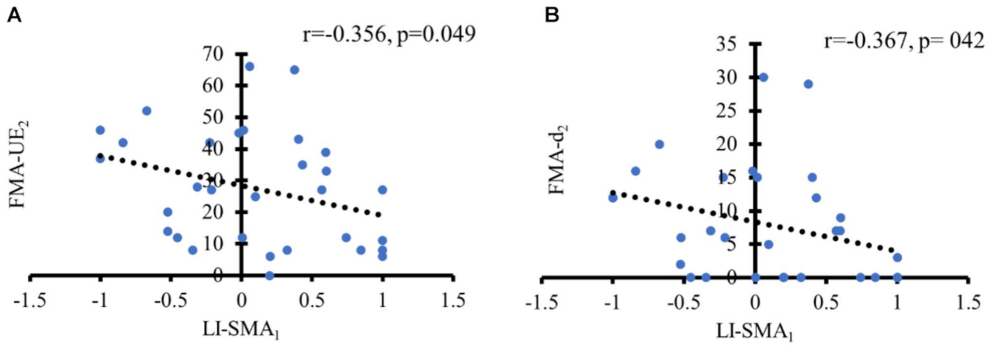

FIGURE 4
Significant correlations of motor function with LI of motor cortical activity. **(A)** Negative correlation between LI-SMA at baseline and FMA-UE at 1 month later; **(B)** Negative correlation between LI-SMA at baseline and FMA-d at 1 month later.

TABLE 2 Comparison between g1 and g2 with FMA-UE and FMA-d at different times.

Group	$FMA\text{-}UE_1$	$FMA\text{-}UE_2$	$FMA\text{-}d_1$	$FMA\text{-}d_2$
	M (P25, P75)	M (P25, P75)	M (P25, P75)	M (P25, P75)
g1 ($n=16$)	24 (11.3,40)	36 (15.5, 45.8)	6.5 (0,14.5)	12 (3.0, 15.8)
g2 ($n=15$)	12 (6, 26)	12 (8.0, 33.0)	0 (0, 7.0)	0 (0, 7.0)
Z	−1.622	−2.278	−1.707	−2.187
p	0.105	0.023*	0.088	0.029*

$g1$, the group of the value from $LI\text{-}SMA_1 + LI\text{-}RMT_1 <$ mean; $g2$, the group of the value from $LI\text{-}SMA_1 + LI\text{-}RMT_1 >$ mean; *Significant median difference at $p < 0.05$.

In the $d(R) < 0$ group, $FMA\text{-}d_2$ had a negative relation with $LI\text{-}RMT_2$ ($r = -0.541$, $p = 0.037$). However, no significant associations were found between fNIRS metrics and TMS metrics in the $d(R) < 0$ (see Figure 7D).

4. Discussion

It is known that the anatomic structure of the left and the right brain is generally symmetrical (Tang et al., 2015). A functional balance exists between the two hemispheres of the healthy brain, regulated by interhemispheric inhibition. This balance is disrupted after the onset of stroke (Shen et al., 2022). However, the role of the motor cortex of both hemispheres in the recovery of motor function remains controversial, especially the UH (Ni et al., 2022). Some studies show that activation of the UH increases interhemispheric inhibition in the AH (Dionisio et al., 2018; Lefaucheur et al., 2020), while others suggest that activation of the UH plays a compensatory role for the inactivation of the AH (Bradnam et al., 2012; Bertolucci et al., 2018). Therefore, predicting motor function outcomes based on the asymmetry of cortical excitability and motor cortical activation is important for developing rehabilitation programs.

The RMT measured by TMS is a standard measure of corticospinal excitability, and the ΔHBO measured by fNIRS is used to assess brain activation (Lee et al., 2019; Badran et al., 2020). To date, no combination of the two assessment methods to assess the imbalance in brain asymmetry has been reported. Our study is the first to combine TMS and fNIRS for investigating motor function outcome after stroke. We calculated the LI of RMT and ΔHBO, which reflects the asymmetry between the cerebral hemispheres, and investigated its relationship with motor function recovery. Exploring the underlying neural mechanisms of functional recovery after stroke will help us to develop new rehabilitation interventions.

In the current study, the patients had recovery of hemiplegic upper limb motor function after one month. It may have been a spontaneous neurological recovery or benefited from conventional rehabilitation. In these patients, those who initially had better motor function subsequently also had corticospinal excitability lateralized to the AH. Similarly, the more corticospinal excitability was lateralized to the AH at baseline, the better motor outcome after a month of recovery time. The result is consistent with the common pattern of motor function recovery. The lateralization of corticospinal excitability reflected by LI-RMT to the AH indicates that the functional integrity of the affected CST is not completely disrupted. The CST in the AH plays an important role in motor function recovery in the hemiplegic limb. It has been shown that the surviving neurons on the AH contribute to axonal remodeling of the CST, which promotes motor recovery after stroke (Okabe et al., 2017). Our result suggests that functional integrity of the CST measured by TMS-induced MEP helps predict motor function outcomes, which is consistent with previous studies suggesting that MEP deficits in the AH are associated with poorer motor recovery after stroke (Chen et al., 2023).

However, TMS assessment is obtained by evoking MEP in M1. It can only reflect the excitability of the corticospinal pathway emanating from M1. Compared to TMS, fNIRS can measure the activation of the entire motor cortex. Our study suggests that combining fNIRS with TMS provides complementary information superior to that of imaging methods in isolation. We found that the patients with SMA activation lateralized to the UH at baseline had better motor outcomes.

The SMA is a secondary motor area that plays a pivotal role in complex hand movements (Shirota et al., 2012). SMA and M1 both have a direct influence on force production during fine manual motor tasks (Entakli et al., 2014). A previous study using fMRI also found a correlation between task-related brain activation patterns and final motor status. They found that greater brain activation in the SMA at baseline was associated with better motor outcomes after stroke (Du et al., 2018). This may be specific recruitment of SMA to provide motor control in order to produce motion output during the motor

task. Previous studies found that better motor outcomes were associated with higher baseline activation in bilateral SMA (Du et al., 2018; Xu et al., 2021), whereas we found that it was SMA activation lateralized to the UH that led to better motor outcomes, especially in distal upper extremity motor function. Our data support the critical role of SMA activation lateralized to the UH in stroke recovery.

Furthermore, the relationship between the lateralization of corticospinal excitability in TMS and the lateralization of motor cortical activation in fNIRS was analyzed. At baseline, if M1 activation was lateralized to the AH, the improvement in motor function was accompanied by lateralization of corticospinal excitability to the AH. It is consistent with the model that motor functional recovery after stroke is dominated by M1 neural remodeling in the AH (Buetefisch, 2015; Yang et al., 2021). If SMA activation was lateralized to the UH, recovery of motor function was accompanied by lateralization of corticospinal excitability to the AH. A previous study has shown that improved motor function after stroke might be highly correlated with the functional connectivity of the ipsilesional M1 to the contralateral SMA (Chen et al., 2021). In this case, the SMA in the AH may play a compensatory role.

Our study shows that a multimodal model combining fNIRS, TMS, and clinical assessment predicts motor outcomes after stroke. It may have important clinical implications in guiding neuromodulation rehabilitation strategies. Previous studies have shown that inhibitory or facilitative rehabilitation techniques can be used based on the imbalance in interhemispheric cortical excitability (Du et al., 2019; Veldema et al., 2021). It is well known that M1 is the major motor output pathway for motor control (Lam et al., 2018) and is also the most commonly used stimulation target for neuromodulation (Hallett et al., 2017; Lefaucheur et al., 2020). However, our results show that activation of SMA lateralized to the UH is also associated with good motor outcome. Besides, the improvement in motor function was most significant when both the corticospinal excitability predominantly in the AH (LI-RMT$_1$) and SMA activation predominantly in the UH (LI-SMA$_1$) conditions were met at baseline (Figure 3). Thus, it is reasonable to assume that the best motor outcome may be obtained when stimulating the M1 of the AH is added with excitatory stimulation of the SMA of the UH. We hypothesize that the SMA of the UH may play a compensatory role in motor recovery, especially in the distal limb motor. So, the SMA may also be a suitable target for rTMS stimulation to develop specific rehabilitation methods. However, the underlying mechanism needs further clinical study.

In addition, we calculated R-values using the RMT measured by TMS, which reflects the interhemispheric imbalance of corticospinal excitability. According to the difference in R-values before and after one month, the patients were divided into two groups. In the d(R) < 0 group, corticospinal excitability changes were dominated by AH, while in the d(R) > 0 group, corticospinal excitability changes were dominated by UH. In the group dominated by the AH, motor outcome of the distal upper limb was positively correlated with altered AH corticospinal excitability. In other words, good motor function of the distal upper limb depended on the degree of recovery of CST function emanating from the AH.

Notably, in the group dominated by UH corticospinal excitability, motor outcomes in the upper limb as well as in the proximal were

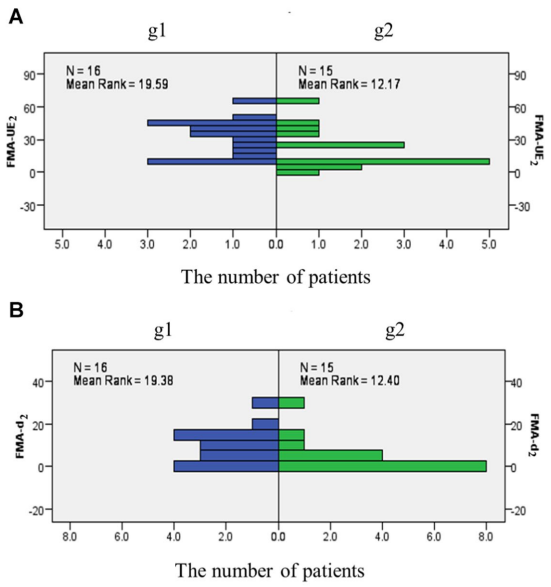

FIGURE 5
The frequency of FMA-UE$_2$ and FMA-d$_2$ in different groups. **(A)** The frequency distribution map as FMA-UE at 1 month later; **(B)** The frequency distribution map as FMA-d at 1 month later.

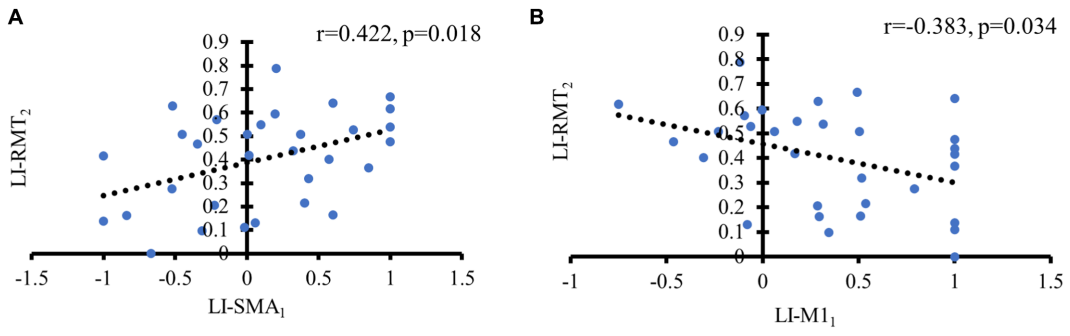

FIGURE 6
Significant correlations of TMS with fNIRS metrics. **(A)** Positive correlation between LI-SMA at baseline and LI-RMT at 1 month later; **(B)** Negative correlation between LI-M1 at baseline and LI-RMT at 1 month later.

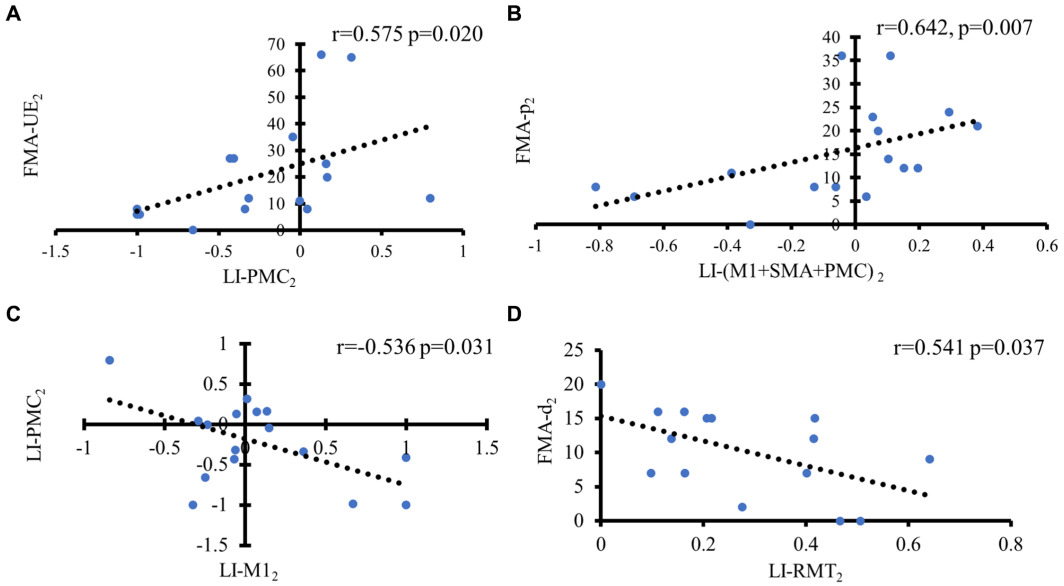

FIGURE 7
Correlation analysis of motor outcome in different groups based on hemispheric asymmetry of corticospinal function. In the d(*R*) > 0 group, **(A)** Positive correlation between LI of PMC and FMA-UE at 1 month later; **(B)** Positive correlation between LI of M1 + SMA + PMC and FMA-p at 1 month later; **(C)** Negative correlation between LI-M1 and LI-PMC at 1 month later. In the d(*R*) < 0 group, **(D)** Negative correlation between FMA-d and LI-RMT at 1 month later.

associated with AH-dominated PMC activation. We hypothesize that the CST emanating from AH is severely impaired in this group, and therefore the corticospinal excitability emanating from UH is dominant. This also implies that the anterior CST emanating from the UH has enhanced conduction signals, which can innervate the ipsilateral hemiplegic limb. Moreover, this compensatory neural pathway innervates more proximal muscles than distal muscles (Wang et al., 2019). On the other hand, it has been demonstrated that PMC has fiber connections to M1 in both the ipsilateral and contralateral hemispheres and that PMC in AH can function instead of M1 (Dum and Strick, 1991; Kantak et al., 2012). Meanwhile, our results show that AH-dominant PMC activation is positively correlated with UH-dominant M1, suggesting that recovery in the motor may be accompanied by enhanced functional connectivity between these two brain areas. It also plausibly explains the positive correlation between motor outcome and AH-dominated PMC activation observed in the proximal of the upper limb in this group. We demonstrate from the interhemispheric imbalance of corticospinal excitability combined with the lateralization of cortical activation that multiple mechanisms may be involved in the process of motor function recovery. These may include the compensation of the PMC within the AH and the compensating effect of the UH.

The structure of the brain is complex, and the connections between brain regions are also variable. Our study suggests that combining fNIRS with TMS provides complementary information superior to that of imaging methods in isolation. It helps to deepen our understanding of brain diseases and provides valuable information for further exploration of neural mechanisms.

However, due to the limited sample size in our study, stratified analysis could not be performed. It is the limitation of our present study. Future studies will need to enroll more post-stroke patients to conduct stratified analysis by disease duration, disease severity, and disease type.

5. Conclusion

In conclusion, the present study provided evidence that the interhemispheric imbalance between corticospinal excitability and motor cortex activation can be a biomarker for predicting motor recovery. The combined assessment of TMS and fNIRS can infer the role of both hemispheres in recovery and contribute to the development of effective individualized neuromodulation strategies. Further studies should include more participants with stroke to obtain a reliable relationship between these features and motor function state.

Data availability statement

The original contributions presented in the study are included in the article/supplementary material, further inquiries can be directed to the corresponding authors.

Ethics statement

The studies involving human participants were reviewed and approved by the Ethics Committee of Shanghai No.3 Rehabilitation Hospital. The patients/participants provided their written informed consent to participate in this study.

Author contributions

SC, XZ, and XC are the co-first authors of this paper. They participated in all studies, analyzed the data, drafted and finalized the manuscript. CS and WL are co-corresponding authors of this paper. They contributed to conception and design of the study, supervised the progression, and revised the manuscript. ZZ consulted on data analysis. KC coordinated data collection and performed the statistical analysis. WC and JW collected and sorted out the related materials. QX and ZL were involved in the recruitment of participants. All authors contributed to the manuscript revision, read and approved the submitted version.

Funding

This work was supported by National Natural Science Fund (Grant No. 82272612), Shanghai Jing'an District Health Research Project (Grant No. 2021MS19), Shanghai Clinical Research Center for Rehabilitation Medicine (21MC1930200) and Key Subjects Construction Program of the Health System in Jing'an District (Grant No. 2021PY04).

Acknowledgments

The authors thank all staff members and participants in this study.

Conflict of interest

The authors declare that the research was conducted in the absence of any commercial or financial relationships that could be construed as a potential conflict of interest.

Publisher's note

References

Andrews, S. C., Curtin, D., Coxon, J. P., and Stout, J. C. (2022). Motor cortex plasticity response to acute cardiorespiratory exercise and intermittent theta-burst stimulation is attenuated in premanifest and early Huntington's disease. *Sci. Rep.* 12:1104. doi: 10.1038/s41598-021-04378-2

Avan, A., Digaleh, H., Di Napoli, M., Stranges, S., Behrouz, R., Shojaeianbabaei, G., et al. (2019). Socioeconomic status and stroke incidence, prevalence, mortality, and worldwide burden: an ecological analysis from the global burden of disease study 2017. *BMC Med.* 17:191. doi: 10.1186/s12916-019-1397-3

Badran, B. W., Caulfield, K. A., Cox, C., Lopez, J. W., Borckardt, J. J., DeVries, W. H., et al. (2020). Brain stimulation in zero gravity: transcranial magnetic stimulation (TMS) motor threshold decreases during zero gravity induced by parabolic flight. *NPJ Microgravity* 6:26. doi: 10.1038/s41526-020-00116-6

Bejot, Y., Bailly, H., Durier, J., and Giroud, M. (2016). Epidemiology of stroke in Europe and trends for the 21st century. *Presse Med.* 45, e391–e398. doi: 10.1016/j.lpm.2016.10.003

Bertani, R., Melegari, C., De Cola, M. C., Bramanti, A., Bramanti, P., and Calabro, R. S. (2017). Effects of robot-assisted upper limb rehabilitation in stroke patients: a systematic review with meta-analysis. *Neurol. Sci.* 38, 1561–1569. doi: 10.1007/s10072-017-2995-5

Bertolucci, F., Chisari, C., and Fregni, F. (2018). The potential dual role of transcallosal inhibition in post-stroke motor recovery. *Restor. Neurol. Neurosci.* 36, 83–97. doi: 10.3233/RNN-170778

Borrell, J. A., Fraser, K., Manattu, A. K., and Zuniga, J. M. (2023). Laterality index calculations in a control study of functional near infrared spectroscopy. *Brain Topogr.* 36, 210–222. doi: 10.1007/s10548-023-00942-3

Bradnam, L. V., Stinear, C. M., Barber, P. A., and Byblow, W. D. (2012). Contralesional hemisphere control of the proximal paretic upper limb following stroke. *Cereb. Cortex* 22, 2662–2671. doi: 10.1093/cercor/bhr344

Buetefisch, C. M. (2015). Role of the Contralesional hemisphere in post-stroke recovery of upper extremity motor function. *Front. Neurol.* 6:214. doi: 10.3389/fneur.2015.00214

Chen, N., Qiu, X., Hua, Y., Hu, J., and Bai, Y. (2023). Effects of sequential inhibitory and facilitatory repetitive transcranial magnetic stimulation on neurological and functional recovery of a patient with chronic stroke: a case report and literature review. *Front. Neurol.* 14:1064718. doi: 10.3389/fneur.2023.1064718

Chen, C., Yuan, K., Wang, X., Khan, A., Chu, W. C., and Tong, R. K. (2021). Neural correlates of motor recovery after robot-assisted training in chronic stroke: a multimodal neuroimaging study. *Neural Plast.* 2021, 8866613–8866612. doi: 10.1155/2021/8866613

Cunningham, D. A., Machado, A., Janini, D., Varnerin, N., Bonnett, C., Yue, G., et al. (2015). Assessment of inter-hemispheric imbalance using imaging and noninvasive brain stimulation in patients with chronic stroke. *Arch. Phys. Med. Rehabil.* 96, S94–S103. doi: 10.1016/j.apmr.2014.07.419

de Freitas, Z. A., Romeiro, D. S. A., Baltar, D. R. M. A., Shirahige, G. D. N. L., Bezerra, D. S. A., Piscitelli, D., et al. (2022). Sensory and motor cortical excitability changes induced by rTMS and sensory stimulation in stroke: a randomized clinical trial. *Front. Neurosci.* 16:985754. doi: 10.3389/fnins.2022.985754

Delorme, M., Vergotte, G., Perrey, S., Froger, J., and Laffont, I. (2019). Time course of sensorimotor cortex reorganization during upper extremity task accompanying motor recovery early after stroke: An fNIRS study. *Restor. Neurol. Neurosci.* 37, 207–218. doi: 10.3233/RNN-180877

Di Lazzaro, V., Pellegrino, G., Di Pino, G., Ranieri, F., Lotti, F., Florio, L., et al. (2016). Human motor cortex functional changes in acute stroke: gender effects. *Front. Neurosci.* 10:10. doi: 10.3389/fnins.2016.00010

Di Pino, G., Pellegrino, G., Assenza, G., Capone, F., Ferreri, F., Formica, D., et al. (2014). Modulation of brain plasticity in stroke: a novel model for neurorehabilitation. *Nat. Rev. Neurol.* 10, 597–608. doi: 10.1038/nrneurol.2014.162

Diao, Q., Liu, J., Wang, C., Cao, C., Guo, J., Han, T., et al. (2017). Gray matter volume changes in chronic subcortical stroke: a cross-sectional study. *Neuroimage Clin.* 14, 679–684. doi: 10.1016/j.nicl.2017.01.031

Dionisio, A., Duarte, I. C., Patricio, M., and Castelo-Branco, M. (2018). The use of repetitive transcranial magnetic stimulation for stroke rehabilitation: a systematic review. *J. Stroke Cerebrovasc. Dis.* 27, 1–31. doi: 10.1016/j.jstrokecerebrovasdis.2017.09.008

Du, J., Yang, F., Hu, J., Hu, J., Xu, Q., Cong, N., et al. (2019). Effects of high- and low-frequency repetitive transcranial magnetic stimulation on motor recovery in early stroke patients: evidence from a randomized controlled trial with clinical, neurophysiological and functional imaging assessments. *Neuroimage Clin.* 21:101620. doi: 10.1016/j.nicl.2018.101620

Du, J., Yang, F., Zhang, Z., Hu, J., Xu, Q., Hu, J., et al. (2018). Early functional MRI activation predicts motor outcome after ischemic stroke: a longitudinal, multimodal study. *Brain Imaging Behav.* 12, 1804–1813. doi: 10.1007/s11682-018-9851-y

Dum, R. P., and Strick, P. L. (1991). The origin of corticospinal projections from the premotor areas in the frontal lobe. *J. Neurosci.* 11, 667–689. doi: 10.1523/JNEUROSCI.11-03-00667.1991

Entakli, J., Bonnard, M., Chen, S., Berton, E., and De Graaf, J. B. (2014). TMS reveals a direct influence of spinal projections from human SMAp on precise force production. *Eur. J. Neurosci.* 39, 132–140. doi: 10.1111/ejn.12392

Gladstone, D. J., Danells, C. J., and Black, S. E. (2002). The Fugl-Meyer assessment of motor recovery after stroke: a critical review of its measurement properties. *Neurorehabil. Neural Repair* 16, 232–240. doi: 10.1177/154596802401105171

Groppa, S., Oliviero, A., Eisen, A., Quartarone, A., Cohen, L. G., Mall, V., et al. (2012). A practical guide to diagnostic transcranial magnetic stimulation: report of an IFCN committee. *Clin. Neurophysiol.* 123, 858–882. doi: 10.1016/j.clinph.2012.01.010

Hallett, M., Di Iorio, R., Rossini, P. M., Park, J. E., Chen, R., Celnik, P., et al. (2017). Contribution of transcranial magnetic stimulation to assessment of brain connectivity and networks. *Clin. Neurophysiol.* 128, 2125–2139. doi: 10.1016/j.clinph.2017.08.007

Huo, C., Xu, G., Li, Z., Lv, Z., Liu, Q., Li, W., et al. (2019). Limb linkage rehabilitation training-related changes in cortical activation and effective connectivity after stroke: a functional near-infrared spectroscopy study. *Sci. Rep.* 9:6226. doi: 10.1038/s41598-019-42674-0

Kantak, S. S., Stinear, J. W., Buch, E. R., and Cohen, L. G. (2012). Rewiring the brain: potential role of the premotor cortex in motor control, learning, and recovery of

function following brain injury. *Neurorehabil. Neural Repair* 26, 282–292. doi: 10.1177/1545968311420845

Kelley, B. J., Harel, N. Y., Kim, C. Y., Papademetris, X., Coman, D., Wang, X., et al. (2014). Diffusion tensor imaging as a predictor of locomotor function after experimental spinal cord injury and recovery. *J. Neurotrauma* 31, 1362–1373. doi: 10.1089/neu.2013.3238

Kemlin, C., Moulton, E., Lamy, J. C., Houot, M., Valabregue, R., Leder, S., et al. (2019). Elucidating the structural and functional correlates of upper-limb Poststroke motor impairment. *Stroke* 50, 3647–3649. doi: 10.1161/STROKEAHA.119.027126

Kinoshita, S., Tamashiro, H., Okamoto, T., Urushidani, N., and Abo, M. (2019). Association between imbalance of cortical brain activity and successful motor recovery in sub-acute stroke patients with upper limb hemiparesis: a functional near-infrared spectroscopy study. *Neuroreport* 30, 822–827. doi: 10.1097/WNR.0000000000001283

Kumar, P., Kathuria, P., Nair, P., and Prasad, K. (2016). Prediction of upper limb motor recovery after subacute ischemic stroke using diffusion tensor imaging: a systematic review and Meta-analysis. *J. Stroke* 18, 50–59. doi: 10.5853/jos.2015.01186

Lam, T. K., Binns, M. A., Honjo, K., Dawson, D. R., Ross, B., Stuss, D. T., et al. (2018). Variability in stroke motor outcome is explained by structural and functional integrity of the motor system. *Sci. Rep.* 8:9480. doi: 10.1038/s41598-018-27541-8

Lee, S. H., Jin, S. H., and An, J. (2019). The difference in cortical activation pattern for complex motor skills: a functional near- infrared spectroscopy study. *Sci. Rep.* 9:14066. doi: 10.1038/s41598-019-50644-9

Lefaucheur, J. P., Aleman, A., Baeken, C., Benninger, D. H., Brunelin, J., Di Lazzaro, V., et al. (2020). Evidence-based guidelines on the therapeutic use of repetitive transcranial magnetic stimulation (rTMS): An update (2014-2018). *Clin. Neurophysiol.* 131, 474–528. doi: 10.1016/j.clinph.2019.11.002

Long, H., Wang, H., Zhao, C., Duan, Q., Feng, F., Hui, N., et al. (2018). Effects of combining high- and low-frequency repetitive transcranial magnetic stimulation on upper limb hemiparesis in the early phase of stroke. *Restor. Neurol. Neurosci.* 36, 21–30. doi: 10.3233/RNN-170733

Matsunaga, K., Maruyama, A., Fujiwara, T., Nakanishi, R., Tsuji, S., and Rothwell, J. C. (2005). Increased corticospinal excitability after 5 Hz rTMS over the human supplementary motor area. *J. Physiol.* 562, 295–306. doi: 10.1113/jphysiol.2004.070755

Najib, U., and Horvath, J. C. (2014). "Transcranial Magnetic Stimulation (TMS) Safety Considerations and Recommendations," in *Transcranial Magnetic Stimulation,* eds A. Rotenberg, J. Horvath, and A. Pascual-Leone (New York, NY: Humana Press), 89, 15–30. doi: 10.1007/978-1-4939-0879-0_2

Ni, J., Jiang, W., Gong, X., Fan, Y., Qiu, H., Dou, J., et al. (2022). Effect of rTMS intervention on upper limb motor function after stroke: a study based on fNIRS. *Front. Aging Neurosci.* 14:1077218. doi: 10.3389/fnagi.2022.1077218

Okabe, N., Narita, K., and Miyamoto, O. (2017). Axonal remodeling in the corticospinal tract after stroke: how does rehabilitative training modulate it? *Neural Regen. Res.* 12, 185–192. doi: 10.4103/1673-5374.200792

Patel, S., Ghimire, P., Lavrador, J. P., Jung, J., Gullan, R., Ashkan, K., et al. (2020). Patient-reported experience measures in patients undergoing navigated transcranial magnetic stimulation (nTMS): the introduction of nTMS-PREMs. *Acta Neurochir.* 162, 1673–1681. doi: 10.1007/s00701-020-04268-y

Plow, E. B., Cunningham, D. A., Varnerin, N., and Machado, A. (2015). Rethinking stimulation of the brain in stroke rehabilitation: why higher motor areas might be better alternatives for patients with greater impairments. *Neuroscientist* 21, 225–240. doi: 10.1177/1073858414537381

Prion, S., and Haerling, K. A. (2014). Making sense of methods and measurement: Pearson product moment correlation coefficient. *Clin. Simul. Nurs.* 10, 587–588. doi: 10.1016/j.ecns.2014.07.005

Shen, Q. R., Hu, M. T., Feng, W., Li, K. P., and Wang, W. (2022). Narrative review of noninvasive brain stimulation in stroke rehabilitation. *Med. Sci. Monit.* 28:e938298. doi: 10.12659/MSM.938298

Shirota, Y., Hamada, M., Terao, Y., Ohminami, S., Tsutsumi, R., Ugawa, Y., et al. (2012). Increased primary motor cortical excitability by a single-pulse transcranial magnetic stimulation over the supplementary motor area. *Exp. Brain Res.* 219, 339–349. doi: 10.1007/s00221-012-3095-7

Stinear, C. M., Petoe, M. A., and Byblow, W. D. (2015). Primary motor cortex excitability during recovery after stroke: implications for neuromodulation. *Brain Stimul.* 8, 1183–1190. doi: 10.1016/j.brs.2015.06.015

Tamashiro, H., Kinoshita, S., Okamoto, T., Urushidani, N., and Abo, M. (2019). Effect of baseline brain activity on response to low-frequency rTMS/intensive occupational therapy in poststroke patients with upper limb hemiparesis: a near-infrared spectroscopy study. *Int. J. Neurosci.* 129, 337–343. doi: 10.1080/00207454.2018.1536053

Tang, Q., Li, G., Liu, T., Wang, A., Feng, S., Liao, X., et al. (2015). Modulation of interhemispheric activation balance in motor-related areas of stroke patients with motor recovery: systematic review and meta-analysis of fMRI studies. *Neurosci. Biobehav. Rev.* 57, 392–400. doi: 10.1016/j.neubiorev.2015.09.003

van Lieshout, E., van der Worp, H. B., Visser-Meily, J., and Dijkhuizen, R. M. (2019). Timing of repetitive transcranial magnetic stimulation onset for upper limb function after stroke: a systematic review and Meta-analysis. *Front. Neurol.* 10:1269. doi: 10.3389/fneur.2019.01269

Veldema, J., Nowak, D. A., and Gharabaghi, A. (2021). Resting motor threshold in the course of hand motor recovery after stroke: a systematic review. *J. Neuroeng. Rehabil.* 18:158. doi: 10.1186/s12984-021-00947-8

Wang, H., Arceo, R., Chen, S., Ding, L., Jia, J., and Yao, J. (2019). Effectiveness of interventions to improve hand motor function in individuals with moderate to severe stroke: a systematic review protocol. *BMJ Open* 9:e032413. doi: 10.1136/bmjopen-2019-032413

Wang, D., Wang, J., Zhao, H., Liang, Y., Zhang, W., Li, M., et al. (2023). The relationship between the prefrontal cortex and limb motor function in stroke: a study based on resting-state functional near-infrared spectroscopy. *Brain Res.* 1805:148269. doi: 10.1016/j.brainres.2023.148269

Xu, Y. W., Lin, P., Yao, P. S., Zheng, S. F., and Kang, D. Z. (2021). Structure and function of corticospinal projection originating from supplementary motor area. *Neuroradiology* 63, 1283–1292. doi: 10.1007/s00234-021-02669-z

Yang, Y., Pan, H., Pan, W., Liu, Y., Song, X., Niu, C. M., et al. (2021). Repetitive transcranial magnetic stimulation on the affected hemisphere enhances hand functional recovery in subacute adult stroke patients: a randomized trial. *Front. Aging Neurosci.* 13:636184. doi: 10.3389/fnagi.2021.636184

frontiers | Frontiers in Neuroscience

TYPE Review
PUBLISHED 07 September 2023
DOI 10.3389/fnins.2023.1269880

OPEN ACCESS

EDITED BY
Feng Zhang,
Third Hospital of Hebei Medical University, China

REVIEWED BY
Changming Wang,
Capital Medical University, China
Jiuxing Liang,
South China Normal University, China
Yan Wang,
Chinese Academy of Sciences (CAS), China

*CORRESPONDENCE
Di Zhao
✉ dizhao_sunset@163.com

RECEIVED 31 July 2023
ACCEPTED 23 August 2023
PUBLISHED 07 September 2023

CITATION
Shan J, Gu Y, Zhang J, Hu X, Wu H, Yuan T and Zhao D (2023) A scoping review of physiological biomarkers in autism. *Front. Neurosci.* 17:1269880. doi: 10.3389/fnins.2023.1269880

A scoping review of physiological biomarkers in autism

Jiatong Shan[1,2], Yunhao Gu[3], Jie Zhang[4], Xiaoqing Hu[5,6], Haiyan Wu[7], Tifei Yuan[1] and Di Zhao[1]*

[1]Shanghai Key Laboratory of Psychotic Disorders, Brain Health Institute, National Center for Mental Disorders, Shanghai Mental Health Center, Shanghai Jiao Tong University School of Medicine, Shanghai, China, [2]Department of Arts and Sciences, New York University Shanghai, Shanghai, China, [3]Graduate School of Education, University of Pennsylvania, Philadelphia, PA, United States, [4]Department of Neurology, Institute of Neurology, Sichuan Provincial People's Hospital, School of Medicine, University of Electronic Science and Technology of China, Chengdu, China, [5]Department of Psychology, The State Key Laboratory of Brain and Cognitive Sciences, The University of Hong Kong, Hong Kong, Hong Kong SAR, China, [6]HKU, Shenzhen Institute of Research and Innovation, Shenzhen, China, [7]Center for Cognitive and Brain Sciences and Department of Psychology, Macau, China

Autism spectrum disorder (ASD) is a neurodevelopmental condition characterized by pervasive deficits in social interaction, communication impairments, and the presence of restricted and repetitive behaviors. This complex disorder is a significant public health concern due to its escalating incidence and detrimental impact on quality of life. Currently, extensive investigations are underway to identify prospective susceptibility or predictive biomarkers, employing a physiological biomarker-based framework. However, knowledge regarding physiological biomarkers in relation to Autism is sparse. We performed a scoping review to explore putative changes in physiological activities associated with behaviors in individuals with Autism. We identified studies published between January 2000 and June 2023 from online databases, and searched keywords included electroencephalography (EEG), magnetoencephalography (MEG), electrodermal activity markers (EDA), eye-tracking markers. We specifically detected social-related symptoms such as impaired social communication in ASD patients. Our results indicated that the EEG/ERP N170 signal has undergone the most rigorous testing as a potential biomarker, showing promise in identifying subgroups within ASD and displaying potential as an indicator of treatment response. By gathering current data from various physiological biomarkers, we can obtain a comprehensive understanding of the physiological profiles of individuals with ASD, offering potential for subgrouping and targeted intervention strategies.

KEYWORDS

autism spectrum disorder, physiological biomarkers, electroencephalography, magnetoencephalography, electrodermal activity markers, eye-tracking markers, neurodevelopmental deficits

1. Introduction

1.1. Definition and overview of autism spectrum disorder

Autism spectrum disorder (ASD) represents a neurodevelopmental condition characterized by pervasive deficits in social interaction, communication impairments, and the presence of restricted and repetitive behaviors. This intricate disorder impacts individuals across a wide spectrum, exhibiting varying degrees of severity and manifestations. According to the World Health Organization, it is estimated that the median prevalence of ASD children in studies from

2012 to 2021 worldwide is about 1 in 100 children, with a trend of increasing prevalence over time (Zeidan et al., 2022), and however, the 1% prevalence may still underestimate the prevalence in low- and middle-income countries (Elsabbagh et al., 2012). And in Asia, ASD is probably more common than previously thought. The average prevalence of ASD before 1980 was around 1.9/10,000 while in China the median prevalence of ASD among only 2–6-year-old children who are reported from 2000 upwards was 10.3/10,000 (Sun and Allison, 2010). Fundamentally, ASD involves aberrant patterns of brain development and functioning. Neuroscientific investigations have shed light on the underlying neural mechanisms associated with ASD, revealing alterations in brain connectivity, structural anomalies, and disruptions in neurotransmitter systems.

Impaired social interaction stands out as a prominent feature of ASD. Individuals with ASD commonly encounter difficulties in comprehending and responding to social cues, including facial expressions and gestures (Lord et al., 2018). Challenges in establishing and maintaining reciprocal relationships, coupled with deficits in empathetic understanding, further contribute to the observed social impairments in this disorder. Communication deficits also feature prominently in ASD. Language development may be delayed or absent in certain individuals, while others exhibit atypical speech patterns, such as repetitive or idiosyncratic language usage (Mitchell et al., 2006). Difficulties in understanding and employing nonverbal communication, encompassing gestures and body language, are also prevalent among individuals with ASD. Restricted and repetitive behaviors serve as defining characteristics of ASD (Harrop et al., 2014). These behaviors manifest in diverse forms, including repetitive movements, insistence on sameness, highly focused interests, and adherence to routines. Sensory sensitivities, ranging from hypersensitivity to hyposensitivity to sensory stimuli, are frequently observed in individuals with ASD.

The etiology of ASD is multifactorial, encompassing genetic and environmental factors. Advancements in genetic research have identified numerous genes associated with ASD, contributing to our understanding of the underlying biological mechanisms. Additionally, prenatal, and perinatal factors, such as maternal immune activation and exposure to environmental toxins, have been implicated in ASD development.

1.2. Significance of investigating physiological biomarkers in ASD research

The absence of a discernible biological signature for ASD, most likely attributable to its inherent heterogeneity, poses challenges in accurate prognosis, including the prediction of treatment response and even diagnosis, thereby complicating the clinical landscape (Shen et al., 2020). The field of ASD faces challenges due to the lack of robust, reliable, and valid biomarkers that can facilitate objective diagnosis and personalized treatment recommendations for patients. In this review, we examine and assess the evidence supporting the most promising biomarkers in ASD. The candidate biomarkers under scrutiny encompass electroencephalography markers (EEG), magnetoencephalography markers (MEG), electrodermal activity markers (EDA), and eye-tracking markers. Our aim is to provide a scoping review of the prevalent views on abnormal physiological behaviors in individuals with ASD.

2. Methods

In this study, we conducted a scoping review using Google Scholar as well as PubMed with specific keywords. Subsequently, we implemented three rounds of meticulous screening to identify relevant studies. First, we got 1,544 records from January 2000 to June 2023 by searching relative keywords on PubMed and Google Scholar, and we removed 1,377 records because of duplication. Then we included 81 reports out of 167 records according our inclusion criteria: (1) utilization of a neurophysiological measure; (2) inclusion of an ASD group, encompassing individuals diagnosed with autism, ASD, Asperger syndrome, autistic disorder, or pervasive developmental disorder – not otherwise specified (PDD-NOS); (3) presence of a typically developing (TD) control group; (4) publication in English; and (5) peer-reviewed status. In the third screening process, we examined again based on the previous criteria, and further excluded 31 records further (8 records did not include ASD subjects, 12 records were review, 8 records were non-relevant studies, 1 record was animal model, and 2 were duplicate records). Finally, 50 records were included and analyzed in this scoping review. This whole screening process was done by Jiatong Shan and Di Zhao separately and decision was moderated if there is a difference. As the third party, Yunhao rated each record included, and all included records have relatively high quality.

3. Results

3.1. Event-related potentials in ASD and its connection to abnormal sensory perception

Researchers employ event-related potentials (ERPs) to assess the processing of sensory stimuli, including social cues. No matter for N1, P1, MMN or P300 waves, the experimenters did not get a unified conclusion on the rules of ASD's abnormal amplitude and latency. Some studies think that ASD patients are insensitive to stimuli, that is, the amplitude decreases and the latency increases; some studies show that ASD patients are too sensitive to stimuli, that is, the amplitude increases and the latency decreases. Different types of stimuli also lead to different results; and the result within the ASD group itself is different from that between ASD and the control group (Brandwein et al., 2015).

First, as for N1&P1, studies have shown that the amplitude of N1b is related to the severity of ASD symptoms, for example, the more severe the symptoms of ASD, the smaller the amplitude of N1b (Brandwein et al., 2015). However, a unified conclusion has not been reached in the comparison of P1&N1 waves between the ASD group and the control group. For example, some researchers believe that the N1b amplitude of the ASD group is smaller than that of the control group, which may be due to their insensitivity to sound, resulting in a smaller ERP amplitude (Bruneau et al., 1999); there are also results showing that the N1b amplitude of the ASD group is higher than that of the control group, and the latency is reduced. It was caused by the oversensitivity of the ASD group to sound stimuli (Oades et al., 1988). Both conclusions make sense somehow. In addition, it has been shown in the literature that the type of auditory stimulus also affects the amplitude of early auditory components in children with ASD. For

example, ASD children will not have an increased P1 amplitude under the stimulation of exaggerated verbal stimuli, while normal children tend to increase significantly. It may explain that ASD children lack the neural reinforcement of verbal grandiosity (Chen et al., 2021). This may also explain the inability of children with ASD to understand some emotional words and sentences. But no studies have shown whether this phenomenon persists as children with ASD grow up.

Second, as for the MMN wave, some literature has shown that ASD children respond poorly to changes in some emotional stimuli (such as fear), so they have reduced MMN wave amplitude and prolonged latency to fearful sound stimuli (Korpilahti et al., 2007; Yoshimura et al., 2018). However, the researchers also did not get a unified conclusion on the amplitude and latency of MMN. Another literature believes that the MMN latency of ASD patients is smaller, and the amplitude is larger, indicating that ASD patients are more sensitive to differential stimuli (Gomot et al., 2002; Ferri et al., 2003). There is also literature showing that there is no significant difference in the MMN amplitude of ASD and the control group (Ceponiene et al., 2003). Like the auditory early component, it has been shown that stimulus type also plays a role in the properties of the MMN. For example, MMN waves disappear when ASD children change consonants, suggesting that ASD children have abnormal insensitivity to consonants (Lepistö et al., 2005).

Third, as for the P3 wave (which reflects a shift toward stimuli that requires a change in attention), some results show that there is no change in P3a amplitude in adults with ASD but there is an increased P3a amplitude in children with ASD (Gomot et al., 2002; Ferri et al., 2003), other results show that there is an increased P3a amplitude in adults (Iwanami et al., 2014). It seems that the amplitude of P3a is related to the subject's age. Also, the type of stimulus is equally important. ASD children will only have a disappearance of P3a towards verbal stimuli, and they will not have a disappearance of P3a towards non-verbal stimuli (Ceponiene et al., 2003; Lepistö et al., 2005). This suggests that deficits in children with ASD occur when verbal attention is diverted. In addition, some literature pointed out that the two parameters dP3a and fP3a in P3a should be analyzed separately. The dP3a latency of the ASD group was shorter than that of the control group, and the more severe the symptoms of ASD, the shorter the dP3a latency. And only in the ASD group, the latency of fP3a becomes smaller with age, and there is no such trend in the control group; the more severe the symptoms of the ASD group (such as rejection of physical contact, etc.), the smaller the latency of fP3a (Chien et al., 2018). It is certain that ASD severity seems to be related to the latency of P3a reduction.

Finally, as for the N170 wave, the range of subjects discussed in current papers is wide: from ASD patients, ASD + TSC (tuberous sclerosis), ASD + ADHD, to family members of ASD children. At present, the generally accepted conclusions are: (1) ASD patients have poor ability to process faces. Most of the literature points out that the N170 latency of the control group was shorter when processing faces than when processing objects, but there was no significant difference between the processing of faces and objects in ASD children (Tye et al., 2015). The latency of N170 when processing faces in ASD patients is longer than that in the control group, and 6 literatures have reached this conclusion (McPartland et al., 2004; Webb et al., 2006; O'Connor et al., 2007; McPartland et al., 2011; Jeste et al., 2013; Tye et al., 2013); (2) 12 literatures point out that control group is more sensitive to upside-down faces than positive faces, and the latency of N170 is larger when observing upside-down faces, while ASD patients had no significant difference in N170 latency between upside-down and positive faces (Dawson et al., 2002; McPartland et al., 2004; Dawson et al., 2005; O'Connor et al., 2005, 2007; Webb et al., 2006; McCleery et al., 2009; Batty et al., 2011; Hileman et al., 2011; McPartland et al., 2011; Webb et al., 2012; Tye et al., 2015); in addition, for the lateralization of brain processing faces, 8 literatures believed that normal subjects' N170 is right-sided (reflected in larger amplitude and shorter latency in the right hemisphere), by contrast, ASD patients' N170 is left-sided or no significant difference between two hemispheres (Schultz et al., 2000; Pierce et al., 2001; Carver and Dawson, 2002; McPartland et al., 2004; Senju et al., 2005; McCleery et al., 2009; Tye et al., 2013, 2015); (3) ASD patients also have abnormal eye direction. Some studies suggest that the N170 latency of ASD to averted gaze is longer than that of direct gaze, and the processing of direct gaze is faster, while the control group has no significant difference between the two kinds of gazes (Senju et al., 2005). Some other literature pointed out that there is no significant difference between averted gaze and direct gaze in the ASD group. While the control group process direct gaze much faster. An interesting phenomenon is that the parents of ASD children do not seem to show the effect of left hemisphere lateralization in facial expression processing. While their N170 amplitude is larger in their right hemisphere than in their left hemisphere (Márquez et al., 2019).

3.2. Resting-state EEG abnormalities in ASD and its connection to attention diversion and memory

First, the literature shows that there is no significant difference between the ASD group and the control group in the resting EEG with eyes-closed conditions (Mathewson et al., 2012); however, when the eyes are open and there is visual stimulation, there are some differences in the power and coherence of delta, theta, beta, gamma, alpha in the ASD group. There are 9 literatures that show that the delta, theta, beta, gamma energy of ASD patients is higher than that of the control group, and the alpha energy is lower than that of the control group (Chan et al., 2007; Klimesch et al., 2007; Murias et al., 2007; Coben et al., 2008; Chan et al., 2009; Wang et al., 2013; Mably and Colgin, 2018; Brito et al., 2019; Neuhaus et al., 2021). And there are also 3 literatures showing that the alpha energy of the ASD group is higher than that of the control group (Cantor et al., 1986; Dawson et al., 1995; Mathewson et al., 2012). Because coherence and power are positively correlated, and phase synchronization is closely related to one's ability to prepare for upcoming behaviors. For example, a lower alpha energy could explain a weaker ability to prepare for future behavior due to a lack in spike frequency or insufficient precision for ASD patients (Mathewson et al., 2012; Guyon et al., 2021).

Second, the degree of ASD symptoms is also a factor. Studies have shown that the more severe the ASD, the smaller the energy of gamma, delta, theta, and alpha, which is somewhat different from the above conclusions (Maxwell et al., 2015; Shephard et al., 2018). Gender is also a factor. As men grow older, the gamma energy decreases; and the stronger the social interaction ability of men with ASD, the lower theta, and alpha energies, but there is no such trend for women (Mathewson et al., 2012). Compared with the control group, the alpha frequency decreased more rapidly with age in the ASD group, which

also seems to explain the faster loss of ASD's ability to shift attention (Dickinson et al., 2022).

Finally, about long-range connectivity, only two literature believed that the temporal and frontal lobes connections of ASD were enhanced (Courchesne and Pierce, 2005; Murias et al., 2007), 17 papers believed that the ASD brain connection was weakened (Castelli et al., 2002; Belmonte et al., 2004; Just et al., 2004; Courchesne and Pierce, 2005; Villalobos et al., 2005; Cavanna and Trimble, 2006; Mottron et al., 2006; Boly et al., 2007; Just et al., 2007; Coben et al., 2008; Ben-Sasson et al., 2009; Weng et al., 2010; Marco et al., 2011; Cheng et al., 2015; Padmanabhan et al., 2017; Martínez et al., 2020; Wantzen et al., 2022). The scopes of insufficient connection involve frontal and bilateral temporal & occipital regions; and some higher-order regions which are related with neuron aging processes and pre-existing neuropathology; their default mode network (DMN), the sensorimotor network (SMN), the dorsal attention network (DAN) internal and inter-connection are also insufficient (Cheng et al., 2015; Padmanabhan et al., 2017; Wantzen et al., 2022). These deficiencies lead to memory loss, language deficits, decreased perception of environmental stimuli, and reduced ability to shift attention in ASD patients, which are some common behavioral symptoms in ASD subjects.

3.3. Magnetoencephalography markers

3.3.1. Introduction to MEG and its advantages in measuring neural activity

Since MEG has ability to extract detailed information on the phase and frequency of neural and relative to EEG, MEG has a high temporal resolution and moderate spatial resolution responses, some research literature uses MEG to study the power band of different frequencies both under resting state and task states in patients with ASD. Functional connectivity and complexity in patients with ASD were also studied. Among the selected articles, a total of 8 discussed the application of MEG in ASD, two of which were measured under resting state and the other six were measured under task state.

3.3.2. MEG findings related to sensory processing in ASD

There are 4 literature which point out that ASD children have an abnormal visual processing pattern as well as right lateralization. Besides, all of them study gamma band. Because of different tasks, these literatures draw different conclusions of gamma response. One study of visual tasks (Kikuchi et al., 2013) show that ASD children have a significant rightward connectivity between parietotemporal areas, which is also pointed out by another two reports (Koshino et al., 2005; Monk et al., 2009), *via* an excess of gamma band oscillation (Orekhova et al., 2007). It indicates that ASD children have an abnormal cortical information processing pattern during visual perception and attention (Jensen et al., 2007; Wang, 2010; Kikuchi et al., 2013). Another non-verbal visual reasoning task also achieved similar conclusions (Takesaki et al., 2016). This study shows that some of ASD patients have a better performance in visual reasoning tasks, because they have an increased connectivity with the visual area/stronger connectivity from the occipital area/increased gamma synchronization in V1 supragranular layers and influences V4 through feedforward projections (Khan et al., 2015), and there is a right lateralization (Kikuchi et al., 2013). It shows that the magnitude of feedforward connectivity associated with visual information represents a neurophysiological index of autistic visual strengths (Grandin, 2009a,b).

Two other experiments on visual processing concluded that ASD children's gamma power was smaller in emotional processing and maternal face processing. One used the mother's face to compare with non-facial stimuli (Hasegawa et al., 2023), showing that when ASD children look at their mother's face, their low-frequency (30–59 Hz) gamma power in the right banks of superior temporal sulcus, right fusiform gyrus, right pericalrine cortex decrease compared to TD group; their high frequency (61–90 Hz) gamma power in right banks of superior temporal sulcus, bilateral fusiform gyrus and bilateral pericalcarine cortex also decrease compared to TD group, also revealing the right-sided gamma anomaly in children with ASD and its problems in social communication and face-processing. Another study concludes that young people with ASD have increased response times when looking at emotional faces, The intrinsic mechanism is that gamma responses from right occipital cortex to occipital-fusiform areas and occipital pole is largely absent (Bentin et al., 1996; Bailey et al., 2005; Wright et al., 2012). The conclusion may reveal a potential mechanism that may explain difficulties in face and emotion processing in ASD.

For auditory abnormalities of ASD hearing, studies have shown that the latency of M100 increases, and the more severe the ASD symptoms, the longer the latency of M100 is (100 ms is bilateral primary/secondary auditory cortex time duration). Besides, the transient gamma-band evoked power of ASD children decreases. It shows that ASD children have a perturbed auditory cortex neural activity/reduced conduction velocity (Gage et al., 2003; Wilson et al., 2007; Edgar et al., 2015a,b; Port et al., 2016). As for the factors of hemispheric laterality and age, another study showed that M100 was significantly delayed in the right hemisphere of ASD, and only the normal group had a decrease in M100 latency with increasing age, and ASD did not show this trend (Roberts et al., 2010). Only one study suggested that the M100 latency of ASD was smaller than that of TD (Ferri et al., 2003).

3.3.3. MEG -based connectivity studies in ASD

In an experiment of resting state activity, the functional connectivity (also the coherence between brain regions) of ASD and its complexity surprisingly compensate for each other, with one being higher and the other lower. ASD has a lower complexity in frontal regions in the delta band and occipital-parietal regions in alpha band and a higher complexity in parietal regions in the delta band, central and temporal regions in theta band, frontal-central boundary regions in the gamma band (Khan et al., 2013; Ghanbari et al., 2015). Comparatively, ASD has an increased short-range connectivity in frontal lobe in the delta band and increased long-range connectivity in temporal, parietal and occipital lobes in alpha band (Courchesne and Pierce, 2005; Barttfeld et al., 2011; Ghanbari et al., 2015). This is similar to the conclusion of another study that also studied resting state (Cornew et al., 2012). ASD's relative delta power increases at frontal regions (Cantor et al., 1986; Murias et al., 2007) and alpha band power increases at temporal and parietal regions. In addition, results show that ASD has increased power of all delta and alpha band, theta band, beta and gamma band power (Orekhova et al., 2007; Cornew et al., 2012). Although a few studies believed that the alpha band power of ASD decreased (Cantor

et al., 1986; Murias et al., 2007), this may be related to the fact that the experiment was done in the opening-eye state. This suggests that resting-state oscillatory activity in ASD is location-specific and supports the conclusion that connectivity in these regions increases (Figure 1).

3.4. Electrodermal activity markers

Overview of EDA as a measure of sympathetic nervous system activity and its application in ASD research. Electrodermal activity (EDA) is a property of our human bodies which causes continuous variation in the electrical characteristics of the skin. Our skin resistance varies with the state of sweat glands which is controlled by the sympathetic nervous system. The skin conductance is related with psychological or physiological arousal. If the sympathetic branch in the autonomic nervous system is aroused, the sweat gland activity increases, the skin conductance also increases. So currently, it is mostly used in clinic to track ASD children's both psychologically and physiologically induced autonomic changes. It shows that ASD children have an abnormal pattern of EDA as well as a reduced average EDA in ASD children's resting autonomic regulation. Also, evidence shows that there is a relationship between EDA and sensory symptoms or emotional dysregulation like anxiety as well as some repetitive behaviors in ASD children.

3.4.1. Relationship between EDA markers and emotional regulation difficulties in ASD

The feasibility of using autonomic nervous system (ANS) activity as a marker of anxiety in ASD was explored in a study. Both typically developing children and children with ASD were examined, and significant changes in heart rate and electrodermal activity were observed during anxiety-inducing tasks. However, a differential pattern of response was found between the two groups, indicating an atypical autonomic response to anxiety in ASD characterized by sympathetic

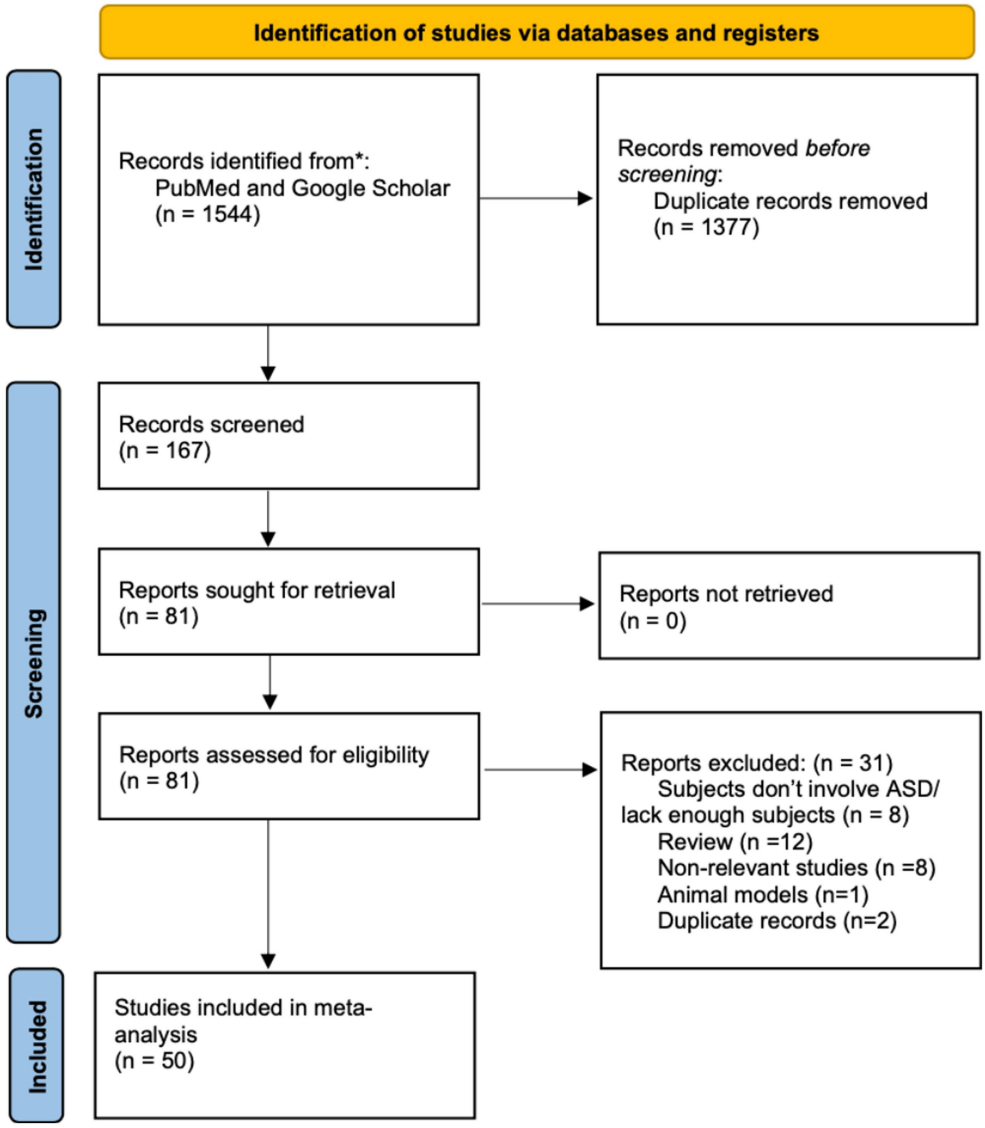

FIGURE 1
The screening process through this scoping review.

over-arousal and parasympathetic under-arousal. Variability in sympathetic nervous system arousal was further examined in relation to symptom severity in children with ASD. The study revealed that EDA in high-anxiety ASD group is different from low-anxiety ASD group. Low-anxiety ASD group has a relatively higher arousal (elevated EDA magnitudes, faster latencies, slower habituation) and high-anxiety ASD group has a lower arousal (lower EDA magnitudes, slower latencies, faster habituation; Panju et al., 2015).

Additionally, the relationship between EDA, sensory symptoms, and repetitive behaviors in children with ASD was explored. Although parents reported higher levels of sensory symptoms and repetitive behaviors in their children with ASD, no significant differences in EDA measures were found between the ASD and typically developing groups. This indicates that the reported differences in symptoms may not be directly related to measured EDA arousal or reactivity (McCormick et al., 2014).

Finally, a study examined the changes in skin conductance level (ΔSCL) in toddlers with ASD and typically developing toddlers in response to anger, joy, and fear emotions. Toddlers with ASD exhibited attenuated ΔSCL in the fear condition, which may predict the emergence of internalizing and externalizing problems. The study suggests that ΔSCL can serve as a dimension associated with behavioral responses in negatively emotionally challenging events in young children (Vernetti et al., 2020). In conclusion, the reviewed studies provide evidence for atypical autonomic function in ASD, particularly in sympathetic activity. The findings underscore the heterogeneity within ASD and emphasize the role of anxiety, autonomic features, and individual variability in understanding the autism spectrum. EDA shows promise as a potential measure of physiological arousal, anxiety, and individual differences within ASD, although further research is needed to fully elucidate its clinical utility.

3.5. Eye-tracking markers

3.5.1. Importance of eye-tracking technology in studying social attention in ASD

Eye-tracking technology is the process of measuring either the point of gaze (eye positions) or the motion of an eye relative to the head (eye movement). Because eye-tracking technology can be used in both static tasks as well as dynamic tasks with videos and study abnormal ASD patients' gaze pattern. Density including response time, fixation frequency, fixation duration, saccade amplitude can be studied in ASD group versus TD group. Several reviewed studies explain the potential relationship between ASD's abnormal gazing pattern and their deficits in social attention and social motivation.

3.5.2. Eye-tracking findings in individuals with ASD

ASD patients have failure to develop normal social relationships, and they also have sensory-perceptual processing deficits that weaken their abilities to attend and perceive social stimuli in daily living contexts. These behavioral abnormalities have something to do with their deficits in interpreting dynamic and interactive social stimuli, especially in reduced gaze at the organs like eyes and mouth. They are less sensitive to their motherese which is opposite in TD group. ASD children have a central coherence weakness (CWW) as well as worse gaze shift in joint attention following others, which means they focus more on specific things instead of global social context as well as they fail to focus on their attention as normal people do.

3.5.3. Correlation between eye-tracking markers and social-communicative deficits in ASD

Different stimuli are studied in a study to test whether there is a significant difference between ASD group and TD group (Chevallier et al., 2015). Result shows that unlike static visual exploration task and dynamic visual exploration (faces and objects presented side-by-side), ASD children show a much less fixation time in the interactive visual exploration task (children are playing with objects) compared to TD group, which also indicates that ASD children have deficits in social attention because they have an abnormal gazing pattern in daily dynamic social stimuli depicting interaction.

Besides, in another study which explores the parts of face ASD patients prefer to gaze at (Jiang et al., 2019), ASD patients are relatively more sensitive to forehead, hair, ears, and chin which are irrelevant to emotion, and they are less sensitive to eyes and mouth compared to TD group. In general, ASD patients have a longer response time, fixation number (the number of fixations subjects make in each trial) and fixation duration, while they have a shorter in fixation frequency (the average number of fixation subjects make in each second of trial). This explains why ASD have difficulties in understanding others' emotions and non-verbal communication.

Additionally, combining with results in fMRI, ASD children have a decreased eye-tracking related attention motherese with reduced activation in superior temporal area. However, TD group has the strongest response to motherese compared to mild and moderate affect speech. This indicates that ASD children have deficits in close relationship. Several studies propose mechanisms behind ASD patients' deficits in social attention (Xiao et al., 2022). First one is CWW. This study analyzes ASD patients' gazing pattern including what part of image and how long they gaze at, as well as let ASD patients to verbally report what they see on the screen. Results show that ASD children have more fixation number in localized AOIs instead of global picture. They cannot understand the whole picture of social context, failing to integrate social cues arising from the recognition of emotions in faces or from the environment in order to understand people's interactions and relationship between social stimuli (Tsang and Chu, 2018; Tassini et al., 2022). Second one is both delay in response and shorter fixation time to visual attention to social stimuli, suggesting ASD patients may misinterpret social information and subsequent social cognitive processing because of skipping registering important momentary social information (Tsang and Chu, 2018). The third one is a reduced ability to engage in joint attention. ASD patients have less gaze shifts and lower gaze accuracy following others' attention. And the more severe ASD symptoms are, the less the gaze shifts are, and lower gaze accuracy is. ASD patients' gaze accuracy is lower when only eye gaze information is available than both eye gaze and head movement are available. This also shows that ASD children have difficulties in communication and social cognition (de Belen et al., 2023).

4. Conclusion

4.1. Recap of physiological biomarkers in ASD

In our review, we screened over 160 literatures, and we focused on 50 literatures in details. Through EEG, MEG, EDA, and

eye-tracking, we conducted a complete and accurate review of ASD patients' abnormal physiological biomarkers as well as their relationship with abnormal social behaviors. In general, ASD patients have abnormal latency, amplitude and power of EEG and MEG wave, suggesting they have abnormal sensory processing, and they also have an abnormal functional connectivity and complexity. Besides, ASD patients have an abnormal EDA and sympathetic nervous system activity, with higher possibility to have emotional regulation difficulties. ASD patients also have deficits in social attention with abnormal gazing pattern to faces and interpreting social context.

4.2. Potential applications and implications of these biomarkers in diagnosis and intervention

These biomarkers imply the abnormalities in social interaction, emotion, sensory processing in ASD patients' daily life, which are what we expect. Through physiological biomarkers, researchers can find a bridge between neural abnormalities and behavioral deficits. For example, a low EDA level shows that patients have a high level of anxiety compared to the typical subjects; less fixation time to the interactive visual exploration tasks shows that patients have deficits in interaction and social communication; and a reduced MMN amplitude and a prolonged MMN latency show that patients have deficits in perceiving emotions. The potential applications of physiological biomarkers in ASD have bright future. For example, researchers can use these physiological biomarkers to detect early symptoms of ASD in children and do some interventions towards ASD. For example, early symptoms may include: no difference of N170 latency to upright and inverted faces; a lower complexity in frontal regions in the delta band and occipital-parietal regions in alpha band and a higher complexity in parietal regions in the delta band, central and temporal regions in theta band, frontal-central boundary regions in the gamma band, etc. Besides, researchers can use certain level of abnormalities in physiological biomarkers to grade the severity of ASD. For instance, the more severe ASD is, the smaller the latency of P3a is; the more severe the symptoms of ASD are, the smaller the amplitude of N1b is; and the more severe the ASD, the smaller the energy of gamma, delta, theta, and alpha are, etc.

4.3. Future directions for research and advancements in the field

Future research should focus more on the studies about EDA and eye-tracking because there are not so many pieces of records on these topics, which means that single and separate result may not ensure the generalizability of the conclusion. Besides, more unified results about EEG and MEG should be made because currently, results really diverge on the amplitude and latency of magnetoencephalogram and electroencephalogram, increasing the difficulty of recognizing and treating ASD patients. More accurate devices, more rigorous measuring methods, and more subjects should be considered in the future studies.

5. Limitation

In this research, we did not include the studies of fNIRS and fMRI as our first proposed title is "A Scoping Review of Electrophysiological Markers in Autism." However, it will be complete to also study what have been done for fNIRS and fMRI. Besides, because we initially wanted to do a systematic review with all literatures in this field, we failed to focus on the novelty of studies, especially for the studies in latest 3 years. In the future, we will include more recent study results. Last but not least, we will modify our review format into a systematic review and do relative meta-analysis to provide a more complete and effective review in the future.

Author contributions

JS: Conceptualization, Formal analysis, Investigation, Methodology, Validation, Visualization, Writing – original draft, Writing – review & editing. YG: Conceptualization, Formal analysis, Investigation, Methodology, Validation, Visualization, Writing – original draft, Writing – review & editing. JZ: Conceptualization, Formal analysis, Investigation, Methodology, Validation, Visualization, Writing – original draft, Writing – review & editing. XH: Conceptualization, Formal analysis, Investigation, Validation, Visualization, Writing – original draft, Writing – review & editing. HW: Conceptualization, Formal analysis, Investigation, Resources, Validation, Writing – original draft, Writing – review & editing. TY: Conceptualization, Formal analysis, Investigation, Validation, Visualization, Writing – original draft, Writing – review & editing. DZ: Conceptualization, Formal analysis, Investigation, Supervision, Validation, Visualization, Writing – original draft, Writing – review & editing.

Funding

The author(s) declare financial support was received for the research, authorship, and/or publication of this article. This study was supported by National Science and Technology Innovation 2030 Major Project of China (2021ZD0203900), NSFC grants (81822017, 82271530, 32241015, 31900765), the Lingang Laboratory (grant no. LG-QS-202203-10), the Science and Technology Commission of Shanghai Municipality (23ZR1480800, 22QA1407900, 21YF1439700), Shanghai Municipal Commission of Health (2022JC016), Shanghai Municipal Education Commission - Gaofeng Clinical Medicine Grant Support (20181715), Innovation teams of high-level universities in Shanghai, Project of Sichuan Department of Science and Technology (grant no. 2023YFS0267, 2022NSFSC1374, and 2021YFS0385), and Project of Sichuan Provincial People's Hospital (grant no. 2022QN04).

Conflict of interest

The authors declare that the research was conducted in the absence of any commercial or financial relationships that could be construed as a potential conflict of interest.

Publisher's note

References

Bailey, A. J., Braeutigam, S., Jousmäki, V., and Swithenby, S. J. (2005). Abnormal activation of face processing systems at early and intermediate latency in individuals with autism spectrum disorder: a magnetoencephalographic study. *Eur. J. Neurosci.* 21, 2575–2585. doi: 10.1111/j.1460-9568.2005.04061.x

Barttfeld, P., Wicker, B., Cukier, S., Navarta, S., Lew, S., and Sigman, M. (2011). A big-world network in ASD: dynamical connectivity analysis reflects a deficit in long-range connections and an excess of short-range connections. *Neuropsychologia* 49, 254–263. doi: 10.1016/j.neuropsychologia.2010.11.024

Batty, M., Meaux, E., Wittemeyer, K., Rogé, B., and Taylor, M. J. (2011). Early processing of emotional faces in children with autism: An event-related potential study. *J. Exp. Child Psychol.* 109, 430–444. doi: 10.1016/j.jecp.2011.02.001

Belmonte, M. K., Allen, G., Beckel-Mitchener, A., Boulanger, L. M., Carper, R. A., and Webb, S. J. (2004). Autism and abnormal development of brain connectivity. *J. Neurosci.* 24, 9228–9231. doi: 10.1523/jneurosci.3340-04.2004

Ben-Sasson, A., Hen, L., Fluss, R., Cermak, S. A., Engel-Yeger, B., and Gal, E. (2009). A meta-analysis of sensory modulation symptoms in individuals with autism spectrum disorders. *J. Autism Dev. Disord.* 39, 1–11. doi: 10.1007/s10803-008-0593-3

Bentin, S., Allison, T., Puce, A., Perez, E., and McCarthy, G. (1996). Electrophysiological studies of face perception in humans. *J. Cogn. Neurosci.* 8, 551–565. doi: 10.1162/jocn.1996.8.6.551

Boly, M., Balteau, E., Schnakers, C., Degueldre, C., Moonen, G., Luxen, A., et al. (2007). Baseline brain activity fluctuations predict somatosensory perception in humans. *Proc. Natl. Acad. Sci. U. S. A.* 104, 12187–12192. doi: 10.1073/pnas.0611404104

Brandwein, A. B., Foxe, J. J., Butler, J. S., Frey, H. P., Bates, J. C., Shulman, L. H., et al. (2015). Neurophysiological indices of atypical auditory processing and multisensory integration are associated with symptom severity in autism. *J. Autism Dev. Disord.* 45, 230–244. doi: 10.1007/s10803-014-2212-9

Brito, N. H., Elliott, A. J., Isler, J. R., Rodriguez, C., Friedrich, C., Shuffrey, L. C., et al. (2019). Neonatal EEG linked to individual differences in socioemotional outcomes and autism risk in toddlers. *Dev. Psychobiol.* 61, 1110–1119. doi: 10.1002/dev.21870

Bruneau, N., Roux, S., Adrien, J. L., and Barthélémy, C. (1999). Auditory associative cortex dysfunction in children with autism: evidence from late auditory evoked potentials (N1 wave-T complex). *Clin. Neurophysiol.* 110, 1927–1934. doi: 10.1016/s1388-2457(99)00149-2

Cantor, D. S., Thatcher, R. W., Hrybyk, M., and Kaye, H. (1986). Computerized EEG analyses of autistic children. *J. Autism Dev. Disord.* 16, 169–187. doi: 10.1007/bf01531728

Carver, L. J., and Dawson, G. (2002). Development and neural bases of face recognition in autism. *Mol. Psychiatry* 7, S18–S20. doi: 10.1038/sj.mp.4001168

Castelli, F., Frith, C., Happé, F., and Frith, U. (2002). Autism, Asperger syndrome and brain mechanisms for the attribution of mental states to animated shapes. *Brain* 125, 1839–1849. doi: 10.1093/brain/awf189

Cavanna, A. E., and Trimble, M. R. (2006). The precuneus: a review of its functional anatomy and behavioural correlates. *Brain* 129, 564–583. doi: 10.1093/brain/awl004

Ceponiene, R., Lepistö, T., Shestakova, A., Vanhala, R., Alku, P., Näätänen, R., et al. (2003). Speech-sound-selective auditory impairment in children with autism: they can perceive but do not attend. *Proc. Natl. Acad. Sci. U. S. A.* 100, 5567–5572. doi: 10.1073/pnas.0835631100

Chan, A. S., Cheung, M. C., Han, Y. M., Sze, S. L., Leung, W. W., Man, H. S., et al. (2009). Executive function deficits and neural discordance in children with autism Spectrum disorders. *Clin. Neurophysiol.* 120, 1107–1115. doi: 10.1016/j.clinph.2009.04.002

Chan, A. S., Sze, S. L., and Cheung, M. C. (2007). Quantitative electroencephalographic profiles for children with autistic spectrum disorder. *Neuropsychology* 21, 74–81. doi: 10.1037/0894-4105.21.1.74

Chen, F., Zhang, H., Ding, H., Wang, S., Peng, G., and Zhang, Y. (2021). Neural coding of formant-exaggerated speech and nonspeech in children with and without autism spectrum disorders. *Autism Res.* 14, 1357–1374. doi: 10.1002/aur.2509

Cheng, W., Rolls, E. T., Gu, H., Zhang, J., and Feng, J. (2015). Autism: reduced connectivity between cortical areas involved in face expression, theory of mind, and the sense of self. *Brain* 138, 1382–1393. doi: 10.1093/brain/awv051

Chevallier, C., Parish-Morris, J., McVey, A., Rump, K. M., Sasson, N. J., Herrington, J. D., et al. (2015). Measuring social attention and motivation in autism spectrum disorder using eye-tracking: stimulus type matters. *Autism Res.* 8, 620–628. doi: 10.1002/aur.1479

Chien, Y. L., Hsieh, M. H., and Gau, S. S. (2018). Mismatch negativity and P3a in adolescents and young adults with autism Spectrum disorders: behavioral correlates and clinical implications. *J. Autism Dev. Disord.* 48, 1684–1697. doi: 10.1007/s10803-017-3426-4

Coben, R., Clarke, A. R., Hudspeth, W., and Barry, R. J. (2008). EEG power and coherence in autistic spectrum disorder. *Clin. Neurophysiol.* 119, 1002–1009. doi: 10.1016/j.clinph.2008.01.013

Cornew, L., Roberts, T. P., Blaskey, L., and Edgar, J. C. (2012). Resting-state oscillatory activity in autism spectrum disorders. *J. Autism Dev. Disord.* 42, 1884–1894. doi: 10.1007/s10803-011-1431-6

Courchesne, E., and Pierce, K. (2005). Why the frontal cortex in autism might be talking only to itself: local over-connectivity but long-distance disconnection. *Curr. Opin. Neurobiol.* 15, 225–230. doi: 10.1016/j.conb.2005.03.001

Dawson, G., Carver, L., Meltzoff, A. N., Panagiotides, H., McPartland, J., and Webb, S. J. (2002). Neural correlates of face and object recognition in young children with autism spectrum disorder, developmental delay, and typical development. *Child Dev.* 73, 700–717. doi: 10.1111/1467-8624.00433

Dawson, G., Klinger, L. G., Panagiotides, H., Lewy, A., and Castelloe, P. (1995). Subgroups of autistic children based on social behavior display distinct patterns of brain activity. *J. Abnorm. Child Psychol.* 23, 569–583. doi: 10.1007/bf01447662

Dawson, G., Webb, S. J., and McPartland, J. (2005). Understanding the nature of face processing impairment in autism: insights from behavioral and electrophysiological studies. *Dev. Neuropsychol.* 27, 403–424. doi: 10.1207/s15326942dn2703_6

de Belen, R. A., Pincham, H., Hodge, A., Silove, N., Sowmya, A., Bednarz, T., et al. (2023). Eye-tracking correlates of response to joint attention in preschool children with autism spectrum disorder. *BMC Psychiatry* 23:211. doi: 10.1186/s12888-023-04585-3

Dickinson, A., Jeste, S., and Milne, E. (2022). Electrophysiological signatures of brain aging in autism spectrum disorder. *Cortex* 148, 139–151. doi: 10.1016/j.cortex.2021.09.022

Edgar, J. C., Fisk Iv, C. L., Berman, J. I., Chudnovskaya, D., Liu, S., Pandey, J., et al. (2015a). Auditory encoding abnormalities in children with autism spectrum disorder suggest delayed development of auditory cortex. *Mol. Autism.* 6:69. doi: 10.1186/s13229-015-0065-5

Edgar, J. C., Khan, S. Y., Blaskey, L., Chow, V. Y., Rey, M., Gaetz, W., et al. (2015b). Neuromagnetic oscillations predict evoked-response latency delays and core language deficits in autism spectrum disorders. *J. Autism Dev. Disord.* 45, 395–405. doi: 10.1007/s10803-013-1904-x

Elsabbagh, M., Divan, G., Koh, Y. J., Kim, Y. S., Kauchali, S., Marcín, C., et al. (2012). Global prevalence of autism and other pervasive developmental disorders. *Autism Res.* 5, 160–179. doi: 10.1002/aur.239

Ferri, R., Elia, M., Agarwal, N., Lanuzza, B., Musumeci, S. A., and Pennisi, G. (2003). The mismatch negativity and the P3a components of the auditory event-related potentials in autistic low-functioning subjects. *Clin. Neurophysiol.* 114, 1671–1680. doi: 10.1016/s1388-2457(03)00153-6

Gage, N. M., Siegel, B., and Roberts, T. P. (2003). Cortical auditory system maturational abnormalities in children with autism disorder: an MEG investigation. *Brain Res. Dev. Brain Res.* 144, 201–209. doi: 10.1016/s0165-3806(03)00172-x

Ghanbari, Y., Bloy, L., Christopher Edgar, J., Blaskey, L., Verma, R., and Roberts, T. P. (2015). Joint analysis of band-specific functional connectivity and signal complexity in autism. *J. Autism Dev. Disord.* 45, 444–460. doi: 10.1007/s10803-013-1915-7

Gomot, M., Giard, M. H., Adrien, J. L., Barthelemy, C., and Bruneau, N. (2002). Hypersensitivity to acoustic change in children with autism: electrophysiological evidence of left frontal cortex dysfunctioning. *Psychophysiology* 39, 577–584. doi: 10.1111/1469-8986.3950577

Grandin, T. (2009a). How does visual thinking work in the mind of a person with autism? A personal account. *Philos. Trans. R. Soc. Lond. Ser. B Biol. Sci.* 364, 1437–1442. doi: 10.1098/rstb.2008.0297

Grandin, T. (2009b). Visual abilities and sensory differences in a person with autism. *Biol. Psychiatry* 65, 15–16. doi: 10.1016/j.biopsych.2008.11.005

Guyon, N., Zacharias, L. R., Fermino de Oliveira, E., Kim, H., Leite, J. P., Lopes-Aguiar, C., et al. (2021). Network asynchrony underlying increased broadband gamma power. *J. Neurosci.* 41, 2944–2963. doi: 10.1523/jneurosci.2250-20.2021

Harrop, C., McConachie, H., Emsley, R., Leadbitter, K., and Green, J. (2014). Restricted and repetitive behaviors in autism spectrum disorders and typical

development: cross-sectional and longitudinal comparisons. *J. Autism Dev. Disord.* 44, 1207–1219. doi: 10.1007/s10803-013-1986-5

Hasegawa, C., Ikeda, T., Yoshimura, Y., Kumazaki, H., Saito, D., Yaoi, K., et al. (2023). Reduced gamma oscillation during visual processing of the mother's face in children with autism spectrum disorder: a pilot study. *Psychiatry Clin Neurosci Rep* 2:e68. doi: 10.1002/pcn5.68

Hileman, C. M., Henderson, H., Mundy, P., Newell, L., and Jaime, M. (2011). Developmental and individual differences on the P1 and N170 ERP components in children with and without autism. *Dev. Neuropsychol.* 36, 214–236. doi: 10.1080/87565641.2010.549870

Iwanami, A., Okajima, Y., Ota, H., Tani, M., Yamada, T., Yamagata, B., et al. (2014). P300 component of event-related potentials in persons with Asperger disorder. *J. Clin. Neurophysiol.* 31, 493–499. doi: 10.1097/wnp.0000000000000080

Jensen, O., Kaiser, J., and Lachaux, J. P. (2007). Human gamma-frequency oscillations associated with attention and memory. *Trends Neurosci.* 30, 317–324. doi: 10.1016/j.tins.2007.05.001

Jeste, S. S., Hirsch, S., Vogel-Farley, V., Norona, A., Navalta, M. C., Gregas, M. C., et al. (2013). Atypical face processing in children with tuberous sclerosis complex. *J. Child Neurol.* 28, 1569–1576. doi: 10.1177/0883073812465122

Jiang, M., Francis, S. M., Srishyla, D., Conelea, C., Zhao, Q., and Jacob, S. (2019). Classifying individuals with ASD through facial emotion recognition and eye-tracking. *Annu Int Conf IEEE Eng Med Biol Soc* 2019, 6063–6068. doi: 10.1109/embc.2019.8857005

Just, M. A., Cherkassky, V. L., Keller, T. A., Kana, R. K., and Minshew, N. J. (2007). Functional and anatomical cortical underconnectivity in autism: evidence from an FMRI study of an executive function task and corpus callosum morphometry. *Cereb. Cortex* 17, 951–961. doi: 10.1093/cercor/bhl006

Just, M. A., Cherkassky, V. L., Keller, T. A., and Minshew, N. J. (2004). Cortical activation and synchronization during sentence comprehension in high-functioning autism: evidence of underconnectivity. *Brain* 127, 1811–1821. doi: 10.1093/brain/awh199

Khan, S., Gramfort, A., Shetty, N. R., Kitzbichler, M. G., Ganesan, S., Moran, J. M., et al. (2013). Local and long-range functional connectivity is reduced in concert in autism spectrum disorders. *Proc. Natl. Acad. Sci. U. S. A.* 110, 3107–3112. doi: 10.1073/pnas.1214533110

Khan, S., Michmizos, K., Tommerdahl, M., Ganesan, S., Kitzbichler, M. G., Zetino, M., et al. (2015). Somatosensory cortex functional connectivity abnormalities in autism show opposite trends, depending on direction and spatial scale. *Brain* 138, 1394–1409. doi: 10.1093/brain/awv043

Kikuchi, M., Shitamichi, K., Yoshimura, Y., Ueno, S., Hiraishi, H., Hirosawa, T., et al. (2013). Altered brain connectivity in 3-to 7-year-old children with autism spectrum disorder. *Neuroimage Clin* 2, 394–401. doi: 10.1016/j.nicl.2013.03.003

Klimesch, W., Sauseng, P., and Hanslmayr, S. (2007). EEG alpha oscillations: the inhibition-timing hypothesis. *Brain Res. Rev.* 53, 63–88. doi: 10.1016/j.brainresrev.2006.06.003

Korpilahti, P., Jansson-Verkasalo, E., Mattila, M. L., Kuusikko, S., Suominen, K., Rytky, S., et al. (2007). Processing of affective speech prosody is impaired in Asperger syndrome. *J. Autism Dev. Disord.* 37, 1539–1549. doi: 10.1007/s10803-006-0271-2

Koshino, H., Carpenter, P. A., Minshew, N. J., Cherkassky, V. L., Keller, T. A., and Just, M. A. (2005). Functional connectivity in an fMRI working memory task in high-functioning autism. *NeuroImage* 24, 810–821. doi: 10.1016/j.neuroimage.2004.09.028

Lepistö, T., Kujala, T., Vanhala, R., Alku, P., Huotilainen, M., and Näätänen, R. (2005). The discrimination of and orienting to speech and non-speech sounds in children with autism. *Brain Res.* 1066, 147–157. doi: 10.1016/j.brainres.2005.10.052

Lord, C., Elsabbagh, M., Baird, G., and Veenstra-Vanderweele, J. (2018). Autism spectrum disorder. *Lancet* 392, 508–520. doi: 10.1016/S0140-6736(18)31129-2

Mably, A. J., and Colgin, L. L. (2018). Gamma oscillations in cognitive disorders. *Curr. Opin. Neurobiol.* 52, 182–187. doi: 10.1016/j.conb.2018.07.009

Marco, E. J., Hinkley, L. B., Hill, S. S., and Nagarajan, S. S. (2011). Sensory processing in autism: a review of neurophysiologic findings. *Pediatr. Res.* 69, 48r–54r. doi: 10.1203/PDR.0b013e3182130c54

Márquez, C., Nicolini, H., Crowley, M. J., and Solís-Vivanco, R. (2019). Early processing (N170) of infant faces in mothers of children with autism spectrum disorder and its association with maternal sensitivity. *Autism Res.* 12, 744–758. doi: 10.1002/aur.2102

Martínez, K., Martínez-García, M., Marcos-Vidal, L., Janssen, J., Castellanos, F. X., Pretus, C., et al. (2020). Sensory-to-cognitive systems integration is associated with clinical severity in autism Spectrum disorder. *J. Am. Acad. Child Adolesc. Psychiatry* 59, 422–433. doi: 10.1016/j.jaac.2019.05.033

Mathewson, K. J., Jetha, M. K., Drmic, I. E., Bryson, S. E., Goldberg, J. O., and Schmidt, L. A. (2012). Regional EEG alpha power, coherence, and behavioral symptomatology in autism spectrum disorder. *Clin. Neurophysiol.* 123, 1798–1809. doi: 10.1016/j.clinph.2012.02.061

Maxwell, C. R., Villalobos, M. E., Schultz, R. T., Herpertz-Dahlmann, B., Konrad, K., and Kohls, G. (2015). Atypical laterality of resting gamma oscillations in autism spectrum disorders. *J. Autism Dev. Disord.* 45, 292–297. doi: 10.1007/s10803-013-1842-7

McCleery, J. P., Akshoomoff, N., Dobkins, K. R., and Carver, L. J. (2009). Atypical face versus object processing and hemispheric asymmetries in 10-month-old infants at risk for autism. *Biol. Psychiatry* 66, 950–957. doi: 10.1016/j.biopsych.2009.07.031

McCormick, C., Hessl, D., Macari, S. L., Ozonoff, S., Green, C., and Rogers, S. J. (2014). Electrodermal and behavioral responses of children with autism spectrum disorders to sensory and repetitive stimuli. *Autism Res.* 7, 468–480. doi: 10.1002/aur.1382

McPartland, J., Dawson, G., Webb, S. J., Panagiotides, H., and Carver, L. J. (2004). Event-related brain potentials reveal anomalies in temporal processing of faces in autism spectrum disorder. *J. Child Psychol. Psychiatry* 45, 1235–1245. doi: 10.1111/j.1469-7610.2004.00318.x

McPartland, J. C., Wu, J., Bailey, C. A., Mayes, L. C., Schultz, R. T., and Klin, A. (2011). Atypical neural specialization for social percepts in autism spectrum disorder. *Soc. Neurosci.* 6, 436–451. doi: 10.1080/17470919.2011.586880

Mitchell, S., Brian, J., Zwaigenbaum, L., Roberts, W., Szatmari, P., Smith, I., et al. (2006). Early language and communication development of infants later diagnosed with autism spectrum disorder. *J. Dev. Behav. Pediatr.* 27, S69–S78. doi: 10.1097/00004703-200604002-00004

Monk, C. S., Peltier, S. J., Wiggins, J. L., Weng, S. J., Carrasco, M., Risi, S., et al. (2009). Abnormalities of intrinsic functional connectivity in autism spectrum disorders. *NeuroImage* 47, 764–772. doi: 10.1016/j.neuroimage.2009.04.069

Mottron, L., Dawson, M., Soulières, I., Hubert, B., and Burack, J. (2006). Enhanced perceptual functioning in autism: an update, and eight principles of autistic perception. *J. Autism Dev. Disord.* 36, 27–43. doi: 10.1007/s10803-005-0040-7

Murias, M., Webb, S. J., Greenson, J., and Dawson, G. (2007). Resting state cortical connectivity reflected in EEG coherence in individuals with autism. *Biol. Psychiatry* 62, 270–273. doi: 10.1016/j.biopsych.2006.11.012

Neuhaus, E., Lowry, S. J., Santhosh, M., Kresse, A., Edwards, L. A., Keller, J., et al. (2021). Resting state EEG in youth with ASD: age, sex, and relation to phenotype. *J. Neurodev. Disord.* 13:33. doi: 10.1186/s11689-021-09390-1

Oades, R. D., Walker, M. K., Geffen, L. B., and Stern, L. M. (1988). Event-related potentials in autistic and healthy children on an auditory choice reaction time task. *Int. J. Psychophysiol.* 6, 25–37. doi: 10.1016/0167-8760(88)90032-3

O'Connor, K., Hamm, J. P., and Kirk, I. J. (2005). The neurophysiological correlates of face processing in adults and children with Asperger's syndrome. *Brain Cogn.* 59, 82–95. doi: 10.1016/j.bandc.2005.05.004

O'Connor, K., Hamm, J. P., and Kirk, I. J. (2007). Neurophysiological responses to face, facial regions and objects in adults with Asperger's syndrome: an ERP investigation. *Int. J. Psychophysiol.* 63, 283–293. doi: 10.1016/j.ijpsycho.2006.12.001

Orekhova, E. V., Stroganova, T. A., Nygren, G., Tsetlin, M. M., Posikera, I. N., Gillberg, C., et al. (2007). Excess of high frequency electroencephalogram oscillations in boys with autism. *Biol. Psychiatry* 62, 1022–1029. doi: 10.1016/j.biopsych.2006.12.029

Padmanabhan, A., Lynch, C. J., Schaer, M., and Menon, V. (2017). The default mode network in autism. *Biol Psychiatry Cogn Neurosci Neuroimaging* 2, 476–486. doi: 10.1016/j.bpsc.2017.04.004

Panju, S., Brian, J., Dupuis, A., Anagnostou, E., and Kushki, A. (2015). Atypical sympathetic arousal in children with autism spectrum disorder and its association with anxiety symptomatology. *Mol. Autism.* 6:64. doi: 10.1186/s13229-015-0057-5

Pierce, K., Müller, R. A., Ambrose, J., Allen, G., and Courchesne, E. (2001). Face processing occurs outside the fusiform 'face area' in autism: evidence from functional MRI. *Brain* 124, 2059–2073. doi: 10.1093/brain/124.10.2059

Port, R. G., Edgar, J. C., Ku, M., Bloy, L., Murray, R., Blaskey, L., et al. (2016). Maturation of auditory neural processes in autism spectrum disorder - a longitudinal MEG study. *Neuroimage Clin* 11, 566–577. doi: 10.1016/j.nicl.2016.03.021

Roberts, T. P., Khan, S. Y., Rey, M., Monroe, J. F., Cannon, K., Blaskey, L., et al. (2010). MEG detection of delayed auditory evoked responses in autism spectrum disorders: towards an imaging biomarker for autism. *Autism Res.* 3, 8–18. doi: 10.1002/aur.111

Schultz, R. T., Gauthier, I., Klin, A., Fulbright, R. K., Anderson, A. W., Volkmar, F., et al. (2000). Abnormal ventral temporal cortical activity during face discrimination among individuals with autism and Asperger syndrome. *Arch. Gen. Psychiatry* 57, 331–340. doi: 10.1001/archpsyc.57.4.331

Senju, A., Tojo, Y., Yaguchi, K., and Hasegawa, T. (2005). Deviant gaze processing in children with autism: an ERP study. *Neuropsychologia* 43, 1297–1306. doi: 10.1016/j.neuropsychologia.2004.12.002

Shen, L., Liu, X., Zhang, H., Lin, J., Feng, C., and Iqbal, J. (2020). Biomarkers in autism spectrum disorders: current progress. *Clin. Chim. Acta* 502, 41–54. doi: 10.1016/j.cca.2019.12.009

Shephard, E., Tye, C., Ashwood, K. L., Azadi, B., Asherson, P., Bolton, P. F., et al. (2018). Resting-state neurophysiological activity patterns in young people with ASD, ADHD, and ASD + ADHD. *J. Autism Dev. Disord.* 48, 110–122. doi: 10.1007/s10803-017-3300-4

Sun, X., and Allison, C. (2010). A review of the prevalence of autism Spectrum disorder in Asia. *Res. Autism Spectr. Disord.* 4, 156–167. doi: 10.1016/j.rasd.2009.10.003

Takesaki, N., Kikuchi, M., Yoshimura, Y., Hiraishi, H., Hasegawa, C., Kaneda, R., et al. (2016). The contribution of increased gamma band connectivity to visual non-verbal reasoning in autistic children: a MEG study. *PLoS One* 11:e0163133. doi: 10.1371/journal.pone.0163133

Tassini, S. C. V., Melo, M. C., Bueno, O. F. A., and de Mello, C. B. (2022). Weak central coherence in adults with ASD: evidence from eye-tracking and thematic content analysis of social scenes. *Appl. Neuropsychol. Adult* 1–12. doi: 10.1080/23279095.2022.2060105

Tsang, V., and Chu, P. C. K. (2018). Comparing eye-tracking data of children with high-functioning ASD, comorbid ADHD, and of a control watching social videos. *J. Vis. Exp*. 142:e58694. doi: 10.3791/58694

Tye, C., Farroni, T., Volein, Á., Mercure, E., Tucker, L., Johnson, M. H., et al. (2015). Autism diagnosis differentiates neurophysiological responses to faces in adults with tuberous sclerosis complex. *J. Neurodev. Disord*. 7:33. doi: 10.1186/s11689-015-9129-2

Tye, C., Mercure, E., Ashwood, K. L., Azadi, B., Asherson, P., Johnson, M. H., et al. (2013). Neurophysiological responses to faces and gaze direction differentiate children with ASD, ADHD and ASD+ADHD. *Dev. Cogn. Neurosci.* 5, 71–85. doi: 10.1016/j.dcn.2013.01.001

Vernetti, A., Shic, F., Boccanfuso, L., Macari, S., Kane-Grade, F., Milgramm, A., et al. (2020). Atypical emotional electrodermal activity in toddlers with autism Spectrum disorder. *Autism Res.* 13, 1476–1488. doi: 10.1002/aur.2374

Villalobos, M. E., Mizuno, A., Dahl, B. C., Kemmotsu, N., and Müller, R. A. (2005). Reduced functional connectivity between V1 and inferior frontal cortex associated with visuomotor performance in autism. *NeuroImage* 25, 916–925. doi: 10.1016/j.neuroimage.2004.12.022

Wang, X. J. (2010). Neurophysiological and computational principles of cortical rhythms in cognition. *Physiol. Rev.* 90, 1195–1268. doi: 10.1152/physrev.00035.2008

Wang, J., Barstein, J., Ethridge, L. E., Mosconi, M. W., Takarae, Y., and Sweeney, J. A. (2013). Resting state EEG abnormalities in autism spectrum disorders. *J. Neurodev. Disord*. 5:24. doi: 10.1186/1866-1955-5-24

Wantzen, P., Clochon, P., Doidy, F., Wallois, F., Mahmoudzadeh, M., Desaunay, P., et al. (2022). EEG resting-state functional connectivity: evidence for an imbalance of external/internal information integration in autism. *J. Neurodev. Disord.* 14:47. doi: 10.1186/s11689-022-09456-8

Webb, S. J., Dawson, G., Bernier, R., and Panagiotides, H. (2006). ERP evidence of atypical face processing in young children with autism. *J. Autism Dev. Disord.* 36, 881–890. doi: 10.1007/s10803-006-0126-x

Webb, S. J., Merkle, K., Murias, M., Richards, T., Aylward, E., and Dawson, G. (2012). ERP responses differentiate inverted but not upright face processing in adults with ASD. *Soc. Cogn. Affect. Neurosci.* 7, 578–587. doi: 10.1093/scan/nsp002

Weng, S. J., Wiggins, J. L., Peltier, S. J., Carrasco, M., Risi, S., Lord, C., et al. (2010). Alterations of resting state functional connectivity in the default network in adolescents with autism spectrum disorders. *Brain Res.* 1313, 202–214. doi: 10.1016/j.brainres.2009.11.057

Wilson, T. W., Rojas, D. C., Reite, M. L., Teale, P. D., and Rogers, S. J. (2007). Children and adolescents with autism exhibit reduced MEG steady-state gamma responses. *Biol. Psychiatry* 62, 192–197. doi: 10.1016/j.biopsych.2006.07.002

Wright, B., Alderson-Day, B., Prendergast, G., Bennett, S., Jordan, J., Whitton, C., et al. (2012). Gamma activation in young people with autism spectrum disorders and typically-developing controls when viewing emotions on faces. *PLoS One* 7:e41326. doi: 10.1371/journal.pone.0041326

Xiao, Y., Wen, T. H., Kupis, L., Eyler, L. T., Goel, D., Vaux, K., et al. (2022). Neural responses to affective speech, including motherese, map onto clinical and social eye tracking profiles in toddlers with ASD. *Nat. Hum. Behav.* 6, 443–454. doi: 10.1038/s41562-021-01237-y

Yoshimura, Y., Kikuchi, M., Hiraishi, H., Hasegawa, C., Hirosawa, T., Takahashi, T., et al. (2018). Longitudinal changes in the mismatch field evoked by an empathic voice reflect changes in the empathy quotient in autism spectrum disorder. *Psychiatry Res. Neuroimaging* 281, 117–122. doi: 10.1016/j.pscychresns.2018.05.003

Zeidan, J., Fombonne, E., Scorah, J., Ibrahim, A., Durkin, M. S., Saxena, S., et al. (2022). Global prevalence of autism: a systematic review update. *Autism Res.* 15, 778–790. doi: 10.1002/aur.2696

frontiers | Frontiers in Neuroscience

TYPE Original Research
PUBLISHED 12 September 2023
DOI 10.3389/fnins.2023.1255354

OPEN ACCESS

EDITED BY
Ying Shen,
The First Affiliated Hospital of Nanjing Medical University, China

REVIEWED BY
Qian Ding,
Guangdong Provincial People's Hospital, China
Huixian Yu,
Capital Medical University, China

*CORRESPONDENCE
Jia-Ning Xi
✉ wmf19920910@126.com

RECEIVED 08 July 2023
ACCEPTED 29 August 2023
PUBLISHED 12 September 2023

CITATION
Yang Z-Q, Wei M-F and Xi J-N (2023) Prefrontal activation in response to a plantar contact task under open and closed eye conditions in patients with cerebral infarction.
Front. Neurosci. 17:1255354.
doi: 10.3389/fnins.2023.1255354

Prefrontal activation in response to a plantar contact task under open and closed eye conditions in patients with cerebral infarction

Zhi-Quan Yang[1,2], Meng-Fan Wei[2] and Jia-Ning Xi[1]*

[1]Beijing Rehabilitation Hospital, Capital Medical University, Beijing, China, [2]Beijing Zhongguancun Hospital/Zhongguancun Hospital, Chinese Academy of Sciences, Beijing, China

Objective: This study investigates the effect of a bilateral (paralyzed side, healthy side) plantar contact task on dorsolateral prefrontal activation in patients recovering from cerebral infarction under open and closed eye conditions.

Methods: We selected 10 patients with cerebral infarction, admitted to the neurorehabilitation center of Beijing Rehabilitation Hospital, affiliated with Capital Medical University, from January 2019 to July 2020, who met our established criteria. Under open-eye and closed-eye conditions, the paralyzed and healthy sides performed the plantar contact tasks separately. The dorsolateral prefrontal region was monitored simultaneously with functional near-infrared spectroscopy (fNIRS), and activation was analyzed according to the curve-type changes of oxyhemoglobin and deoxyhemoglobin changes in the dorsolateral prefrontal cortex with 560 near-infrared monitoring channels.

Results: After stratifying the data based on the eyes-open and eyes-closed conditions, some degree of heterogeneity was observed between the layers. Under the eyes-closed condition, the Pearson χ^2 was 0.142, with a p value of 0.706, indicating no significant impact of the eyes-closed condition on the activation of the dorsolateral prefrontal cortex during the plantar task, whether performed on the paralyzed or the healthy side.

In contrast, the Pearson χ^2 value was 15.15 for the eyes-open condition, with a p value of 0.002. This suggests that carrying out the plantar task, either on the paralyzed or the healthy side, with eyes open significantly influenced the activation of the dorsolateral prefrontal cortex. Furthermore, activation of the dorsolateral prefrontal cortex was 1.55 times higher when the task was executed with the paralyzed side compared to the healthy side. This implies that the paralyzed side was more likely to activate the dorsolateral prefrontal lobe when performing the plantar contact task under eyes-open conditions.

Conclusion: Observations via fNIRS revealed that the plantar contact task elicited dorsolateral prefrontal cortex activation. Moreover, the activation effect was intensified when performed on the paralyzed side under eyes-open conditions. Therapeutic methods that leverage these findings—namely cognitive-motor therapies that promote the recovery of motor functions by activating cognitive control brain regions via perception (information construction)—may hold promise.

KEYWORDS

fNIRS, plantar contact task, cerebral infarction, dorsolateral prefrontal lobe, rehabilitative

1. Introduction

Stroke is a disease caused by impaired cerebral blood circulation with a high rate of disability (Maenza et al., 2020). Studies indicate that approximately 90% of individuals recovering from stroke experience varying levels of functional impairment, with walking dysfunction among the most prominent (Hobbs and Artemiadis, 2020). Hemiparesis (Bogousslavsky et al., 1996), the most common functional deficit among patients with cerebral infarction, often results in patients' inability to walk independently, necessitating reliance on assistance from others or wheelchair use for mobility. Even those who regained independent walking face challenges such as decreased foot contouring ability, compromised lower limb stability, and diminished walking efficiency due to foot drop during the swing phase and foot lateral edge contact at the end of the stance phase. These complications contribute to reduced ambulatory capabilities and a significantly increased fall risk. This severely affects patients' mobility, safety, and quality of life, acting as a major barrier for stroke survivors with hemiplegia to reintegrate into their families and society.

Regaining walking ability is a major task for motor function and activities of daily living (ADL) rehabilitation in hemiplegic stroke patients. In clinical practice, cognitive-motor therapy, which emphasizes perceptual input and cognitive-driven movement, has been increasingly practiced clinically in improving walking ability in patients with cerebral infarction, especially in tasks requiring attention and processing speed, such as multitasking and gait adaptation tasks (Montero-Odasso et al., 2012). Some studies demonstrated the importance of cortical function for locomotion, as well as a greater emphasis on some methods to improve motor function by activating cognitive processes in the cortex (Fritz et al., 2015; Pothier et al., 2018; Hazra et al., 2022). In addition, cognitive-motor training, in which a cognitive task is performed alongside motor training, can more effectively strengthen the functional brain network connections between motor-cognitive brain areas and facilitate the activation of the cerebral cortex, thus promoting brain functional network remodeling and improving the patient's functional impairment (Caetano et al., 2017; Pang et al., 2018). However, the mechanism of action may involve brain functional remodeling, motor relearning, and neural facilitation, but its neurophysiological mechanism is not established.

Hence, we designed a plantar contact task based on the therapeutic principles of cognitive-motor therapy and used a portable fNIRS technique to monitor its effects on dorsolateral prefrontal activation during the treatment to analyze and explore the possible mechanisms of perception (constructing information) to promote motor function recovery. We hypothesize that cognitive-motor therapy can promote the recovery of motor function in cerebral infarction patients by activating cognitive control of brain areas through perceptual haptics.

Abbreviations: fNIRS, Functional near-infrared spectroscopy; ADL, Activities of daily living; Oxy-Hb, Oxygenated hemoglobin; Deoxy-Hb, Deoxygenated hemoglobin; NIR, near-Infrared; PFC, Prefrontal cortex; Fp, Frontopolar midline point; ROIs, Regions of interest; RDPFC, Right dorsolateral prefrontal cortex; LDPFC, Left dorsolateral prefrontal cortex; OR, Odds ratio.

2. Research subjects and methods

2.1. Research subjects

We selected 10 patients with cerebral infarction, admitted to the neurorehabilitation center of Beijing Rehabilitation Hospital, affiliated with Capital Medical University, from January 2019 to July 2020, who met our established criteria. The inclusion criteria included: ① Patients who met the diagnostic criteria of cerebral infarction formulated by the Fourth Academic Conference on Cerebrovascular Diseases (Neurology CSo, 2015) and confirmed as the first onset by cranial CT or MRI examination; ② Aged between 18 and 65 years; ③ Duration of disease less than 6 months, stable vital signs, clear consciousness, and ability to follow instructions; ④ Absence of serious acute or chronic heart valve disease, cardiomyopathy, frequent recent attacks of angina pectoris, unstable angina pectoris, or other organic heart diseases; ⑤ The ability to maintain an independent sitting position with knees capable of more than 90 degrees flexion and feet capable of sliding backward; ⑥ Normal vestibular system function and proprioception.

The exclusion criteria included: ① Pregnant or lactating women; ② Those with involuntary twitching, tremor, or other severe organic diseases and neurological diseases, who were unable to cooperate with the completion of the examination; ③ Aphasia; ④ Mental impairment, hearing impairment, comprehension impairment, or severe cognitive impairment; ⑤ History of orthopedic surgery, hip dislocation, unhealed fractures, or severe osteoporosis; ⑥ Presence of scoliosis and other spinal deformities; ⑦ Malignant tumors, bleeding tendency; ⑧ Patients with deteriorating conditions, with new infarct foci, or cerebral hemorrhage.

The study was approved by the Ethics Committee of Beijing Rehabilitation Hospital, Capital Medical University, and all study subjects provided written informed consent.

2.2. Research methods

2.2.1. Apparatus for fNIRS test

This study used a portable fNIRS brain imaging system, from Shimadzu, Japan (Figure 1). This system employs a 3-wavelength (780 nm, 805 nm, and 830 nm) absorbance meter algorithm to measure the changes in oxygenated hemoglobin (Oxy-Hb),

FIGURE 1
Portable fNIRS brain imaging system.

deoxygenated hemoglobin (Deoxy-Hb), and total hemoglobin concentrations. The light source of this system is a 3-wavelength near-infrared (NIR) semiconductor laser, and the detector is an avalanche photodiode. The device is powered by a 15 V AC adapter or a lithium battery, and the external output includes a 3-bit digital signal and a 10-bit analog signal. The dimensions are W253 × D222 × H68 mm (excluding protruding parts), and the weight is approximately 1,600 g (excluding the computer, battery, and fiber).

The equipment comprises an optical fiber, a probe, fNIRS detection equipment, and a laptop computer. The probe is color-coded, with red representing an integrated LED light source head combining 780, 805, and 830 nm wavelengths, while blue indicates the near-infrared light detection head. The probe converts the NIR light signals detected during the experiment into electrical signals for further processing in the computer. The testing machine communicates wirelessly with the computer. During testing, the light source probe and detection receiving probe are secured using fiber optic cap jacks, forming a 2×8 array with 22 sampling channels (Figure 2). Each testing area, or sampling channel, is determined by the area between every two adjacent light source heads and receiving heads.

2.2.2. Test procedure

The experimental conditions were set to an ambient temperature of 15–30°C, with a temperature variation within 5°C/h, relative humidity of 45–85% (ensuring no dew or ice formation), and air pressure between 700 and 1,060 hPa.

The subjects were dressed in loose clothing and barefoot, though socks were allowed. They wore portable fNIRS head caps. Using continuous wave (CW) technology mode, we monitored the dorsolateral prefrontal cortex (PFC) with a time resolution of 0.075 s and a 2.0–3.0 cm depth to measure the concentrations of Oxy-Hb and Deoxy-Hb.

For optode placement, 8 emitting optodes (red dots) and 8 receiving optodes (blue dots) were positioned on the subject's dorsolateral prefrontal lobe, maintaining a 3 cm spacing. The detection area was the region between the emitting and receiving optodes, constituting a total of 22 detection channels. We focused on the 14 channels covering the dorsolateral prefrontal lobe. The frontopolar midline point (Fp) was determined according to the international 10–20 electrode configuration method, ensuring the central emitting optode was positioned on the Fp point (Figure 2).

Before the experiment, we cleared the patient's hair from the scalp area where the optodes were placed. Following installation, an instrument self-test was performed to confirm the smooth optical path.

The procedure involved (1) the patient relaxing, sitting, and stepping on a small 6 cm diameter red elastic ball (Figures 3, 4) under Light NIRS monitoring; (2) while seated, the patient was asked to perform a plantar contact task, moving the ball from heel to toe and vice versa at a controlled speed, flexing and extending the knee joint, and feeling the trajectory changes of the ball under their foot; (3) the activation of the dorsolateral prefrontal lobe was tested under eyes-open and eyes-closed conditions, with both the paralyzed and healthy side of the lower limb performing the task.

During the procedure, a professional staff member was present. If a patient experienced pain or the ball slid from under their foot, the test was paused, adjustments were made for comfort or to restore the ball's position, and then the test resumed.

2.2.3. Observed indicators

The plantar contact task designed for this trial was based on cognitive-motor therapy principles designed to promote improved motor function in the affected knee and ankle by reconstituting the cognitive process of the plantaris minor (Cabral et al., 2022). Because of the limited number of optodes lined up for fixation and test optodes in the fiber optic cap used for testing, the cortical domain of the dorsolateral prefrontal area, a key brain region associated with many higher cognitive functions, was selected for fNIRS monitoring. The Brodmann areas were used as the basis for the localization of prefrontal cortical areas, while the 10–20 systematic map, frequently used in EEG for brain functional area localization, aided in determining the distribution of each channel at different regions of interest (ROIs). Among the channels, the right dorsolateral prefrontal cortex (RDPFC) was primarily covered by channels 1, 2, 8, 9, 10, 16, and 17. In contrast, channels 6, 7, 13, 14, 15, 21, and 22 mainly focused on the left dorsolateral prefrontal cortex (LDPFC). Subjects in the experiment were tested for a total of four separate testing sessions, included the plantar contact task on the paralyzed side of the eyes-open condition, the healthy side of the eyes-open condition, the paralyzed side of the eyes-closed condition, and the healthy side of the eyes-closed condition, respectively (Figure 5). In this experiment, our primary attention was on 560 channels (ch; 14ch/case × 10 cases/session × 4 sessions = 560ch).

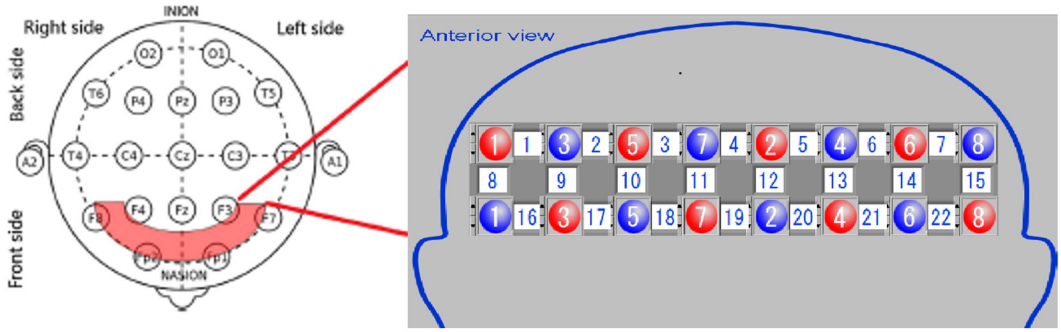

FIGURE 2
Placement of optical poles and test area.

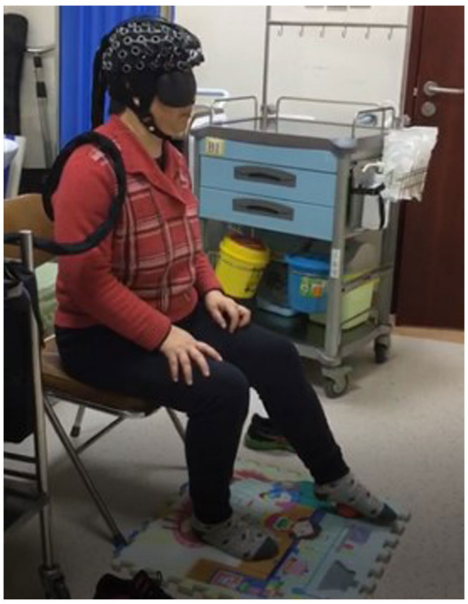

FIGURE 3
Plantar contact task (the patient was asked to perform a plantar contact task, moving the ball from heel to toe and vice versa at a controlled speed, flexing and extending the knee joint, and feeling the trajectory changes of the ball under their foot).

FIGURE 4
Red soft elastic sphere (diameter 6 cm).

2.2.4. Methods for analysis of brain activation

Oxy-Hb has been identified as the most sensitive indicator of regional cerebral blood flow among fNIRS signals (Hoshi et al., 1985). Cognitive-related tasks are known to induce changes in brain rheological parameters, serving as a stable parameter for brain oxygenation. Activation of brain regions leads to dilation of local blood supply, increasing blood flow by approximately 30–50% and boosting blood oxygen consumption by around 5%. These changes prompt a hemodynamic response that often results in elevated levels of blood Oxy-Hb and decreased Deoxy-Hb levels (Suto et al., 2004; Nakahachi et al., 2008). Therefore, in this study, the relationship between the changes in the Oxy-Hb and Deoxy-Hb curves during the time phase of performing the plantar contact task was divided into four types (Figure 6), and subsequent statistical analyses were performed with the characteristic curve changes of all channels.

2.2.5. Statistical analysis

SPSS 26.0 software was used to complete the data processing. The total number of channels in this experiment was 560ch (14ch/case × 10 cases/ session × 4 sessions = 560ch), and the effect on the activation of each channel in the prefrontal lobe was hierarchical listing information in the open-eye condition, paralyzed side versus healthy side, and the statistical inference of its independence test was made by stratified χ^2 test. $p < 0.05$, statistically significant.

3. Results

3.1. Activation of each channel in the dorsolateral prefrontal lobe

The dorsolateral prefrontal cortex, a crucial cerebral region linked to numerous advanced cognitive operations, was chosen for fNIRS monitoring. This region comprised seven channels on the left and right sides, resulting in 14 channels. According to the four types of changes in the relationship between the main components of the Oxy-Hb and Deoxy-Hb curves during the execution phase of the plantar contact task, A + B (Type A and B in Figure 6) was considered activated, and C + D (Type C and D in Figure 6) was the inactive state. The number of each curve type is shown in Tables 1, 2. 64 dorsolateral prefrontal channels were activated, 76 were inactivated in the paralyzed side, 33 dorsolateral prefrontal channels were activated, and 107 were inactivated in the healthy side during the open-eye and closed-eye conditions, respectively. In the closed-eye condition, the paralyzed side performed the task with 47 activated and 93 inactive dorsolateral prefrontal channels and the healthy side performed the task with 50 activated and 90 inactive dorsolateral prefrontal channels.

3.2. Effect of open and closed-eye conditions on paralyzed versus healthy side performing the task

The stratified chi-square test was employed to compute the chi-square test results separately for the aggregate data under both open and closed eyes conditions (Table 3). The Test of Homogeneity of Odds Ratio (OR), utilized for determining the consistency of OR values across varying strata, is also called the test of homogeneity of OR values. The statistics associated with these two homogeneity tests and their test results are documented in Table 4. For the Breslow-Day method, χ^2 was 9.259 with $p = 0.002$, while for the

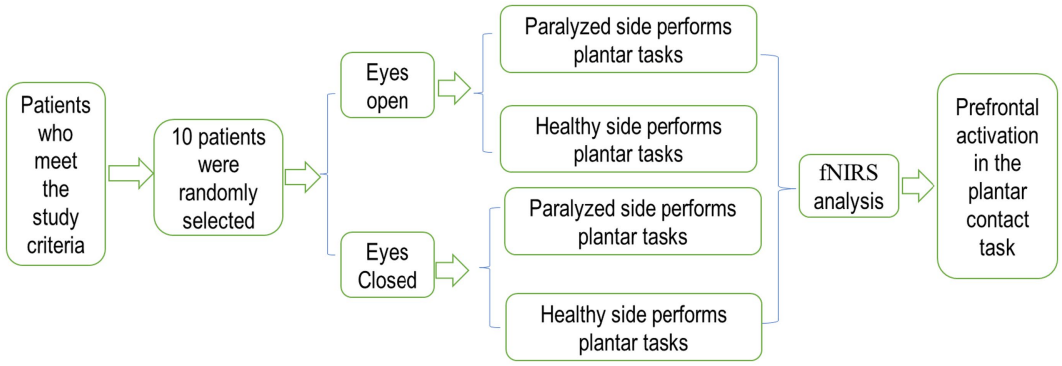

FIGURE 5
The study protocol.

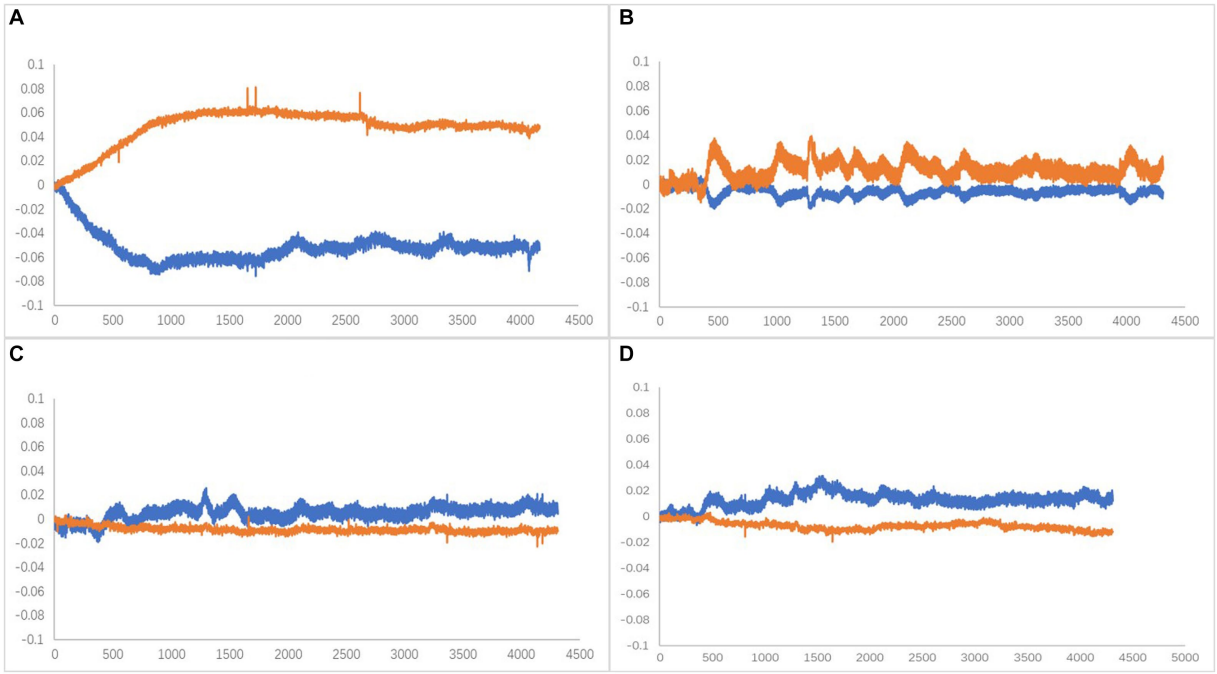

FIGURE 6
(A) Type A, Oxy-Hb upstream separated (activated). **(B)** Type B, Companion Oxy-Hb up (activated). **(C)** Type C, Companion Oxy-Hb downstream. **(D)** Type D, Oxy-Hb downstream separated. X-axis is time (ms),Y-axis is compound concentration (mmol/L).

TABLE 1 Number of each curve type for the relationship between Oxy-Hb and Deoxy-Hb in the dorsolateral prefrontal brain region under the eyes-open condition.

	Paralysis side		Healthy side	
Curve type	Left dorsolateral prefrontal	Right dorsolateral prefrontal	Left dorsolateral prefrontal	Right dorsolateral prefrontal
A	4	6	0	0
B	24	30	22	11
C	34	24	17	36
D	8	10	31	23

Tarone method, χ^2 was 9.258 with $p = 0.002$. Both methodologies exhibited $p < 0.05$, which implies that post-stratification, according to whether the eyes were open or closed, there exists a degree of heterogeneity in the OR values between strata. Combining OR values at this time is inappropriate, and stratification is recommended for reporting.

TABLE 2 Number of each curve type for the relationship between Oxy-Hb and Deoxy-Hb in dorsolateral prefrontal brain regions under closed-eye condition.

	Paralysis side		Healthy side	
Curve type	Left dorsolateral prefrontal	Right dorsolateral prefrontal	Left dorsolateral prefrontal	Right dorsolateral prefrontal
A	12	15	7	18
B	13	7	20	5
C	18	14	33	17
D	27	34	10	30

TABLE 3 Pearson chi-square test results.

Item	χ^2	p
Closed-eye conditions	0.142	0.706
Eyes-open condition	15.15	0.000

TABLE 4 Odds ratio homogeneity test.

Methods	χ^2	p
Breslow-Day	9.259	0.002
Tarone's	9.258	0.002

TABLE 5 Independence test of the conditions.

Methods	χ^2	p
Cochran's	6.183	0.013
Mantel–Haenszel	5.729	0.017

In the closed-eye condition, performing the plantar task on either the paralyzed or healthy side showed no significant effect on dorsolateral prefrontal activation (Pearson $\chi2 = 0.142$, $p = 0.706$). In the eyes-open condition, we found a statistically significant difference (Pearson $\chi2 = 15.15$, $p = 0.002$) in dorsolateral prefrontal lobe activation between the paralyzed and healthy sides, suggesting that the side on which the plantar task is performed influences activation.

3.3. Activation of the dorsolateral prefrontal lobe in the eyes-open condition with paralysis versus the healthy side performing the task

The previous results indicated that the eyes-open condition was influential in the execution of the plantar contact task on the paralyzed side versus the healthy side. Therefore, after removing the eyes-open and eyes-closed factors, the relationship between the paralyzed side versus the healthy side in performing the task and the activation of the dorsolateral prefrontal lobe was tested using both Cochran's and Mantel–Haenszel chi-square tests, the former being a modified version of the latter, and the results are shown in Table 5. p-values were found to be less than 0.05, indicating that the paralyzed side of the patient versus the healthy side differed in activation of the dorsolateral prefrontal lobe when performing the plantar contact task.

The Mantel–Haenszel odds ratio was estimated to be 0.646. In this study, the variables were set as follows: for 'side' (1 = paralyzed, 2 = healthy) and for 'activation' (1 = unactivated/C + D, 2 = activated/A + B). Hence, an OR of 0.646 indicates that dorsolateral prefrontal activation was 0.646 times higher on the healthy side than the paralyzed one during task performance. In other words, the dorsolateral prefrontal activation during task performance on the paralyzed side was 1.55 times greater than on the healthy side. In the eyes-open condition, the paralyzed side was more likely to activate the dorsolateral prefrontal during the plantar contact task.

4. Discussions

The role of cognitive function in motor tasks has gained increasing attention in research, and the significance of cortical function in the neuromodulatory mechanisms associated with walking has been highlighted. In this study, we examined the impact of a plantar contact task on the activation of the dorsolateral prefrontal cortex in patients with post-stroke hemiplegia under both eyes-open and eyes-closed conditions. The patients carried out the task at a self-determined pace, sequentially transitioning the ball from the heel to the toe by flexing and extending the knee joint and continuously experiencing the trajectory change of the ball on the foot sole. Based on the fNIRS observations, the execution of the plantar contact task was effective in activating the dorsolateral prefrontal lobe. This task requires sensory input to the plantar surface of the foot regarding the blob's trajectory and movement, generating a perceptual experience. Patients in a stable sitting posture primarily innervated the knee and ankle joints of the lower limbs to control the small ball planetary, signifying substantial cognitive engagement in this motor process.

Cortical afferents to the frontal motor cortex come from three sources: parietal somatosensory cortex, prefrontal cortex, and cingulate cortex (Fuster, 1993; Yip and Lui, 2023). In contrast, previous studies in rhesus monkeys have shown that the prefrontal cortex, primarily responsible for cognitive functions, has interactive fiber connections with the optic cortex (striate area), temporal lobe, and parietal lobe. It has direct or indirect fiber connections with the basal forebrain, cingulate gyrus, and hippocampus, extending fiber projections to the basal ganglia and hypothalamus. The prefrontal cortex has a well-developed granular layer IV that receives direct projections from the dorsomedial thalamic nucleus, the only neocortex with interactive fiber connections to this cortical information "portal. It is the only neocortex that interacts with this cortical information "portal." This complex fiber connection pattern enables it to play a key role in perceiving abstract rules, working memory, attentional regulation, and cognitive functions such as planning and strategy of behavior, thinking, and reasoning (Kandel et al., 2000). Radiological studies have shown that cognitive

task training combined with motor training enhances the hemodynamics in the dorsolateral prefrontal cortex (Erickson et al., 2007). Watanabe and Funahashi (2018) suggested that the parallel processing of multitask information mainly occurs due to the involvement of the dorsolateral prefrontal lobe, selectively activating different prefrontal cortex regions when processing various task modules. Stroke patients demonstrated enhanced activation of brain regions in the superior frontal gyrus, inferior frontal gyrus, bilateral cingulate gyrus, and right precentral gyrus associated with motor performance and learning, somatosensory, motor planning, and conflict information processing (Peters et al., 2019).

We also observed variability in dorsolateral prefrontal lobe activation related to whether the eyes were open or closed. After considering the stratified influences of open and closed eyes, in the closed-eye situation, the execution of the plantar contact task on the paralyzed side or healthy side did not affect dorsolateral prefrontal activation. In contrast, in the eyes-open condition, the execution of the plantar contact task on the paralyzed side or the healthy side was an important influence on dorsolateral prefrontal activation, and the dorsolateral prefrontal activation was 1.55 times higher on the paralyzed side than on the healthy side during the task. It is suggested that the change in motor control difficulty associated with performing the task on the paralyzed or healthy side with eyes open and external visual influences can enhance the activation of the cognitive control cortex represented by the dorsolateral prefrontal lobe. Studies have also probed motor cortical excitability by open versus closed eyes and similarly found that the stimulus–response curve obtained with eyes open was steeper than that obtained with eyes closed and that the closed-eye state may affect the recruitment of cortical circuits and thus reduce evoked motor output, which is also consistent with our results (Chen and Huang, 2018). In the eyes-open condition, the paralyzed side of the task is more activated to the dorsolateral prefrontal lobe and less activated to the healthy side. Compared to the healthy side, the increased difficulty of performing the plantar task on the paralyzed side necessitates greater activation of the cognitive control cortex. This allows for more robust information input to the regions of the brain processing the stimulus. Moreover, increasing the complexity of cognitive-motor tasks enhances the activation and interconnectedness of cortical networks (Rietschel et al., 2012). The plantar contact task involves visual conduction as well as proprioception in the eyes-open condition and proprioceptive conduction in the eyes-closed condition. It has been found that motor and cognitive tasks compete with each other for attentional resources and reorganize their allocation when a person is completing a cognitive-motor task. Allocating a portion of the resources fully devoted to cognition and proprioception to vision when eyes are open, the effective attentional resources allocated to the proprioceptive task are reduced (Snijders et al., 2007). Some scholars have argued (Walker et al., 2000; Ruffieux et al., 2015) that the visual system ensures the stability of the body by collecting information about its spatial position and other information, and that plantar tasks can be better accomplished. When the visual input is blocked when the eyes are closed, the visual feedback will be reduced, and the function of the vestibular system and proprioceptive system of the human body will be reduced. As a result, the human body's postural adjustment ability decreases when performing tasks with eyes closed compared to eyes open, making it more difficult to complete the task. Some scholars have also found (Remaud et al., 2012; Kabbaligere et al., 2017) that visual, vestibular and cognitive functions are all important factors in the control of human position and movement. When a dual task is performed with normal visual input, the visual center will compensate for the completion of the cognitive task. It has also been found that brain activity recorded by electroencephalogram (EEG) is strongly modulated by the closed-eye state compared to the open-eye state. The use of fNIRS to measure cortical activity implies that a decrease in activity may reflect reduced utilization of a brain region (Lustig et al., 2009; Cabeza et al., 2018), whereas an increase in activity may signal a compensatory recruitment mechanism (Cabeza et al., 2002; Schneider-Garces et al., 2010). The higher the task difficulty, the greater the need for mobilization and recruitment within the compensable range for motor control, resulting in stronger activation of cognitive control brain regions (Qiao et al., 2020).

Interestingly, no type A curves were observed during the execution of the plantar contact task on the healthy side, with type A representing typical activation curve changes. This suggests that less difficult conditions are less likely to evoke a substantial blood oxygen response in the prefrontal lobe, leading to a typical activation pattern. Information from the occipital and parietal lobes related to vision and somatosensation forms perceptions translated into actual actions (motor output), primarily via the dorsolateral prefrontal cortex, which directly connects with the motor cortex (Miller and Cohen, 2001; Wallis et al., 2001; Szczepanski and Knight, 2014). This is consistent with earlier theories proposing a hierarchical organization in the prefrontal cortex, with the anterior end controlling abstract cognitive abilities and the posterior end regulating motor functions (Badre and D'esposito, 2009). However, it has also been suggested that the frontopolar and medial prefrontal cortex are closely related to the limbic system of the medial temporal lobe (Medial temporal) and thus have a stronger role in long-term memory, emotion, and motivation. Although various subdivisions of the prefrontal cortex control different aspects of cognitive function and play a major role in a specific function, they operate in concert when performing a specific task (Erickson et al., 2007). The most important neuromodulatory function performed by the dorsolateral prefrontal lobe is related to the inhibitory effect of this region on the amygdala and the hypothalamic–pituitary–adrenal axis. It usually relies on connections with other subcortical areas, which are then translated into action motivation via the limbic and mesocortical dopamine systems (Bigliassi and Filho, 2022). As stroke patients recover, external stimuli trigger endogenous neural repair mechanisms. These mechanisms are stimulated by motor training and cognitive behaviors, which together promote cortical activation. It promotes neural regeneration and increases the number of cortical neuronal synapses, which leads to faster information processing (Pang et al., 2018).

5. Conclusion

The execution of the plantar contact task, as observed through fNIRS, can effectively stimulate the dorsolateral prefrontal lobe. When combined with conditions of open and closed eyes, this activation effect can be enhanced by implementing the plantar task through the paralyzed side of the patient and moderately increasing task difficulty. Therapies rooted in such cognitive-motor techniques may provide a novel approach to promote motor function recovery through the perception and stimulation of cognitive control brain regions; however, their therapeutic impacts warrant further exploration. This study has certain limitations as it focused solely on the channels encompassing the dorsolateral prefrontal brain region and included a small patient population suffering from cerebral infarction.

Data availability statement

The raw data supporting the conclusions of this article will be made available by the authors, without undue reservation.

Ethics statement

The studies involving humans were approved by Ethics Committee of Beijing Rehabilitation Hospital, Capital Medical University. The studies were conducted in accordance with the local legislation and institutional requirements. The participants provided their written informed consent to participate in this study.

Author contributions

Z-QY: Methodology, Writing – original draft. M-FW: Data curation, Writing – original draft. J-NX: Funding acquisition, Writing – review and editing.

Acknowledgments

We wish to thank our colleagues for mentorship, help and guidance in experimental design.

Conflict of interest

The authors declare that the research was conducted in the absence of any commercial or financial relationships that could be construed as a potential conflict of interest.

Publisher's note

All claims expressed in this article are solely those of the authors and do not necessarily represent those of their affiliated organizations, or those of the publisher, the editors and the reviewers. Any product that may be evaluated in this article, or claim that may be made by its manufacturer, is not guaranteed or endorsed by the publisher.

References

Badre, D., and D'esposito, M. (2009). Is the rostro-caudal axis of the frontal lobe hierarchical? *Nat. Rev. Neurosci.* 10, 659–669. doi: 10.1038/nrn2667

Bigliassi, M., and Filho, E. (2022). Functional significance of the dorsolateral prefrontal cortex during exhaustive exercise. *Biol. Psychol.* 175:108442. doi: 10.1016/j.biopsycho.2022.108442

Bogousslavsky, J., Bernasconi, A., and Kumral, E. (1996). Acute multiple infarction involving the anterior circulation. *Arch. Neurol.* 53, 50–57. doi: 10.1001/archneur.1996.00550010068017

Cabeza, R., Albert, M., Belleville, S., Craik, F. I. M., Duarte, A., Grady, C. L., et al. (2018). Maintenance, reserve and compensation: the cognitive neuroscience of healthy ageing. *Nat. Rev. Neurosci.* 19, 701–710. doi: 10.1038/s41583-018-0068-2

Cabeza, R., Anderson, N. D., Locantore, J. K., and McIntosh, A. R. (2002). Aging gracefully: compensatory brain activity in high-performing older adults. *NeuroImage* 17, 1394–1402. doi: 10.1006/nimg.2002.1280

Cabral, D. F., Fried, P., Koch, S., Rice, J., Rundek, T., Pascual-Leone, A., et al. (2022). Efficacy of mechanisms of neuroplasticity after a stroke. *Restor. Neurol. Neurosci.* 40, 73–84. doi: 10.3233/RNN-211227

Caetano, M. J. D., Menant, J. C., Schoene, D., Pelicioni, P. H. S., Sturnieks, D. L., and Lord, S. R. (2017). Sensorimotor and cognitive predictors of impaired gait adaptability in older people. *J. Gerontol. A Biol. Sci. Med. Sci.* 72, 1257–1263. doi: 10.1093/gerona/glw171

Chen, K. H., and Huang, Y. Z. (2018). The change of motor cortical excitability between eyes open and closed conditions. *Neuroreport* 29, 214–218. doi: 10.1097/WNR.0000000000000955

Erickson, K. I., Colcombe, S. J., Wadhwa, R., Bherer, L., Peterson, M. S., Scalf, P. E., et al. (2007). Training-induced functional activation changes in dual-task processing: an FMRI study. *Cereb. Cortex* 17, 192–204. doi: 10.1093/cercor/bhj137

Fritz, N. E., Cheek, F. M., and Nichols-Larsen, D. S. (2015). Motor-cognitive dual-task training in persons with neurologic disorders: a systematic review. *J. Neurol. Phys. Ther.* 39, 142–153. doi: 10.1097/NPT.0000000000000090

Fuster, J. M. (1993). Frontal lobes. *Curr. Opin. Neurobiol.* 3, 160–165. doi: 10.1016/0959-4388(93)90204-C

Hazra, D., Yoshinaga, S., Yoshida, K., Takata, N., Tanaka, K. F., Kubo, K. I., et al. (2022). Rhythmic activation of excitatory neurons in the mouse frontal cortex improves the prefrontal cortex-mediated cognitive function. *Cereb. Cortex* 32, 5243–5258. doi: 10.1093/cercor/bhac011

Hobbs, B., and Artemiadis, P. (2020). A review of robot-assisted lower-limb stroke therapy: unexplored paths and future directions in gait rehabilitation. *Front. Neurorobot.* 14:19. doi: 10.3389/fnbot.2020.00019

Hoshi, Y., Kobayashi, N., and Tamura, M. (1985). Interpretation of near-infrared spectroscopy signals: a study with a newly developed perfused rat brain model. *J. Appl. Physiol.* 90, 1657–1662. doi: 10.1152/jappl.2001.90.5.1657

Kabbaligere, R., Lee, B. C., and Layne, C. S. (2017). Balancing sensory inputs: sensory reweighting of ankle proprioception and vision during a bipedal posture task. *Gait Posture* 52, 244–250. doi: 10.1016/j.gaitpost.2016.12.009

Kandel, E. R., Schwartz, J. H., Jessell, T. M., Siegelbaum, S. A., and Hudspeth, A. J. (2000). *Principles of neural science*. New York: McGraw-hill.

Lustig, C., Shah, P., Seidler, R., and Reuter-Lorenz, P. A. (2009). Aging, training, and the brain: a review and future directions. *Neuropsychol. Rev.* 19, 504–522. doi: 10.1007/s11065-009-9119-9

Maenza, C., Good, D. C., Winstein, C. J., Wagstaff, D. A., and Sainburg, R. L. (2020). Functional deficits in the less-impaired arm of stroke survivors depend on hemisphere of damage and extent of paretic arm impairment. *Neurorehabil. Neural Repair* 34, 39–50. doi: 10.1177/1545968319875951

Miller, E. K., and Cohen, J. D. (2001). An integrative theory of prefrontal cortex function. *Annu. Rev. Neurosci.* 24, 167–202. doi: 10.1146/annurev.neuro.24.1.167

Montero-Odasso, M., Verghese, J., Beauchet, O., and Hausdorff, J. M. (2012). Gait and cognition: a complementary approach to understanding brain function and the risk of falling. *J. Am. Geriatr. Soc.* 60, 2127–2136. doi: 10.1111/j.1532-5415.2012.04209.x

Nakahachi, T., Ishii, R., Iwase, M., Canuet, L., Takahashi, H., Kurimoto, R., et al. (2008). Frontal activity during the digit symbol substitution test determined by multichannel near-infrared spectroscopy. *Neuropsychobiology* 57, 151–158. doi: 10.1159/000147467

Neurology CSo (2015). Chinese classification of cerebrovascular diseases. *Chin. J. Neurol.* 50, 168–171.

Pang, M. Y. C., Yang, L., Ouyang, H., Lam, F. M. H., Huang, M., and Jehu, D. A. (2018). Dual-task exercise reduces cognitive-motor interference in walking and falls after stroke. *Stroke* 49, 2990–2998. doi: 10.1161/STROKEAHA.118.022157

Peters, S., Eng, J. J., Liu-Ambrose, T., Borich, M. R., Dao, E., Amanian, A., et al. (2019). Brain activity associated with dual-task performance of ankle motor control during cognitive challenge. *Brain Behav.* 9:e01349. doi: 10.1002/brb3.1349

Pothier, K., Gagnon, C., Fraser, S. A., Lussier, M., Desjardins-Crépeau, L., Berryman, N., et al. (2018). A comparison of the impact of physical exercise, cognitive training and combined intervention on spontaneous walking speed in older adults. *Aging Clin. Exp. Res.* 30, 921–925. doi: 10.1007/s40520-017-0878-5

Qiao, L., Xu, M., Luo, X., Zhang, L., Li, H., and Chen, A. (2020). Flexible adjustment of the effective connectivity between the fronto-parietal and visual regions supports cognitive flexibility. *NeuroImage* 220:117158. doi: 10.1016/j.neuroimage.2020.117158

Remaud, A., Boyas, S., Caron, G. A., and Bilodeau, M. (2012). Attentional demands associated with postural control depend on task difficulty and visual condition. *J. Mot. Behav.* 44, 329–340. doi: 10.1080/00222895.2012.708680

Rietschel, J. C., Miller, M. W., Gentili, R. J., Goodman, R. N., McDonald, C. G., and Hatfield, B. D. (2012). Cerebral-cortical networking and activation increase as a function of cognitive-motor task difficulty. *Biol. Psychol.* 90, 127–133. doi: 10.1016/j.biopsycho.2012.02.022

Ruffieux, J., Keller, M., Lauber, B., and Taube, W. (2015). Changes in standing and walking performance under dual-task conditions across the lifespan. *Sports Med.* 45, 1739–1758. doi: 10.1007/s40279-015-0369-9

Schneider-Garces, N. J., Gordon, B. A., Brumback-Peltz, C. R., Shin, E., Lee, Y., Sutton, B. P., et al. (2010). Span, CRUNCH, and beyond: working memory capacity and the aging brain. *J. Cogn. Neurosci.* 22, 655–669. doi: 10.1162/jocn.2009.21230

Snijders, A. H., van de Warrenburg, B. P., Giladi, N., and Bloem, B. R. (2007). Neurological gait disorders in elderly people: clinical approach and classification. *Lancet Neurol.* 6, 63–74. doi: 10.1016/S1474-4422(06)70678-0

Suto, T., Fukuda, M., Ito, M., Uehara, T., and Mikuni, M. (2004). Multichannel near-infrared spectroscopy in depression and schizophrenia: cognitive brain activation study. *Biol. Psychiatry* 55, 501–511. doi: 10.1016/j.biopsych.2003.09.008

Szczepanski, S. M., and Knight, R. T. (2014). Insights into human behavior from lesions to the prefrontal cortex. *Neuron* 83, 1002–1018. doi: 10.1016/j.neuron.2014.08.011

Walker, C., Brouwer, B. J., and Culham, E. G. (2000). Use of visual feedback in retraining balance following acute stroke. *Phys. Ther.* 80, 886–895. doi: 10.1093/ptj/80.9.886

Wallis, J. D., Anderson, K. C., and Miller, E. K. (2001). Single neurons in prefrontal cortex encode abstract rules. *Nature* 411, 953–956. doi: 10.1038/35082081

Watanabe, K., and Funahashi, S. (2018). Toward an understanding of the neural mechanisms underlying dual-task performance: contribution of comparative approaches using animal models. *Neurosci. Biobehav. Rev.* 84, 12–28. doi: 10.1016/j.neubiorev.2017.08.008

Yip, D. W., and Lui, F. (2023). Physiology, Motor Cortical. StatPearls. Treasure Island (FL) ineligible companies. Disclosure: Forshing Lui declares no relevant financial relationships with ineligible companies; StatPearls Publishing Copyright © 2023, StatPearls Publishing LLC.

frontiers | Frontiers in Neuroscience

TYPE Clinical Trial
PUBLISHED 16 November 2023
DOI 10.3389/fnins.2023.1282496

OPEN ACCESS

EDITED BY
Feng Zhang,
Third Hospital of Hebei Medical University, China

REVIEWED BY
Daniel Tozer,
University of Cambridge, United Kingdom
Wenliang Fan,
Huazhong University of Science and Technology, China

*CORRESPONDENCE
Nan Yang
✉ srsyang@126.com
Shuxue Liu
✉ lius_2@126.com

RECEIVED 24 August 2023
ACCEPTED 16 October 2023
PUBLISHED 16 November 2023

CITATION
Chen S, Huang R, Zhang M, Huang X, Ling S, Liu S and Yang N (2023) Altered brain spontaneous activity in patients with cerebral small vessel disease using the amplitude of low-frequency fluctuation of different frequency bands.
Front. Neurosci. 17:1282496.
doi: 10.3389/fnins.2023.1282496

Altered brain spontaneous activity in patients with cerebral small vessel disease using the amplitude of low-frequency fluctuation of different frequency bands

Sina Chen[1], Ruiwang Huang[2], Mingxian Zhang[2], Xiaohuang Huang[1], Shuiqiao Ling[1], Shuxue Liu[1]*and Nan Yang[1]*

[1]Zhongshan Hospital of Traditional Chinese Medicine, Zhongshan, Guangdong, China, [2]Center for Study of Applied Psychology, School of Psychology, South China Normal University, Guangzhou, Guangdong, China

Background: Previous studies showed that cerebral small vessel disease (cSVD) is a leading cause of cognitive decline in elderly people and the development of Alzheimer's disease. Although brain structural changes of cSVD have been documented well, it remains unclear about the properties of brain intrinsic spontaneous activity in patients with cSVD.

Methods: We collected resting-state fMRI (rs-fMRI) and T1-weighted 3D high-resolution brain structural images from 41 cSVD patients and 32 healthy controls (HC). By estimating the amplitude of low-frequency fluctuation (ALFF) under three different frequency bands (typical band: 0.01–0.1 Hz; slow-4: 0.027–0.073 Hz; and slow-5: 0.01–0.027 Hz) in the whole-brain, we analyzed band-specific ALFF differences between the cSVD patients and controls.

Results: The cSVD patients showed uniformly lower ALFF than the healthy controls in the typical and slow-4 bands ($p_{FWE} < 0.05$). In the typical band, cSVD patients showed lower ALFF involving voxels of the fusiform, hippocampus, inferior occipital cortex, middle occipital cortex, insula, inferior frontal cortex, rolandic operculum, and cerebellum compared with the controls. In the slow-4 band, cSVD patients showed lower ALFF involving voxels of the cerebellum, hippocampus, occipital, and fusiform compared with the controls. However, there is no significant between-group difference of ALFF in the slow-5 band. Moreover, we found significant "group × frequency" interactions in the left precuneus.

Conclusion: Our results suggested that brain intrinsic spontaneous activity of cSVD patients was abnormal and showed a frequency-specific characteristic. The ALFF in the slow-4 band may be more sensitive to detecting a malfunction in cSVD patients.

KEYWORDS

spontaneous brain activity, amplitude of low-frequency fluctuation, cerebral small vessel disease, mild cognitive impairment, white matter hyperintensity, lacune, cerebral microbleed

Highlights

- cSVD patients showed uniformly lower ALFF than controls at typical frequency band and slow-4 band.
- At The typical frequency band (0.01–0.1 Hz), cSVD patients Had lower ALFF In The cerebellum, occipital cortex, and hippocampus compared To healthy controls.

1. Introduction

Cerebral small vessel disease (cSVD) refers to an intracranial vascular disease that involves various pathological and neurological processes affecting brain blood vessels (Feng et al., 2021). The disease of cSVD exhibits a high prevalence, which largely exceeds that of large-vessel stroke (Dey et al., 2016). Up to 45% of dementia cases may be brought on by CSVD, which also causes 20% of all strokes worldwide, 25% of which are ischemic strokes (also known as lacunar strokes). It is responsible for roughly 20% of all strokes worldwide and 25% of ischemic strokes (also known as lacunar strokes), of which 20% result in disability for the patient (Pantoni, 2010). Moreover, cSVD is one of main factors leading to vascular cognitive decline and dementia (Cai et al., 2015) and contributing to the pathogenesis of Alzheimer's disease (AD) (Liu et al., 2018; Kim et al., 2020). Recently, structural magnetic resonance imaging (MRI) techniques have been widely applied to identify brain structural neuroimaging markers associated with cSVD (Chen et al., 2019). Although originating from different pathogenesis, cSVD may commonly exhibit similar structural markers including small subcortical infarcts, vascular lacunes, vascular white-matter hyperintensity, cerebral microbleeds, perivascular space and brain atrophy (Staals et al., 2015; De Guio et al., 2016; Chen et al., 2019). In addition to tremendous endeavors made in the structural field, current studies pertaining to brain functional properties are progressively increasing.

The resting-state functional MRI (rs-fMRI) has been applied to investigate the relationship between cognitive impairment and brain functional activity using the amplitude of low-frequency fluctuation (ALFF) (Zang et al., 2007) in patients with cSVD (Zhou et al., 2020; Feng et al., 2021; Li et al., 2021; Mo et al., 2023). Low-frequency oscillation ranging from 0.01 to 0.1 Hz has been identified as a representative indicator of brain spontaneous activity (Zou et al., 2008; Zuo et al., 2010), and the ALFF, the square root of the power spectrum of the frequency range, is supposed to reflect brain regional spontaneous activity (Zang et al., 2007). Moreover, the regional ALFF changes may function as diagnostic biomarker for cSVD (Feng et al., 2021).

Given the fact that different oscillatory bands usually have different generation mechanisms and different physiological functions (Buzsáki and Draguhn, 2004). The detection of different brain tissues may be more sensitive under a specific frequency spectrum (Zuo et al., 2010; Qi et al., 2020; Sasai et al., 2021). Previous studies (Zuo et al., 2010; Qi et al., 2020) subdivided frequency spectrums of BOLD signals into several frequency bands such as the slow-6 (0.0052–0.01 Hz), slow-5 (0.01–0.027 Hz), slow-4 (0.027–0.073 Hz), slow−3 (0.073–0.198 Hz) and slow-2 (0.198–0.25 Hz) to compare frequency-specific ALFF values in different brain regions. For example, the basal ganglia, thalamus, and precuneus were found to show higher ALFF value in the slow-4 band than that in the slow-5 band (Zuo et al., 2010). Several studies showed a strong association between local brain abnormalities in psychiatric disorders and neural activity in specific frequency bands (slow-4 and slow-5 bands) (Wu et al., 2020; Liao et al., 2021; Ren et al., 2021). Wang et al. (2021) compared the difference in ALFF between AD and aMCI patients under three different frequency bands. They suggest that ALFF in the slow-5 band may be able to help identify severe AD and aMCI. So far, little is known about the functional brain activity of cSVD patients with cognitive impairment in response to different frequency bands. Therefore, we attempted to study the characteristic performance of ALFF values in patients with cognitive impairment at different frequency bands.

This study addressed this problem by examining frequency-dependent neural activity in cSVD patients during the resting state. It is the first study to undertake the spontaneous neural activity of specific frequency bands in cSVD. There are two primary aims of this study: 1. To investigate whether cSVD patients would show abnormal ALFF in regions associated with cognitive function; 2. To ascertain whether these abnormalities would be associated with specific frequency bands. The present study detected the brain regions with ALFF alterations (0.01–0.1 Hz) in cSVD patients contrasting with controls. Based on the specificity of sub-bands, we attempted to reveal the brain regions with abnormal ALFF in slow-4 (0.027–0.073 Hz) and slow-5 (0.01–0.027 Hz), separately.

2. Methods

2.1. Subjects

We recruited 41 cSVD patients with right-handedness for this study from December 2016 to December 2018 from the inpatient and outpatient of the Neurology Department of Zhongshan TCM Hospital, Guangdong, China. Two experienced neurologists (XH, Huang; SQ, Ling) screened the participants based on the diagnostic criteria. In addition, we also recruited 32 sex-matched healthy participants as the healthy controls (HCs). This study was approved

Abbreviations: cSVD, Cerebral small vessel disease; AD, Alzheimer's disease; MCI, Mild cognitive impairment; ALFF, Amplitude of low-frequency fluctuation; ReHo, Regional homogeneity; WMH, White matter hyperintensity; LA, Lacune; CMB, Cerebral microbleed; VFT, Verbal fluency test; DST, Digit span test; DSST, Digit symbol substitution test.

by the Institutional Review Board (IRB) of Zhongshan TCM Hospital (ClinicalTrials.gov identifier: 2016ZSZY-LLK-028). Written informed consent for each patient and the healthy participant was obtained before the study. Table 1 lists the clinical and demographic characteristics of the participants.

The cSVD patients were diagnosed according to the Neuroimaging Standards for Research into Small Vessel Disease (Wardlaw et al., 2013). Specifically, the diagnostic standard for imaging of cSVD included: (i) Recent small subcortical infarct: Axial views show an infarct diameter less than 20 mm, which can be larger than 20 mm in the coronal or sagittal view. (ii) Lacunes of presumed vascular origin: round or ovoid in shape, 3-15 mm in diameter, distributed in subcortical regions, filled with the same signals as cerebrospinal fluid (CSF). (iii) white matter hyperintensity (WMH) of presumed vascular origin: abnormal brain white matter (WM) signals, the range of lesions can vary in size, showing a high signal on the T2-weighted or T2-weighted FLAIR images. (iv) Perivascular space: the signal of perivascular space is the same as that of the CSF in all MRI sequences. The shape was linear when the image plane ran parallel to the blood vessels and round or oval when running perpendicular to the blood vessels, usually less than 3 mm in diameter. (v) Cerebral microbleeds: cerebral microbleeds are defined as the following changes in the images obtained with T2*-weighted gradient-echo sensitive to magnetizing effects, for instance, (1) small round or oval, clear boundary, homogeneity, lack of signal focus; (2) diameter in 2-5 mm, maximum 10 mm, and the lesion is surrounded by the brain parenchyma; (3) brain atrophy: reduced brain volume, but it was not associated with mainly specific focal lesions such as trauma and cerebral infarction.

The diagnostic criteria of vascular cognitive impairment (VCI) [37] indicate a continuum of clinical manifestations for cSVD patients. Mild VCI refers to impairment in at least one cognitive domain and mild to no impairment in instrumental activities of daily living (IADLs)/activities of daily living (ADLs) (independent of the motor/sensory sequelae of the vascular event). Major VCI refers to clinically significant deficits of sufficient severity in at least one cognitive domain (deficits may be present in multiple domains) and severe disruption to IADLs/ADLs (independent of the motor/sensory sequelae of the vascular event).

TABLE 1 Demography characteristics for the patients with cerebral small vessel disease (cSVD) and the healthy controls (HCs).

	cSVD (n = 41)	HCs (n = 32)	Value of p
Sex (M/F)	23/18	11/21	0.098[a]
Age (years old)	68 ± 7 (41–80)	42 ± 15 (25–76)	<0.001[b]
Education level	15/19/5/2	4/6/3/19	<0.001[c]
DSST score	11.48 ± 9.08	N/A	N/A
DST score	10.50 ± 2.56	N/A	N/A
VFT score	17.63 ± 6.77	N/A	N/A
Smoke (Y/N)	23/18	21/11	0.409[b]
Diabetes (Y/N)	15/26	7/25	0.174[b]
Hypertension (Y/N)	28/13	18/14	0.290[b]

Education included a primary school, junior high school, senior high school, university and over. N/A, not applicable. Y/N, Yes or No. Level of education refers to the number of people at each level of education: elementary, middle school, high school, and college. [a]The value of p was obtained by a χ^2-test. [b]The value of p was obtained by a two-sample t-test. [c]The value of p was obtained by a Wilcoxon test.

The inclusion criteria for the cSVD patients were as follows: (a) the patients aged in a range of 40–80 years old, (b) the patients or legal guardians agreed and signed informed consents, (c) the patient was confirmed to satisfy the diagnostic imaging criteria for cSVD and the diagnostic criteria for VCI, and (d) the patient was in mild to moderate cognitive impairment with a mini-mental state examination (MMSE) screening score in 9–24 points. Patients meeting all these criteria were included in our study. The exclusion criteria for the patients included: (a) the cognitive dysfunction caused by macrovascular and cardiogenic cerebral embolism confirmed by examination; (b) non-vascular causes of WM degeneration and pure AD; (c) those who have been confirmed to have brain tumors, brain trauma, cerebral parasitic diseases, encephalitis and other diseases that can cause cognitive impairment; (d) patients with severe speech, vision, hearing or mental disorders that affect cognitive testing and cognitive training; (e) patients suffered from depression and other neuropsychological disorders resulting in cognitive impairment; (f) patients have the history of alcohol and drug abuse; (g) patients combined with severe heart, liver, kidney endocrine system, and hematopoietic system diseases; and (h) participating in other clinical trials.

2.2. Assessments

Each patient was requested to attend the clinical assessments, such as a medical history inquiry, a neurological examination, and a series of neuropsychological tests, which included the verbal fluency test (VFT), digit span test (DST), and digit symbol substitution test (DSST).

The VFT is a widely used neuropsychological scale mainly to measure cognitive, verbal, and executive functions (Vaucheret Paz et al., 2020). It consists of three subtests to detect semantic, speech, and motion fluency, respectively. (1) semantic subtest: ask the participants to say as many animals, vegetable, or fruit words as possible in one minute; (2) speech subtest: ask the participants to say as many words as possible, starting with "Fa" in one minute; (3) motion subtest: participants were asked to say as many words as possible in one minute about an event that could occur in a particular location (e.g., kitchen).

The DST (Leung et al., 2011) consists of two parts, a digit forward and a digit backward. During the test process, the participants are asked to remember two numbers simultaneously, read by the researcher with the speed of one digit per second starting with the first set. If the participants pass the 2-digit number, then the 3-digit number is measured, and so on. If the participant does not pass the 8-digit number, the 8-digit number of the second set will be read, and when the participant passes the 8-digit number of the second set, the 9-digit number will be read. If the participant fails to pass the 8-digit number of the second set, his score will be "7-digit."

The DSST was used to evaluate multiple aspects of cognitive function, such as executive function, processing speed, attention, and working memory (Baune et al., 2018). According to the diagram at the top of the scale, the participants filled in the matching numbers under each symbol in the table below as quickly as they could. Rating

instructions are that the number of correct answers in 90 s is the final score, not including the numbers filled in during the practice. The number of correct answers will be counted as the total score.

2.3. Imaging data acquisition

All images were obtained on a GE 3T MRI scanner with an 8-channel phased-array head coil. The participant was requested to keep their eyes closed, relax but not fall asleep, and minimize head movement during the scanning. Functional images were collected with a gradient-echo echo-planar imaging (EPI) sequence with the following parameters: repetition time (TR) = 2,000 ms, echo time (TE) = 30 ms, flip angle (FA) = 90°, field of vision (FOV) = 240 mm × 240 mm, slice thickness = 3.5 mm, inter-slice gap = 0.7 mm, data matrix = 64 × 64, 33 interleaved axial slices coving the whole brain, and 240 volumes acquired in about 8 min. In addition, high-resolution brain structural images were acquired using a T1-weighed 3D BRAVO sequence with the following parameters: TR = 8.0 ms, TE = 3.0 ms, FA = 12°, data matrix = 256 × 256, FOV = 256 mm × 256 mm, slice thickness = 1 mm, and 188 sagittal slices covering the whole brain. The conventional T1-weighted and T2-weighted FLAIR images were acquired for clinical assessment. All MRI images for each participant were acquired in the same session.

2.4. Data pre-processing

The rs-fMRI data were preprocessed using the DPARSF toolbox[1] based on Matlab2012a (Mathworks, Inc., Massachusetts). Before pre-processing the data, we visually inspected both brain functional and structural images and excluded the datasets with significant signal dropouts, distortion, and other quality problems. The procedure of pre-processing included: (1) removing the first 10 volumes to keep the magnetization equilibrium; (2) performing slice-timing and head-movement correction to remove effects caused by slice acquisition time differences and head movements; (3) conducting a linear co-registration between functional images and structural images for each participant; (4) regressed out signals of the WM and CSF, and head-movement parameters (Friston-24 model); (5) performed a non-linear transformation between structural images and template brain images of the Montreal Neurological Institute (MNI) space, and normalized functional images into the MNI space with 3 × 3 × 3 mm^3 voxel size and smoothed with a Gaussian kernel of 5 mm full width at half maximum (FWHM), and (6) performed temporal band-pass filtering for the typical band (0.01–0.1 Hz), the slow-4 band (0.027–0.073 Hz), and the slow-5 band (0.01–0.027 Hz), respectively. In this study, the fMRI data for subjects with head motion displacement >2mm or rotation >2° in any axis (*x*, *y*, and *z*-axis) were discarded. In the calculation, we excluded the datasets for three participants because of their head-movement displacements exceeding 2 mm and the rotation exceeding 2°. A total of 41 cSVD patients and 32 HCs were finally included in the following analysis. There were also no significant group differences in the head motion between the two groups.

2.5. ALFF analysis

We first performed a voxel-wise Fast Fourier Transform (FFT) method for each participant to convert the filtered time series into the frequency domain to obtain the power spectrum. Since the power within a given frequency band is proportional to the square of the magnitude of that frequency component, we calculated the square root of the power spectrum within each frequency band and then averaged these square roots across three frequency bands: 0.01–0.1 Hz (typical band), 0.027–0.073 Hz (slow-4), and 0.01–0.027 Hz (slow-5) at each voxel. This averaged square root was taken as ALFF (Zang et al., 2007), which was assumed to reflect the absolute intensity of spontaneous brain activity.

2.6. Statistical analysis

2.6.1. Demographic

A χ^2-test was used to test between-group differences in sex. A *t*-test was used to test between-group differences in age. The Wilcoxon test was used to test the education level between groups. The statistical significance level was set at $p < 0.05$. Statistical analysis was conducted using SPSS (version 21.0).

2.6.2. ALFF

The between-group difference in ALFF was conducted by PALM that is implemented in the DPARSF toolbox.[2] In the calculations. A general linear model (GLM) was applied, and sex and age factors were regressed. A two-tailed non-parametric permutation test (5,000 times) was conducted to determine the differences between the two groups. For the multiple-comparison correction, we used cluster-forming threshold and family-wise error (FWE) methods. The significance level was set at $p < 0.05$ (cluster-forming threshold >2.3, voxel-wise FWE <0.05).

A mixed effect analysis was performed on the two groups and their ALFF on the slow-5 and slow-4 band, using a two-way repeated measures analysis of variance (ANOVA) to investigate the effects of group and frequency band with age, sex, and head motions (mean FD) as covariates. Group (cSVD and HCs) was used as a between-subjects factor and frequency band (slow-4 and slow-5) as a repeated measurements factor. In addition, *post hoc* tests were performed between slow-5 band and slow-4 bands on the cSVD patients within brain regions showing group and frequency band interactions (Gu et al., 2019; Wang Z. et al., 2020). In addition, we also took a threshold of 50 voxels to remove small clusters, which meant only a cluster size >50 voxels were reported. For the multiple-comparison correction, we used threshold free cluster enhancement (TFCE) and family-wise error (FWE) methods. The significance level was set at $p < 0.01$ (voxel-wise FWE < 0.01). The imaging results after the multiple-comparison correction were reported by the AAL atlas (Rolls et al., 2020).

To determine whether the ALFF value in each region varied with clinical measures, we performed the correlation analyses between the ALFF values for the significantly changed ALFF and each clinical variable (i.e., VFT, DSST, and DST). The threshold was set at $p_{\text{two-tailed}} < 0.05$.

1 http://rfmri.org/dpabi

2 http://rfmri.org/DPABI

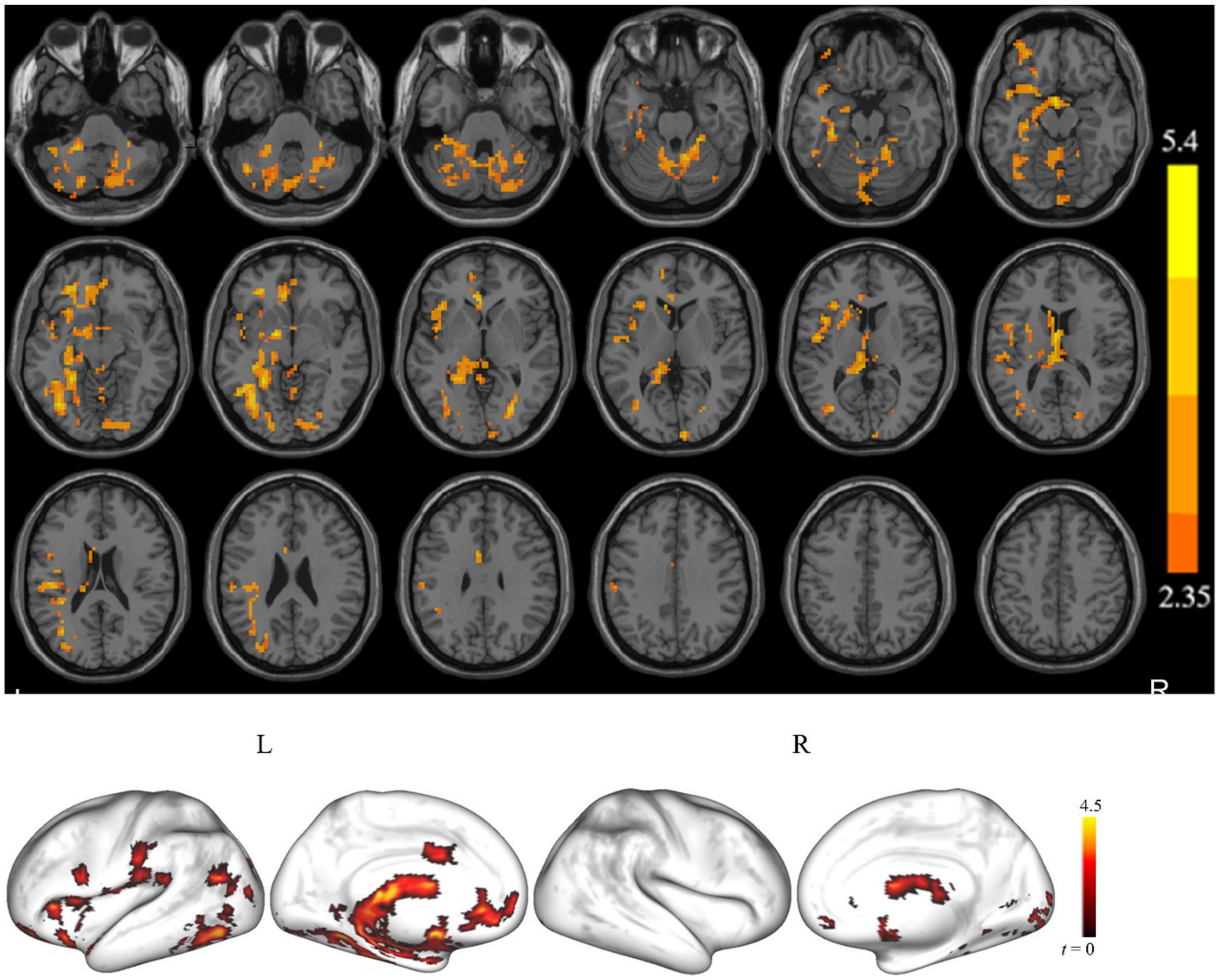

FIGURE 1
The brain regions show a significant difference in the amplitude of low-frequency fluctuation (ALFF) between the cSVD patients and the healthy controls in the typical frequency band ($p < 0.05$, cluster-forming threshold and FWE corrected). We found that the cSVD showed lower ALFF values in the one cluster in the left cerebellum, left hippocampus/parahippocampal, and left inferior occipital gyrus (IOG) of the controls.

3. Results

3.1. Demographic information

Table 1 lists the demographic information for both the cSVD and healthy controls, and clinical information for the cSVD group. No significant difference was found in sex between the two groups. The age and education level of the cSVD group were significantly higher than those of the healthy controls ($p < 0.05$).

3.2. ALFF in the typical frequency band (0.01–0.1 Hz)

Figure 1 displays clusters with significant between-group differences in ALFF. Compared with the controls, the cSVD patients showed significantly reduced ALFF in one cluster (cluster size = 3,019 voxels). The locations of the cluster are listed in Table 2. Specifically, the cSVD patients had significantly lower ALFF than the controls in the left fusiform gyrus/hippocampus/insula/inferior occipital gyrus/middle occipital gyrus/inferior frontal gyrus-medial orbital/rolandic operculum and the bilateral cerebellum.

3.3. ALFF in slow-4 and slow-5

Figure 2 shows the clusters with a significant difference in ALFF between the cSVD and controls for slow-4. For the slow-4, we found that the cSVD patients had significantly reduced ALFF in one cluster (voxel size = 1,383 voxels) in the left hemisphere, including the left cerebellum/hippocampus/fusiform gyrus/inferior occipital gyrus. As for the slow-5, no clusters showed a significant between-group difference in ALFF. The detailed information for the clusters is also listed in Table 2.

3.4. Interaction effect between group and frequency band

We observed a significant interaction between the frequency band and group in the left calcarine, bilateral lingual, left cerebellum,

TABLE 2 Brain areas showing significant differences in ALFF values under the typical (0.01–0.1 Hz) and slow-4 bands (0.027–0.073 Hz) between cSVD patients and HCs.

Frequency bands	Cluster size (Voxels)	MNI (*x y z*)	*t*	Brain regions
Typical	3,019	−6 30 −3	5.09	Cerebelum_8_R/L, Fusiform_L, Hippocampus_L, Cerebelum_Crus1/2_L, Insula_L, Occipital_Mid/Inf_L, Cerebelum_Crus1_R, Cerebelum_4_5_L, Cerebelum_6_L/R, Frontal_Inf_Orb_L, Rolandic_Oper_L
Slow-4	1,383	−3 0 −15	5.43	Cerebelum_crus1/2_L, Cerebelum_8_L, Hippocampus_L, Occipital_Mid_L, Fusiform_L, Cerebelum_crus1_L, Occipital_Inf_L

The significance threshold was set at $p < 0.05$, corrected for multiple comparisons using a cluster-forming threshold and the family-wise error (FWE) correction method. Coordinates of the peak voxel are shown in the Montreal Neurological Institute (MNI) space. The *t*-value corresponds to the peak voxel with a significant between-group difference in ALFF. The positive *t*-value represents a decrease (HCs > cSVD). Oper, operculum; Inf, inferior; Orb, orbital; Mid, middle; Sup, superior; L(R), left (right) hemisphere.

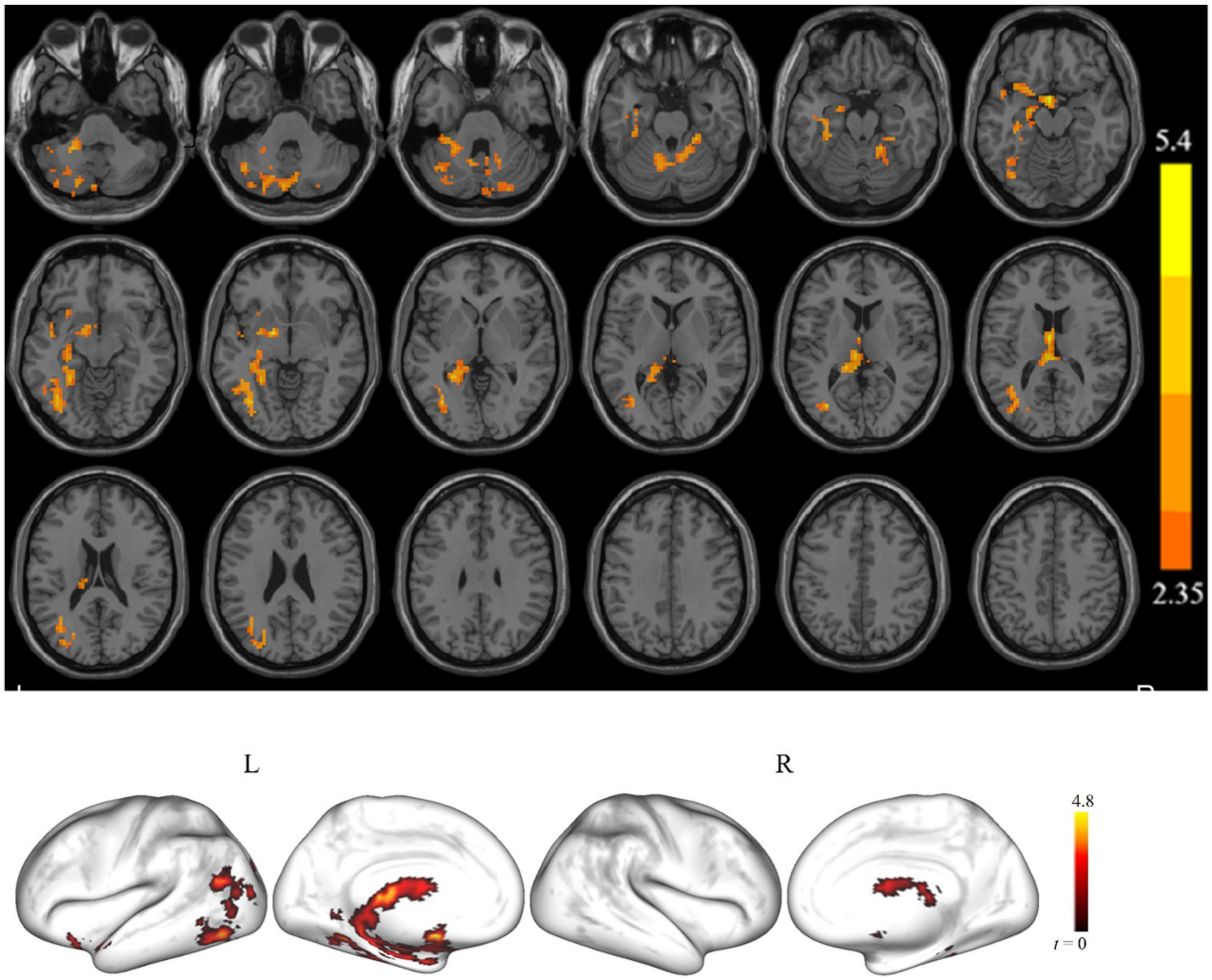

FIGURE 2
The brain regions showed a significant ALFF difference in the slow-4 band between the cSVD patients and the HCs ($p < 0.05$, cluster-forming threshold and FWE corrected). Hot (cold) colors represent higher (lower) ALFF in the HCs than in the cSVD patients.

bilateral precuneus, left cuneus, and right superior parietal gyrus (Table 3). Further *post hoc* tests showed significantly decreased ALFF values were identified in the left precuneus in the slow-4 band (Figures 3, 4).

3.4.1. Relationship between ALFF and clinical performance

For each of the significant clusters, no significant correlation was found between ALFF values and any neuropsychological scales ($p > 0.05$).

4. Discussion

This study identified the specific alteration pattern of ALFF in cSVD patients under different frequency bands through a voxel-based whole-brain analysis. We found that the cSVD patients showed significantly lower ALFF in the cerebellum, hippocampus, and occipital cortex than the controls in the typical band and the slow-4 band. Additionally, *post hoc* analysis indicated that cSVD was associated with a wide range of abnormalities in brain activity with related frequency bands.

TABLE 3 Significant interaction in ALFF between groups and frequency band.

Cluster	Brain regions	Cluster size (#voxels)	MNI (*x y z*)	*t* scores
A	Calcarine_L, Lingual_L, Lingual_R, Cerebelum_4_5_L, Cerebelum_Crus1_L, Cerebelum_6_L	769	−18 −72 12	4.83
B	Precuneus_L, Precuneus_R, Cuneus_L, Parietal_Sup_R	289	−3 −57 60	4.93

The interaction between frequency band and group on ALFF. The clusters were obtained by a two-way repeated-measures ANOVA ($p < 0.01$, TFCE and FWE corrected). Oper, operculum; Inf, inferior; Orb, orbital; Mid, middle; Sup, superior; L(R), left (right) hemisphere; TFCE, Threshold Free Cluster Enhancement.

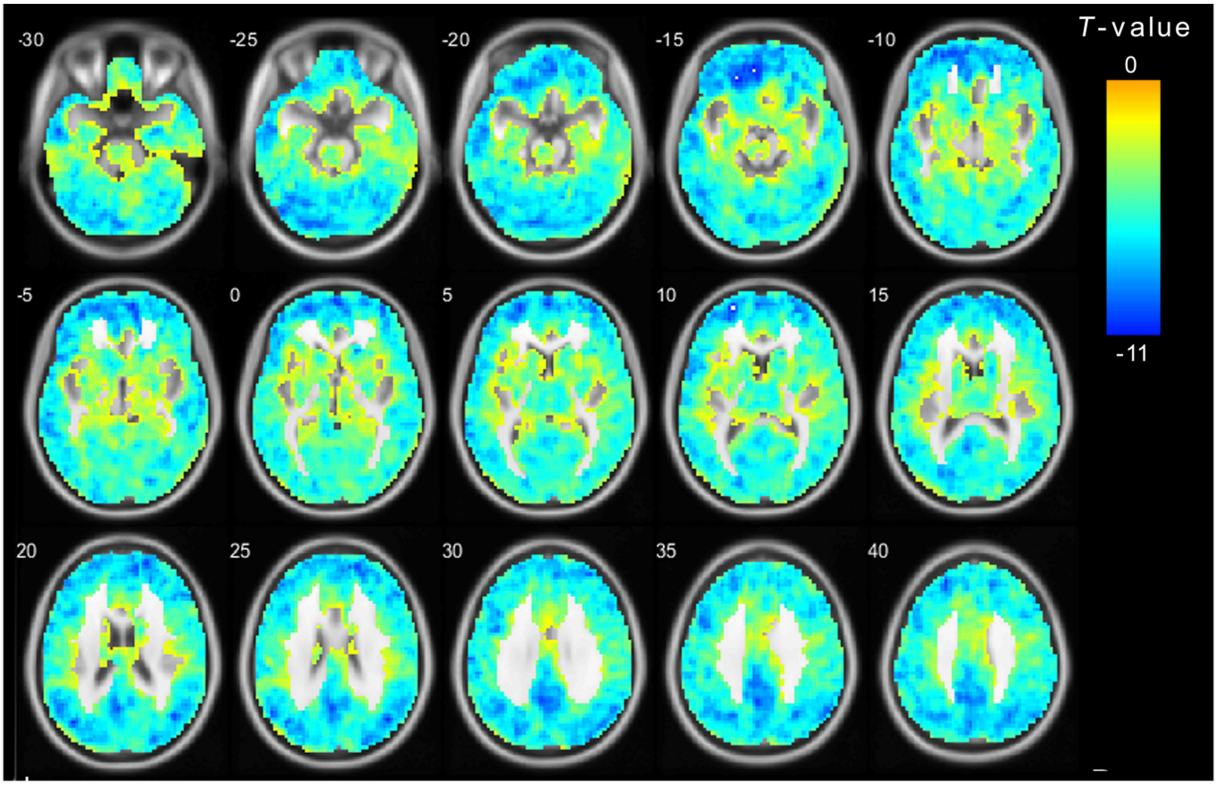

FIGURE 3
The main effect for frequency band on ALFF. The color bar on the right indicates the statistical *t*-value. Blue cold colors represent lower ALFF. The results were obtained by two-way repeated-measures ANOVA (TFCE and FWE corrected, voxel $p < 0.01$). TFCE, Threshold Free Cluster Enhancement.

4.1. ALFF differences between cSVD and HC

We found that cSVD patients showed reduced ALFF in the cerebellum compared with the controls (Figure 1). Although previous studies had noted that the cerebellum is widely believed to be responsible for motor skills (Baune et al., 2018), coordination, and balance of visual-motor (Garfinkle et al., 2020), several studies (Koziol et al., 2014; Thomas et al., 2017; Seese, 2020) indicated that it is also involved in cognitive function and executive function. The decrease of microstructural integrity in the cerebellum of deep white matter hyperintensities patients was associated with dual-task gait speed. Dual-task gait speed was associated with three cognitive domains (global cognition, attention/processing speed, and executive function) (Ghanavati et al., 2018). Schaefer et al. (2014) applied rs-fMRI analysis methods (eigenvector centrality) in cSVD patients and showed reduced connectivity in frontoparietal networks, whereas connectivity increases in the cerebellum. Another important finding is a positive correlation between reaction time in the incongruent condition of the Stroop task with the eigenvector centralities of the cerebellar region. The functional connectome in cerebellar regions was increased while the functional connectome in frontoparietal cognitive networks was decreased; therefore, the author speculated that frontoparietal hypoconnectivity might be compensated by hyper-connectivity. For example, Li et al. (2018) found lower grey matter volume in the cerebellar in patients with early-onset AD than in healthy controls. Several studies (Li et al., 2013; Mascalchi et al., 2014) also found that MCI patients had reduced WM integrity. These studies of AD or MCI provided insight into MCI patients with brain structural or functional impairment in the cerebellum. Previous studies (Castellazzi et al., 2014) in MCI patients also reported that the FC of the cerebellum is lower than that in healthy controls and the cerebellar FC correlates positively with semantic fluency. Thus, we infer that the reduction of spontaneous activity in the cerebellum may be related to the cognitive dysfunction of cSVD patients.

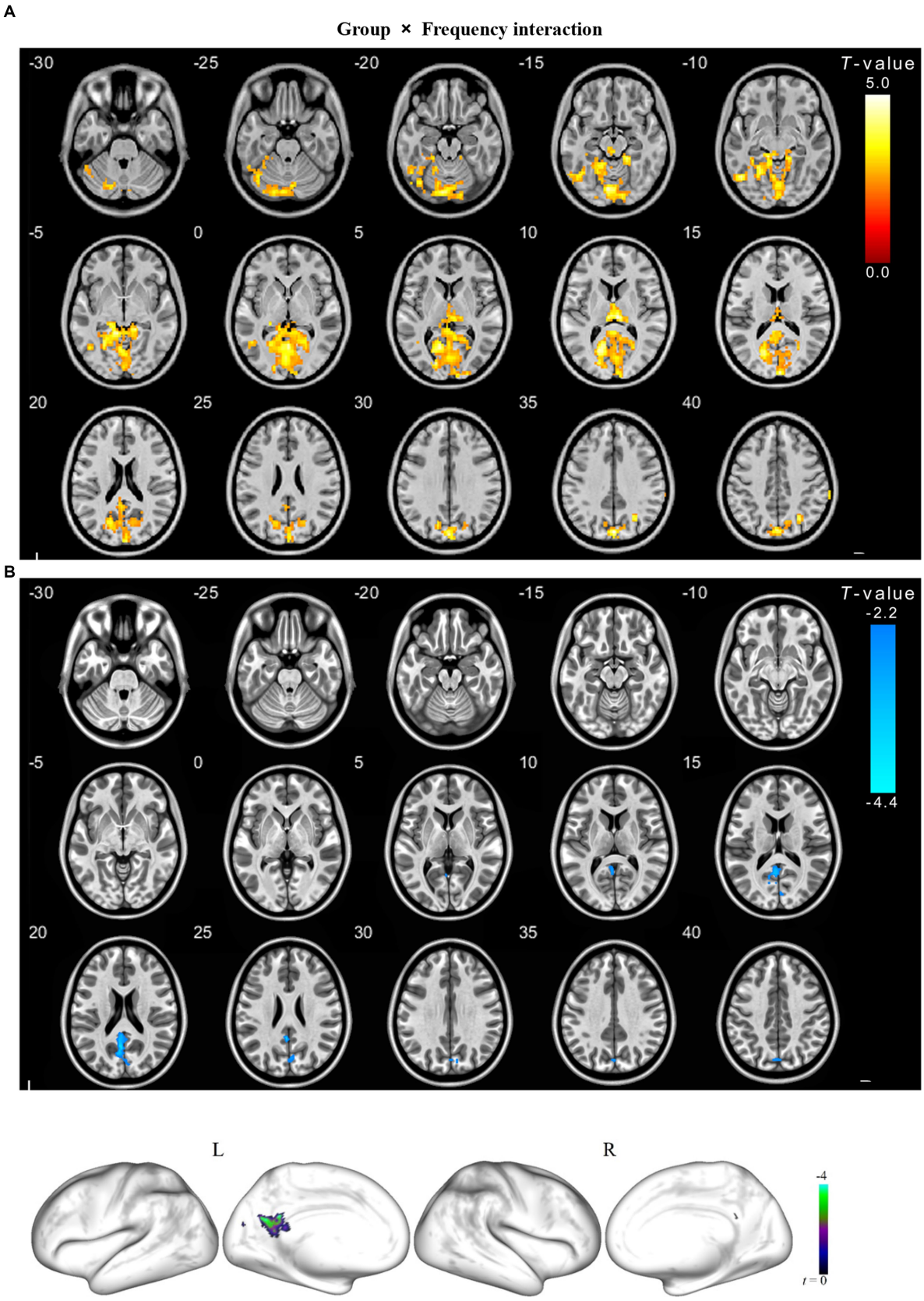

FIGURE 4
The interaction between frequency band and group on ALFF for cSVD patients. The results were obtained by a two-way repeated-measures ANOVA ($p < 0.01$, TFCE and FWE corrected) **(A)**; and then a post-hoc pair *t*-test shown in the **(B)** ($p < 0.025$, TFCE and FWE corrected), compared to the slow-5 band, cold overlays indicate lower ALFF in cSVD patients in the slow-4 band. TFCE, Threshold Free Cluster Enhancement.

This study also found aberrant spontaneous brain activity in the occipital cortex (Figure 1). In the pathological anatomy of cSVD, researchers found that cortical microinfarcts were presented more frequently in the parietal and occipital lobes, which were also related to the severity of cSVD (Ii et al., 2021). A comparison of our findings with those of other studies (De Marco et al., 2017; Marjańska et al., 2019) confirms dysfunction of the occipital lobe during AD and MCI. Gray matter volume of different brain regions was associated with cognitive ability in cSVD patients, and gray matter volume in the occipital thalamus was positively correlated with Montreal Cognitive Assessment scores (Wang Y. et al., 2020). Lambert et al. (2016) did longitudinal research into symptomatic cSVD to investigate. They showed that the rate of white matter hyperintensity progression is associated with increases in cortical gray matter atrophy rates in occipital lobes. Chen et al. (2020) found that the right inferior longitudinal fasciculus had a significantly negative correlation with total cognitive and episodic memory. It could be that the cSVD patients showed a relative decline of spontaneous brain activity in the occipital cortex, which might be part of the underlying brain function mechanism of cognitive dysfunction.

In addition, the current study also found abnormal spontaneous brain activity in the hippocampus of cSVD patients, suggesting that the occurrence of cognitive decline in cSVD may relate to the decreased activity in the hippocampus. The hippocampus is closely related to memory function and spatial navigational ability and plays a crucial role in all forms of declarative memory (including recognition) (Wixted and Squire, 2011). Jokinen et al. (2020) studied the relationship between grey matter volume and clinical symptoms of cSVD. They found a positive correlation between hippocampal volume and Vascular Dementia Assessment Scale–Cognitive Subscale, executive function, and memory. A study evaluated the influence of negative and positive cSVD-hippocampal subfield atrophy on episodic memory and frontal executive function (Wong et al., 2021). Hippocampal subfield atrophy worsened with increasing SVD severity, and atrophy in the subiculum, CA1, CA4, molecular layer, and dentate gyrus of the hippocampal were essential to poor episodic memory and frontal executive function. Xi et al. (2012) found that the low-frequency oscillation amplitudes of the right hippocampus, parahippocampal gyrus, left middle temporal gyrus and right ventromedial prefrontal cortex of MCI patients were reduced. The ALFF values of the hippocampus and parahippocampal gyrus had a positive correlation with the neuropsychological scale score. The hippocampal ALFF value of cSVD patients is abnormally decreased, and it is positively correlated with the MoCA score in our research. Many studies have affirmed the role of the hippocampus in the field of cognitive function, which may be a critical factor in the cognitive dysfunction of cSVD patients.

4.2. Group × frequency interaction

Different neurophysiological mechanisms have different physiological functions, including different oscillatory bands (Buzsáki and Draguhn, 2004). Previous studies had explored the differences in ALFF between brain areas in the slow-4 and slow-5 bands (Xiao et al., 2018; Wang Z. et al., 2020). Neural oscillations of different frequencies in the human brain may be sensitive to activities in different regions and can reflect different physiological functions of brain activities (Knyazev, 2007). Low-frequency oscillations are related to long-distance connections and the integration of large neuronal systems. In contrast, the high-frequency oscillations synchronization constitutes a functionally important neuronal peak time relationship in brain activity (Arnulfo et al., 2020). Connectivity between distal cortical regions is a valuable but expensive feature of cortical tissue and exists mainly between heterotypic (Oligschläger et al., 2017). It is generally believed that the slow-5 band is the main contributor of resting-state fluctuations in healthy humans (Zuo et al., 2010), and is more sensitive in the cortex (such as the temporal and Rolandic lobes). Our results are dissimilar to previous rs-fMRI studies in AD, showing more varied areas in the slow-5 band than the slow-4 band (Yang et al., 2020). Liu et al. (2014) also found that several temporal regions were more significant in the slow-5 band than the slow-4 band in AD patients. Our results are similar to previous studies in patients with cognitive impairment, which suggested that most cortical areas had more robust low-frequency oscillations and higher functional activities in the slow-5 band.

We observed a significant group × frequency interaction effect on the ALFF value in the left precuneus. These findings showed that the ALFF changes in CSVD patients with cognitive dysfunction are related to frequency bands, and the neurophysiological mechanism is unclear. Thus, we conclude that certain pathologic conditions in the precuneus may increase the influence of specific frequency bands. However, studies have found that precuneus plays a central role in many highly integrated tasks, including visual space imagery, situational memory extraction, and self-processing operations (Cavanna and Trimble, 2006). Hebscher et al. (2020) have also confirmed that the precuneus was closely related to human autobiographical memory. Luo et al. (2020) studied the functional connection between the precuneus and the cortical using resting-state fMRI and found that the human precuneus can be subdivided into six symmetrical and connected parcels. The precuneus has four sub-regions and acts as a mediator in the interaction of the default mode, multi-faceted attention, and frontoparietal control network. Precuneus and posterior cingulate cortex together belong to the posterior default mode network (DMN). The DMN is a specific neuronal circuitry to global brain function. Damage to the DMN often occurs in diseases such as Alzheimer's disease, Parkinson's disease, Epilepsy and attention deficit hyperactivity disorder (ADHD) (Mohan et al., 2016). A meta-analysis compared amnestic mild cognitive impairment patients (aMCI) with healthy control suggested that aMCI is associated with widespread aberrant regional spontaneous brain activity, predominantly involving the default mode, salience, and visual networks. In contrast, the increased severity of cognitive impairment in aMCI patients was associated with more significant decreases in ALFFs in the cuneus/precuneus cortices (Pan et al., 2017).

These findings indicated that frequency-specific ALFF could supplement important information for disease diagnosis as well as supply a new perspective for our understanding of the pathology of CSVD.

5. Limitations

This study has several limitations. First, the number of samples is not large enough, and age differences across cSVD patients or between patients and healthy control groups were not well addressed.

Second, one of limitations of the present study is the 8-channel phased-array head coil employed for data acquisition, which represents the minimal number of channels. Using an advanced scanning sequence may need to be considered in future studies, which may potentially enhance qualities of scanned images. Third, we did not classify the sub-type of cSVD although there are many types of imaging performance and various pathophysiology of cSVD. Future study needs to recruit more patients and distinguish between different imaging findings to evaluate the degree of impairment of brain function in different types to guide the treatment. Fourth, the current study used the rs-fMRI only. It would be better to use multi-modal neuroimaging data, such as arterial spin labeling (ASL) and diffusion tensor imaging (DTI). The combination of multi-modal neuroimaging and neuropsychological scales might help us understand cognitive dysfunction progression in cSVD more thoroughly. Finally, the healthy controls included in our study were different in age from the CSVD group. Because age is a high-risk factor for the development of cerebral small vessel disease, we had great difficulty in finding age-matched healthy controls.

6. Conclusion

This study analyzed spontaneous brain activity in cSVD patients and showed abnormal ALFF in distinct brain regions in patients compared with controls. These abnormal brain regions were found in the cerebellum, occipital, and hippocampus in cSVD patients. These findings could reflect the pathogenesis of specific clinical manifestations of cSVD, especially cognitive decline.

Data availability statement

The original contributions presented in the study are included in the article/supplementary materials, further inquiries can be directed to the corresponding authors.

Ethics statement

The studies involving humans were approved by the Institutional Review Board of Zhongshan TCM Hospital (ClinicalTrials.gov identifier: 2016ZSZY-LLK-028). The studies were conducted in accordance with the local legislation and institutional requirements. The participants provided their written informed consent to participate in this study.

Author contributions

SC: Data curation, Writing – original draft. RH: Methodology, Writing – original draft. MZ: Writing – original draft. XH: Writing – review & editing. SLing: Writing – review & editing. SLiu: Resources, Writing – review & editing. NY: Methodology, Writing – review & editing.

Funding

The author(s) declare that no financial support was received for the research, authorship, and/or publication of this article.

Acknowledgments

This study was approved by the Institutional Review Board of Zhongshan TCM Hospital (ClinicalTrials.gov identifier: 2016ZSZY-LLK-028).

Conflict of interest

The authors declare that the research was conducted in the absence of any commercial or financial relationships that could be construed as a potential conflict of interest.

Publisher's note

References

Arnulfo, G., Wang, S. H., Myrov, V., Toselli, B., Hirvonen, J., Fato, M. M., et al. (2020). Long-range phase synchronization of high-frequency oscillations in human cortex. *Nat. Commun.* 11:5363. doi: 10.1038/s41467-020-18975-8

Baune, B. T., Brignone, M., and Larsen, K. G. (2018). A network meta-analysis comparing effects of various antidepressant classes on the digit symbol substitution test (DSST) as a measure of cognitive dysfunction in patients with major depressive disorder. *Int. J. Neuropsychopharmacol.* 21, 97–107. doi: 10.1093/ijnp/pyx070

Buzsáki, G., and Draguhn, A. (2004). Neuronal oscillations in cortical networks. *Science* 304, 1926–1929. doi: 10.1126/science.1099745

Cai, Z., Wang, C., He, W., Tu, H., Tang, Z., Xiao, M., et al. (2015). Cerebral small vessel disease and Alzheimer's disease. *Clin. Interv. Aging* 10, 1695–1704. doi: 10.2147/CIA.S90871

Castellazzi, G., Palesi, F., Casali, S., Vitali, P., Sinforiani, E., Wheeler-Kingshott, C. A., et al. (2014). A comprehensive assessment of resting state networks: bidirectional modification of functional integrity in cerebro-cerebellar networks in dementia. *Front. Neurosci.* 8:223. doi: 10.3389/fnins.2014.00223

Cavanna, A. E., and Trimble, M. R. (2006). The precuneus: a review of its functional anatomy and behavioural correlates. *Brain* 129, 564–583. doi: 10.1093/brain/awl004

Chen, H. F., Huang, L. L., Li, H. Y., Qian, Y., Yang, D., Qing, Z., et al. (2020). Microstructural disruption of the right inferior fronto-occipital and inferior longitudinal fasciculus contributes to WMH-related cognitive impairment. *CNS Neurosci. Ther.* 26, 576–588. doi: 10.1111/cns.13283

Chen, X., Wang, J., Shan, Y., Cai, W., Liu, S., Hu, M., et al. (2019). Cerebral small vessel disease: neuroimaging markers and clinical implication. *J. Neurol.* 266, 2347–2362. doi: 10.1007/s00415-018-9077-3

De Guio, F., Jouvent, E., Biessels, G. J., Black, S. E., Brayne, C., Chen, C., et al. (2016). Reproducibility and variability of quantitative magnetic resonance imaging markers in cerebral small vessel disease. *J. Cereb. Blood Flow Metab.* 36, 1319–1337. doi: 10.1177/0271678X16647396

De Marco, M., Duzzi, D., Meneghello, F., and Venneri, A. (2017). Cognitive efficiency in Alzheimer's disease is associated with increased occipital connectivity. *J. Alzheimers Dis.* 57, 541–556. doi: 10.3233/jad-161164

Dey, A. K., Stamenova, V., Turner, G., Black, S. E., and Levine, B. (2016). Pathoconnectomics of cognitive impairment in small vessel disease: a systematic review. *Alzheimers Dement.* 12, 831–845. doi: 10.1016/j.jalz.2016.01.007

Feng, M., Wen, H., Xin, H., Zhang, N., Liang, C., and Guo, L. (2021). Altered spontaneous brain activity related to neurologic dysfunction in patients with cerebral small vessel disease. *Front. Aging Neurosci.* 13:731585. doi: 10.3389/fnagi.2021.731585

Garfinkle, J., Guo, T., Synnes, A., Chau, V., Branson, H. M., Ufkes, S., et al. (2020). Location and size of preterm cerebellar hemorrhage and childhood development. *Ann. Neurol.* 88, 1095–1108. doi: 10.1002/ana.25899

Ghanavati, T., Smitt, M. S., Lord, S. R., Sachdev, P., Wen, W., Kochan, N. A., et al. (2018). Deep white matter hyperintensities, microstructural integrity and dual task walking in older people. *Brain Imaging Behav.* 12, 1488–1496. doi: 10.1007/s11682-017-9787-7

Gu, L., Hong, S., Jiang, J., Liu, J., Cao, X., Huang, Q., et al. (2019). Bidirectional alterations in ALFF across slow-5 and slow-4 frequencies in the brains of postherpetic neuralgia patients. *J. Pain Res.* 12, 39–47. doi: 10.2147/jpr.S179077

Hebscher, M., Ibrahim, C., and Gilboa, A. (2020). Precuneus stimulation alters the neural dynamics of autobiographical memory retrieval. *NeuroImage* 210:116575. doi: 10.1016/j.neuroimage.2020.116575

Ii, Y., Ishikawa, H., Shindo, A., Matsuyama, H., Matsuura, K., Matsuda, K., et al. (2021). Association between cortical microinfarcts and total small vessel disease burden in cerebral amyloid angiopathy on 3-tesla magnetic resonance imaging. *Eur. J. Neurol.* 28, 794–799. doi: 10.1111/ene.14610

Jokinen, H., Koikkalainen, J., Laakso, H. M., Melkas, S., Nieminen, T., Brander, A., et al. (2020). Global burden of small vessel disease-related brain changes on MRI predicts cognitive and functional decline. *Stroke* 51, 170–178. doi: 10.1161/strokeaha.119.026170

Kim, H. W., Hong, J., and Jeon, J. C. (2020). Cerebral small vessel disease and Alzheimer's disease: A Review. *Review* 11:927. doi: 10.3389/fneur.2020.00927

Knyazev, G. G. (2007). Motivation, emotion, and their inhibitory control mirrored in brain oscillations. *Neurosci. Biobehav. Rev.* 31, 377–395. doi: 10.1016/j.neubiorev.2006.10.004

Koziol, L. F., Budding, D., Andreasen, N., D'Arrigo, S., Bulgheroni, S., Imamizu, H., et al. (2014). Consensus paper: the cerebellum's role in movement and cognition. *Cerebellum* 13, 151–177. doi: 10.1007/s12311-013-0511-x

Lambert, C., Benjamin, P., Zeestraten, E., Lawrence, A. J., Barrick, T. R., and Markus, H. S. (2016). Longitudinal patterns of leukoaraiosis and brain atrophy in symptomatic small vessel disease. *Brain* 139, 1136–1151. doi: 10.1093/brain/aww009

Leung, J. L., Lee, G. T., Lam, Y. H., Chan, R. C., and Wu, J. Y. (2011). The use of the digit span test in screening for cognitive impairment in acute medical inpatients. *Int. Psychogeriatr.* 23, 1569–1574. doi: 10.1017/s1041610211000792

Li, H., Jia, X., Li, Y., Jia, X., and Yang, Q. (2021). Aberrant amplitude of Low-frequency fluctuation and degree centrality within the default mode network in patients with vascular mild cognitive impairment. *Brain Sci.* 11:1534. doi: 10.3390/brainsci11111534

Li, H., Liang, Y., Chen, K., Li, X., Shu, N., Zhang, Z., et al. (2013). Different patterns of white matter disruption among amnestic mild cognitive impairment subtypes: relationship with neuropsychological performance. *J. Alzheimers Dis.* 36, 365–376. doi: 10.3233/jad-122023

Li, K. C., Luo, X., Zeng, Q. Z., Xu, X. J., Huang, P. Y., Shen, Z. J., et al. (2018). Distinct patterns of interhemispheric connectivity in patients with early- and late-onset Alzheimer's disease. *Front. Aging Neurosci.* 10:261. doi: 10.3389/fnagi.2018.00261

Liao, H., Yi, J., Cai, S., Shen, Q., Liu, Q., Zhang, L., et al. (2021). Changes in degree centrality of network nodes in different frequency bands in Parkinson's disease with depression and without depression. *Front. Neurosci.* 15:638554. doi: 10.3389/fnins.2021.638554

Liu, Y., Braidy, N., Poljak, A., Chan, D. K. Y., and Sachdev, P. (2018). Cerebral small vessel disease and the risk of Alzheimer's disease: a systematic review. *Ageing Res. Rev.* 47, 41–48. doi: 10.1016/j.arr.2018.06.002

Liu, X., Wang, S., Zhang, X., Wang, Z., Tian, X., and He, Y. (2014). Abnormal amplitude of low-frequency fluctuations of intrinsic brain activity in Alzheimer's disease. *J. Alzheimers Dis.* 40, 387–397. doi: 10.3233/jad-131322

Luo, Z., Zeng, L. L., Qin, J., Hou, C., Shen, H., and Hu, D. (2020). Functional Parcellation of human brain Precuneus using density-based clustering. *Cereb. Cortex* 30, 269–282. doi: 10.1093/cercor/bhz086

Marjańska, M., McCarten, J. R., Hodges, J. S., Hemmy, L. S., and Terpstra, M. (2019). Distinctive neurochemistry in Alzheimer's disease via 7 T in vivo magnetic resonance spectroscopy. *J. Alzheimers Dis.* 68, 559–569. doi: 10.3233/jad-180861

Mascalchi, M., Ginestroni, A., Toschi, N., Poggesi, A., Cecchi, P., Salvadori, E., et al. (2014). The burden of microstructural damage modulates cortical activation in elderly subjects with MCI and leuko-araiosis. A DTI and fMRI study. *Hum. Brain Mapp.* 35, 819–830. doi: 10.1002/hbm.22216

Mo, Y., Mao, C., Yang, D., Ke, Z., Huang, L., Yang, Z., et al. (2023). Altered neuroimaging patterns of cerebellum and cognition underlying the gait and balance dysfunction in cerebral small vessel disease. *Front. Aging Neurosci.* 15:1117973. doi: 10.3389/fnagi.2023.1117973

Mohan, A., Roberto, A. J., Mohan, A., Lorenzo, A., Jones, K., Carney, M. J., et al. (2016). The significance of the default mode network (DMN) in neurological and neuropsychiatric disorders: a review. *Yale J. Biol. Med.* 89, 49–57.

Oligschläger, S., Huntenburg, J. M., Golchert, J., Lauckner, M. E., Bonnen, T., and Margulies, D. S. (2017). Gradients of connectivity distance are anchored in primary cortex. *Brain Struct. Funct.* 222, 2173–2182. doi: 10.1007/s00429-016-1333-7

Pan, P., Zhu, L., Yu, T., Shi, H., Zhang, B., Qin, R., et al. (2017). Aberrant spontaneous low-frequency brain activity in amnestic mild cognitive impairment: a meta-analysis of resting-state fMRI studies. *Ageing Res. Rev.* 35, 12–21. doi: 10.1016/j.arr.2016.12.001

Pantoni, L. (2010). Cerebral small vessel disease: from pathogenesis and clinical characteristics to therapeutic challenges. *Lancet Neurol.* 9, 689–701. doi: 10.1016/s1474-4422(10)70104-6

Qi, R., Luo, Y., Zhang, L., Weng, Y., Surento, W., Jahanshad, N., et al. (2020). FKBP5 haplotypes and PTSD modulate the resting-state brain activity in Han Chinese adults who lost their only child. *Transl. Psychiatry* 10:91. doi: 10.1038/s41398-020-0770-5

Ren, F., Ma, W., Zong, W., Li, N., Li, X., Li, F., et al. (2021). Brain frequency-specific changes in the spontaneous neural activity are associated with cognitive impairment in patients with Presbycusis. *Front. Aging Neurosci.* 13:649874. doi: 10.3389/fnagi.2021.649874

Rolls, E. T., Huang, C.-C., Lin, C.-P., Feng, J., and Joliot, M. (2020). Automated anatomical labelling atlas 3. *NeuroImage* 206:116189. doi: 10.1016/j.neuroimage.2019.116189

Sasai, S., Koike, T., Sugawara, S. K., Hamano, Y. H., Sumiya, M., Okazaki, S., et al. (2021). Frequency-specific task modulation of human brain functional networks: a fast fMRI study. *NeuroImage* 224:117375. doi: 10.1016/j.neuroimage.2020.117375

Schaefer, A., Quinque, E. M., Kipping, J. A., Arélin, K., Roggenhofer, E., Frisch, S., et al. (2014). Early small vessel disease affects frontoparietal and cerebellar hubs in close correlation with clinical symptoms--a resting-state fMRI study. *J. Cereb. Blood Flow Metab.* 34, 1091–1095. doi: 10.1038/jcbfm.2014.70

Seese, R. R. (2020). Working memory impairments in cerebellar disorders of childhood. *Pediatr. Neurol.* 107, 16–23. doi: 10.1016/j.pediatrneurol.2020.02.005

Staals, J., Booth, T., Morris, Z., Bastin, M. E., Gow, A. J., Corley, J., et al. (2015). Total MRI load of cerebral small vessel disease and cognitive ability in older people. *Neurobiol. Aging* 36, 2806–2811. doi: 10.1016/j.neurobiolaging.2015.06.024

Thomas, A. R., Lacadie, C., Vohr, B., Ment, L. R., and Scheinost, D. (2017). Fine motor skill mediates visual memory ability with microstructural neuro-correlates in cerebellar peduncles in prematurely born adolescents. *Cereb. Cortex* 27, 322–329. doi: 10.1093/cercor/bhw415

Vaucheret Paz, E., Puga, C., Ekonen, C., Pintos, P., Lascombes, I., De Vita, S., et al. (2020). Verbal fluency test in children with neurodevelopmental disorders. *J. Neurosci. Rural Pract.* 11, 95–99. doi: 10.1055/s-0039-3400347

Wang, L., Feng, Q., Wang, M., Zhu, T., Yu, E., Niu, J., et al. (2021). An effective brain imaging biomarker for AD and aMCI: ALFF in Slow-5 frequency band. *Curr. Alzheimer Res.* 18, 45–55. doi: 10.2174/1567205018666210324130502

Wang, Z., Liu, Y., Ruan, X., Li, Y., Li, E., Zhang, G., et al. (2020). Aberrant amplitude of Low-frequency fluctuations in different frequency bands in patients with Parkinson's disease. *Front. Aging Neurosci.* 12:576682. doi: 10.3389/fnagi.2020.576682

Wang, Y., Yang, Y., Wang, T., Nie, S., Yin, H., and Liu, J. (2020). Correlation between white matter Hyperintensities related gray matter volume and cognition in cerebral small vessel disease. *J. Stroke Cerebrovasc. Dis.* 29:105275. doi: 10.1016/j.jstrokecerebrovasdis.2020.105275

Wardlaw, J. M., Smith, E. E., Biessels, G. J., Cordonnier, C., Fazekas, F., Frayne, R., et al. (2013). Neuroimaging standards for research into small vessel disease and its contribution to ageing and neurodegeneration. *Lancet Neurol.* 12, 822–838. doi: 10.1016/S1474-4422(13)70124-8

Wixted, J. T., and Squire, L. R. (2011). The medial temporal lobe and the attributes of memory. *Trends Cogn. Sci.* 15, 210–217. doi: 10.1016/j.tics.2011.03.005

Wong, F. C. C., Yatawara, C., Low, A., Foo, H., Wong, B. Y. X., Lim, L., et al. (2021). Cerebral small vessel disease influences hippocampal subfield atrophy in mild cognitive impairment. *Transl. Stroke Res.* 12, 284–292. doi: 10.1007/s12975-020-00847-4

Wu, Z., Luo, Q., Wu, H., Wu, Z., Zheng, Y., Yang, Y., et al. (2020). Amplitude of Low-frequency oscillations in major depressive disorder with childhood trauma. *Front. Psych.* 11:596337. doi: 10.3389/fpsyt.2020.596337

Xi, Q., Zhao, X., Wang, P., Guo, Q., Jiang, H., Cao, X., et al. (2012). Spontaneous brain activity in mild cognitive impairment revealed by amplitude of low-frequency fluctuation analysis: a resting-state fMRI study. *Radiol. Med.* 117, 865–871. doi: 10.1007/s11547-011-0780-8

Xiao, F., Wang, T., Gao, L., Fang, J., Sun, Z., Xu, H., et al. (2018). Frequency-dependent changes of the resting BOLD signals predicts cognitive deficits in asymptomatic carotid artery stenosis. *Front. Neurosci.* 12:416. doi: 10.3389/fnins.2018.00416

Yang, L., Yan, Y., Li, Y., Hu, X., Lu, J., Chan, P., et al. (2020). Frequency-dependent changes in fractional amplitude of low-frequency oscillations in Alzheimer's disease: a resting-state fMRI study. *Brain Imaging Behav.* 14, 2187–2201. doi: 10.1007/s11682-019-00169-6

Zang, Y. F., He, Y., Zhu, C. Z., Cao, Q. J., Sui, M. Q., Liang, M., et al. (2007). Altered baseline brain activity in children with ADHD revealed by resting-state functional MRI. *Brain Dev.* 29, 83–91. doi: 10.1016/j.braindev.2006.07.002

Zhou, X., Zhang, C., Li, L., Zhang, Y., Zhang, W., Yin, W., et al. (2020). Altered brain function in cerebral small vessel disease patients with gait disorders: a resting-state functional MRI study. *Front. Aging Neurosci.* 12:234. doi: 10.3389/fnagi.2020.00234

Zou, Q.-H., Zhu, C.-Z., Yang, Y., Zuo, X.-N., Long, X.-Y., Cao, Q.-J., et al. (2008). An improved approach to detection of amplitude of low-frequency fluctuation (ALFF) for resting-state fMRI: fractional ALFF. *J. Neurosci. Methods* 172, 137–141. doi: 10.1016/j.jneumeth.2008.04.012

Zuo, X. N., Di Martino, A., Kelly, C., Shehzad, Z. E., Gee, D. G., Klein, D. F., et al. (2010). The oscillating brain: complex and reliable. *NeuroImage* 49, 1432–1445. doi: 10.1016/j.neuroimage.2009.09.037

frontiers | Frontiers in Neuroscience

TYPE Original Research
PUBLISHED 13 December 2023
DOI 10.3389/fnins.2023.1281160

OPEN ACCESS

EDITED BY
Guang-qing Xu

REVIEWED BY
Jitka Veldema,
Bielefeld University, Germany
Hongwu Wang,
University of Florida, United States
Massimiliano Toscano,
Sapienza University of Rome, Italy

*CORRESPONDENCE
Jianxian Wu
✉ ay2fyjianxianwu@126.com

RECEIVED 22 August 2023
ACCEPTED 27 November 2023
PUBLISHED 13 December 2023

CITATION
Shen X, Yu Y, Xiao H, Ji L and Wu J (2023) Cortical activity associated with focal muscle vibration applied directly to the affected forearm flexor muscle in post-stroke patients: an fNIRS study.
Front. Neurosci. 17:1281160.
doi: 10.3389/fnins.2023.1281160

Cortical activity associated with focal muscle vibration applied directly to the affected forearm flexor muscle in post-stroke patients: an fNIRS study

Xianshan Shen[1,2], Yang Yu[1,2], Han Xiao[1,2], Leilei Ji[1,2] and Jianxian Wu[1,2]*

[1]Department of Rehabilitation Medicine, The Second Affiliated Hospital of Anhui Medical University, Hefei, China, [2]Department of Rehabilitation and Sports Medicine, The Second Clinical College of Anhui Medical University, Hefei, China

Objective: The purpose of this study was to utilize functional near-infrared spectroscopy (fNIRS) to identify changes in cortical activity caused by focal muscle vibration (FMV), which was directly administered to the affected forearm flexor muscles of hemiplegic stroke patients. Additionally, the study aimed to investigate the correlation between these changes and the clinical characteristics of the patients, thereby expanding the understanding of potential neurophysiological mechanisms linked to these effects.

Methods: Twenty-two stroke patients with right hemiplegia who were admitted to our ward for rehabilitation were selected for this study. The fNIRS data were collected from subjects using a block-design paradigm. Subsequently, the collected data were analyzed using the NirSpark software to determine the mean Oxyhemoglobin (Hbo) concentrations for each cortical region of interest (ROI) in the task and rest states for every subject. The stimulation task was FMV (frequency 60 Hz, amplitude 6 mm) directly applied to belly of the flexor carpi radialis muscle (FCR) on the affected side. Hbo was measured in six regions of interest (ROIs) in the cerebral cortex, which included the bilateral prefrontal cortex (PFC), sensorimotor cortex (SMC), and occipital cortex (OC). The clinical characteristics of the patients were assessed concurrently, including Lovett's 6-level muscle strength assessment, clinical muscle tone assessment, the upper extremity function items of the Fugl-Meyer Assessment (FMA-UE), Bruunstrom staging scale (BRS), and Modified Barthel index (MBI). Statistical analyses were conducted to determine the activation in the ROIs and to comprehend its correlation with the clinical characteristics of the patients.

Results: Statistical analysis revealed that, except for right OC, there were statistically significant differences between the mean Hbo in the task state and rest state for bilateral SMC, PFC, and left OC. A positive correlation was observed between the muscle strength of the affected wrist flexor group and the change values of Hbo (Hbo-CV), as well as the beta values in the left SMC, PFC, and OC. However, no statistical correlation was found between muscle strength and Hbo-CV or beta values in the right SMC, PFC, and OC. The BRS of the affected upper limb exhibited a positive correlation with the Hbo-CV or beta values in the left SMC and PFC. In contrast, no statistical correlation was observed in the right SMC, PFC, and bilateral OC. No significant correlation was found between the muscle tone of the affected wrist flexor group, FMA-UE, MBI, and Hbo-CV or beta values of cortical ROIs.

Conclusion: FMV-evoked sensory stimulation applied directly to the FCR belly on the paralyzed side activated additional brain cortices, including bilateral PFC and ipsilesional OC, along with bilateral SMC in stroke patients. However, the clinical characteristics of the patients were only correlated with the intensity of ipsilesional SMC and PFC activation. The results of this study provide neurophysiological theoretical support for the expanded clinical application of FMV.

KEYWORDS

focal muscle vibration, stroke, cortical excitability, cortical activity, functional near-infrared spectroscopy

1 Introduction

Stroke is a widespread disease that endangers the lives and health of the middle-aged and elderly. According to the Global Burden of Disease (GBD) study, stroke continues to be the second main reason for mortality and the third cause of both mortality and disability (measured by disability-adjusted life-years lost-DALYs) in individuals (Feigin et al., 2022). After experiencing a stroke, roughly 26% of individuals continue to face disability in essential daily tasks, while half of them endure restricted mobility caused by hemiparesis (Kelly-Hayes et al., 2003). Stroke can induce altered muscle tone in the affected upper limbs and hands, decreased coordination, impaired sensation, muscle weakness, and impaired motor control, affecting activities of daily living and social participation. Scholars have commonly expressed their concern regarding how to enhance the effectiveness of limb function in patients with hemiplegic stroke. The main clinical treatments for post-stroke limb dysfunction include physical therapy (European and Rehabilitation Medicine Bodies, 2018), occupational therapy (Powell et al., 2016), transcutaneous electrical nerve stimulation (Mahmood et al., 2019), functional electrical stimulation (Eraifej et al., 2017), transcranial direct current stimulation (Van Hoornweder et al., 2021), repetitive transcranial magnetic stimulation (Starosta et al., 2022), motor imagery (Monteiro et al., 2021), virtual reality (Kim et al., 2020), constraint induced movement therapy (Rocha et al., 2021), brain-computer interface technology (Xue et al., 2021), and robotics (Bruni et al., 2018), etc. These intervention strategies have limitations due to the need for trained professionals, lack of precision, consensus evidence, and high implementation costs (Wang et al., 2020). Pursuing a safe and effective method for neurorehabilitation poses a significant and complex challenge.

Disruption of the sensory system after stroke plays an essential role in the motor dysfunction of hemiplegic limbs (Bolognini et al., 2016). The loss of proprioception can impact the correction of motor errors, and stroke often leads to the loss of tactile sensation, which can affect the control of limb movements (Hughes et al., 2015). The motor recovery process after stroke may be attributed to the ongoing reorganization of neural networks, and inducing plasticity in neural networks may be facilitated by activating cortical or thalamic circuits (Zhou et al., 2022). From this perspective, one of the most effective modulators of cortical motor and somatosensory structures is repetitive sensory input (Ward and Cohen, 2004). In recent years, many scholars have applied vibration therapy (VT) to stroke rehabilitation, and related studies have shown that vibration therapy is effective for post-stroke limb dysfunction and spasticity (Moggio et al., 2022). Two categories of VT are whole body vibration (WBV) and focal muscle vibration (FMV). FMV is a therapeutic method using a mechanical device to provide vibrational stimulation to the belly of a specific muscle or its tendons. Studies have concluded that it is advantageous in facilitating the restoration of limb motor function in stroke patients during both the acute (Toscano et al., 2019) and chronic phases of stroke (Marconi et al., 2011). However, there are currently no standardized protocols or regulations for using FMV. Additionally, there is still ongoing debate about its exact efficacy. Moreover, the specific mechanism of its application is yet to be fully understood, necessitating further clinical research and verification. Cortical activation and neural network remodeling are the internal recovery processes in most neurological diseases; the activation and reconstruction of neurocircuitry is the natural procedure to achieve functional recovery. Available evidence suggests that FMV acts as a powerful proprioceptive stimulus, which modulates brain and spinal cord plasticity for clinical therapeutic effects (Viganò et al., 2023). Several studies have explored the cortical activation changes in stroke patients in response to FMV. Positron emission tomography (PET), electroencephalography (EEG), and functional magnetic resonance imaging (fMRI) have been used to investigate the neural mechanisms of focal vibration in healthy individuals (Naito et al., 1999; Golaszewski et al., 2002; Naito, 2004; Casini et al., 2006; Lopez et al., 2017). There have been limited reports on cortical activation changes in stroke patients in response to FMV, particularly in real-time. The advancement of noninvasive functional brain imaging technology provides us with an essential tool for detecting various brain function dysfunctions. The detection of fMRI is limited because the focal vibration therapies used in the clinic are metal devices. Fortunately, functional near-infrared spectroscopy (fNIRS) is a cutting-edge method of imaging the brain's activity, possessing various benefits such as being safe, noninvasive, portable, resistant to motion and electromagnetic interference, offering excellent spatial and temporal resolution, as well as enabling prolonged monitoring (Wang et al., 2023b). The main objective of this study was to use fNIRS to identify changes in cortical activity caused by FMV, which was directly administered to the affected belly of the flexor carpi radialis muscle (FCR) of hemiplegic stroke patients. Furthermore, the study sought to investigate how these changes relate to the clinical characteristics of the patients, ultimately improving our understanding of the possible neurophysiological mechanisms involved in these effects. Moreover, the efforts described above will help provide a dependable reference for developing optimal protocols for focal vibration therapy.

2 Materials and methods

2.1 Subjects

This study included 22 patients who had right hemiplegia after suffering a stroke and were admitted to the Second Affiliated Hospital of Anhui Medical University in 2022. The group consisted of 16 male and 6 female patients, with 18 of them having cerebral infarction and the remaining four having cerebral hemorrhage. Additionally, all patients were right-handed and had been suffering from the disease for a duration of 2 weeks to 1 year upon admission to the hospital (as shown in Table 1).

2.2 Inclusion and exclusion criteria

The following criteria were used for inclusion: (1) Patients had to meet the stroke diagnostic criteria revised by the World Health Organization definition (Stroke, 1989) and undergo cranial CT and MRI to confirm the stroke; (2) Patients must be more than 2 weeks post-stroke onset; (3) Vital signs needed to be stable; (4) Patients must have the ability to sit for at least 30 min; (5) Patients and their family members had to agree to participate in this study. The following criteria were used for exclusion: (1) Severe cognitive impairment; (2) History of previous brain injury or complicating neurodegenerative diseases; (3) History of mental illness; (4) Presence of serious diseases affecting the liver, kidney, hematopoietic system, endocrine system, and osteoarthritis; (5) Peripheral vascular disease in the upper extremities such as deep vein thrombosis, vasculitis, Raynaud's disease, etc.

2.3 Methods for assessing clinical characteristics

Professor Lovett's 6-point scale (0–5), developed at Harvard University, United States, in 1916 assessed muscle strength. The subsequent information provides a brief overview of each level of muscle strength: Grade 0 indicates the absence of any muscle contraction. Grade 1 denotes the presence of slight muscle contraction without resulting in joint movement. Grade 2 suggests the ability to generate some muscle movement, albeit not against the force of gravity. Grade 3 signifies the capability to counter mild resistance, though incapable of overcoming significant resistance. Grade 4 denotes the capacity to counter moderate resistance, yet insufficient to completely overcome maximum resistance. Finally, Grade 5 signifies combatting maximum resistance and maintaining normal muscle strength (Hidayat et al., 2015).

TABLE 1 Demographic and clinical characteristics of the patients.

Characteristics	Subjects ($N = 22$)
Age (years)[b]	63.05 ± 8.81
Gender, male/female[a]	16/6
Infarction/hemorrhage[a]	18/4
Dominant arm (right/left)[a]	22/0
Right hemiplegia/left hemiplegia[a]	22/0
Muscle strength (affected wrist flexor group)[b]	1.86 ± 1.32
Muscle tone (affected wrist flexor group)[b]	1.23 ± 0.92
BRS (affected upper limb)[b]	2.55 ± 1.22
FMA-UE (affected upper limb)[b]	16.59 ± 16.89
MBI[b]	55.45 ± 17.99

[a]The number of participants; [b]Mean ± standard deviation.

Muscle tone was evaluated on a scale ranging from grade 0 (low) to grade 4 (severely increased), with grade 1 indicating normal muscle tone, grade 2 indicating slightly increased muscle tone, and grade 3 indicating greater muscle tone.

The upper extremity function items of the Fugl-Meyer Assessment (FMA-UE) and the Bruunstrom Recovery Stage (BRS) were employed to assess the severity of post-stroke paralysis. FMA-UE is composed of 9 main items and 33 subitems, with each subitem graded on a scale of 0, 1, or 2. This results in 66 points, wherein higher scores indicate superior upper extremity function (Fugl-Meyer et al., 1975). BRS is a model that linearly describes the process of motor recovery in six different stages, each representing a different motor pattern and muscle control, and the motor recovery of most stroke patients after the disease onset conforms to the BRS pattern (Huang et al., 2016).

The Modified Barthel Index (MBI) was used to measure activities of daily living, which included 10 activities: eating, bathing, grooming, dressing, bed and chair transfer, ambulation (walking, wheelchair use), stair walking, bowel control, and urinary control. Each activity was rated on a graded scale, ranging from fully independent to entirely dependent, and the total score was 100.

2.4 Measurement of fNIRS

2.4.1 Probe positioning and measurement points

For this study, a fNIRS system called Nirscan-6000A, manufactured by Danyang Huichuang Medical Equipment Co., Ltd. in China, was used to detect changes in Hbo signals. This device has been previously used in previous studies (Deng et al., 2022; Lin et al., 2022; Ma et al., 2023). The sampling rate for this study was set at 11 Hz, and the wavelengths used were 730 nm, 808 nm, and 850 nm. The system's design included 32 probes, consisting of 16 sources and 16 detectors, following the 10/20 international standard line system. 34 channels were present in these probes, covering the cortical regions of interest (ROIs). The left and right prefrontal cortex (PFC) had seven channels each, while the left and right sensorimotor cortex (SMC) had nine channels each. Each left and right occipital cortex (OC) had one channel, as shown in Figure 1.

2.4.2 Activation task

The fNIRS data was collected using a block-design paradigm. The stimulation task involved FMV of the flexor carpi radialis in the upper limb of the affected side (Celletti et al., 2020), which was administered using a deep muscle stimulation therapy device (ZEPU-K5000A, ZEPU Medical Equipment Co. Ltd., China), with the stimulation position located at the muscle belly of the flexor carpi radialis on the affected side. The stimulation was carried out at 60 Hz and an amplitude of 6 mm.

The fNIRS test was conducted in a quiet room with only the experimenter and participant present. The participant was instructed to ensure they had enough sleep and were in a normal mental state

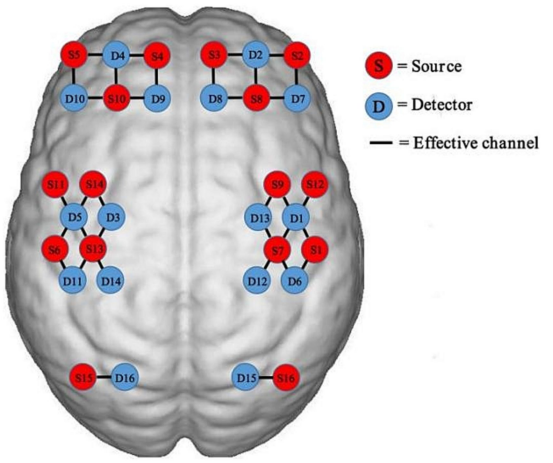

FIGURE 1
Functional near-infrared spectroscopy (fNIRS) probe positioning and measurement points.

before the test. They were also instructed to avoid consuming stimulating foods and drugs, such as tobacco, alcohol, tea, and coffee. The participant was seated in a bent-legged position, with their upper limbs naturally resting on soft pillows. Their elbows were bent, and their forearms were rotated outward. They were instructed to remain relaxed, not to move their head or speak, and to minimize distractions. The tester used simple and accurate verbal cues to initiate and conclude each task. The subjects received FMV on the affected FCR in the following order (block-design paradigm): 30 s of FMV followed by 30 s of rest. This pattern continued for 5 cycles. Throughout both the task and rest states, the fNIRS device was used to measure Oxyhemoglobin concentrations (hereinafter referred to as Hbo) in all channels.

2.4.3 Data analysis of fNIRS

This research used the NirSpark software to analyze the fNIRS data. Data preprocessing involved six steps: eliminating experimentally irrelevant time intervals, removing artifacts unrelated to the experimental data, transforming light intensity to luminous density, choosing band-pass filters (0.01–0.2 Hz) to filter out the noise and interfering signals, changing luminous density to blood oxygen concentration, and configuring the initial time of the hemodynamic response function (HRF) to −2 s and the end time to 60 s. The retained baseline state was from −2 s to 0 s, while the time of the single block paradigm was from 0 s to 60 s. Under the task state time setting of 30 s, the blood oxygen concentrations of the five blocking paradigms were superimposed and averaged to produce a blocking average result. The time-series data of Hbo was analyzed using a generalized linear model (GLM). The data was preprocessed for each channel and each subject. Subsequently, a t-test was conducted to compare the baseline and task statuses, with a significance level set at $p < 0.05$. The GLM facilitated the generation of an ideal hemodynamic response function (HRF) for each task. Following this, a comparison was made between the experimental and ideal HRF values to determine the corresponding range. The beta value, which shows the extent of cortical activation, served as an indicator for estimating the HRF prediction of the Hbo signal (Kawabata Duncan et al., 2019).

All participants completed the clinical scale assessment and fNIRS testing within 48 h of admission. Before completing the assessment, subjects had not received any rehabilitation therapy to ensure that such treatment did not influence the results. A highly skilled professional physiotherapist conducted the clinical scale assessment, while the fNIRS test was administered by a systematically trained master's student.

2.5 Statistical analysis

The statistical analysis of the data was conducted using IBM SPSS (v.26.0). In order to examine the effects of cortical activity induced by FMV, t-tests were used to analyze the difference between the mean Hbo values of the task state and rest state in each cortical region of interest (ROI) at the group level. To determine if the sample data adhered to a normal distribution, the Shapiro–Wilk test was used. If the data followed a normal distribution, the paired samples t-test was utilized for statistical analysis to derive the T-value. On the other hand, if the sample data did not conform to a normal distribution, the Wilcoxon signed-rank test was applied to derive the Z-value. To gain further insight into the relationship between cortical activity and clinical characteristics, the change values of Hbo (Hbo-CV) in the task and rest states for each cortical ROI, along with the beta values and the patient's clinical assessment data, were analyzed using Pearson's correlation analysis or Spearman's correlation analysis. Pearson correlation analysis was employed for sample data conforming to a normal distribution, while for sample data not conforming to a normal distribution, Spearman correlation analysis was used. A significance level of $p < 0.05$ was regarded as statistically significant.

2.6 Protocol approvals

The study was conducted at the Department of Rehabilitation Medicine of the Second Affiliated Hospital of Anhui Medical University. The Ethics Committee of the Second Affiliated Hospital of Anhui Medical University approved the experimental methods (approval number YX2022-018F1) and ensured compliance with the ethical standards stated in the 1975 Declaration of Helsinki, with revisions in 2008.

3 Results

3.1 Effects of cortical activity induced by FMV

The fNIRS data were analyzed using the NirSpark software to capture the mean Hbo values for each cortical ROI in both the task and rest state for each subject. Statistical analysis indicated that, except for right OC, the differences between the mean Hbo in the task and rest states were statistically significant for bilateral SMC, bilateral PFC, and left OC. This suggests that the FMV treatment of the upper limb effectively activates the cortical regions of bilateral SMC, bilateral PFC, and left OC (Table 2; Figure 2). Figures 3A,B depict anatomical maps of cortical activation in two distinct phases, task state and rest state, at the group level. This visualization was plotted using the NirSpark

TABLE 2 The difference between the mean Hbo values of the task state and rest state in each ROI at the group level.

Cortical ROI	Hbo (task state)	Hbo (rest state)	*T*	*Z*	*P*
LSMC	0.0275 ± 0.0312	0.0037 ± 0.0231	5.59		**0.000*****
RSMC	0.0274 ± 0.0353	0.0015 ± 0.0226		−4.01	**0.000*****
LPFC	0.0244 ± 0.0274	0.0117 ± 0.0204	3.61		**0.002****
RPFC	0.0222 ± 0.0284	0.0095 ± 0.0232	3.11		**0.005****
LOC	0.0312 ± 0.0521	0.0114 ± 0.0356		−2.516	**0.012***
ROC	0.0094 ± 0.0504	0.0041 ± 0.0431		−0.633	0.527

Bold indicates statistical significance (**P* < 0.05; ***P* < 0.01; ****P* < 0.001). Hbo (Task state), the average concentration of oxygenated hemoglobin in the task state; Hbo (Rest state), The average concentration of oxygenated hemoglobin in the rest state; LSMC, the left sensorimotor cortex; RSMC, the right sensorimotor cortex; LPFC, the left prefrontal cortex; RPFC, the right prefrontal cortex; LOC, the left occipital cortex; ROC, the right occipital cortex; *T*, *T*-value derived from paired *t*-test; *Z*, *Z*-value in nonparametric statistical tests.

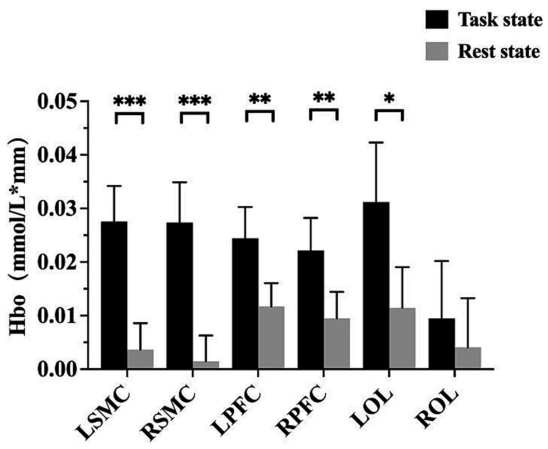

FIGURE 2
A bar chart with a summary date showing the activation of each cortical ROI. **p* < 0.05; ***p* < 0.01; ****p* < 0.001. LSMC, the left sensorimotor cortex; RSMC, the right sensorimotor cortex; LPFC, the left prefrontal cortex; RPFC, the right prefrontal cortex; LOC, the left occipital cortex; ROC, the right occipital cortex.

software. Different colors on the images indicate these phases. The channel's color corresponds to the mean Hbo level, with a redder tone indicating a higher mean Hbo and a bluer tone indicating a lower mean Hbo. Noteworthy color changes were observed in brain cortices such as bilateral SMC, bilateral PFC, and left OC, aligning with the findings of the aforementioned data analysis.

3.2 Correlation between the cortical activity and clinical assessment data

The Hbo-CV (change values of Hbo) in the task and rest states for each cortical ROI were calculated by subtracting the mean Hbo of the rest state from that of the task state. By analyzing the correlation between the Hbo-CV and the clinical assessment data, we can gain some insight into the association between the activation of different brain cortices and the patient's clinical characteristics. Through Spearman correlation analysis, we found a positive correlation between the muscle strength of the affected wrist flexor group and the Hbo-CV in left SMC, PFC, and OC. However, no statistical correlation was found between muscle strength and Hbo-CV in the right SMC, PFC, and OC. The BRS (Bruunstrom Recovery Stage) of the affected upper limb showed a positive correlation with the Hbo-CV in left SMC and PFC, while no statistical correlation was observed in right SMC, PFC, and bilateral OC. No statistical correlation was found between the muscle tension of the affected wrist flexor group, FMA-UE, MBI, and the Hbo-CV of each cortical ROI (Table 3; Figure 4).

To gain a better understanding of the relationship between the patient's clinical characteristics and the cortical activity produced by FMV, we conducted a Spearman correlation analysis using the beta values of each cortical ROI obtained from a GLM model and the clinic assessment. The results were consistent with the findings mentioned above. The muscle strength of the affected wrist flexor group showed a positive correlation with the beta values of left SMC, PFC, and OC. However, no statistical correlation was found in right SMC, PFC, and OC. The patient's BRS on the affected upper limb exhibited a positive correlation with the beta values of left SMC and PFC. In contrast, no statistical correlation was found with the beta values of right SMC, PFC, and bilateral OC. Overall, no statistical correlation was observed between the patient's affected wrist flexor group muscle tone, FMA-UE, MBI, and the beta values in each cortical ROI (Table 4; Figure 5).

4 Discussion

Several studies have used neurophysiological and neurofunctional imaging techniques, such as PET, fMRI, EEG, and TMS, to explore the neural mechanisms of focal vibration in healthy individuals. Naito et al. (1999) used PET scans to study the brain excitability of blindfolded subjects experiencing illusory arm movements through bicep tendon vibration. The study found significant excitability in contralateral motor areas and S1. (Golaszewski et al. (2002) used fMRI to study the cortical activity of healthy individuals during 50 Hz vibration of the right-hand palm. Results showed contralateral precentral and postcentral gyrus activation in all subjects, while some also exhibited ipsilateral activation. Naito (2004)) used fMRI to examine the cortical activity of focal vibration to produce a "motion illusion" in healthy subjects. The study found that the contralateral primary SMC, dorsal premotor cortex (PMd), supplementary motor area (SMA), cingulate motor cortex, and ipsilateral cerebellum were all activated. Casini et al. (2006) found that focal vibrating of the wrist tendons induced a "motor illusion" in healthy subjects, activating the contralateral primary SMC, SMA, and angular gyrus by using magnetoencephalography. Imai et al. (2014) used fNIRS to measure cortical activity during wrist tendon vibration at different frequencies in healthy subjects. They observed increased excitability in both cerebral hemispheres' premotor cortex and parietal areas. An EEG-based study found that focal vibration applied to limb muscles modulated neurophysiological oscillations and increased contralateral S1-M1 excitability in healthy volunteers (Lopez et al., 2017). A randomized controlled study was conducted by Marconi et al. (2011) involving 30 hemiplegia patients who had suffered from a stroke. The experimental group, which received focal vibration stimulation in addition to physiotherapy, exhibited a

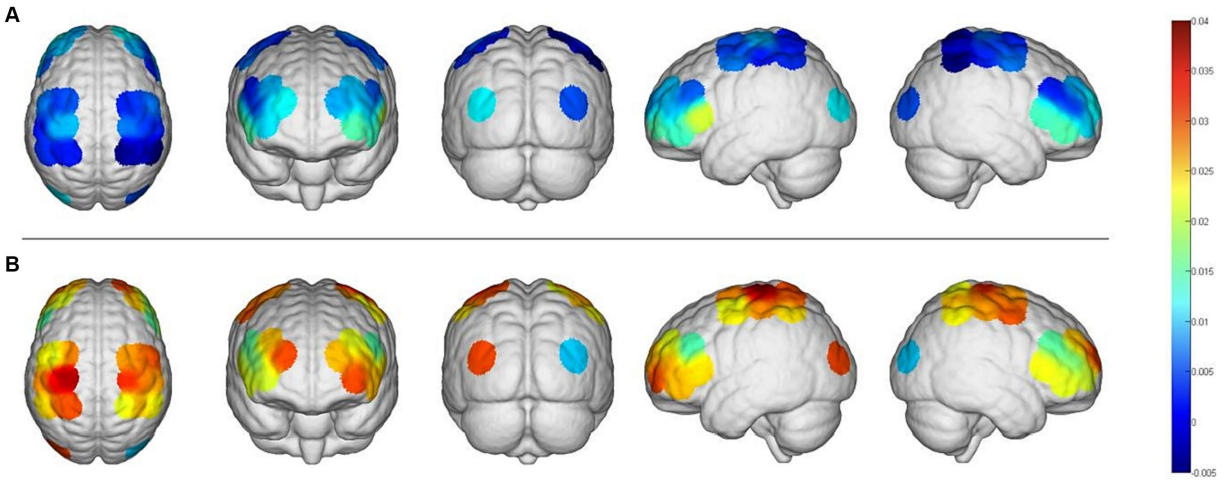

FIGURE 3
An anatomical view of cortical activation during two different phases, the task and the rest stages, is represented using different colors. **(A)**, Rest stage; **(B)**, task stage.

TABLE 3 The correlation coefficient between the Hbo-CV and clinical characteristics for each cortical ROI ($N = 22$).

	Hbo change value (Hbo-CV)					
	LSMC	RSMC	LPFC	RPFC	LOC	ROC
Muscle strength[a]	**0.501***	0.392	**0.516***	0.291	**0.553****	0.249
Muscle tone[a]	0.298	0.247	0.24	−0.044	0.109	0.157
BRS[b]	**0.491***	0.35	**0.490***	0.335	0.397	0.081
FMA-UE[b]	0.256	0.139	0.334	0.143	0.238	−0.054
MBI	0.308	0.139	0.266	0.015	0.367	0.084

LSMC, the left sensorimotor cortex; RSMC, the right sensorimotor cortex; LPFC, the left prefrontal cortex; RPFC, the right prefrontal cortex; LOC, the left occipital cortex; ROC, the right occipital cortex; [a]affected wrist flexor group; [b]affected upper limb; Bold indicates statistical significance (*$P < 0.05$, **$P < 0.01$).

lower resting motor threshold (RMT), an increased motor evoked potential (MEP) index, and an increased short-interval intracortical inhibition (SICI) compared to the control group, which only received physiotherapy. Another EEG study found that focal vibration (75 Hz) of the biceps brachii muscle on the affected side of subacute stroke can enhance contralateral S1-M1 excitability and alter the functional brain network (Li et al., 2019). An EEG study by Li et al. (2022) found that applying focal vibration (87 Hz, 0.28 mm) on the triceps of chronic stroke patients resulted in bilateral activation of the SMC. In summary, the majority of the studies mentioned above were conducted in healthy subjects due to the design of the study protocol and the experimental conditions, and the studies focused mainly on the SMC. Most of the studies found that focal vibration activated the contralateral sensorimotor cortex in healthy subjects, and there was only one EEG study (Li et al., 2022), which found that focal vibration activated the sensorimotor cortex bilaterally in stroke patients. The present study using fNIRS demonstrates that directly applying FMV on the affected FCR in stroke hemiplegic patients can immediately activate more brain cortex, such as the bilateral PFC and ipsilateral OC, in addition to the bilateral SMC. Based on the above findings, it is stated that hyperactivation of muscle proprioceptors induced by FMV can produce long-term potentiation (LTP) -like plastic changes that do not involve the sole ipsilesional sensorimotor cortex but probably entail a whole motor network relearning achieved through the plasticity-based modulation of the effective connectivity (Viganò et al., 2023).

Previous neuroimaging studies have reported contralateral brain activation in healthy subjects during active hand movements (Rao et al., 1993; Sabatini et al., 1993; Bonnal et al., 2023) In contrast, stroke patients more often experience increased excitability in both cerebral hemispheres during active movements of the affected hand (Marshall et al., 2000; Staudt et al., 2002; Rehme et al., 2011; Favre et al., 2014). The activation of bilateral sensorimotor areas induced by FMV was comparable to the results of some previous studies using fMRI or EEG which observed the activation of brain areas induced by motor imagery (Veverka et al., 2012), active movement (Veverka et al., 2014) and passive movement (Manganotti et al., 2010) as a task for the affected hand. Therefore, FMV, which acts as a potent proprioceptive stimulus, has some similar effectiveness to the activation of the brain produced by the movement-as-task paradigm. Previous studies on the activation of brain functions by FMV in stroke patients have rarely reported PFC and OC activation. This study showed that FMV applied to the flexor muscle of the forearm activated the bilateral PFC and the contralateral OC in addition to the bilateral SMC. Earlier studies have suggested that FMV applied to the limb can create "motor illusion" that can produce effective motor control and facilitate motor learning (Naito, 2004) (Imai et al., 2014). The PFC is an anterior region of the brain associated

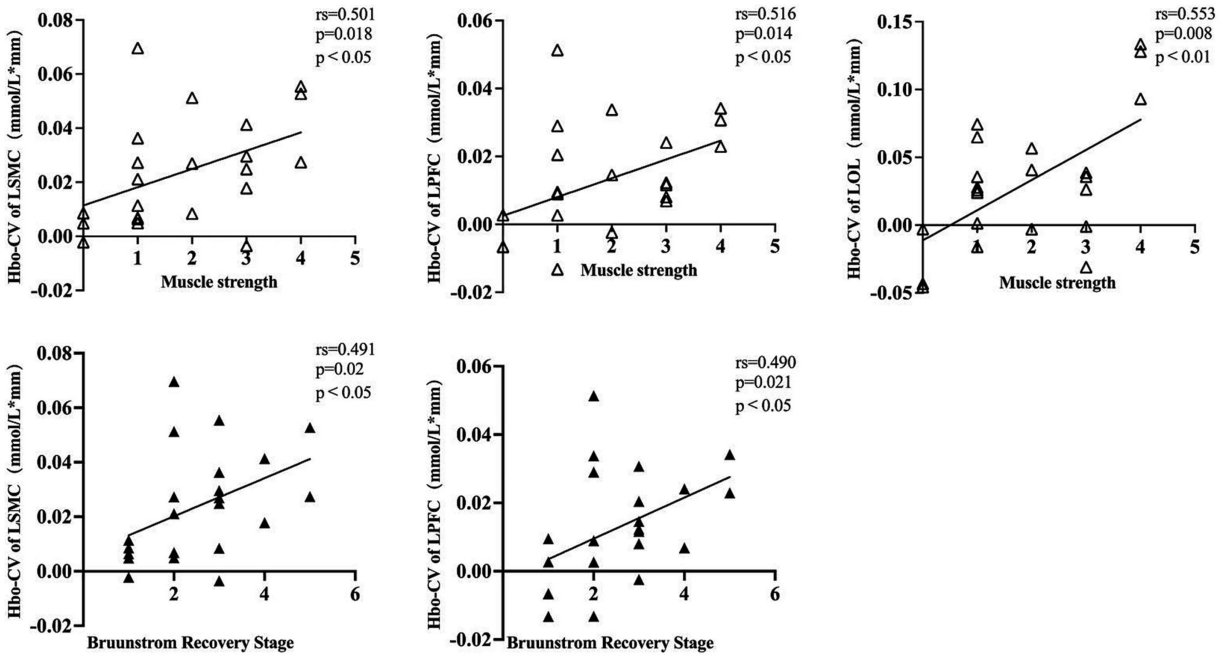

FIGURE 4
A dot plot showing the correlation between Hbo-CV and clinical assessment information for each cortical ROI. rs, Spearman correlation analysis correlation coefficient. LSMC, the left sensorimotor cortex; LPFC, the left prefrontal cortex; LOC, the left occipital cortex; muscle strength was assessed in the affected wrist flexor groups; Brunnstrom Recovery Stage was evaluated on the affected upper limb.

TABLE 4 The correlation coefficient between the beta value and clinical characteristics for each cortical ROI ($N = 22$).

	Beta value					
	LSMC	RSMC	LPFC	RPFC	LOC	ROC
Muscle strength[a]	**0.488***	0.286	**0.575****	0.27	**0.553****	0.249
Muscle tone[a]	0.326	0.15	0.332	0.112	0.109	0.157
BRS[b]	**0.433***	0.224	**0.574****	0.181	0.397	0.081
FMA-UE[b]	0.187	0.036	0.32	−0.03	0.238	−0.054
MBI	0.385	0.046	0.298	−0.114	0.367	0.084

LSMC, the left sensorimotor cortex; RSMC, the right sensorimotor cortex; LPFC, the left prefrontal cortex; RPFC, the right prefrontal cortex; LOC, the left occipital cortex; ROC, the right occipital cortex; [a]affected wrist flexor group; [b]affected upper limb; Bold indicates statistical significance (*$P < 0.05$; **$P < 0.01$).

with cognitive control and executive functions (Friedman and Robbins, 2022). We hypothesize that the PFC may be involved in the perception, interpretation, and cognitive processes of the motion illusion produced by FMV to help understand how it is consistent with prior motion experience and intrinsic modeling. The OC is located in the posterior part of the brain and is primarily involved in the processing of visual information (Barton and Brewer, 2013). However, when FMV induces motion illusions, the OC may play a role in generating internal visual images, motion simulation, and pictorial motion illusions. Motion illusions induced by vibration can activate the processing of visual information in the occipital lobe, which in turn enhances and supports the perception of motion illusions.

Spasticity is one of the frequent complications after stroke, which affects the motor performance and rehabilitation process of stroke patients. The exact mechanism of post-stroke spasticity is not fully understood. Studies have shown that, among the downstream conduction tracts, the ventral medial reticulospinal tract from the pontine reticular formation and the vestibulospinal tract from the vestibular nucleus contribute to the increase in muscle tone; The dorsal reticulospinal tract from the bulbar reticular formation inhibited the excitability of the stretch reflex. The cerebral cortex modulates the stretch reflex by excitation of the bulbar reticular formation through the cortical reticular tracts (Trompetto et al., 2014; Naro et al., 2017; Bruni et al., 2018). The positive effect of FMV in reducing hemiplegic upper and lower limb spasticity in stroke patients has been confirmed by several reviews (Murillo et al., 2014; Alashram et al., 2019; Yang, 2020). A previous study applied FMV directly to the spastic muscles (Biceps brachii, Wrist flexor muscles, and Finger flexor muscles) of post-stroke hemiplegic patients and found that it was effective in decreasing spasticity of the target muscles as well as improving upper extremity function (Noma et al., 2009). The study discovered that vibratory stimulation resulted in a decrease in both the F-wave amplitude and the F/M ratio, which indicates a decline in motor neuron excitability. The current work discovered by fNIRS that FMV of the

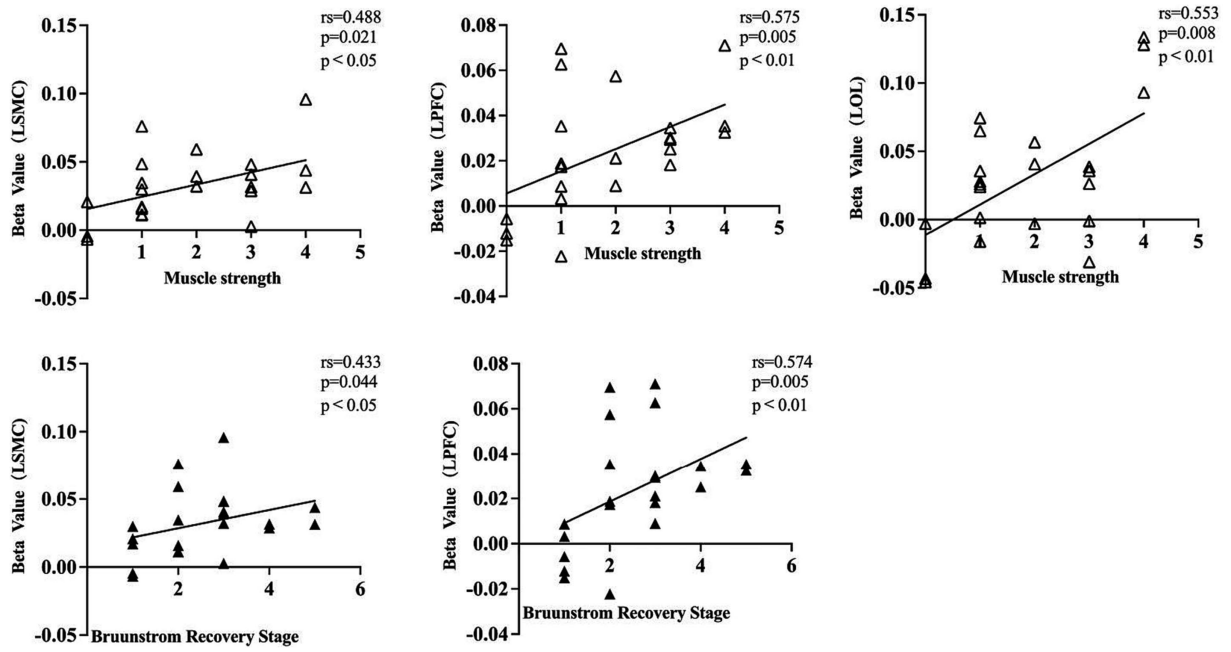

FIGURE 5
A dot plot showing the correlation between beta value and clinical assessment information for each cortical ROI. rs, Spearman correlation analysis correlation coefficient. LSMC, the left sensorimotor cortex; LPFC, the left prefrontal cortex; LOC, the left occipital cortex; muscle strength was assessed in the affected wrist flexor groups; Brunnstrom recovery stage was evaluated on the affected upper limb.

spastic muscle of the hemiplegic upper limb (wrist flexor muscle), leads to elevated cortical activity. The increase in sensorimotor cortical activation could indicate an improvement in inhibitory circuits, which helps to decrease spasticity (Vazquez et al., 2018). The possible mechanism is the aforementioned alteration of cortical activity, followed by excitation of the bulbar reticular formation through the corticoreticular bundle, as a result of a modulatory effect on the stretch reflex. The study found no correlation between the initial levels of muscle spasticity and the intensity of cortical activation induced by FMV. This suggests that there is no significant causal relationship between the level of muscle spasticity and the intensity of activation in the individual cerebral cortex following a stroke. Some articles suggest that FMV helps reduce spasticity by rebalancing interhemispheric interactions through the activation of bilateral S1-M1 (Li et al., 2022). Future longitudinal studies are necessary to better understand the relationship between FMV-induced spasticity relief and cortical activation when applied directly to the affected flexor muscles.

One previous meta-study found that the intensity of upper limb impairments in stroke patients was strongly linked to the level of activation in the ipsilesional M1 during movement of the paralyzed hand, as measured using fMRI (Rehme et al., 2012). The authors were inspired by the results of the above studies, and a search of the database did not reveal any relevant studies on the relationship between the activation of functional brain regions and movement performances in stroke patients as detected by fNIRS or fMRI studies using sensory stimulation as a task. In this study, we used fNIRS (a block-design paradigm) as a detection tool to perform a correlation analysis between the excitation intensity of cortical ROI and the clinical data of stroke patients using the FMV applied to the affected FCR (target muscle) as a task. The results revealed that the muscle strength grades of the target muscles were statistically positively correlated with the activation intensity in the ipsilesional ROIs, and not in the contralesional ROIs. The above results suggest that the muscle strength of the target muscles of the affected limb is closely related to the integrity of the sensory-motor nerve pathway and the functional status of the ipsilateral cortex of the lesion, which is also in accordance with the rules of traditional structural and functional anatomy. The outcomes of the ongoing study demonstrated that the BRS of the affected upper limb was positively correlated with the activation intensity of the ipsilesional SMC and LPFC, while it was not statistically correlated with the activation intensity of the contralesional SMC, PFC, and bilateral OC. The above results suggest that good activation of ipsilesional SMC and PFC induced by FMV-evoked sensory stimulation predicts a better motor recovery of the affected limb in stroke patients, which in part reflects the patient's motor performance ability. This is somehow in line with the results of a previous meta-analysis that used fMRI and PET scans to study active or passive sensorimotor tasks involving the upper limb (Favre et al., 2014). A recent fNIRS study found that touching the affected shoulder in stroke patients can activate both sides of the motor cortex, the intensity of this activation was correlated with the baseline clinical characteristics of the patients. The authors attributed this result to functional compensation in uninjured brain regions (Zhang et al., 2023). This functional compensation is seen both within the affected hemisphere and between the unaffected hemispheres (Viganò et al., 2023; Zhang et al., 2023).

The design of an intervention program for focal vibration therapy mainly includes the settings of device parameters (such as frequency, amplitude, intensity, etc.), vibration duration, the targeted site for vibration action (such as flexor, extensor, muscle belly, tendon, etc.), and the varied timing in relation to stroke onset for recruited patients. it is widely reported that FMV's capability of inducing

synaptic plasticity using the proprioceptive pathway depends on vibration parameters that can deeply affect clinical results in RCT (Wang et al., 2020; Avvantaggiato et al., 2021; Viganò et al., 2023). Those aspects probably explain the absence of statistical correlations found in the present study between FMA-UE and MBI and the activation intensity of all cortical ROIs. Focal vibration stimulates the muscle spindle, and impulses are transmitted via Ia afferent fibers to alpha motor neurons and Ia inhibitory interneurons in the spinal cord. This afferent pathway produces an involuntary contractile response in the vibrated muscle, also known as a tonic vibration reflex (TVR), and a so-called "reciprocal inhibition" in the antagonist muscle, which inhibits spasticity in the antagonist muscle (De Gail et al., 1966; Hagbarth and Eklund, 1966). Therefore, there have been many previous studies of vibratory stimulation of antagonist muscles of spastic muscles to reduce spasticity in hemiplegic limbs (Bishop, 1975; Desmedt, 1983; Ageranioti, 1990; Casale et al., 2014; Constantino et al., 2014; Annino et al., 2019). Clinical observations have shown that vibration stimulation applied directly to spastic muscles produces an initial TVR in stroke patients, with significant relief of spasticity after several minutes of continuous stimulation (Noma et al., 2009). Hence, in recent years, many studies have used focal vibration to directly stimulate the spastic muscles (flexor muscles) in stroke patients, and have also achieved good efficacy (Noma et al., 2009; Marconi et al., 2011; Aprile et al., 2020). In recent years, the vibration frequency of local vibration applied to stroke rehabilitation ranges from 30 to 300 Hz, and the amplitude ranges from 0.01-10 mm (Wang et al., 2020, 2022; Viganò et al., 2023). It has been shown that vibrations of approximately 10 Hz or higher than 220 Hz do not produce a reliable and vivid "motion illusion." Vibrations without the illusion of motion tend to activate the sensory areas of the brain, whereas vibrations with the illusion of motion activate the motor areas in addition to the sensory areas of the brain, and illusory limb movements activate the motor areas normally involved in executing and controlling limb movements (Naito, 2004). Previous studies have reported that in studies of vibration interventions for patients with spinal cord injury, multiple sclerosis, and other movement disorders, vibration amplitudes of 0.01 mm–2 mm, which were used for stroke rehabilitation, were comparable to vibration amplitudes of 0.005 mm to 10 mm (Murillo et al., 2014; Souron et al., 2017; Yang, 2020). Based on the above reasons, the present study adopted a treatment protocol of direct focal vibration (frequency: 60 Hz; amplitude: 6 mm) to the spastic muscles of the upper limb in stroke, using a therapeutic device (ZEPU-K5000A, ZEPU Medical Equipment Co., Ltd., China) that is widely used in neurological rehabilitation institutions in China, and which can induce "motion illusions" and TVR. In my clinical work, I found that applying this device to the flexor muscles of the hemiplegic upper limbs of stroke patients can reduce muscle spasticity and improve motor function of the upper limbs (ready for submission), without any side effects. A recent study using this same device in the treatment of hemiplegic stroke patients also showed that it was effective in improving upper limb motor function (Wang et al., 2023a). However, the decision on the selection of the above vibration parameters is still debated. It has been suggested that different vibration frequencies may preferentially activate different cortical areas (Chung et al., 2013; Avvantaggiato et al., 2021). Most literature currently uses vibration frequencies between 80 and 120 Hz, with 100 Hz being the most common. This frequency is believed to more easily induce plastic changes in the brain and spinal cord through cortical hyperactivity and motoneuron excitability, respectively; The optimal vibratory stimulus amplitude is <0.5 mm, as it activates Ia afferents via primary muscle spindle discharge. Higher amplitudes cause overflow, leading to TVR via amplified Ia inputs from persistent stimulation, which is still unclear if it is necessary for clinical effects (Viganò et al., 2023). Randomized controlled studies with different vibration frequencies and amplitudes are necessary in the future to further understand their effects on cortical activity and clinical function in stroke patients.

In addition, there are some other limitations of this study that can lead to bias in the results. First, the number of subjects was relatively small, the type of stroke (cerebral hemorrhage or cerebral infarction) was not restricted, and the exact location and size of the lesions were inconsistent, although the lesions were in the left cerebral hemisphere in all subjects. Therefore, more stroke patients must be recruited, the type of stroke needs to be limited, and the results can be better validated by controlling for the site and size of the injury in the patients. Second, adaptive neuroplasticity declines with time since acute stroke and improvement in clinical function peaks 3–6 months after stroke (Kwakkel and Kollen, 2013; Viganò et al., 2023). However, the duration of illness of the subjects recruited for this study ranged from 2 weeks to 1 year, which can also lead to bias in the results, so it would be preferable to recruit patients with acute or subacute stages of stroke as study subjects in future studies. Third, the current study used a block-design paradigm to detect changes in cortical activity, with the task being 30 s of FMV, which actually observed cortical activity during the FMV-induced TVR, not involving the cortical activity or brain networks after a TVR lasting several minutes, which needs to be added to future studies as well. Finally, assessment of functional activation of motor-related systems as an imaging biomarker has been suggested as a predictive method for prognosis after stroke (Zhang et al., 2022). The present study analyzed the correlation between FMV-induced changes in cortical activity and baseline clinical characteristics and did not perform a correlation analysis of changes in distant clinical characteristics. Therefore, further studies are necessary to confirm whether the prognosis of stroke patients can be predicted by analyzing FMV-induced changes in cortical activity.

5 Conclusion

The application of FMV-evoked sensory stimulation directly to the muscle belly of the FCR on the paralyzed side of the upper limb in stroke patients activated additional brain cortices, such as bilateral PFC and ipsilesional OC, in addition to bilateral SMC. This suggests that FMV induces neural plasticity across multiple brain regions. However, only the intensity of ipsilesional SMC and PFC activation showed a correlation with the clinical characteristics of the patients. The results of this study provide neurophysiological theoretical support for the expanded clinical application of FMV. Furthermore, the fNIRS test, which utilized a block-design paradigm of FMV, has the potential to be used as an objective assessment tool for hemiplegic stroke patients. Further studies are necessary to confirm whether the prognosis of stroke patients can be predicted by fNIRS detection of altered cortical activity induced by sensory stimuli evoked by FMV.

Data availability statement

The original contributions presented in the study are included in the article/supplementary material, further inquiries can be directed to the corresponding author.

Ethics statement

The studies involving humans were approved by the Ethics Committee of the Second Affiliated Hospital of Anhui Medical University. The studies were conducted in accordance with the local legislation and institutional requirements. The participants provided their written informed consent to participate in this study.

Author contributions

XS: Conceptualization, Funding acquisition, Methodology, Writing – original draft, Writing – review & editing, Data curation, Formal analysis, Investigation, Project administration, Resources, Software, Supervision, Validation, Visualization. HX: Investigation, Writing – review & editing, Validation. LJ: Investigation, Project administration, Resources, Writing – review & editing. JW: Conceptualization, Methodology, Resources, Supervision, Writing – review & editing. YY: Data curation, Investigation, Software, Validation, Visualization.

Funding

The author(s) declare financial support was received for the research, authorship, and/or publication of this article. This work was supported by the Clinical Research Cultivation Program of the Second Affiliated Hospital of Anhui Medical University (grant no. 2020LCYB16) and the Research Fund Project of Anhui Medical University (grant no. 2022xkj196).

Conflict of interest

The authors declare that the research was conducted in the absence of any commercial or financial relationships that could be construed as a potential conflict of interest.

Publisher's note

All claims expressed in this article are solely those of the authors and do not necessarily represent those of their affiliated organizations, or those of the publisher, the editors and the reviewers. Any product that may be evaluated in this article, or claim that may be made by its manufacturer, is not guaranteed or endorsed by the publisher.

References

Ageranioti, S. (1990). Effect of vibration on hypertonia and hyperreflexia in the wrist joint of patients with spastic hemiparesis. *Physiother. Can.* 42, 24–33.

Alashram, A. R., Padua, E., Romagnoli, C., and Annino, G. (2019). Effectiveness of focal muscle vibration on hemiplegic upper extremity spasticity in individuals with stroke: a systematic review. *NeuroRehabilitation* 45, 471–481. doi: 10.3233/NRE-192863

Annino, G., Alashram, A. R., Alghwiri, A. A., Romagnoli, C., Messina, G., Tancredi, V., et al. (2019). Effect of segmental muscle vibration on upper extremity functional ability poststroke: a randomized controlled trial. *Medicine (Baltimore)* 98:e14444. doi: 10.1097/MD.0000000000014444

Aprile, I., Iacovelli, C., Pecchioli, C., Cruciani, A., Castelli, L., and Germanotta, M. (2020). Efficacy of focal muscular vibration in the treatment of upper limb spasticity in subjects with stroke outcomes: randomized controlled trial. *J. Biol. Regul. Homeost. Agents* 34, 1–9.

Avvantaggiato, C., Casale, R., Cinone, N., Facciorusso, S., Turitto, A., Stuppiello, L., et al. (2021). Localized muscle vibration in the treatment of motor impairment and spasticity in post-stroke patients: a systematic review. *Eur. J. Phys. Rehabil. Med.* 57, 44–60. doi: 10.23736/S1973-9087.20.06390-X

Barton, B., and Brewer, A. A. (2013). Visual working memory in human cortex. *Psychology* 4, 655–662. doi: 10.4236/psych.2013.48093

Bishop, B. (1975). Vibratory stimulation: part II. Vibratory stimulation as an evaluation tool. *Phys. Ther.* 55, 28–34. doi: 10.1093/ptj/55.1.28

Bolognini, N., Russo, C., and Edwards, D. J. (2016). The sensory side of post-stroke motor rehabilitation. *Restor. Neurol. Neurosci.* 34, 571–586. doi: 10.3233/RNN-150606

Bonnal, J., Ozsancak, C., Monnet, F., Valery, A., Prieur, F., and Auzou, P. (2023). Neural substrates for hand and shoulder movement in healthy adults: a functional near infrared spectroscopy study. *Brain Topogr.* 36, 447–458. doi: 10.1007/s10548-023-00972-x

Bruni, M. F., Melegari, C., De Cola, M. C., Bramanti, A., Bramanti, P., and Calabro, R. S. (2018). What does best evidence tell us about robotic gait rehabilitation in stroke patients: a systematic review and meta-analysis. *J. Clin. Neurosci.* 48, 11–17. doi: 10.1016/j.jocn.2017.10.048

Casale, R., Damiani, C., Maestri, R., Fundaro, C., Chimento, P., and Foti, C. (2014). Localized 100 Hz vibration improves function and reduces upper limb spasticity: a double-blind controlled study. *Eur. J. Phys. Rehabil. Med.* 50, 495–504.

Casini, L., Romaiguere, P., Ducorps, A., Schwartz, D., Anton, J. L., and Roll, J. P. (2006). Cortical correlates of illusory hand movement perception in humans: a MEG study. *Brain Res.* 1121, 200–206. doi: 10.1016/j.brainres.2006.08.124

Celletti, C., Suppa, A., Bianchini, E., Lakin, S., Toscano, M., La Torre, G., et al. (2020). Promoting post-stroke recovery through focal or whole body vibration: criticisms and prospects from a narrative review. *Neurol. Sci.* 41, 11–24. doi: 10.1007/s10072-019-04047-3

Chung, Y. G., Kim, J., Han, S. W., Kim, H. S., Choi, M. H., Chung, S. C., et al. (2013). Frequency-dependent patterns of somatosensory cortical responses to vibrotactile stimulation in humans: a fMRI study. *Brain Res.* 1504, 47–57. doi: 10.1016/j.brainres.2013.02.003

Constantino, C., Galuppo, L., and Romiti, D. (2014). Efficacy of mechano-acoustic vibration on strength, pain, and function in poststroke rehabilitation: a pilot study. *Top. Stroke Rehabil.* 21, 391–399. doi: 10.1310/tsr2105-391

De Gail, P., Lance, J. W., and Neilson, P. D. (1966). Differential effects on tonic and phasic reflex mechanisms produced by vibration of muscles in man. *J. Neurol. Neurosurg. Psychiatry* 29, 1–11. doi: 10.1136/jnnp.29.1.1

Deng, X., Jian, C., Yang, Q., Jiang, N., Huang, Z., and Zhao, S. (2022). The analgesic effect of different interactive modes of virtual reality: a prospective functional near-infrared spectroscopy (fNIRS) study. *Front. Neurosci.* 16:1033155. doi: 10.3389/fnins.2022.1033155

Desmedt, J. E. (1983). Mechanisms of vibration-induced inhibition or potentiation: tonic vibration reflex and vibration paradox in man. *Adv. Neurol.* 39, 671–683.

Eraifej, J., Clark, W., France, B., Desando, S., and Moore, D. (2017). Effectiveness of upper limb functional electrical stimulation after stroke for the improvement of activities of daily living and motor function: a systematic review and meta-analysis. *Syst. Rev.* 6:40. doi: 10.1186/s13643-017-0435-5

European and Rehabilitation Medicine Bodies (2018). White book on physical and rehabilitation medicine in Europe. Introductions, executive summary, and methodology. *Eur. J. Phys. Rehabil. Med.* 54, 125–155. doi: 10.23736/S1973-9087.18.05143-2

Favre, I., Zeffiro, T. A., Detante, O., Krainik, A., Hommel, M., and Jaillard, A. (2014). Upper limb recovery after stroke is associated with ipsilesional primary motor cortical activity: a meta-analysis. *Stroke* 45, 1077–1083. doi: 10.1161/STROKEAHA.113.003168

Feigin, V. L., Brainin, M., Norrving, B., Martins, S., Sacco, R. L., Hacke, W., et al. (2022). World stroke organization (WSO): global stroke fact sheet 2022. *Int. J. Stroke* 17, 18–29. doi: 10.1177/17474930211065917

Friedman, N. P., and Robbins, T. W. (2022). The role of prefrontal cortex in cognitive control and executive function. *Neuropsychopharmacology* 47, 72–89. doi: 10.1038/s41386-021-01132-0

Fugl-Meyer, A. R., Jaasko, L., Leyman, I., Olsson, S., and Steglind, S. (1975). The post-stroke hemiplegic patient. 1. A method for evaluation of physical performance. *Scand. J. Rehabil. Med.* 7, 13–31. doi: 10.2340/1650197771331

Golaszewski, S. M., Siedentopf, C. M., Baldauf, E., Koppelstaetter, F., Eisner, W., Unterrainer, J., et al. (2002). Functional magnetic resonance imaging of the human

sensorimotor cortex using a novel vibrotactile stimulator. *NeuroImage* 17, 421–430. doi: 10.1006/nimg.2002.1195

Hagbarth, K. E., and Eklund, G. (1966). Tonic vibration reflexes (TVR) in spasticity. *Brain Res.* 2, 201–203. doi: 10.1016/0006-8993(66)90029-1

Hidayat, A. A., Arief, Z., and Happyanto, D. C. (2015). LOVETT scaling with flex sensor and MYO armband for monitoring finger muscles therapy of post-stroke people. *Int J Eng Technol.* 3, 60–76. doi: 10.24003/emitter.v3i2.45

Huang, C. Y., Lin, G. H., Huang, Y. J., Song, C. Y., Lee, Y. C., How, M. J., et al. (2016). Improving the utility of the Brunnstrom recovery stages in patients with stroke: validation and quantification. *Medicine* 95:e4508. doi: 10.1097/MD.0000000000004508

Hughes, C. M., Tommasino, P., Budhota, A., and Campolo, D. (2015). Upper extremity proprioception in healthy aging and stroke populations, and the effects of therapist- and robot-based rehabilitation therapies on proprioceptive function. *Front. Hum. Neurosci.* 9:120. doi: 10.3389/fnhum.2015.00120

Imai, R., Hayashida, K., Nakano, H., and Morioka, S. (2014). Brain activity associated with the illusion of motion evoked by different vibration stimulation devices: an fNIRS study. *J. Phys. Ther. Sci.* 26, 1115–1119. doi: 10.1589/jpts.26.1115

Kawabata Duncan, K., Tokuda, T., Sato, C., Tagai, K., and Dan, I. (2019). Willingness-to-pay-associated right prefrontal activation during a single, real use of cosmetics as revealed by functional near-infrared spectroscopy. *Front. Hum. Neurosci.* 13:16. doi: 10.3389/fnhum.2019.00016/full

Kelly-Hayes, M., Beiser, A., Kase, C. S., Scaramucci, A., D'Agostino, R. B., and Wolf, P. A. (2003). The influence of gender and age on disability following ischemic stroke: the Framingham study. *J. Stroke Cerebrovasc. Dis.* 12, 119–126. doi: 10.1016/S1052-3057(03)00042-9

Kim, W. S., Cho, S., Ku, J., Kim, Y., Lee, K., Hwang, H. J., et al. (2020). Clinical application of virtual reality for upper limb motor rehabilitation in stroke: review of technologies and clinical evidence. *J. Clin. Med.* 9:3369. doi: 10.3390/jcm9103369

Kwakkel, G., and Kollen, B. J. (2013). Predicting activities after stroke: what is clinically relevant? *Int. J. Stroke* 8, 25–32. doi: 10.1111/j.1747-4949.2012.00967.x

Li, W., Li, C., Xiang, Y., Ji, L., Hu, H., and Liu, Y. (2019). Study of the activation in sensorimotor cortex and topological properties of functional brain network following focal vibration on healthy subjects and subacute stroke patients: an EEG study. *Brain Res.* 1722:146338. doi: 10.1016/j.brainres.2019.146338

Li, W., Luo, F., Xu, Q., Liu, A., Mo, L., Li, C., et al. (2022). Brain oscillatory activity correlates with the relief of post-stroke spasticity following focal vibration. *J. Integr. Neurosci.* 21:96. doi: 10.31083/j.jin2103096

Lin, Q., Zhang, Y., Zhang, Y., Zhuang, W., Zhao, B., Ke, X., et al. (2022). The frequency effect of the motor imagery brain computer Interface training on cortical response in healthy subjects: a randomized clinical trial of functional near-infrared spectroscopy study. *Front. Neurosci.* 16:810553. doi: 10.3389/fnins.2022.810553

Lopez, S., Bini, F., Del Percio, C., Marinozzi, F., Celletti, C., Suppa, A., et al. (2017). Electroencephalographic sensorimotor rhythms are modulated in the acute phase following focal vibration in healthy subjects. *Neuroscience* 352, 236–248. doi: 10.1016/j.neuroscience.2017.03.015

Ma, Y., Yu, Y., Gao, W., Hong, Y., and Shen, X. (2023). Cerebral hemodynamic changes during unaffected handgrip exercises in stroke patients: an fNIRS study. *Brain Sci.* 13:141. doi: 10.3390/brainsci13010141

Mahmood, A., Veluswamy, S. K., Hombali, A., Mullick, A. N. M., and Solomon, J. M. (2019). Effect of transcutaneous electrical nerve stimulation on spasticity in adults with stroke: a systematic review and Meta-analysis. *Arch. Phys. Med. Rehabil.* 100, 751–768. doi: 10.1016/j.apmr.2018.10.016

Manganotti, P., Acler, M., Formaggio, E., Avesani, M., Milanese, F., Baraldo, A., et al. (2010). Changes in cerebral activity after decreased upper-limb hypertonus: an EMG-fMRI study. *Magn. Reson. Imaging* 28, 646–652. doi: 10.1016/j.mri.2009.12.023

Marconi, B., Filippi, G. M., Koch, G., Giacobbe, V., Pecchioli, C., Versace, V., et al. (2011). Long-term effects on cortical excitability and motor recovery induced by repeated muscle vibration in chronic stroke patients. *Neurorehabil. Neural Repair* 25, 48–60. doi: 10.1177/1545968310376757

Marshall, R. S., Perera, G. M., Lazar, R. M., Krakauer, J. W., Constantine, R. C., and DeLaPaz, R. L. (2000). Evolution of cortical activation during recovery from corticospinal tract infarction. *Stroke* 31, 656–661. doi: 10.1161/01.str.31.3.656

Moggio, L., de Sire, A., Marotta, N., Demeco, A., and Ammendolia, A. (2022). Vibration therapy role in neurological diseases rehabilitation: an umbrella review of systematic reviews. *Disabil. Rehabil.* 44, 5741–5749. doi: 10.1080/09638288.2021.1946175

Monteiro, K. B., Cardoso, M. D. S., Cabral, V., Santos, A., Silva, P. S. D., Castro, J. B. P., et al. (2021). Effects of motor imagery as a complementary resource on the rehabilitation of stroke patients: a Meta-analysis of randomized trials. *J. Stroke Cerebrovasc. Dis.* 30:105876. doi: 10.1016/j.jstrokecerebrovasdis.2021.105876

Murillo, N., Valls-Sole, J., Vidal, J., Opisso, E., Medina, J., and Kumru, H. (2014). Focal vibration in neurorehabilitation. *Eur. J. Phys. Rehabil. Med.* 50, 231–242.

Naito, E. (2004). Sensing limb movements in the motor cortex: how humans sense limb movement. *Neuroscientist* 10, 73–82. doi: 10.1177/1073858403259628

Naito, E., Ehrsson, H. H., Geyer, S., Zilles, K., and Roland, P. E. (1999). Illusory arm movements activate cortical motor areas: a positron emission tomography study. *J. Neurosci.* 19, 6134–6144. doi: 10.1523/JNEUROSCI.19-14-06134.1999

Naro, A., Leo, A., Russo, M., Casella, C., Buda, A., Crespantini, A., et al. (2017). Breakthroughs in the spasticity management: are non-pharmacological treatments the future? *J. Clin. Neurosci.* 39, 16–27. doi: 10.1016/j.jocn.2017.02.044

Noma, T., Matsumoto, S., Etoh, S., Shimodozono, M., and Kawahira, K. (2009). Anti-spastic effects of the direct application of vibratory stimuli to the spastic muscles of hemiplegic limbs in post-stroke patients. *Brain Inj.* 23, 623–631. doi: 10.1080/02699050902997896

Powell, J. M., Rich, T. J., and Wise, E. K. (2016). Effectiveness of occupation- and activity-based interventions to improve everyday activities and social participation for people with traumatic brain injury: a systematic review. *Am. J. Occup. Ther.* 70:7003180040p1. doi: 10.5014/ajot.2016.020909

Rao, S. M., Binder, J. R., Bandettini, P. A., Hammeke, T. A., Yetkin, F. Z., Jesmanowicz, A., et al. (1993). Functional magnetic resonance imaging of complex human movements. *Neurology* 43, 2311–2318. doi: 10.1212/wnl.43.11.2311

Rehme, A. K., Eickhoff, S. B., Rottschy, C., Fink, G. R., and Grefkes, C. (2012). Activation likelihood estimation meta-analysis of motor-related neural activity after stroke. *NeuroImage* 59, 2771–2782. doi: 10.1016/j.neuroimage.2011.10.023

Rehme, A. K., Eickhoff, S. B., Wang, L. E., Fink, G. R., and Grefkes, C. (2011). Dynamic causal modeling of cortical activity from the acute to the chronic stage after stroke. *NeuroImage* 55, 1147–1158. doi: 10.1016/j.neuroimage.2011.01.014

Rocha, L. S. O., Gama, G. C. B., Rocha, R. S. B., Rocha, L. B., Dias, C. P., Santos, L. L. S., et al. (2021). Constraint induced movement therapy increases functionality and quality of life after stroke. *J. Stroke Cerebrovasc. Dis.* 30:105774. doi: 10.1016/j.jstrokecerebrovasdis.2021.105774

Sabatini, U., Chollet, F., Rascol, O., Celsis, P., Rascol, A., Lenzi, G. L., et al. (1993). Effect of side and rate of stimulation on cerebral blood flow changes in motor areas during finger movements in humans. *J. Cereb. Blood Flow Metab.* 13, 639–645. doi: 10.1038/jcbfm.1993.82

Souron, R., Besson, T., Millet, G. Y., and Lapole, T. (2017). Acute and chronic neuromuscular adaptations to local vibration training. *Eur. J. Appl. Physiol.* 117, 1939–1964. doi: 10.1007/s00421-017-3688-8

Starosta, M., Cichon, N., Saluk-Bijak, J., and Miller, E. (2022). Benefits from repetitive transcranial magnetic stimulation in post-stroke rehabilitation. *J. Clin. Med.* 11:2149. doi: 10.3390/jcm11082149

Staudt, M., Grodd, W., Gerloff, C., Erb, M., Stitz, J., and Krageloh-Mann, I. (2002). Two types of ipsilateral reorganization in congenital hemiparesis: a TMS and fMRI study. *Brain* 125, 2222–2237. doi: 10.1093/brain/awf227

Stroke (1989). Recommendations on stroke prevention, diagnosis, and therapy. Report of the WHO task force on stroke and other cerebrovascular disorders. *Stroke* 20, 1407–1431. doi: 10.1161/01.str.20.10.1407

Toscano, M., Celletti, C., Vigano, A., Altarocca, A., Giuliani, G., Jannini, T. B., et al. (2019). Short-term effects of focal muscle vibration on motor recovery after acute stroke: a pilot randomized sham-controlled study. *Front. Neurol.* 10:115. doi: 10.3389/fneur.2019.00115

Trompetto, C., Marinelli, L., Mori, L., Pelosin, E., Curra, A., Molfetta, L., et al. (2014). Pathophysiology of spasticity: implications for neurorehabilitation. *Biomed. Res. Int.* 2014:354906. doi: 10.1155/2014/354906

Van Hoornweder, S., Vanderzande, L., Bloemers, E., Verstraelen, S., Depestele, S., Cuypers, K., et al. (2021). The effects of transcranial direct current stimulation on upper-limb function post-stroke: a meta-analysis of multiple-session studies. *Clin. Neurophysiol.* 132, 1897–1918. doi: 10.1016/j.clinph.2021.05.015

Vazquez, A. L., Fukuda, M., and Kim, S. G. (2018). Inhibitory neuron activity contributions to hemodynamic responses and metabolic load examined using an inhibitory Optogenetic mouse model. *Cereb. Cortex* 28, 4105–4119. doi: 10.1093/cercor/bhy225

Veverka, T., Hlustik, P., Hok, P., Otruba, P., Tudos, Z., Zapletalova, J., et al. (2014). Cortical activity modulation by botulinum toxin type a in patients with post-stroke arm spasticity: real and imagined hand movement. *J. Neurol. Sci.* 346, 276–283. doi: 10.1016/j.jns.2014.09.009

Veverka, T., Hlustik, P., Tomasova, Z., Hok, P., Otruba, P., Kral, M., et al. (2012). BoNT-A related changes of cortical activity in patients suffering from severe hand paralysis with arm spasticity following ischemic stroke. *J. Neurol. Sci.* 319, 89–95. doi: 10.1016/j.jns.2012.05.008

Viganò, A., Celletti, C., Giuliani, G., Jannini, T. B., Marenco, F., Maestrini, I., et al. (2023). Focal muscle vibration (fMV) for post-stroke motor recovery: multisite neuroplasticity induction, timing of intervention, clinical approaches, and prospects from a narrative review. *Vibration.* 6, 645–658. doi: 10.3390/vibration6030040

Wang, H., Chandrashekhar, R., Rippetoe, J., and Ghazi, M. (2020). Focal muscle vibration for stroke rehabilitation: a review of vibration parameters and protocols. *Appl. Sci.* 10:8270.

Wang, H., Ghazi, M., Chandrashekhar, R., Rippetoe, J., Duginski, G. A., Lepak, L. V., et al. (2022). User participatory Design of a Wearable Focal Vibration Device for home-based stroke rehabilitation. *Sensors* 22:3308. doi: 10.3390/s22093308

Wang, L., Wang, S., Zhang, S., Dou, Z., and Guo, T. (2023a). Effectiveness and electrophysiological mechanisms of focal vibration on upper limb motor dysfunction in patients with subacute stroke: a randomized controlled trial. *Brain Res.* 1809:148353. doi: 10.1016/j.brainres.2023.148353

Wang, X., Luo, Z., Zhang, M., Zhao, W., Xie, S., Wong, S. F., et al. (2023b). The interaction between changes of muscle activation and cortical network dynamics during isometric elbow contraction: a sEMG and fNIRS study. *Front. Bioeng. Biotechnol.* 11:1176054. doi: 10.3389/fbioe.2023.1176054

Ward, N. S., and Cohen, L. G. (2004). Mechanisms underlying recovery of motor function after stroke. *Arch. Neurol.* 61, 1844–1848. doi: 10.1001/archneur.61.12.1844

Xue, X., Tu, H., Deng, Z., Zhou, L., Li, N., and Wang, X. (2021). Effects of brain-computer interface training on upper limb function recovery in stroke patients: a protocol for systematic review and meta-analysis. *Medicine (Baltimore)* 100:e26254. doi: 10.1097/MD.0000000000026254

Yang, F. (2020). Application of vibration training in people with common neurological disorders. *Man. Vib. Exer. Vib. Ther.*, 343–353.doi: 10.1007/978-3-030-43985-9_25

Zhang, J. J., Sanchez Vidana, D. I., Chan, J. N., Hui, E. S. K., Lau, K. K., Wang, X., et al. (2022). Biomarkers for prognostic functional recovery poststroke: a narrative review. *Front. Cell Dev. Biol.* 10:1062807. doi: 10.3389/fcell.2022.1062807

Zhang, Y., Wang, D., Wang, D., Yan, K., Yi, L., Lin, S., et al. (2023). Motor network reorganization in stroke patients with dyskinesias during a shoulder-touching task: a fNIRS study. *J. Innov. Opt. Health Sci.* 16:2340003. doi: 10.1142/s1793545823400035

Zhou, Z., Chen, S., Li, Y., Zhao, J., Li, G., Chen, L., et al. (2022). Comparison of sensory observation and somatosensory stimulation in Mirror neurons and the sensorimotor network: a task-based fMRI study. *Front. Neurol.* 13:916990. doi: 10.3389/fneur.2022.916990

Frontiers in Neuroscience

Provides a holistic understanding of brain function from genes to behavior

Part of the most cited neuroscience journal series which explores the brain - from the new eras of causation and anatomical neurosciences to neuroeconomics and neuroenergetics.

Discover the latest Research Topics

See more →

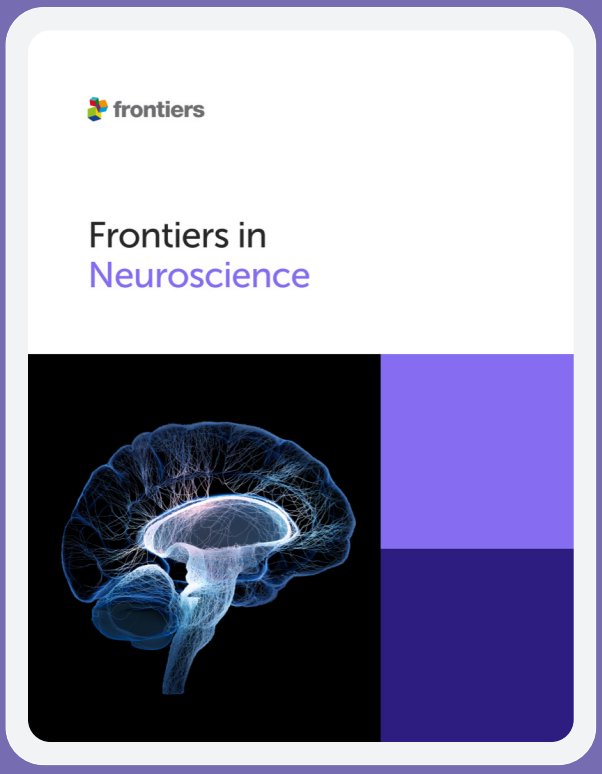

Frontiers

Avenue du Tribunal-Fédéral 34
1005 Lausanne, Switzerland
frontiersin.org

Contact us

+41 (0)21 510 17 00
frontiersin.org/about/contact